/
Article / Book Information

( )	
Title(English)	A Fundamental Study on Mechanical Behavior of Piled Raft Foundation in Sand Subjected to Horizontal and Moment Loads
( )	
Author(English)	Kouhei Sawada
( )	: ( ), : , : 10153 , :2016 3 26 , : , : , , ,
Citation(English)	Degree:Doctor (Engineering), Conferring organization: Tokyo Institute of Technology, Report number: 10153 , Conferred date:2016/3/26, Degree Type:Course doctor, Examiner:,,,,
( )	
Type(English)	Doctoral Thesis

A Fundamental Study on Mechanical Behavior of Piled Raft Foundation in Sand Subjected to Horizontal and Moment Loads

Kouhei Sawada

Dissertation

submitted in partial fulfillment of requirements for the degree of

DOCTOR OF ENGINEERING

at

Tokyo Institute of Technology

2016

Abstract

Recently, the design concept of the foundation in the geotechnical field has been shifting to the performance design, and the rational and economical foundation system is therefore required. In the conventional design of the pile group foundation although the raft base touches the ground surface, the contribution of the raft base is ignored from the safety point of view. The piled raft foundation is widely recognized as an economical and rational foundation system with the combined effect of the raft and piles. The concept of the piled raft foundation is to take advantage of the bearing capacity of the raft and to reduce the settlement to an acceptable level by installing a few friction piles.

Therefore, considerable researches on the settlement behavior of the piled raft foundation have been published to develop the concept of the piled raft, and the performance of the vertically loaded piled raft is gradually clarified. However, the behavior of the laterally loaded piled raft has not been well clarified due to the uncertainties in the complicated interaction of raft-ground-piles when it is subjected to seismic and horizontal loads. In particular, it is seemed that when the relatively large moment and rotation are acting on the piled raft, the behavior of the piled raft becomes much complex because the contact conditions between the raft and ground is varied during the loading.

Therefore, to clarify the mechanical behavior of piled raft subjected to horizontal and moment loads is required in highly seismic area such as Japan. The accumulation of the observed data under seismic and horizontal loads is crucial to address above issue. However, it is very rare case to record actual field data of the piled raft foundation during an earthquake. Physical models can play important role in the study of the piled raft under seismic and horizontal loadings because it can solve the difficulties in the field observations, whereas there should be rooms in the modeling techniques to obtain reliable test result and to accelerate future researches. In the present thesis newly developed centrifuge modeling techniques are proposed. In addition to this, the mechanical behavior of the piled raft foundation subjected to horizontal and moment load such as the complex interaction of raft-ground-piles is examined using proposed modeling techniques.

This thesis consists of following six chapters.

Chapter 1 is the introduction of this thesis.

Chapter 2 reviewed the experimental and analytical researches on the piled raft foundation, as well as reports on the construction case histories of the piled raft. The literature review examines the limitation of research on the laterally loaded piled raft.

Chapter 3 briefly describes the basic principal of the centrifuge modeling, and modeling concept and model preparation procedures are explained. In addition to this, the newly developed centrifuge modeling techniques is proposed. One of the most important conditions or parameters of the piled raft foundation is the load proportions between the piles and the raft. In the measurement of the load proportion for the piled raft foundation, the forces acting on the piles are first measured and then load carried by the raft part is estimated from the strain gauges, especially for the relatively small foundation with a few numbers of piles. Therefore, the accurate measurements of strain in the piles are crucial in the modeling of piled raft foundation. The measurement accuracy of the strain gauge is carefully discussed in this chapter.

Chapter 4 examined the behavior of the piled raft subjected to the vertical load. The foundations are experienced three vertical loading steps prior to the horizontal loading tests during the model preparation. The main objective of this chapter is to verify the initial conditions before the vertical loading tests. Beside this, the mechanical behavior of the vertically loaded piled raft foundation such as the influence of the raft pressure on the vertical pile response is examined. The principal findings are; the raft vertical proportion RVLP can be controlled by loading and unloading process; the vertical bearing load is larger for the piled raft than the pile group because the bearing load of the raft can be obtained and raft pressure enhanced the shaft friction load.

Chapter 5 examines the mechanical behavior of the piled raft foundation subjected to horizontal and moment loads in sand was examined. The much focus was placed on the influence of the raft base pressure on the pile response. The findings from this chapter are; although the piled raft foundation can restrain the settlement caused by the alternate horizontal loading, the upward movement of the pull-out pile might be critical issue in the piled raft foundation; the horizontal and moment resistance of the piled raft foundation is higher for the piled raft than the pile group because the base resistance can be obtained in the piled raft and raft pressure gives the positive influence on the pile part. However, the raft part has negative effect on the pull-out pile.

Chapter 6 described the conclusions derived from the present thesis.

Acknowledgement

This dissertation concludes the research work which was carried out at Tokyo Institute of Technology, Graduate School of Science and Engineering, between October 2009 and March 2016.

First, I would like to thank my research supervisor Associate professor Jiro Takemura of Tokyo Institute of Technology for his continuous support and kind guidance. I could not completed this dissertation without his support.

My thanks should be extended to the other committee members of this thesis, Professor Junichiro Niwa, Professor Masaki Kitazume, Professor Akihiro Takahashi, Pipatpongsa Thirapong, and Anil C. Wijeyewickrema for their careful reviews and kind advice.

Other members of Tokyo Institute of Technology, Geotechnical Engineering Group faculty were particularly helpful with specific areas of this work. I spent valuable and pleasant time in the laboratory during my doctoral course. Professor Osamu Kusakabe, Dr. Jun Izawa of Railway Technical Research Institute, who was formally Research Associate at Tokyo Institute of Technology, Associate Professor Tomohide Takeyama, who was formally Research Associate at Tokyo Institute of Technology, and Mr. Sakae Seki, Technician. Professor Osamu Kusakabe suggested valuable references, and guided my project for the better. Dr. Jun Izawa and Associate Professor Tomohide Takeyama helped my research and gave valuable and pleasant time in the laboratory life. Mr. Sakae Seki also helped my research. He taught me the various knowledge of centrifuge model tests. Chapter 3 in my thesis could not have concluded without his cooperation. I would like to thank them for all their cooperation and help.

I would like to show my sincere appreciation to the support of Japan Society for the Promotion of Science for my JSPS Research Fellow (DC 12J08185).

Words are not enough to thank my parents for the support they have given me during my doctoral course.

Kouhei SAWADA

Contents

CHAPTER 1

INTRODUCTION

1.1 Background

Types of foundation can be mainly divided into two, one is raft (shallow) foundation, and the other is piled (deep) foundation (Fig. 1.1.1). From the economic point of view, the raft foundation will generally be applied. In the design of the raft foundation, it is required to confirm that bearing capacity of the raft is sufficient and the settlement of the foundation is an acceptable level. In sandy grounds, the enough bearing capacity could be mostly secured from the ground for the raft foundation because the bearing capacity increased with the foundation size.
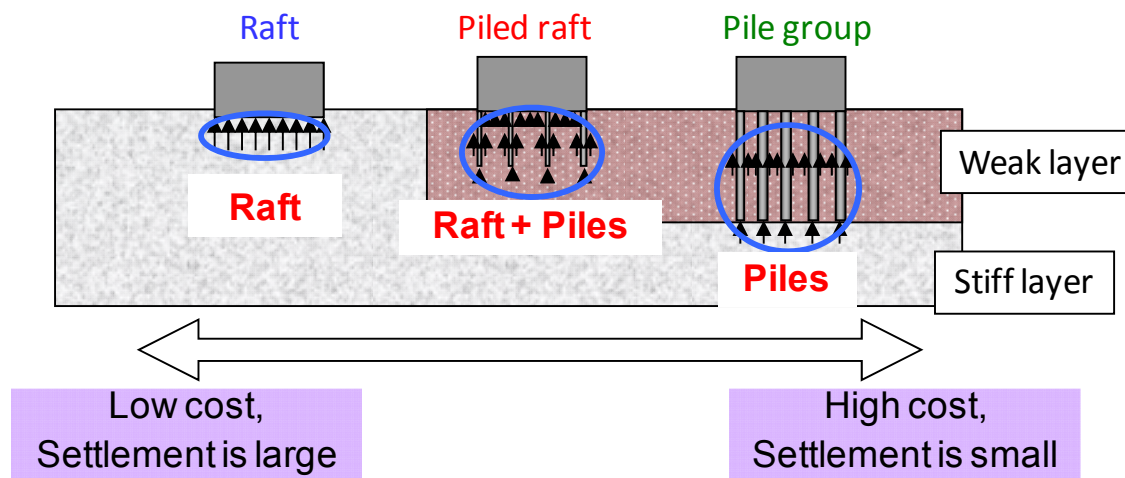

Figure 1.1.1 Foundation type and bearing capacity mechanism

However, the estimated total and differential settlements might be excessive even though the bearing capacity of the raft is sufficient. In such case, a piled foundation is employed, and piles are installed beneath the raft in order to reduce the raft settlement. In the conventional piled foundation design, pile specifications, such as number of piles, pile length ant diameter, are determined by assuming that all loads are supported by only piles, and ignoring the contribution from the raft or the pile cap even though the raft base has a contact with the ground surface. This design concept is derived from two reasons. One is complex interaction of raft-ground-piles, which makes it much difficult to analyze actual load sharing between the raft and the piles. Another is from the safety view point. In the application of the piled foundations, the pile tip generally reached at stiff layer, and therefore, the vertical movement of the structure is quite small. However, there is a potential for the soil above the support layer to settle down during and after the construction, which leads uncertainty in securing the contact condition between the raft base and the ground surface. Consequently, the bearing capacity of the foundation

system is overestimated when the contribution from the raft base is taken into account in the foundation design.

The piled raft foundation has been recognized as an economical and rational foundation system since Burland et al. (1977) presented the concept of the "settlement reducers". The concept of the piled raft foundation is to take the advantage of the bearing capacity of the raft and to reduce the settlement of foundation to an acceptable level by installing friction piles beneath the raft base. Piles in the piled raft foundation play the roles of reducing the settlement and transferring a part of the load to the deep ground. Although the settlement of the piled raft foundation can be restrained in an acceptable level by the friction piles, it is actually larger for the piled raft than the conventional piled foundation. However, this relatively larger settlement can secure the ~~strict~~ contact condition between the raft base and the ground, resulting that the bearing capacity from the raft base could be positively considered in the piled raft design.

Thus, the piled raft foundation is economical and rational foundation system because the contribution from the raft base can be taken in the design, and specifications of piles could be reduced. A design code of the piled raft foundations has been published in Japan (Architectural Institute of Japan 2001), and the piled raft foundations have been applied recently to the actual buildings in Japan (Yamashita 2012). However, the behavior of the piled raft foundation is not well clarified due to the complicated interaction among the raft, ground and piles, especially under the seismic or horizontal loadings as shown in Fig. 1.1.2. Therefore for introducing a rational design of the piled raft foundation in highly seismic area such as Japan, it is crucial to clarify the mechanical behavior of the piled raft foundation subjected to seismic and horizontal loading.

1.2 Objectives

The concept of the piled raft foundation is to use the piles as "settlement reducers", which originated from Burland et al. (1977). Therefore, researches on the settlement behavior of the piled raft foundation have been actively reported to develop this concept. On the other hand, the researches on the piled raft foundation subjected to horizontal loading are relatively limited. In order to clarify the complicated behavior of the piled raft foundations, accumulation of the observed data under horizontal loading is required.
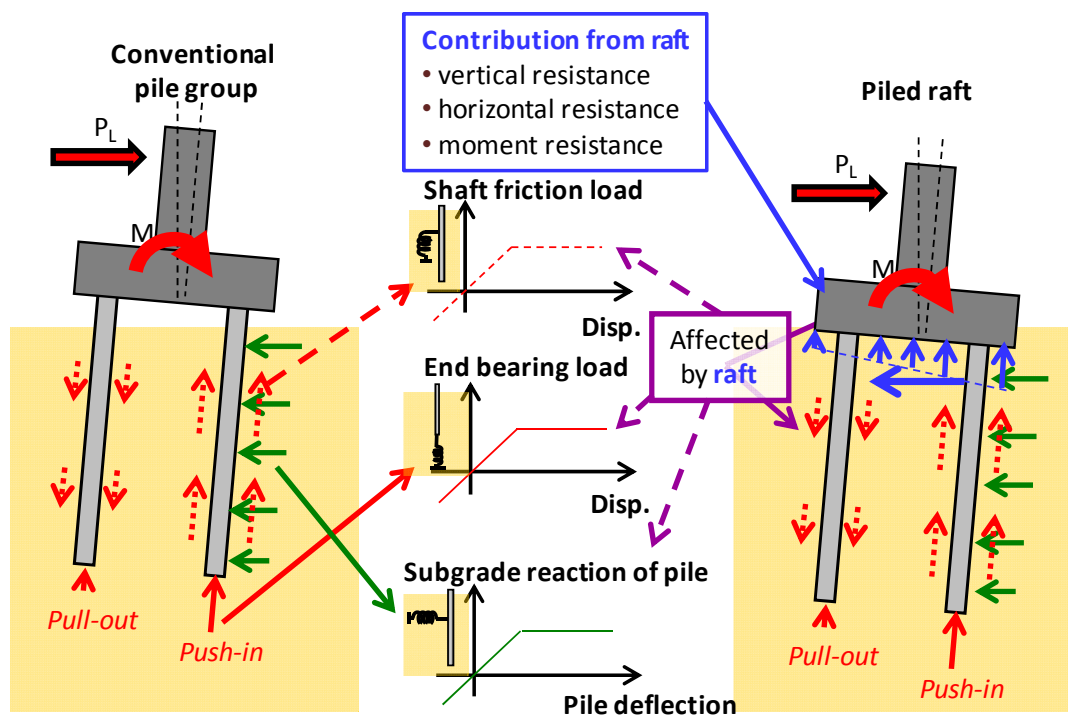
Figure 1.1.2 Complicated behavior of the piled raft subjected to horizontal and moment loads

Field observations of the piled rafts have accumulated especially during the construction period. However, field records on the performance of the piled raft foundation attacked by the actual seismic loading are still very limited. Furthermore, from a single observed event, it is very difficult to obtain a general mechanical behavior of the foundation and develop a design method for the piled raft foundation due to the complexity of the site boundary conditions.

Physical modeling tests can an important role in the study of the piled rat because it can solve the difficulties of field observations with its capability of investigating the various factors under clear boundary and initial conditions. Consequently, researches on the piled raft using physical modeling are increasing in a last decade (Horikoshi et al. (2002 a, b); Matsumoto et al. (2004); Hamada et al. (2012)). However, the behavior of the piled raft foundation subjected to horizontal loading is not still well understood especially when the large moment load and rotation arise on the structure. The behavior of the piled raft under relatively large moment load and rotation becomes much complex because the contact conditions between the raft base and the ground surface, i.e., interaction among the raft, ground and piles, might vary during the loading. It is crucial to clarify the mechanical behavior of the piled raft subjected to the moment load and

3

rotation because relatively high moment load is occurs during the earthquake for the civil engineering structure, especially for the relatively small size foundations, such as those for viaducts. Therefore, the present research carried out centrifuge model tests on a small size piled raft foundation to clarify its mechanical behavior. Much focus was placed on the performance of the piled raft under relatively large moment load and rotation.

Although the expectations for the physical modeling on the piled raft have been raised as mentioned above, modeling techniques on the piled raft have not been well discussed and established. It is required to develop modeling techniques to make the research much reliable and thus to enhance the study on the performance of the piled raft. Therefore developing physical modeling techniques on the piled raft foundation is also one of main objectives in this thesis.

1.3 Thesis structure

The present thesis consists of the following six chapters.

- Experimental researches and analytical researches on the piled raft foundation are reviewed in Chapter 2, as well as reports on case histories of piled raft foundation. The literature review will explain the limitation of the various techniques and will indicate the current problem of the piled raft foundation. And then, the objectives and thesis stream will be presented.

- In Chapter 3, basic principal of the centrifuge is discussed and the centrifuge modeling technique of the piled raft is proposed. The procedure of the foundation preparation and the model foundation used in the present study are explained. In particular, the measurement accuracy of the strain gauge was carefully discussed because shared loads between the raft and the piles are generally estimated by the strain gauge.

- The piled raft foundation subjected to vertical load was examined in Chapter 4. The foundations experienced the three vertical loading processes before the horizontal loading tests. The main objectives of the present chapter was to examine the mechanical behavior of the piled raft foundation subjected to vertical load and to verify the initial conditions of the foundation before the horizontal loading tests.

- In Chapter 5 the mechanical behavior of the piled raft foundation subjected to horizontal and moment loads in sand was examined. The much focus was placed on the influence of the raft base pressure on the pile response.

- The conclusions derived from the present thesis are summarized in Chapter 6.

CHAPTER 2

LITERATURE REVIEW

2.1 Introduction

The piled raft foundation has been widely recognized as an economical and rational foundation system because the settlement of the structure can be restrained in an acceptable level by the combined effect of the raft and piles. However, the interaction among the raft, ground and piles must be considered and hence the design of the piled raft becomes rather complex. It is sure that the design code of the piled raft foundation is published by Architectural Institute of Japan and the piled raft foundations are applied to the actual foundations, especially for the architectural structures such as tall building, but almost foundation designs employ a very simple and non-rational method in which the contribution of piles is ignored, the horizontal load is therefore assumed to be carried only by the raft because of the complex interaction among the raft, ground and piles. In order to adequately evaluate the performance of the piled raft foundation, accumulation of observed data by the field measurement and the physical modeling, and establishment of practical analysis method are required.

Considerable researches on the settlement behavior of the piled raft foundation have been reported because the concept of the piled raft foundation has been developed with the design philosophy in which the settlement of the structure is reduced in a required settlement by friction piles. On the other hand, researches on the horizontally loaded piled raft foundation are relatively limited. In this chapter, the literature review will firstly examine the theories and the experiment data of pile group foundation which is the component of the piled raft. Then, the literature review on the piled raft foundation will examine the differences between the present thesis and previous works will be focused.

2.2 Single pile and pile group foundation

In this section, literature review will focus on the theories and experimental data of the pile, which is consisting of the piled raft foundation.

2.2.1 Bearing capacity of single pile

The behavior of the isolated pile subjected to the horizontal loading is generally evaluated by the following equation in which the interaction between the pile and the soil is represented as a spring.

$$EI\frac{d^4y}{dz^4}+D\cdot p(z,y)=0 \tag{2.2.1}$$

E : Young's modulus of pile

I : Moment inertia of pile

D : Outer diameter of pile

y : Horizontal deflection

z : Depth

$p(z,y)$: Horizontal subgrade reaction

In particular, the relationship between p and y in this equation stands for the lateral soil resistance-deflection relation, and it is so-called p-y relationship in general. The evaluation method basing on the pile-soil spring can be identified into three categories by the spring type such as the elastic subgrade reaction method、 ultimate subgrade reaction method、 and composite subgrade reaction method. Considerable researches on the p-y relationship have been published as follows.

i) Elastic subgrade reaction method

In the elastic subgrade reaction method, the horizontal resistance of the pile is calculated by assuming that the soil around pile is treated as the perfect elastic material and the pile itself is modeled as the beam. In this method, it can be said that the soil horizontal resistance, p, is the function of the pile deflection, y, and depth, z as below equation, where k_h is the coefficient of subgrade reaction.

$$p(z,y) = k_h z^m y^n \tag{2.2.2}$$

The horizontal resistance of pile is significantly depending on parameters of m and n in this method, various ideas to decide them have been proposed.

Chang (1937) solved eq. (2.2.1) using eq. (2.2.3) in which the horizontal soil resistance has a linear relationship with deflection, y ($n=1$), and it is independent value against depth, z ($m=0$).

$$p(z,y) = k_h y \tag{2.2.3}$$

The general solution of eq. (2.2.1) using eq. (2.2.3) is given as bellows, where $C_1 \sim C_4$ are the integral constant, and β is the characteristic value of pile and it is described by eq. (2.2.5).

$$y_z = e^{\beta z}(C_1 \cos\beta z + C_2 \sin\beta z) + e^{-\beta z}(C_3 \cos\beta z + C_4 \sin\beta z) \tag{2.2.4}$$

$$\beta = \sqrt[4]{\frac{D \cdot k_h}{4EI}} \tag{2.2.5}$$

Chang (1937) also proposed that the pile type can be divided into two, such as Long pile and Short pile, using β and the pile embedment length, L_0,

$$\beta \cdot L_0 > \pi \qquad \rightarrow \qquad \text{Long pile}$$

$$\beta \cdot L_0 < \pi \qquad \rightarrow \qquad \text{Short pile}$$

According to the beam bending theory, slope-deflection θ_z、 bending moment M_z、 shear force S_z、 horizontal soil resistance p_z along the pile shaft can be estimated as bellows.

$$\theta_z = -\frac{dy_z}{dz}, \quad M_z = -EI\frac{d^2 y_z}{dz^2}, \quad S_z = -EI\frac{d^3 y_z}{dz^3}, \quad p_z = k_h z, \qquad (2.2.6)$$

Chang (1937) compared the simulated result with the large scale horizontal loading tests done by Feagin (1937), in which the pile head rotation was fixed. By this comparison, Chang (1937) confirmed that even if the horizontal subgrade reaction, k_h, is assumed as a constant value of k_h at first fixed point along the ground depth, the pile behavior can be predicted with a high accuracy.

As well as Chang (1937), Broms (1964a, b) also solved the governing eq. (2.2.1) using eq. (2.2.3), and validate these equation by comparing with the horizontal loading tests on the isolate pile done by previous researches. Broms (1964a, b) confirmed that k_h was the constant against the depth ($m=0$) for the cohesive soil, on the other hand, in the cohesionless soil, he supported eq. (2.2.7) established by Terzaghi (1955), where k_h varies inversely with the depth and the pile diameter, D, respectively.

$$p(z, y) = n_h \frac{z}{D} y \qquad (2.2.7)$$

The n_k in this equation is a kind of constant value, and Terzaghi (1955) proposed approximate value for each soil type.

Thus, Chang (1937) and Broms (1964a, b) proposed that there was a linearity between the horizontal soil resistance, p, and the pile deflection, y ($n=1$), however, Kubo (1961, 1962, 1964, 1965) found that n value in eq. (2.2.2) is around 0.5 through a number of small and large scale model tests. Additionally, they proposed m value in eq. (2.2.2) has two different values according to the soil conditions. For Type S soil where the soil strength such as N value derived from the standard penetration tests linearly increased with the ground depth, the coefficient of subgrade reaction is also proportional to the depth

(*m*=1). The soil having constant N value along the ground depth is named Type C soil, where the coefficient of subgrade reaction is considered constant value regardless the depth (*m*=0). Kubo (1961, 1962, 1964, 1965) confirmed that discrimination of Type S and C soils is not required at the deep area of the ground, and it is enough to determine the soil type at the area shallower than a certain depth where the bending moment acting on the piles is zero. He also proposed that the behavior of the prototype pile can be estimate from the loading tests on the standard pile using the scaling law. Terashi (1989) et al. testified this method, which assumed the value of *n* is 0.5, by comparing the results of horizontal loading tests on the pile.

However, the restriction of "Elastic subgrade reaction method" is limitation to relatively small pile displacement, and it cannot treat the large displacement problem.

ii) Ultimate subgrade reaction method

Ultimate subgrade reaction method proposed by Broms (1965) assumes the profile of the horizontal soil resistance at the ultimate state, and estimates the pile horizontal resistance using equilibrium of external force acting on the pile, horizontal soil resistance, *p*, is therefore a function of *z* (*p=p(z)*). Broms (1965) expressed the horizontal soil resistance for the sandy soil as three times Rankin's passive earth pressure shown in eq. (2.2.8).

$$p_{\max} = 3K_P \sigma_v{}'$$
<div align="right">(2.2.8)</div>

The p_{max} in this equation is ultimate horizontal soil resistance, K_p is the coefficient of Rankin's passive earth pressure and $\sigma_v{}'$ is the effective vertical stress. However, this method cannot deal with the pile displacement problem because the horizontal resistance of the pile is determined by the equilibrium of force at the ultimate state.

iii) Composite subgrade reaction method

The composite subgrade reaction method is the combination of the elastic subgrade reaction and ultimate subgrade reaction methods. The cross-sectional force of pile and soil resistance at relatively large deformation can be taken into account by this method. Reese et al. (1974) introduced the ultimate subgrade reaction into the *p-y* relationship, where *p-y* relationship up to ultimate state was expressed by the line and parabolic function. This method has been adopted in API (American Petroleum Institute). Kishida and Nakai (1979) simply expressed the non-linear *p-y* relationship as the bi-linear model using the coefficient of subgrade reaction k_h and the ultimate horizontal soil resistance p_{max}. Kishida and Nakai (1979) confirmed that *p-y* relation using bi-linear models can represent accurately

the actual pile behavior by comparing with the horizontal loading tests on small and large scale pile done by Kubota (1977) and Suzuki (1976).

Yamakata et al. (1968, 1969, 1970) and Siva (1970) employed the plasticity into the soil resistance around the ground surface where the soil deformation might be relatively large. Wu (1998) proposed the p-y curve described by hyperbolic function. Li and Peter (1992) used p-y curve with parabolic, and justified the validation of this method by comparing the horizontal loading tests of the pile done by Morison (1986) and *p-y* curve from API method. Furthermore, Georgiandis et al (1992), Det Norske Verias (1980), Scott (1980), Murchison and O'Neil (1984) also proposed various methods about *p-y* curve.

Thus, *p-y* relationship is of considerable significance to comprehend the behavior of the horizontally loaded pile, especially the coefficient of subgrade reaction and the ultimate soil resistance, which determines the initial gradient of *p-y* curve and maximum soil resistance respectively, are crucial. However, due to the non-linearity of the soil and the complexity of the interaction between the pile and soil, p-y curves employed in the various design method as expressed below have been empirically or semi-empirically determined.

Japan Port and Harbor Association:

$$p(z,y) = k_{hs} z y^{0.5} \tag{2.2.9}$$

Japan Road Association、 Railway Technical Research Institute:

$$\begin{aligned} p(z,y) &= k_h y \qquad p \le p_{max} \\ p &= p_{max} \qquad p \ge p_{max} \end{aligned} \tag{2.2.10}$$

$$\text{API:} \quad p(z,y) = p_{max} \tanh\left(\frac{k_h \dfrac{z}{D} y}{p_{max}}\right) \tag{2.2.11}$$

2.2.2 Researches on Pile group

Previous section summarized the horizontal response of the isolated pile, while piles in the actual piled foundation behaved not as the isolated pile but as the pile group because many piles are installed beneath the raft base in the actual piled foundation. Consequently, the interaction of pile-soil-pile in the pile group must be considered, and the problems are much complex compared with the isolated pile. In this section, literature review will focus on the behavior of the pile group subjected to horizontal load.
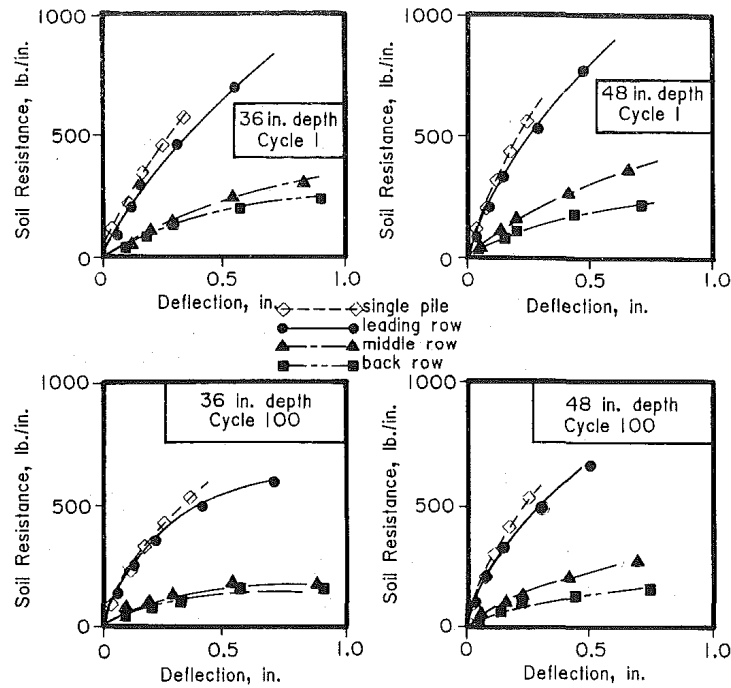
Figure 2.2.1 Typical p-y curves by row position for piles in group. (Brown et al. (1988))

Brown et al. (1988) carried out horizontal loading test on the single pile and pile group with nine piles (*s/D* is three, where *s* is the pile spacing and *D* is the pile diameter) in the sandy soil using the stainless steel pile with 273mm diameter, 9.27mm thickness and 3m length. Several strain gauges were attached at the model piles to measure the bending moment acting on piles. From the bending moments, *p-y* curve was estimated using method proposed by Matlock and Ripperger (1956). Brown et al. (1988) confirmed that piles in the front row and the single pile showed similar tendency of *p-y* curve, but the coefficient of subgrade reaction was much smaller for piles in the trailing row than the single pile as shown in Fig. 2.2.1 because of the influence of the piles in the leading row. This reduced efficiency of the trailing piles in the group was called the effect of "shadowing". Reduction ration of piles in the group against the single pile are therefore defined by employing the *p-multiplier* P_m as shown in Fig. 2.2.2. From the result of horizontal loading tests, it was found that only 40% of horizontal resistance was observed for the piles in the trailing row than the single pile as shown in Fig. 2.2.3. Remaud et al. (1998) also conducted the horizontal loading tests on the pile group in the sand by varying the pile spacing, and similar result as Brown et al. (1988) was derived. They also found that reduced resistance in the trailing piles can be ignored over the ratio of pile spacing on the pile diameter of six.
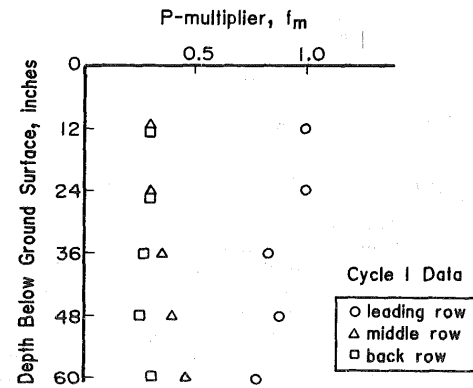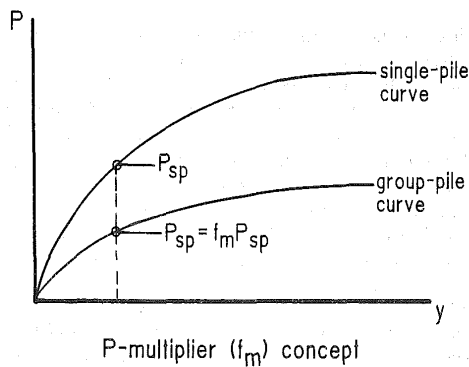
Figure 2.2.2 p-multiplier concept. (Brown et al. (1988))

Figure 2.2.3 Experimental p-multipliers vs. depth. (Brown et al. (1988))

Table 2.2.1 p-multiplier values from large-scale experiments. (Rollins et al.(1998))

Soil properties (reference) (1)	Pile properties (2)	Deflection range (mm) (3)	Front row (4)	2nd row (5)	3rd row (6)	4th row (7)
Clayey slit (CL-ML, ML); S_u = 50 to 75 kPa (1,000 to 1,500 psf); PI = 5–20; LL = 25–40 (this study)	Driven 324 mm OD steel pipe pile with concrete fill	25–60	0.6	0.4	0.4	—
Loose fine sand (SP); D_r ~ 20–40%; ϕ = 32° (Ruesta and Townsend 1997)	Jetted/driven 760 mm square pre-stressed concrete pile	25–75	0.8	0.7	0.3	0.3
Clean medium sand (SP); D_r ~ 50%; ϕ = 38°; sand placed after pile driving was completed (Brown et al. 1988)	Driven 272 mm OD steel pipe with grout fill	25–38	0.8	0.4	0.3	—
Stiff clay (CL to CH); overconsolidated by decissation; S_u = 70 to 180 kPa (1,400 to 3,600 psf); PI = 30–50, LL = 40–70; (Brown et al. 1987)	Driven 272 mm OD steel pipe pile with grout fill	30 / 50	0.7 / 0.7	0.6 / 0.5	0.5 / 0.4	— / —
Silty Clay (CL); S_u = 25 kPa (500 psf); ϕ' = 38–42°; c' = 0; PI = 15–25; LL = 35–45; (Meimon et al. 1986)	Driven 284 × 270 mm steel H-pile with side plates to form a box section.	15	0.9	0.5	—	—

Brown et al. (1987) carried out horizontal loading tests on the single pile and the pile group using the same pile as research by Brown et al (1988). They reported that although the p-y curves were almost same between the single pile and piles in the group at the relatively small pile deflection, the smaller coefficient of subgrade reaction was observed for the piles in the group than the single pile at the large deflection of pile.

Rollins et al. (1998) carried out the horizontal loading tests on the single pile and pile group in a 3×3 configuration and with a nominal spacing of three-pile diameters center to center. The model pile is stainless steel pile with 305mm in inner diameter, 9.5mm in thickness and 9.1m in length. Rollins et al. (1998) compared the tests result done by them and by others (Sparks and Rollins (1997), Ruesta and Townsend (1997), Brown et al. (1987, 1988) and Meimon et al. (1986)) with the computing analysis, GROUP, developed by Reese et al. (1996), and *p-multiplier* (P_m) which was proposed by Broms (1988) was back-calculated (Table 2.2.1). By this comparison, it was found that the p-multipliers did not appear to be sensitive over nominal pile spacing of six-pile diameters

(Fig. 2.2.4). This trend had an agreement with the research findings derived from Cox et al. (1984), who confirmed that the effect of pile group can be ignored at the pile spacing-pile diameter ration of six.
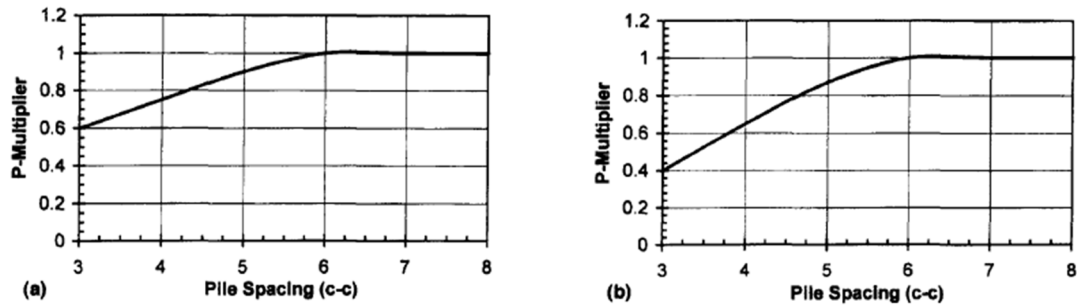
Figure 2.2.4 Interim design curves for p-multipliers as function of pile spacing. (Rollins et al. (1998))

Llyas et al. (2004) carried out horizontal loading tests on the pile group in normal and over consolidated clay. Much focus was placed on the influence of the pile spacing and number of piles on the performance of horizontally loaded pile group. It was found that shadowing effect proposed by Brown (1988) was observed at pile spacing of less than three-pile diameter, however, there was no difference between the single pile and piles in the pile group at pile spacing of more than five-pile diameter (Fig. 2.2.5). The slight group effect at the pile spacing of more than five-pile diameter was also confirmed by McVay et al (1994). Furthermore, Llyas et al. (2004) described Table 1, where the *p-multiplier* (P_m) obtained from previous research was summarized.
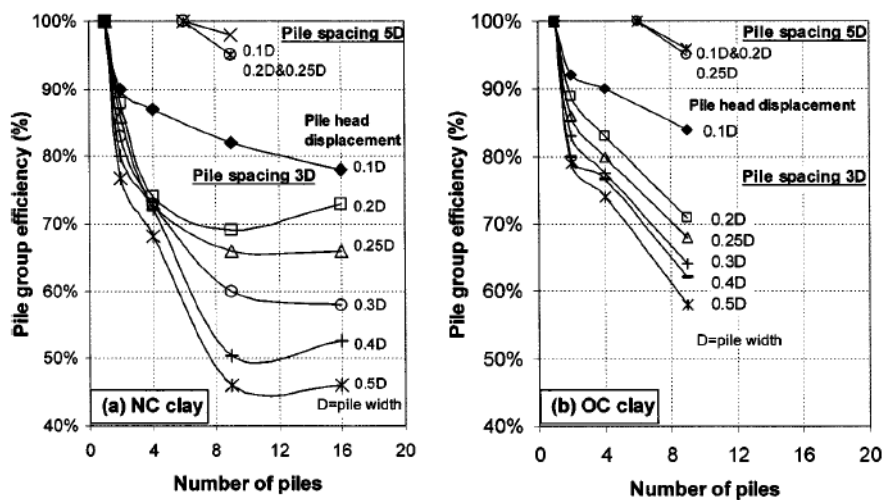
Figure 2.2.5 Pile group efficiency (p-multiplier) at various pile head displacement. (Llyas et al. (2004))

12

Thus, it has been widely recognized that the behaviors of the isolated pile and piles in the group were significantly different, i.e., the smaller pile spacing is, the smaller pile horizontal resistance in the group is. The reduction ratio of piles in the group on the single pile has been determined experimentally, it can be therefore said that the routine design of piled foundation relies largely on empirical or semi-empirical approaches, owing to the complicated interactions between the components.

2.3 Piled raft foundation

2.3.1 Settlement behavior of piled raft foundation

2.3.1.1 Analytical study

Analytical methods of estimating piled raft behavior are major concerns in this section. Several methods of analyzing piled rafts have been developed, which are summarized by Poulos et al. (1997, 2001) and Randolph (1994). Two broad classes of analysis method have been identified.

i) Simplified calculation methods

Poulos and Davis (1980) introduced a simple method of estimating the overall load-settlement curve to failure for the piled foundation. It is assumed that a part of the pile group is replaced by the equivalent pier. This method is therefore called "equivalent pier method". They presented two types of equivalent piers; single equivalent pier of the same cross-sectional area as the original and of equivalent pile length, L_{eq}; single equivalent pier of the same pile length as the original, but with an equivalent pier diameter, d_{eq}. The resultant load-settlement curve is tri-linear, reflecting the three main portions such as no yielding, piles yielding and piles and raft yielding regions. However, it should be noted that the shared load by the raft and piles cannot be taken into account.

A useful extension to Poulos's method can be made by using the simple method of estimating the load sharing between the raft and piles, as outlined by Randolph (1983, 1994). The stiffness of piled raft and ratio of shared load carried by components are represented:

$$k_{pr} = \frac{k_p + k_r \left(1 - 2\alpha_{rp}\right)}{1 - \left(k_r / k_p\right)\alpha_{rp}^2} \tag{2.3.1}$$

$$\frac{P_r}{P_p} = \frac{1 - \alpha_{rp}}{1 - \left(k_r / k_p\right)\alpha_{rp}} \times \frac{k_r}{k_p} \tag{2.3.2}$$

where k_{pr} is stiffness of piled raft, k_r is stiffness of raft, k_p is stiffness of piles, α_{rp} is

13

interaction factor of pile group on raft, P_r is load carried by raft and P_p is load carried by piles. The raft stiffness k_r can be estimated via elastic theory, for example using the solutions of Mindlin (1936), Fraser and Wardle (1976) and Mayne and Poulos (1999). The pile group stiffness can be also estimated from elastic theory such as that described by Poulos and Davis (1980) and Poulos (1989). α_{rp} is given by following:

$$\alpha_{pr} = 1 - \frac{\ln(r_r/r_p)}{\ln(r_m/r_p)}$$

(2.3.3)

where r_r is radius of raft, r_p is pile radius and r_m is maximum radius of influence of each individual pile. α_{rp} approached a value of approximately 0.8 for a wide range of the number of piles, pile spacing and pile stiffness.

ii) Hybrid method and Numerical approach

A boundary element method (BEM) to predict the settlement of piles and pile groups with incompressible pile and perfectly rigid pile cap was developed by Poulos and Davis (1968) and Poulos (1968). Referring to Fig. 2.3.1, the displacement p_i of the soil adjacent to the center of the periphery of an element i on pile 1 due to pile 1 itself and the adjacent pile 2 is

$$p_i = \sum_{j=1}^{j=n} p_j \left({}_1 I_{ij} + {}_2 I_{ij} \right) + p_b \left({}_1 I_{ib} + {}_2 I_{ib} \right)$$
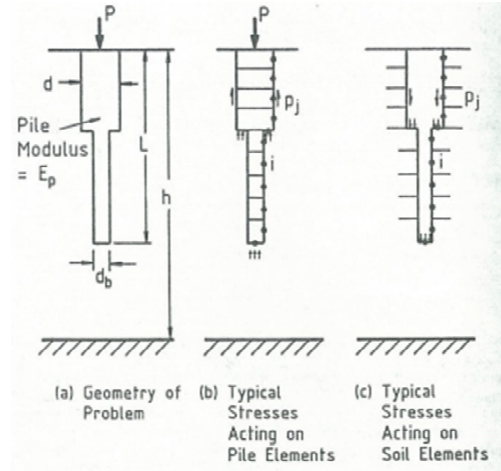
Figure 2.3.1 Boundary element analysis of single pile. (Poulos and Davis (1968))

(2.3.4)

where ${}_1 I_{ij}$ is the displacement influence factor at element i due to a uniform ring load on element j on pile 1, ${}_2 I_{ij}$ is the displacement influence factor at element i due to a uniform ring load on element j on pile 2 and ${}_1 I_{ib}$ is the displacement influence factor at element i due to a uniform load on the base of pile 1, and similarly for ${}_2 I_{ib}$. Similar expression for the displacement of pile tip p_b was proposed.

$$p_b = \sum_{j=1}^{j=n} p_j \left({}_1 I_{bj} + {}_2 I_{bj} \right) + p_b \left({}_1 I_{bb} + {}_2 I_{bb} \right)$$

(2.3.5)

where ${}_1 I_{bj}$ is the displacement factor for the pile base due to a uniform ring load on element j on pile 1, and similarly for ${}_2 I_{bj}$ and ${}_1 I_{bb}$ is the displacement factor for pile base due to a uniform load on the base of pile 1, and similarly for ${}_2 I_{bb}$. These

displacement factors can be obtained by integration of the Mindlin's equation.

A rigorous boundary element method for pile groups with rigid raft was reported by Butterfield and Banerjee (1971a, b), in which pile compressibility and influence of pile cap on the group can be taken into account. Mindlin's solution based on elastic theory for a point load embedded in the interior of semi-infinite elastic solid is adopted as a convenient singular solution. The result show that the load displacement characteristics of similar pile group with and without pile cap were different, i.e., the contacting cap increased the foundation stiffness by 5-15%. This increase was dependent on the group size and the pile spacing. Although the pile compressibility and pile cap existing can be considered, the differential settlement of the raft was not dealt with because the raft was assumed fully rigid.

Ottaviani (1975) analyzed a pile group with and without a rigid cap in a homogeneous elastic medium by using the three dimensional finite element approach. Ottaviani reported that the contacting cap greatly reduced the shear stress in the soil around the upper portion of the piles, and, at the same time, increase the vertical stresses in the soil underneath the pile base.

Hain (1975) and Hain and Lee (1978) analyzed the piled raft having a flexible raft in an elastic homogeneous or non-homogeneous material. The pile group-supporting soil system is modeled by the Mindlin's equation for a deep homogeneous soil mass. The failure of individual piles at loads less than the total group capacity was represented by applying an excess load cut-off procedure. Interaction factor method was employed to consider the interaction between each component. The raft was composed of rectangular plate bending finite elements, and the raft stiffness ratio was introduced:

$$K_R = \frac{4E_R t_R B_R (1 - v_s^2)}{3\pi E_S L_R^4} \tag{2.3.6}$$

where K_R is the raft-supporting soil relative stiffness, E_R, E_P and E_S are Young's modulus of the raft, pile and soil mass respectively, v_S is Poisson's ratio of the soil and L_R, B_R, t_R are length, breadth and thickness of the raft respectively. Two piled raft application on actual site, namely, La Azteca building, Mexico City and Hyde Park Cavalry Barracks, London reported by Zeevaert (1957) and Hooper (1973) respectively were reanalyzed. There was encouraging agreement between measured and predicted settlements and pile load.

Brown and Wiesner (1975) analyzed uniformly loaded piled raft, where the raft and piles were modeled as the strip footing and incompressible pile respectively. In order to obtain the displacement, the integration technique described by Poulos and Davis (1968) and Mindlin's solution were employed. They introduced different raft stiffness ratio K_{st} from Hain and Lee (1978):

$$K_{st} = \frac{16EI(1-v_s^2)}{\pi E_S L^4} \qquad (2.3.7)$$

where E is Young's modulus of the footing, I is second moment of area of the footing, v_s is the Poisson's ratio of the soil, E_s is the Young's modulus of the soil and L is the footing length. Analytical result showed the significant reduction of displacement, differential displacement and positive bending moment acting on the footing for the piled raft. However, addition of piles gave rise to negative bending moment, and when the footing is flexible (K_{st}<0.001) the positive moment are larger than would have occurred without piles.

A boundary element analysis based on elastic theory was performed by Kuwabara (1989) to analyze the behavior of piled raft foundation subjected to vertical load. Compared with the pile group with and without raft contact, the reduction of the settlement caused by the present of the rat is very small, although the raft transmits 20-40% of the applied load direct to the soil.

Chow (1986) presented method analyzing linear and no-linear responses of vertically loaded pile groups, in which the approximate solution for a single pile response presented by Randolph and Wroth (1978) was employed. Chow and Teh (1991) extended the work by Chow (1986) to analyze piled rafts on a non-homogeneous soil with a finite depth. The raft was assumed rigid and discretised into sub-elements. Piles were discretised into some elements with an axial mode of deformation. They reported that the effect of contact pressure by rigid raft had a slight influence on the stiffness of the piled raft. Note that the differential settlement cannot be treated in this method.

Clancy and Randolph (1993) extended the work by Chow (1986) and Chow and Teh(1991) to analyze a flexible piled raft on a homogeneous soil. The treatment of the pile group and of interactions between piles and the raft were based on Mindlin's solution, but the load transfer model of Randolph and Wroth (1978) was used for each single pile response. The flexible raft was modeled using plate-bending finite elements. The schematic concept of this approach is shown in Fig. 2.3.2.

1. One-dimensional pile element
2. Ground resistance at each pile node represented by non-linear 'T-Z' springs
3. Two-dimensional plate-bending finite element raft mesh
4. Ground resistance at each raft node represented by an equivalent spring
5. Pile-soil-pile interaction effects calculated between pairs of nodes using Mindlin's equation
6. Pile-soil-raft interaction
7. Raft-soil-raft interaction

Figure 2.3.2 Numerical representation of piled raft. (Clancy and Randolph (1993))

Poulos (1991) proposed the "strip on springs approach", in which a section of the raft is represented by a strip, and the supporting piles by springs. Approximate allowance is made for all four components of interaction (raft-raft, pile-pile, raft-pile and pile-raft), and the effects of the parts of the raft outside the strip section being analyzed are taken into account by computing the free-field soil settlement due to these parts. These settlements are then incorporated into the analysis, and the strip section is analyzed to obtain the settlements and moments due to the applied loading on that strip section and the soil settlements due to the sections outside the raft.

Poulos (1994) described a plate on springs approach, in which the raft is represented by an elastic plate, the soil is represented by an elastic continuum and piles are modeled as springs. This analysis has been implemented via a program GARP (Geotechnical Analysis of Raft wit Piles). Allowance has been made for layering of the soil profile, the effects of piles reaching their ultimate capacity, the development of bearing capacity failure below the raft and the presence of free-field soil settlements acting on the foundation system. This method is so-called "plate on springs approach".

Russo (1998) have described a similar approach to the above "plate on springs method". To model the non-linear behavior of piles, the analytical expression of the Chin's hyperbola (1970) is used in this method. The interaction factor method is employed to model pile-pile interactions is represented:

$$\alpha_{pp}(s) = \frac{w_2(s)}{w_1} \qquad\qquad (2.3.8)$$

where $\alpha_{pp}(s)$ is pile-pile interaction factor, w_i represents the elastic settlement of the pile i, and the load free pile 2 is located at a spacing s, away from the loaded pile 1. A preliminary BEM (Boundary Element Method) analysis, via a computer code, allows to calculating this interaction factor. The raft of any geometry and stiffness is then calculated by FEM analysis. The numerical procedure is implemented via the computer program NAPRA. Russo (1998) compared the analytical results with results from the Poulos's plate on springs approach and from the centrifuge model test done by Horikoshi and Randolph (1996). The details of centrifuge model tests will be presented in later section. The comparisons carried out indicated that the computer program NAPRA may satisfactory solutions both in linear and non-linear range.

Ta and Small (1996) analyzed the piled raft systems constructed in layered soils. The raft was modeled using the finite element method and treated as a thin elastic plate, and therefore this method can be used to analyze a raft with any geometry and stiffness. The soil can be considered to be an isotropic or cross-anisotropic horizontally layered material. Solution can be obtained for most of the quantities required by designers such as differential settlement and moment in the raft, loads in the piles and raft.

Prakoso and Kulhawy (2000) carried out analysis on the piled raft using simplified linear elastic and non-linear plane strain finite element models. The effects of raft an pile group system geometries and pile group compression capacity were evaluated on the average and differential displacements, raft bending moment, and pile butt load ratio of the piled rafts.

Thus, a lot of analytical studies have been reported. The main stream for analyzing method of the piled raft foundation subjected to vertical load is the so-called Hybrid method, in which the raft in the piled raft is modeled as the thin plate or strip on the springs and the interaction among the raft, piles and ground is considered using the elastic theory such as Mindlin's solution as shown above.

2.3.1.2 Field measurement

The piled raft foundations have been applied to actual foundation design over the world. The design code of the piled raft foundation was published by Architectural

Institute of Japan (2001), and a number of piled raft application have been reported in Japan as well since a piled raft was first fused in the construction of a four-story building in Urawa in 1987 (Yamashita and Kakurai (1991)). In this section, some literature review will explain the case history of piled raft application. In particular, much focus will be placed on the load sharing of the piles and the raft.
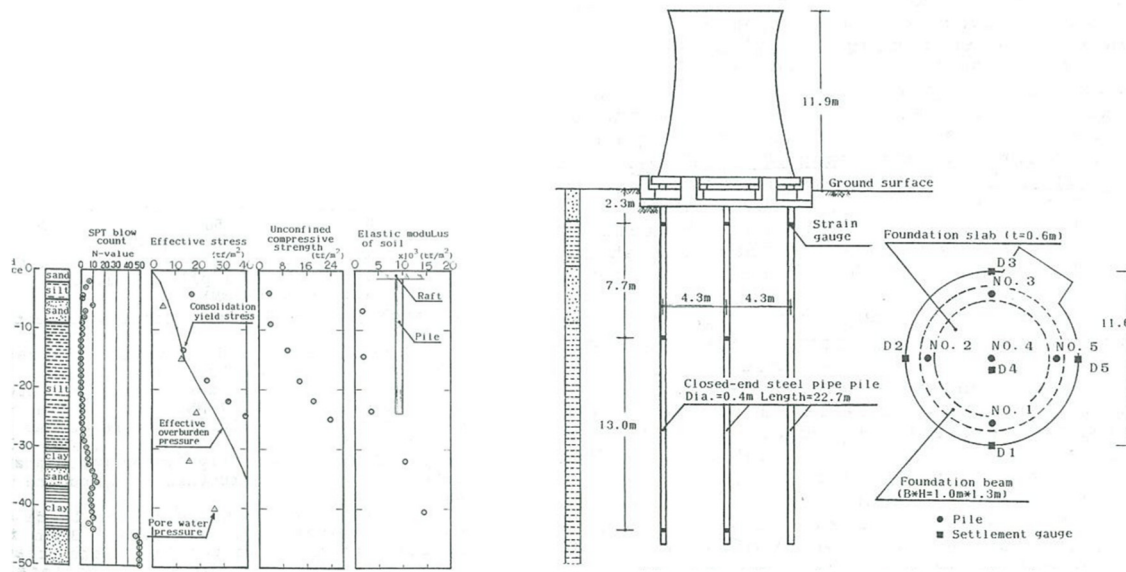
Figure 2.3.3 Schematic illustration of foundation and soil profile. (Kakurai et al. (1987))

Kakurai et al. (1987) reported that observed data reinforced concrete silo supported by the piled raft foundation. The schematic illustration and soil profile are shown in Fig. 2.3.3. The settlement gauge and strain gauges were installed to measure the silo settlement and axial load along pile. The base pressure was 74kPa, and if a raft foundation was used to support the superstructure, its bearing capacity was 111kPa and more than 80mm of total consolidation settlement were predicted.
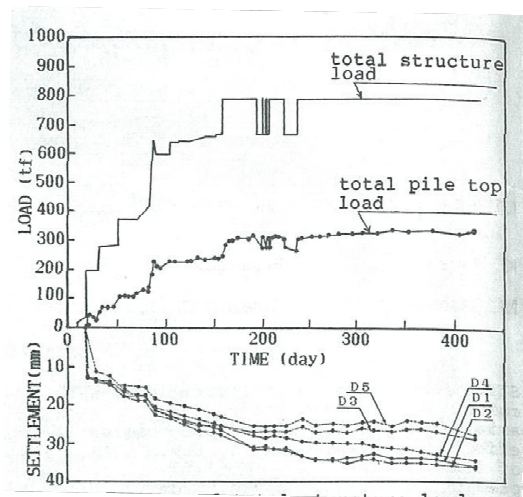
Figure 2.3.4 Time histories of load and settlement. (Kakurai et al. (1987))

Thus raft foundation with five friction piles was employed aiming at reducing the consolidation settlement. The observed settlement after 420 days was 31mm as shown in Fig. 2.3.4, implying that five friction piles can

19
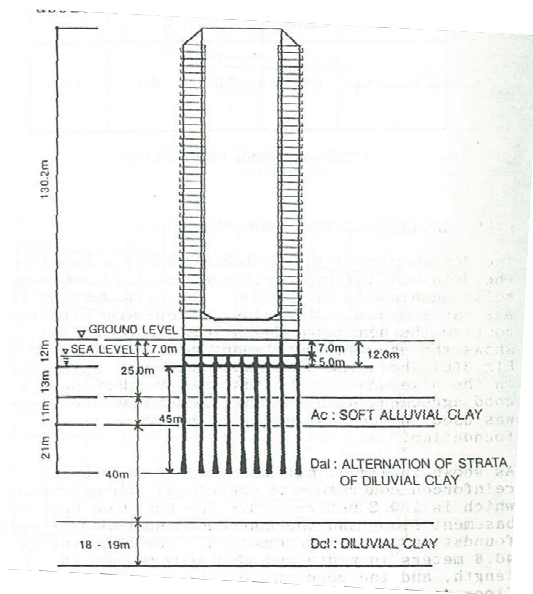
Figure 2.3.5 Soil profiles and section of the building. (Kishida (1991))
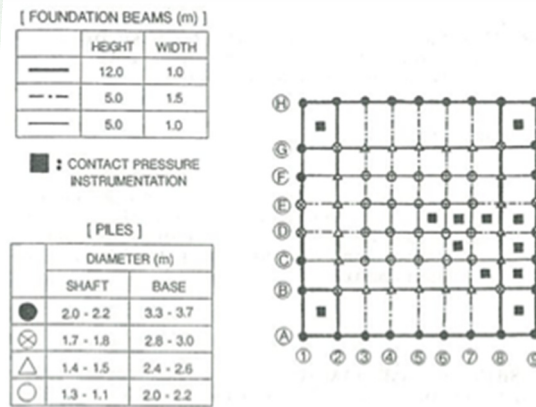
Figure 2.3.6 Location of instrumentations. (Kishida (1991))

restrain the consolidation settlement. They also simulating the observed data using analytical method proposed by Tomono et al. (1987), which was similar method as that proposed by Hain and Lee (1978). The calculated behavior showed a fairly good agreement with observed behavior in load-settlement relationship, axial load distribution and load division between the raft and the piles.
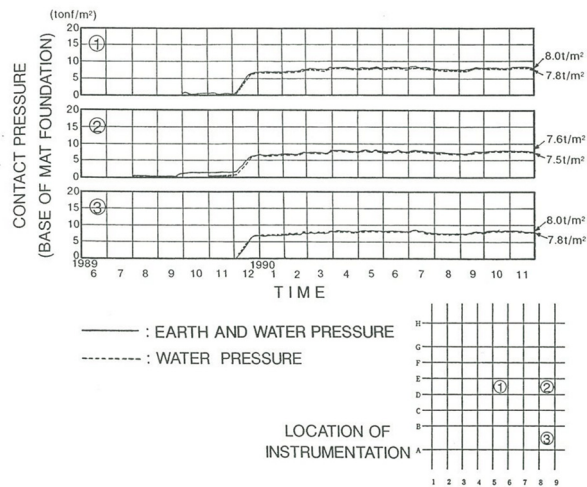
Figure 2.3.7 Measured earth pressure and water pressure. (Kishida (1991))

Kishida (1991) reported that the behavior of the tall building supported by piled raft in Rokko Island from 1989.6 to 1990.11. The schematic illustration is described in Fig. 2.3.5. The building supported by 72 bell-shaped bore piles is 46.8m in width, 45.0m in length and 130.2m in height from the ground surface. The average base contact pressure is about 450kPa. The size and location of the piles is shown in Fig. 2.3.6. The measurement targets are settlements of the foundation and the ground and earth

20

pressure beneath the raft base. The author confirmed that there was almost no empty space between the base of the raft and the ground using the measured settlement at the foundation and at the ground. The proportion of the vertical load carried by the raft part on the total vertical load (RVLP) was almost 22% (calculated from Fig. 2.3.7) after the construction.

Yamashita et al. (1994) also reported the observation of the piled raft on layered ground (Fig. 2.3.8). They designed piles with relatively larger pile spacing (s/D=8, where s is pile spacing and D is pile diameter) to reduce the overall and differential settlement effectively as proposed by Cooke (1986). In the case of this building design requirements are as follows. The maximum contact pressure is lower than the one-third of the ultimate value of 490kPa, and allowable axial loads determined by pile material are larger than design column loads. Measured were the settlement of the foundation and axial load acting on piles. The RVLP for this case is approximately 51% as shown in Fig. 2.3.9.
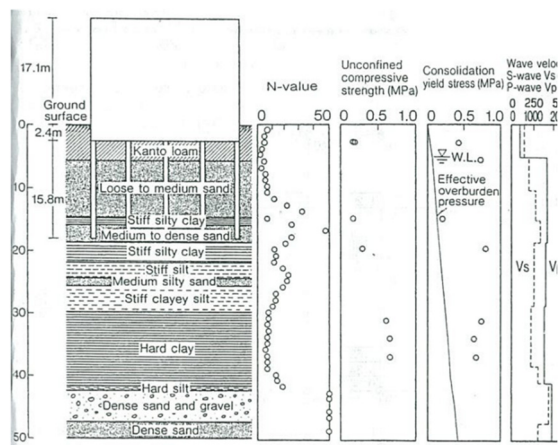
Figure 2.3.8 Schematic illustration of building and soil profiles. (Yamashita et al. (1994))
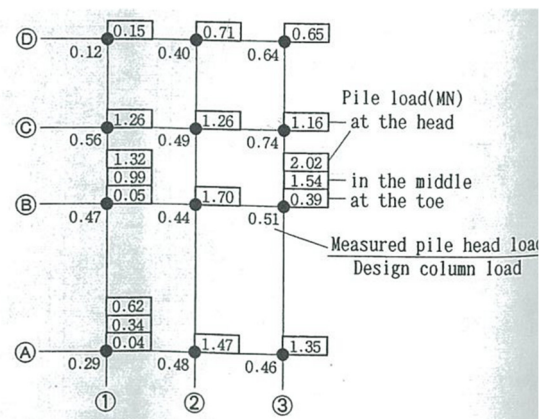
Figure 2.3.9 Measured pile loads at the time of completion. (Yamashita et al. (1994))

Katzenbach et al. (2000) also reported the behavior of the piled raft foundation supporting the 121m high office building in Berlin. On the fist 3m below ground level the subsoil consists of fill, followed by loose sand and medium dense to dense sands in a depth of 40m. The building is founded on a piled raft foundation with 54 bored piles of 0.88m diameter (Fig. 9). The RVLP after the construction was about 52%.

Yamashita et al. (2011) summarized five recent case histories of the piled raft foundations in Japan. To confirm the validity of the foundation design, field measurements were performed on the foundation settlements and the load sharing

between the rafts and piles by monitoring the five structures from the beginning of their construction to 17 to 60 months after the end of their construction. All the constructions described by Yamashita et al. (2011) were based on the following common design criteria under the working condition. 1) It has to be proved that the factor of safety against the ultimate bearing capacity of a piled raft foundation is larger than 3. The ultimate bearing capacity of the piled raft foundation can be replaced with the ultimate bearing capacity of the raft foundation alone (ignoring bearing capacity of the piles). 2) It has to be proved that the maximum settlement and the differential settlement are less than the allowable values.

The design criteria under seismic loading conditions are as follows. 1) It has to be proved that the factor of safety against ultimate bearing capacity of the piled raft is larger than 1.5 under vertical loading together with lateral loading. 2) It generally has to be proved that the factor of safety against the ultimate bearing capacity of the piles is larger than 1.5 against the maximum axial load assumed in the design load sharing. 3) The influence of lateral loading on the piled raft has to be considered, i.e., the maximum bending moment and the shear force on the cross sections of the piles evaluated by the analytical method should be less than the design structural strength of the piles (Hamada et al. (2009)).

i) 11-story office building on medium sand

The 11-story office building, 60.8m in height is located in Aichi. The piled raft foundation consisting of 40 piles was proposed. The RVLP 60 months after the end of construction was about 35%.

ii) 13-story hospital on soft clay

This building is located at Osaka and the dimensions are 51.3m in height, 55m in width and 45m in length. The raft base pressure is 169kPa and the base is supported by 17piles with 19m of length and 0.8-1.0m of diameter. 42% of the RVLP was observed 52 months after the end of the construction.

iii) Hardron Experimental Hall on medium to dense sand

This building is located in Ibaraki and the average contact pressures over the raft were from 259kPa to 442kPa. 371 piles with 22.0-25.7m in length and 0.6-0.8m in diameter were prepared beneath the raft base. After 42 months after the end of the construction the RVLP of 14% and 33% were observed for P1 and P2 respectively.

iv) 47-story residential tower on medium sand

The 47-story residential tower, 162m in height and measuring 50m by 34m in plan, is located in Nagoya. The average base pressure over the raft is about 600kPa. 36 piles were used and the piles have a diameter varying from 1.5 to 1.9m and an enlarged bell

at the pile bottom varying from 1.8 to 2.2m. The layout of piles with locations of monitoring devices is shown in Fig. 26. The RVLPs 17 months after the end of construction were 7% and 13% for 5D and 7D respectively.

v) 19-story residential building on loose sand

The 19-story reinforced-concrete residential building, 75.8m above the ground surface, is located in Kagoshima. The average pressure is 257kPa, and 27 bell shaped piles with 62.8m in length and 1.2 or 1.3m in diameter were employed. 30% and 24% of the RVLP were observed 22 months after the end of construction.

Form these case histories, Yamashita et al. (2011) confirmed that the RVLP increased with pile spacing ration s/D, where s is the pile spacing and D is the pile diameter. Similar tendencies were reported by Cooke (1986) and Mandolini et al. (2005).
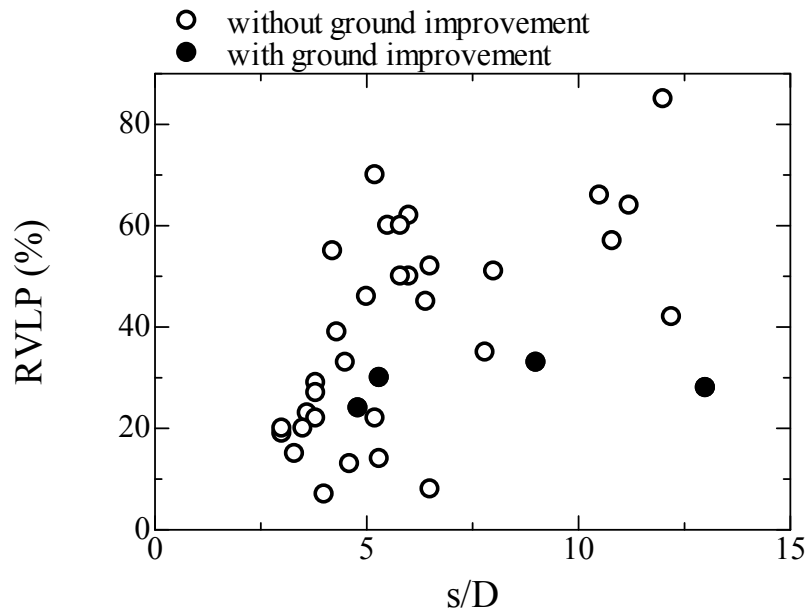
Figure 2.3.10 Relationship between pile spacing ratio (s/D) and RVLP.

Table 2.3.1 summarizes the case histories reported by the previous researches. The relationship between s/D and RVLP is plotted in Fig. 2.3.10. As been seen, the RVLP generally decreased as the pile spacing ration was increased. The RVLP seems to have significantly increased as the pile spacing ratio was increased from about four to six. However, the RVLPs for the piled raft with ground improvement were almost constant against the pile spacing.

Table 2.3.1 Case histories of piled raft applications.

Structure	Height (m)	Contact pressure (kPa)	Piles (mm)			RVLP after construction (%)	Reported by
			Number (Ag/A)	Length (L/B)	Diameter (s/D)		
Stonebridge park	-	-	(0.9)	(0.65)	(3.6)	23	Cooke et al.
5-stories building		2.7	504	18-24	0.2 (10)		Tan, Y. C. et al.
Dashwood house	-	-	(0.9)	(0.5)	(3)	19	Hight & Green (1976)
Apartment block	-	-	(0.9)	(0.5)	(5.2)	22	Joustra et al. (1977)
National Westimnster Bank	-	-	(0.91)	(0.5)	(3.8)	29	Hooper (1979)
Hide Park Cavalry Barracs	-	-	(0.72)	(0.9)	(4.3)	39	Hooper (1979)
House 1	-	-	(0.9)	(2.1)	(6.5)	8	Jendeby (1986)
House 2	-	-	(0.9)	(2.2)	(10.5)	66	Jendeby (1986)
Uppsala house	-	-	(0.9)	(2.2)	(11.2)	64	Jendeby (1986)
Silo	11.9	74	5	22.7	0.4 (10.8)	57	Kakurai et al. (1987)
Tall building	130.2	441	72	45	1.1-2.2 (4.1-3.5)	22	Kishida (1991)
Messe Turm	-	-	(0.83)	(0.52)	(6.4)	45	Sommer et al. (1991)
5-story building	17.1	84	20 (0.9)	15.8 (0.64)	0.7-0.8 (8)	51	Yamashita, K. et al. (1994)
Multi-span bridge	-	-	(0.7)	(1)	(3.8)	27	Van Impe et al. (1994)
Tower	121	-	189	24-33	1.2	.	Ergun (1995)
Garigliano bridge	-	-	(0.88)	(4.5)	(3)	20	Russo (1996)
Messe Torhaus	-	-	(0.8)	(1.14)	(3.5)	20	Katzenbach et al. (2000)
Wetend 1-DG Bank	-	-	(0.52)	(0.63)	(6)	50	Katzenbach et al. (2000)
Japan Centre	-	-	(0.45)	(0.6)	(5.5)	60	Katzenbach et al. (2000)
Forum	-	-	(0.55)	(0.7)	(6)	62	Katzenbach et al. (2000)
Congress Centre	-	-	(0.62)	(1)	(5.8)	60	Katzenbach et al. (2000)
Main Tower	-	-	(0.7)	(0.5)	(3.3)	15	Katzenbach et al. (2000)
Eurotheum	-	-	(0.55)	(0.8)	(5.2)	70	Katzenbach et al. (2000)
TREPTOWER	121	365	54	12.5-16	0.88 (6.5)	52	Katzenbach et al. (2000)
Tall building	60	275	10	20.7	1.8 (4.2)		

4-story building	-	72	93	12	0.5 (12)	85	Matsuo et al. (2003)
Tank 12 Harbour Napoli	-	-	(0.82)	(0.92)	(5.8)	50	Mandolini et al. (2005)
Tank 14 Harbour Napoli	-	-	(0.82)	(1.1)	(5)	46	Mandolini et al. (2005)
47-story residential tower	161.9	600	36	50.2	1.5-1.8 (4.6-4.0)	13-7	Yamashita, K. et al. (2010)
11-story office building	60.8	181	40	27.5	1.5 (7.8)	35	Yamashita, K. et al. (2011)
13-story hospital	51.3	169	17	19	0.8-1.0 (12.2)	42	Yamashita, K. et al. (2011)
Hadron experimental hall	19	259-442	371	22-25.7	0.6, 0.8 (5.3, 4.5)	14-33	Yamashita, K. et al. (2011)
19-story residential building	75.8	257	28	62.8	1.2, 1.3 (5.3, 4.8)	30-24	Yamashita, K. et al. (2011)
7-story office building	29.4	100	70	29.8	0.7, 0.9 (15, 12)	28	Yamashita, K. et al. (2011)
12-story residential building	38.7	199	16	45	1.0, 1.2 (10, 8)	33	Yamashita, K. et al. (2012)

2.3.1.3 Physical modeling test

Liu et al. (1985) carried out 74 series of field tests on bored single pile and pile group in the non-dense sandy soil. Varied parameters were: pile diameter (D=125-330mm); pile length (L=8-23D); pile spacing ration (s/D=2-6); number of pile (n=2-10); pile arrangement (square, rectangle and single range); pile cap position (the pile cap did not touch the ground for the high-rise cap, and it touched the ground for the low-rise cap). From a number of series tests, it was found that the ultimate shaft friction load was smaller for the high-rise cap than the low-rise cap. However, the end bearing load increased by the existing of the pile cap having the contact with the ground.

Cooke (1986) conducted extensive series of model tests on the unpiled rafts, free-standing pile groups and piled rafts with various raft size, number of piles, pile spacing. Cooke found that at the pile spacing that are closer than the critical spacing at which block behavior of free-standing groups occurred, the piled raft and free-standing pile group of the same size followed the theoretical block failure mechanism (eq. (2.3.9)) and have similar ultimate bearing capacities and similar immediate settlement.

$$\frac{P_g}{c_u d^2} = \left[4(n-1)k + \pi\right]\frac{L}{d} + \left[(n-1)k + 1\right]^2 N_c \tag{2.3.9}$$

A pile spacing that are wider than the critical spacing the ultimate bearing capacity of a pile group can be increased significantly by a raft formed on the clay surface. The stiffness of the piled rafts was at most 30% greater than those of the free-standing pile groups at large pile spacing ratio as shown in Fig.2.3.11. Similar trend can be observed for the case histories (Fig. 2.3.10)
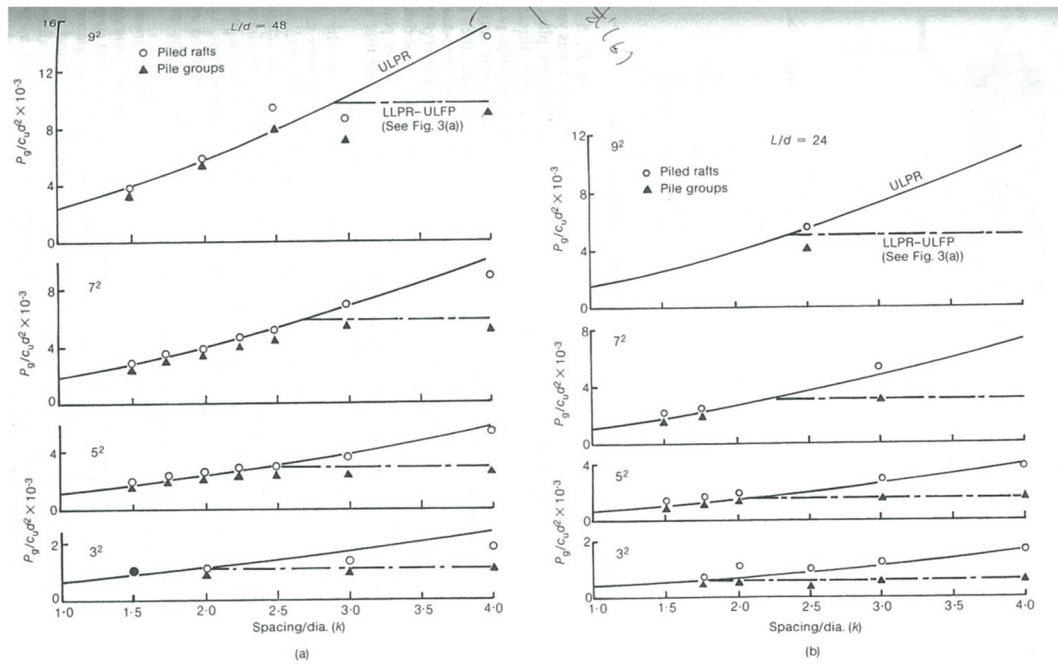
Figure 2.3.11 Comparisons of ultimate load capacities of piled rafts and free-standing pile groups. (Cooke (1986))

Thaher and Jessberger (1991) carried out a centrifuge model tests on the piled raft on over consolidated clay. A centrifuge acceleration of 50g was employed. The effects of pile number, pile length and pile diameter on the performance of vertically loaded piled raft foundation were examined. Moreover, additional centrifuge model test simulating the foundation of the Fair Tower in Frankfurt was conducted. Basic finding from this research was the ratio of pile spacing to pile diameter (s/D) is a key figure for piled raft foundation design. Similar suggestion were made by Cooke et al. (1986), Yamashita et al. (2011) and Mandolini et al. (2005), i.e., the wider pile spacing is, the larger contribution from the raft base (RVLP) is.
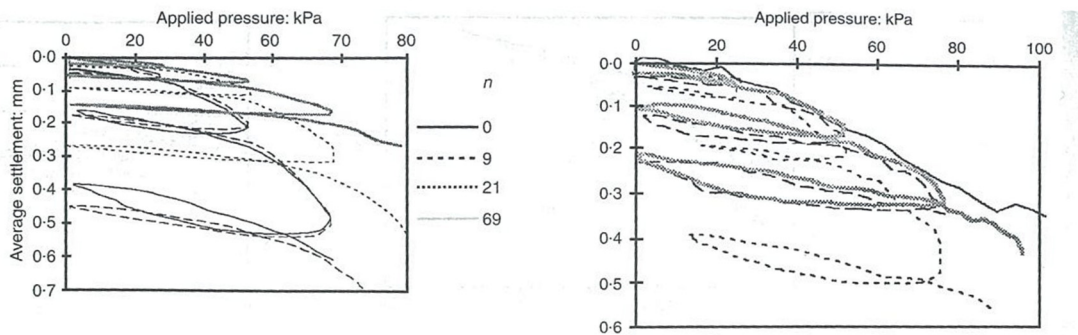
Figure 2.3.12 Average settlement of raft during loading tests. (Horikoshi and Randolph (1996))

Horikoshi and Randolph (1996) carried out six series of centrifuge model tests of the piled raft and unpiled model with various pile number of 9, 21 and 69 on clay. The centrifugal acceleration employed in this research was 50g. The piles were uniformly arranged beneath the raft base for the piled raft with 21 and69 piles, while piles were installed only central part for the piled raft with 9 piles. Beside the loading tests on the piled raft and unpiled raft, the vertical loading tests on the capped pile and uncapped pile were also done. It was found that the vertical stiffness was higher for the capped pile than the uncapped pile. It was also confirmed that although the average settlement of the piled raft with nine piles was almost same as that of the unpiled raft (Fig. 2.3.12), the differential settlement can be reduced by 70% for the piled raft (Fig. 2.3.13), implying that the central piles can effectively reduce the differential
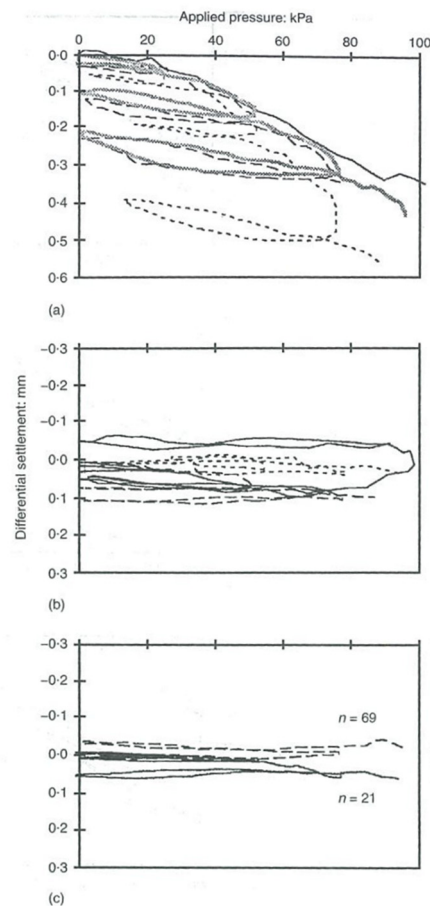
Figure 2.3.13 Differential settlement of raft during loading tests: (a) unpiled raft; (b) piled raft with 9 piles; (c) piled raft with 21 and 69 piles. (Horikoshi and Randolph (1996))

settlement. Horikoshi and Randolph (1998) carried out the parametric study using the analytical approach developed by Clancy and Randolph (1993). They also compared with the analytical results and experimental results derived from Horikoshi and Randolph (1996). From these extensive works, it was proposed for the optimum piled raft design

27

that piles should be installed over the central 16-25% of the raft area to effectively reduce the differential settlement.

Poulos (2001) summarized recent extensive works on the piled raft including the analytical and experimental methods and case history. An interesting aspect of piled raft behavior is introduced using the experimental result derived from Katzenbach et al. (1998). The ultimate shaft friction developed by piles within a piled raft can be significantly greater than that for a single pile or a pile in a conventional pile group as shown in Fig. 17 (2.3.14). This is because of the increased normal stresses generated between the soil and the pile shaft by the loading on the raft. The piles within the piled raft foundation develop more than twice the shaft resistance of a single isolated pile or a pole within a normal pile group.
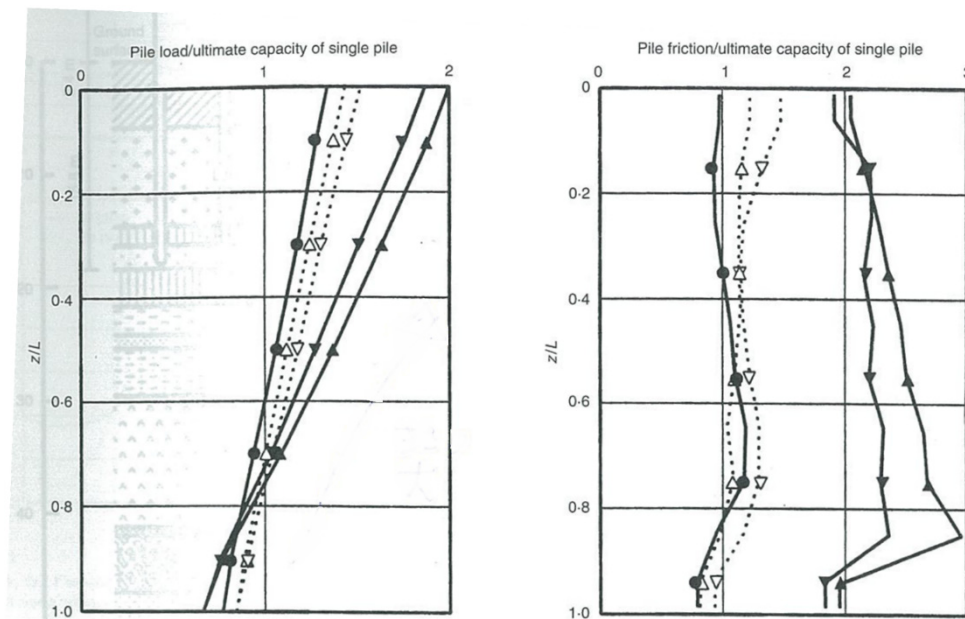
Figure 2.3.14 Distribution of pile load and skin friction. (Poulos (2001))

Blakumar et al. (2005) carried out vertical loading tests on the piled raft, free standing pile group and isolated pile on medium dense sand in the gravity field. The model ground was prepared by pouring and compacting method. The pile part in the piled raft foundation took much higher vertical load than the free standing pile group. In the free standing pile group, it appeared that shaft friction load was fully mobilized for a settlement around 2mm. However, the pile part in the piled raft continued to offer higher resistance even for the settlements beyond 2mm settlement. They concluded that this

28

additional resistance offered by the piles in the piled raft was due to the increase in normal stress. This higher shaft friction on the piled raft was also reported by Poulos (2001).

Tejchman et al. (2005) carried out vertical loading tests on the piled raft, free-standing pile group, single pile and raft alone model on the medium dense sand in the laboratory floor. The pile number was changed (n=1, 4, 5, 6, 7, 8, 9) and contribution of the piles and raft in transmission of loads into the subsoil was discussed by introducing α_{CPRF} and effective coefficient η as expressed below.

$$\alpha_{CPRF} = \frac{R_{pile}}{R_{total}} \qquad (2.3.10)$$

$$\eta = \frac{R_{total}}{R_{fsp} + R_{raft}} \qquad (2.3.11)$$

where R_{pile} is vertical load carried by pile part, R_{total} is vertical load of piled raft, R_{fsp} is vertical load of corresponding free standing pile group and R_{raft} is vertical load of raft alone model. As been seen in Fig. 2.3.15, the larger number of piles was, i.e., the narrower pile spacing was, the higher α_{CPRF} was. This trend can be clearly observed by Cooke et al. (1986), Thaher and Jessberger (1991) and in the field observation as explained in previous section. It was also confirmed from effective coefficient η that the load transmitted into the subsoil by the piled raft foundation is higher than the algebraic sum of loads transmitted by the corresponding free standing pile group and shallow foundation (see Fig. 2.3.16).
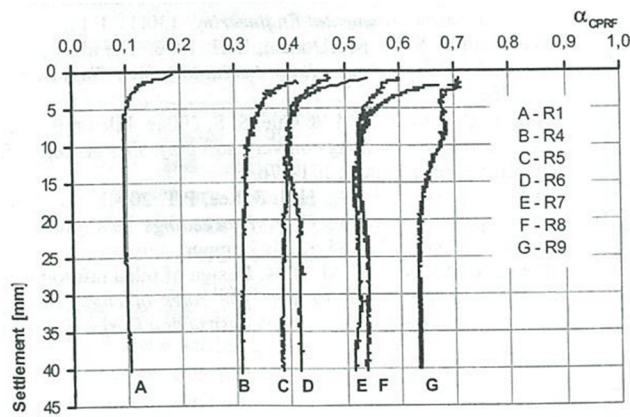
Figure 2.3.15 α_{CPRF} ratio determined by model tests (Tejchman et al. (2005))
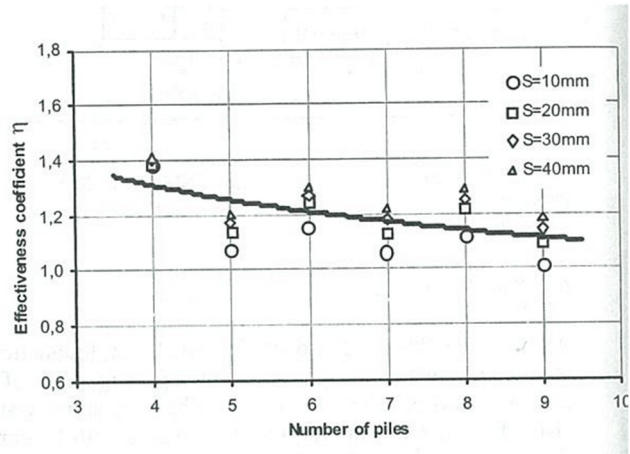
Figure 2.3.16 Effective coefficient η of piled raft foundaiton. (Tejchman et al.(2005))

From the literature review on the settlement behavior of the piled raft foundation, it

seems that vertically loaded piled raft foundation have been relatively well discussed using case histories, analytical and experimental approach. Consequently, the effectiveness of friction piles to reduce the average and differential settlements of superstructure is widely recognized and the complicated load sharing mechanism between the piles and the raft is gradually clarified. Therefore, the piled raft foundation has been positively employed (Table 2.3.1) with intention to reduce the settlement.

2.3.2 Researches on the laterally loaded piled raft foundation

It is crucial to clarify the behavior of laterally loaded piled raft foundation in seismic area such as Japan. Details of researches on the laterally loaded piled raft foundation will be described in the following chapter.

2.3.2.1 Analytical study
i) Simplified method

Ishii et al. (2003) proposed the simplified method using cone model as shown in Fig. 2.3.17. The cone model is method to calculate the soil deformation profile $\delta(z)$ caused by the raft base using below equation.

$$\delta(z) = \delta_0 \frac{Z_{h0}}{z} \quad , \quad \delta_0 = \frac{Q_r}{K_{hb}}$$

$$K_{hb} = \pi G \frac{r_{h0}^2}{Z_{h0}}, \quad Z_{h0} = \pi r_{h0} \frac{2-v}{8} \tag{2.3.12}$$

where δ_0 is horizontal displacement of the raft, Q_r is the horizontal load carried by the raft, Z_{h0} is the height of the cone top from the ground surface, z is the depth from the cone top, $\delta(z)$ is the soil deformation at the depth of z, G is the shear stiffness of the soil, v is Poisson's ration of the soil and r_{h0} is the radius of the raft.

Then, the horizontal deformation obtained from eq. (2.3.12) is applied to the piles in the piled raft through the soil spring, and the horizontal load Q_p is given at the pile head until the horizontal displacement at the pile head equals to raft horizontal displacement δ_0. The total horizontal load of the piled raft can be estimated by sum of Q_r and Q_p. They
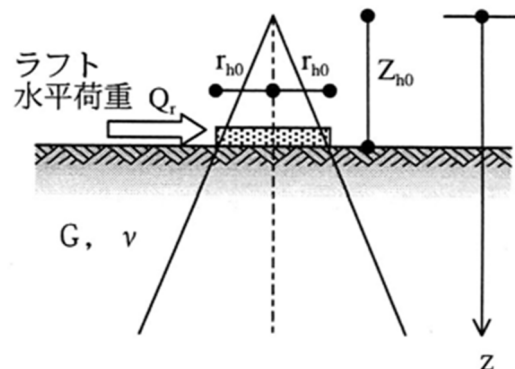
Figure 2.3.17 Concept of the cone model. (Ishii et al. (2003))

verified this simplified approach by comparing the results of the centrifuge model tests on the piled raft done by Fujimori et al. (2003) and Nishiyama et al. (2003). The details of centrifuge model tests will be given later section.

Nagao et al. (2004) proposed simple model which consists of two dimensional beam elements of piles and Winkler's type of soil springs. Pile behavior is modeled using the beam-spring model and the shear spring putting on the ground surface is treated as the horizontal resistance of the raft part as shown in Fig. 2.3.18. By comparing the results of model tests on the piled raft (Nagao et al. (2002)), it was confirmed that if the proper soil spring is used for the model, the behavior of the piled raft foundation can be predicted. The results derived from model tests will be described at later section.
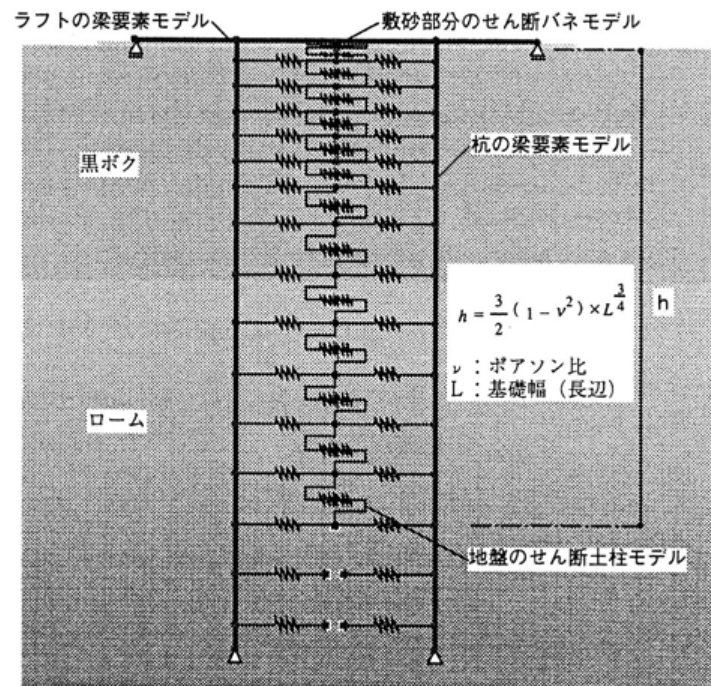
Figure 2.3.18 Concept of the simple model proposed by Nagano et al. (2004)

ii) Hybrid method

Tsuchiya et al. (2001) extended the Hybrid method (see section 2.4.1.1) to the method which can treat the horizontal problem such as horizontal load, moment load and locking. The raft and pile is modeled as the thin elastic plate element and elastic beam element respectively. Interaction of raft-soil-pile is considered using the elastic theory such as Mindlin's solution as shown in Fig. 2.3.19. The bi-linear or tri-linear soil spring were used to consider the nonlinearity of the soil. Because the interactions for both vertical

and horizontal direction are taken into account at the same time, horizontal displacement, rotation, settlement of the foundation can be calculated. Nagao and Tsuchiya (2004) developed the Tsuchiya's method by taking in the non-linearity of the soil using bi-linear or tri-linear soil springs. Some comparison with the field tests done by Nagai and Tsuchiya (2004) was done.
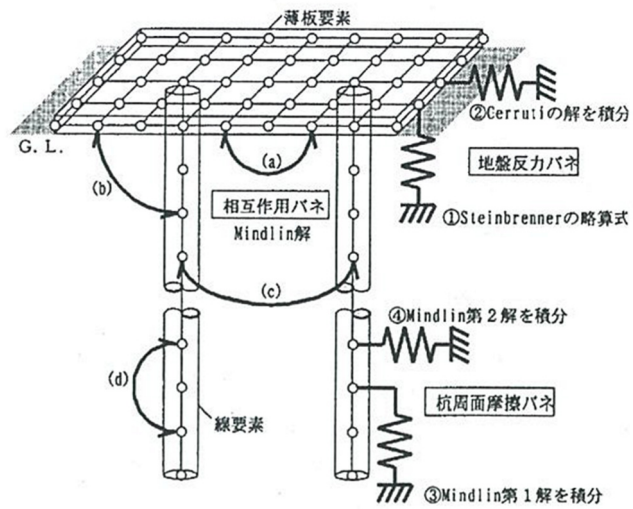
Figure 2.3.19 Concept of Hybrid approach proposed by Tsuchiya et al. (2001)

Kitiyodom and Matsumoto (2002) also proposed the Hybrid approach. The raft and piles are took place by the plate and beam. Soil springs are added on the raft and piles for both vertical and horizontal direction as shown in Fig. 2.3.20. An important feature of the proposed method is that pile-soil-pile, pile-soil-raft, raft-soil-raft interactions due to lateral forces as well as vertical forces are
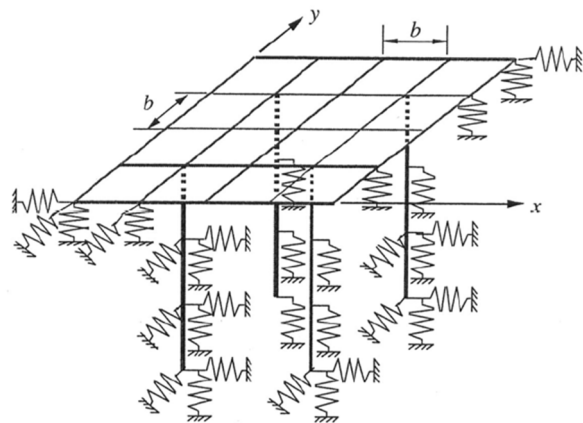
Figure 2.3.20 Hybrid model proposed by Kitiyodom and Matsumoto (2002).

incorporated in the analysis. They verified this method through comparisons with the results from previous research. Kitiyodom and Matsumoto (2003) developed this approach further. The developed approach can deal with the pile in the non-homogeneous soil and load distribution along the piles can be calculated. Hamada et al. (2003, 2012) proposed similar Hybrid approach, in which the interaction is considered using Mindlin's solution and nonlinearity of the soil and pile can be taken into account. The model tests on the piled raft done by Tsuchiya et al. (2003) were simulated using this approach, and the validation of this method was confirmed.

iii) Finite layer method

Small and Zhang (2002) proposed a new method of analysis of piled raft as shown in

Fig. 2.3.21. The soil is divided into multiple horizontal layers depending on the accuracy of solution required and each layer may have different properties. The raft is modeled as a thin plate and the piles as elastic beams. Finite layer theory is employed to analyze the layered soil while finite element theory is used to analyze the raft and piles. The behavior of the piled raft subjected to vertical, horizontal and moment load in any direction can be calculated. Comparisons of forces in piles, moments in the raft an piles and displacement of piled raft subjected to either vertical and horizontal loadings show that this solutions agree closely with those provided by the finite element method. However, this method was applicable only for the elastic soils.
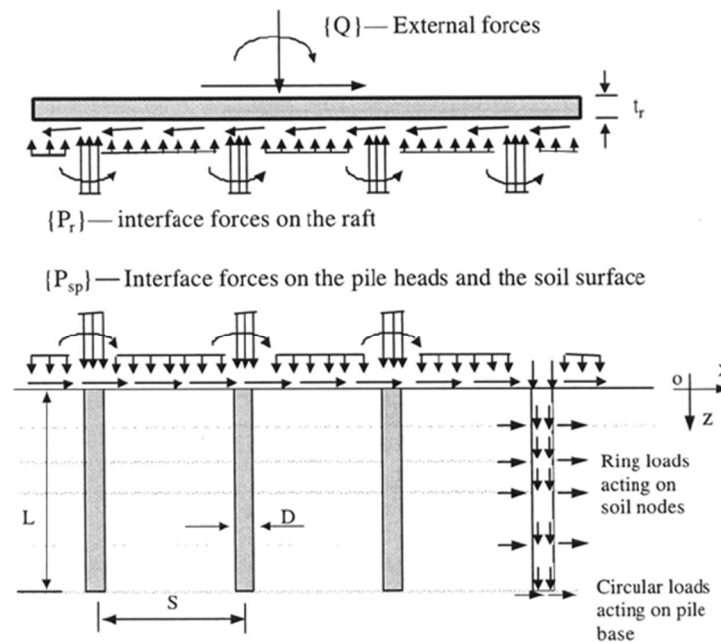
Figure 2.3.21 Finite layer method. (Small and Zhang (2002))

Thus, from the literature review on the analytical studies on the laterally loaded piled raft, the almost approaches are the Hybrid method where the raft and piles are replaced by the thin plate and elastic beam, and the interactions of the raft-soil-piles are modeled using the elastic theory such as Mindlin's solution. Recently, this approach has been extended to deal with the nonlinearity of the soil, however, it is difficult to determine the proper parameters used for the analysis such as coefficient of subgrade reaction. So, there should be still rooms in the analytical method to improve and obtain reliable results.

2.3.2.2 Field measurement

Yamada et al. (2001) reported the observation data on the twelve-story building in Osaka City from 1991 to 1996. During this period, Hyogoken-Nambu Earthquake was hit this building. The maximum ground-surface acceleration recorded in Osaka City was about 200Gal or more. This was very rare case to record the piled raft behavior attacked by the earthquake. The schematic illustration and soil profile was described in Fig. 2.3.22. The building plan measures 39.2m by 24,3m, and the average contact pressure of the building is 275kPa. Ten piles and soil cement wall pile was installed beneath the raft base, and some of piles were instrumented to measure the axial force acting on piles as shown in Figs. 2.3.23. The piles were cast-in-place concrete piles which were 1.8m in shaft diameter, 2.5m in toe diameter and 20.7m in length. The soil cement wall pile was 0.9m in diameter and 16.1m in length. Beside the axial force, the settlement of the foundation, the earth pressure and the water pressure beneath the raft base were measured. Figure 2.3.24 show the variation of settlement, axial force, earth pressure, water pressure, shared load and shared load ration (RVLP) with time. The RVLP one year after the end of construction was about 55%. The most unique data was that the trend of observed data did not change before and after the earthquake.

Yamshita et al. (2012) also reported the behavior of the piled raft during the earthquake. The piled raft
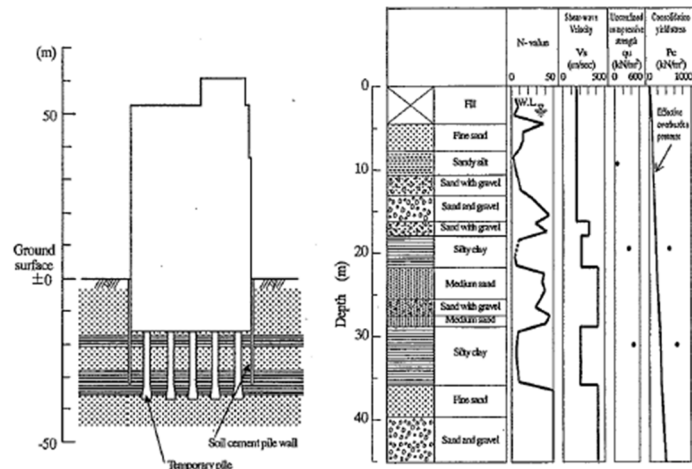
Figure 2.3.22 Schematic illustration of building and soil profile. (Yamashita et al. (2001))
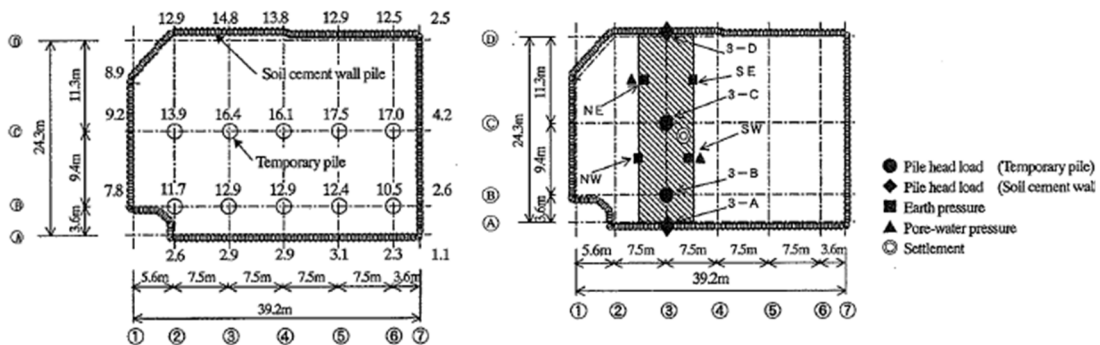
Figure 2.3.23 Foundation plan and monitoring position. (Yamada et al. (2001))

(a) Development of the settlement of the building

(b) Development of the axial forces of the temporary piles

(c) Development of the axial forces of the soil cement wall piles

(d) Development of the earth pressures underside of the foundation slab

(e) Development of the water pressures underside of the foundation slab

(a) Load carried by the raft and the piles

(b) Ratio of load carried by the raft and the piles to the total load

Figure 2.3.24 Measured results. (Yamashita et al. (2001))

35

foundation supporting a 12-story base-isolated building is located in Tokyo, and the schematic view of building and the foundation with soil profile is shown in Fig. 2.3.25. The contact pressure of the raft base is about 200kPa. An assessment of the potential for liquefaction during earthquakes was carried out using the simplified method (Tokimatsu and Yoshimi (1983)). It indicated that the loose silty sand between depths of 3 and 7m below the ground surface had the potential for liquefaction with a peak horizontal ground acceleration of $0.2m/s^2$. Therefore, to cope with the liquefiable sand and to ensure the bearing capacity of the raft, grid-form deep cement mixing walls (the TOFT method) were employed. Furthermore, to reduce the settlement and the differential settlement to acceptable levels, sixteen 45m long precast piles, 0.8-1.2m in diameter, were used. Field measurements were performed on the foundation settlement, the axial loads of the piles and the contact pressure between the raft and the soil, as well as the pore water pressure beneath the raft, from the beginning of the construction to 43 months after the end of the construction. During this period, the 2011 off the Pacific coast of Tohoku earthquake struck the building site. Fig. 2.3.26 shows the time histories of EW accelerations of ground and structure. A peak horizontal ground acceleration of $1.748m/s^2$ was observed near the ground surface, and no significant differences can be seen in the envelopes of the waveforms at all observation points. Load sharing among piles, deep mixing walls and soil, and ratio of load carried by piles during earthquake are shown in Figs. 2.3.27 and 2.3.28 respectively. The increment in total load was small and carried mainly by the piles. The ratio of shared load by the
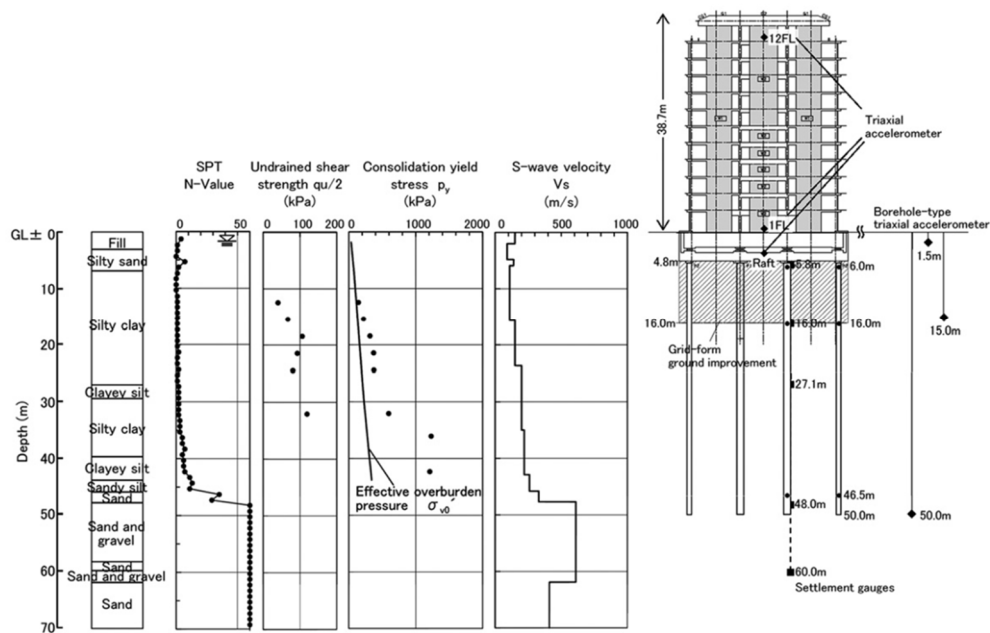
Figure 2.3.25 Schematic view of building and soil profile. (Yamashita et al. (2012))
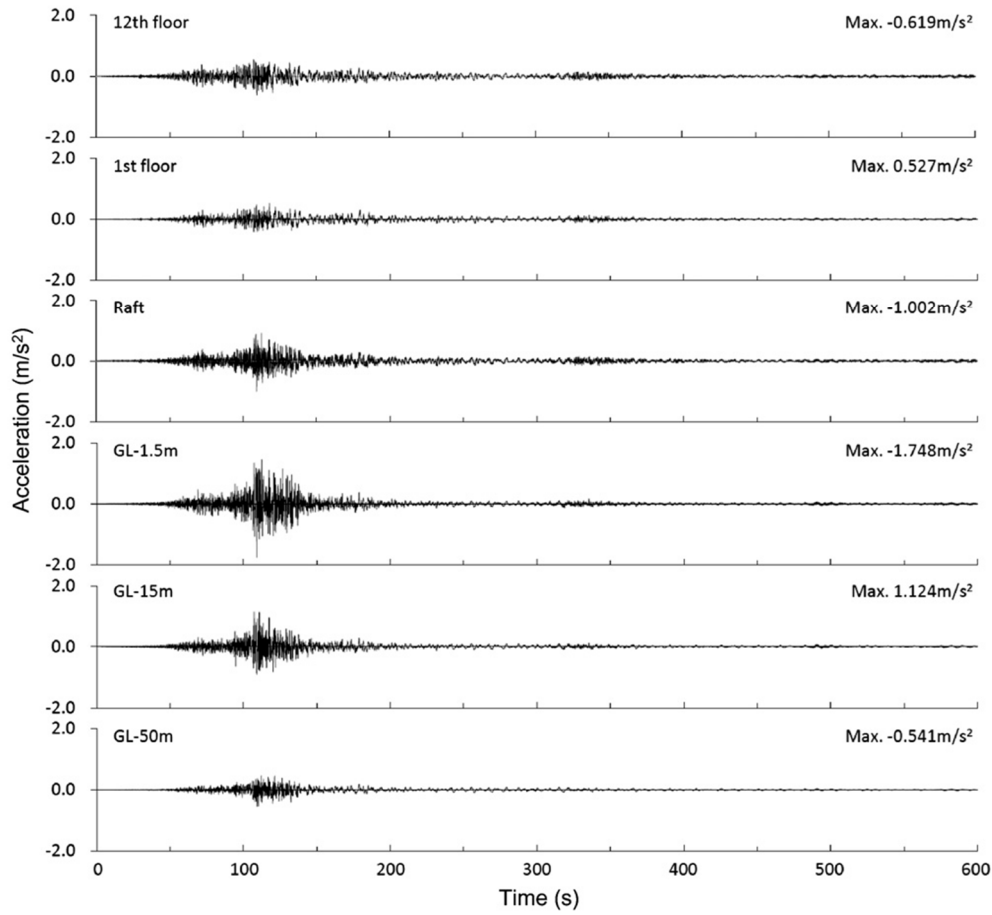
Figure 2.3.26 Time histories of acceleration at ground and superstructure. (Yamashita et al. (2012))
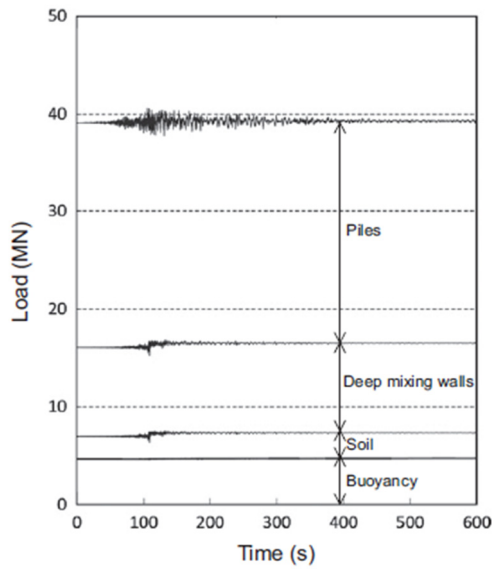
Figure 2.3.27 Load sharing among piles, deep mixing walls and soil during earthquake. (Yamashita et al. (2012))
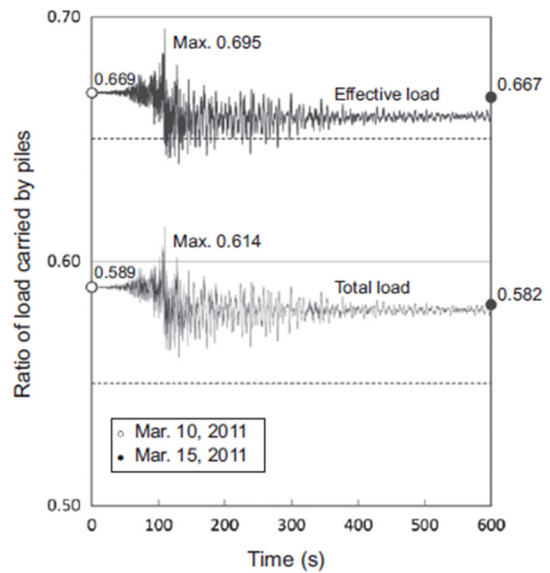
Figure 2.3.28 Ratio of load carried by piles during earthquake. (Yamashita et al. (2012))

piles slightly decreased during the earthquake, but the ratio was almost same before and after the earthquake.

Thus, according to the reports on the behavior of the piled raft foundation struck by the earthquake, there are no significant difference in the observed data such as shared load proportion by the raft and piles between before and after the earthquake. This is probably because the rotation of the foundation is restrained for the relatively wide foundation width such as architectural buildings, and the contact pressure, i.e., the interaction among the raft, ground and piles is therefore does not vary during the earthquake. However, in order to confirm the performance of laterally loaded piled raft, the case histories on the behavior of the piled raft during the earthquake are extremely few.

2.3.2.3 Physical modeling test

As mentioned in previous section, it is difficult to record the actual field data of the piled raft foundation during the earthquake. Furthermore, to generalize the field data is also difficult due to the un-uniformity of the soil profile in the site. Therefore, physical models can play an important role in the study of the piled raft foundation under seismic and horizontal loadings. In this section, literature review will focus on the physical model tests on the laterally loaded piled raft foundation.

Robert et al. (2001) carried out the field tests on the single piles and pile groups with pile cap in the natural soil to discuss the effect of the pile cap on the performance of laterally loaded pile groups. Totally thirty-one cases were conducted to evaluate the lateral load resistance of pile caps by comparing the response of pile groups with caps fully embedded ad with soil removed from around the caps. It was found that the pile caps embedded in the soil provided approximately 50% of the overall lateral resistance of the pile groups to lateral loads. They pointed out neglecting this resistance can lead to excessively conservative estimates of the lateral load capacities of pile groups.

Nagao et al. (2002) conducted the horizontal loading tests on the piled raft and its components of pile group and raft foundations. Four piles having 3m pile length were rigidly fixed to the raft with the pile spacing of 1m as described in Fig. 2.3.29. The initial raft vertical load proportion (RVLP) was 40%. The basic findings were as follows: 1) Although the horizontal resistance of the piled raft was slightly smaller than the sum of horizontal resistance of the pile group and the raft in the small horizontal displacement

range, that was larger for the piled raft in the large horizontal displacement range. This was mainly due to the increase of the contact pressure at the relatively large horizontal displacement. By comparing piled raft with pile group, 2.5 times larger horizontal resistance was observed for the piled raft foundation (Fig. 2.3.30). 2) The piles in the piled raft showed the kind of anchor for both front and rear piles, and the axial load at pile head decreased even for the front piles (Fig. 2.3.31). This was because the positive dilatancy by the shear stress beneath the raft base forced piles to move upward. 3) The bending moment acting on piles was smaller for the piled raft compared with the pile group at the same horizontal displacement, because the relative displacement of the piles against the soil was smaller for the piled raft.
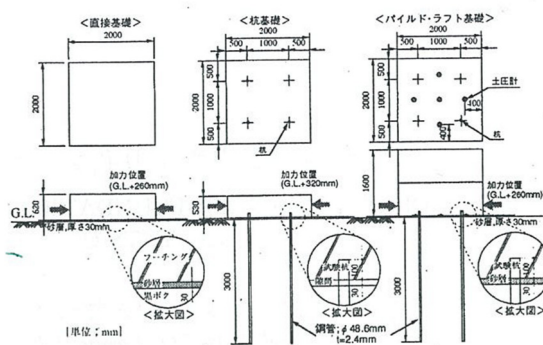
Figure 2.3.29 Schematic view of model foundations. (Nagano et al. (2002))
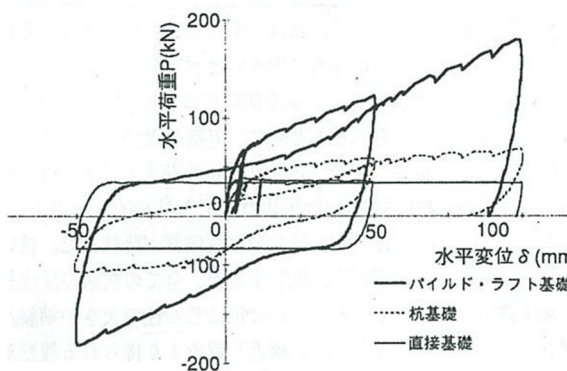
Figure 2.3.30 Relationship between horizontal displacement and horizontal load (Nagano et al. (2002))
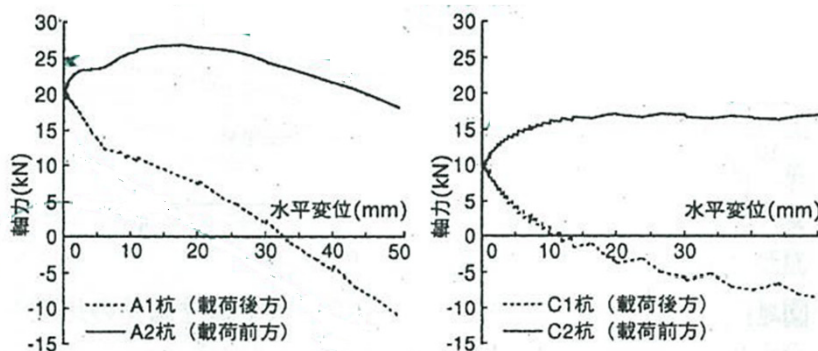
Figure 2.3.31 Relationship between horizontal displacement and axial load at pile head. (Nagano et al. (2002))

Mano et al. (2002, 2003) carried out static horizontal loading tests on the piled raft, pile group and raft models under 30g centrifugal acceleration. Nine piles were rigidly fixed to the raft with the pile spacing of 72mm as shown in Fig. 2.3.32. The model pile was brass made pipe with 12mm in diameter and 0.5mm in thickness. The strain gauges

were attached at five points along the depth. The initial RVLP in the flight was 75%. It was found that for the piled raft larger horizontal resistance was observed for the front pile than that of the rear pile (Fig. 2.3.33) because the raft base slightly moved upward at the rear side and the confining stress beneath the raft base decreased. The horizontal subgrade reaction was smaller for the piled raft than the pile group due to the smaller relative horizontal displacement of pile against the soil for the piled raft. This kind of smaller relative horizontal displacement effect was also reported by Nagao et al. (2002) in the bending moment profile. However, the total horizontal resistance of the piled raft was higher than the corresponding pile group foundation because the horizontal resistance could be obtained from the raft. Nakai et al. (2002) carried out the dynamic loading tests using the same model foundation as Mano's model. The input acceleration was about 200gal. They confirmed that the loads acting on the piles such as the bending moment and the shear force were similar for both static and dynamic loading tests.
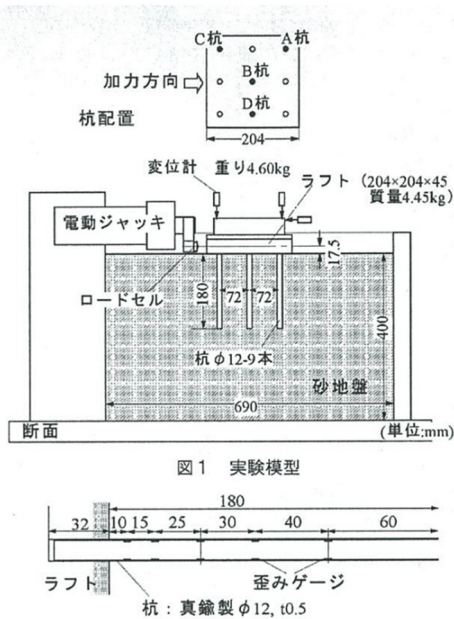
Figure 2.3.32 Model setup. (Mano et al. (2002, 2003))
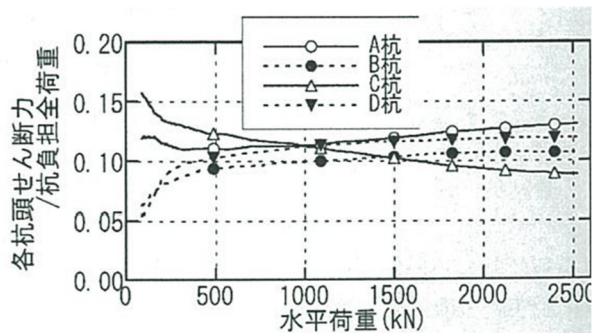
Figure 2.3.33 Ratio of shared load by each pile to toal pile resistance. (Mano et al. (2002, 2003))

Tsuchiya et al. (2003) and Nagano et al. (2003) reported the result of static horizontal loading tests on the piled raft, pile group and raft foundation in the laboratory floor. The piled raft and pile group consisted of 16 piles and 1m x 1m raft as shown in Fig. 2.3.34. The initial RVLP was 68%. It was confirmed that the horizontal resistance of the front pile was smaller than that of the middle pile and rear pile because the base contact pressure made the soil stiffness in front of the middle and rear piles larger. It was also found that the horizontal resistance of the piled raft was higher than the sum of horizontal resistance of the pile group and raft foundation, especially for the relatively

large horizontal displacement (Fig. 2.3.35). This was because the high confining stress around piles could be expected at large horizontal displacement range.
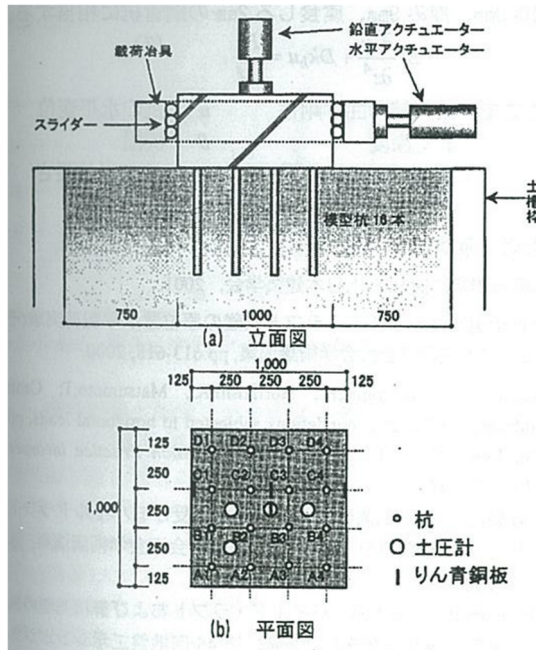
Figure 2.3.34 Schematic view of model setup. (Tsuchiya et al. (2003))
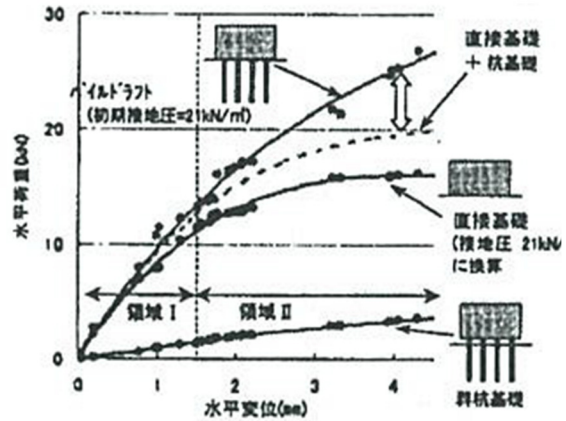
Figure 2.3.35 Relationship between horizontal displacement and horizontal load for the piled raft and sum of pile group and raft (Tsuchiya et al. (2003))

Horikoshi et al. (2003a, b) carried out the static horizontal and dynamic loading tests on the piled raft, raft and single pile under 50g centrifugation. Model piled raft having different pile head conditions, i.e., rigid and hinged pile head connection, consisted of four model pile with the pile spacing of 40mm. Much focus was placed on the effect of pile head
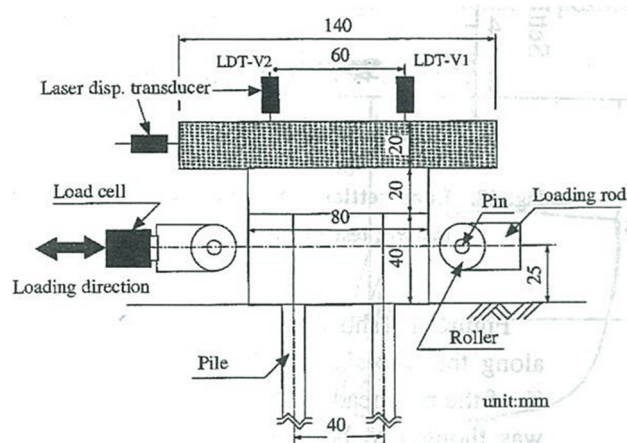
Figure 2.3.36 Illustration of horizontal loading system. (Horikoshi et al. (2003a)

rigidity on the performance of the laterally loaded piled raft foundation. Figure 2.3.36 shows the illustration of horizontal loading system. The principle findings from this research were as follows: 1) The stiffness and the ultimate resistance of the pile in piled raft foundations are different from those observed in the single pile, due to the difference in the confining stress condition around the piles. In the piled raft with the rigid pile head connection, the horizontal resistances carried by the piles were larger than that of

the single pile for both front and rear piles (Fig. 24 (2.3.37)). 2) As for the proportion of the horizontal load carried by each component, the raft initially carried more load than the piles. With larger displacements, the piles carried more load than the raft in the piled raft with rigid pile head connection. In the piled raft with hinged pile head connection, the contribution of the piles was much smaller.
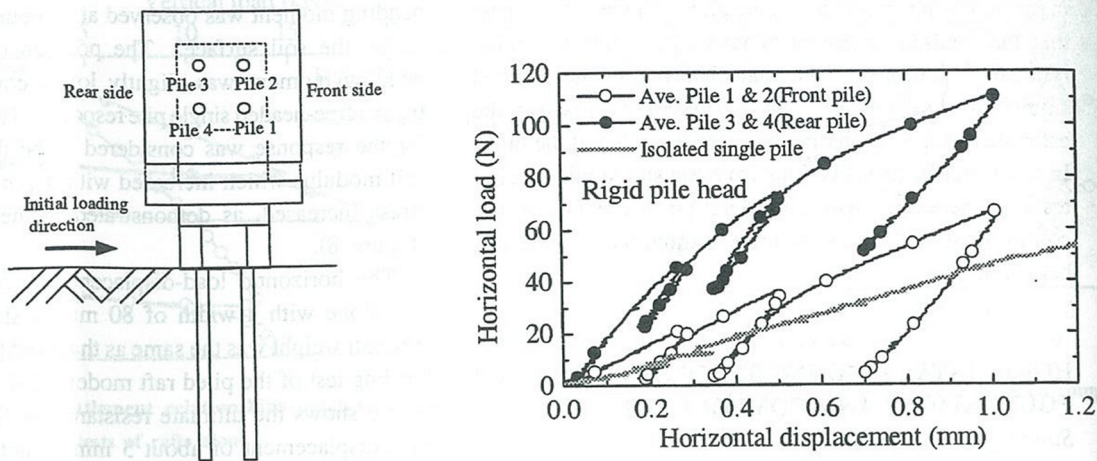
Figure 2.3.37 Horizontal load-displacement relationship of piles in the piled raft, together with that of single pile. (Horikoshi et al. (2003a)

Matsumoto et al. (2004a, b) also conducted static horizontal and shaking table tests in gravity field using the piled raft model with two different rigidity of the pile head connection: rigid connection and hinged connection. Four piles having 170mm length were attached to the model raft with 40mm of pile spacing. Horizontal load was applied at various height from the ground surface for the static loading tests, and the height of centre gravity of superstructure was changed for the shaking table tests to discuss the effects of the loading height. The loading height was relatively higher (Fig. 2.3.38) compared with other previous literatures. The findings derived from this research were as follows: 1) Initial horizontal stiffness of both of the rigid and hinged connection piled rafts decreased as the
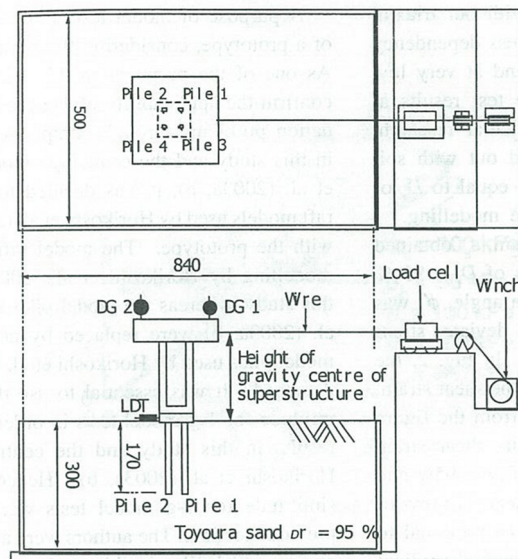
Figure 2.3.38 Schematic illustration of test setup. (Matsumoto et al. (2004a))

height o horizontal loading point increased. The initial horizontal stiffness of the hinged connection piled raft was larger than that of the corresponding rigid connection piled raft (Fig. 2.3.39). 2) Comparing the rigid and hinged connection, the inclination of former one was larger than that of the latter one when the horizontal loading height was middle or high, while the reverse behavior was observed when the height of the loading point was low (Fig. 2.3.40).
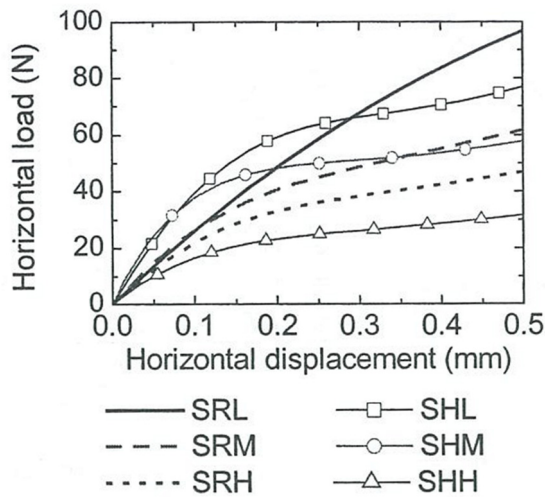
Figure 2.3.39 Horizontal load-horizontal displacement relationship (Matsumoto et al. (2004a))
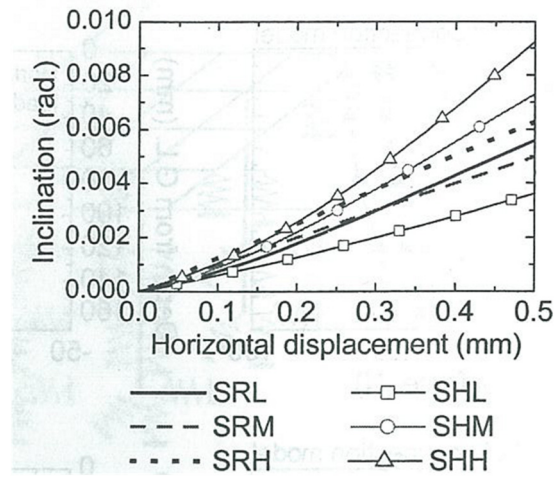
Figure 2.3.40 Horizontal displacement - inclination relationship (Matsumoto et al. (2004a)

Nagai and Tsuchiya (2004) carried out static horizontal loading tests on the piled raft and single pile at the site. The piled raft consisted of two instrumented piles with the pile spacing ratio (*s/D*, where *s* is pile spacing and *D* is diameter) of 10. The pile diameter and length were 114.3mm and 10m respectively. The different rigidity of pile head connection was mainly discussed in this paper. The findings were as follows: 1) The axial load at pile head decreased with the horizontal loading for both front and rear piles (Fig. 2.3.41) because the effect of raft rocking was smaller than the pull-out force by the
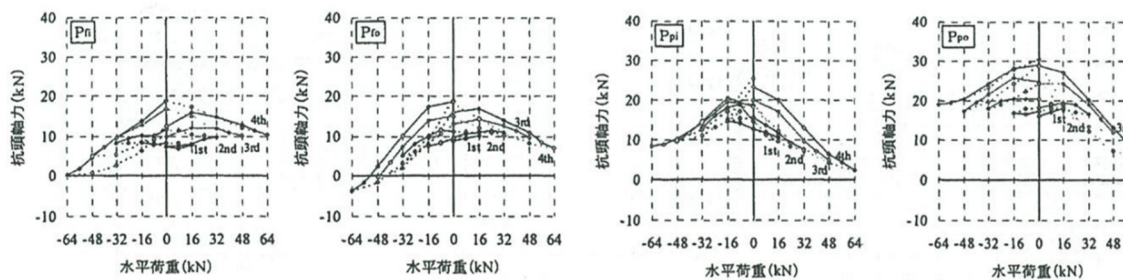
Figure 2.3.41 Variation of axial load at pile head during horizontal loading. (Nagai and Tsuchiya (2004))

43

positive dilatancy just beneath the raft base. Similar tendency was also reported by Nagao et al. (2002). 2) The average horizontal resistance of piles in the piled raft was larger than that of single pile for both rigid and hinged pile head connection. This was because confining stress around piles increased due to the contact stress from the raft and positive dilatancy (Fig. 2.4.42).
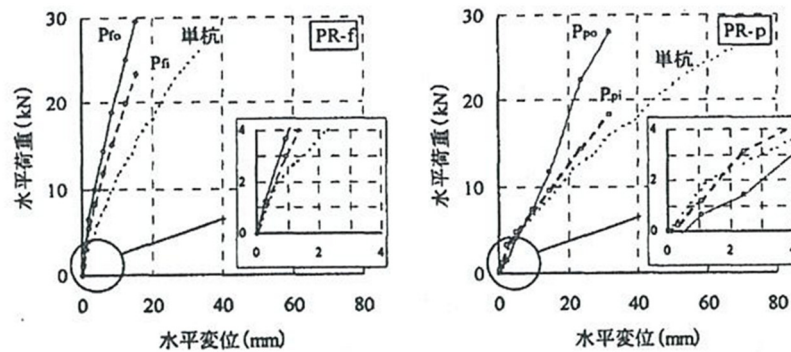
Figure 2.3.42 Relationship between horizontal displacement and horizontal resistance of pile. (Nagai and Tsuchiya (2004))

Katzenbach and Turek (2004) carried out the static horizontal loading tests on the piled raft, pile group and raft models in the gravitational field. Five piles were rigidly fixed by the raft with the pile spacing of 127mm between corner and centre piles and 180mm between corner piles. Two types of model ground was prepared, one is loose sand (density is 1.534g/cm^3) and the other is dense sand (density is 1.712g/cm^3). Prior to the horizontal loading tests, different vertical loads, 1000N, 3000N and 5000N, were applied to each foundation to discuss the effect of the pre-load on the performance of laterally loaded piled raft. The conclusions derived from this research were as follows: 1) Higher vertical loading led to a higher horizontal resistance of the piled raft foundation. However, no significant increase of horizontal resistance due to the increase of vertical loading was observed for the pile group. 2) The horizontal resistance of piled raft foundation was about 2.5-6 times higher than that of the pile group.

Matsumoto et al. (2010) presented the result from the experimental and analytical studies on the behaviors of model pile group and piled raft in dry sand subjected to static cyclic horizontal loading. Much focuses were placed on the influence of various pile head connection conditions between the raft and the piles on the behavior of the foundation and the applicability of a simplified analytical method to simulate the load tests. The analytical method was so-called Hybrid method, which was explained in detail by Kitiyodom and Matsumoto (2002, 2003). There were four types of pile head connection

conditions such as rigid, semi-rigid, semi-hinged and hinged as shown in Fig. 2.3.43. The piled raft and pile group consisted of four instrumented piles and the model raft with 400mm width. Following conclusions were derived from this research: 1) The horizontal stiffness of the piled raft was larger than that of the pile group with the same configuration as the piled raft, because the raft acted effectively as a 'horizontal displacement reducer' (Fig. 2.3.44). 2) The bending moments of the piles in the piled raft were reduced, compared with those in the pile group.
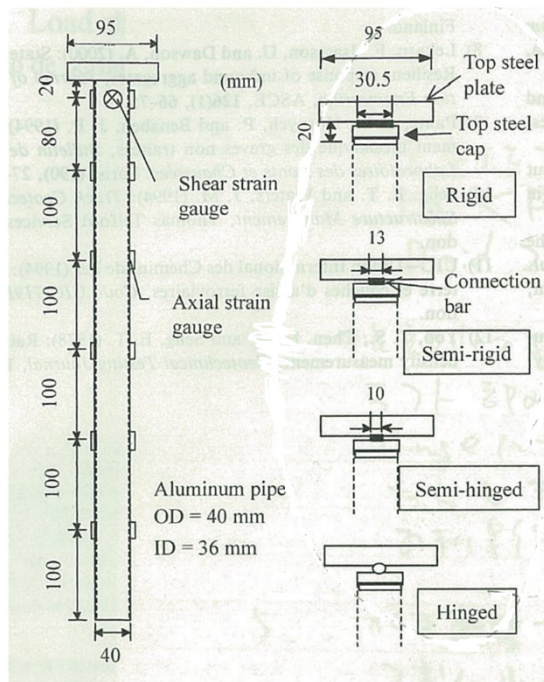
Figure 2.3.43 Model piles with different pile head connection conditions. (Matsumoto et al. (2010))
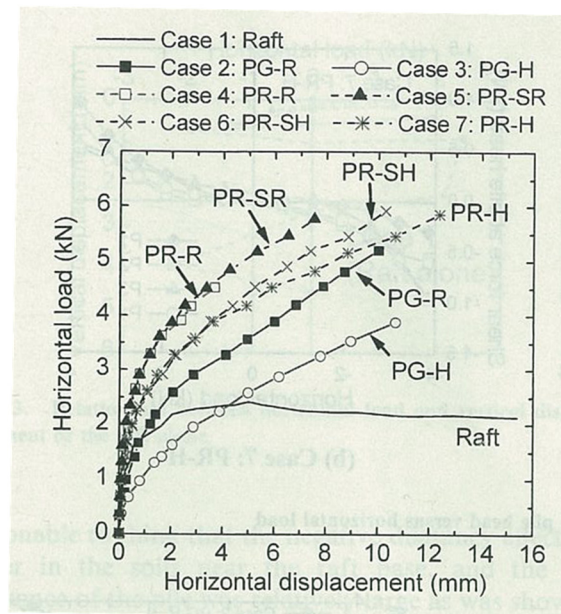
Figure 2.3.44 Horizontal load vs. Horizontal displacement at maximum load in each cycle. (Matsumoto et al. (2010))

Test conditions of previous researches on the laterally loaded piled raft foundation were summarized in Table 2.3.2. In the almost previous researches, it seems that the rotation and moment load acting on the foundation during the horizontal loading was made smaller by applying the horizontal load at relatively low height. In particular, the rotation of the foundation was absolutely restrained using outer and inner flame in the research done by Tsuchiya et al. (2003). This was probably because the model foundation in the previous researches modeled the architectural foundation, in which the foundation width is relatively wide against the loading height and rotation of the foundation is therefore very small. In such case, the rotation and moment resistance of the foundation was not critical issue compared with the horizontal resistance of the foundation. However,

it is crucial for the foundation having relatively narrow width such as viaduct to clarify the moment resistance of the piled raft foundation.

Table 2.3.2 Summary of previous researches on piled raft foundations subjected to horizontal load.

	Test condition	Loading condition	Pile length h	s/D	h/S	RVLP	Observed load-disp. curve	Foundation type	Sensors for estimating shared load
Nagao et al. (2002)	1g	S	3	20.6	0.26	40	δ-P_L	PR, PG, R	Strain gauge (4/4)
Mano et al. (2002)	30g	S	0.18	6	0.24	75	δ-P_L	PR	Strain gauge (4/9)
Nakai et al. (2002)	30g	D	0.18	6	-	75	δ-P_L	PR	Strain gauge (3/9)
Mano et al. (2003)	30g	S	0.18	6	0.24	75	δ-P_L	PR, PG, R	Strain gauge (3/9)
Fujimori et al. (2003)	50g	D	0.3	12	0.83	80	δ-P_L	PR, PG	Strain gauge
Nishiyama et al. (2003)	50g	S	0.3	12	0.83	80	δ-P_L	PR, PG	Strain gauge
Tsuchiya et al. (2003)	1g	S	0.7, 1	3.3, 13	No rotation	47-74	δ-P_L	PR, PG, R	Strain gauge (16/16)
Horikoshi et al. (2003a)	50g	S	0.18	4	0.625	55	δ-P_L	PR, SP, R	Strain gauge (4/4)
Horikoshi et al. (2003b)	50g	D	0.18	4	-	55-60	δ-P_L	PR, PG	Strain gauge (4/4)
Matsumoto et al. (2004a)	1g	S	0.17	4	1.2-4.7	10-43	δ-P_L θ-P_L	PR	Strain gauge (4/4)
Matsumoto et al. (2004b)	1g	D	0.17	4	1.2-4.7	21-29	δ-P_L θ-P_L	PR	Strain gauge (4/4)
Nagai and Tsuchiya (2004)	1g	S	10	10	0.1	50	δ-P_L	PR, PG	Strain gauge (2/2)
Katzenbach and Turek (2004)	1g	S	0.64	4	0.47	-	δ-P_L	PR, PG, R	Strain gauge (?/5)
Matsumoto et al. (2010)	1g	S	0.6	5	0.1	25-50	δ-P_L θ-P_L	PR, PG, R	Strain gauge (4/4)

2.4 Summary

From the above discussion, it seems that settlement behavior of the piled raft foundation has been well discussed for a long time because the concept of the piled raft foundation is to reduce the settlement to an acceptable level installing few friction piles. As a result, the behavior of the vertically loaded piled raft foundation has been relatively well clarified, and the design code of the piled raft foundation was published in Japan. Some application of the piled raft foundation to the actual foundation has been also reported. However, researches on the behavior of laterally loaded piled raft foundation were not carried out until recent year and there are therefore still many uncertainties. In the actual piled raft foundation design, very simple design methodology is usually employed where the all horizontal load is supported by only the raft by ignoring the contribution of the piles. It is crucial for establishing seismic design of the piled raft to clarify the mechanical behavior of the laterally loaded piled raft in detail.

To address above issue, accumulation of the observed data of laterally loaded piled raft is required, but as mentioned in section 2.3.2.2, it is difficult to record the actual field data of the piled raft foundation during the earthquake. Therefore, physical models can play an important role in the study of the piled raft foundation under seismic and horizontal loadings. However, from the above literature review, it can be said that the researched on the laterally loaded piled raft foundation were mostly carried out under the limited condition where the rotation and moment load acting on the foundation were very small. This was probably because the almost previous researches dealt with the relatively wide structures such as architectural building. In such case, the distribution of the contact pressure does not vary during the horizontal loading. However, for the relatively small size foundation supporting tall superstructures, such as a viaduct, rotation of the foundation becomes large, and distribution of the contact pressure varies during the loading, resulting in more complicated interaction among raft base, ground and piles. The author is aware that it is essential to clarify the mechanical behavior of the piled raft foundation subjected to relatively large rotation and moment load for its seismic design.

Although the physical model tests have advantages for this kind of complex problem as mentioned above, modeling technique of piled raft foundation has not been discussed and there should be rooms in the modeling technique to improve and obtain reliable results. Particularly, it is required to exactly evaluate the shared loads by the raft and pile part for clarifying the performance of the piled raft. These shared loads are generally

measured by the strain gauges attached at model piles, but the validity and accuracy of strain gauges attached at small piles has not been discussed.

Therefore, in this thesis main objectives are to establish the centrifuge modeling technique of the piled raft, and to clarify the mechanical behavior of the piled raft foundation subjected to large rotation and moment load using a geotechnical centrifuge.

CHAPTER 3

DEVELOPMENT OF CENTRIFUGE MODELING OF
PILED RAFT FOUNDATION

3.1 Introduction

As explained in previous chapter, the main aim of the present thesis is to develop the modeling technique of piled raft foundation and to clarify the mechanical behavior of piled raft subjected to large rotation and moment load by using developed technique. Centrifuge model tests were carried out on the piled raft and its component such as the pile group and the raft alone model in dry Toyoura sand. By comparing the piled raft foundation and the pile group which has no raft-ground-piles interaction, it is possible to evaluate the complex interaction of raft-ground-piles in the piled raft foundation.

In this chapter, the principle of centrifuge model tests will be described in the beginning, and then modeling technique will be explained. In addition to this, method to improve the accuracy of the strain gauge attached at small model pile, which is essential for evaluating the performance of the piled raft will be proposed.

3.2 Centrifuge modeling principles

Physical modeling tests have advantages in reducing time and cont, compared with the field observations and in-situ tests. The performance of soil structures generally depend on the stress level of the soil, and the physical modeling test done in the gravitational field therefore have a problem because it cannot duplicate the stress condition of the actual ground. The basic principal of the centrifuge model is to apply the Ng centrifugal acceleration to the small model and to make the same stress level as that of the actual ground as shown in Fig. 3.2.1. The detailed information about centrifuge model test was summarized by Schofield (1980).
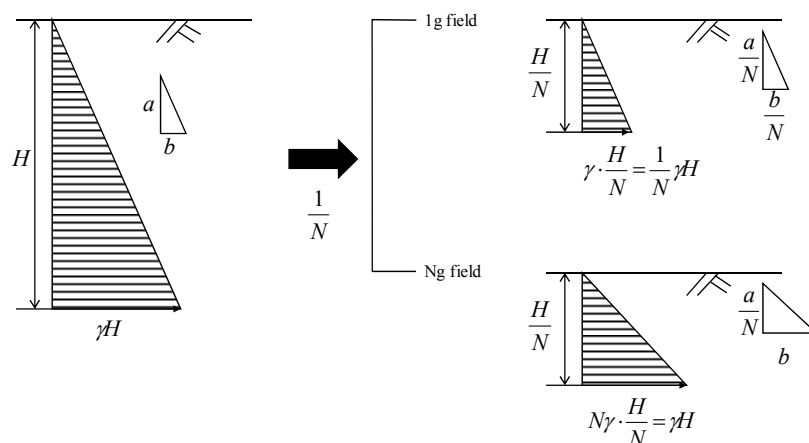
Figure 3.2.1 Stress conditions in actual site and small model.

49

When Ng centrifugal acceleration is applied to 1/N model, the relationships between the model scale (subscript is m) and prototype scale (subscript is p) are as follows.

$$\text{Length}: \quad l_m = l_p / N \tag{3.2.1}$$

$$\text{Cross-sectional area}: \quad A_m = A_p / N^2 \tag{3.2.2}$$

$$\text{Volume}: \quad V_m = V_p / N^3 \tag{3.2.3}$$

Because the unit weight of soil is $\gamma_m = n\gamma_p$, the following equation about $W_m \left(= V_m \gamma_m \right)$ has a quality.

$$W_m = W_p / N^2 \tag{3.2.4}$$

The vertical stress σ_m at depth of z_m is

$$\sigma_m = \gamma_m z_m = \left(N\gamma_p \right)\frac{z_p}{N} = \gamma_p z_p = \sigma_p \tag{3.2.5}$$

and the vertical stresses in the prototype scale and model scale are agreed. Table 3.2.1 summarized the scaling law for the Ng centrifugation. It should be recognized that the centrifuge model tests have following problems.

Table 3.2.1 Scaling law for 1/N centrifuge model

Quantity	Ratio
Gravity: g [m/s²]	N
Density: ρ [kg/m³]	1
Unit weight: γ [N/m³]	N
Length: l [m]	1/N
Area: A [m²]	1/N²
Volume: V [m³]	1/N³
Stress: σ [N/m²]	1
Strain: ε [-]	1
Force: F [N]	1/N²
Moment load: M [Nm]	1/N³
Young's modulus: E [N/m²]	1
Bending rigidity: EI [Nm²]	1/N⁴
Axial rigidity: EA [N]	1/N²

i) Distribution of centrifugal acceleration along the centrifuge radius

The centrifugal acceleration applied to the model depends on the centrifugal radius. This cause a parabolic distribution of the vertical stress in the model soil rather than linear as shown in Fig. 3.2.2. This effect becomes larger as the centrifugal radius decreases, since the ratio of model depth to centrifugal radius generally becomes larger.
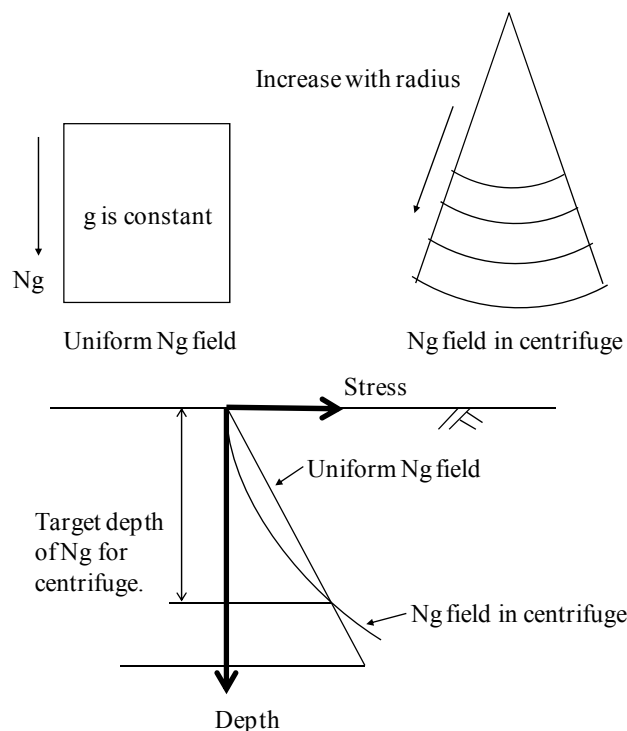
Figure 3.2.2 Difference between uniform Ng field and Ng field in centrifuge flight.

ii) Size effect of soil particles

In centrifuge models, identical soil is generally used in the model and prototype, in order to ensure the same stress-strain response. This means that proportion of the particle size to structure size is larger for the model compared with the prototype, which may lead to scale effects. For Toyoura sand used in the present research is enough fine (Fig. 3.4.11) to ignore the scale effects.

3.3 Centrifuge specifications

A geotechnical centrifuge used in the present research is Mark III centrifuge installed at Tokyo Institute of Technology n 1995 (Fig. 3.3.1). The detailed specifications of this centrifuge were described by Takemura et al. (1999), and main specifications are as follows.

Effective radius : 2.3 m

Maximum centrifugal acceleration：150G

Maximum rotation speed：300rpm

Maximum load capability：50g*ton

Capacity of platform：width 0.9m、breadth 0.9m、height 0.97m

Electrical sliprings for operation：20 sliprings

Electrical sliprings for instrumentation：72 sliprings

Available channels for measurement：64ch

The centrifuge is a beam type having a pair of parallel arms that hold two platforms. The model is mounted on the platform, and the counterweight was placed on the other platform to make a counter balance. The electrical sliprings are installed above the rotational center, and the measurements can be done through them. Rotary joint is also installed at the center to supply the air and water during the centrifugation.
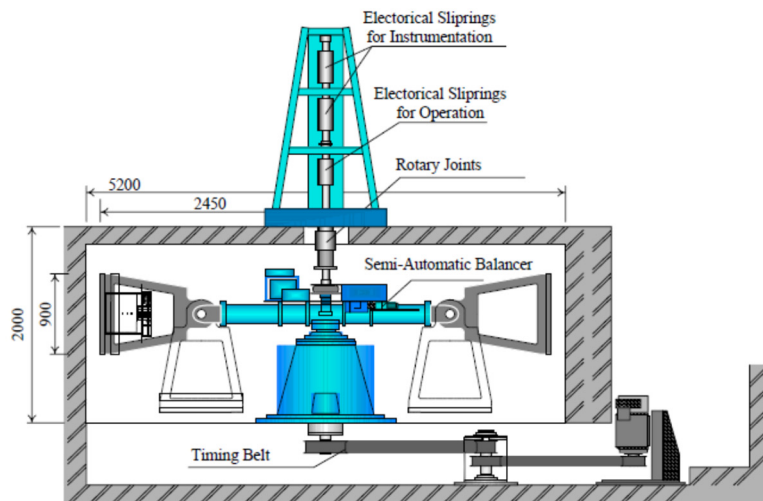
Figure 3.3.1 Tokyo Tech Mark III centrifuge.

3.4 Centrifuge package and model foundation

3.4.1 Centrifuge package

In the present research, a series of static vertical and horizontal loading tests was carried out on the

piled raft and its components such as the pile group and the raft foundation. Schematic illustration of the centrifuge package is described in Fig. 3.4.1. The total height of the model including the actuator is 1.3m, however, there is a height limitation of 1.0m on the left hand side of the swing platform. The model foundation is therefore placed on the relatively right side of the container, where is 140mm from the container center. The CCD camera is installed at the top and in front of the container in order to observe the model foundations during the tests.
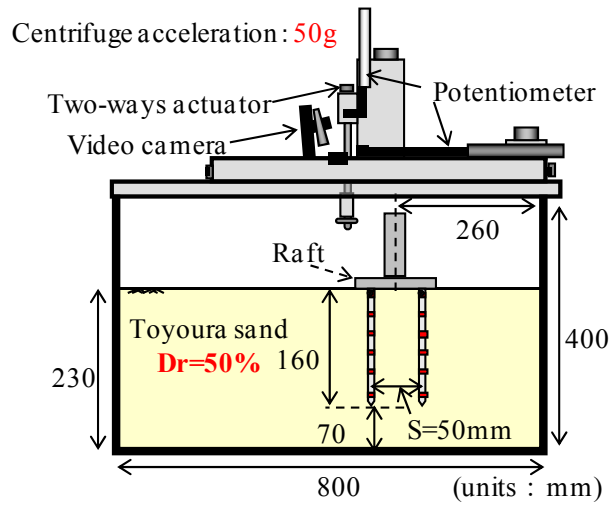
Figure 3.4.1 Schematic illustration of centrifuge package.
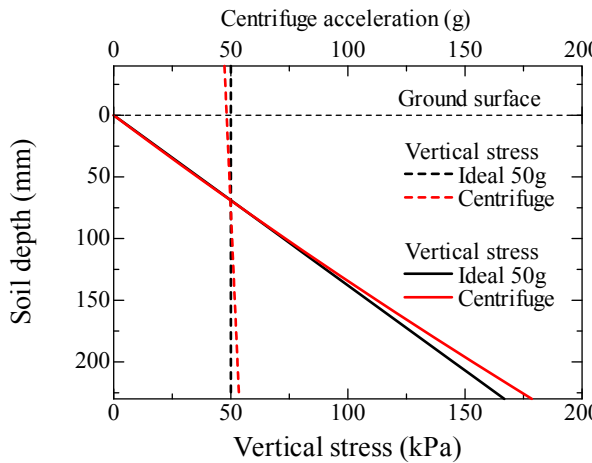
Figure 3.4.2 Distribution of vertical stress in model ground for ideal stress field and centrifuge stress field.
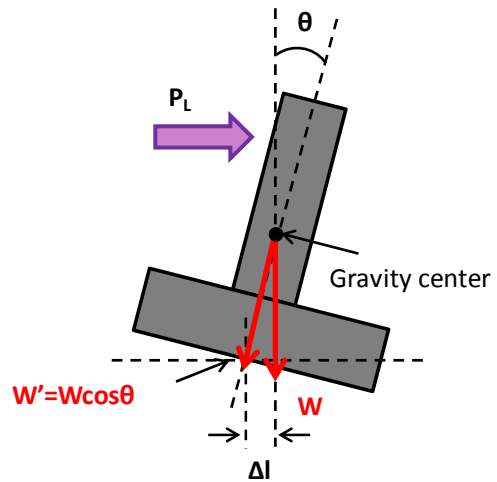
Figure 3.4.3 Influence of foundation rotation on the vertical load of the foundation.

The centrifugal acceleration of 50g was applied to 1/N scale model shown in Fig. 3.4.1. As already explained, when the centrifugation is given by the geotechnical centrifuge, the centrifugal acceleration is distributed along the centrifuge radius. The target centrifugal acceleration of 50g was applied at 1/3 depth of the ground height in the present experiments. Fig. 3.4.2 shows the variation of the ideal centrifugal acceleration, which is 50g, and actual centrifugal acceleration in the present study with ground depth. The centrifugal acceleration at the gravity center of the foundation was approximately 47.5g. The vertical load of the foundation is estimated using this acceleration in the following discussion. Basically, the vertical load of the foundation is constant during the horizontal loading tests. However, it may decrease from *W* to *W'* due to the foundation inclination as shown in Fig. 3.4.3, which

is less than 0.05%. Therefore, the decreased vertical load of the foundation is not taken into account in the present thesis. Furthermore, the vertical load may be varied during the horizontal loading because the gravity center of the foundation shifts to lower by the settlement. However, this effect is less than 0.3% in the present experiment, and it is therefore neglected in the present study.

The vertical stresses under the ideal uniform acceleration and under the same conditions as the present tests are also described in the figure. The difference of the vertical stress between them is 7% at the bottom of the ground, while only 3% difference is seen at the depth around the pile tip. Therefore, this distributed centrifugal acceleration has no significant influence on the performance of the model foundation.

3.4.2 Model raft, superstructure and piles

3.4.2.1 Model raft

The model raft employed is stainless steel block (Fig.3.4.4), implying the model raft is enough stiff to regard it as perfectly rigid. In fact the actual raft is generally made by the concrete slab, and the raft might deform during the static condition and horizontal loading. The model raft used in the present study is not modeled as the certain actual raft, and the deformation of the raft is not discussed in this thesis. The reasons for using stiff raft are to simplify the behavior of the foundation and to rigidly clutch the model piles by the raft. Two types of model raft were prepared, one is the dimension of 80 x 80 x 20mm and the other is 80 x 80 x 40mm. The total mass of superstructure (explained latter) and each raft are 2.7kg and 3.7kg, which are equivalent to 1320N and 1810N in the centrifugation of 50g
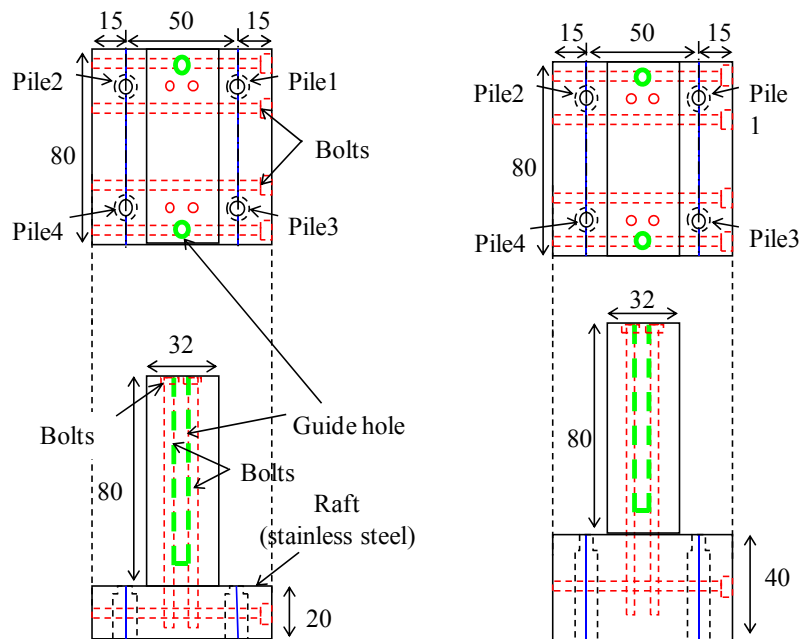
Figure 3.4.4 Model raft and superstructure.

54

respectively. The test cases using the light and heavy raft are defined as light case and heavy case respectively. By comparing the result derived from different mass, the influence of the vertical load of the superstructure on the performance of the piled raft and the pile group can be discussed.

This raft can be divided into three parts, by which four model piles were rigidly clutched using screws. The clutched length is 17mm for the light raft and 37mm for the heavy raft, and latter raft can make more rigid connection condition of the pile head than the former. Four model piles were employed in the previous researches summarized in Chapter 2 as well (Horikoshi et al., 2003a, b; Katzenbach & Turek, 2005; Matsumono et al., 2004a, b; Matsumono et al., 2010), and the results can be therefore easily compared with the present study. Because the frictional resistance at the raft base cannot be expected for the stainless steel raft, the sandpaper is pasted beneath the raft base to make a rough base condition (Fig. 3.4.5). In almost previous researches using the stainless steel or aluminum raft model, the rough base contact condition was artificially created. Mano et al. (2002, 2003) glued the sand on the raft base, Horikoshi et al. (2003a, b), Matsumoto et al. (2004a, b, 2010) made the rough base by scratching the raft base.
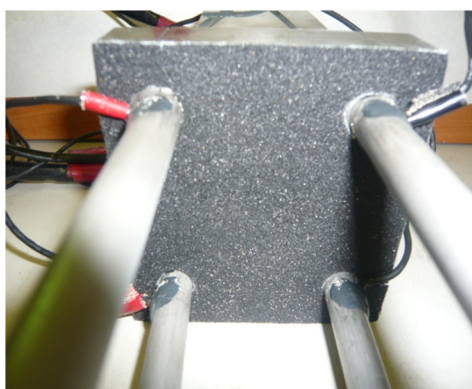
Figure 3.4.5 Sand paper glued on the raft base.

3.4.2.2 Model superstructure and guide rods

The stainless steel block was used for the model superstructure as well. The superstructure is rigidly fixed on both light and heavy rafts using four screws. Its dimensions are 32mm in width, 80mm in breadth and 80mm in height. Because the vertical and horizontal loads are applied at this superstructure, the stiff stainless steel is used to prevent the deformation of the superstructure. On top of the superstructure, two guide holes are made with a depth of 70mm to insert the guide rod shown in Fig. 3.4.6. This guide rod is fixed to the actuator thorough the load cell, and vertical load can be applied to the foundation by hemisphere part at the center as shown in Fig. 3.4.7. The guide rod and holes can secure the verticality of the foundation during the vertical loading.

Figure 3.4.6. Guide rod.
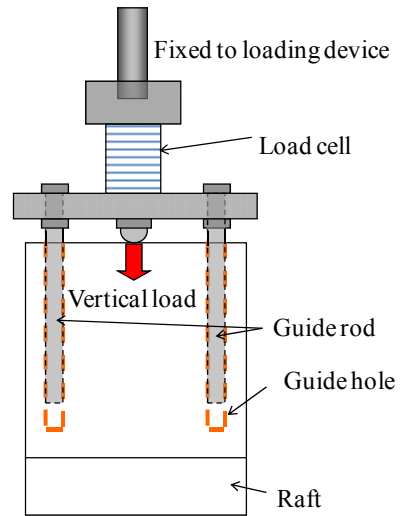
Figure 3.4.7 Guide rod and guide holes.
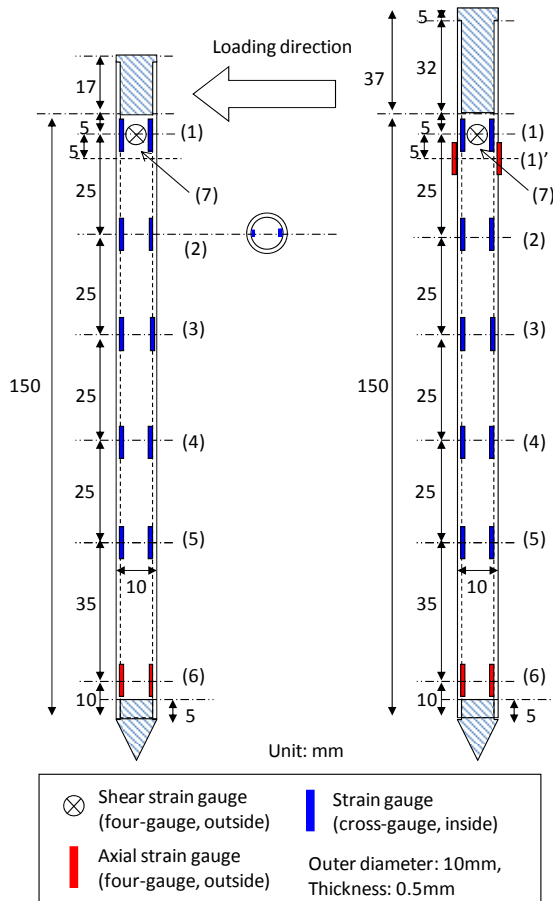
Figure 3.4.8 Model piles for light and heavy cases.

Figure 3.4.9 Picture of model pile.

3.4.2.3 Model piles

Figure 3.4.8 and 3.4.9 shows the model piles used. Model piles are made of stainless steel pipe with 10mm in outer diameter, 0.5mm in thickness and 160mm in embedment length. The model piles were

penetrated into the ground in the 50g centrifugal acceleration (detail explanation will be done latter). Therefore, the pile tip is closed by the brass made cone to easily penetrate piles in the flight. The pile head is also filled by the brass made cap in order to obtain enough stiffness of the pile head when the pile head is clutched by the raft.

The axial and bending rigidity of the model pile should be carefully considered because pile is subjected to vertical, horizontal and moment loads during the tests. Specifications of model pile are summarized in Table 3.4.1 n both model scale and prototype scale. For reference, the axial and bending rigidity of the solid concrete pile with 35Gpa in Young's modulus and 500mm in diameter. The general thickness of stainless steel pile having 500mm diameter is from 9mm to 14mm. From this fact and Table 3.4.1, the model pile used in the present study, which pile thickness is 25mm in the prototype scale, has relatively large rigidity compared with the actual stainless steel pile and solid concrete pile. Therefore, it thought to be that the deformation and strain acting on the pile during the experiments is restrained compared with the actual stainless steel or concrete piles. The maximum bending strain observed in the horizontal loading tests was approximately 800μ, implying that the model pile behaved within the elastic region. However, considering the smaller strain in the model pile used, this bending strain might be sufficient to collapse the actual stainless steel and concrete piles, especially for the tension side of the concrete pile. So, it should be noted that the model pile during the experiments showed only elastic response, and piled raft behavior under condition in which the model pile is collapsed cannot be discussed in the present thesis.

Table 3.4.1. Physical properties of model pile

Properties	Model	Prototype	Concrete pile
Material	Stainless steel	Stainless steel	Concrete
Diameter	10mm	500mm	500mm
Thickness	0.5mm	25mm	Solid
Embedment depth	160mm (piled raft) 155mm (pile group)	8m 7.75m	8m 7.75m
Cross section area, A_P	14.9 mm^4	3.73×10^{-2} m^2	7.85×10^{-1} m^2
Moment of inertia, I_P	169 mm^4	1.06×10^{-3} m^4	3.07×10^{-3} m^4
Young's modulus, E_P	205 GPa	205 GPa	35 GPa
Longitudinal rigidity, $E_P A_P$	3.06×10^{-3} GN	7.65 GN	6.87 GN
Bending rigidity, $E_P I_P$	3.46×10^{-8} GNm^2	0.216 GNm^2	0.107 GNm^2

The interface friction between the model pile and the soil is estimated by following equation, which was proposed by Durgunoglu and Mitchell (1975a, b) and Endra Susila and Roman (2003).

$$\delta\!\!\Big/_{\!\phi'} = 0.50 \qquad\qquad\qquad\qquad (3.4.1)$$

δ is interface friction angle between the steel and sandy soil, and φ' is internal friction angle of soil. The internal friction angle of soil φ' is 37 degree at the middle depth of the model ground for the present study as explained in latter section of 3.4.3. The δ for the present study in 18.5 degree (coefficient of friction $\mu=\tan\delta=0.33$), implying that the model pile used is relatively smooth pile).
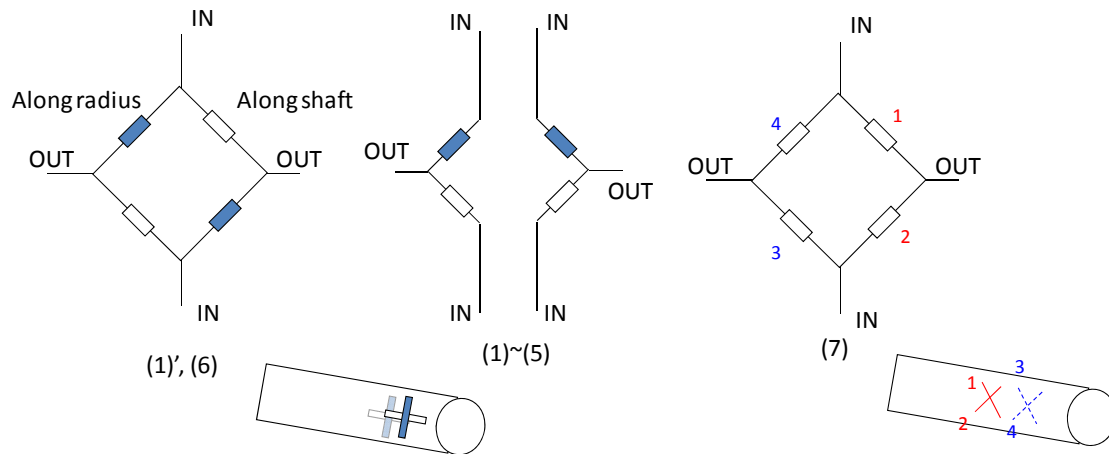
Figure 3.4.10 Bridge circuit for each strain gauge type.

Table 3.4.2 Specifications of strain gauges used for model piles

Specification	Strain gauges (1)', (1)-(6)	Shear strain gauge (7)
Model	FCA-1-17-3LH	KFG-1-120-D16
Resistance at 24℃ (Ω)	120±0.2%	120±0.2%
Gauge factor at 24℃	2.14	2.05

In the study of the piled raft, it is crucial to exactly measure the forces acting on piles because the interaction of raft-ground-piles is evaluated by them. Therefore, strain gauges are attached at the pile at several depths along the shaft. For gauge (1)-(5) in Fig. 3.4.10 cross-gauge is attached at both sides of inside the pile. Strains are individually measured at the both sides, and the axial and bending strains can be therefore measured at the same time. The strain gauges are attached inside of the pile tip by four-gauge method (gauge (6)), which can measure only axial strain, because the bending strain is considered almost zero at the pile tip. A set of shear strain gauges is attached outside surface of the pile head by the four-gauge method (gauge (7)) to measure the shear force at the pile head. The same strain gauge is used for shear strain gauge and others, but the shear strain gauge is attached with inclination of 45 degree as shown in Fig. 3.4.10. These strain gauges are prepared for both light case and heavy case pile, only for the heavy case pile additional strain gauge is attached at the outside of the pile head by the four-gauge method in order to measure the axial strain. The specifications of strain

gauge are summarized in Table 3.4.2.

The reasons why almost strain gauges are attached inside the pile are to keep the constant pile diameter along the pile shaft and to reduce the disturbance of the model ground during the pile penetration. Note that the method to make bridge circuit for each strain gauge and calibration technique will be described latter (Section 3.6).

Using above mentioned model raft, superstructure and piles, the piled raft and the pile group model are prepared as shown in Fig. 3.4.11. The raft foundation model uses the same raft and superstructure as the piled raft and the pile group, but four columnar caps are inserted in substitution of piles to make flat base condition.
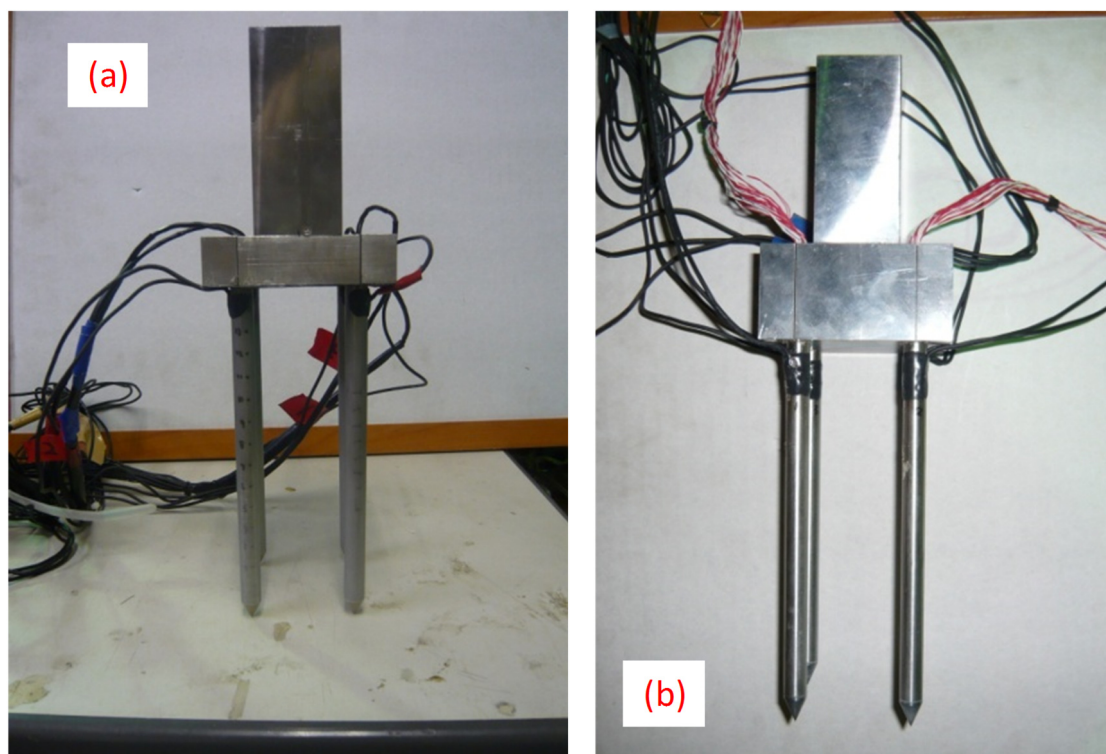
Figure 3.4.11 Model piled raft and pile group (a) for light case, (b) for heavy case.

3.4.3 Soil model

The dry Toyoura sand is employed for the model ground in present tests because the physical properties of Toyoura sand have been well studied and known. The model ground was made with a depth of 230mm and a target relative density of 50%. In this section, the physical properties, deformation characteristics and strength characteristics of Toyoura sand and conditions of model ground will be explained.

From the grain size accumulation curve of Toyoura sand shown in Fig. 3.4.12, it can be said that the particle size from 0.15 to 0.25mm account for 90% of total, and Toyoura sand has almost uniform particle size. Other physical properties are summarized in Table 3.4.3. The dry density ρ_d for 50% of relative density is 0.791g/cm^3, and profile of vertical stress under 50g centrifugal acceleration is already described in Fig. 3.4.2.
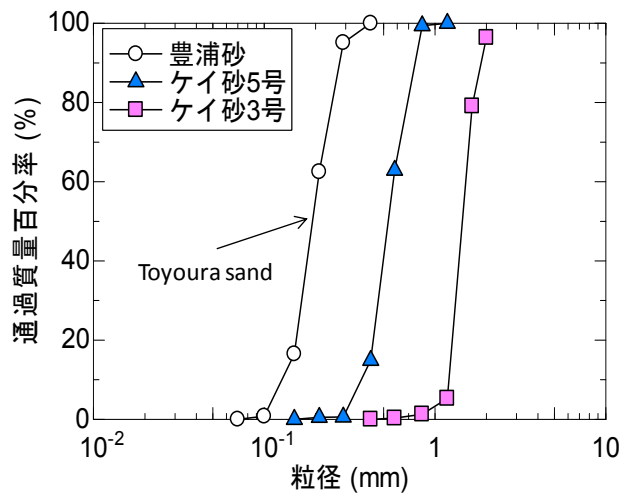
Figure 3.4.12 Cumulative frequency curve for Toyoura sand.

Table 3.4.3 Physical properties of Toyoura sand

Property	Value
Particle density G_s (g/cm^3)	2.65
Mean grain size D_{50} (mm)	0.162
Uniformity coefficient U_c	1.56
Coefficient of curvature U_c'	0.95
Maximum void ratio e_{max}	0.973
Minimum void ratio e_{min}	0.609

The Young's modulus is one of important deformation characteristic of soil. Kaku et al. (1996) carried out tri-axial compression tests using Toyoura sand with relative density of 50%. Figure 3.4.13 shows relationship between confining stress σ_3'and Young's modulus E_{50} derived from them. From this relationship, the following approximate equation can be obtained for the relative density of 50%.

$$E_{50} = 1059 \times \sigma_3^{0.675} \tag{3.4.2}$$
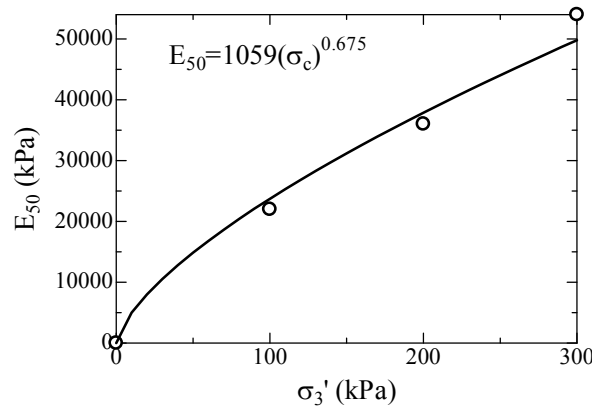
Figure 3.4.13 Relationship between confining stress σ_3' and Young's modulus E_{50} for Toyoura sand with relative density of 50% (Kaku (1996))

The following equation was proposed by Jaky (1948) for the coefficient of earth pressure at rest.

$$K_0 = 1 - \sin \phi' \tag{3.4.3}$$

Next, the strength characteristics of Toyoura sand are explained. Fukushima and Tanaka (1984) carried out drained tri-axial compression tests using Toyoura sand by varying relative density. The relationship between principle stress ratio and strain for the relative density of 60%, which is almost same as the present t tests, is shown in Fig. 3.4.14. From this figure, it can be observed that the principle stress ratio, i.e., internal friction angle of sand φ' decreased with increase of confining stress σ_3'.
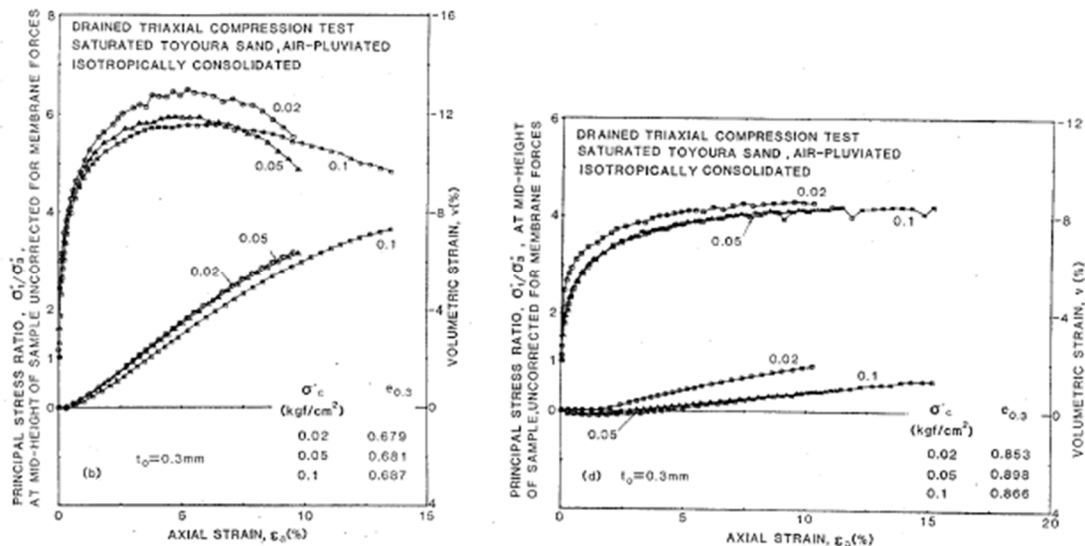
Figure 3.4.14 Typical relationships between principal stress ratio for loose sample (a) σ_3'=10~400kPa, (b) σ_3'=2~10kPa. (Fukushima and Tatsuoka (1984))

Tatsuoka et al. (1986) carried out plane strain compression tests by varying the relative density, the angle between direction of principle stress σ_1' and depositional surface δ. They plotted φ' evaluated by following equation against void ratio e in Fig. 3.4.15.
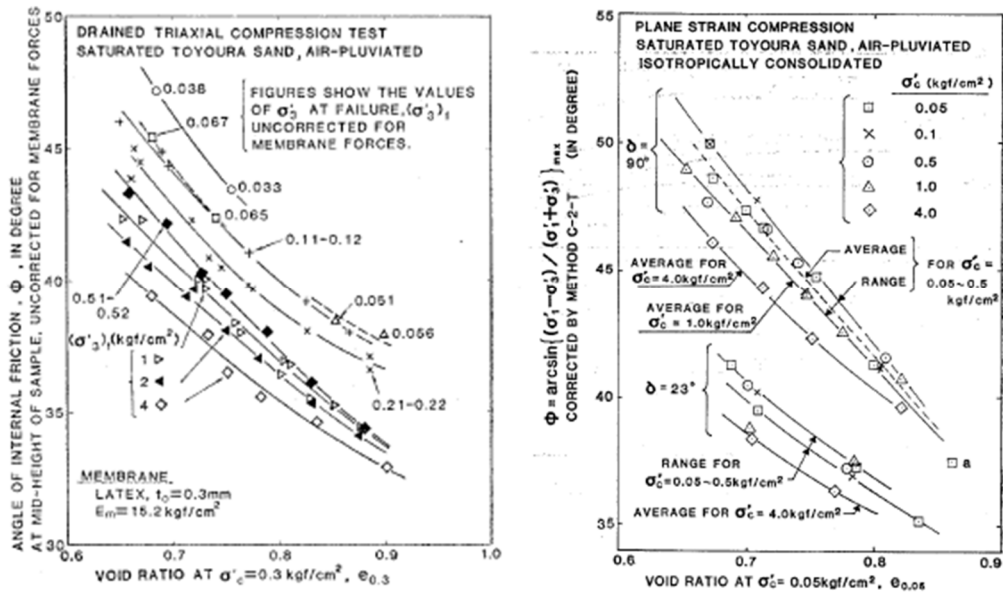
Figure 3.4.15 Relationship between internal friction angle φ' and void ratio for (a) triaxial compression tests at σ3' of 30kPa (Fukushima and Tatsuoka (1984)), (b) plane strain compression tests at σ3' of 5kPa (Tatsuoka et al. (1986)).

$$\phi' = \sin^{-1}\left(\frac{\sigma_1' - \sigma_3'}{\sigma_1' + \sigma_3'}\right)_{max} \qquad (3.4.4)$$

In the figure, the result from tri-axial test done by Fukushima and Tatsuoka (1984) is also described. From this figure it can be confirmed that the internal friction angle φ' decreased with the void ratio e. The relationship between the confining stress σ3' and internal friction angle φ' at the void ratio of 0.7 and 0.8 is shown in Fig. 3.4.16. They pointed out that although the internal friction angle decreases with the increase of the confining stress, the internal friction angle

Figure 3.4.16 Relationship between internal friction angle φ' and σ3' for (a) e=0.7, (b) e=0.8. (Tatsuoka et al. (1986))

is almost constant when the confining stress is less than 50kPa. Because the stress condition of the present tests is similar with that of tri-axial tests, the internal friction angle is approximately 37% using the result from tri-axial test in Fig. 3.4.16.

By summarizing the above discussion, the vertical stress σ_v', horizontal stress σ_h', Young's modulus E_{50}, the coefficient of earth pressure at rest K_0 and internal friction angle φ' are plotted against the ground depth in Fig. 3.4.17.
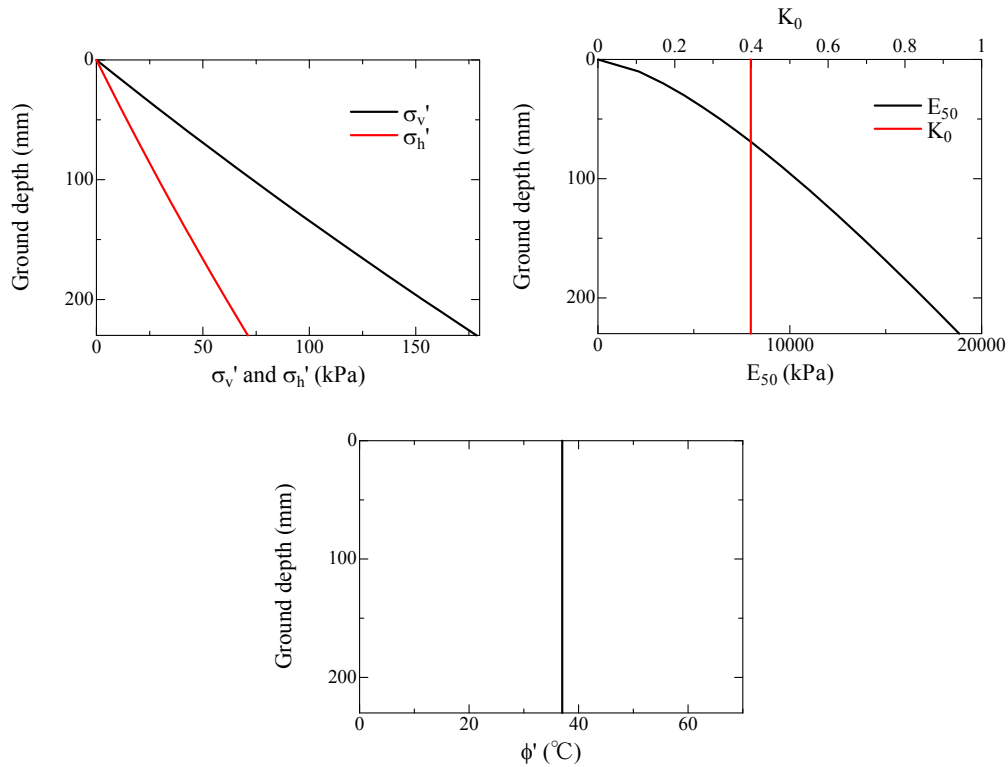
Figure 3.4.17 Variation of (a) stress level, (b) deformation characteristics and (c) strength characteristic with ground depth for present model.

3.4.4 Apparatus and instrumentations used in the tests

i) Rigid container (Fig. 3.4.18)

A rigid container is employed in the present tests. Inner dimension is 800mm in width, 250mm in breadth and 400mm in height, and outer dimension is 920mm in width, 450mm in breadth and 465mm in height. The acrylic plate is attached in front of the container, and the loading sequences in the flight can be checked by the video camera.

ii) Two-ways actuator (Fig. 3.4.19)

The vertical and horizontal loads were applied by two-ways actuator, which is driven by the electrical motor. The schematic illustration of the actuator is shown in Fig. 3.4.20. The range of motion is about 180mm for vertical direction, 250mm for horizontal direction. The loading rates can be controlled from 0.01mm/sec to 3.3mm/sec for the vertical and more than 0.2mm/sec for the horizontal.

iii) Two-directional load cell (Fig. 3.4.21)

A two-directional load cell is fixed to the two-ways actuator, by which the vertical and horizontal loads are measured. The maximum horizontal load during the experiments is considered as a relatively

small value by the literature reviews, and the load cell having small capacity of 5kN is therefore used for the horizontal loading tests.

iv) One-directional load cell (Fig. 3.4.22)

For the vertical loading tests, the One-directional load cell, which can measure only the vertical load, is fixed to the two-ways actuator. Because relatively large vertical load is applied to the foundation during the vertical loading tests, one-directional load cell with large capacity of 10kN is used.

v)   Horizontal loading device (Fig. 3.4.23)

The horizontal load was applied to the foundation through the horizontal loading device attached at the two-directional load cell. This horizontal loading device has two hemisphere parts at the sides, by which the pin horizontal load can be applied to the foundation. At the bottom of it, the flat bolt is attached in order to apply the vertical load. The verticality of the foundation is secure because the vertical load is applied by the surface using the flat bolt

v) Potentiometer (Fig. 3.4.24)

Four potentiometers were placed at the corner of the model raft to measure the total settlement and the vertical displacement of each pile.

vi) Laser displacement transducer (Fig. 3.4.25)

Two laser displacement transducers (LDTs) were installed to measure the horizontal displacement. The rotation of the foundation is also estimated from the difference between the displacements measured by them. The principle of the LDT is applying the laser with 780mm of wavelength to the objective, and measuring the phase difference between applied and reflected laser. The LDTs is not available for the stainless steel raft and superstructure because the stainless steel cannot reflect the laser properly. Therefore, the thin acrylic plate, on which the white tape was glued, was used as a target. The measurement range of LDTs used is 40±10mm.

vii) CCD Camera (Fig. 3.4.26)

Two CCD cameras were installed at the top and in front of container to record the tests in the flight.

viii) Sand hopper (Fig. 3.4.27)

The model ground was made by the air-pluviation method using the sand hopper shown. The target relative density and ground depth are 50% and 230mm respectively.
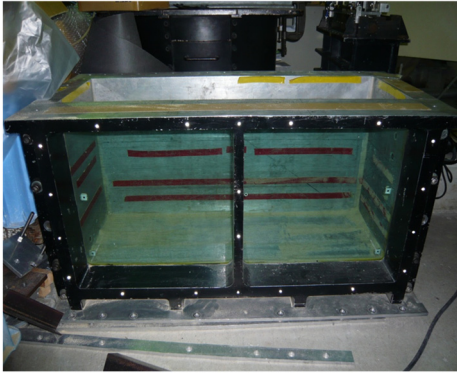
Figure 3.4.18 Rigid container

Figure 3.4.19 Two-ways actuator.
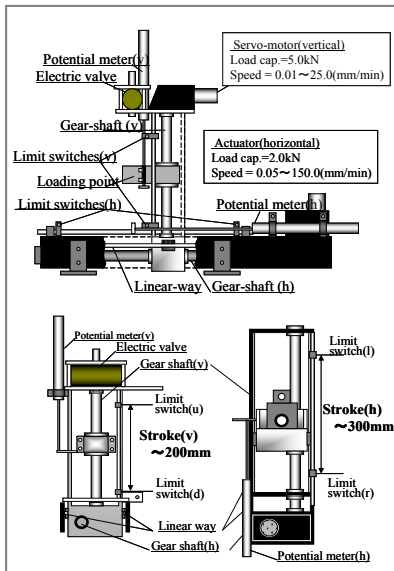
Figure 3.4.20 Details of two-ways actuator.

Figure 3.4.21 Two-directional load cell.

Figure 3.4.22 One-directional load cell.
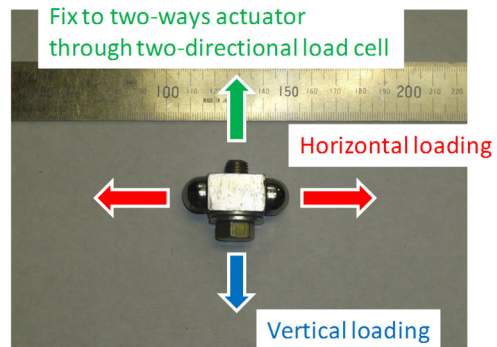
Figure 3.4.23 Horizontal loading device.

Figure 3.4.24 Potentiometer.

Figure 3.4.25 Laser displacement transducer.

Figure 3.4.26 CCD camera.

Figure 3.4.27 Sand hopper.

3.5 Test procedures

3.5.1 Test series

Totally 10 series of vertical and horizontal loading tests on the piled raft and its components such as the pile group and the raft were carried out in the present research as listed in Table 3.5.1. The same model was used for both piled raft and pile group foundation models. The piled raft model had a contact with the ground surface, but 5mm gap between the raft base and the ground surface was provided to avoid the interaction between them for the pile group model. The design concept of conventional pile group was made by this gap. The complex interaction among the raft, ground and piles can be evaluated by comparison of the piled raft and pile group, which are with and without interaction of the raft and the ground.

Table 3.5.1 Test cases.

Case	Foundation type	Test type[1]	Max. vertical load in pre-vertical loading process (N)	Applied horizontal disp. at lower LDT (mm)	Vertical load by raft and superstructure (N)	Initial RVLP[3] (%)
R_L1	Raft	H		±1mm (h/S=1, 1.8) +4mm (h/S=1)	1320	100
R_L2	Raft	H		±1mm (h/S=1, 1.8) +4mm (h/S=1.8)	1320	100
R_L3	Raft	V		———	1320	100
P_L	Pile group	H	2440	±1mm (h/S=1, 1.8) ±2mm (h/S=1, 1.8)	1320	0
PR_L1	Piled raft	H	3190	±1mm (h/S=1, 1.8) ±2mm (h/S=1, 1.8)	1320	27
PR_L2	Piled raft	V	9800[2]	———	1320	———
R_H1	Raft	H		±1mm (h/S=1, 1.8) +4mm (h/S=1)	1810	100
R_H2	Raft	H		±1mm (h/S=1, 1.8) +4mm (h/S=1.8)	1810	100
P_H	Pile group	H	2320	±1mm (h/S=1, 1.8) ±2mm (h/S=1, 1.8)	1810	0
PR_H	Piled raft	H	4530	±1mm (h/S=1, 1.8) ±2mm (h/S=1, 1.8)	1810	27

[1]Test type; H is horizontal loading test and V is vertical loading test.
[2] Maximum vertical load during vertical loading test.
[3]Initial proportion of vertical load carried by raft part before horizontal loading.

3.5.2 Test procedures for vertical loading tests

3.5.2.1 Preparation of model foundations for vertical loading tests

The model preparing and loading processes for the vertical loading tests are summarized in Table 3.5.2. A part of procedures was same for both vertical and horizontal loading tests, which was from Step I to VI in the table.

Table 3.5.2 Model preparation procedures for pile group and piled raft models.

Step	Vertical loading test	Horizontal loading test	Step name	Pile embedment length at each step* Light case	Heavy case
I	Preparation of model ground with a depth of 230mm		———	———	———
II	Penetration of piles by deadweight (putting foundation on ground for raft foundation) with guide rod in gravity field		———	35mm (PR_L1) 40mm (PR_L2) 40mm (P_L)	60mm (PR_H) 55mm (P_H)
III	Penetration of piles by deadweight (applying deadweight of foundation to model ground for raft foundation) with guide rod during increase of centrifugation		———	75mm (PR_L1) 80mm (PR_L2) 90mm (P_L)	125mm (PR_H) 115mm (P_H)
IV	Penetration of piles (applying vertical load to raft foundation) using actuator with guide rod in flight		Penetration process	157mm (PR_L1) 157mm (PR_L2) 150mm (P_L)	156mm (PR_H) 150mm (P_H)
V	Stop of centrifugation and installation sensors		———	Same as above	Same as above
VI	Increase of centrifuge acceleration		———	Same as above	Same as above
VII	Vertical loading using electric jack with guide rod	Vertical loading using two-ways actuator with guide rod	Vertical loading process	160mm (PR_L1) 160mm (PR_L2) 152mm (P_L)	160mm (PR_H) 150mm (P_H)
VIII	———	Stop of centrifugation, removal of guide rod and installation of horizontal loading device	———	160mm (PR_L1) 152mm (P_L)	160mm (PR_H) 150mm (P_H)
IX	———	Increase of centrifugal Acceleration	———	Same as above	Same as above
X	———	Pre-vertical loading using two-ways actuator without guide rod	Pre-vertical loading process	160mm (PR_L1) 154mm (P_L)	160mm (RP_H) 153mm (P_H)
XI	———	Horizontal loading using two-ways actuator	Horizontal loading process	———	———

* PR_L1 and PR_H1 are case of horizontal loading tests on piled raft; PR_L2 is case of vertical loading test on piled raft
  P_L and P_H are case of horizontal loading tests on pile group (see Table 4)

Firstly, the model ground was made from dry Toyoura sand by air-pluviation method with the depth of 230mm and the target relative density of 50% (Fig. 3.5.1). After pouring the sand into the container, the perfectly flat ground surface was made using the vacuum. The conditions of model ground were explained in Fig. 3.4.17.

Having completed the model ground, the actuator was mounted on top of the container. For the piled raft and the pile group model, the foundations were fixed to the actuator through the load cell and guide rod, and they were hung above the ground surface (Fig. 3.5.2). The spring ties were used for fixing the foundations and guide rods. The raft foundation was also fixed to the actuator through the load cell and guide rod, but it was placed on the ground surface. As mentioned in Section 3.4.2.2, the verticality of the foundation can be secure by the guide rod. Then, the spring ties were removed for the piled raft and the pile group foundations, and the foundations were penetrated into the ground by their deadweight in the gravitational field (Fig.3.5.3). At this time (Step II), the piles were penetrated into the ground about 40mm and 60mm for the light case and heavy case respectively.

Centrifugal acceleration was then increased up to 50g, and the piles were further penetrated by the self weight during this period. The total pile penetration lengths were approximately 80mm and 120mm for the light case and the heavy case respectively. Under 50g centrifugation, piles were penetrated at a rate of 0.26mm/sec using the two-ways actuator until the raft base reached about 3mm above the ground surface for the piled raft and 10mm above for the pile group foundation. The vertical load was applied in the flight for the raft foundation as well in order to give the same centrifugation and loading histories as those of the piled raft and the pile group to the raft foundation. This penetration step using the actuator in the first flight was named "penetration process" (Step IV).

After the penetration process, the centrifugation was once stopped (Fig. 3.5.4), and four potentiometers were arranged at the corner of the model raft (Fig. 3.5.5). The electrical actuator having larger capacity than the two-ways actuator was placed in substitution of the two-ways actuator only for the vertical loading tests. Then, the centrifugation was again done up to 50g. The same preparation procedures were used for both vertical and horizontal loading tests up to this step (Step VI).
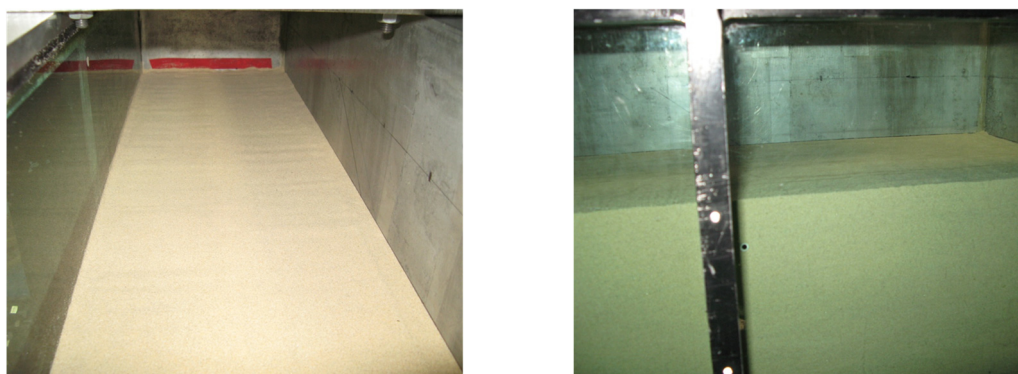
Figure 3.5.1 Model ground prepared by air-pluviation method.

Figure 3.5.2 Model foundation fixed to actuator using guide rods for (a) piled raft and pile group, (b)raft.
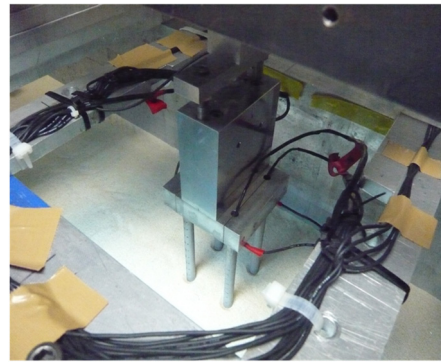
Figure 3.5.3 Penetrated piles by deadweight in gravitational field.

Figure 3.5.4 Model piled raft and pile group after penetration process.

Figure 3.5.5 Model piled raft and pile group after setting instrumentations.

In almost previous literatures listed in Chapter 2, different model preparing procedure was employed (Mano et al. (2002, 2003); Tsuchiya et al. (2003); Horikoshi et al., 2003a, b; Katzenbach & Turek, (2005); Matsumono et al. (2004a, b); Matsumono et al. (2010)). After making the model ground, the piles were penetrated in the flight in the present research. On the other hand, the model piles were firstly fixed to the container using rigid flame, and the model ground was then made in the previous research. It can be said that the piles prepared by the former method (present research) was behaved as the "displacement pile", and piles prepared by the latter one (almost previous literature) was acted as the "non-displacement pile".

There are two reasons for employing this method in the present research. One is to make the flat ground. One of the most important things in the modeling of the piled raft is to make the contact condition between the raft base and the ground surface uniform. However, it is difficult to make flat ground in the condition where piles are fixed to the container. Therefore, the method in which the level ground was firstly made was adopted in the present study.

The other reason is to increase the mobilized shaft friction of pile. The concept of the piled raft foundation is reducing the total and differential settlement by few friction piles. Therefore, it is preferred to design the model piles as the friction piles for the physical modeling tests as well. However, the model pile used had small interface friction angle between the pile surface and the soil of 17.5 degree as explained in Section 3.4.2.2, and its surface was relatively smooth. According to Sherif et al. (1995), the displacement piles showed three times larger for the shaft friction and four times larger for the coefficient of earth pressure compared with the non-displacement pile. Meyehof (1976) also reported that similar tendencies, i.e., although the coefficient of earth pressure in the non-displacement pile was almost same as the coefficient of earth pressure at rest K_0, that in the displacement pile is four times larger than them. Therefore, the model preparing procedures in which the piles were penetrated into the ground under the centrifugation was employed to make the shaft friction along the piles larger.

For the reference, the variation of end bearing load and shaft friction load with the settlement for PR_L2 is shown in Fig. 3.5.6. The relationship derived from the loading tests on the pile group done by Yamana (2009) also described in the figure. For PR_L2 there was about 3mm gap between the raft base and the ground surface as explained above, implying that the foundation behaved as the pile group foundation for the settlement less than 3mm and it acted as the piled raft foundation after the settlement reached 3mm. The model pile group foundation used in Yamana (2009) consisted of four
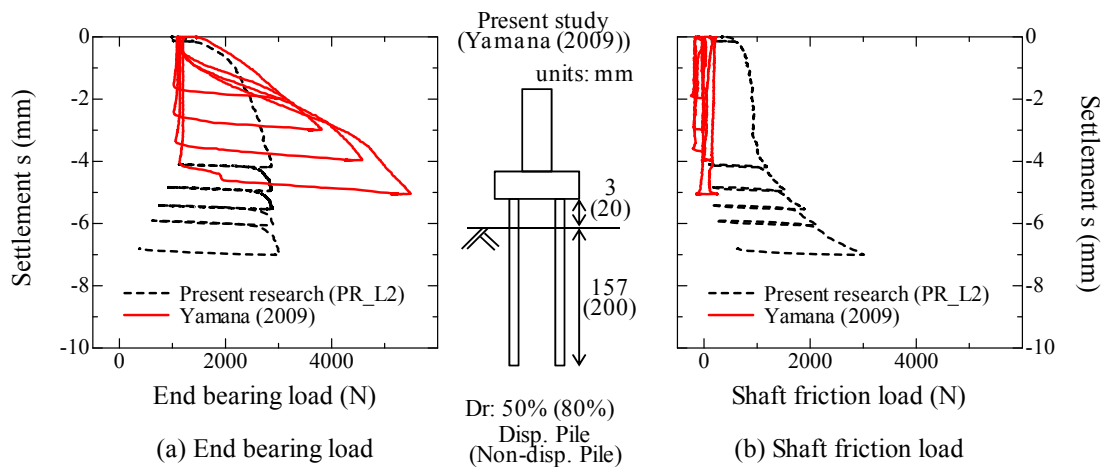
Figure 3.5.6 Variation of pile load with settlement during vertical loading test.

stainless steel pile with the pile spacing of 50mm. The model pile was 10mm in outer diameter, 0.5mm in thickness and 200mm in embedment length. The relative density of the model ground was 80%. The model pile group was prepared as the non-displacement pile, that is, four piles were fixed to the container with the rigid flame and then the ground was prepared using dry Toyoura sand by the air-pluviation method. In the behavior of end bearing load, the effect of soil density and embedment length can be clearly seen. The larger the density and embedment depth are, the larger the bearing load is. However, mobilized shaft friction load is much larger for the displacement pile (present study) than the non-displacement pile (Yamana's research), confirming the effectiveness of pile installation procedures in this study for modeling the friction piles.

3.5.2.2 Procedures of vertical loading tests

After the centrifugation reached 50g (Step VI), the vertical loading tests on the piled raft (PR_L2) and the raft (R_L3) were conducted. The schematic illustration of the vertical loading tests is shown in Fig. 3.5.7. The vertical load applied by the actuator was measured by the load cell and settlement of the foundation was measured by the potentiometers. And the forces acting on the model piles were measured by strain gauges.
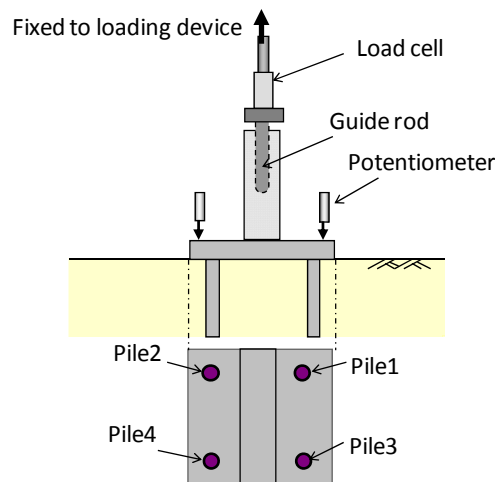
Figure 3.5.7 Schematic illustration of vertical loading tests.

As mentioned in previous section, the raft base was not in contact to the ground in the beginning for PR_L2. From the evaluation of the raft base 3mm above the ground surface the foundation was vertically loaded with the guide rod using a large capacity electric actuator at a rate of 0.16mm/sec until the raft base reached 4mm below the ground surface. This vertical loading period in the second flight was named as the "vertical loading process".

3.5.3 Test procedures for horizontal loading tests

3.5.3.1 Preparation of model foundations for horizontal loading tests

The preparing procedures of the horizontal loading tests were same as those of the vertical loading process from Step I to Step VI, which was explained in Section 3.5.2.1. After Step VI, the vertical load was applied to the foundation by the two-ways actuator with the guide rod securing the verticality of the foundation. For the piled raft the vertical load was applied to the foundation until the raft base touched the ground and the proportion of the vertical load carried by the raft part (RVLP) reached approximately 30%. The vertical load was also applied to the foundation to have 2mm settlement for the pile group case, and the raft foundation was subjected to vertical load of 1500N. This vertical loading stage in the second flight was named as the "vertical loading process".

After the vertical loading, the centrifugation was once stopped to remove the guide rod and to install the laser displacement transducers (LDTs , Fig. 3.4.23) and horizontal loading device (Fig. 3.4.25) as shown in Fig. 3.5.8. The centrifugation was done again up to 50g, and the pre-vertical load was then applied to the piled raft foundation without the guide rod. The reason for applying the pre-load prior to the horizontal loading tests was to confirm that each piled raft case had the same initial RVLPs of about 30%. The vertical load was applied to the pile group and the raft as well in order to give the same loading history as the piled raft. As already explained, the piled raft foundation had RVLP of 30% in the vertical loading process (in the second flight). However, the RVLP became smaller and reached few percent after the centrifugation was once stopped and increased again. Therefore, the pre-vertical load was applied just before the horizontal loading tests to increase and control the initial RVLP. The relationship between the settlement and RVLP was discussed in detail latter (Chapter 4), but one example for this relationship are shown in Fig. 3.5.9. From this figure, it can be said that the RVLP increased with the settlement, and therefore, it also can be confirmed that the RVLP can be controlled by the vertical load. This pre-loading period prior to the horizontal loading tests was named
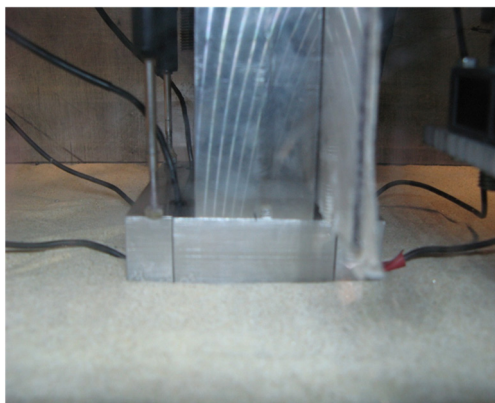
Figure 3.5.8 Model foundation before horizontal loading tests.
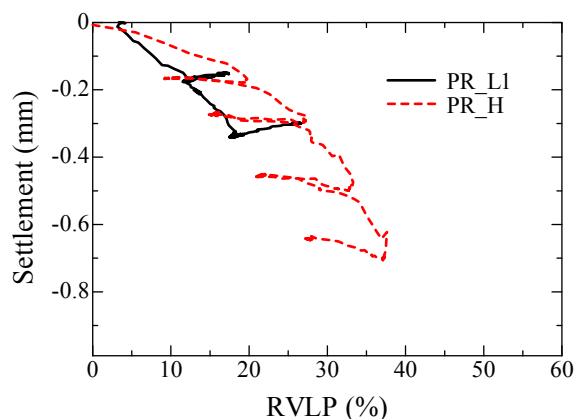
Model 3.5.9 Relationship between RVLP – settlement for PR_L1 and PR_H during pre-vertical loading process.

as "pre-vertical loading process". According to Yamashita (2012), the RVLP significantly affected by pile spacing ratio (s/D), that is, the smaller the pile spacing ratio is, the larger the RVLP is. As summarized in Fig. 2.3.10, RVLP observed in the actual foundation was distributed from 10% to 70% at the pile spacing ratio s/D of five (s/D is 5 in the present study), and therefore the RVLP of 50% was applied to the piled raft in the present study. The initial RVLP for the previous researches are already summarized in Table 2.3.2. In the centrifuge model tests (Mano et al. (2002, 2003); Fujimori et al. (2003); Nishiyama et al. (2003); Horikoshi et al. (2003a, b)), the initial RVLP before the horizontal loading tests was not intended value but the resultant one due to the centrifugation. It seemed that this resultant RVLP was determined by the foundation specifications, pile preparation procedures and ground conditions. Although the RVLP was not intentionally controlled in almost previous researches done in the gravitational field (Nagano et al. (2002); Matsumoto et al. (2004a, b, 2010)), the RVLP was controlled in some researches in 1g environment (Tsuchiya et al. (2003); Nagai and Tsuchiya (2004)). In the research done by Tsuchiya et al. (2003) the RVLP was controlled by pulling out the foundation, and in the research carried by Nagai and Tsuchiya (2004) the RVLP of 50% was prepared by putting the soil bags on the foundation.

3.5.3.2 Procedures of horizontal loading tests

After pre-vertical loading process, the horizontal loading tests were done with a loading rate of 0.155mm/sec. The schematic illustration of horizontal loading tests is shown in Fig. 3.5.10. The horizontal loading tests were controlled by the horizontal displacement measured at lower LDT, δ_{LDT} as shown in Fig. 3.5.11. Horizontal displacement with an amplitude of $\delta_{LDT} = \pm 1$mm was first imposed from the left side and then right side at h/S=1. The same amplitude of δ_{LDT} was applied at h/S=1.8. After the first loading series, the same sequence as that in the first loading series but with $\delta_{LDT} = \pm 2$mm was conducted for the piled raft and pile group foundations. The $\delta_{LDT} = 4$mm was applied at h/S=1 for R_L1 and R_H1, and at h/S=1.8 for R_L2 and R_H2 after the first loading series of $\delta_{LDT} = \pm 1$mm.
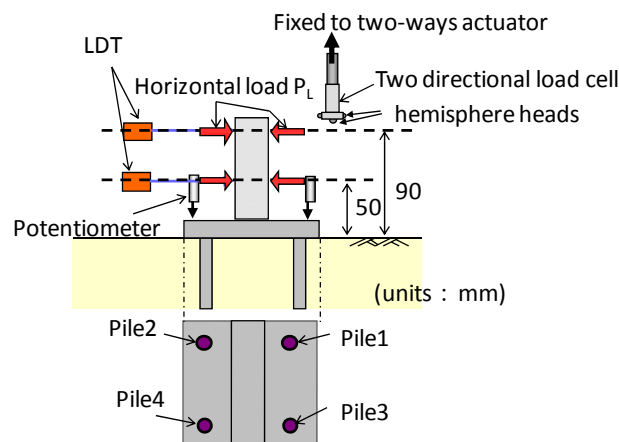
Figure 3.5.10 Schematic illustration of horizontal loading tests.

74
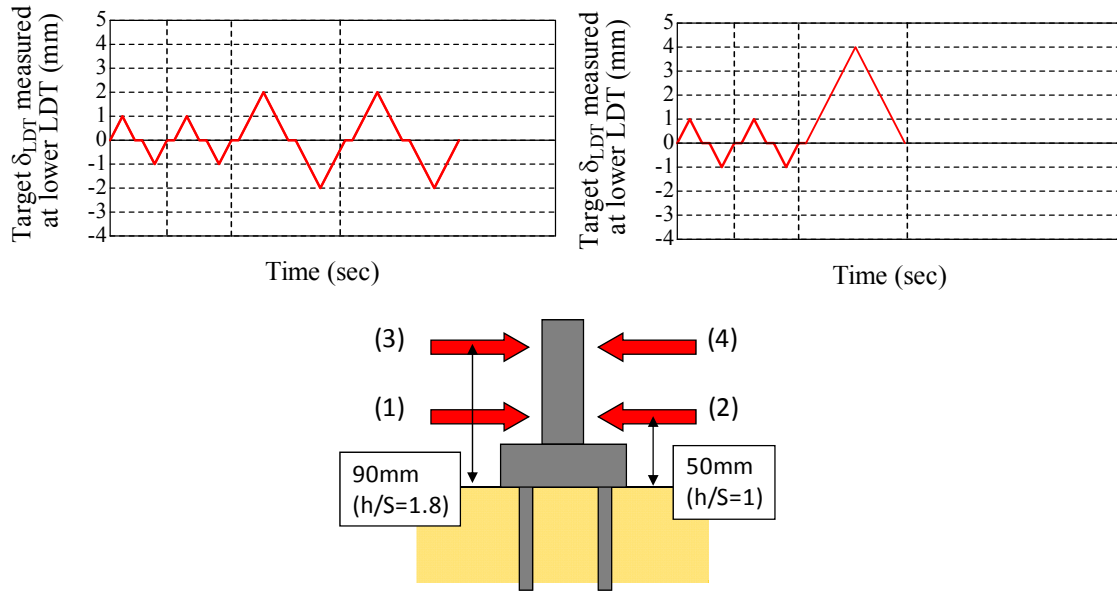
Figure 3.5.11 Applied horizontal displacement at lower LDT, δ_{LDT}, during horizontal loading tests.

Rightward horizontal load and displacement, and clockwise moment are taken positive in the present study.

The instrumentations used for the horizontal loading tests were the load cell, LDTs, potentiometers and strain gauges, by which the values listed in Fig. 3.5.12, were measured or calculated. The vertical load P_V and the horizontal load P_L were measured by the two-directional load cell, where the P_V included the deadweight of the raft and the superstructure. The moment load applied M_L was calculated by multiplying the P_L and the loading height from the raft base h. The settlement of each pile was measured by potentiometer, and the settlement at the center of the raft base s was calculated by the average settlement measured by four potentiometers. The horizontal displacement of the raft base δ and the rotation of the foundation θ were calculated by two LDTs. Forces acting on pile such as axial load, bending moment and shear force were measured by strain gauges (Fig. 3.4.8), and the vertical load and the horizontal load carried by pile part (P_{PV} and P_{PH} respectively) were estimated from the total axial load at pile head Q_{PV} and the total shear force at pile head Q_{PH} respectively. The vertical load carried by the raft part P_{RV} was calculated by subtracting P_{PV} form P_V, and the horizontal load carried by the raft part P_{RH} was estimated by subtracting P_{PH} from P_L. Thus, the shared load between the raft and piles, which were important in the study of the piled raft, were estimated from the measured values by strain gauges (Q_{PV} and Q_{PH}). The same method was also employed to evaluate the shared load in the almost previous literature listed in Chapter 2. Therefore, the accuracy of the strain gauges is crucial for the model tests on the piled raft foundation. The validity of evaluating the shared load between the raft and piles by the strain gauges, and the method which can improve the measurement

P_V: vertical load
P_L: horizontal load
h: horizontal loading height
M_L: moment load=P_L × h
δ_LDT: horizontal displacement measured by lower LDT
s: settlement at the center of raft base
δ: horizontal displacement at the center of raft base
θ: rotation of foundation
Q_PV: total axial load at pile head
Q_PH: total shear force at pile head
P_RV: vertical load carried by raft
P_PV: vertical load carried by piles
P_RH: horizontal load carried by raft
P_PH: horizontal load carried by piles
RVLP: P_RV/P_V
RHLP: P_RH/P_L

Figure 3.5.12 Measured and calculated values.

accuracy of the strain gauges will be discussed in Section 3.6.

3.6 Pile calibration technique and improvement method of strain gauge accuracy

The accuracy of the strain gauges is important for the study of the piled raft as explained in the previous section. This chapter will explain the basic mechanism of the strain gauge, the calibration method used in the present study and will discuss the measurement accuracy of the strain gauge. Moreover, method improving the measurement accuracy of the strain gauge will be proposed.

3.6.1 Theory of strain gauges

The strain gauge used is already shown in Fig. 3.4.8 and Fig. 3.4.10. Gauge (1)-(5) is attached inside the pile by the cross-gauge method, by which the strain can be individually measured at the both sides. Therefore, from the strains measured both sides (defined as ε_1, ε_3) the axial strain (ε_a) and bending strain (ε_m) are estimated by the following equations.

$$\varepsilon_a = \frac{(\varepsilon_1 + \varepsilon_3)}{2}$$
$$\varepsilon_m = \frac{(\varepsilon_1 - \varepsilon_3)}{2}$$

(3.6.1)

Gauge (1)' and (6) were attached by the four-gauge method, and only axial strain was measured by them. Gauge (7) was also attached by the four-gauge method, by which the shear strain was measured. Note that the gauge (1)'were attached outside surface of the pile head only for the heavy case pile.

The principal of strain gauge measurement is to make the bridge circuit consisted of four strain gauges, and to measure the voltage difference Δe (output value) generated by the deformation of the gauge as shown in Fig. 3.6.1. The theoretical relationship between the Δe and strain ε are as bellows.

$$\Delta e = \frac{VK}{4}\left(\varepsilon_1 - \varepsilon_2 + \varepsilon_3 - \varepsilon_4\right) \tag{3.6.2}$$

$$\text{Gauge factor } K: \quad K = \frac{\Delta R / R}{\varepsilon} \tag{3.6.3}$$

V: input voltage, K: gauge factor, ε_n: strain of each gauge, R: resistance of each gauge, ΔR: resistance variation of each gauge.

The gauge factor K is the material dependent value, and that used for the present study is shown in Table 3.4.2. Although the gauge (1)-(5) were cross-gauge, the bridge circuit can be made by introducing two dummy gauges into R_3 and R_4 (Fig. 3.6.1) using the bridge box. It should be noted that the resistance of dummy gauge does not changed.
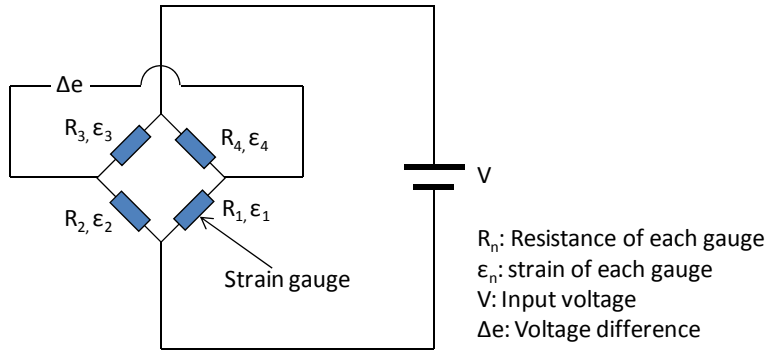
Figure 3.6.1 Bridge circuit for strain gauge.

In particular, the theoretical relationships between output value Δe and strain ε can be obtained by following equations, which are derived from eq. (3.6.2).

$$\text{Cross-gauges (gauge (1)-(5)): } \quad \Delta e = \frac{(1+\nu_p)V}{4} K\varepsilon \tag{3.6.3}$$

$$\text{Four-gauges for axial strain (gauge (1)', (6)): } \quad \Delta e = \frac{(1+\nu_p)V}{2} K\varepsilon \tag{3.6.4}$$

$$\text{Four-gauges for shear strain (gauge (7)): } \quad \Delta e = \frac{VK}{2}\gamma \tag{3.6.5}$$

ν_p is the Poisson's ratio of the pile, γ is shear strain. From above equations the theoretical calibration number C_n can be estimated as follows.

$$\text{Cross-gauges (gauge (1)-(5)): } \quad C_n = \frac{\varepsilon}{\Delta e} = \frac{4}{(1+\nu_p)VK} \tag{3.6.6}$$

$$\text{Four-gauges for axial strain (gauge (1)', (6)): } \quad C_n = \frac{\varepsilon}{\Delta e} = \frac{2}{(1+\nu_p)VK} \tag{3.6.7}$$

$$\text{Four-gauges for shear strain (gauge (7)):} C_n = \frac{\gamma}{\Delta e} = \frac{2}{VK} \qquad (3.6.8)$$

However, actual calibration number is influenced by the cable length, accuracy of gauge attaching and Poisson's ratio, and therefore the pile calibration was carried out in order to get the actual calibration number for each gauge.

3.6.2 Calibration method

Fig. 3.6.2 shows the schematic illustration of the pile calibration. The pile fixed as the cantilever, and the load was applied 20mm from the pile tip. In this calibration method only bending strain and shear strain were applied to the model pile but the axial strain was not applied. Therefore, note that the gauge (1)' and (6), which measure only axial strain, cannot be calibrated by this method. The calibration number was evaluated by comparing the output value and applied bending strain ε and shear strain γ calculated by following equations.

$$\text{Applied bending strain:} \quad \varepsilon = \frac{M}{E_p I_p} y = \frac{Wl}{\frac{\pi}{64}\left(d_1^4 - d_2^4\right)}\frac{d_2}{2} \qquad (3.6.9)$$

$$\text{Applied shear strain:} \quad \gamma = \frac{\tau}{G_p} = \frac{\tau}{\dfrac{E_p}{2\left(1+v_p\right)}} \qquad (3.6.710)$$

M: Applied moment, E_p: Young's modulus of pile, I_p: Moment of inertia, W: Applied load, l: Distance between strain gauge and loading point, d_1: Outer diameter of pile, d_2: Inner diameter of pile, τ: Shear stress, G_p: Shear modulus of pile, v_p: Poisson's ration of pile.
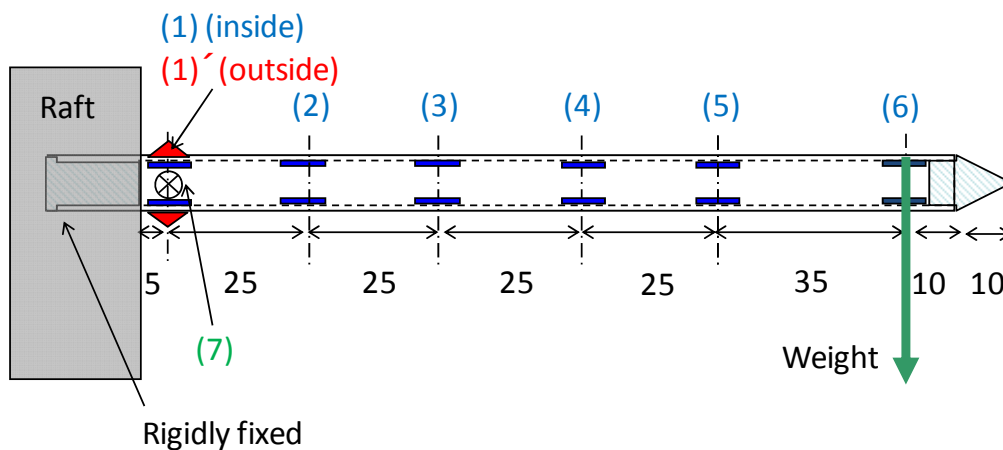
Figure 3.6.2 Calibration method of model pile.

3.6.3 Calibration result

3.6.3.1 Calibration number of each strain gauge

i) Calibration number C_n of gauge (1)-(5)

The relationships between the output value Δe and applied bending strain of Pile 1 and Pile 2 for the light case pile and heavy case pile were described in Fig. 3.6.3 and Fig. 3.6.4 respectively. The calibration results from all piles (Pile1~4) are shown in Appendix (A. 3.6.1, 3.6.2). The theoretical relationship derived from eq. (3.6.3) is also shown in the figure. It can be observed that the Δe had a good linearity with the applied strain, and the calibration number (slop of this relationship) obtained from this calibration method was therefore reliable. It is also found that the calibration number from the pile calibration was 5% larger than theoretical calibration number.

(a) Pile 1   (b) Pile 2
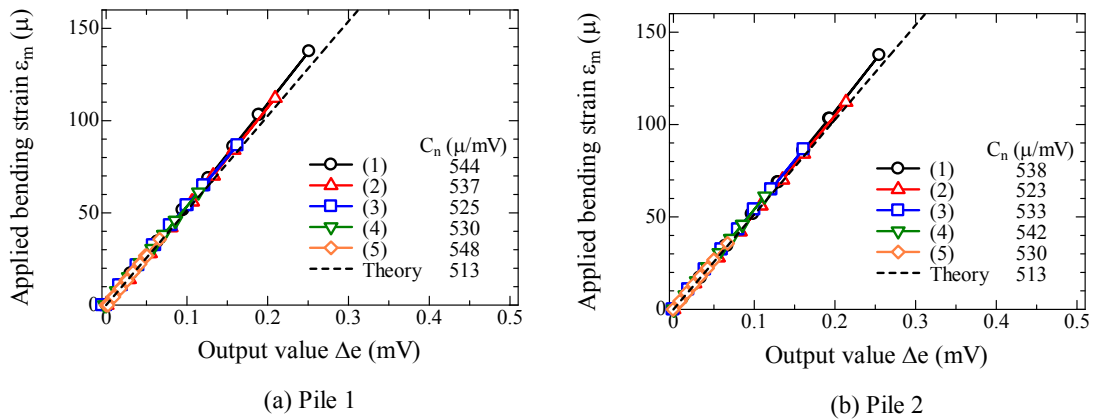
Figure 3.6.3 Relationship between output value and applied bending strain for light case pile.

(a) Pile 1   (b) Pile 2
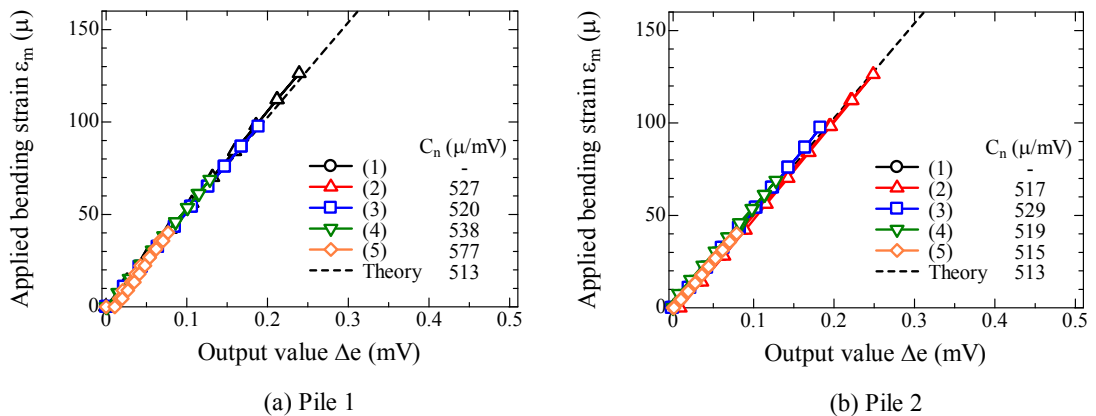
Figure 3.6.4 Relationship between output value and applied bending strain for heavy case pile.

Here, the error of the calibration number caused by the accuracy of the gauge attaching. This error by the gauge attaching can be divided into two components, such as error by the angular declination and the position gap. The error by the angular declination of gauge is firstly discussed. If the gauge is
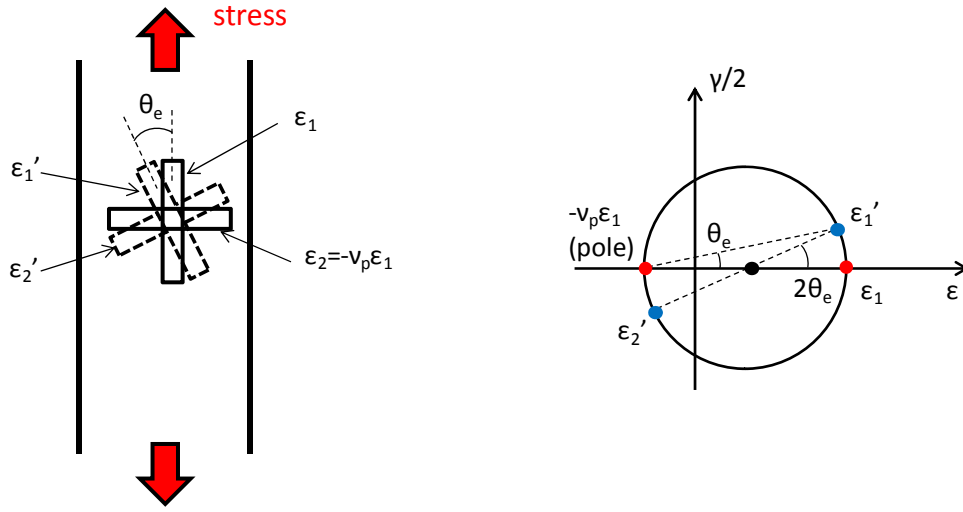
(a) Illustration of angular declination of strain gauges.　　　(b) Mohr circle of strain

Figure 3.6.5 Measurement error of strain gauge by angular declination.

not attached at the different angle of θ_e against the proper angle as shown in Fig. 3.6.5, the strain gauge measure the ε_1' and ε_2' instead of ε_1, $\varepsilon_2=-v_p\varepsilon_1$ which are intrinsically measured. The ε_1' and ε_2' can be estimated from the Mohr's circle for strain shown in Fig. 3.6.5 (b) as follows.

$$\varepsilon_1^{'} = \frac{\varepsilon_1}{2}\left\{\left(1-v_p\right)+\left(1+v_p\right)\cos 2\theta_e\right\}$$
$$\varepsilon_2^{'} = \frac{\varepsilon_1}{2}\left\{\left(1-v_p\right)-\left(1+v_p\right)\cos 2\theta_e\right\}$$

(3.6.11)

By substituting these formulas into the ε_1 and ε_2 in eq. (3.6.2), the following equation is obtained (ε_3 and ε_4 are zero they are dummy gauges).

$$\Delta e = \frac{(1+v_p)V}{4}K\varepsilon_1 \cos 2\theta_e$$

(3.6.12)

The calibration number evaluated from this equation C_n' is as follows.

$$C_n^{'} = \frac{4}{VK(1+v)\cos 2\theta}$$

(3.6.13)

The difference ratio between theoretical C_n (obtained from eq. (3.6.6)) and C_n' are plotted against θ_e in Fig. 3.6.6. The difference ratio increased at an accelerated pace with θ_e.

The error by the position gap is illustrated in Fig. 3.6.7. If the strain gauge is attached at the proper position, the distance between the neutral axis and the strain gauge is $d_2/2$ as shown in the figure. The strain at this position is $\varepsilon_1 = \frac{M}{E_pI_p}\frac{d_2}{2}$ obtained from eq. (3.6.9), and the calibration number is
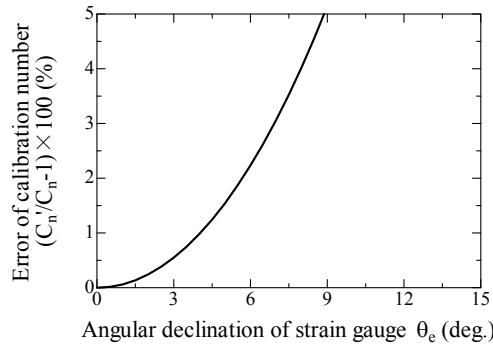
Figure 3.6.6 Error of calibration number caused by angular declination θ_e.

estimated by eq. (3.6.6). However, when the strain gauge is attached at the wrong position with δ_e from the proper position, the distance between the neutral axis and the strain gauge is

$y' = \sqrt{(d_2/2)^2 - \delta_e^2}$. In such case, the strain measured by the strain gauge at the wrong position is

$\varepsilon_1' = \dfrac{M\sqrt{(d_2/2)^2 - \delta_e^3}}{E_p I_p} = \dfrac{\sqrt{(d_2/2)^2 - \delta_e^3}}{d_2/2}\varepsilon_1$. By assigning this ε_1' into eq. (3.6.3), the calibration

number can be obtained as bellows.

$$C_n' = \frac{4}{(1+\nu)VK}\frac{d_2/2}{\sqrt{(d_2/2)^2 - \delta_e^2}} \tag{3.6.14}$$

The difference ratio between theoretical C_n (eq. (3.6.6)) and C_n' are plotted against δ_e in Fig. 3.6.8. The difference increased with δ_e as with the θ_e. If the strain gauge is attached at wrong position with 1.5mm from the proper position, the difference of the calibration number from the theory and the pile calibration is 5%.
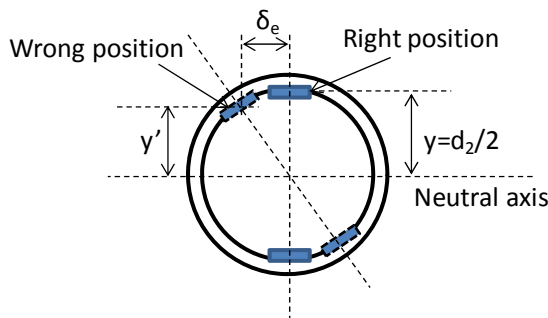
Figure 3.6.7 Measurement error of strain gauge by position gap.
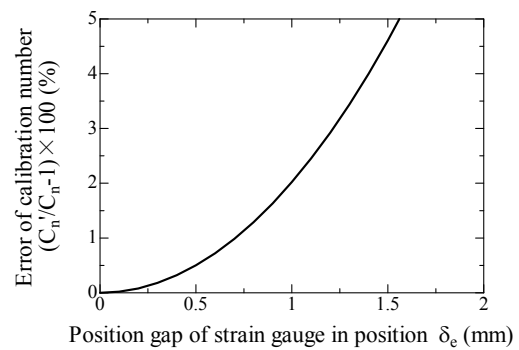
Figure 3.6.8 Error of calibration number caused by position gap δ_e.

It seemed that 5% difference of the calibration number from the theory and the pile calibration caused by the angular declination and the position gap of attaching strain gauge. However, the calibration number can be exactly evaluated by the pile calibration introduced in the present section.

81

ii) Calibration number C_n of gauge (7)

Fig. 3.6.9 shows the relationship output Δe value and shear strain γ observed during the pile calibration. The relationship obtained by eq. (3.6.5) is also shown in the figure. The calibration number estimated by the pile calibration was almost half of that calculated theoretically. This was probably because the shear stress τ was not uniformly distributed in the pile cross-section as shown in Fig. 3.6.10. The shear stress τ profile in the pipe having slight thickness is the function of the distance from the neutral axis as following equation.

$$\tau = 2\frac{Q}{A}\left\{1 - \left(\frac{y}{r}\right)^2\right\} \tag{3.6.15}$$

Q: applied shear force, A: cross-sectional area, r: outer radius of pipe, y: distance from the neutral axis.

	C_n (μ/mV)
Pile 1	151
Pile 2	146
Pile 3	147
Pile 4	140
Theory	325

(a) Light case

	C_n (μ/mV)
Pile 1	224
Pile 2	135
Pile 3	147
Pile 4	195
Theory	325

(b) Heavy case
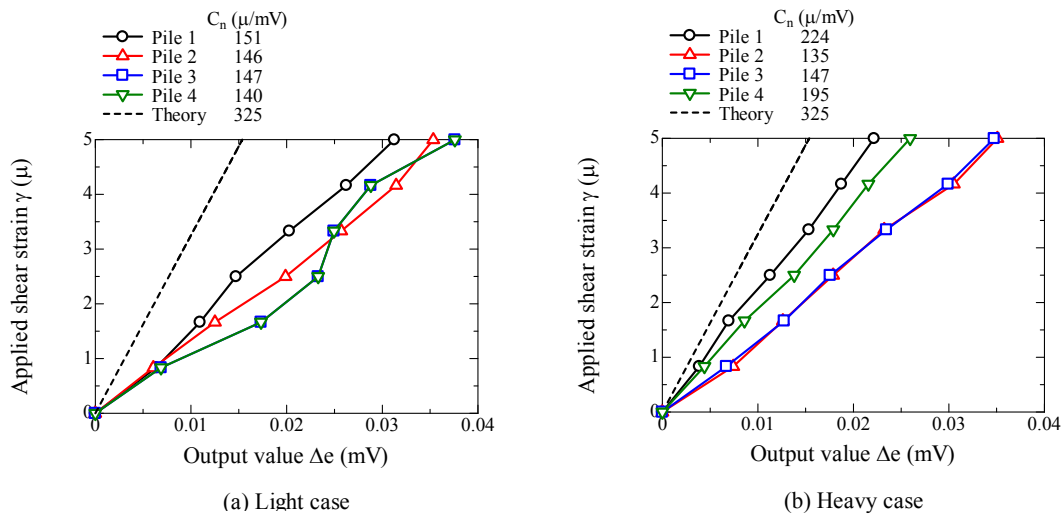
Figure 3.6.9 Relationship between output value and applied shear strain.
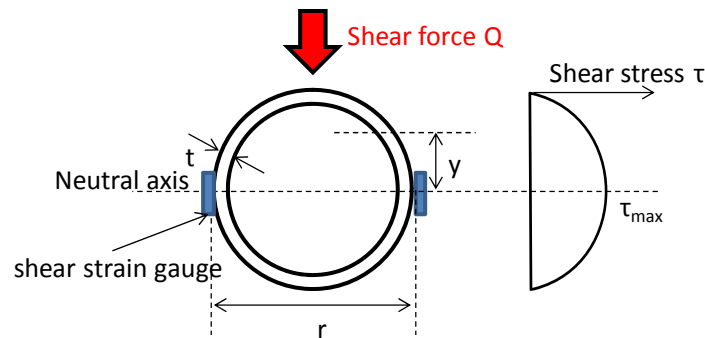
Figure 3.6.10 Distribution of shear stress on pile.

The maximum shear stress, which is twice larger than average shear stress, is observed at $y=0$ where the shear strain gauge was attached. Therefore, the output value detected during the pile calibration
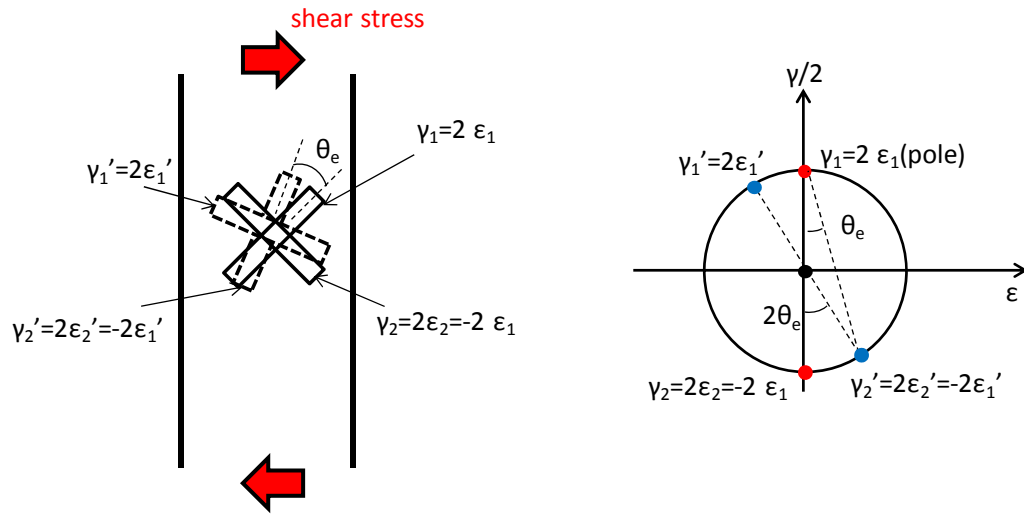
(a) Illustration of angular declination of strain gauge.   (b) Mohr circle of shear strain.

Figure 3.6.11 Measurement error of shear strain gauge caused by angular declination.
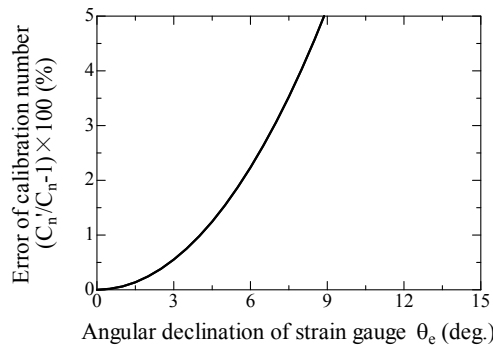
Figure 3.6.12 Error of calibration number caused by angular declination θ_e.

became to be twice, and the calibration number evaluated from the calibration was half of the theoretical one.

The relationship between the shear strain and the output value shows worse linearity than that observed in the relationship between the bending strain and output value (Fig. 3.6.3, Fig. 3.6.4). This could be mainly attributed by two reasons. One is the applied shear strain was much less than the applied bending strain. As a result, the measurement error was relatively dominant for the shear strain compared with the bending strain. The other reason is difficulty in attaching shear strain gauge at the proper position of small model pile. If the shear strain gauge is not attached at the right position and has an angular declination of θ_e as shown in Fig. 3.6.11 (a), the shear strain measured is not γ_1 and γ_2 but γ_1' and γ_2'. The γ_1' and γ_2' can be calculated by the Mohr's circle for strain (Fig. 3.6.11 (b)) as follows.

$$\gamma_1' = 2\varepsilon_1' = \gamma_1 \cos 2\theta_e$$
$$\gamma_2' = 2\varepsilon_2' = -\gamma_1 \cos 2\theta_e$$

(3.6.16)

If the same strains are occurred at the shear strain gauge at the opposite side ($\varepsilon_1'=\varepsilon_3'$ and $\varepsilon_2'=\varepsilon_4'$), the following calibration number C_n' is estimated from eq. (3.6.2) and eq. (3.6.16).

$$C_n' = \frac{2}{VK \cos 2\theta}$$
(3.6.14)

The difference ration between C_n' and theoretical C_n (eq. (3.6.8)) are plotted against θ_e in Fig. 3.6.12. Although the shear strain gauge was attached at the outside of the pile, it was difficult to attach the gauge at the proper position because the shear strain gauge was attached with the inclination of 45 degree against the pile shaft direction. Therefore, the variability of calibration number at each gauge became larger as shown in Fig. 3.6.9.

iii) Calibration number C_n of gauge (1)' and (6)

The gauge (1)' and (6) measured only axial strain, and the calibration number cannot be therefore obtained the calibration method introduced above. It was confirmed form the above discussion that there was only 5% difference between the calibration number obtained by the pile calibration and the theoretical one for the gauge (1)-(5) attached inside the pile. Therefore, the calibration number of gauge (6) was estimated by multiplying 1.05 with the theoretical calibration number (eq. (3.6.7)) by assuming that the calibration number of gauge (6) attached inside also included 5% error against the theory. This 5% difference between the calibration number calculated by the calibration and theory was mainly derived from the accuracy of pile attaching as mentioned in the previous section. From this fact, it could be said that the difference became smaller for the gauge attached outside of the pile than that inside the pile. Therefore, the theoretical calibration number was employed for that of the gauge (1)' attached outside.

The calibration numbers evaluated in this section are summarized in Appendix (A.3 and A.4).

3.6.3.2 Interference strain and proposal of method to remove it

This section will focus on the axial strain observed in the pile calibration. Figure 3.6.13 and 3.6.14 show the relationship between the applied bending strain and detected axial strain. Only for light case Pile 1 (Fig. 3.6.13 (a)), relatively large bending strain was applied. In the pile calibration only bending and shear strains are applied to the model pile implying no axial strain acting on pile. However, the axial strain was measured as described in these figure showing the axial strain included the error when the bending moment is given to the pile. This axial strain caused by the bending moment is defined as "interference strain".

It was thought to be that this interference strain was mainly caused by attaching strain gauges at incorrect positions as shown in Fig. 3.6.5, 3.6.7. The larger interference strain was observed for the

(a) Pile 1 (light case)

(b) Pile 2 (light case)

(c) Pile 3 (light case)

(d) Pile 4 (light case)
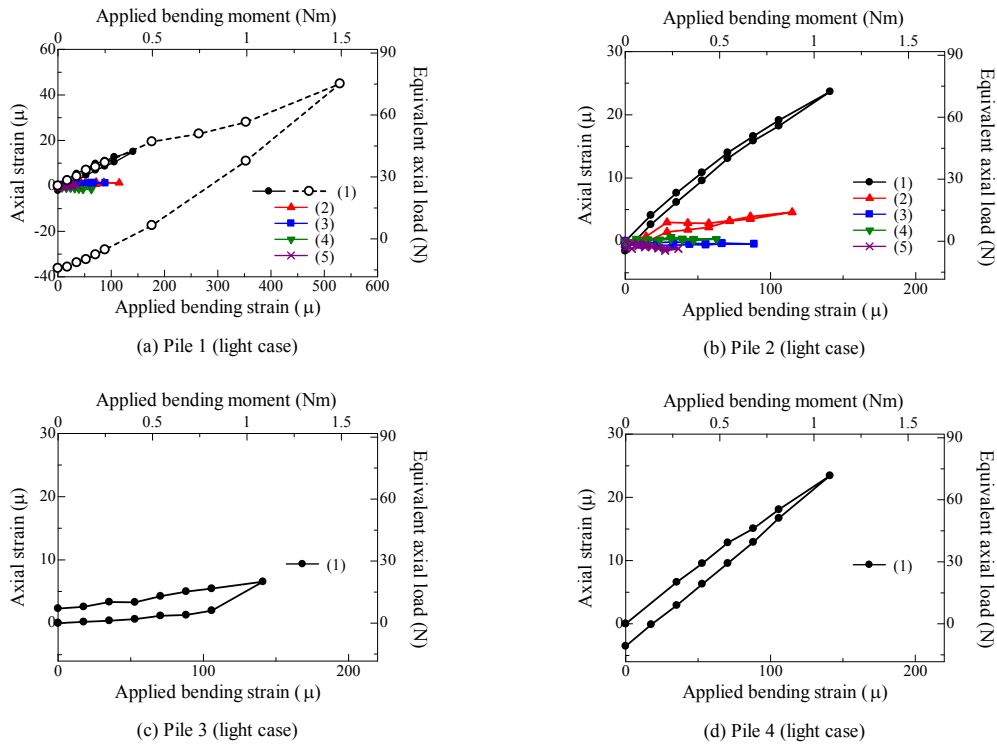
Figure 3.6.13 Relationship between applied bending strain and axial strain for light case pile during calibration

(a) Pile 1 (heavy case)

(b) Pile 2 (heavy case)

(c) Pile 3 (heavy case)

(d) Pile 4 (heavy case)
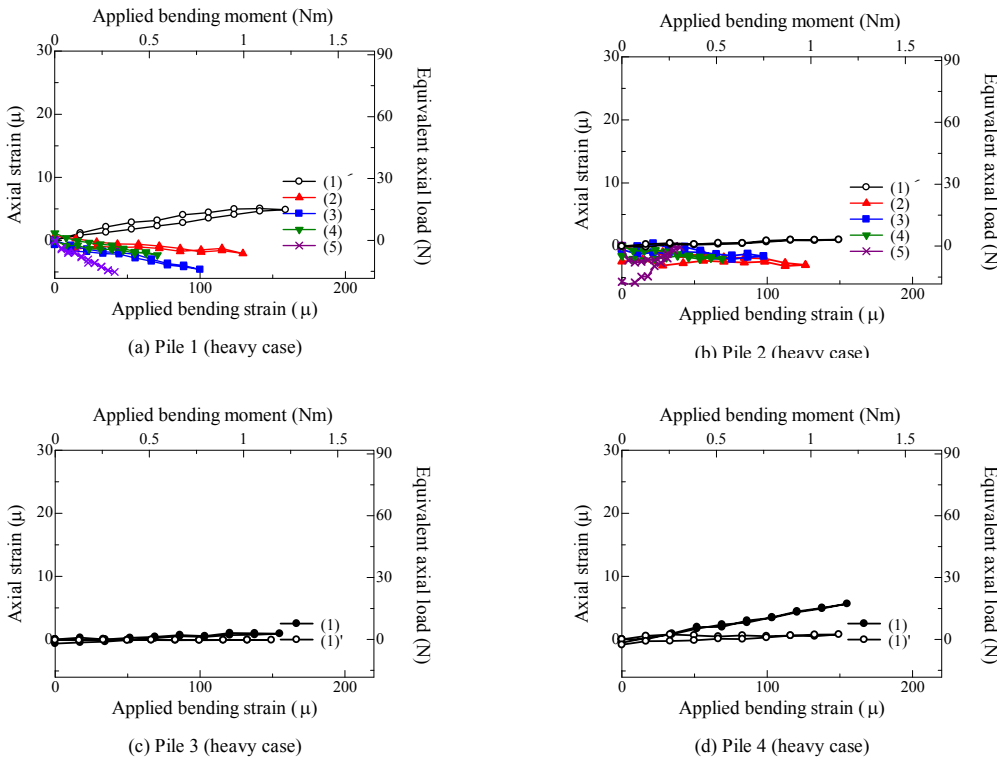
Figure 3.6.14 Relationship between applied bending strain and axial strain for heavy case pile during calibration

85

gauge at pile head than other gauges, especially for the light case pile. For the strain gauges at the pile head clutched part by the raft also generated the interference strain. However, this interference strain can be corrected using following method. The gauge (1)' in the heavy case pile can restrain the interference strain compared with the gauge (1) in the light case pile. Furthermore, comparing the interference strain observed in Pile 3 and Pile 4 for heavy case (Fig. 3.6.14 (c) and (d)) it can be clearly seen that the interference strain was larger for strain gauge attached at inside than outside strain gauge. It would be considered that the interference strain depended on the gauge attaching accuracy resulting in smaller interference strain for gauge (1)' attached outside of pile. Thus, the axial strain may have an error (interference strain) caused by the bending moment. However, the interference strain had almost linear relationship with the bending strain as shown in Fig. 3.6.13 and 3.6.14. From this fact it can be said that the axial strain can be corrected by removing the interference strain using this linear relationship. However, when the relatively large bending strain was acting on pile, the interference strain did not be back to the original strain (Fig. 3.6.13 (a)), showing the hysteresis in the bending strain and the interference strain relationship. This fact implies that the interference strain cannot be modified using the above linear relationship if the relatively large bending strain is applied to the model pile. This hysteresis made the error in measured axial load larger when the horizontal loading tests as shown latter (Fig. 3.6.16).

(a) PR_L1

(b)PR_H
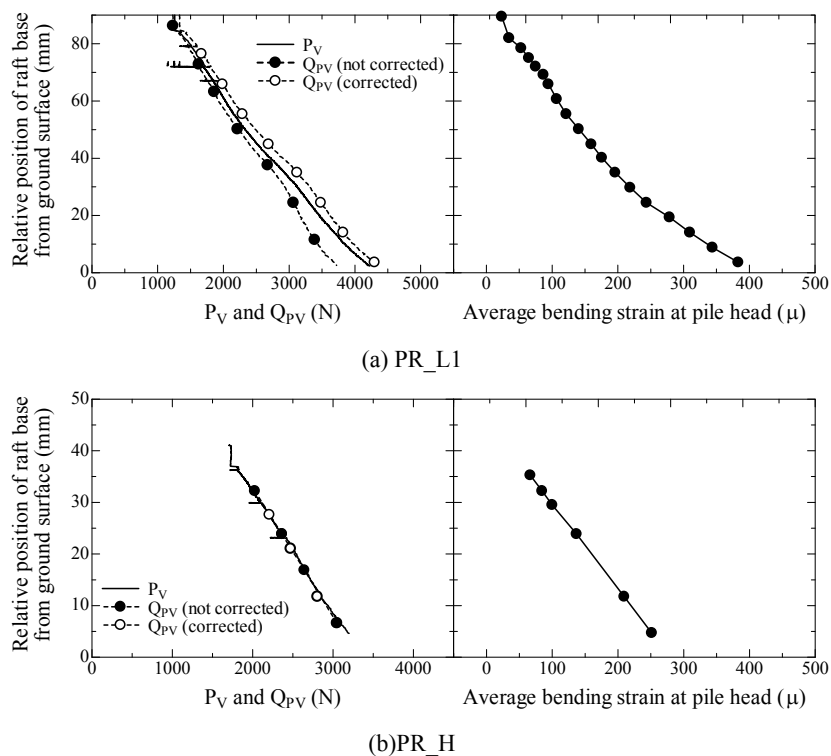
Figure 3.6.15 Variation of PV, QPV and bending strain at pile head with settlement for PR_L1 and P_H during penetration process.

86

3.6.4 Validation and limitation of strain gauge accuracy

This section will verify the accuracy of calibration number obtained in the previous section. In addition to this, it will be also verified the proposed method which can improve the measurement accuracy of the strain gauges by removing the interference strain. Figs. 3.6.15 show the variation of the vertical load P_V, the total axial load at pile head Q_{PV} and the average bending strain at the pile head with the settlement s for PR_L1 and PR_H observed in the penetration process. As been seen, the bending strain acting on the pile during the penetration process, which was probably due to the slight inclination of the foundation. The results obtained from other cases are shown in Appendix (A. 3.6.5~3.6.9) in which not only the total pile response but also the each pile response are also shown. Corrected Q_{PV} considering the interference strain by the moment strain is also shown in these figures. The axial load at pile head with and without correction, and bending strain at pile head for each pile are also shown in the figure. Axial load without correction for the light case indicated about 10% difference from Q_{PV}, whereas that for the heavy case had a good agreement with P_V due to smaller interference strain for the heavy case pile as explained in Fig. 3.6.13 and 3.6.14. Although applied bending strain in the calibration was about 150μ, that observed in the penetration process was approximately 400μ (in max., 700μ bending strain was observed in Pile 1of PR_L1, see A.3.6.5 (b)) at a maximum and 300μ at an average. However, the difference of P_V and Q_{PV} can be significantly reduced by correcting the interference strain, and the Q_{PV} had a good agreement with P_V. This fact justified the correction method removing the interference strain even when relatively large bending moment was applied to the pile. Therefore, the vertical load carried by the piles P_{PV} can be estimated from the corrected axial load at the pile head (corrected Q_{PV}) with reasonable accuracy, and the vertical load carried by the raft P_{RV} can also be estimated by subtracting corrected Q_{PV} (P_V) from P_V.

The time histories of the total axial load at pile head and the average bending strain at pile head for P_L and P_H observed in the horizontal loading tests are shown in Fig. 3.6.16. The corrected axial load is also shown in the figures. The observed these pile response for each pile is shown in Appendix (A. 3.6.10, 3.6.11). In the horizontal loading tests constant vertical loads were applied to the piles form the superstructure for the pile group models, i.e., 1260N and 172 0N for the light case and the heavy case respectively, which are indicated as dotted horizontal line in the figures. Note that the vertical load of the foundation was estimated with the consideration about centrifuge acceleration distribution along the centrifuge radius as explained in Fig. 3.4.2. However, the measured Q_{PV} varied during the loading and the gap between the vertical load of superstructure and Q_{PV} was observed. The gap between them can be reduced by the correction, however, it should be noted that corrected axial load still have a difference of 10%, implying that measured P_{PV} and P_{RV} might have an uncertainty in the magnitude during the horizontal loading tests. This error in the measured axial load was probably owing to the hysteresis of the bending strain and the interference strain relation as
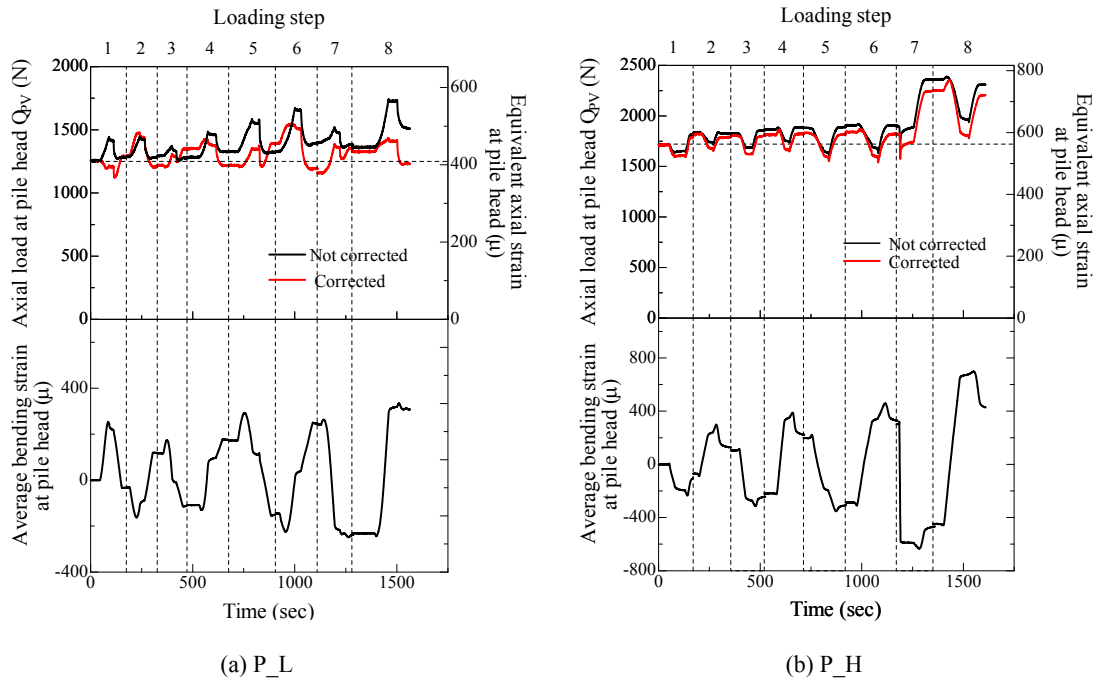
Figure 3.6.16 Variation of axial load and bending strain at pile head with time for P_L and P_H during horizontal loading tests.

shown in Fig. 3.6.13 (a). Relatively large bending strain for the positive and negative direction was alternately acting on the pile during the horizontal loading tests as shown in Fig. 3.6.16. The interference strain gradually accumulated with the alternate loading procedures, which made the error of axial load measurement large during the horizontal loading tests. Further discussion is required to improve the axial load measurement.

Only influence of bending strain on the axial strain was discussed as above but it seemed that the interference bending strain is also occurred by the axial strain. Here, the maximum average axial and bending strains observed during the penetration process and horizontal loading tests are summarized in Table 9. The interference axial strain was generated up to 10% of applied bending strain as described in Fig. 3.6.12 and 3.6.13. Assuming 10% of axial strain is also included in the bending strain as the interference bending strain, the each interference strain observed in the penetration process and horizontal loading tests can be calculated as shown in Table 9. The calculated ratio of interference strain to maximum average axial and bending strains during the penetration process were 13% and 7.5%, implying that the bending strain also had an uncertainty of 7.5%. However, it was not required to make consideration of the interference bending strain because the bending strain during the penetration process was not important value. The ratio of interference strain to maximum average axial strain and bending strain during the horizontal loading test were 30% and 5% respectively. Thus, although the influence of interference strain on the axial strain was significant, that on the bending

88

strain was slight and negligible. Therefore in the present research only interference axial strain caused by the bending strain was corrected.

Next the measurement accuracy of the shear strain gauge is explained. Fig. 3.6.17 shows the variation of the horizontal load P_L and the total shear force at the pile head Q_{PH} with the horizontal displacement of the raft base δ for the piled raft and the pile group with the loading cycle of $h/S=1$ and $\delta_{LDT}=\pm2$mm. The P_L and Q_{PH} were measured by the two-directional load cell and the shear strain gauge (gauge (7)) respectively. The horizontal load P_L was supported by only piles for the pile group foundation. The Q_{PH} had a good agreement with the P_L for the pile group, which means that the high accuracy of the shear strain gauge can be confirmed. Therefore, it can be said that the horizontal load carried by the pile part P_{PH} can be evaluated from the total shear force at pile head Q_{PH} and the difference between P_L and Q_{PH} can be regarded as the horizontal load carried by the raft part P_{RH} for the piled raft foundation.

(a) Light case (PR_L1 and PR_L)   (b) Heavy case (PR_H and P_H)
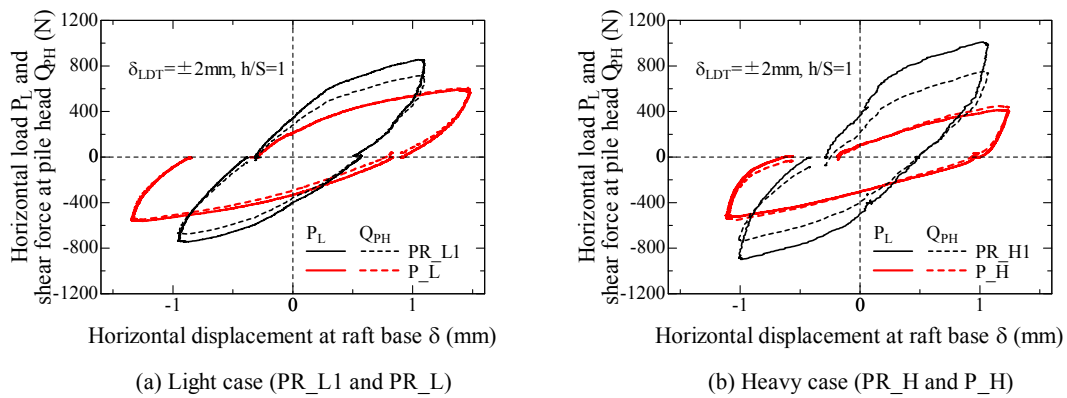
Figure 3.6.17 Variation of P_L and Q_{PH} with δ for $\delta_{LDT}=\pm2$mm, $h/S=1$.

3.7 Summary

This chapter explained the basic principal of centrifuge and d information of centrifuge model test carried by the present study, and also proposed the modeling technique on the piled raft. In particular, the measurement accuracy of the strain gauge was carefully discussed because shared loads between the raft and the piles are generally estimated by the strain gauge. Followings are the basic findings and the modeling technique proposed in this chapter.

In almost previous research the piled raft foundation was prepared using the "non-displacement pile" method in which the piles were rigidly fixed to the container and the sand was poured into the container. However, in the present study the model piles were installed as the "displacement pile", that is, the level model ground was firstly made, and the piles were penetrated into the ground in the

centrifugation. Preparing the model foundation by this method, the uniform contact condition between the raft base and the ground surface can be made, and relatively large shaft friction can be secured compared with the piled raft with the "non-displacement pile" method. The concept of the piled raft is to reduce the settlement using a few friction piles. Therefore, the piled raft foundation installed as "displacement pile" introduced in the present thesis can model the actual piled raft concept accurately.

It was found that the proportion of the vertical load carried by the raft (RVLP) increased with the piled raft settlement. The initial RVLP before the horizontal loading tests was controlled by applying the pre-load to the foundation.

The pile calibration technique was proposed, by which the forces acting on the pile can be evaluated accurately. However, it was found that the axial strain measured by the gauge included the error due to the interference strain when the pile was subjected to bending moment. The method to improve the measurement accuracy of strain gauge was proposed. That is, the axial strain was corrected by removing the interference strain using the relationship between the bending strain and interference strain observed in the pile calibration. It was also confirmed that the validity of the calibration number obtained by the present calibration method and the effectiveness of correction method. This implied that he shared load between the raft and piles can be evaluated with high accuracy.

VERTICAL RESPONSE OF THE PILED RAFT

4. Vertical response of the piled raft

4.1 Introduction

In this chapter, the vertical response of the piled raft foundation will be examined. The piled raft foundation was experienced three vertical loading processes such as the penetration process, the vertical loading process and the pre-vertical loading process before the horizontal loading tests. Beside the discussion about the vertical response of the piled raft foundation, main objectives of the present chapter is to verify the initial conditions of the piled raft foundation before the horizontal loading tests.

4.2 Penetration process

In the present centrifuge model tests, the foundation was mainly penetrated into the ground during the penetration process in the first flight. In this section, the behavior of each foundation observed in the penetration process will be examined. Much focus will be focused on the foundation conditions prepared as the displacement pile.

4.2.1 Influence of penetration depth in the flight on pile response

4.2.1.1 Overall response of pile penetrated in centrifugation

Figure 4.2.1.1 show the variation of the vertical load P_V, total axial load at pile head P_{PV} with the relative position of raft base from ground surface for PR_L1 and PR_H. The y-axis of zero represents the ground surface. The P_V was measured by the load cell and P_{PV} was measured by the strain gauges at the pile heads. The P_{PV} in these figures were axial load, which was corrected by the method proposed in Chapter 3. The results observed in other cases are shown in Appendix (A. 4.2.1.1, 4.2.1.2). As explained in the previous chapter, the accuracy of the corrected axial load can be confirmed from these figures. As been seen, the piles were penetrated into the ground until the raft base reached approximately 10mm above the ground surface in the penetration process. As a

(a) PR_L1   (b) PR_H
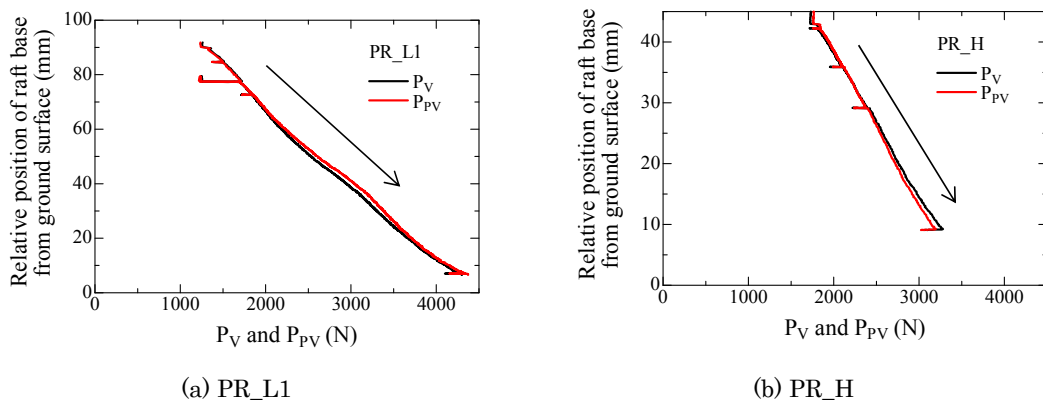
Figure 4.2.1.1 Variation of PV, PPV with relative position of raft base from ground surface during penetration process for (a) PR_L1 and (b) PR_H. (Other cases are shown in A. 4.2.1.1 and 4.2.1.2)
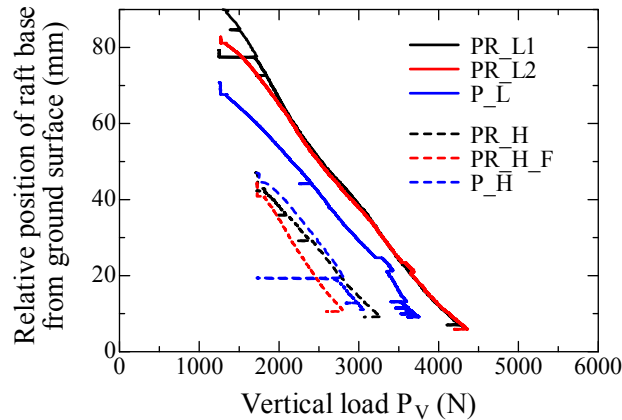
Figure 4.2.1.2 Variation of PV with relative position of raft base from ground surface observed in the penetration process for all cases.

result, the penetration depth in the flight was 70mm and 40mm for the light case and the heavy case respectively.

Figure 4.2.1.2 shows the relationship between the vertical load P_V and the relative position of raft base from ground surface. From this figure, it can be said that the vertical load was smaller for the heavy case with smaller penetration depth in the flight than the light case. And for the P_L with relatively small penetration depth under the centrifugation also showed smaller vertical load compared with other light case. This was probably owing to the different pile preparation procedures, that is, the difference of the penetration depth in the 1g field and the centrifugation.

The vertical load can be divided into two parts such as the end bearing load and shaft friction load. Figure 4.2.1.3 shows the variation of the end bearing load and the shaft friction load with the relative position of raft base from ground surface. If the piles were prepared as the non-displacement pile, the mobilized shaft friction load is quite smaller than the piles prepared as the displacement pile as shown in the Fig. 3.5.6. However, the shaft friction load was almost same between the light case and the heavy case regardless the different penetration depth in the flight. Therefore, it can be said that the piles penetrated into the ground about 40mm under the centrifugation can be regarded as the displacement pile.

On the other hand, the mobilized end bearing load was significantly affected by the penetration depth in the flight, that is, the longer the penetration depth in the flight was, the larger end bearing load was. From this fact, it can be confirmed the difference of the

(a) End bearing load   (b) Shaft friction load
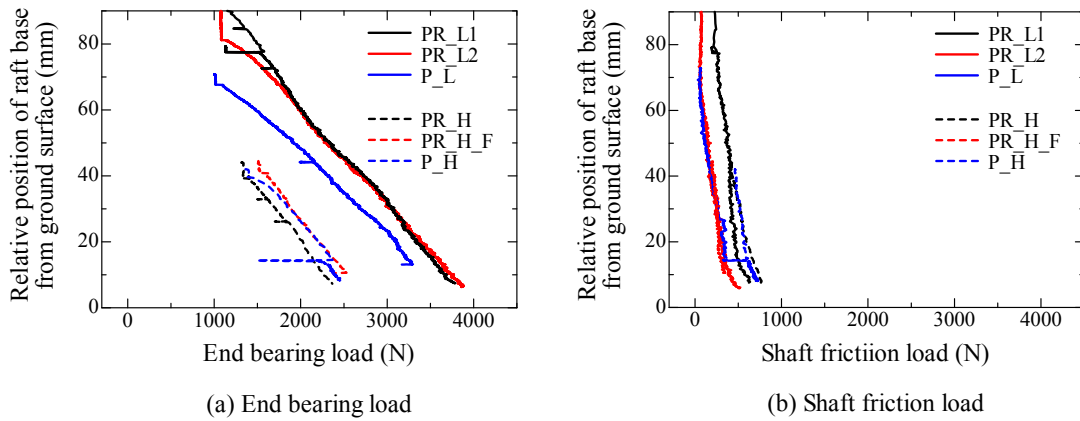
Figure 4.2.1.3 Relationship between pile force and relative position of raft base from ground surface during penetration process for all cases.

vertical load between the light case and the heavy case was mainly attributed the difference of the end bearing load. This difference of end bearing load difference may affect the performance of foundation during the horizontal loading tests. In order to mitigate this difference, the pre-vertical load was applied to the foundation prior to the horizontal loading test, and the almost same end bearing loads were mobilized for all cases before the horizontal loading tests as shown in latter Fig. 4.4.2.3. This end bearing load can be treated as a kind of cone resistance. Compared with the end bearing loads for cases having almost same penetration depth in the flight, the end bearing loads were almost same, confirming the good repeatability, except for P_L. The soil condition in P_L might be slightly weak compared with PR_L1 and PR_L2.
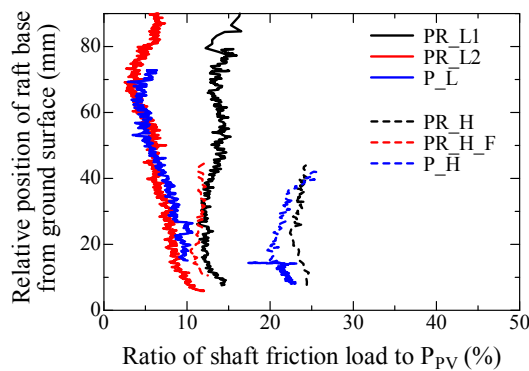
Figure 4.2.1.4 Ratio of shaft friction load to vertical load carried by piles PPV during penetration process for all cases.

Figure 4.2.1.4 shows the variation of the proportion of the shaft friction load against the vertical load of the pile part P_{PV} with the relative position of raft base from ground

surface during the penetration process. The proportion was scattered little bit, but it showed 10%-25%. The proportion was slightly larger for the heavy case than the light case. Although there was no difference between the shaft friction load between the light case and the heavy case, the end bearing load was larger for the light case than the heavy case as shown in Fig. 4.2.1.3. As a result, the proportion of the shaft friction load was larger for the heavy case. As been seen, the shaft friction load was still smaller than the end bearing load, the larger shaft friction load was mobilized by penetrating piles in the flight as explained in Fig. 3.5.6. Furthermore, the larger shaft friction was further enhanced by the base pressure for the piled raft foundation as discussed latter. Therefore, the combining effect of the pile penetration in the flight and the raft base pressure create the key conditions in the piled raft having larger shaft friction load.
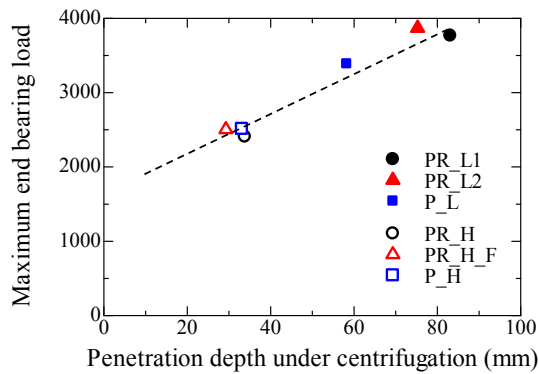
Figure 4.2.1.5 Relationship between penetration depth in the flight and maximum end bearing load.
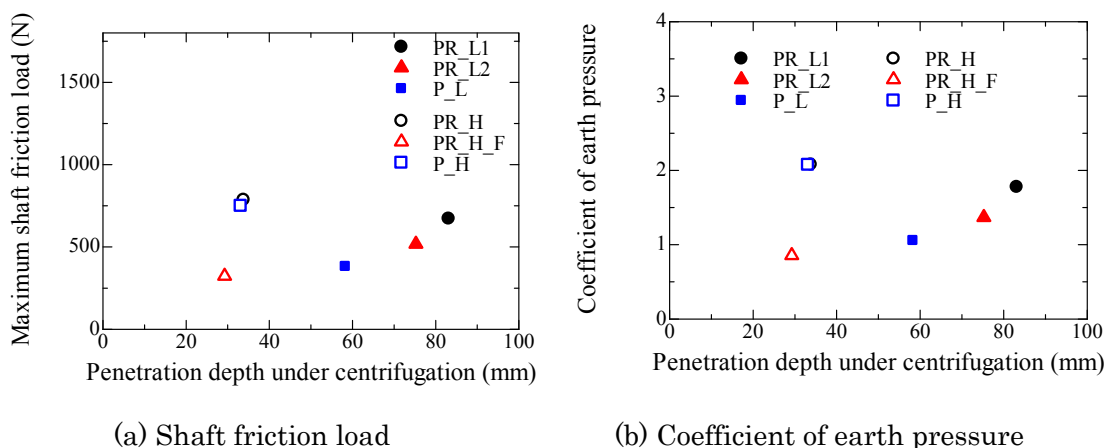
(a) Shaft friction load   (b) Coefficient of earth pressure

Figure 4.2.1.6 Relationship between penetration depth in the flight and (a) shaft friction load and (b) coefficient of earth pressure during penetration process.

Figure 4.2.1.5 and 4.2.1.6 shows variation of maximum end bearing load, maximum

shaft friction load and coefficient of earth pressure observed in the penetration process with penetration depth under the centrifugation. The coefficient of earth pressure was estimated from the shaft friction load using interface friction angle between the pile and the soil, which is 0.33.. From the variation of the maximum end bearing load, there was linear relationship between the end bearing load and the penetration depth in the flight. On the other hand, it seemed that the shaft friction load had no correlation with the penetration depth. The coefficient of earth pressure estimated from the shaft friction load also scattered with the penetration depth. Comparing the coefficient of earth pressure at rest (K_0=0.4), the average coefficient of earth pressure was approximately 1.5, which was 3.8 times higher than that at rest. According to Meyehof (1976) and Sherif et al. (1995), the coefficient earth pressure mobilized in the driven pile was four times larger than the coefficient of earth pressure at rest. Therefore, it seemed that the present results had a good agreement with their research. From these figures it can be said that the mobilization of pile load was different between the light case and the heavy case owing to the different penetration depth in the flight, especially for the end bearing load. In order to mitigate the different pile load mobilization caused by the model preparation process, the pre-vertical loads were applied to all foundations prior to the horizontal loading tests, and reduce this difference. This will be discussed in Section 4.4.
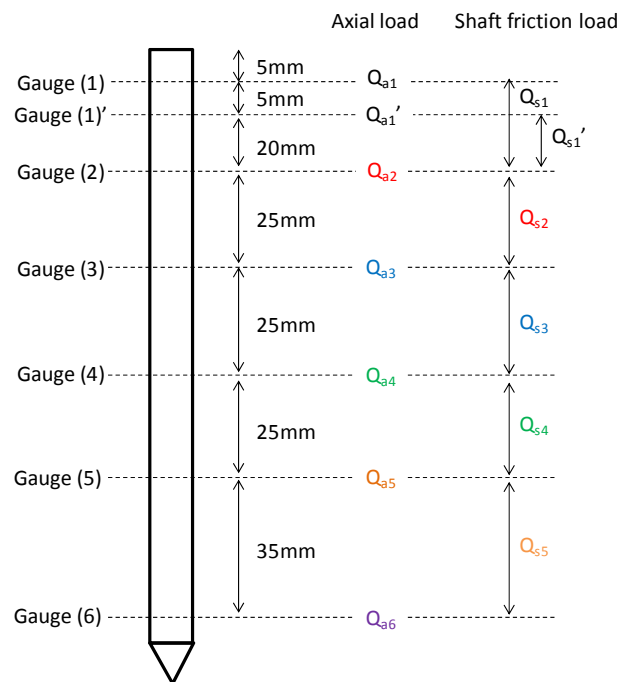
Figure 4.2.1.7 Definition of axial load and shaft friction load acting on ple.

(a) PR_L1   (b) PR_H
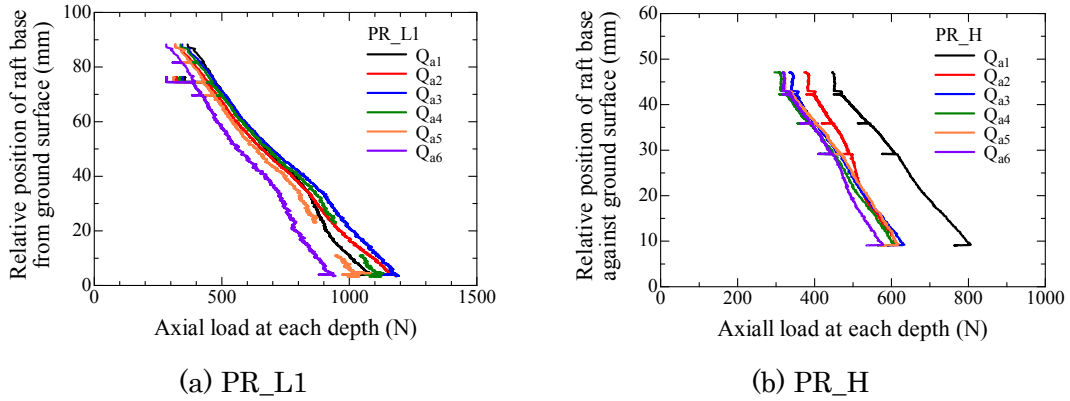
Figure 4.2.1.7 Variation of axial load at each depth with relative position of raft base from ground surface for PR_L1 and PR_H during penetration process.

(a) PR_L1   (b) PR_H
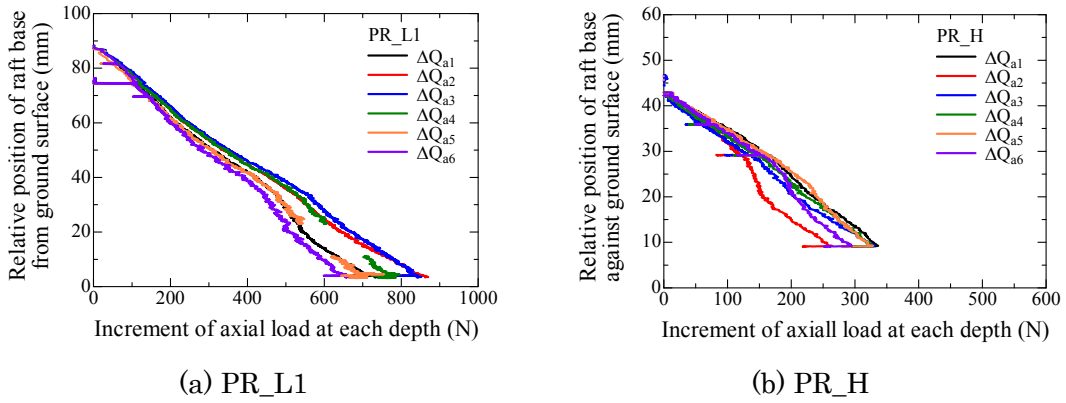
Figure 4.2.1.8 Variation of axial load increment at each depth with relative position of raft base from ground surface for PR_L1 and PR_H during penetration process. (A. 4.2.1.3-4.2.1.8)

4.2.1.2 Axial loads along pile shaft

The axial load measured at several depths will be examined in the present section. The axial load at each depth measured by stain gauges Q_{an} were defined as Fig. 4.2.1.6. The shaft friction loads at depths were calculated using Q_{an} as follows

$$Q_{sn} = Q_{an} - Q_{an+1} \qquad (4.2.1.1)$$

Figure 4.2.1.7 show the relationship between Q_{an} and the settlement s for PR_L1 and PR_H. Q_{an} in the figure was shown as the average of Pile 1 and Pile 2. The increment of axial load $\varDelta Q_{an}$, which was the increment of Q_{an} from the beginning of loading, is shown in Fig. 4.2.1.8. The variation of axial load for other cases, and that of Pile 1 and Pile 2 are shown in Appendix (A. 4.2.1.3-4.2.1.8). The axial load Q_{a6} (end bearing load) was smaller than the axial load at other depth for all cases because the positive shaft friction

96

load was mobilized along the pile. The shaft friction load will be examined latter. There was no clear trend in the axial load measured at other depths, and this trend can be seen in the increment of axial load for light case. On the other hand, the significantly large axial load was mobilized for heavy case, owing to the large shaft friction load at the pile head as discussed latter section. This fact indicated that the ground condition at the shallower part might be different between the light case and the heavy case. The The ΔQ_{an} observed in heavy case was distributed in the narrow wide compared with Q_{an}. This means that the larger axial load at pile head was mobilized during increasing the centrifugation.

(a) PR_L1   (b) PR_H
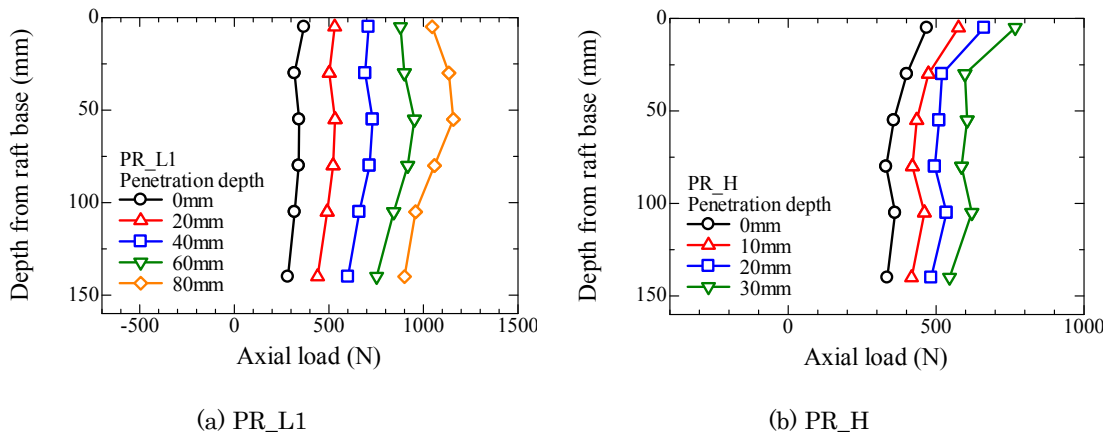
Figure 4.2.1.9 Profiles of axial load for PR_L1 and PR_H during penetration process.

(a) PR_L1   (b) PR_H
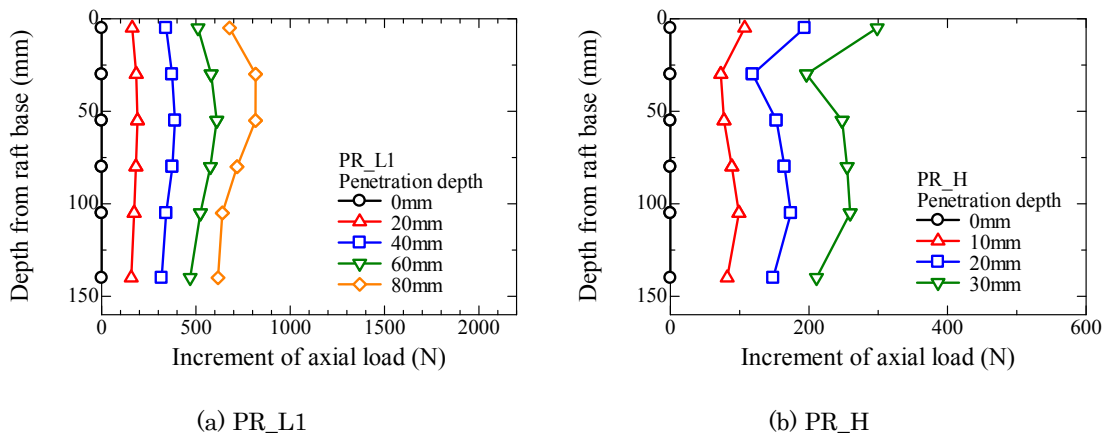
Figure 4.2.1.10 Profiles of axial load increment for PR_L1 and PR_H during penetration process.
(A. 4.2.1.9-4.2.1.14)

Figure 4.2.1.9 show the axial load profile for PR_L1 and P_H. The axial load was in the figure is average value of Pile 1 and Pile 2. The profiles of axial load increments for

same cases are shown in Fig. 4.2.1.10. Result from other cases and each pile response such as Pile 1 and Pile 2 are shown in Appendix (A. 4.2.1.9-4.2.1.14). For the PR_L1, the axial load decreased with the depth at deep ground, but it was almost constant or slight increase with depth at shallower depth. This was probably because the large positive shaft friction load was mobilized at the deep part due to high ground stress, and by contrast, the shaft friction load at shallow depth was small. The shallower ground was subjected to relatively large shear during the penetration in the flight as shown in Fig. 4.2.1.11. The shaft friction load reached at peak and gradually decreased when the ground was sheared, and therefore, the shaft friction near the ground surface showed smaller shaft friction load, which led that the axial load increased with the depth as shown in Fig. 4.2.1.7-4.2.1.8.
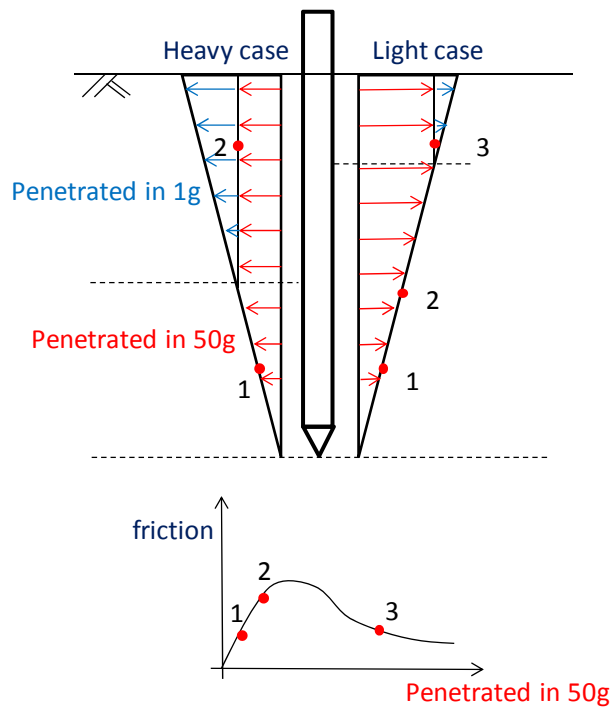
Figure 4.2.1.11 Pile penetration length along soil depth.

The axial load at the deep part decreased with the ground depth for both light and heavy case due to the positive shaft friction load. The axial load near the ground surface also decreased with the ground depth for the heavy case. This trend was totally different from the light case. This was because the penetration depth in the flight was relatively small for the heavy case, and the reduction of the shaft friction load at the shallower part like the light case was not occurred. Furthermore, the penetration length in gravitational field was larger for the heavy case than the light case. The soil around

98

(a) PR_L1   (b) PR_H
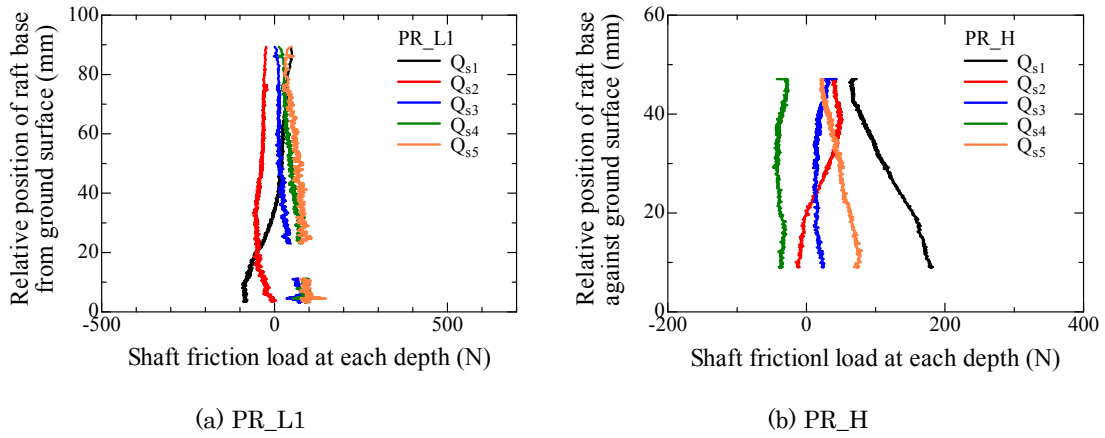
Figure 4.2.1.12 Variation of shaft friction at each depth with relative position of raft base from ground surface for PR_L1 and PR_H during penetration process.

(a) PR_L1   (b) PR_H
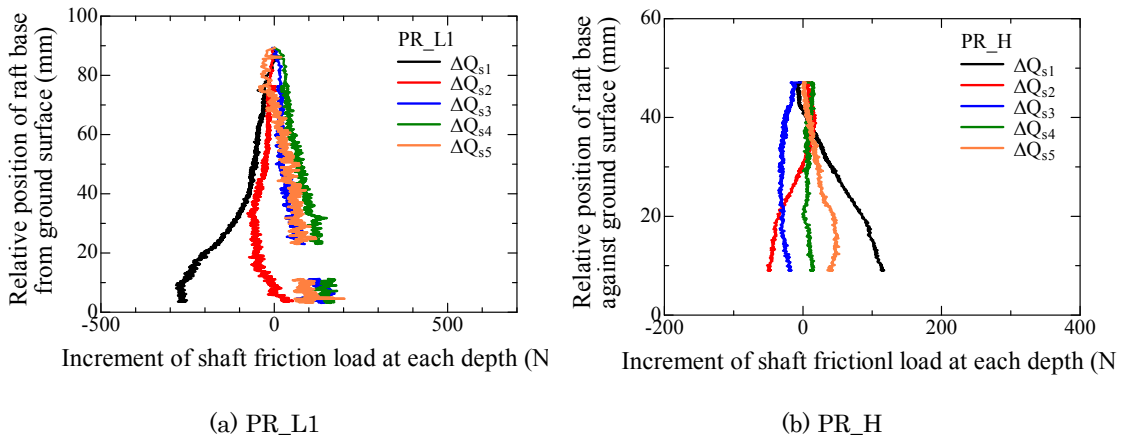
Figure 4.2.1.13 Variation of shaft friction at each depth with relative position of raft base from ground surface for PR_L1 and PR_H during penetration process. (A. 4.2.1.15-4.2.1.20)

pile may be deformed and showed the negative dilatancy by the shear in 1g. As a result, the soil at the shallower part became much dense for the heavy case than the light case. Therefore, the mobilized shaft friction load was larger for the heavy case, which led that the axial load decreased with the depth for the heavy case.

4.2.1.3 Shaft friction along pile shaft

Figure 4.2.1.12 show the variation of shaft friction at each depth Q_{sn} and relative position of raft base from the ground surface. The increment of shaft friction load ΔQ_{sn} from the beginning of the loading is also shown in Fig. 4.2.1.13. The Q_{sn} is defined in eq. (4.2.1.1) and Fig. 4.2.1.7, and the shaft friction loads in these figures are the average value of Pile 1 and Pile 2. The result from all cases and variations of Pile 1 and Pile 2 are shown in Appendix (A. 4.2.1.15-4.2.1.20). For the PR_L1, the larger shaft friction load was observed at the deep part because the ground stress became larger associated

with the penetration length (settlement). However, the shaft friction load near the pile head Q_{s1} decreased with the settlement. This was because the shaft friction load at shallower part passed the peak and showed residual value as explained in Fig. 4.2.1.11.

(a) PR_L1   (b) PR_H
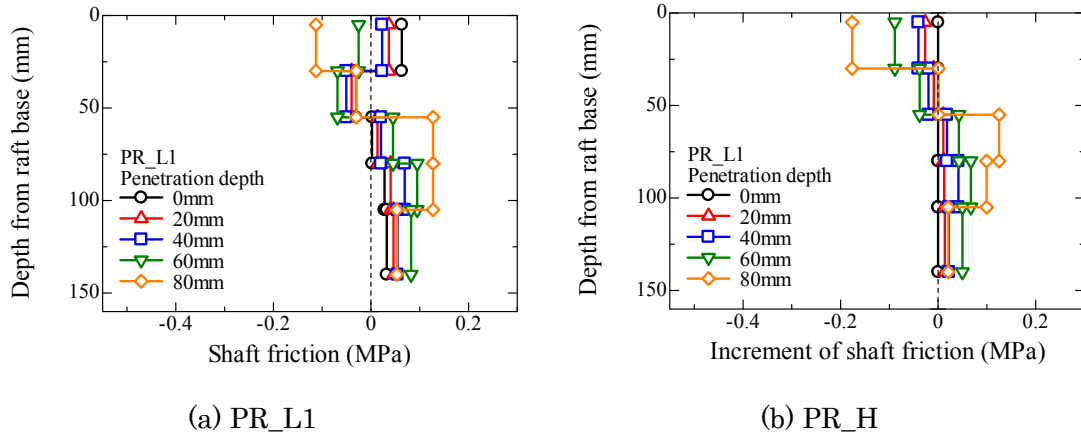
Figure 4.2.1.14 Profiles of shaft friction and shaft friction increment for PR_L1 and PR_H during penetration process.

(a) PR_L1   (b) PR_H
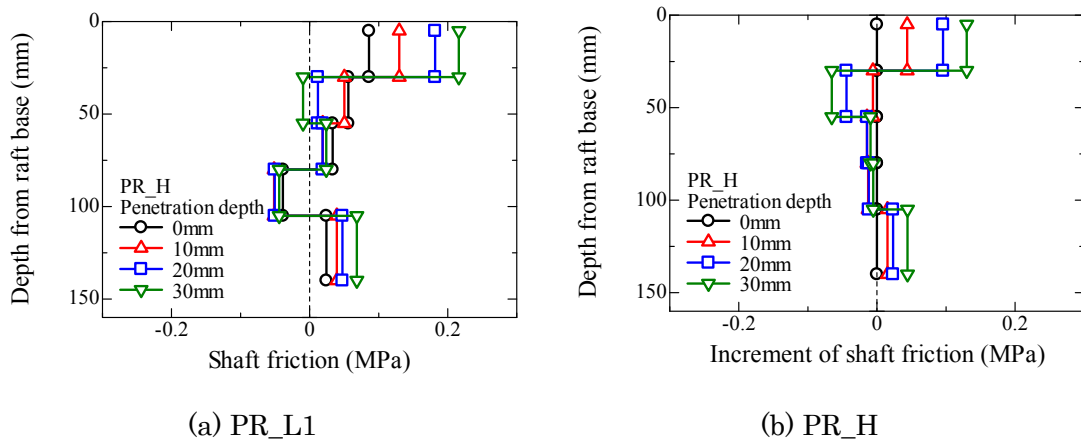
Figure 4.2.1.15 Profiles of shaft friction and shaft friction increment for PR_L1 and PR_H during penetration process. (A.4.2.1.21-4.2.1.26)

The shaft friction load at the deep part increased with the settlement for the PR_H as well. However, the shaft friction load at shallower part also increased with the settlement. This was because the reduction of the shaft friction load at the shallower depth was not occurred in the heavy case. Furthermore, the soil near the ground surface became much dense compared with the light case because the soil around piles was strongly sheared by the pile in the 1g environment. As a result, the larger shaft friction load was mobilized near the pile head as shown in Fig. 4.2.1.12 and 4.3.1.13.

Figure 4.2.1.14 shows the shaft friction profile at several penetration depths for PR_L1

(a) ΔQ_{s1}

(b) ΔQ_{s2}

(d) ΔQ_{s4}

(c) ΔQ_{s3}

(e) ΔQ_{s5}
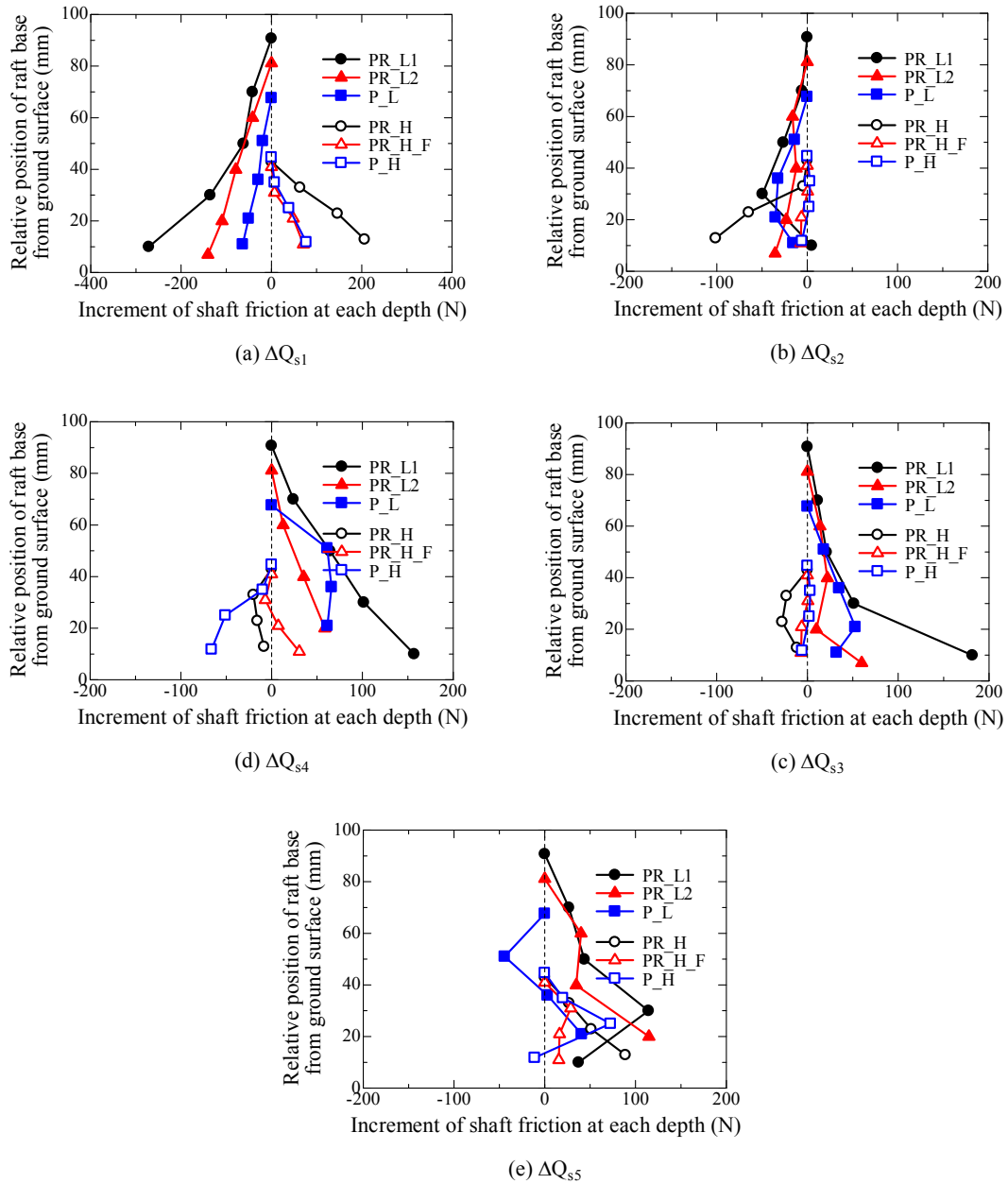
Figure 4.2.1.16 Variation of shaft friction increment at each depth with relative position of raft base from ground surface.

and PR_H. The profile of shaft friction increment from the beginning of the loading for PR_L1 and PR_H is shown in Fig. 4.2.1.15. The shaft friction in these figures is the average of Pile 1 and Pile 2. The shaft friction profiles of other cases are shown in Appendix (A. 4.2.1.21-4.2.1.26). The shaft frictions of Pile 1 and Pile 2 are also shown in the Appendix. As mentioned above, the shaft friction near the pile head gradually decreased with the settlement for the light case. On the other hand, the positive shaft friction load was mobilized at the shallower part for the heavy case. Generally, the

maximum shaft friction was mobilized at the deep part of the ground due to the high soil stress. The shaft friction observed in the heavy case showed totally different trend. That is, the maximum shaft friction load in the heavy case was occurred at the pile head. This trend verified that the pile penetration in 1g field made the soil around pile much denser.

The above mentioned difference of shaft friction mobilization between the light case and heavy case, in other words, between the different penetration depth in 1g and flight, could be clearly seen in Fig. 4.2.1.16, where the ΔQ_{sn} was plotted against the penetration depth.

(a) P_{PV} (b) End bearing and shaft friction loads
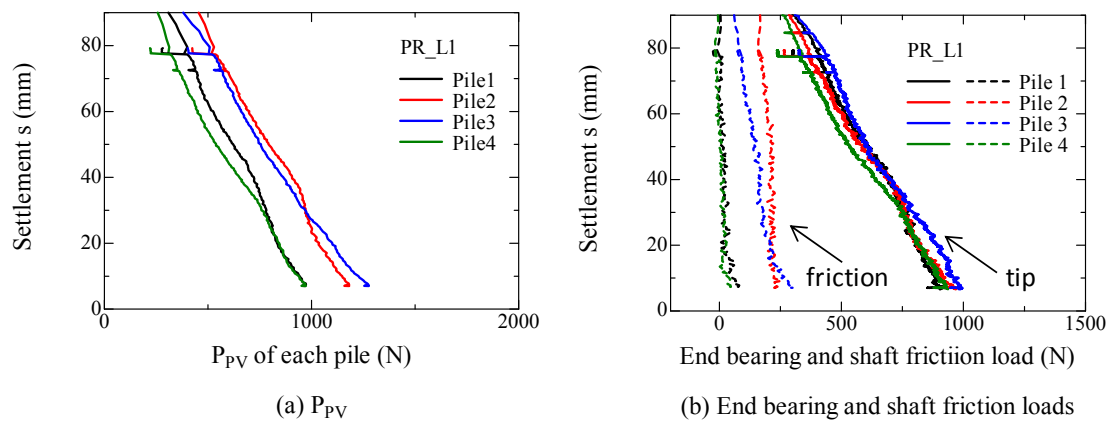
Figure 4.2.2.1 Relationship between pile load acting on each pile and settlement for PR_L1 observed in penetration process.

(a) P_{PV} (b) End bearing and shaft friction loads
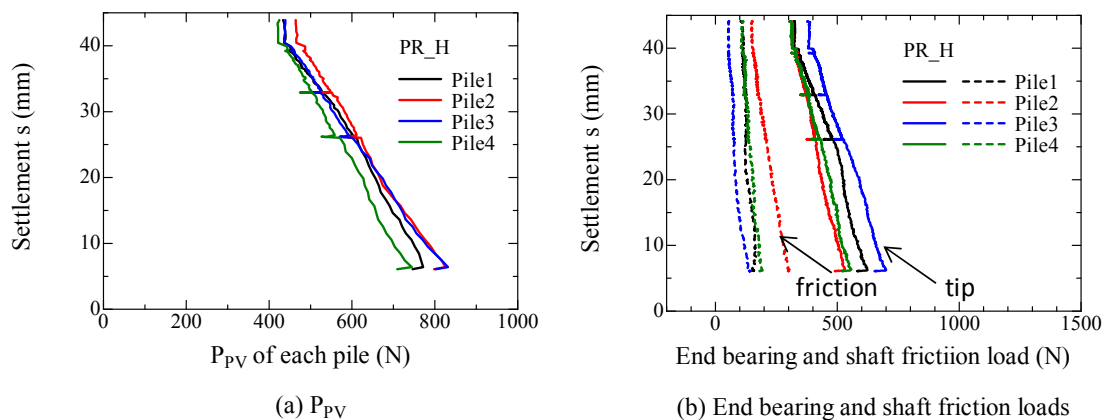
Figure 4.2.2.2 Relationship between pile load acting on each pile and settlement for PR_H observed in penetration process. (A. 4.2.2.1-4.2.2.12)

4.2.2 Variability of each pile response

In the present section, the variability of the pile response during the pile penetration process will be discussed. Figure 4.2.2.1 and 4.2.2.2 show the variation of axial load, end
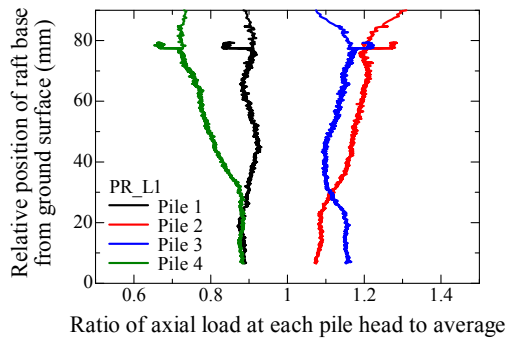
(a) Axial load at pile head
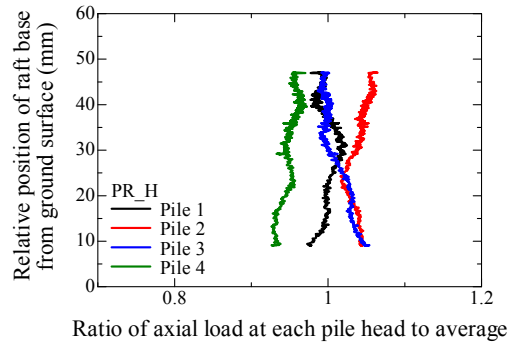
(a) Axial load at pile head
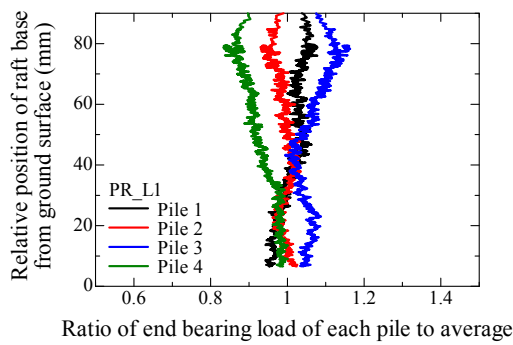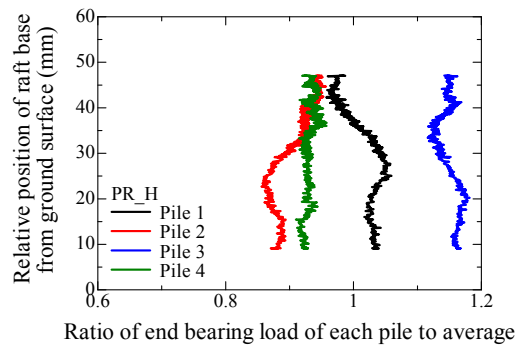
(b) End bearing load

(b) End bearing load
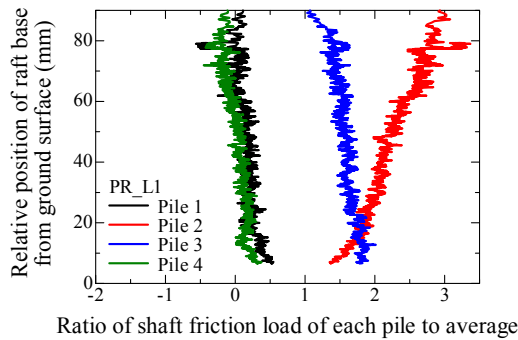
(c) Shaft friction load
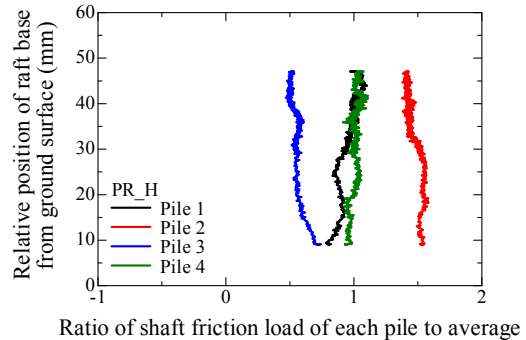
(c) Shaft friction load

Figure 4.2.2.3 Relationship between variability of pile forces and relative position of raft base from ground surface for PR_L1 observed in penetration process.

Figure 4.2.2.4 Relationship between variability of pile forces and relative position of raft base from ground surface for PR_L1 observed in penetration process.

(A. 4.2.2.13-4.2.2.24)

bearing load and shaft friction load with the relative position of the raft baser from the ground surface observed in the pile penetration for PR_L1 and PR_H respectively. These pile loads are the average values of Pile 1 and Pile 2. The results from other cases and the pile load of Pile 1 and Pile 2 are shown in Appendix (A. 4.2.2.1-4.2.2.12). The ratio of the each pile load to the average pile load at this stage is shown in Fig. 4.2.2.3 and

4.2.2.4. The ratios of other cases are summarized in Appendix (A. 4.2.2.13-4.2.2.24). In particular, the variability of the end bearing load was useful to discuss the ground uniformity because it could be regarded as a kind of result of cone penetration test.

It was seemed that the piles showing the large end bearing load also had a large shaft friction load because the stiffness of soil around this pile was relatively high. However, this trend can be seen in only PR_L1, and there was no correlation between the end bearing load and shaft friction load in other cases. This was probably because the soil around pile was disturbed by the pile penetration, and therefore the soil around pile showed more complicated uniformity compared with the soil beneath the pile tip.

The variability of the end bearing load was relatively small, and the variability ratio was less than 10%. Therefore, it can be confirmed that the uniform model ground was made in the present study. The variability range of the shaft friction load was almost same as that of the end bearing load as shown in Fig. 4.2.2.1 and 4.2.2.2. However, the variability ratio was much larger for the shaft friction load as shown in Fig. 4.2.2.3 and 4.2.2.4 because the shaft friction load was smaller than the end bearing load, and small difference between each pile was significant for the shaft friction load. Thus, the shaft friction load was much sensitive to the experimental uncertainties such as the slight uniformity of the model ground. Sometimes, all model piles were not instrumented assuming that the loads acting on piles was same as the symmetrical pile. However, the shaft friction load cannot be evaluated with a high accuracy in such case. In order to evaluate the pile load, it is required to measure the load acting on all piles used in the tests.

4.3 Vertical loading process in the second flight

In the present section, the result of the vertical loading process in the second centrifugation will be summarized.

4.3.1 Overall behavior of piled raft, pile group and raft foundation

Figure 4.3.1.1 and 4.3.1.2 show the relationship between the vertical load P_V and relative position of the raft base from the ground surface for the PR_L1 and PR_H. The same relationships obtained from other cases are summarized in Appendix (A. 4.3.2.1 and 4.3.2.2). The result of vertical load carried by pile part P_{PV} and raft part P_{RV} are also shown in the figure. When the relative position of the raft base is positive, the raft base did not touch the ground yet, implying the foundation behaves as the pile group

foundation. On the other hand, foundation behaves as the piled raft foundation for the negative relative position of the raft base from the ground surface. Some loading, unloading and reloading steps were repeated in the vertical loading process as shown in the figure. A set of loading-unloading cycle was defined as one loading step. The vertical load of the pile part in the piled raft foundation was fully mobilized before the raft base touched the ground because the relatively large settlement was already imposed to the foundation. And the vertical load carried by the raft part gradually increased after the raft base had a contact with the ground surface. Therefore, the vertical load was mainly supported by the piles in the beginning for the piled raft foundation.

(a) PR_L1　　　　　　　　　　(b) PR_H
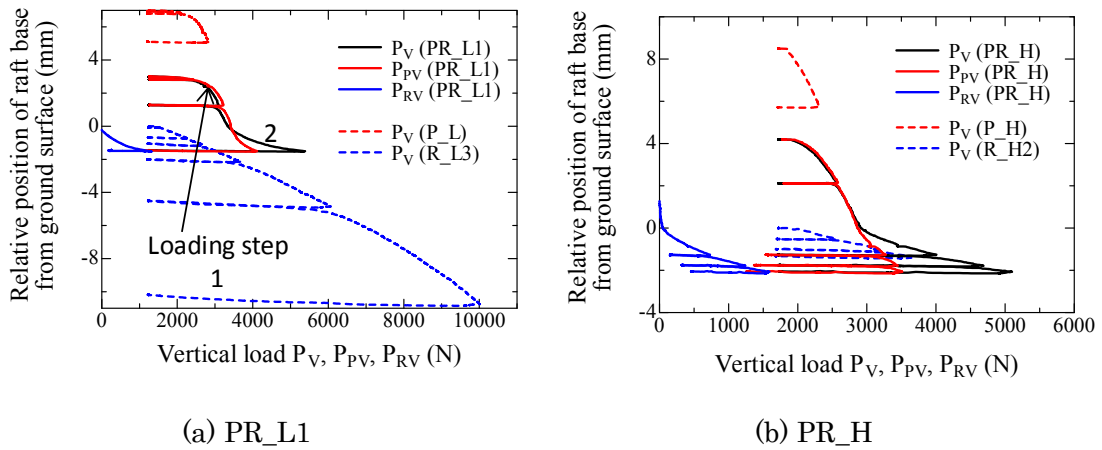
Figure 4.3.1.1 Variation of P_V, P_{PV} and P_{RV} for PR_L1 and PR_H with settlement observed in the vertical loading process. (A. 4.3.2.1 and 4.3.2.2)

4.3.2 Shared load by the raft

Figure 4.3.2.1 shows the variation of the vertical load P_V, the vertical load of the raft part P_{RV} and the vertical load of the pile part P_{PV} with the relative position of the raft base from the ground surface for all cases. The vertical load of the raft part rapidly increased with the settlement after the raft base touched the ground. The almost linier load-settlement curve can be observed for the raft part in the piled raft and the raft foundation, implying the raft load was still in the elastic region. The vertical load of pile part also increased after the raft base had a contact with the ground surface. The reason for this increment of pile part will be discussed in the next section. The vertical load before the raft base did not touch the ground can be regarded as the vertical load of the pile group foundation. Therefore, it can be said that the increase of the vertical load of raft part and the pile part contributes the higher vertical resistance of the piled raft foundation than the pile group foundation. And increment of the vertical load of the raft part was larger than that of pile part, implying the larger vertical load of the piled raft than the pile group was mainly attributed from the contribution of the raft part. It was also noted that although the raft load showed elastic response at relatively large

(a) Piled raft

(b) Raft part

(c) Pile part
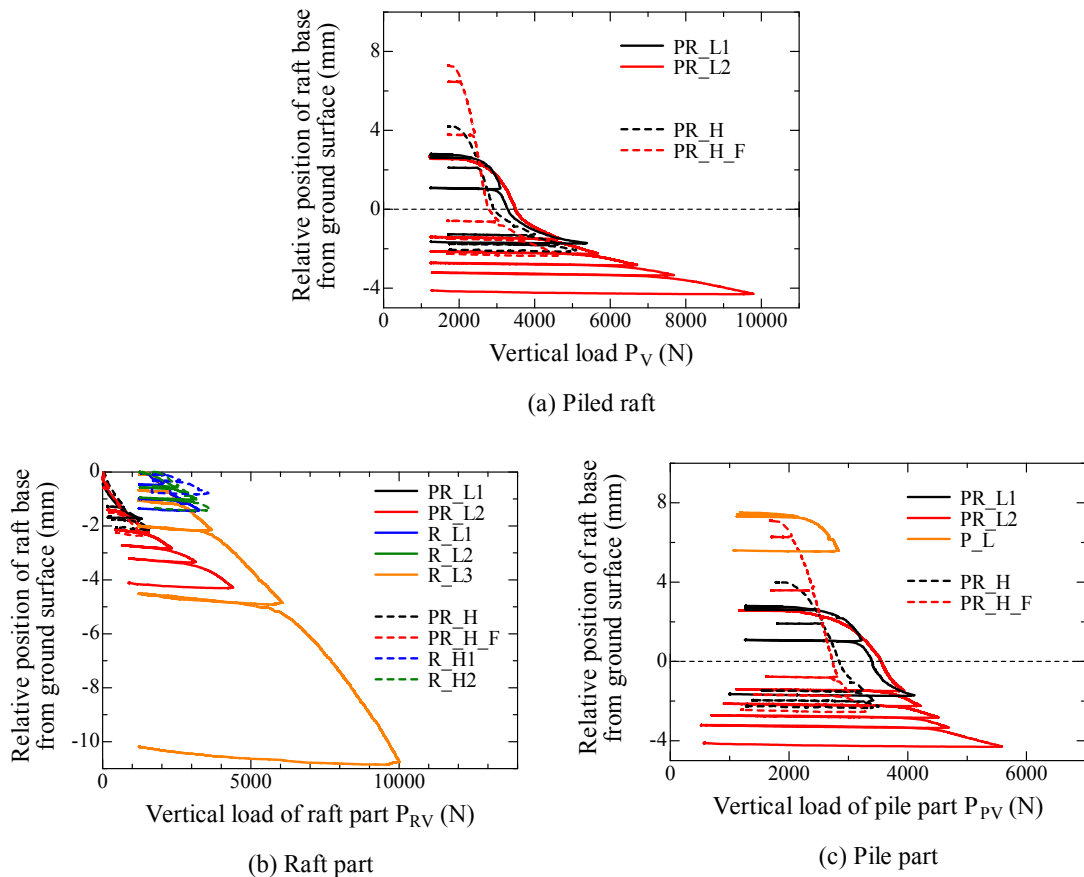
Figure 4.3.2.1 Relationship between vertical load and relative position of raft base from ground surface during vertical loading process.

settlement, the vertical pile response before the raft base touched the ground reached critical state.

Figure 4.3.2.2 shows the relationship between the proportion of the vertical load carried by the raft part (RVLP) and the relative position of the raft base from the ground surface. RVLP increased with the settlement because the increase of the vertical load of the raft part was larger than that of the pile part as explained above. From this fact, it can be said that the RVLP can be controlled by applying the vertical load to the foundation. The trend of the RVLP was almost same between the light case and the heavy case during the loading but that was totally different was observed during the unloading period. That is, the RVLP increased for the light case, and it decreased for the heavy case during the unloading. This was due to the difference of the mobilization of the pile load during the unloading, which will be discussed in latter Fig. 4.3.3.3.

(a) Light case   (b) Heavy case
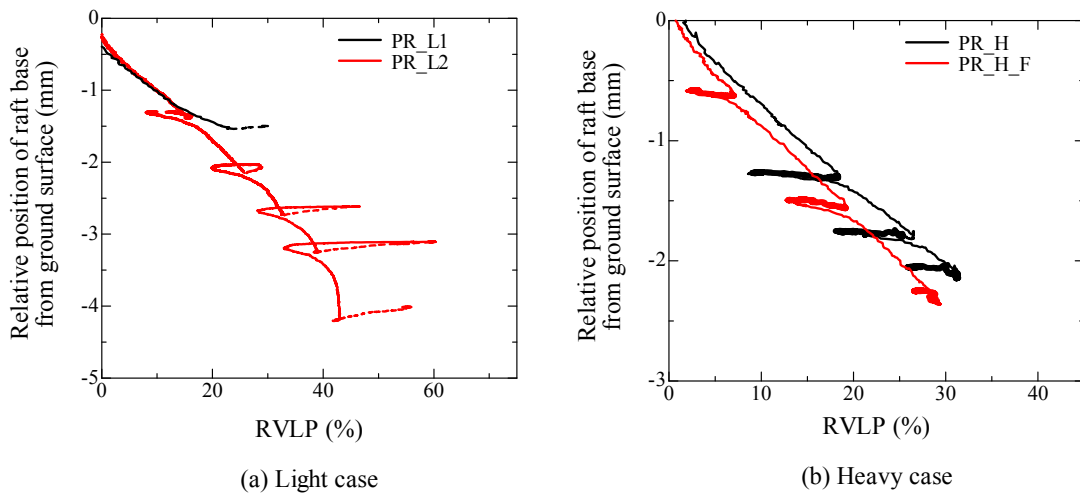
Figure 4.3.2.2 Variation of RVLP with relative position of raft base from ground surface observed in vertical loading process.

Figure 4.3.2.3 shows the relationship between coefficient of subgrade reaction of raft part and raft base pressure or the vertical loading step. The result of the raft foundation is also shown in the figure. The contact pressure in R_L1 and R_L2 was about 200kPa, and that of R_H1 and R_H2 was 270kPa. The coefficient of subgrade reaction was estimated by the slope during the reloading period. It should be noted that these figure was represented in the prototype scale. From these figures, it can be said that the coefficient of subgrade reaction was much smaller for the raft part in the piled raft foundation than the raft foundation due to poor contact condition between the raft base

and the ground surface. However, it gradually increased with the base contact pressure because the settlement made the contact condition better. And it was expected that the coefficient of raft part finally reached that of the raft foundation.
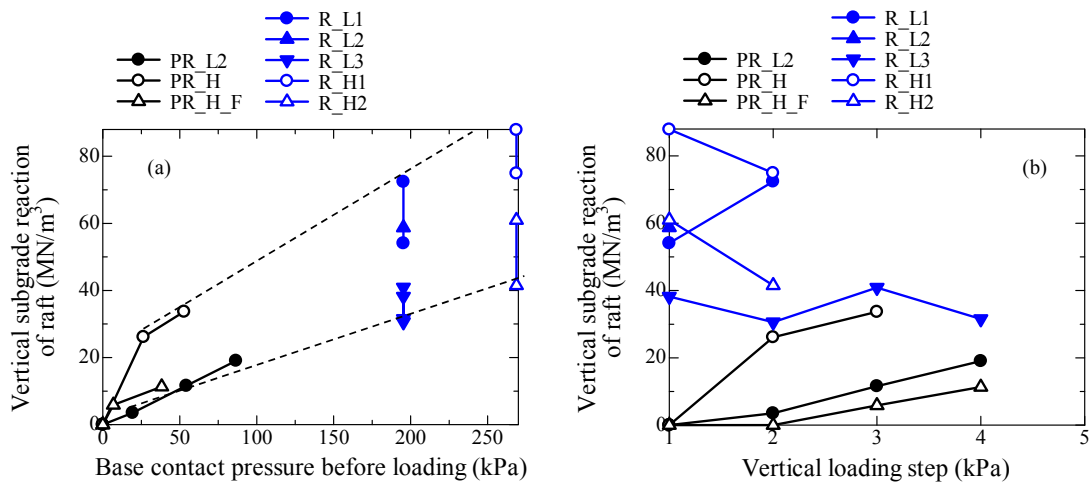
Figure 4.3.2.3 Variation of vertical subgrade reaction of raft with (a) base contact pressure before loading and (b) vertical loading step during vertical loading process.

4.3.3 Shared load by the piles

4.3.3.1 End bearing and shaft friction loads

As been seen in Fig. 4.3.2.1 (c), the trend of the vertical load of the pile part increased with the settlement after the raft base touched the ground surface. This was probably because the raft base pressure affected to the pile response. Here, the vertical response of the pile part will be discussed in detail by dividing the vertical load carried by pile part into the end bearing load and the shaft friction load.

Figure 4.3.3.1 shows the variation of the end bearing load and the shaft friction load with the relative position of the ground surface from the ground surface. When the relative position of the raft base is positive, the raft base did not touch the ground yet, implying the foundation behaves as the pile group foundation. On the other hand, foundation behaves as the piled raft foundation for the negative relative position of the raft base from the ground surface. The larger end bearing load was mobilized in the light case compared with the heavy case because the end bearing load was proportional to the penetration depth in the flight as shown in Fig. 4.3.1.3 and 4.2.1.6. The trend of the end bearing load did not change before and after the raft base touched the ground, implying that there was no influence of the raft base pressure on the pile tip, where was two times depth than the raft width. The end bearing load reached the ultimate capacity. The

(a) End bearing load   (b) Shaft friction load
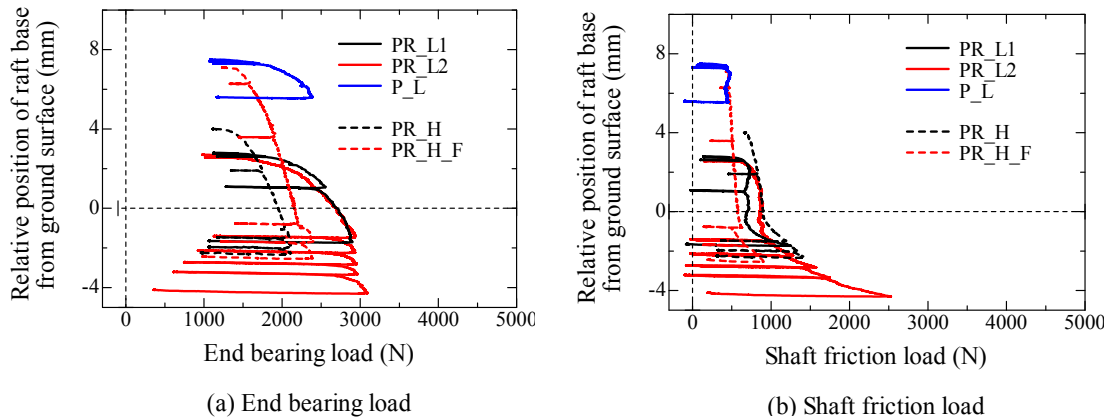
Figure 4.3.3.1 Variation of end bearing and shaft friction loads with relative position of raft base from ground surface for light and heavy cases observed in vertical loading process.

mobilized shaft friction load before the raft base touched the ground surface (foundations behaved as the pile group foundation) also showed almost constant value against the vertical displacement, showing the clear yielding of the shaft friction load. However, it rapidly increased with the settlement after the raft base was in contact to the ground. This was probably due to the increase of the confined stress around piles caused by the raft base pressure. The range of raft pressure influence will be discussed latter. Therefore, larger vertical pile load for the piled raft foundation than the pile group foundation was mainly attributed to the increase of the shaft friction load. It was also noted that the influence of the base pressure on the pile response reached shallower part. This influence range by the raft pressure will be discussed in detail latter.
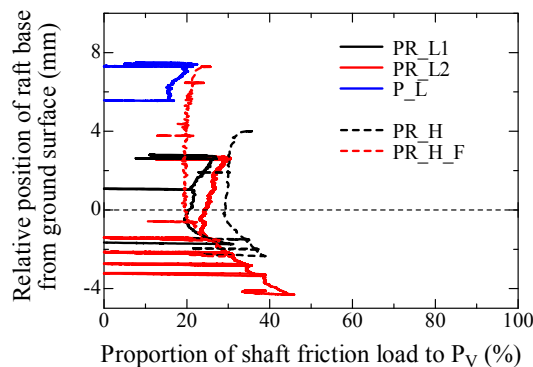
Figure 4.3.3.2 Relationship between proportion of shaft friction load to total vertical load PV and relative position of raft base from ground surface during vertical loading process.

Figure 4.3.3.2 shows the proportion of the shaft friction load against the total vertical load of the pile. The proportion was about 30% before the raft base touched the ground surface, in other words, the foundation behaved as the pile group foundation. During this period the proportion was almost constant with the settlement. However, the ratio

109

increased with the settlement after the raft base touched the ground, in other words, the foundation acted as the piled raft foundation. This was because the trend of end bearing load was almost same between the pile group and the piled raft foundation as shown in Fig. 4.3.3.1, and trend of the shaft friction load increased after the raft base touched the ground.

Figure 4.3.3.3 shows remained end bearing load and shaft friction load after each loading step. The remained shaft friction load gradually decreased with the loading step procedures. In particular, the remained shaft friction significantly reduced and reached almost zero for the light case. The piles were moved upward during the unloading, and this upward movement was larger for the light case than the heavy case. It was well known that the shaft friction load was fully mobilized in the small displacement. Therefore, the remained shaft friction load reached almost zero for the light case.

(a) End bearing load　　　　　　　　(b) Shaft friction load
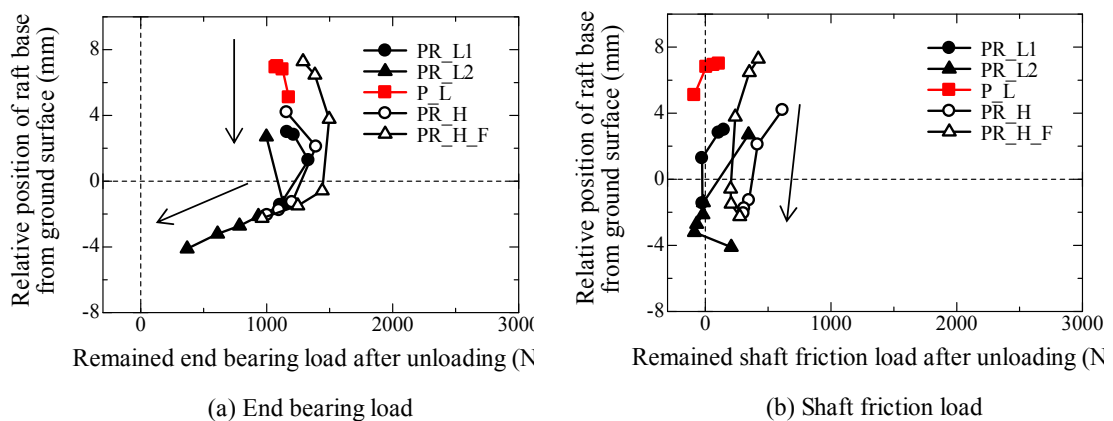
Figure 4.3.3.3 Variation of remained pile loads with relative position of raft base from ground surface observed in vertical loading process.

Although the remained end bearing load was almost constant for each loading step when the foundation behaved as the pile group foundation, it rapidly decreased with the settlement after the raft base touched the ground. This significant reduction of remained end bearing load implied that the piles acted as a kind of anchor and prevented the free heaving of the raft. Considering the remained end bearing load and shaft friction load, the reduction of the pile load during the unloading was larger for the light case than the heavy case. Therefore, the RVLP increased during the unloading period for the light case, and it decreased during the unloading for the heavy case as shown in Fig. 4.3.2.2.

Figure 4.3.3.4 shows the variation of the coefficient of the subgrade reaction of end bearing load and shaft friction load with base contact pressure before each loading step.

And the coefficient plotted against the vertical loading step is shown in Appendix (A.4.3.3.1) It should be noted that the coefficient of subgrade reaction was shown in the proto type scale. The coefficient of subgrade reaction of end bearing load was almost constant with the base pressure, implying that there was no influence of the raft base on a kind of spring constant of the end bearing load. As explained in Fig. 4.3.3.1, the raft base did not affect the end bearing load. Therefore, it can be said that the mobilization of the end bearing load is same between the pile group foundation and the piled raft foundation. Although the coefficient of subgrade reaction of shaft friction load slightly increased at the large base pressure, it seemed that the influence of the base pressure on the spring constant of the shaft friction load. The ultimate shaft friction load was significantly enhanced by the raft base pressure as shown in Fig. 4.3.3.1. Therefore, it can be said that the raft base had a significant influence on the ultimate shaft friction load compared with the spring constant of the shaft friction load.

(a) Pile tip   (b) Pile shaft
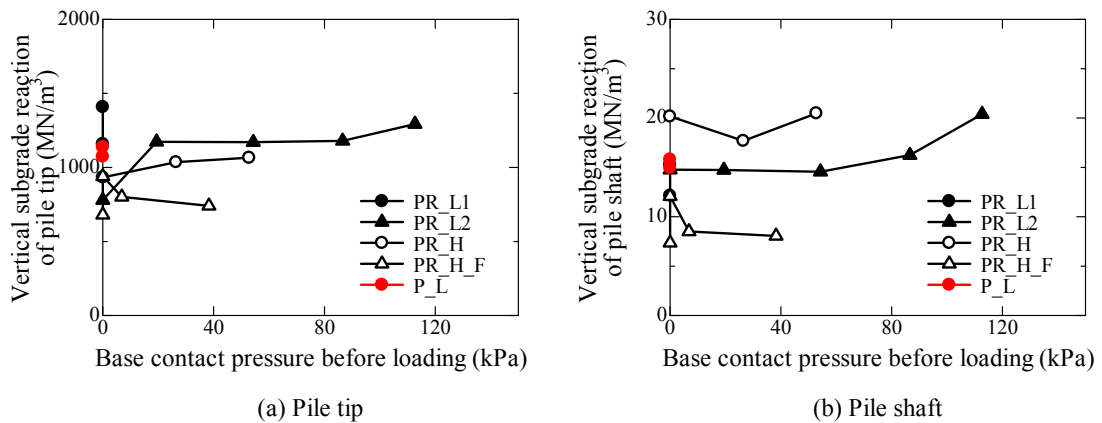
Figure 4.3.3.4 Variation of vertical subgrade reaction of pile with base contact pressure before loading.

(A. 4.3.3.1)

4.3.3.2 Influence of raft base pressure on vertical pile response

It was observed that the base pressure affected on the ultimate shaft friction load in the previous section. In the present section, this influence of raft pressure will be discussed in detail.

Figure 4.3.3.5 (a) shows the relationship between the base contact pressure and the average shaft friction, and Fig. 4.3.3.5 (b) shows the base contact pressure and shaft friction at the peak of each vertical loading step. The shaft friction at the base pressure of zero can be regarded as the shaft friction of the pile group foundation. From this figure, it can be confirmed that the shaft friction of pile linearly increased with the base pressure.
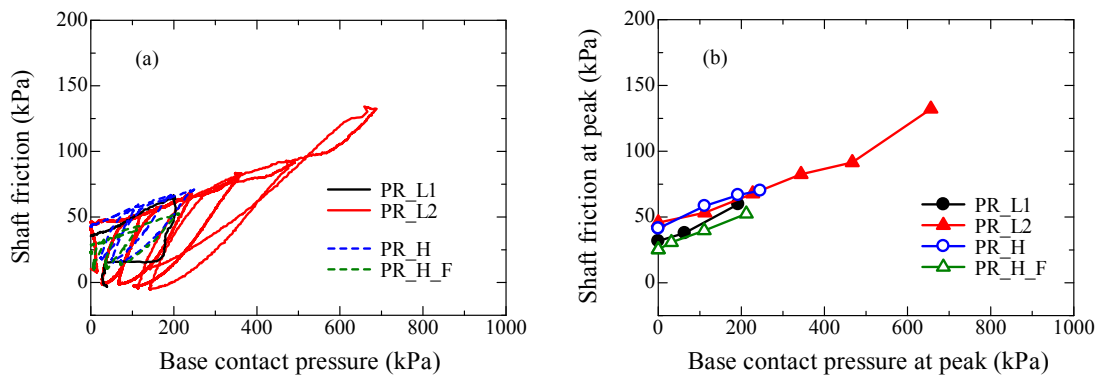
Figure 4.3.3.5 Relationship between base contact pressure and shaft friction during vertical loading process.

That is, the shaft friction of the piled raft consisted of shaft friction of the pile group and the increased shaft friction by raft pressure. It is required for the piled raft design to estimate the additional shaft friction load generated by the raft pressure.
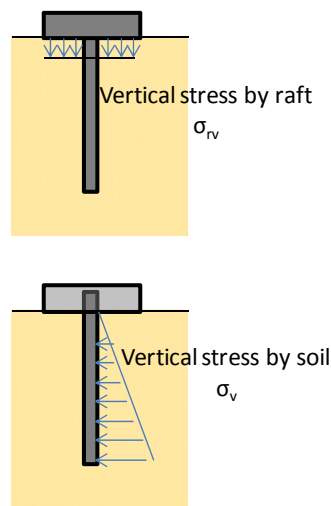
Figure 4.3.3.6 Vertical stress caused by the soil weight and base contact pressure.

The vertical stress distribution of the ground beneath the piled raft foundation consisted of two components such as the vertical stress by the soil weight and the vertical stress by the raft pressure as shown in Fig. 4.3.3.6. The vertical stress by the soil weight was calculated from the unit weight of soil, and it linearly distributed with the ground depth as shown in Fig. 4.3.3.8 (a). It was well known that using the elastic theory the vertical stress of the raft pressure transferred into the ground by the bulb shape as show in Fig. 4.3.3.7. The elastic theory can be employed in the present study because the raft load response was in the elastic as explained in Fig. 4.3.2.1. The model

(a) $L=B$
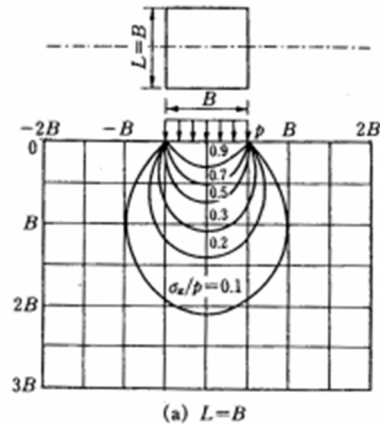
Figure 4.3.3.7 Stress bulb beneath 3D footing.

(a) Vertical

(b) Horizontal
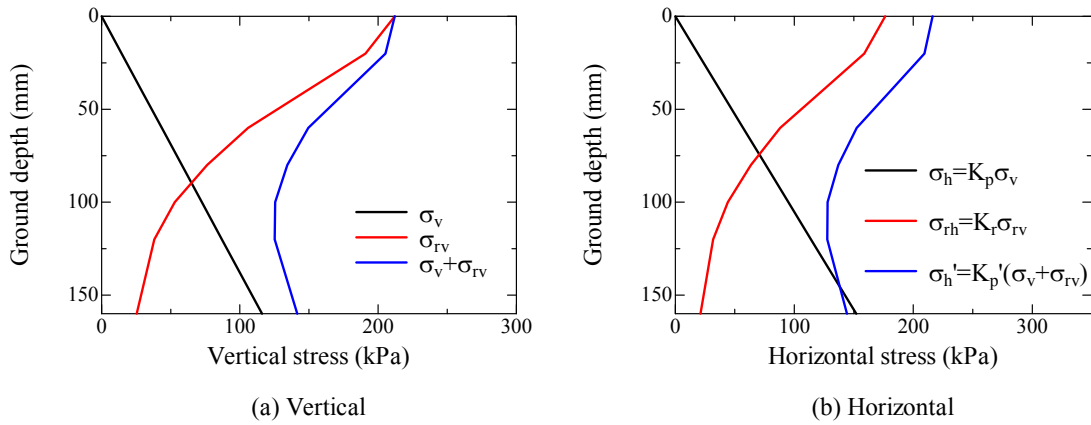
Figure 4.3.3.8 Stress profile in the model ground.

ground was divided into ten layers, and the distribution of the vertical stress by the raft was calculated as described in Fig. 4.3.3.8 (a). σ_v in the figure is vertical stress by the soil and σ_{rv} is the vertical stress by the raft calculated using Fig. 4.3.3.7. Here the three types of coefficient of earth pressure were employed to calculate the shaft friction of the pile such as the coefficient of earth pressure for the vertical stress by the soil weight K_h, that for the vertical stress by the raft pressure K_r and that for the total vertical stress by the soil and the raft pressure K_h'. The horizontal stress in the ground was calculated using these coefficients of earth pressure as shown in Fig. 4.3.3.8 (b). Then,, two types of shaft friction can be calculated as follows.

$$Q_s = \sum \mu \left(K_h \sigma_v + K_r \sigma_{rv} \right)$$
$$Q_s^{'} = \sum K_h^{'} \left(\sigma_v + \sigma_{rv} \right)$$

(4.3.3.1)

μ in the figure is the coefficient of friction between the pile and the soil. The $\Sigma \mu K_h \sigma_v$ is the shaft friction load of the pile group foundation and the $\Sigma \mu K_r \sigma_{rv}$ is the increased shaft

friction load by the raft pressure (Fig. 4.3.3.6 (b)).

The coefficient of earth pressure was back calculated using this equation and the measured shaft friction load. The calculated coefficient of earth pressure is plotted against the base pressure in Fig. 4.3.3.9. The K_p is treated as the coefficient of earth pressure at the base contact pressure of zero because it was the coefficient of the earth pressure for the soil weight. The relatively large coefficient of earth pressure can be observed because the foundation was penetrated into the ground under the centrifugation and soil condition became to be the passive state. However, the K_h' gradually decreased with the contact pressure because the soil condition shifted to the relative active state due to the base pressure. As been seen, K_r was almost constant with the raft base pressure, which was almost zero for the all cases. Therefore, it can be said that the additional shaft friction load in the piled raft foundation can be simply calculated using this K_r value.

(a) K_p & K_p' (b) K_r
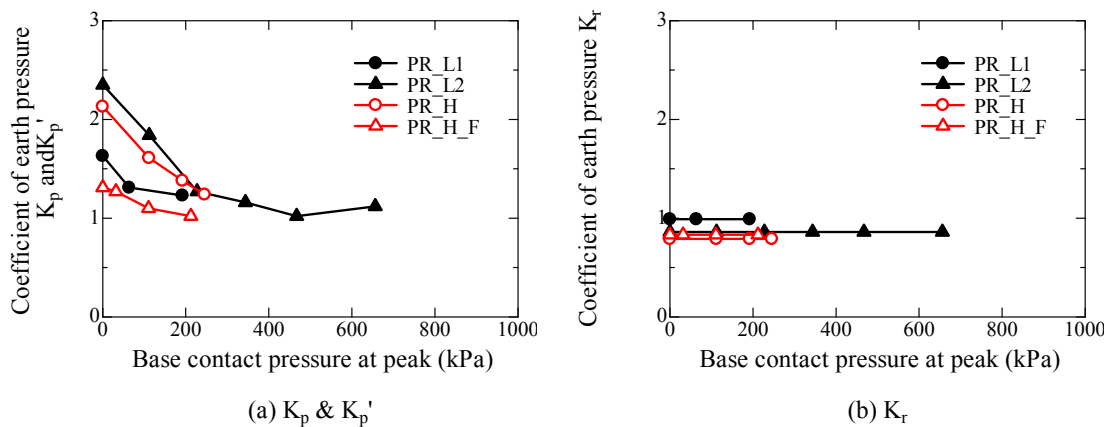
Figure 4.3.3.9 Coefficient of earth pressure back-calculated from the soil weight and raft pressure.

Thus, it was difficult to estimate the shaft friction load in the piled raft foundation using K_h' because it depended on the raft base pressure. However, the shaft friction load mobilized in the piled raft foundation can be simply calculated from sum of the shaft friction of the pile group and the additional shaft friction due to the raft base using K_r. As explained in Fig. 4.3.3.5 and 4.3.3.6, the influence of the raft base on the coefficient of the subgrade reaction of shaft friction was slight. Therefore, it can be confirmed that the raft base can enhance the ultimate shaft friction load in the piled raft foundation.

Next the pile observed in each depth will be examined to clarify the range of base pressure influence. Figure 4.3.3.10 – 4.3.3.12 show the variation of the axial load at
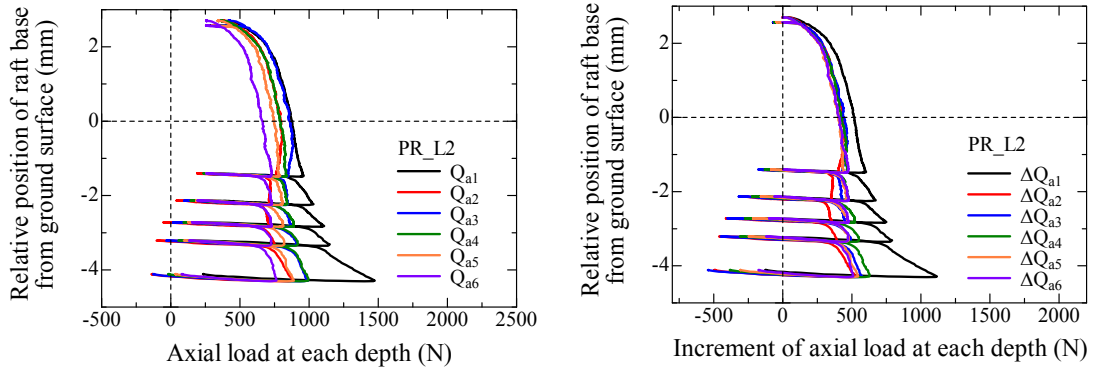
Figure 4.3.3.10 Variation of axial load and axial load increment at each depth with relative position of raft base from ground surface for PR_L2 during penetration process.
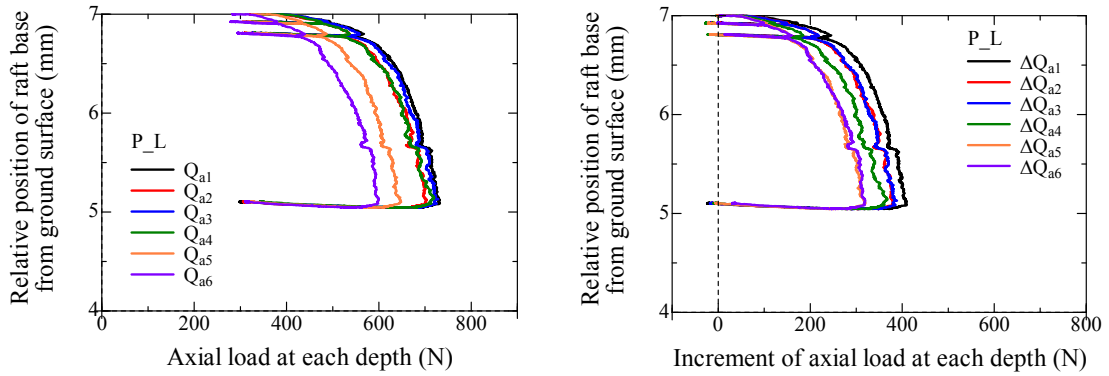
Figure 4.3.3.11 Variation of axial load and axial load increment at each depth with relative position of raft base from ground surface for P_L during penetration process.
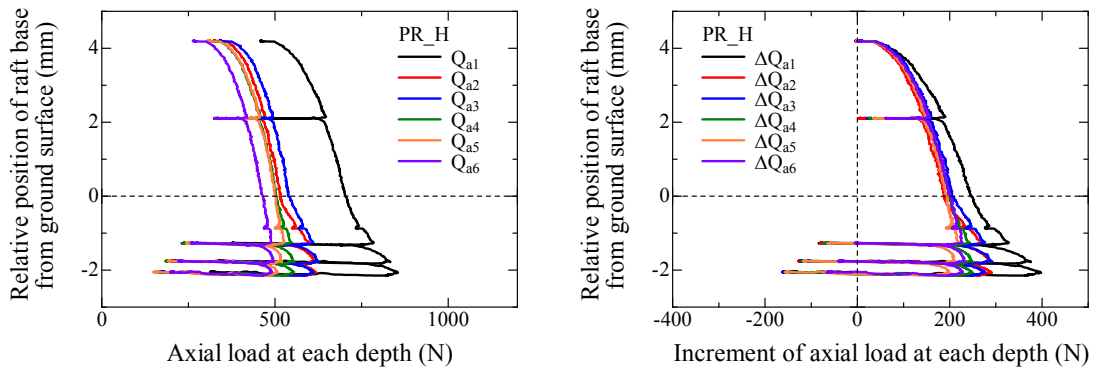
Figure 4.3.3.12 Variation of axial load and axial load increment at each depth with relative position of raft base from ground surface for PR_H during penetration process.
(A. 4.3.3.2-4.3.3.6)

each depth Q_{an} and increment of axial load ΔQ_{an} with the relative position of the raft base from the ground surface for PR_L2, P_L and PR_H respectively. The axial load is the average of Pile 1 and Pile 2. Results from other cases and each pile response such as

Pile 1 and Pile 2 are summarized in Appendix (A. 4.3.3.2-4.3.3.6). When the relative position of the raft base is positive, the raft base did not touch the ground yet, implying the foundation behaves as the pile group foundation. On the other hand, foundation behaves as the piled raft foundation for the negative relative position of the raft base from the ground surface. The axial loads at all depths gradually increased with the settlement before the raft base touched the ground for both piled raft and pile group foundation. In particular, the Q_{a1} in the heavy case showed large value. This was because the pile penetration made the soil near the ground surface much denser for the heavy case, and the shaft friction at shallow part increased as explained in Fig. 4.2.1.9 – 4.2.1.10. The axial load rapidly increased after the raft base touched the ground, especially at the shallower depth. Furthermore, the sudden change of the axial load cannot be seen in the pile group foundation despite of the depth. From this fact it can be said that the shaft friction load at the shallower depth increased due to the contact pressure.

Figures 4.3.3.13 – 4.3.3.15 show the profile of axial load at the peak of each vertical loading step for PR_L2, P_L and PR_H. The axial loads described in the figures are average load of Pile 1 and Pile 2. Axial load observed in other cases, and that observed in each pile (Pile 1 and Pile 2) are shown in Appendix (A.4.3.3.7-4.3.3.11). The increment of axial load from the beginning of first vertical loading is also shown in the figure. The some vertical loading step in the piled raft foundation before the raft base touched the ground can be regarded as the result of the pile group foundation as shown in Fig. 4.3.1.1. So, the PG in the figure represents the profile regarded as the pile group, and the PR represents the profile after the raft base touched the ground. For the pile group foundation (Fig. 4.3.14 and PG in Fig. 4.3.13 and 4.3.1.15), the increment of axial load each depth was almost the same, and the axial load profile moved in parallel with the loading step procedures. On the other hand, in the piled raft foundation the axial load at only pile head rapidly increased with the loading step procedures, implying that the larger shaft friction load was mobilized near the raft base.

(a) Average of Pile 1 & Pile 2

(d) Average of Pile 1 & Pl
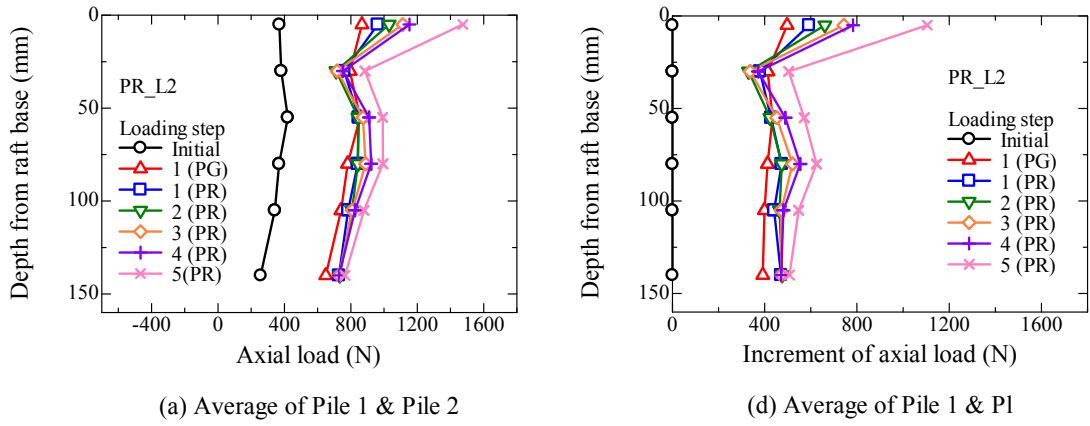
Figure 4.3.3.13 Profiles of axial load and axial load increment for PR_L2 during vertical loading process.

(a) Average of Pile 1 & Pile 2

(d) Average of Pile 1 & Pile 2
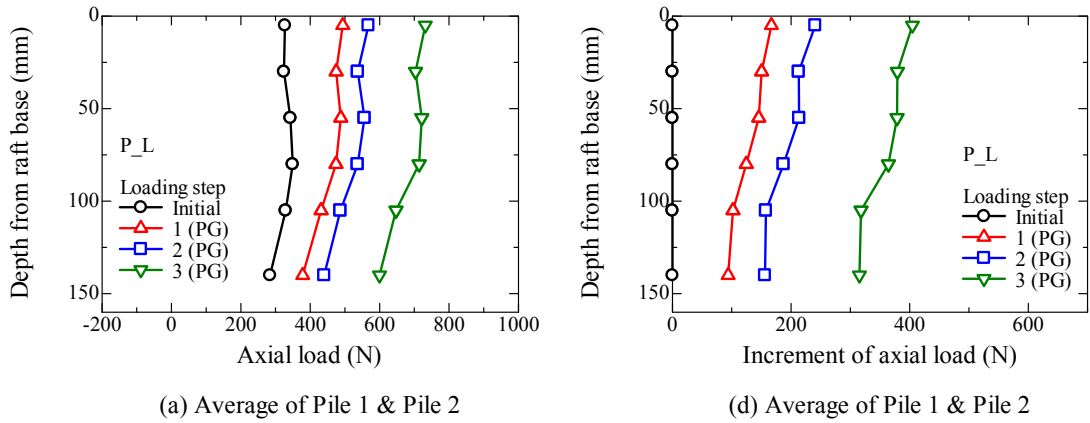
Figure 4.3.3.14 Profiles of axial load and axial load increment for P_L during vertical loading process.

(a) Average of Pile 1 & Pile 2

(d) Average of Pile 1 & Pile 2
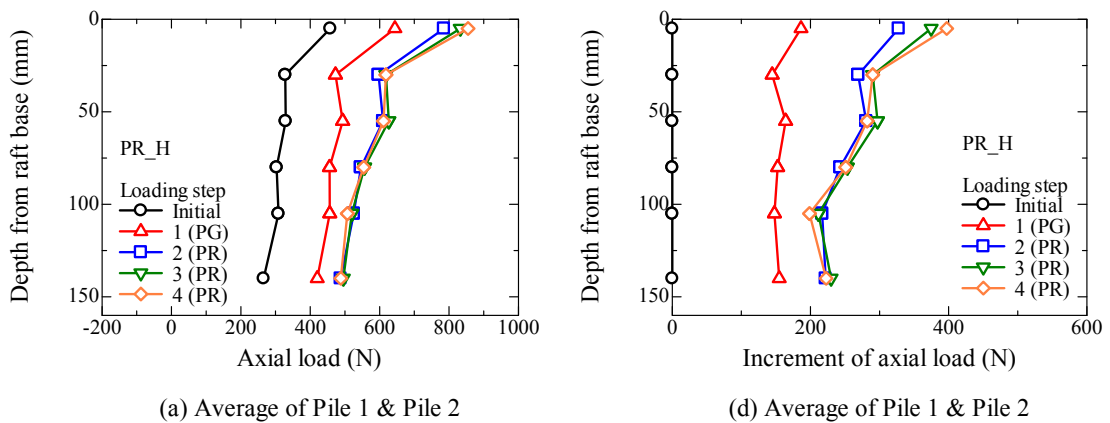
Figure 4.3.3.15 Profiles of axial load and axial load increment for PR_H during vertical loading process.

(A. 4.3.3.7-4.3.3.11)

117
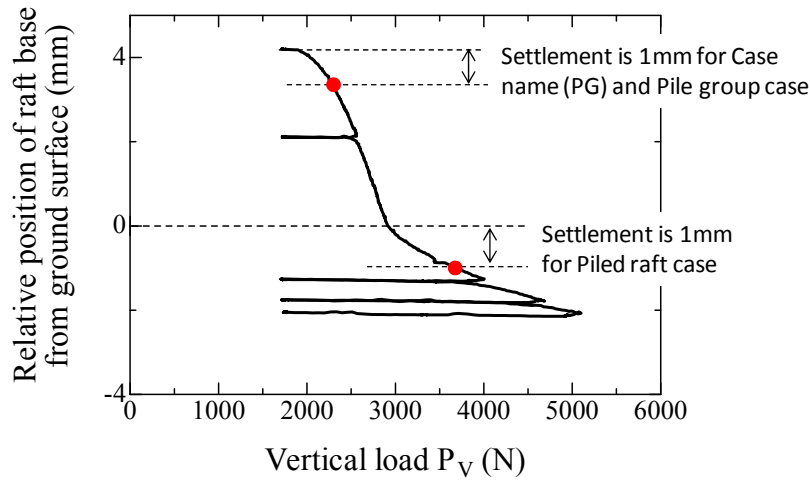
Figure 4.3.3.16 Positions in which axial loads are compared in Fig. 4.3.3.18.
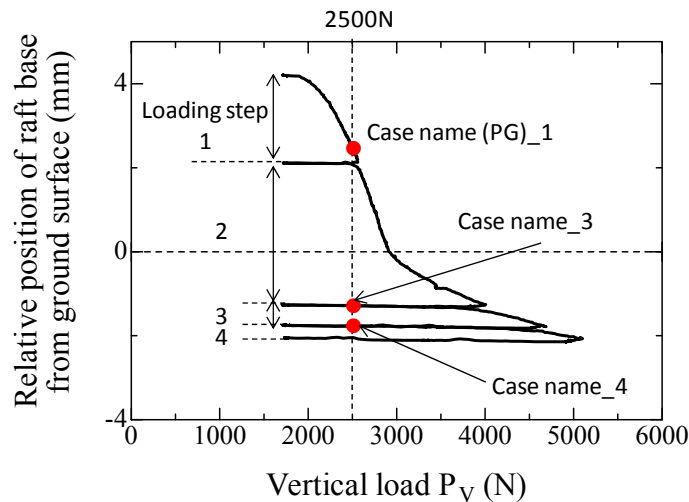
Figure 4.3.3.17 Positions in which axial loads are compared in Fig. 4.3.3.19.

Figure 4.3.3.18 shows the axial load profile at 1mm settlement. The increment of axial load profile is also shown in the figure. The PG in the figure represents the profile before the raft base had a contact with the ground. The 1mm settlement means the settlement from the beginning of the loading for the pile group foundation and the piled raft before the raft base touched the ground. For the piled raft having contact with the raft base and the ground, the 1mm settlement is the settlement after the raft base touched the ground as shown in Fig. 4.3.3.16. Although the axial load was gently distributed for the pile group foundation, the significant large axial load can be observed at the pile head for the piled raft foundation as mentioned above. For the increment of axial load, the axial load increment at each depth was almost same for the pile group, however, unique axial load mobilization can be observed for axial load increment in the piled raft, that is, only axial

118
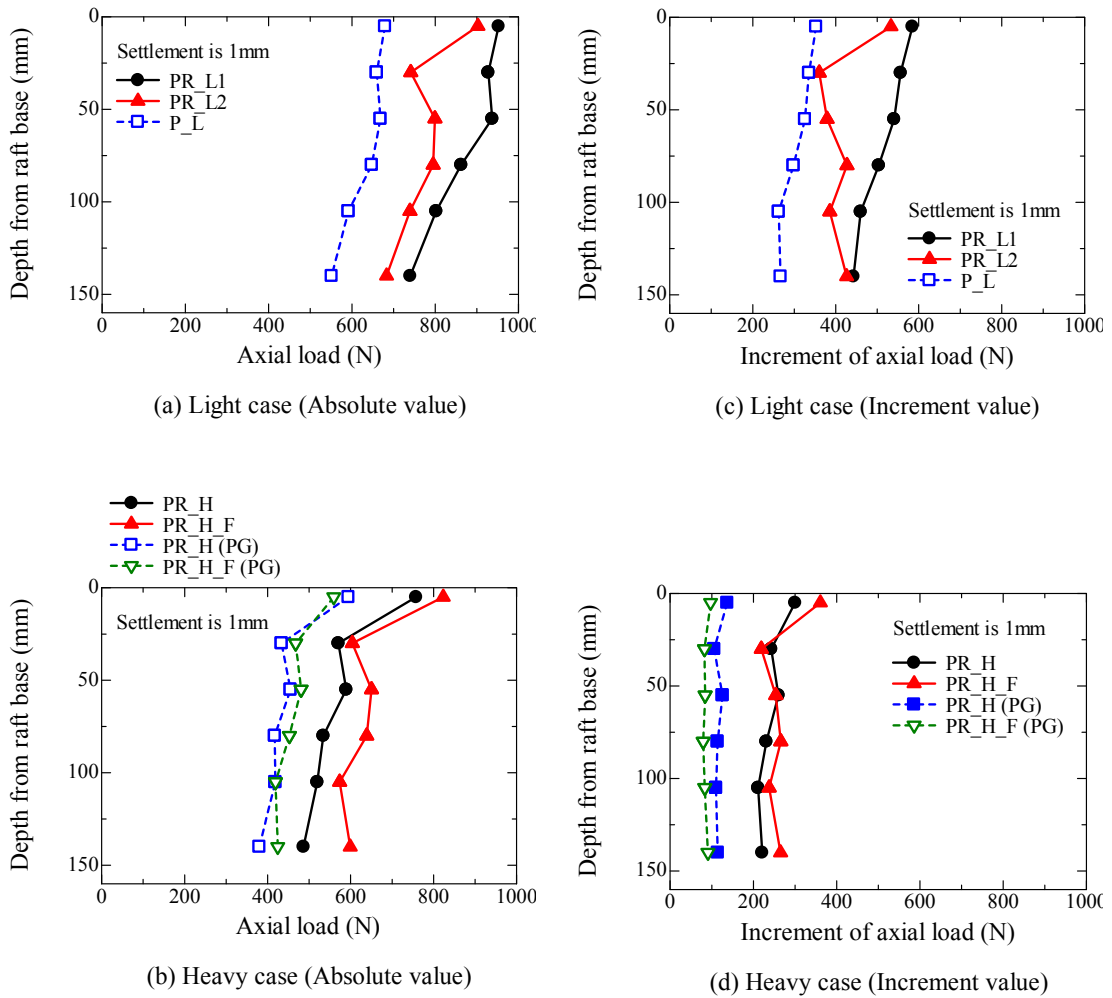
Figure 4.3.3.18 Profile of axial load and axial load increment at settlement of 1mm.

load at shallower part significantly increased. It was also noted that the axial load acting on the pile was larger for the piled raft foundation than the pile group foundation because the relatively large vertical load was imposed to the piled raft foundation at the same settlement as shown in Fig. 4.3.1.1 and 4.3.1.2.

Figure 4.3.3.19 shows the axial load profile at the vertical load of 2500N as shown in Fig .4.3.3.17. The axial load increment was shown in the figure as well. As been seen, the piled raft foundation can reduce the axial load acting on piles compared with the pile group foundation when the same vertical load was applied to the foundation. This was because a part of the vertical load was supported by the raft part, and the vertical load acting on pile decreased. The axial load acting on the piled raft gradually decreased with the loading step procedures because the vertical load supported by the raft part increased with the settlement as shown in Fig. 4.3.2.2.

Figure 4.3.3.20 shows relationship between the RVLP before each loading step and the axial load at each depth with the vertical load of 2500N. The relationship between the
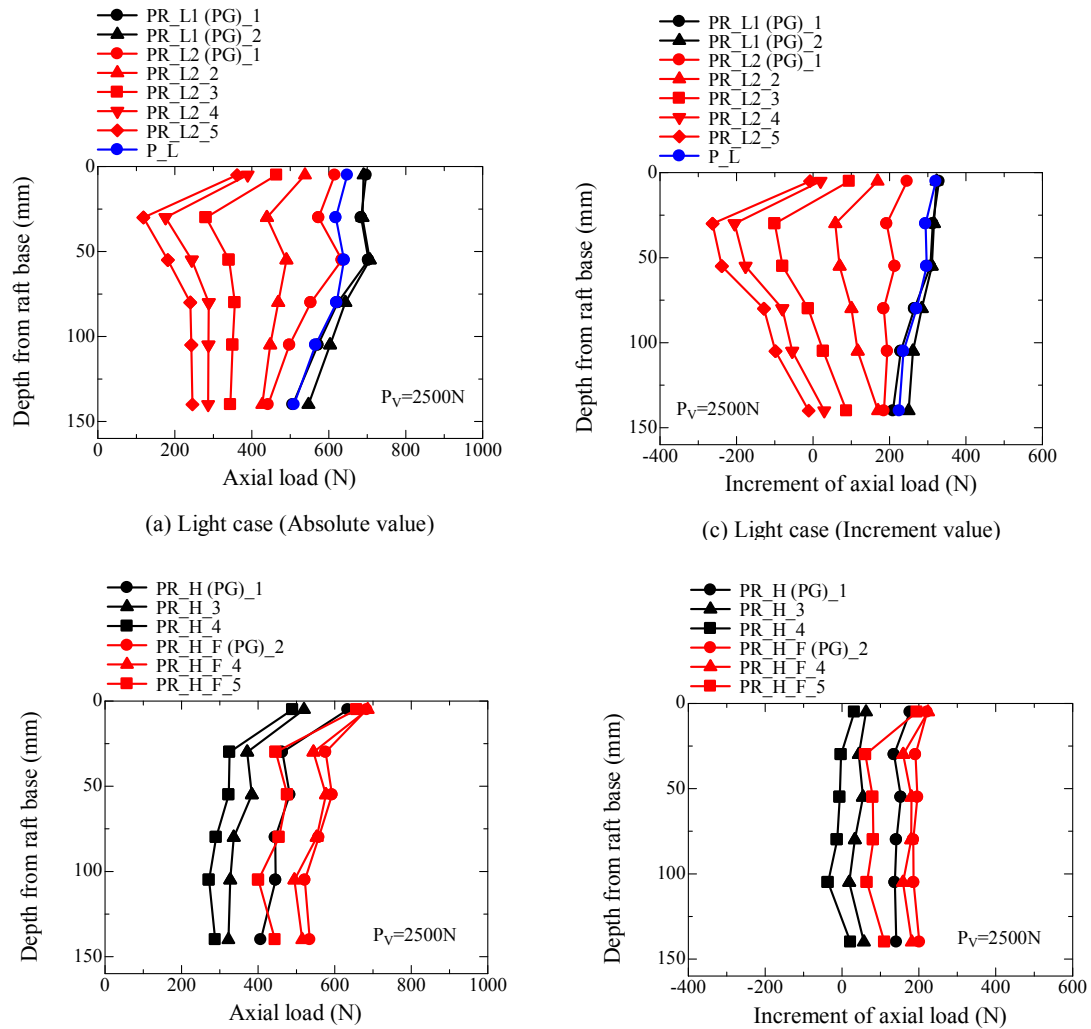
Figure 4.3.3.19 Profile of axial load at Pv of 2500N.

RVLP and the axial load at each depth normalized by that of the pile group foundation is also described in the figure. From this figure, it can be said that the piled raft efficiently reduced the axial load acting on the pile compared with the pilegroup foundation, and this trend can be clearly seen in the large RVLP.

Figures 4.3.3.21 shows the relationship between the shaft friction load observed in each depth and the relative position of the raft base from the ground surface for PR_L2 and P_L. The shaft friction load in this figure is the average value of Pile 1 and Pile 2. The
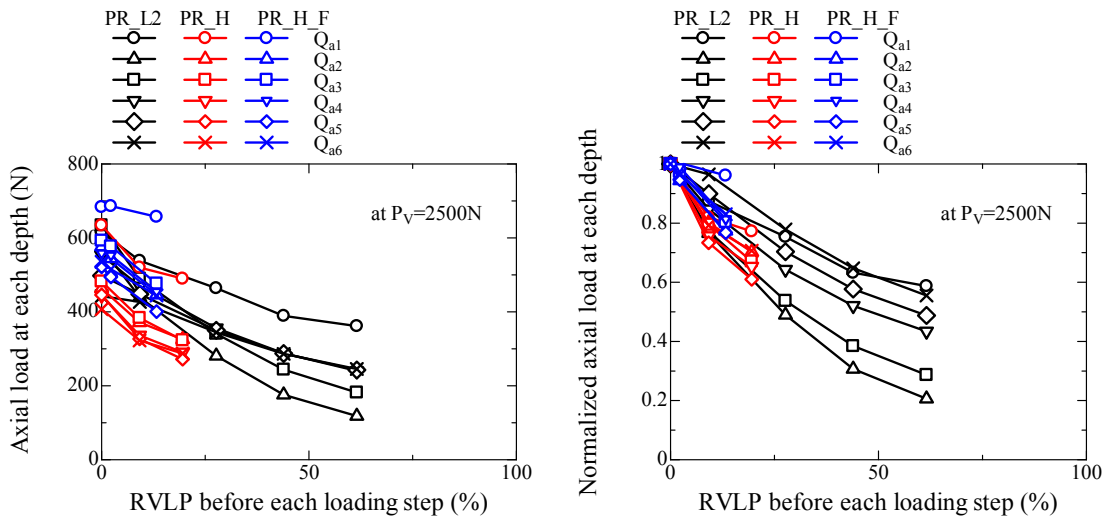
Figure 4.3.3.20 Variation of axial load at each depth and normalized axial load at each depth with RVLP before each loading step.

(a) PR_L2	(b) P_L
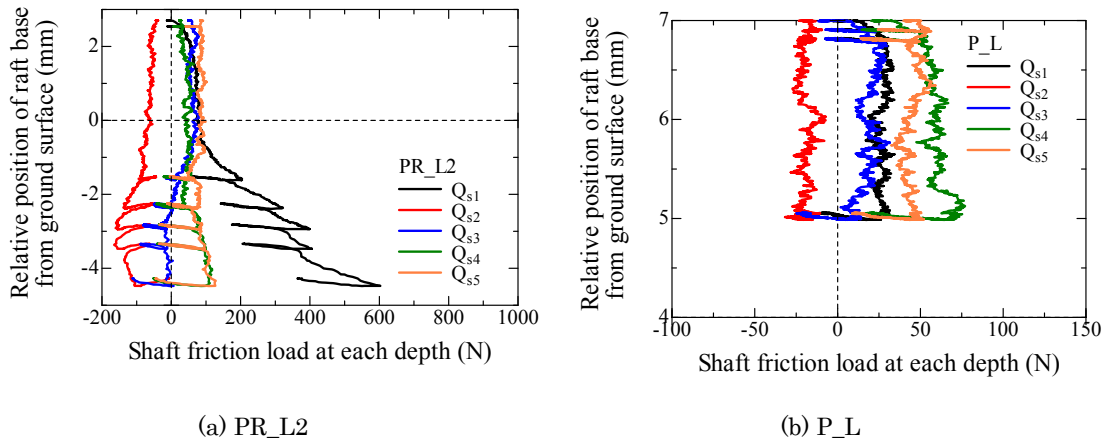
Figure 4.3.3.21 Variation of shaft friction load and shaft friction load increment at each depth with relative position of raft base from ground surface for PR_L2 and P_L during penetration process. (A.4.3.3.12-4.3.3.16)

variation of shaft friction load for other cases and individual pile response of Pile 1 and Pile 2 are summarized in Appendix (A. 4.3.3.12-4.3.3.16). The increment of the shaft friction load is also shown in the figure. The shaft friction load for the pile group and the piled raft before the raft base touched the ground showed almost constant value with the settlement, implying that the shaft friction load was already fully mobilized. However, the shaft friction load rapidly increased with the settlement after the raft base touched the ground, in other words, foundation behaved as the piled raft foundation. This fact can be confirmed by Fig. 4.3.3.22 where the shaft friction profiles at the peak of each loading step for PR_L2 and P_L are described. The result obtained from other cases and each pile response are summarized in Appendix (A. 4.3.3.17-4.3.3.21). The shaft friction was significantly larger at the shallower part than other depth, especially

(a) PR_L2

(b) P_L
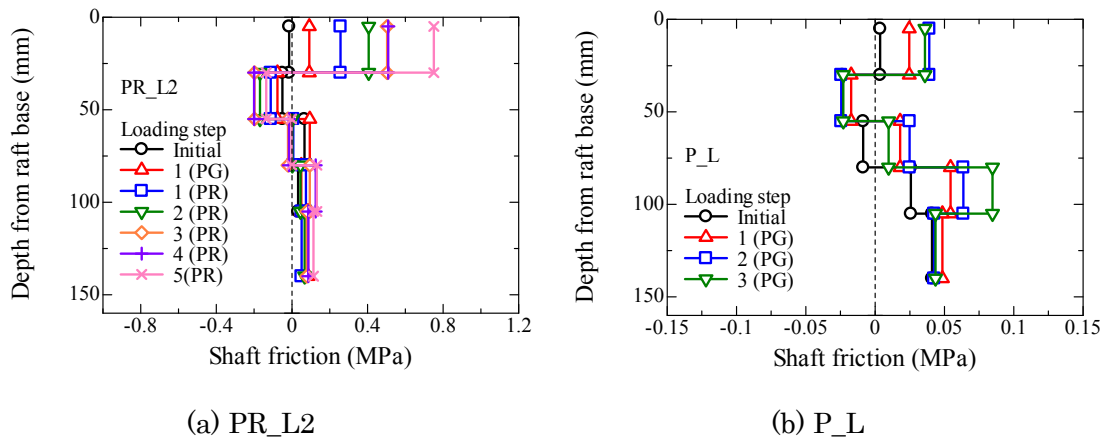
Figure 4.3.3.22 Profiles of shaft friction for PR_L2 and P_L during the vertical loading process.
(A. 4.3.3.17-4.3.3.21)

(a) Light case (Absolute value)

(b) Heavy case (Absolute value)
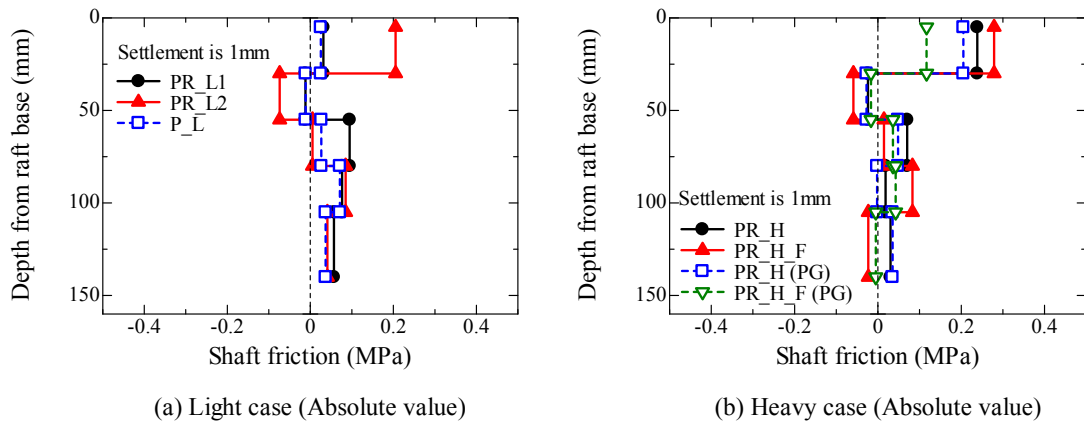
Figure 4.3.3.23 Profile of shaft friction at settlement of 1mm for (a) light case, (b) heavy case.

(A. 4.3.3.22)

for the piled raft foundation, implying that the raft pressure enhanced the shaft friction just beneath the raft base. Therefore, it can be also said that the increment of the shaft friction shown in Fig. 4.3.2.1 was mainly attributed to the increase of shaft friction load near the raft base.

Figure 4.3.3.23 shows the shaft friction profile at the settlement of 1mm for the light case and the heavy case. The profile of shaft friction increment is shown in Appendix (A. 4.3.3.22). The PG in the figure represents the profile of the piled raft before the raft base touched the ground. The 1mm settlement means the settlement from the beginning of the loading for the pile group foundation and the piled raft before the raft base touched the ground. For the piled raft having contact with the raft base and the ground, the 1mm settlement is the settlement after the raft base touched the ground as shown in Fig. 4.3.3.16. The shaft friction load near the pile head was larger for the piled raft than the

122

(a) Light case (b) Heavy case
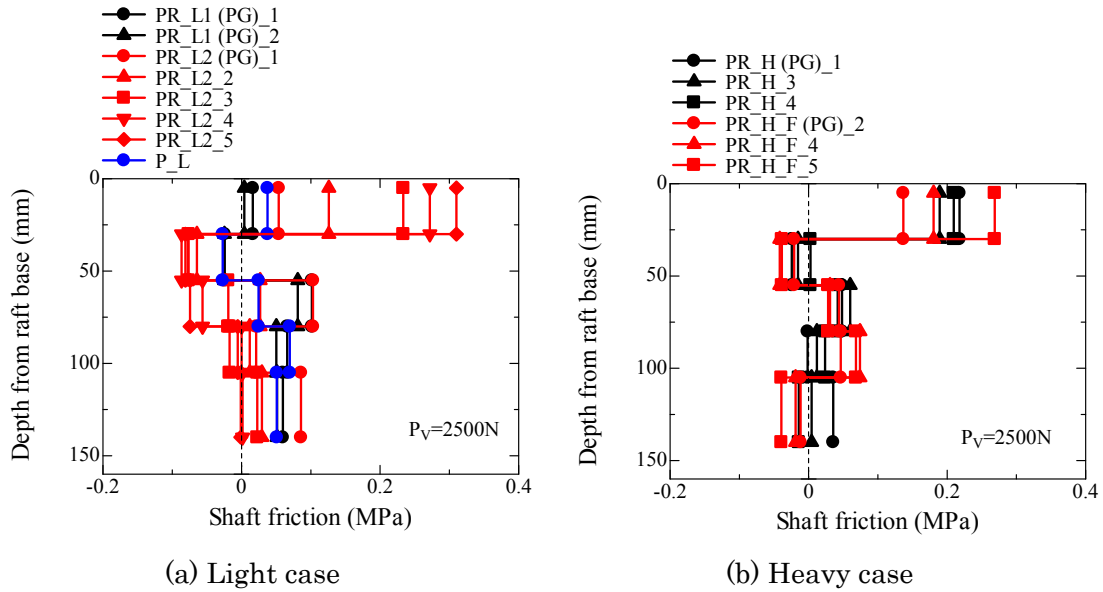
Figure 4.3.3.24 Profile of shaft friction at P_V of 2500N for (a) light case, (b) heavy case.
(A. 4.3.3.23)

pile group because base pressure enhanced the shaft friction as mentioned above and relative large vertical load was applied to the piled raft at the same settlement.

Figure 4.3.3.24 shows the profile of shaft friction at the vertical load of 2500N. The increment of shaft friction profile is also shown in Appendix (A. 4.3.3.23). The larger shaft friction was mobilized at the pile head for the piled raft than the pile group due to the raft base pressure. And the shaft friction at pile head increased with the loading step procedures. This increased shaft friction can reduce the axial load acting on pile in the piled raft as shown in Fig. 4.3.3.19 and 4.3.3.20.

4.4 Pre-vertical loading process in the third flight

In the present section, the result of the pre-vertical loading process in the first centrifugation will be summarized. The pre-vertical loading process determined the initial conditions of the foundation before the horizontal loading tests. Therefore, much focus was placed on clarifying the initial conditions of the foundation.

4.4.1 Overall behavior of piled raft, pile group and raft foundation

Figure 4.4.1.1 shows relationship between the vertical load P_V and the settlement s for PR_L1 and PR_H. The relationships for other cases are summarized in Appendix (A. 4.4.4.1). The vertical loads carried by the raft part P_{RV} and pile part P_{PV} are also shown in the figure. For the piled raft foundation, the vertical load was applied to the foundation until the proportion of the vertical load carried by the raft part RVLP reached the target value of 27%.

| (a) PR_L1 | (d) PR_H |
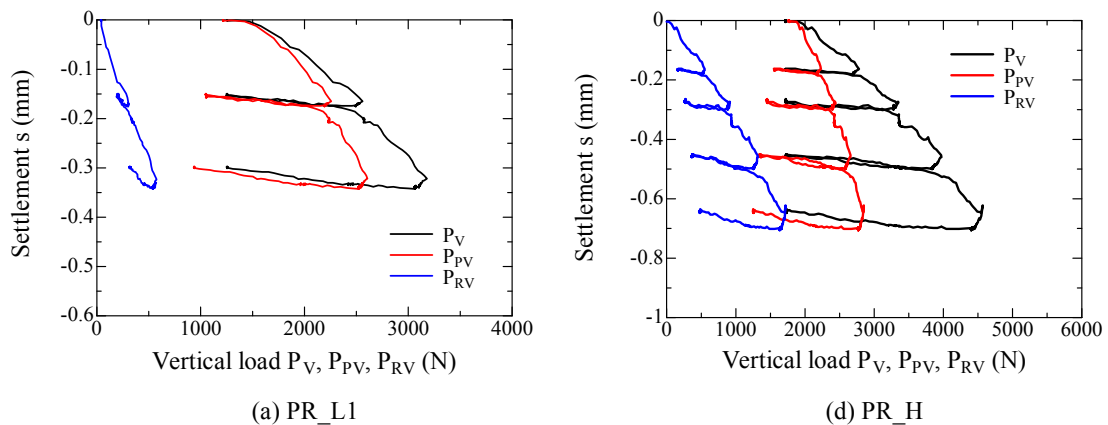
Figure 4.4.1.1 Variation of P_V, P_{PV} and P_{RV} with settlement during pre-vertical loading process.

4.4.2 Initial conditions of foundations before horizontal loading tests
4.4.2.1 Vertical load carried by raft

Figure 4.4.2.1 shows variation of the vertical load P_V, the vertical load carried by the pile part P_{PV} and the vertical load carried by the raft part P_{RV} with the settlement s. The basic behavior of the piled raft subjected to the vertical load was already examined in the Section 4.3. The initial vertical load of the raft part was quite small. As explained in Section 4.3, although the RVLP was increased up to 30% by applying the vertical load in the vertical loading process, the increased vertical load carried by the raft part was diminished once the centrifugation was stopped.

(a) Overall

(b) Pile part

(c) Raft part
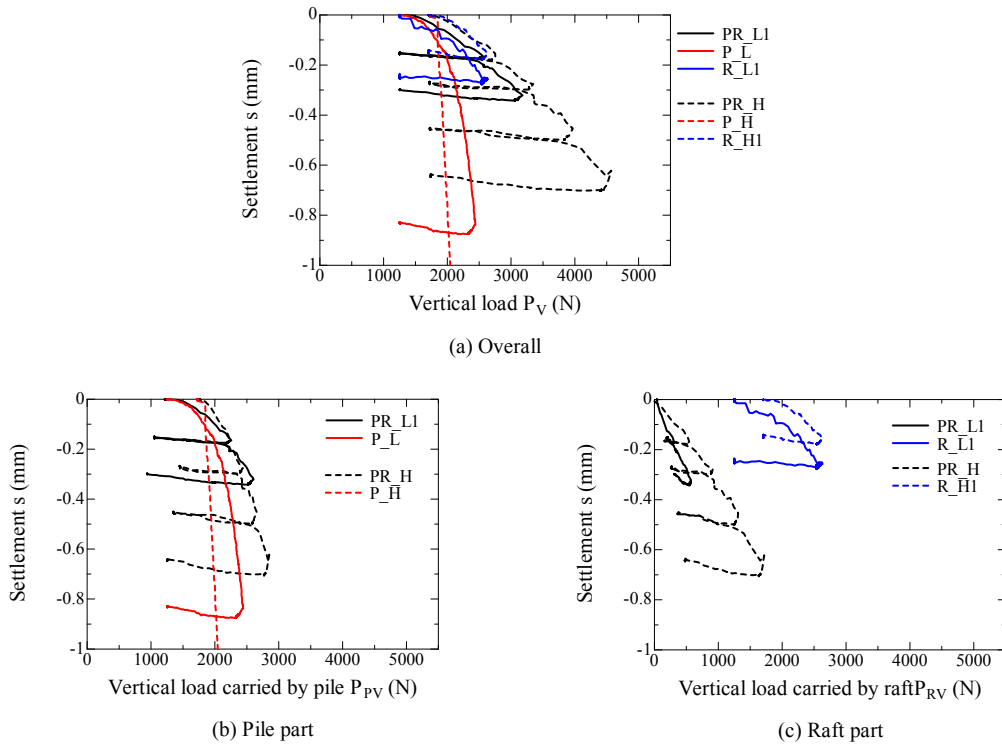
Figure 4.4.2.1 Relationship between vertical load carried by component and settlement.

(a) Light case

(b) Heavy case
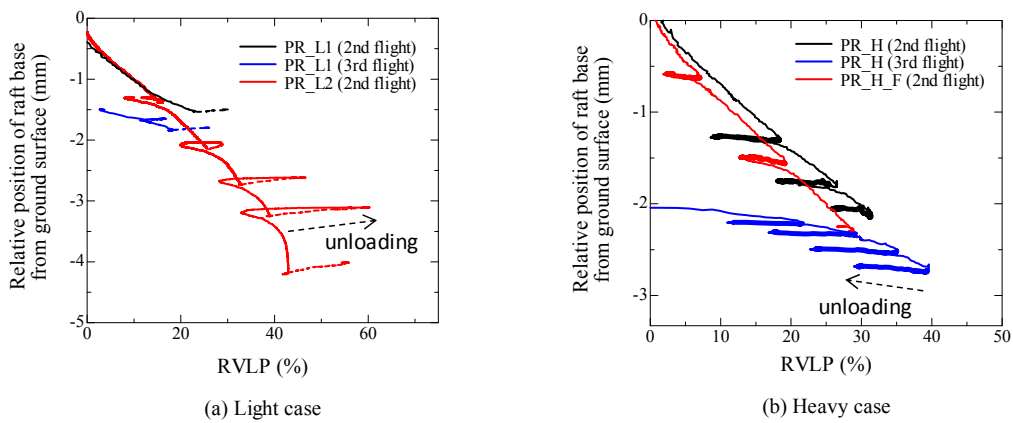
Figure 4.4.2.2 Variation of RVLP with settlement observed in pre-vertical loading process.

Figure 4.4.2.2 shows the relationship between the RVLP and the settlement s. The variation of the RVLP observed in the vertical loading process is also shown in the figure. As been seen, although the RVLP was already increased about 30% in the vertical loading process, the initial RVLP in the third flight decreased. Therefore, the RVLP increased again by applying the pre-vertical load by the two-ways actuator and it finally reached about 30% before the horizontal loading tests. The trend of the RVLP during the

unloading period was totally different between the light case and the heavy case. The reason for this was already explained in Fig. 4.3.2.2 and 4.3.3.3.

4.4.2.2 Vertical load carried by pile

The relatively large vertical load was imposed to the piled raft foundation to control the initial RVLP before the horizontal loading tests. However, applied vertical load on the pile part was almost same for both the piled raft and the pile group foundation as shown in Fig. 4.4.2.1 (b). Therefore, the different vertical load did not affected to the pile response of the piled raft and the pile group foundation. Next the safety factor of pile will be calculated. The safety factor of pile was calculated by dividing the maximum vertical load carried by the pile part P_{PV} during the pre-vertical load by the deadweight of the superstructure. The calculated safety factor of pile was 2.0 for the light case and 1.3 for heavy case. Therefore, it can be said that the piles in the heavy case was relatively weak pile.

Figure 4.4.2.3 shows the variation of the end bearing load and the shaft friction load with the settlement s. The end bearing load was smaller for the heavy case than the light case because the penetration depth in the flight was smaller for the heavy case as explained in Fig. 4.2.1.5. However, the relatively large settlement was imposed to the heavy case foundation, and the mobilized end bearing load was almost same for the light and heavy cases. Therefore, it can be said that the different mobilization of the end bearing load owing to the different penetration process can be reduced in the pre-vertical loading process. The shaft friction load was larger for the piled raft than the pile group due to the higher confined stress around pile.

(a) End bearing load   (b) Shaft friction
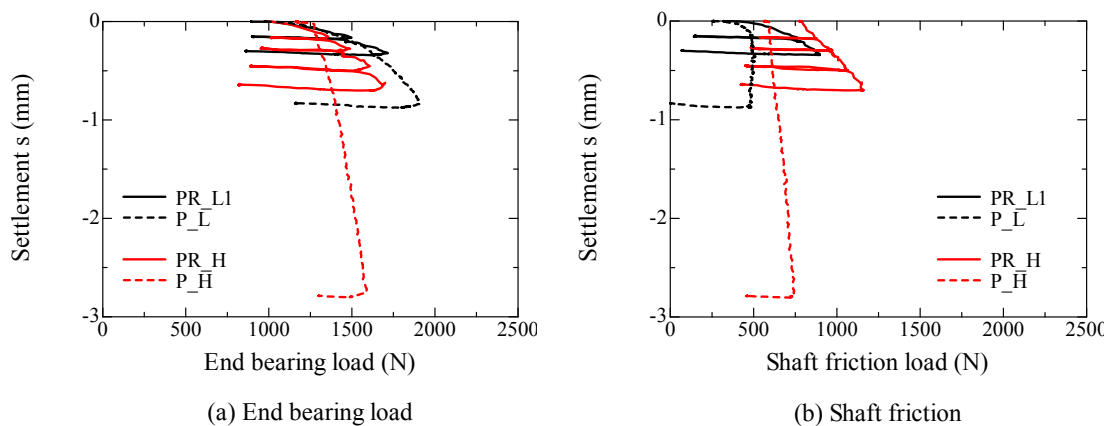
Figure 4.4.2.3 Relationship between pile load and settlement (a) end bearing load, (b) shaft friction load.
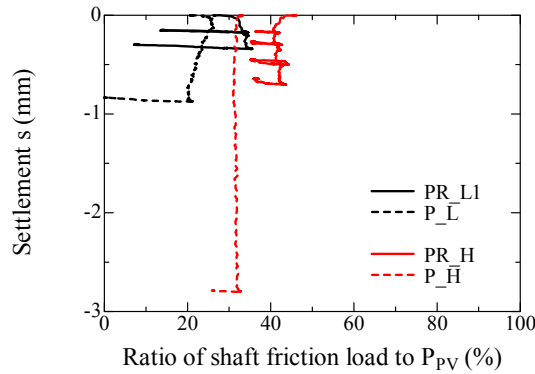
Figure 4.4.2.4 Relationship between ratio of shaft friction load to P$_{PV}$ and settlement s.

Figure 4.4.2.4 shows the relationship between the ratio of shaft friction load to the vertical load of the pile part *P$_{PV}$* and the settlement *s*. The ratio of the piled raft foundation was larger than that of the pile group foundation for both light case and the heavy case. And the ratio was higher for the heavy case than the light case. In the horizontal loading tests, the shaft friction initially dominated 30% of the pile bearing load.

(a) End bearing load

(b) Shaft friction load
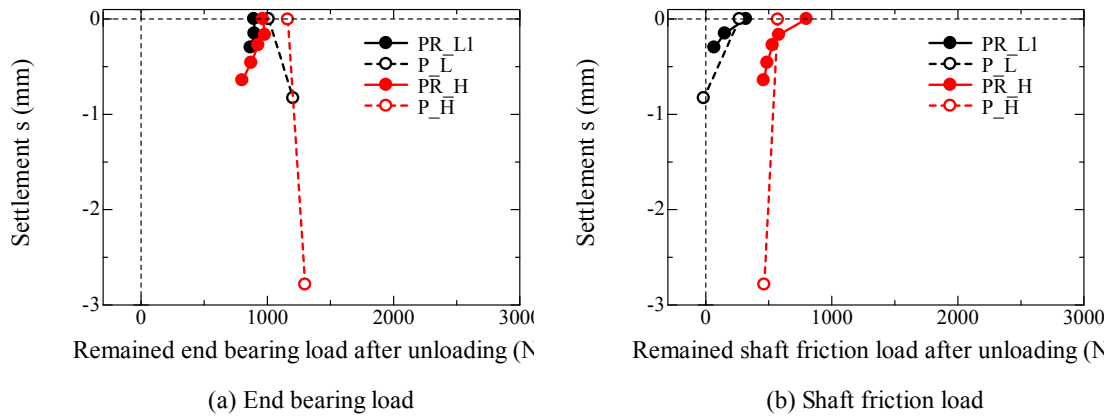
Figure 4.4.2.5 Variation of remained pile load after each unloading period with settlement s, (a) end bearing load, (b) shaft friction load.

Figure 4.4.2.5 shows variation of the remained end bearing load and shaft friction load with the settlement *s* after unloading. The remained end bearing and shaft friction loads during the pre-vertical loading process showed almost same trend as that observed in the vertical loading process (Fig. 4.3.3.3). The remained shaft friction load deceased with the loading procedures. In particular, the remained shaft friction load significantly decreased and reached almost zero for the light case. This was because the upward the

(a) PR_L1

(b) P_L

(c) PR_H

(d) P_H
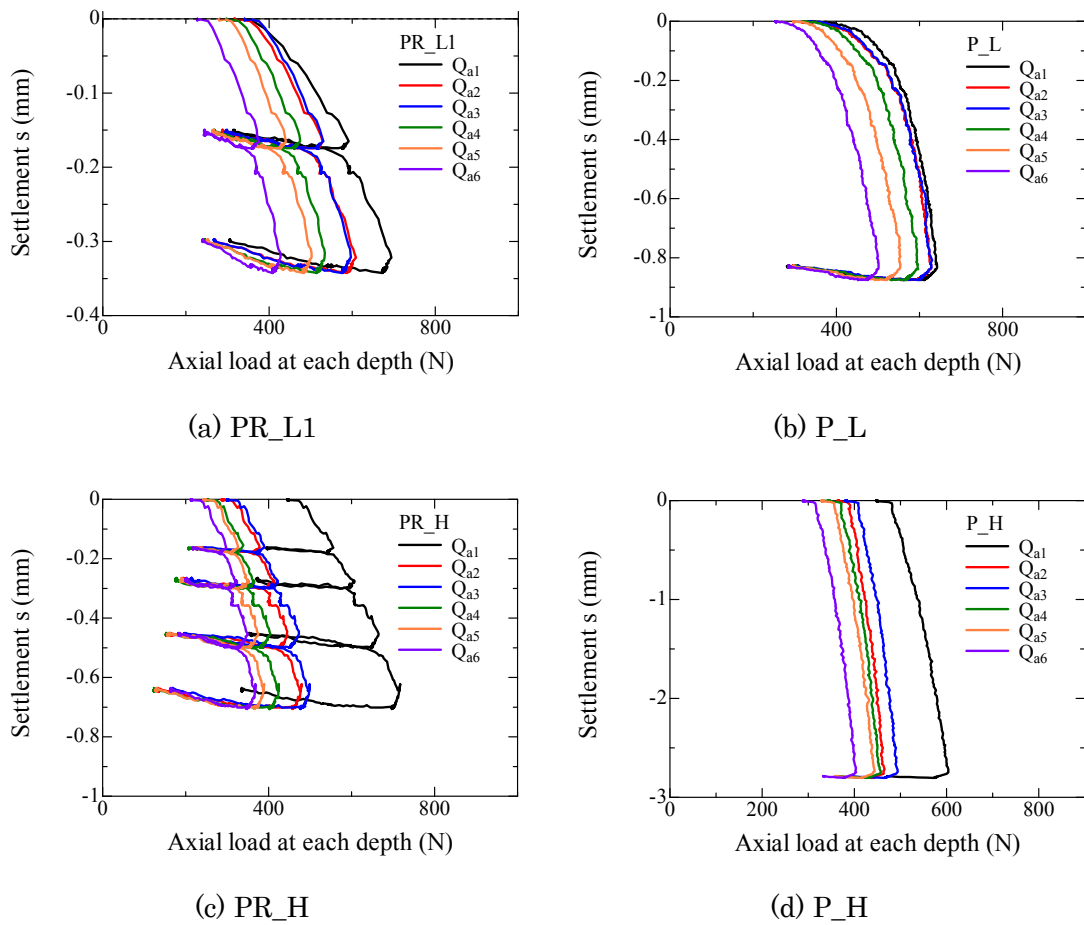
Figure 4.4.2.6 Variation of axial load at each depth Q_{an} with settlement s during pre-vertical loading process. (A. 4.4.2.2-4.4.2.5)

movement during the unloading was larger for the light case than the heavy case, and shaft friction load rapidly decreased during the unloading. The remained end bearing load was decreased for the piled raft foundation, and it increased for the pile group foundation, which implied that the pile in the piled raft foundation acted as the anchor and prevented the free heaving of the raft. Thus, the remained end bearing load and shaft friction load were larger for the heavy case than the light case. As a result, the RVLP increased and decreased during the unloading for the light case and the heavy case respectively as shown in Fig. 4.4.2.2.

Figure 4.4.2.6 shows the variation of the axial load at each depth Q_{an} with settlement s, where the Q_{an} is defined in Fig. 4.2.1.7. The axial load shown in the figure is the average of Pile 1 and Pile 2. The Q_{an} of Pile 1 and Pile 2, and increment of Q_{an} are summarized in Appendix (A. 4.4.2.2-4.4.2.5). The axial load increment is also shown in the figure. As been seen, the shallower was, the larger axial load was, because the

positive shaft friction was mobilized at the pile shaft. In particular, the heavy case showed the larger axial load at pile head compared with the light case, implying the

(a) PR_L1

(b) P_L

(c) PR_H

(d) P_H
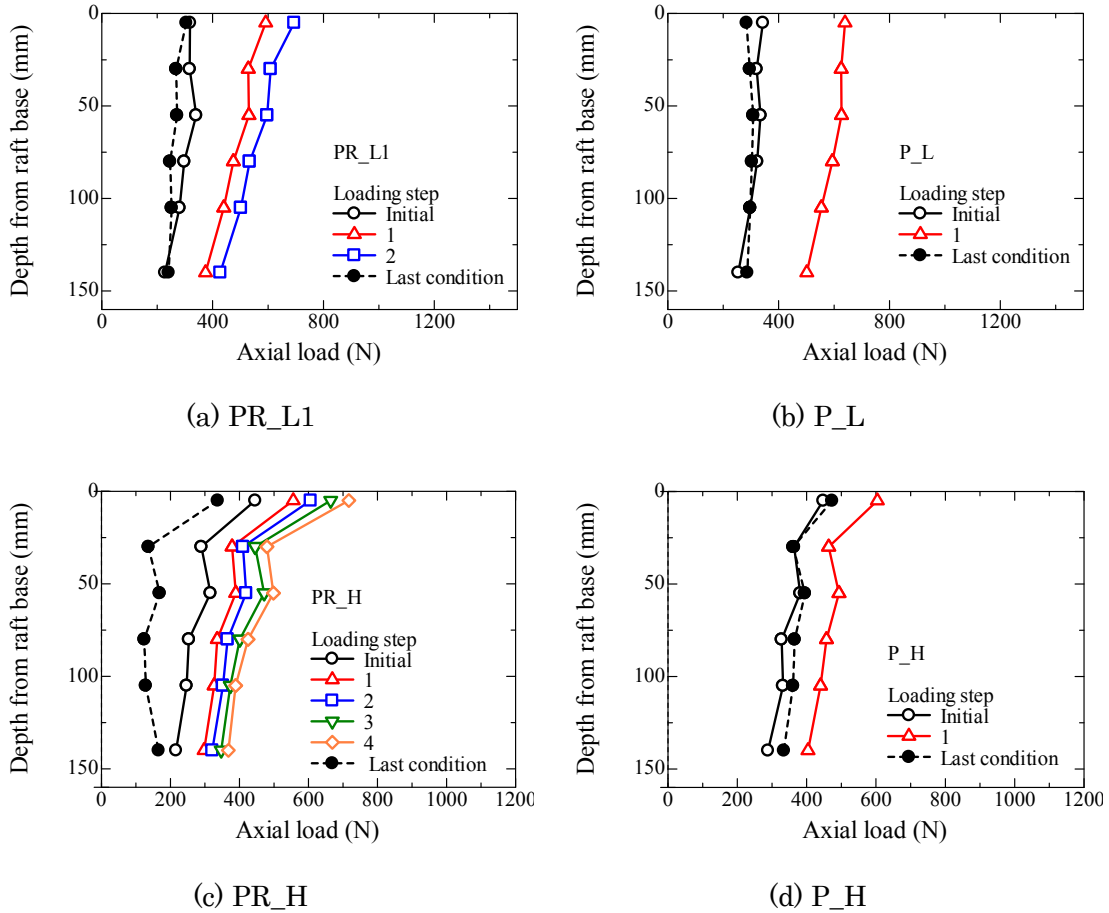
Figure 4.4.2.7 Profiles of axial load during pre-vertical loading process. (A. 4.4.2.6-4.4.2.9)

larger shaft friction at the pile head. Figure 4.4.2.7 shows the axial load profile at the each vertical loading step. The axial load drawn in this figure is the average value of Pile 1 and Pile 2. The profile of axial load increment and profiles of Pile 1 and Pile 2 are summarized in Appendix (A. 4.4.2.6-4.4.2.9). In the figure the profile of axial load just before the horizontal loading tests is also shown. Although the axial load was gently distributed with the ground depth for the light case, the profile of heavy case showed unique shape.

Figure 4.4.2.8 shows the variation of shaft friction load at each depth with the settlement *s*. The shaft friction load in the figure is the average of Pile 1 and Pile 2. The shaft friction load acting on each pile, Pile 1 and Pile 2, are shown in Appendix (A. 4.4.2.10-4.4.2.13). The increment of shaft friction is also shown in the Appendix. For the

pile group foundation, the shaft friction was almost constant with the settlement regardless the ground depth, implying that the shaft friction was fully mobilized in the

(a) PR_L1

(b) P_L

(c) PR_H

(d) P_H
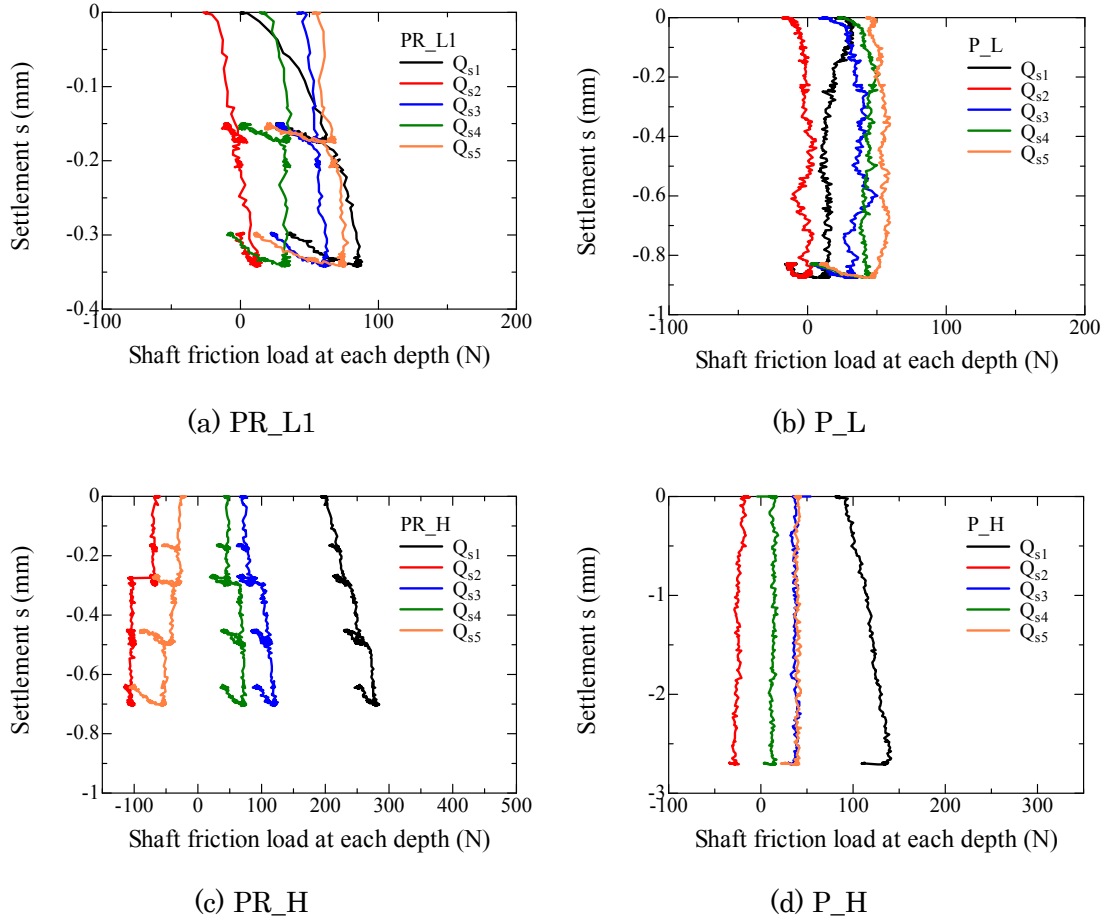
Figure 4.4.2.8 Variation of shaft friction load at each depth with settlement s during pre-vertical loading process. (A. 4.4.2.10-4.4.2.13)

pile group foundation. However, the shaft friction load gradually increased with the settlement for the piled raft foundation, especially at the shallower depth. Therefore, it can be said that the mobilized shaft friction load at pile head was totally different between the pile group and the piled raft before the horizontal loading tests. Figure 4.4.2.9 shows the shaft friction profile at the peak of each loading step. The profile just before the horizontal loading test was also shown in the figure. The shaft friction here is the average of Pile 1 and Pile 2. The increment of shaft friction from beginning of the pre-vertical loading is summarized in Appendix (A.4.4.2.14-4.4.2.17). The larger shaft friction was mobilized near the raft base compared with the pile group foundation.

(a) PR_L1

(b) P_L

(c) PR_H

(d) P_H
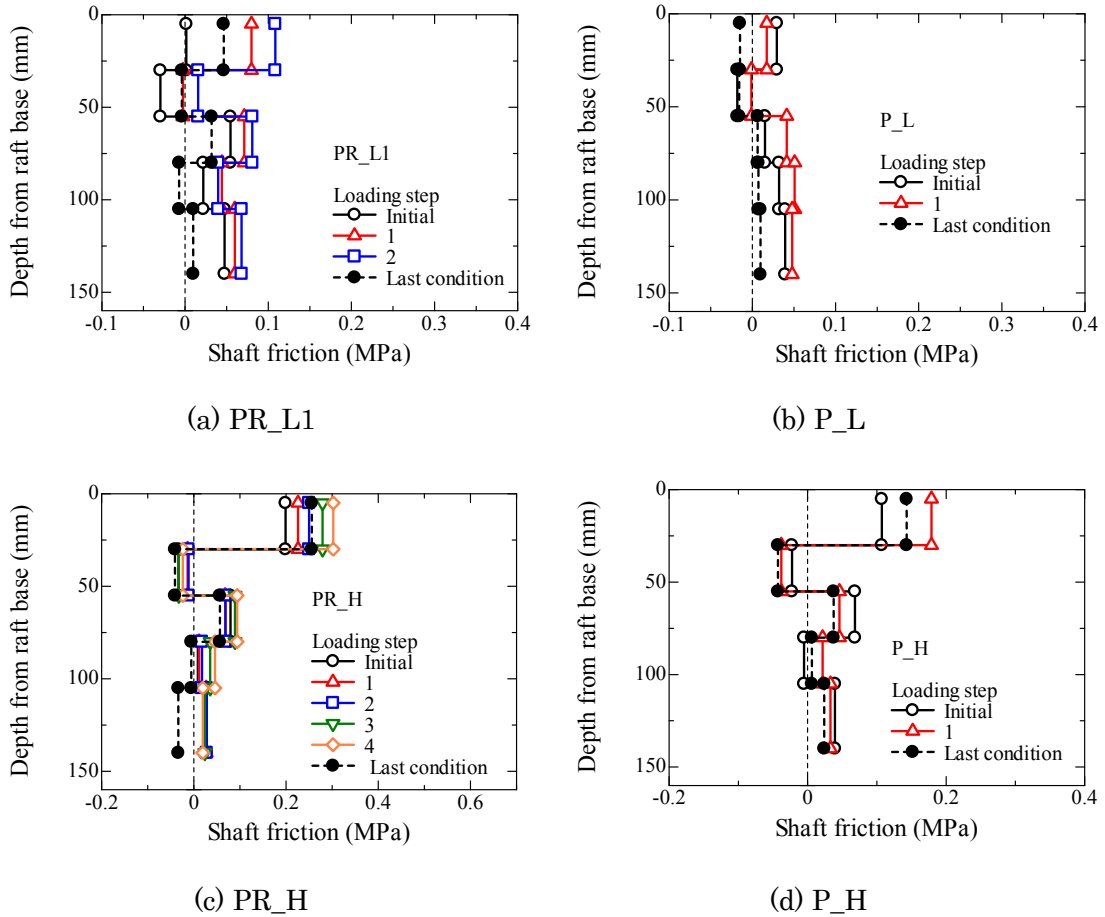
Figure 4.4.2.9 Profiles of shaft friction during pre-vertical loading process. (A. 4.4.2.14-4.4.2.17)

4.5 Summary

The piled raft foundation subjected to vertical load was examined in the present chapter. The foundations experienced the three vertical loading processes such as the penetration process, the vertical loading process and the pre-vertical loading process before the horizontal loading tests. It was crucial to clarify the initial conditions of the foundations before the horizontal loading tests. Therefore, the main objectives of the present chapter was not only to examine the mechanical behavior of the piled raft foundation subjected to vertical load but also to verify the initial conditions of the foundation before the horizontal loading tests. Followings are the findings in this chapter.

The piled raft foundation showed higher vertical resistance than the pile group

foundation, which was attributed to the mobilized resistance of the raft part and the increase of the vertical resistance of the pile part.

Initially the coefficient of the subgrade reaction of raft part in the piled raft foundation was relatively smaller than that of the raft foundation because the contact condition between the raft base and the ground was poor. However, it increased with the settlement, in other words, the vertical load carried by the raft part.

The vertical resistance of the pile part in the piled raft was higher than that of the pile group due to the influence of raft base pressure on the pile response. There was no influence of the raft base on the ultimate end bearing load and the coefficient of the subgrade reaction of end bearing load. On the other hand, the raft base pressure enhanced the ultimate shaft friction load and the coefficient of the subgrade reaction of shaft friction. The additional shaft friction load had a linear relationship with the base pressure, and it can be simply estimated using elastic theory.

The proportion of the vertical load carried by the raft part (RVLP) can be controlled by applying the vertical load. The almost same RVLP of 30% was prepared for the piled raft cases by applying the vertical load before the horizontal loading tests.

The variation of the RVLP depended on the vertical load of the foundation. The piles in the piled raft acted a kind of anchor and prevented the free-heaving of the raft part during the unloading. This anchoring effect can be clearly seen for the piled raft with small vertical load of the foundation. Therefore, the RVLP increased during the unloading for the piled raft with small vertical load.

CHAPTER 5

MECHANICAL BEHAVIOR OF PILED RAFT SUBJECTED TO HORIZONTAL AND MOMENT LOADS

5.1 Introduction

In this chapter the behavior of the piled raft foundation subjected to horizontal and moment loads will be discussed. Much focus is placed on the influence of the raft base pressure on the pile response. Firstly the test conditions such as the applied horizontal displacement applied load will be simply presented, and then the settlement behavior which significantly affects the horizontal and moment resistances of the piled raft foundation. Finally the mechanical behavior of the piled raft foundation subjected to horizontal and moment loads will be examined in detail.

5.2 Test condition of each alternate loading step

Figure 5.2.1 and 5.2.2 show the time histories of the applied horizontal displacement δ_{LDT}, the applied horizontal load P_L and the total axial load at pile head during the horizontal loading tests for light case and heavy case respectively. The axial load at right pile head and left pile head is also shown in the figure. The red number in the loading step represents the loading step with the high loading height of h/S=1.8 and black number represents the low loading height of h/S=1. The details of horizontal loading procedures were already explained in Section 3.5.3.2. Because the horizontal loading tests were manually controlled, there were slight differences in the applied horizontal displacement between cases. The right pile and left pile were alternately pushed in and pulled out during the tests. The left pile was pushed in during the odd number loading step, and it was pulled out during the even number loading step. The total axial load varied during the loading, and it reached different value from the beginning.
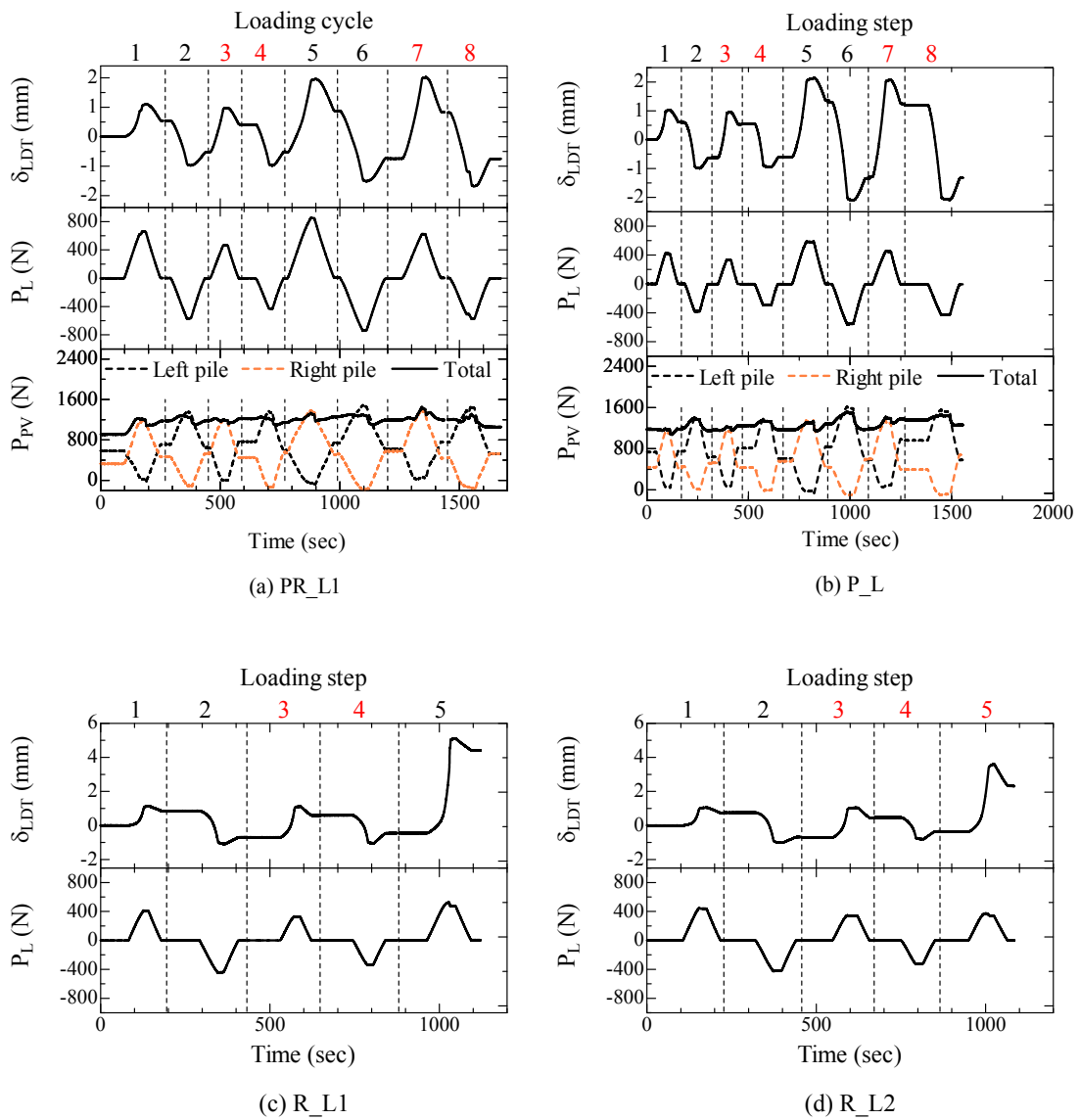
Figure 5.2.1 Applied horizontal displacement at lower LDT δ_{LDT}, applied horizontal load P_L and measured axial load at pile head P_{PV} for light case.

(a) PR_H

(b) P_H

(c) R_H1

(d) R_H2
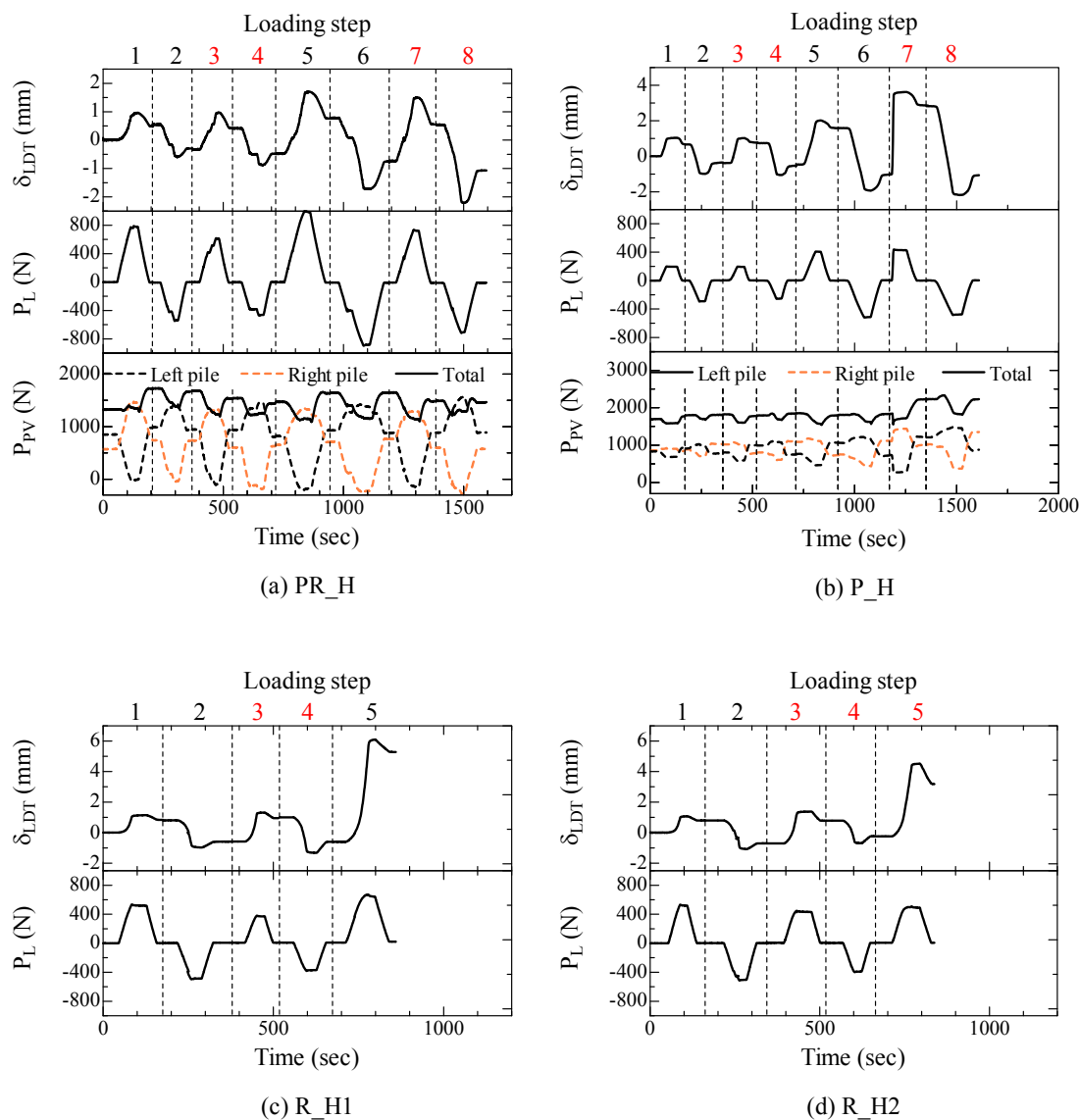
Figure 5.2.2 Applied horizontal displacement at lower LDT δ_{LDT}, applied horizontal load P_L and measured axial load at pile head P_{PV} for heavy case.
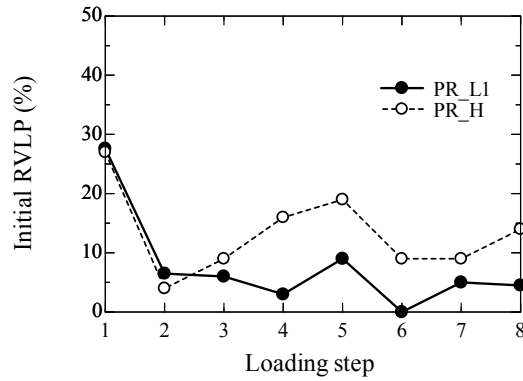
Figure 5.2.3 Initial RVLP for each loading step at each loading step.

Figure 5.2.3 shows the initial RVLP (Raft vertical load proportion) at each loading step. The same RVLPs of 30% were prepared for both light and heavy cases by applying the vertical load to the foundation before the horizontal loading tests. Similar method was employed in the researches done by Tsuchiya et al. (2003); Nagai and Tsuchiya (2004). In the research done by Tsuchiya et al. (2003) the RVLP was controlled by pulling out the foundation, and in the research carried by Nagai and Tsuchiya (2004) the RVLP of 50% was prepared by putting the soil bags on the foundation. The initial RVLP was different at each loading step because the total axial load at pile head varied during the loading as explained above. In particular, the large reduction of RVLP can be observed in the first loading step. This was probably because the effects of pre-vertical load were diminished. As explained in Section 4.4.2.2, the piles acted as a kind of anchor and prevented the free heaving of the raft after the pre-vertical load was applied. This anchoring effect of piles was decreased by the disturbance of soil around pile due to the horizontal loading, and the RVLP was therefore significantly decreased in the first loading step. However, the initial RVLPs in trailing loading step were almost constant, which was 5% for light case (PR_L1) and 15% for heavy case (PR_H). From these observed fact, it can be said that the effect of pre-vertical load such as increased RVLP of the piled raft was diminished in the first loading, and the RVLP in following loading was determined by the conditions of soil, piles, superstructure and pile preparation process. It was also noted that the contact condition between the raft base and the ground was better for the heavy case than the light case due to the larger RVLPs of heavy case, and therefore the larger contribution of the raft can be expected.

5.3 Settlement caused by alternate horizontal loading

5.3.1 Average settlement of foundation

Figure 5.3.1.1 and 5.3.1.2 shows the relationship between the horizontal displacement

(a) PR_L1   (b) All light cases
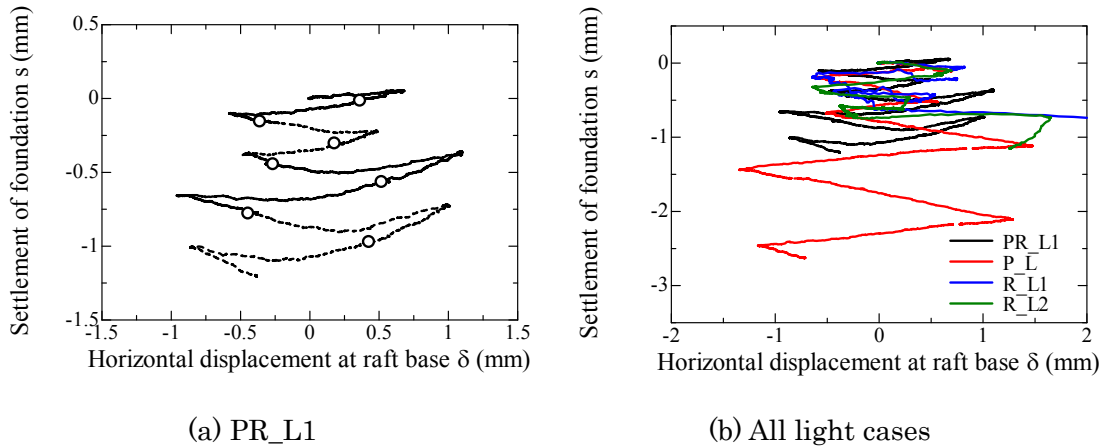
Figure 5.3.1.1 Relationship between horizontal displacement at raft base δ and settlement s for light case. (A.5.3.1.1)

(a) PR_H   (b) All heavy cases
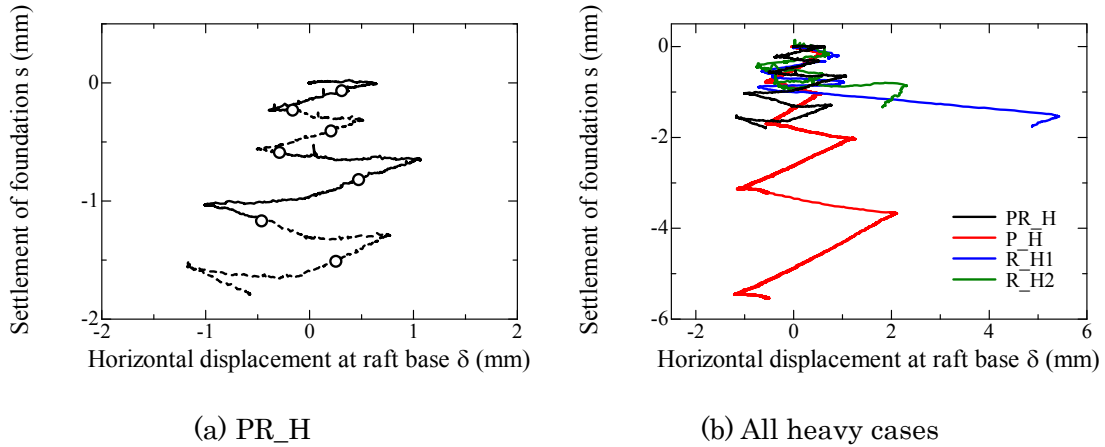
Figure 5.3.1.2 Relationship between horizontal displacement at raft base δ and settlement s for heavy case. (A.5.3.1.2)

at raft base δ and settlement s for light case and heavy case respectively. The settlements observed in the pile group and raft foundations are shown in Appendix (A. 5.3.1.1, 5.3.1.2). The open marks in the figure represent the initial state of each loading step. The solid line and broken line stand for the results with loading height of h/S=1 and 1.8 respectively. The settlement of the pile group foundation linearly increased with horizontal displacement, and the trend of settlement behavior of the piled group foundation were almost same between the loading height of h/S=1 and 1.8. For the raft foundation, although the settlement with loading step of h/S=1 also linearly increased with the horizontal displacement, the non-linear relationship of the settlement can be seen for h/S=1.8. That is, the settlement increased with horizontal displacement at small displacement range, and the trend of the settlement decreased or slightly moved upward at large displacement. The piled raft foundation also showed the nonlinearity of the settlement. The foundation settled down at the small horizontal displacement, but the

foundation moved upward at the large horizontal displacement.
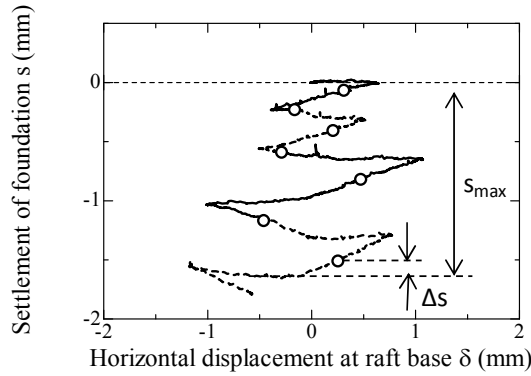
Figure 5.3.1.3 Definition of s_{max} and Δs.

(a) s_{max} (b) Δs
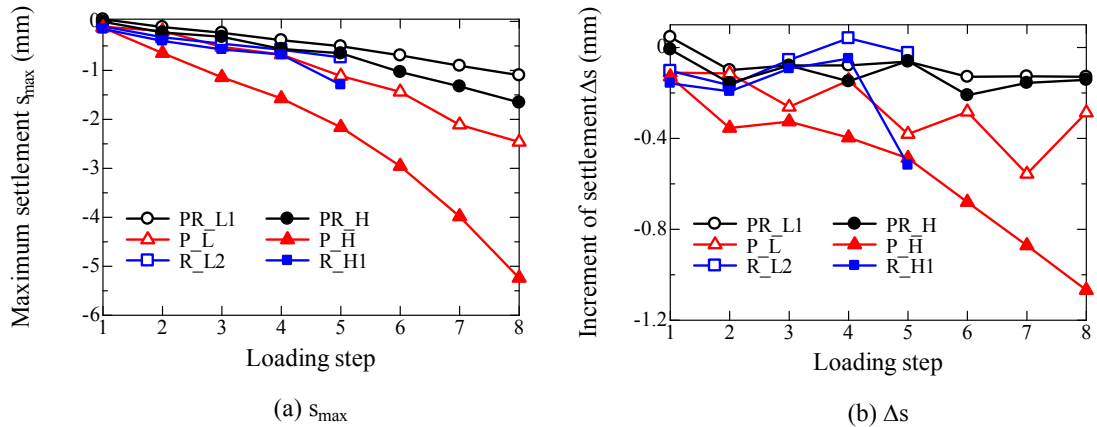
Figure 5.3.1.4 Observed settlement in each loading step.

Figure 5.3.1.4 shows observed s_{max} and Δs at each loading step. The s_{max} and Δs were defined in the Fig. 5.3.1.3. The s_{max} is the maximum settlement during the loading and Δs is the increment of settlement from the beginning of each loading. From this figure, it can be confirmed that the piled raft foundation can restrain the settlement caused by the alternate horizontal loading by the existing of the raft. This could be verified by the smaller settlement of the raft foundation than that of the pile group foundation. The larger settlement was observed in the heavy case compared with the light case for all foundation types. This larger settlement of heavy case secured the larger initial RVLP in each loading step for PR_H as shown in Fig. 5.1.3. In particular, the settlement of P_H was significantly larger than that of other case due to relatively small safety factor of pile (F_S=1.5). Look at the settlement increment Δs, it was gradually increased with the loading step procedures. This was probably because the soil around piles was disturbed

138

by the loading, and the settlement of the foundation gradually increased. On the other hand, the almost constant Δs was observed for the piled raft and raft foundations with the loading step procedures. Piles in the piled raft foundation also easily settled down with the loading procedures, however, the raft part prevented the excessive settlement resulting in the constant Δs. The R_H1 showed larger settlement at the loading step 5 because large horizontal displacement of about 5mm was applied to the raft foundation in loading step 5. However, the R_L2 can restrain the settlement in the loading step 5 because the smaller settlement of the raft foundation was arose for the higher loading height as explained above.

Figure 5.3.1.5 shows the variation of the normalized settlement by that of the pile group foundation and normalized settlement by that of the light case with loading step. The piled raft foundation can restrain the settlement due to alternate horizontal loading by the half of the pile group foundation. Particularly, the settlement at the first loading step was significantly reduced for the piled raft foundation because the RVLP, in other words, the contribution of the raft was larger in the first loading step. Nagao et al. (2002) also reported that the piled raft foundation can restrain the settlement caused by the horizontal loading compared with the pile group foundation.

(a) Normalized by pile group   (b) Normalized by light case
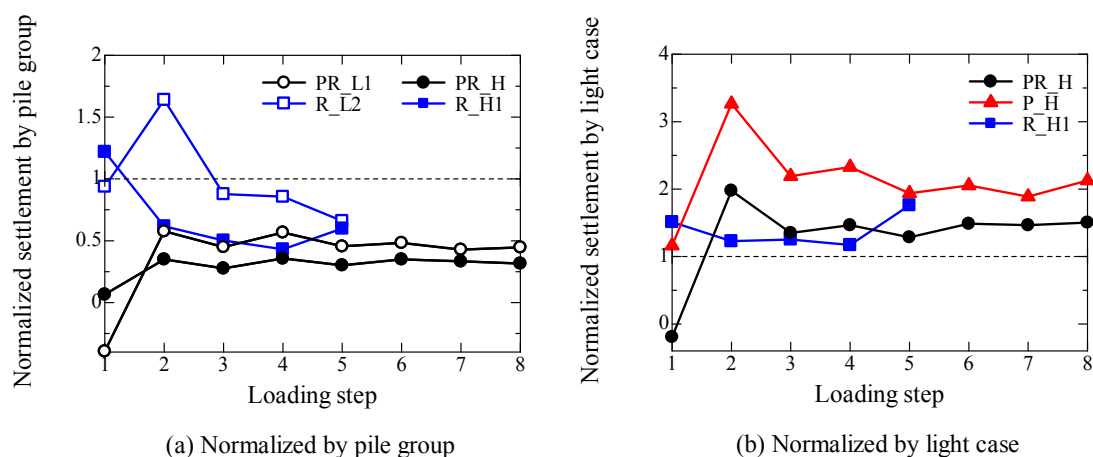
Figure 5.3.1.5 Normalized settlement in each loading step.

5.3.2 Settlement of push-in and pull-out piles

Figure 5.3.2.1 and 5.3.2.2 shows relationship between the horizontal displacement of the raft base δ and the settlement of the left pile for the light case and heavy case respectively. The settlement behavior of the right pile is shown in Appendix (A. 5.3.2.1,
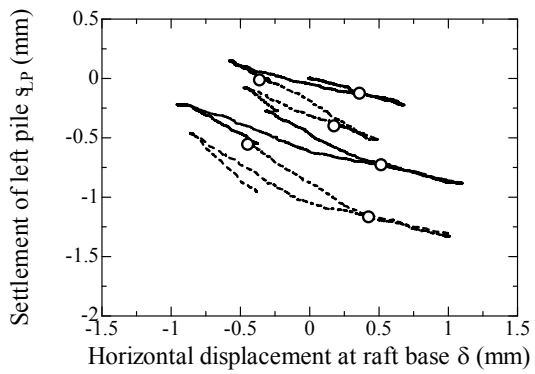
(a) PR_L1
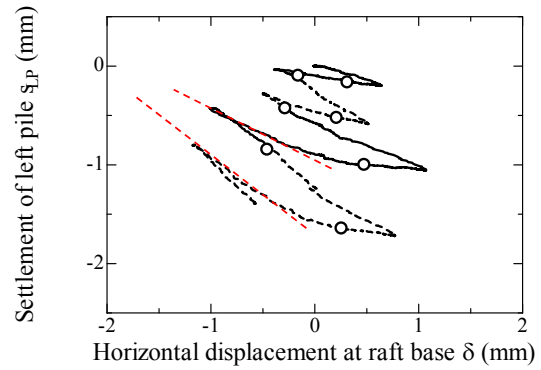
(a) PR_H
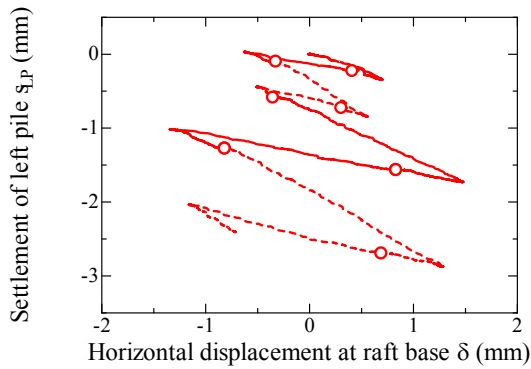
(b) P_L
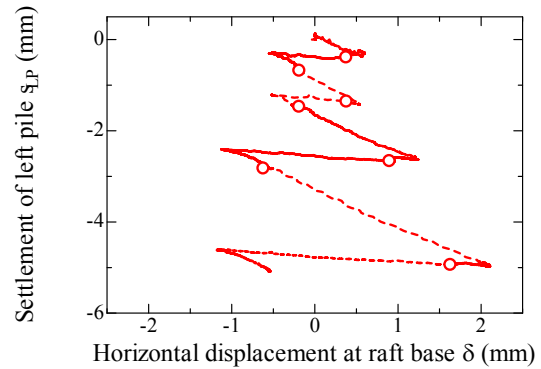
(b) P_H
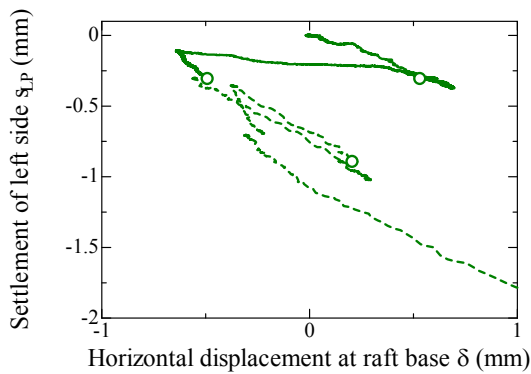
(c) R_L2
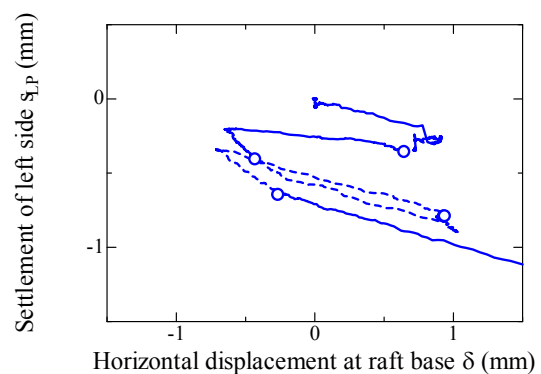
(c) R_H1

Figure 5.3.2.1 Relationship between horizontal displacement at raft base δ and settlement of righ pile s_{RP} and left pile s_{LP} for light case. (A. 5.3.2.1)

Figure 5.3.2.2 Relationship between horizontal displacement at raft base δ and settlement of righ pile s_{RP} and left pile s_{LP} for heavy case. (A. 5.3.2.2)

5.3.2.2). Open marks in the figure represents the beginning of each loading step, and the solid line and broken line stand for the result of the loading step with h/S=1 and 1.8 respectively. The left pile was pushed in first, and the right pile was pulled out in the first loading step. The pile group foundation showed the linear relationship between the

140

settlement and the horizontal displacement. The settlement of the push-in pile was larger than the upward movement of the pull-out pile for the pile group foundation. It was also noted that the trend of the settlement of the pile group foundation was almost same between h/S=1 and 1.8, that is, the loading height had no influence on the settlement behavior.

For the raft foundation, although the settlement of the push-in side was larger compared with the upward displacement of the pull-out side for lower loading height (h/S=1), the upward displacement of pull-out side became larger for the higher loading height (h/S=1.8) and it reached almost same as the settlement of push-in side. From this fact, it can be confirmed that the loading height affected on the settlement behavior of the raft foundation. The upward movement of the pull-out side was critical issues under relatively high loading height, in other words, the relatively large moment load with the horizontal load.

For the piled raft foundation the push-in pile settled down with the small horizontal displacement range, however, the trend of settlement became to be small. This was because the raft part prevented the excessive settlement in the push-in side. By contrast, although the upward movement of the pull-out pile was relatively small at the small horizontal displacement, it rapidly increased at the large horizontal displacement. Therefore, it was seemed that the base contact pressure rapidly decreased at the pull-out side during the horizontal loading tests. The larger upward movement of pull-out pile was because the smaller settlement of the push-in pile at large horizontal displacement enhanced the upward movement of the pull-out piles. As a result, the settlement of the piled raft foundation showed nonlinear settlement behavior as shown in Fig. 5.3.1.1 and 5.3.1.2. It should be also noted that the higher loading height was, the large upward movement of pull-out pile was, as pointed by broken line. Thus, the settlement behavior of the piled raft at relatively large horizontal displacement was similar with that of the raft foundation, implying that the influence of the raft part became larger for the large horizontal displacement.

Figure 5.3.2.4 shows the settlement increment of push-in pile Δs_{PI}, and settlement increment of pull-out pile Δs_{PI} for each loading step. The Δs_{PI}, and Δs_{PO}, are the increment from beginning of each loading step as defined in Fig. 5.3.2.3. The rotation of the foundation was determined from Δs_{PI}, and Δs_{PO}, as following equation.

$$\text{Rotation of foundation: } \theta = (\Delta s_{PI} - \Delta s_{PO})/S \qquad (5.3.2.1)$$

where S is pile spacing.
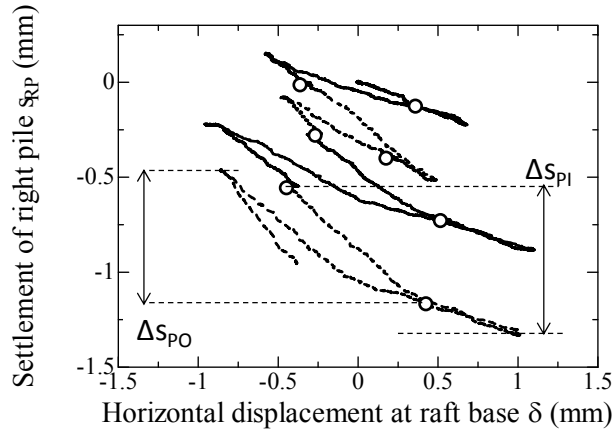
Figure 5.3.2.3 Definition of Δs_{PI} and Δs_{PO}.
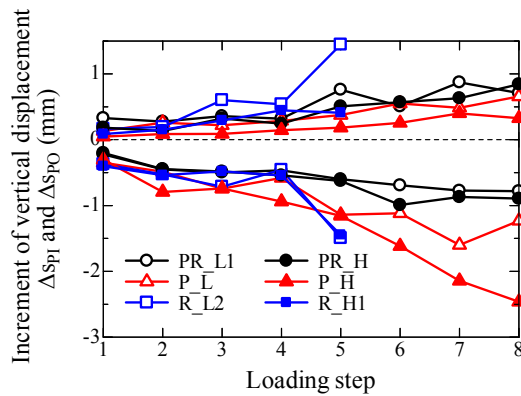
Figure 5.3.2.4 Increment vertical displacements Δs_{PI} and Δs_{PO} observed in each loading step.

In the loading step 5 for the raft foundation, the horizontal load was applied at h/S=1.8 for R_L2 and it was applied at h/S=1.8 for R_H1. The larger settlement of the raft foundation was observed in the loading step 5 because large displacement of 5mm was imposed to the foundation in this loading step as shown in Fig. 5.1.1 and 5.1.2. The almost same settlement of push-in side was observed for R_L2 and R_H1, implying that the loading height had no influence on the settlement of push-in side. However, although the upward movement of R_H1 was quite small, that of R_L2 was large. Look at the settlement in the push-in pile, the piled raft foundation can restrain the settlement compared with the pile group foundation due to the existing of raft part. And, the settlement of push-in pile was larger for the heavy case than the light case. However, the vertical displacement of pull-out pile showed totally different tendencies from that of

push-in pile. That is, the upward movement was larger for the piled raft foundation than the pile group foundation, and was larger for the light case than the heavy case.

Figure 5.3.2.5 shows the ratio of settlement increment of push-in pile Δs_{PI} to the settlement increment of pull-out pile Δs_{PI}. The rotation of the foundation was determined by them as explained in eq.(5.3.2.1), and therefore this ratio examine the influence of vertical displacement of push-in and pull-out piles on the rotation. From this figure, it can be said that the settlement of push-in pile was significantly large for P_H, and it was the dominant factor for the rotation of the foundation. The P_L also showed relatively large settlement of push-in pile, and therefore the upward displacement of pull-out pile was relatively dominant factor in the rotation for the piled raft foundation. Thus, the piled raft foundation can restrain the settlement of push-in pile, whereas the upward displacement of pull-out pile might be critical issues under relative large moment load with the horizontal load for the foundation design.
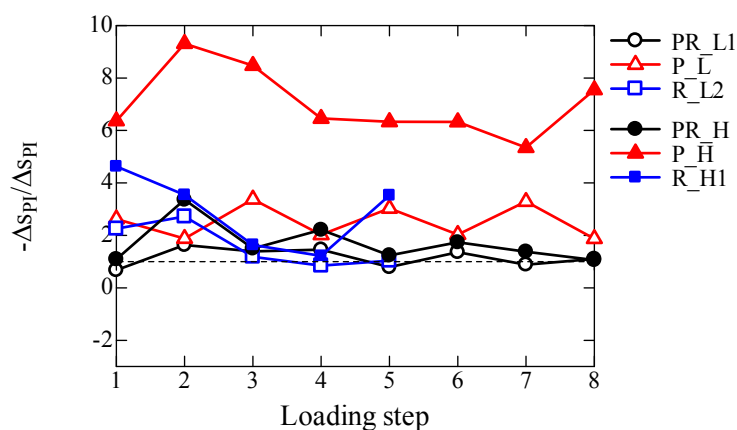
Figure 5.3.2.5 Ratio of Δs_{PI} to Δs_{PO} in each loading step.

5.4 Horizontal resistance of piled raft

5.4.1 Overall resistance of piled raft

Figure 5.4.1.1 and 5.4.1.2 show the relationship between the horizontal displacement at raft base δ and the horizontal load P_L for light case and heavy case respectively. Comparing the different loading height, the horizontal load was larger for h/S=1 than that for h/S=1.8 because the relative large moment load with the horizontal load was applied to the foundation for h/S=1.8. Figure 5.4.1.3 shows the relationship between the horizontal displacement at raft base δ and the horizontal load P_L observed in each loading step. Although the raft foundation showed higher horizontal resistance at small horizontal displacement range, the horizontal resistance was almost constant at the

(a) PR_L1

(b) P_L

(c) R_L1

(d) R_L2
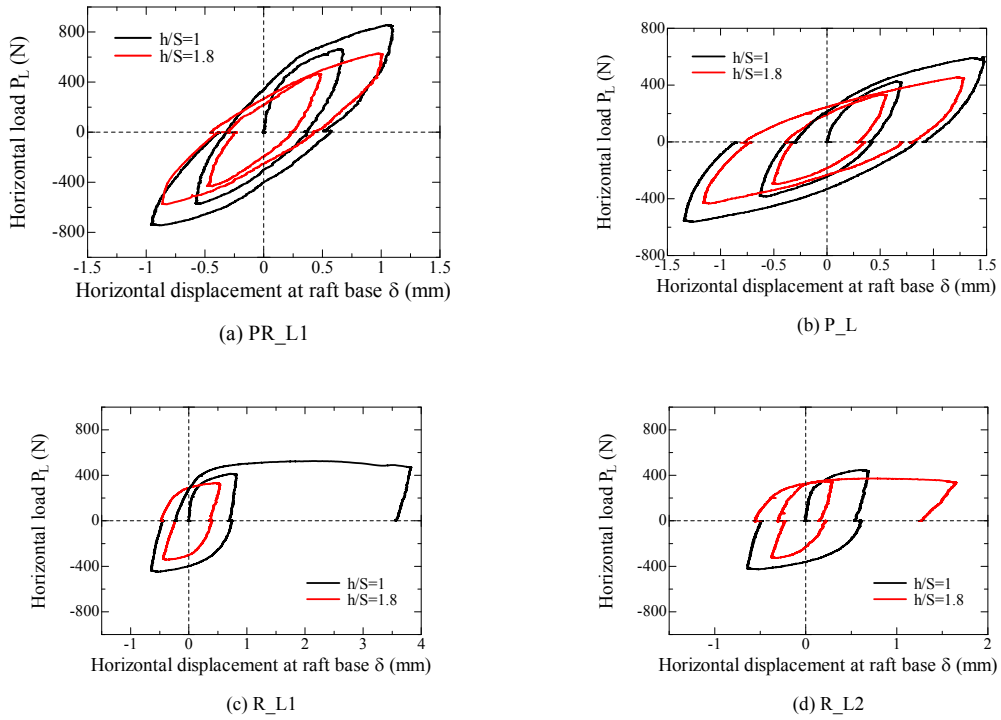
Figure 5.4.1.1 Relationship between horizontal displacement at raft base δ and horizontal load P_L for light case.

(a) PR_H

(b) P_H

(c) R_H1

(d) R_H2
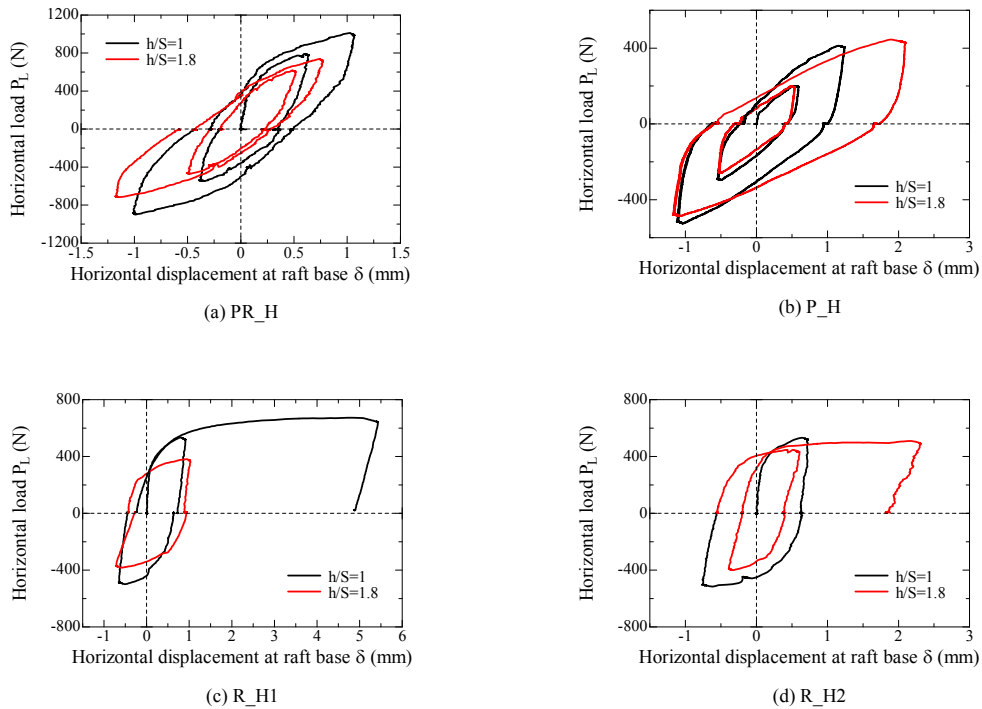
Figure 5.4.1.2 Relationship between horizontal displacement at raft base δ and horizontal load P_L for heavy case.

(a) $\delta_{LDT}=\pm 1mm$, h/S=1

(b) $\delta_{LDT}=\pm 1mm$, h/S=1.8

(c) $\delta_{LDT}=\pm 2mm$, h/S=1

(d) $\delta_{LDT}=\pm 2mm$, h/S=1.8
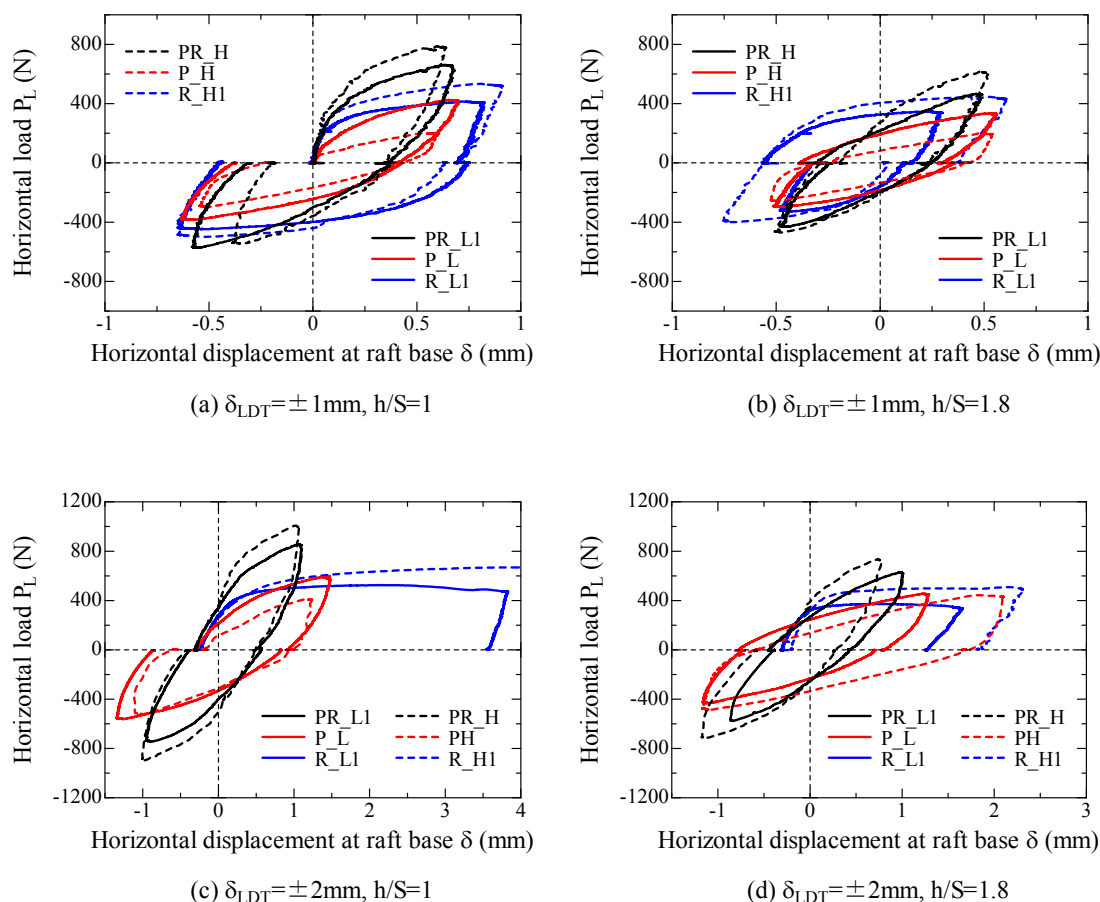
Figure 5.4.1.3 Relationship between horizontal displacement at raft base δ and horizontal load P_L.

large displacement, showing the clear failure of the foundation. On the other hand, the horizontal resistance of the pile group foundation was relatively small at the small displacement. However, it gradually increased with the displacement, and the larger horizontal resistance was observed for the pile group than the raft foundation. The piled raft foundation showed higher horizontal resistance than the pile group regardless the loading height and horizontal displacement range. This kind of unique response of each foundation was also reported by Nagao et al. (2002), Mano et al. (2003), Horikoshi et al. (2003a), Tsuchiya et al. (2003) and Matsumoto et al. (2010). Particularly Nagao et al. (2002) and Tsuchiya et al. (2003) reported that the piled raft foundation showed higher horizontal resistance than the total resistance of the raft foundation and the pile group foundation at the relatively large horizontal displacement due to the influence of the influence of the raft base pressure on the pile response.

Figure 5.4.1.5 shows the relationship between the increment of the horizontal displacement at the raft base $\varDelta\delta$ and the increment of the horizontal load $\varDelta P_L$ for

145
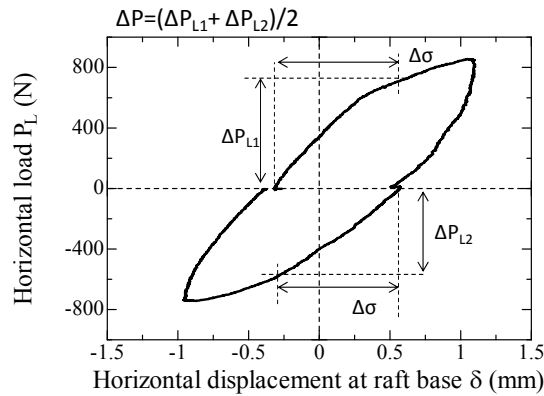
Figure 5.4.1.4 Definition of horizontal load increment ΔP and horizontal displacement increment Δδ.
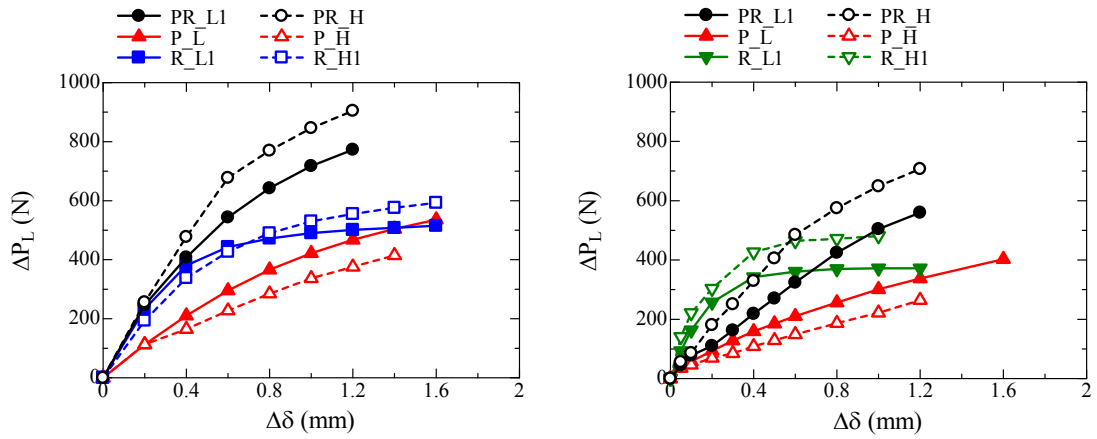
(a) δ_{LDT}=±2mm, h/S=1　　　　　　(b) δ_{LDT}=±2mm, h/S=1.8

Figure 5.4.1.5 Relationship between Δδ and ΔP$_L$ observed in δ_{LDT}=±2mm, h/S=1, 1.8. (A. 5.4.1.1)

δ_{LDT}=±2mm, h/S=1 and 1.8. The results from other loading steps are summarized in Appendix (A.5.4.1.1). The *Δδ* is the increment of the horizontal displacement from the beginning of loading step, and *ΔP$_L$* is average horizontal resistance for the positive and negative direction at the specific horizontal displacement of the raft base Δδ as defined in Fig. 5.4.1.4. As mentioned above, the raft foundation showed larger horizontal resistance at the small horizontal displacement, which was almost equivalent to the piled raft foundation. However, there was clear failure point in the raft foundation, resulting in the constant horizontal resistance at the large horizontal displacement. The horizontal resistance was larger for the heavy case than the light case because the larger base resistance was obtained in the heavy case. From this figure, the coefficient of friction between the raft base and the ground *μ* can be estimated by dividing the ultimate horizontal resistance of the raft foundation by vertical load of the foundation. The calculated *μ* was almost 0.4 for both light and heavy cases. According to Specifications for highway bridges, the coefficient of friction between the concrete slab and the sandy

soil is assumed 0.6. Nagao et al. (2002) and Tsuchiya et al. (2003) verified that the coefficient of interface friction was almost 0.6 for the concreted slab. The almost same coefficient of interface friction of 0.4 was observed in Horikoshi et al. (2003a, b), in which the raft base was scratched by the file. On the other hand, the relatively larger coefficient of friction of 0.7 was observed in Mano et al. (2002, 2003), in which the sand was glued on the raft base.

Although the horizontal resistance of the pile group foundation was smaller than the raft foundation at small displacement, it was larger for the pile group than the raft foundation at the large displacement. Unlike the raft foundation, the horizontal resistance of the pile group foundation was higher for the light case than the heavy case. This was because the safety factor of pile was smaller for the heavy case (Fs=2.1 for light case and Fs=1.5 for heavy case) as explained in Chapter 3, and therefore the piles in the heavy case could be said weak pile. The horizontal resistance of the piled raft foundation was almost same as that of the pile group at the small horizontal displacement, however, the clear failure like the raft foundation was not observed, resulting in higher horizontal resistance than the pile group and the raft foundations at the large displacement. As for the piled raft foundation, the piles in the piled raft was also weaker for the heavy case than the light case due to small safety factor of pile, but mobilized horizontal resistance of the piled raft foundation was larger for heavy than the light case. The reason for this will be discussed latter.

(a) δ_{LDT}=±2mm, h/S=1 　　　　　　　(b) δ_{LDT}=±2mm, h/S=1.8
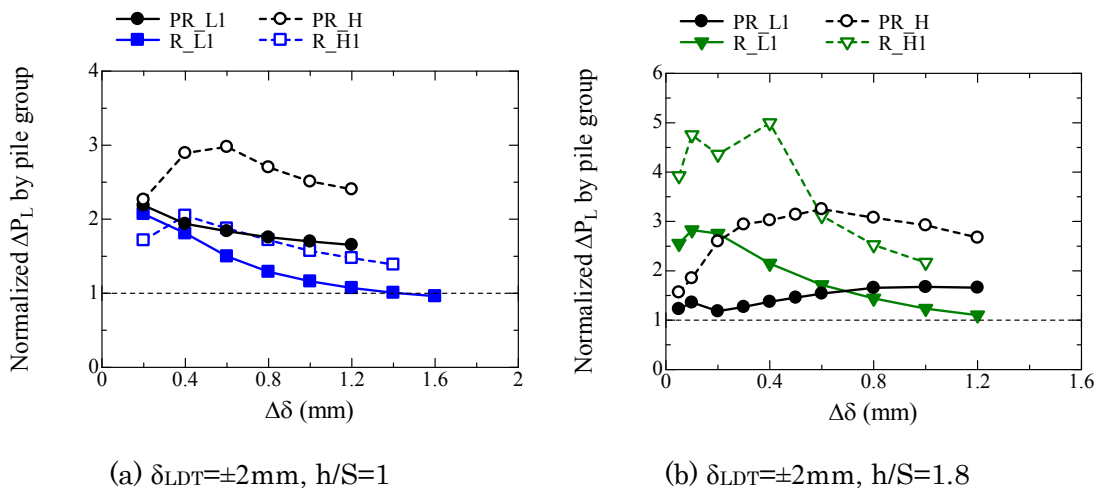
Figure 5.4.1.6 Relationship between $\Delta\delta$ and normalized ΔP_L by that of pile group forδ_{LDT}=±2mm, h/S=1, 1.8. (A. 5.4.1.2)

Figure 5.4.1.6 shows the relationship between $\Delta\delta$ and normalized ΔP_L by that of the pile group foundation for the loading step of δ_{LDT}=±2mm, h/S=1 and 1.8. The results from

other loading steps are summarized in Appendix (A. 5.4.1.2). This normalized horizontal resistance represents the ratio of horizontal resistance to that of the pile group. The horizontal resistance of the raft foundation was larger at small displacement, but the ratio gradually decreased with the displacement. The piled raft showed higher resistance than the pile group, especially for the heavy case.

Figure 5.4.1.7 shows $\Delta\delta$ and normalized ΔP_L of heavy case by that of the light case for the loading step of $\delta_{LDT}=\pm2$mm, h/S=1 and 1.8. The results from other loading steps are summarized in Appendix (A. 5.4.1.3). The P_L having the large safety factor of pile showed larger horizontal resistance than P_H. On the other hand, the larger horizontal resistance was observed for heavy case than the light case in the raft foundation. The piles in the piled raft was also weaker for the heavy case than the light case due to small safety factor of pile, but mobilized horizontal resistance of the piled raft foundation was larger for heavy than the light case because the larger contribution of the raft part can be obtained as explained latter.

(a) δLDT=±2mm, h/S=1   (b) δLDT=±2mm, h/S=1.8
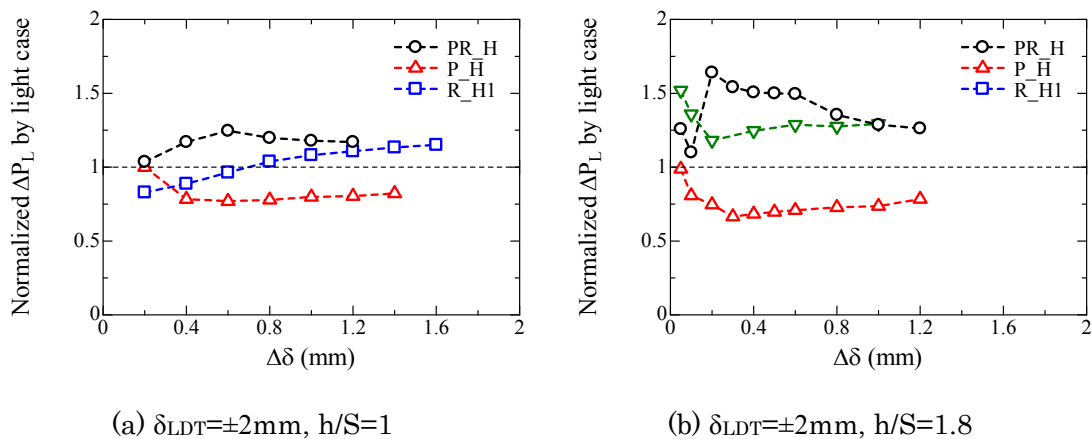
Figure 5.4.1.7 Relationship between Δδ and normalized ΔP_L of heavy case by that of light case forδLDT=±2mm, h/S=1, 1.8. (A.5.4.1.3)

Figure 5.4.1.8 shows the relationship between $\Delta\delta$ and normalized ΔP_L of h/S=1.8 by that of h/S=1. The results of the raft foundation in Fig. 5.4.1.8 (c) and (d) were estimated by normalizing ΔP_L of R_L2 and R_H2 by that of R_L1 and R_H1 respectively. This normalized ΔP_L represented the influence of the loading height on the horizontal resistance of the foundation. As been seen, the normalized ΔP_L of the raft foundation was quite small at small horizontal displacement for $\delta_{LDT}=\pm1$mm, and it gradually increased with the displacement. However, the horizontal resistance of h/S=1.8 was still smaller than that of h/S=1 at large displacement because the relative moment load with the horizontal load was large for h/S=1.8. As for $\delta_{LDT}=\pm2$mm (loading step 5), the totally
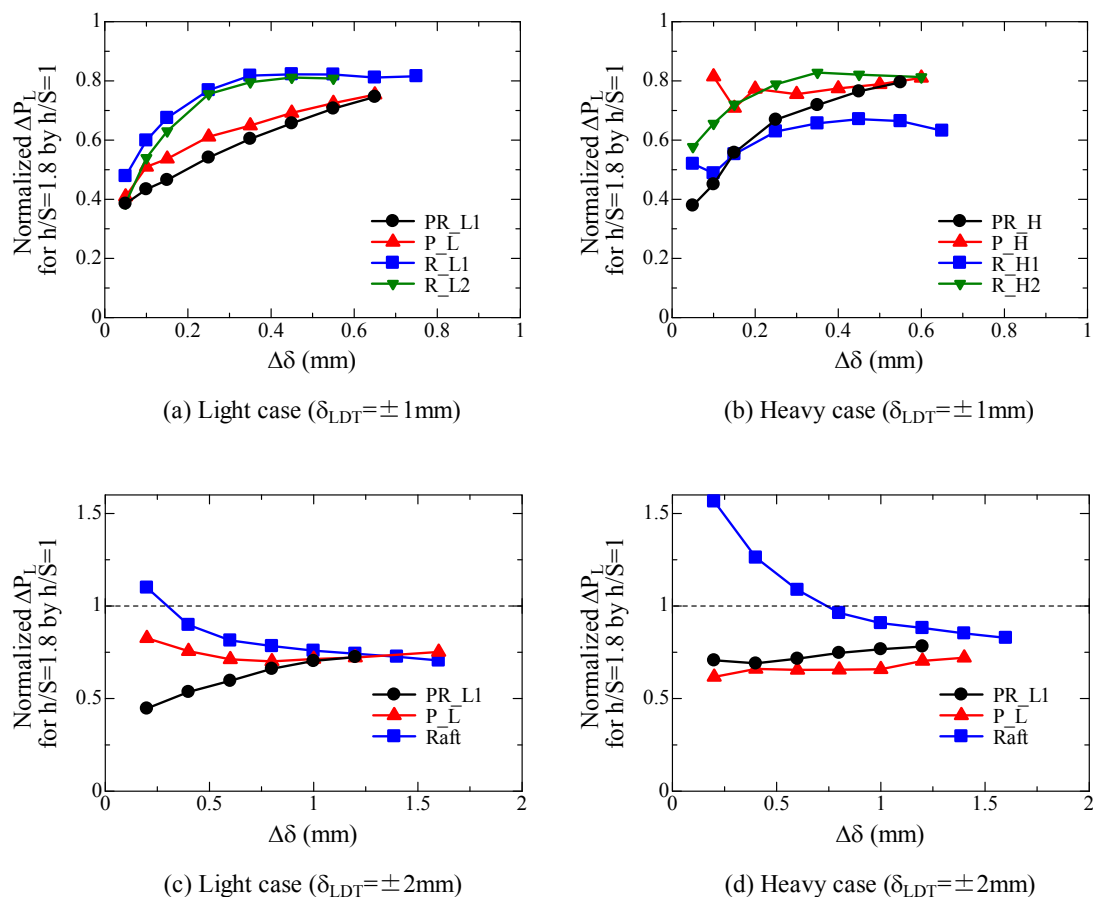
Figure 5.4.1.8 Relationship between $\Delta\delta$ and normalized ΔP_L for h/S=1.8 by that of h/S=1.

different tendency from δ_{LDT}=±1mm was observed in the raft foundation. That is, the horizontal resistance of h/S=1.8 was larger than that of h/S=1 at small horizontal displacement range, and it decreased with the displacement and reached smaller value than h/S=1. In the loading step 4 the loading height was h/S=1.8, and the pull-out side of the raft foundation rapidly moved upward with the higher loading height as explained in Fig. 5.3.2.1, 5.3.2.2, 5.3.2.4 and 5.3.2.5. Therefore, the contact area between the raft and the ground was thought to be loss. Here, the pull-out side in the loading step 4 was the push-in side in the next loading step 5. The loss of contact might be quickly recovered for h/S=1.8 compared with h/S=1 because relative moment load with horizontal load, in other words, the rotation of foundation was large for h/S=1.8. Therefore, the horizontal resistance of h/S=1.8 was larger than that of h/S=1 at the small horizontal displacement. This kind of loading height effect was also reported by Matsumoto et al. (2004a, b, 2010), that is, the higher loading height is, the smaller horizontal resistance of the foundation is. However, they did not the mechanism of the loading height effect in detail because their loading tests were done in the 1g conditions and the interaction of raft-ground-piles

cannot be evaluated. Therefore, in the present study the influence of the loading on the each component was discussed.

Figure 5.4.1.9 and 5.4.1.10 shows relationship between $\Delta\delta$ and ΔP_L for the light case and the heavy case respectively. This figure compared the horizontal resistance of each loading step for the same horizontal loading height. So, the influence of the loading sequence on the horizontal resistance can be discussed in this figure. From this figure, it can be said that the horizontal resistance observed in the first loading step was larger than other loading step, and the horizontal resistances in the following loading step were almost same. This trend can be clearly seen in the piled raft foundation. This was because the effect of the pre-vertical loading was strongly remained in the first loading step. And this effect might be diminished in the following step because the soil around pile and beneath the raft was disturbed with loading as explained in Fig. 5.1.3.

As explained above, the horizontal resistance of the piled raft foundation was higher than the pile group regardless the loading height and horizontal displacement level, especially for the first loading step. To examine the mobilization of pilled raft resistance in detail, authors divide the horizontal resistance of the piled raft foundation into the horizontal resistance of the raft part and pile part and discuss them. The much focus was placed on the influence of the raft base pressure on the pile response.

(a1) PR_L1 (h/S=1)

(a2) PR_L1 (h/S=1.8)

(b1) P_L (h/S=1)

(b2) P_L (h/S=1.8)

(c1) Raft (h/S=1)
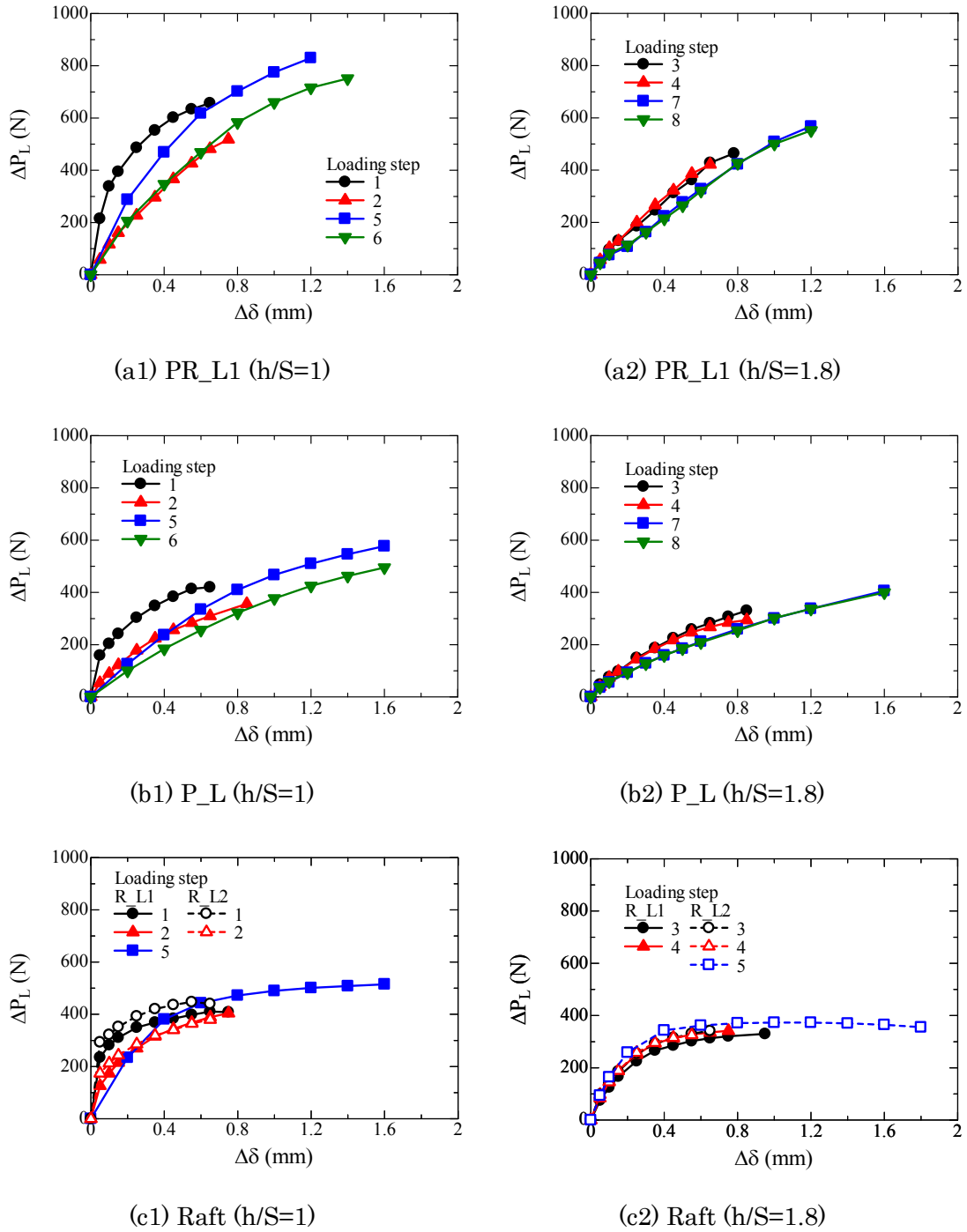
(c2) Raft (h/S=1.8)

Figure 5.4.1.9 Relationship between $\Delta\delta$ and ΔP_L for light case observed in each loading step.
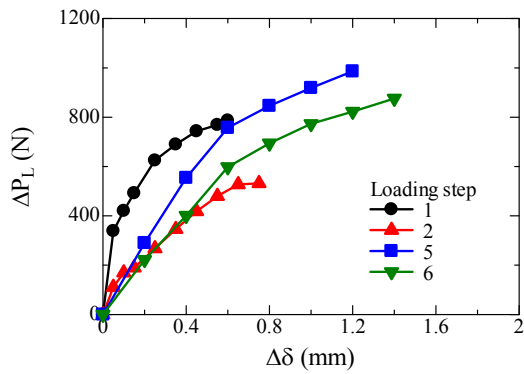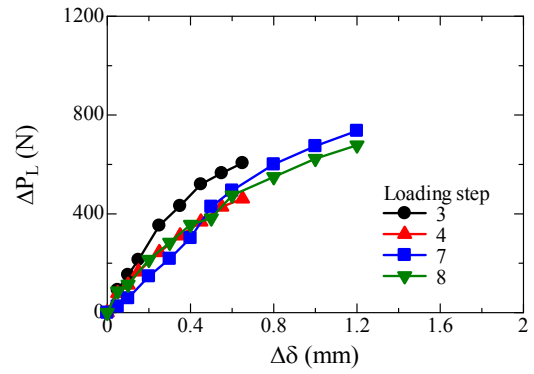
(a1) PR_H (h/S=1)   (a2) PR_H (h/S=1.8)
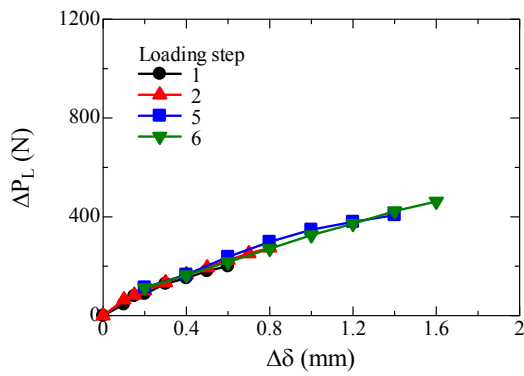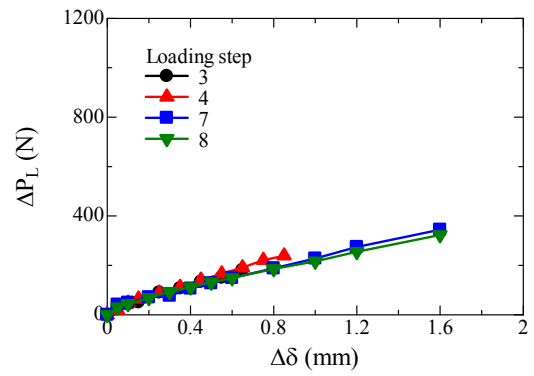
(b1) P_H (h/S=1)   (b2) P_H (h/S=1.8)
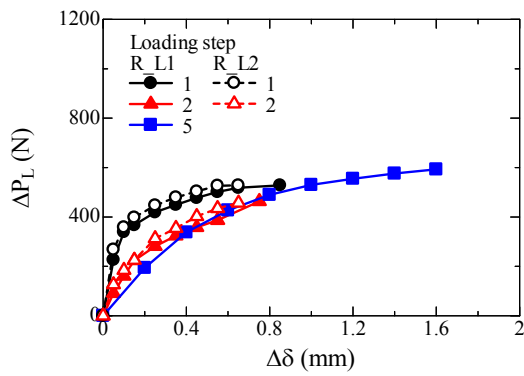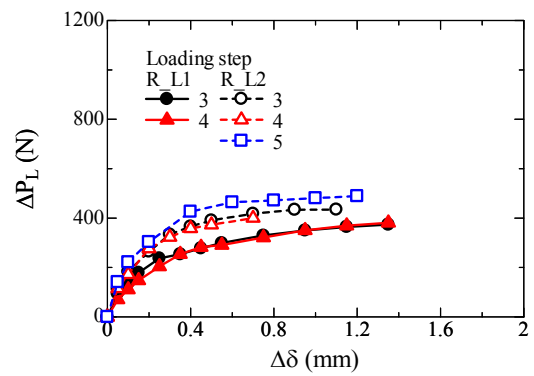
(c1) Raft (h/S=1)   (c2) Raft (h/S=1.8)

Figure 5.4.1.10 Relationship between $\Delta\delta$ and ΔP_L for heavy case observed in each loading step.

5.4.2 Horizontal resistance of raft part

Figure 5.4.2.1 and 5.4.2.2 show the relationship between the horizontal displacement at raft base δ and the horizontal load P_L, the horizontal load carried by pile part P_{PH} and the horizontal load carried by raft part P_{RH} of the piled raft foundation for the light case and heavy case respectively. The result shown in the figure is from only the loading step of $\delta_{LDT}=\pm2$mm, h/S=1 and 1.8. The results from other loading steps are summarized in Appendix (A. 5.4.2.1, 5.4.2.2). The variation of P_L of the pile group and the raft foundations are also described in the figure. As been seen the horizontal resistance of the piled raft mainly consisted of the horizontal resistance of pile part, and that of raft part was relatively small. This was because the initial RVLP of each loading step was small, which was about 5% for the light case and 15% for heavy case as shown in Fig. 5.1.3. It was also observed that the horizontal resistance of the pile part in the piled raft foundation was higher than the pile group foundation.

(a) $\delta_{LDT}=\pm2$mm, h/S=1   (b) $\delta_{LDT}=\pm2$mm, h/S=1.8
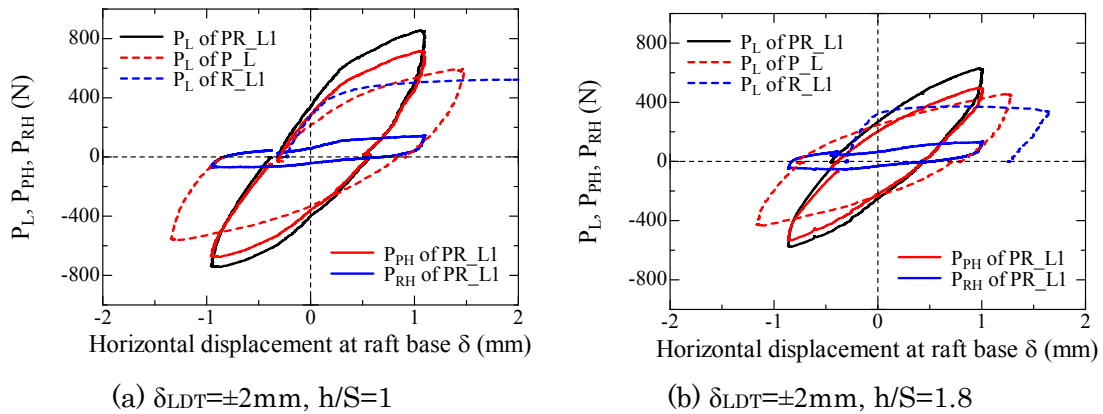
Figure 5.4.2.1 Variation of horizontal load P_L and horizontal load carried by raft P_{RH} and piles P_{PH} with horizontal displacement at raft base δ for light case. (A. 5.4.2.1)

(a) $\delta_{LDT}=\pm2$mm, h/S=1   (b) $\delta_{LDT}=\pm2$mm, h/S=1.8
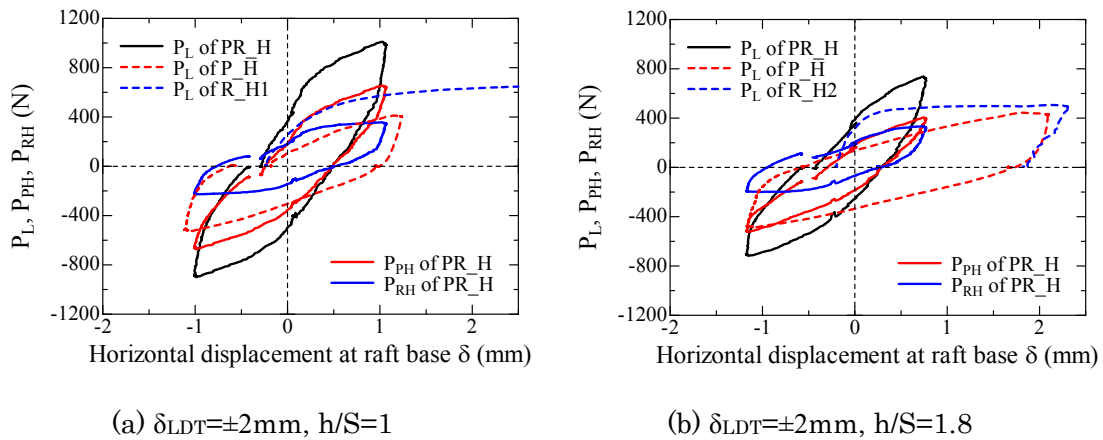
Figure 5.4.2.2 Variation of horizontal load P_L and horizontal load carried by raft P_{RH} and piles P_{PH} with horizontal displacement at raft base δ for heavy case. (A. 5.4.2.2)

Figure 5.4.2.3 shows the relationship between the horizontal displacement at the raft base δ and the horizontal load carried by raft part P_{RH}. From this figure, it can be confirmed that the P_{RH} in all loading step regardless the loading height were involved in on envelope curve. It should be also noted that the horizontal resistance of the raft part was higher for the heavy case than the light case. This was probably due to the larger RVLP for the heavy case as explained in Fig. 5.2.3.

(a) PR_L1　　　　　　　　　　　　　(b) PR_H
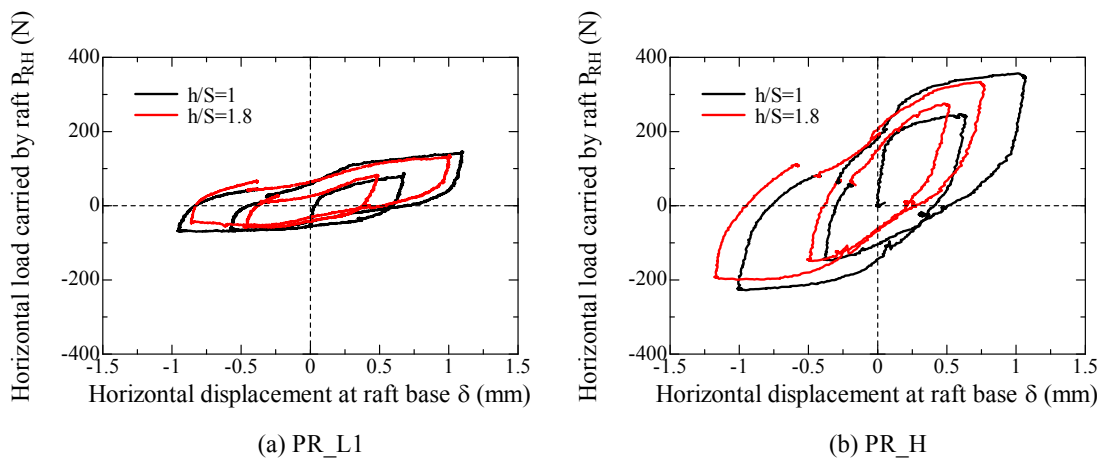
Figure 5.4.2.3 Relationship between δ and horizontal load carried by raft part in piled raft P_{RH}.

Figure 5.4.2.4 and 5.4.2.5 show the variation of the proportion of vertical load carried by raft part RVLP, the proportion of horizontal load carried by raft part RHLP and settlement s with the horizontal displacement at raft base δ for the light case and the heavy case respectively. The result only from δ_{LDT}=+1mm, h/S=1 and δ_{LDT}=-2mm, h/S=1.8, which are first and last loading step respectively, are shown in the figure. Please refer the Appendix (A.5.4.2.3, 5.4.2.4) to see the results from other loading steps. In the figure the results during the unloading period were omitted. There are two broken line in the figure, one is representing the horizontal displacement of zero, and the other is representing the point at which the trend of settlement changed. As explained in Section 5.3, the piled raft foundation settled down in the beginning of loading, but it moved upward at the large horizontal displacement. The second line was represents the transition of these trend. The RVLP was estimated from the total axial load at pile head, implying that the RVLP was significantly influenced by the accuracy of strain gauges. The RVLP less than zero was observed during the loading in the light case because the measurement accuracy of strain gauge involved the uncertainties in the light case pile due to large interference strain as explained in Chapter 3. Therefore, the RVLP during the horizontal loading tests will be discussed using the heavy case. It was also noted that

154

the larger reduction of the RVLP can be observed in the first loading step, especially for the light case because the foundation did not settle down but moved upward in the first step. This was probably because the effect of pre-vertical load was still remained in the first step, resulting in the difficulties in settling down. The trends of RHLP and RVLP increased during the foundation settled down because the contact condition between the raft base and the ground and the contribution of the raft became larger in the period. On the other hand, when the foundation moved upward at large horizontal displacement, RHLP and RVLP kept constant or slightly decreased with the horizontal displacement. From this fact, it can be confirmed that the RHLP and RVLP were strongly affected the settlement of the foundation. It was also noted that the RHLP and RVLP reached almost same value at the end of loading.

(a) Loading step 1 (δ_{LDT}=+1mm, h/S=1)   (b) Loading step 8 (δ_{LDT}=-2mm, h/S=1.8)
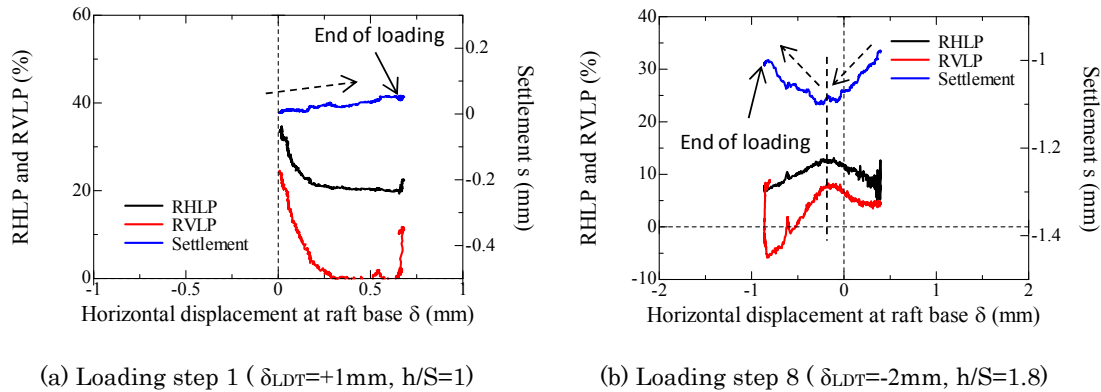
Figure 5.4.2.4 Variation of RHLP, RVLP and settlement s for light case. (A. 5.4.2.3)

(a) Loading step 1 (δ_{LDT}=+1mm, h/S=1)   (b) Loading step 8 (δ_{LDT}=-2mm, h/S=1.8)
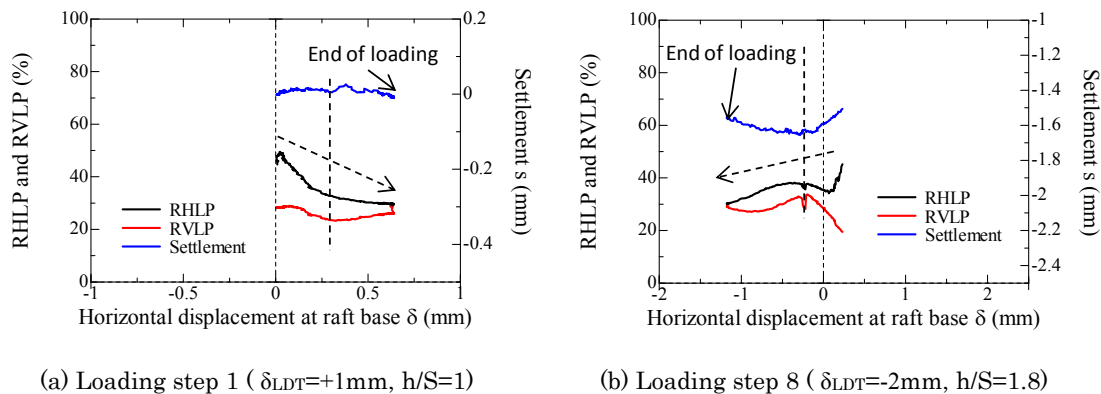
Figure 5.4.2.5 Variation of RHLP, RVLP and settlement s for heavy case. (A. 5.4.2.4)

Figure 5.4.2.6 shows the relationship between the vertical load carried by raft part P_{RV} and the horizontal load carried by the raft part P_{RH}. The broken line in the figure represents the theoretical relationship between them, which was estimated using coefficient of friction between the raft base and the ground μ of 0.4 derived from Fig.
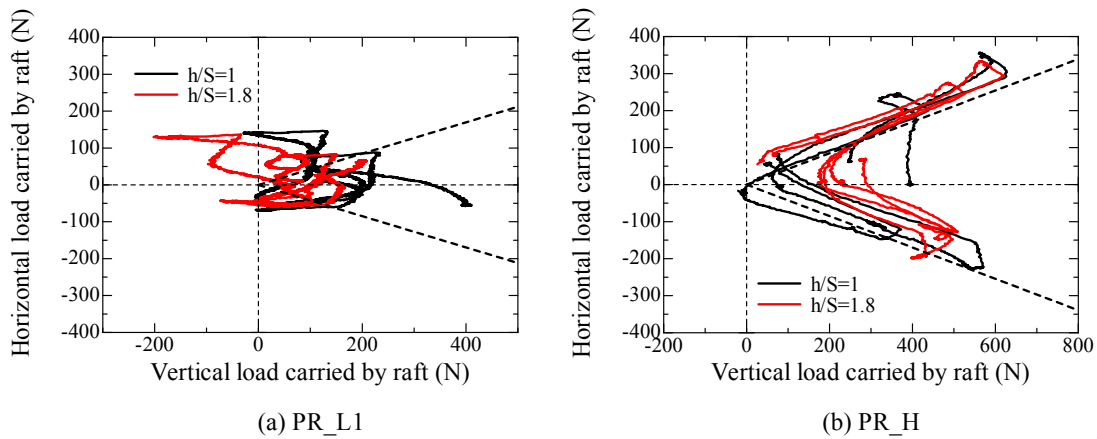
Figure 5.4.2.6 Relationship between vertical load carried by raft P_{RV} and horizontal load carried by raft P_{RH}.

5.4.1.5. There was no clear correlation for light case because the RVLP evaluated from strain gauges included the uncertainties as explained above. However, the relationship between P_{RV} and P_{PH} had a good agreement with the theoretical one. Thus, it can be said that the horizontal resistance of the raft part in the piled raft foundation can be also easily calculated from the coefficient of friction and vertical load of raft part. Nagao et al. (2002) and Tsuchiya et al. (2003) also found that the horizontal resistance of the raft part can be evaluated by the vertical load carried by the raft part.

Figure 5.4.2.7 shows the variation of the horizontal load increment ΔP_L and increment of horizontal load carried by the raft part ΔP_{RH} with horizontal displacement increment $\Delta\delta$ for the loading step of $\delta_{LDT}=\pm 2$mm, h/S=1 and 1.8. The result from other loading step is shown in Appendix (A. 5.4.2.5). ΔP_L, ΔP_{RH}, and $\Delta\delta$ were estimated by the matter shown

(a) $\delta_{LDT}=\pm 2$mm, h/S=1

(b) $\delta_{LDT}=\pm 2$mm, h/S=1
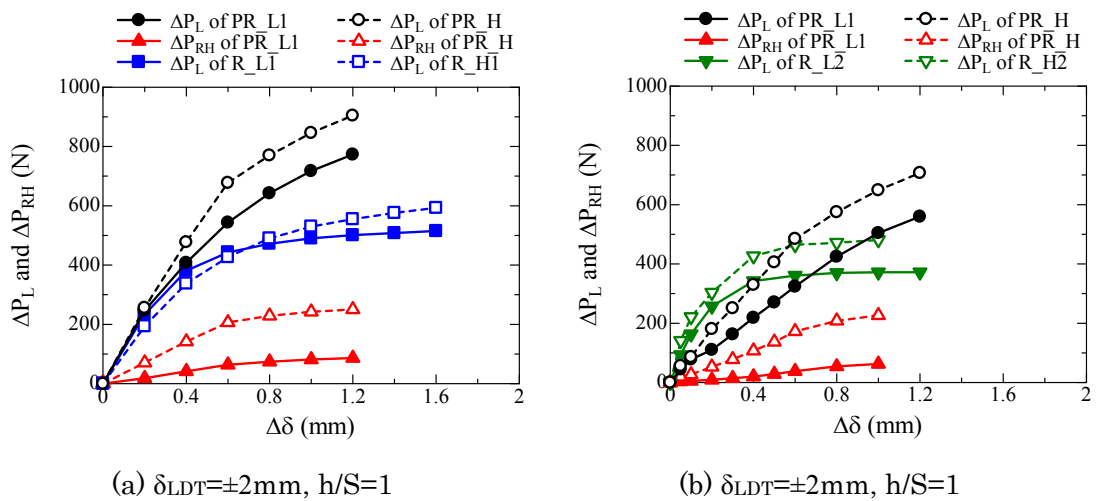
Figure 5.4.2.7 Variation of ΔP_L and ΔP_{RH} with $\Delta\delta$ for each loading step. (A. 5.4.2.5)

156
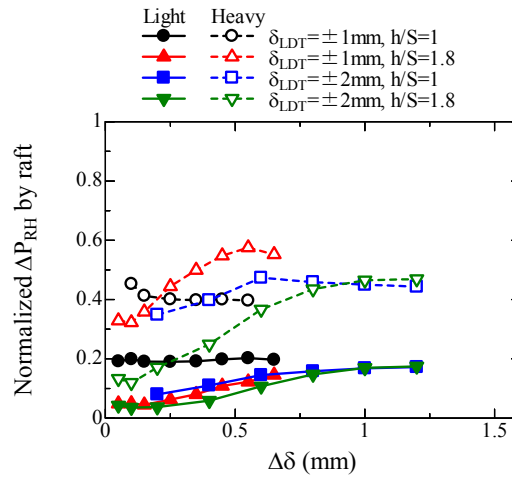
Figure 5.4.2.8 Relationship between Δδ and normalized ΔP$_{RH}$ by that of raft foundation.

in Fig. 5.4.1.4. That is, they are the increment of horizontal load P_L, horizontal load carried by the raft part P_{RH} and the horizontal displacement at raft base δ from the beginning of each loading step respectively. The result from the raft foundation is also shown in the figure. The horizontal resistance of the raft part was larger for the heavy case than the light case due to the larger vertical load of the raft part. Figure 5.4.2.8 shows relationship between the $\Delta\delta$ and the normalized ΔP_{RH} by ΔP_L (ΔP_{RH}) of the raft foundation. The normalized ΔP_{RH} increased with the displacement, and reached constant value. This was because the horizontal resistance of the raft increased at the small horizontal displacement range, and it showed constant value or slightly decreased when the horizontal displacement became larger as explain in Fig. 5.4.2.4 and 5.4.2.5.

(a) δ$_{LDT}$=±2mm, h/S=1   (b) δ$_{LDT}$=±2mm, h/S=1.8
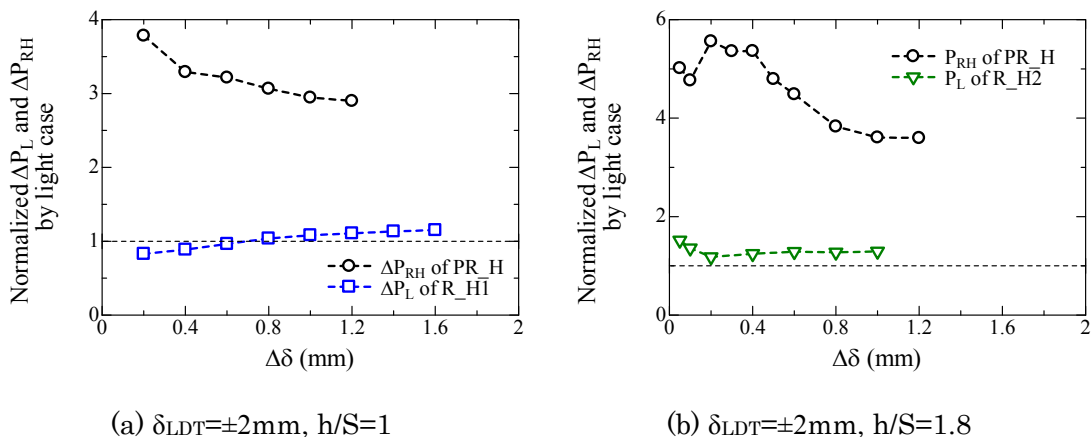
Figure 5.4.2.9 Variation of normalized ΔP$_L$ and ΔP$_{RH}$ of heavy case by those of light case with Δδ.

(A. 5.4.2.6)

Figure 5.4.2.9 shows relationship between the horizontal displacement increment $\Delta\delta$

and the increment of horizontal resistance of the raft part ΔP_{RH} of heavy case normalized by the light case for the loading step of $\delta_{LDT}=\pm 2$mm, h/S=1 and 1.8. Result from other loading step is shown in Appendix (A.5.4.2.6). The normalized resistance of the raft foundation is also shown in the figure. From this normalized resistance, the influence of the vertical load of the foundation on the horizontal resistance of the raft part can be discussed. As for the raft foundation, the horizontal resistance of the heavy case was higher than that of the light case because the raft base resistance was generally proportional to the vertical load. On the other hand, the raft part in the piled raft foundation showed higher horizontal resistance for the heavy case than the light case, and this increased ratio was higher than the ratio of vertical load of heavy case to that of light case. The settlement of the piled raft foundation was larger for the heavy case than the light case, resulting in the better contact conditions for the heavy case. As a result, the influence which was larger than the simple influence of the vertical load was appeared in the horizontal resistance of the raft part. Figure 5.4.2.10 shows the relationship between $\Delta\delta$ and normalized ΔP_L and ΔP_{RH} of h/S=1.8 by those of h/S=1. The result shown in the figure is for the loading step of $\delta_{LDT}=\pm 2$mm. The result from $\delta_{LDT}=\pm 1$mm is shown in the Appendix (A. 5.4.2.7). The horizontal resistance of the raft part was smaller for higher loading height due to the relative large moment load with the horizontal load.

(a) $\delta_{LDT}=\pm 2$mm, h/S=1   (b) $\delta_{LDT}=\pm 2$mm, h/S=1.8
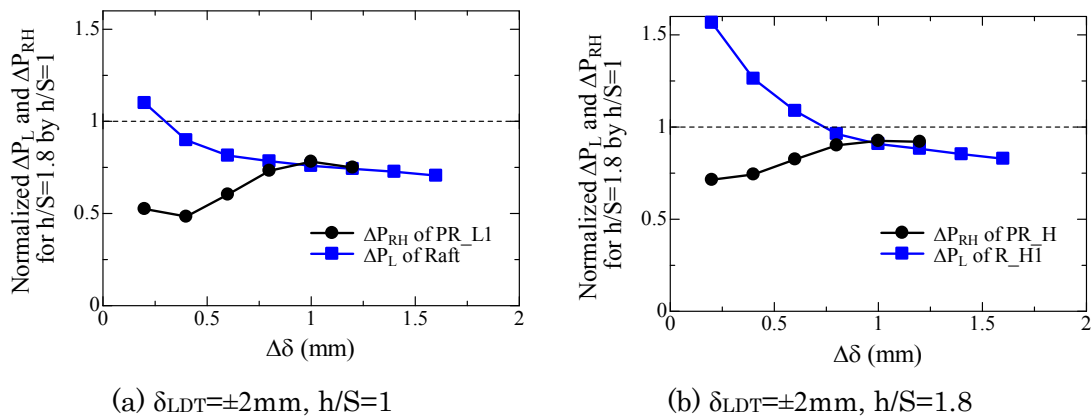
Figure 5.4.2.10 Variation of normalized ΔP_L and ΔP_{RH} of heavy case by those of light case with $\Delta\delta$.
(A. 5.4.2.7)

Figure 5.4.2.11 and 5.4.2.12 show the relationship between $\Delta\delta$ and ΔP_{RH} for each loading step. As been seen, the horizontal resistance of the raft part was higher for the first loading step compared with others. And other loading steps show almost same horizontal resistance of the raft part. This was probably due to the effect of pre-vertical load was remained in only first loading step. However, the effect of the pre-vertical loading was diminished in the first loading due to the disturbance of the soil around piles.

Therefore, it can be confirmed that the pre-vertical load can affect on only the first loading. Same tendency as the horizontal resistance of the raft part was observed in the horizontal resistance of the pile part, which will be explained latter. Consequently, the relatively large total horizontal resistance of the piled raft in the first loading step (Fig. 5.4.1.9 and 5.4.2.10) was attributed to the raft part and pile part.

(a) PR_L1 (h/S=1)   (b) PR_L1 (h/S=1.8)
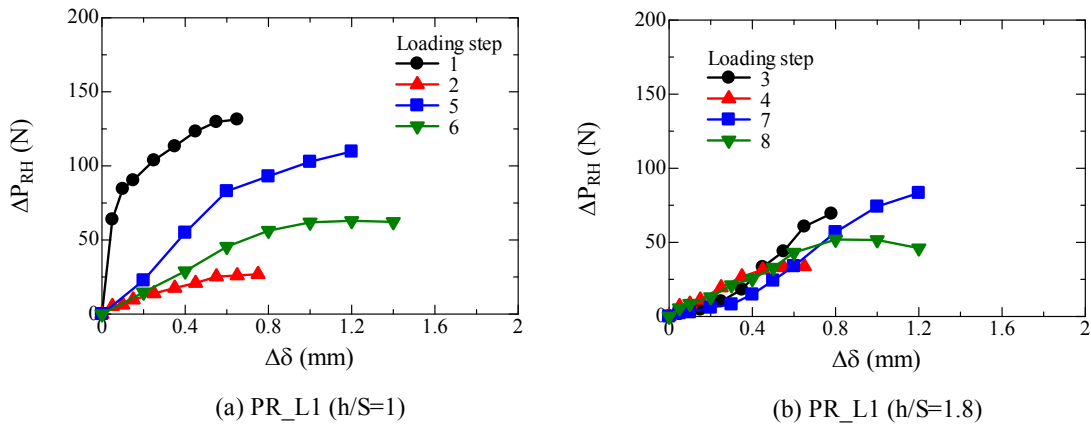
Figure 5.4.2.11 Relationship between Δδ and ΔP_RH for light case observed in each loading step.

(a) PR_H (h/S=1)   (b) PR_H (h/S=1.8)
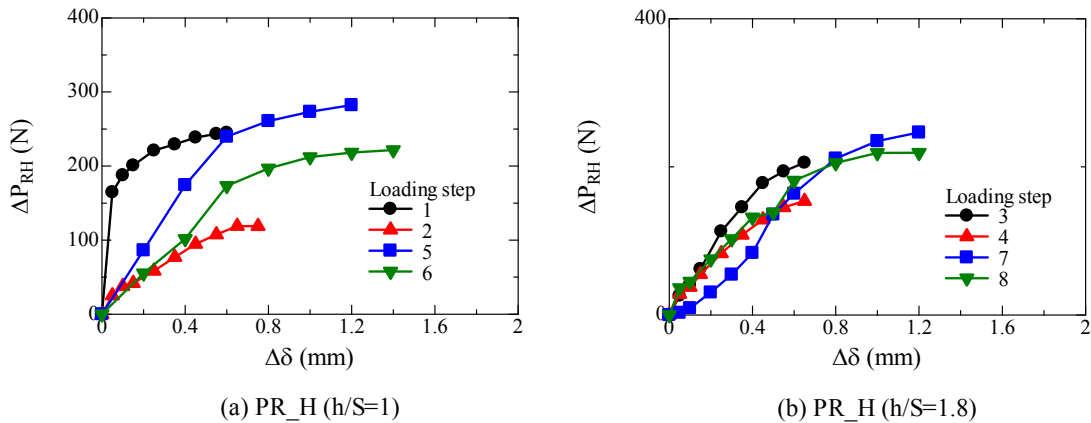
Figure 5.4.2.12 Relationship between Δδ and ΔP_RH for heavy case observed in each loading step.

The horizontal resistance of the raft part in the piled raft foundation was discussed in this section. The higher horizontal resistance of the raft part can be obtained in the piled raft with smaller safety factor of the pile because the strict contact condition between the raft base and ground can be secured during the loading. And the ratio of the horizontal resistance of the raft part in the piled raft (P_{RH}) with smaller safety factor of pile to PRH with larger safety factor was larger than the ratio of the vertical load of the foundation for heavy case to that for light case. Therefore, it can be confirmed that the smaller safety factor of pile is, the larger contribution of the raft is.

5.4.3 Horizontal resistance of pile part

In this section the horizontal resistance of the pile part P_{PH} will be discussed. In particular, the influence of the raft base pressure on the pile response will be examined.

Figure 5.4.3.1 and 5.4.3.2 show the relationship between the horizontal displacement at the raft base δ and the horizontal load P_L, the horizontal load carried by pile part P_{PH} and the horizontal load carried by raft P_{RH} for light case and heavy case, which are already described in Fig. 5.4.2.1 and 5.4.2.2. From this figure, it can be said that the horizontal resistance of pile part in the piled raft foundation was higher than that of the pile group foundation. This was probably because the piles in the piled raft foundation were affected by the raft pressure. And this influence of the raft part on the pile will be discussed in detail.

(a) $\delta_{LDT}=\pm2mm$, h/S=1   (b) $\delta_{LDT}=\pm2mm$, h/S=1.8
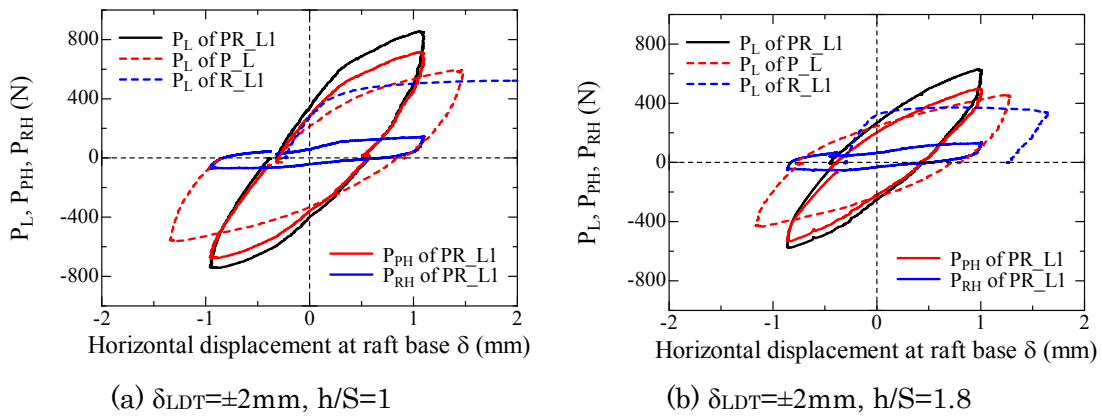
Figure 5.4.3.1 Variation of horizontal load P_L and horizontal load carried by raft P_{RH} and piles P_{PH} with horizontal displacement at raft base δ for light case. (A. 5.4.2.1)

(a) $\delta_{LDT}=\pm2mm$, h/S=1   (b) $\delta_{LDT}=\pm2mm$, h/S=1.8
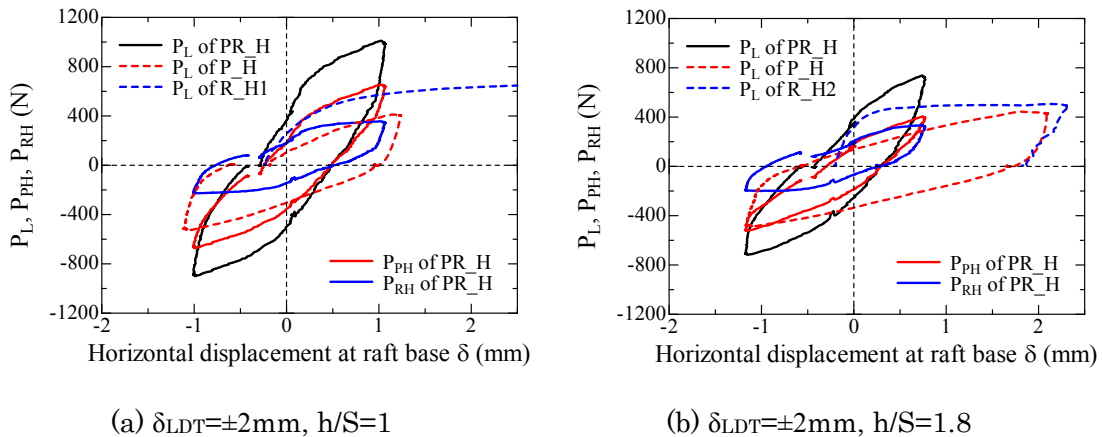
Figure 5.4.3.2 Variation of horizontal load P_L and horizontal load carried by raft P_{RH} and piles P_{PH} with horizontal displacement at raft base δ for heavy case. (A. 5.4.2.2)

160
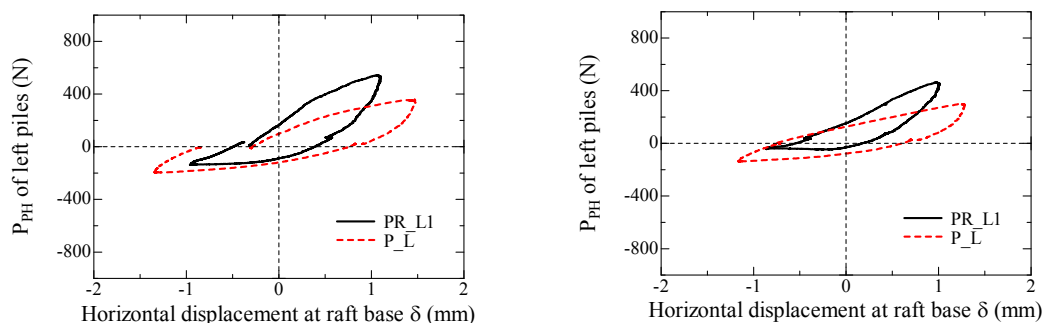
(a) Left pile (δ_{LDT}=±2mm, h/S=1) (b) Left pile (δ_{LDT}=±2mm, h/S=1.8)

Figure 5.4.3.3 Relationship between horizontal displacement at raft base δ and horizontal load carried by pile part P_{PH} for light case. (A.5.4.3.1)
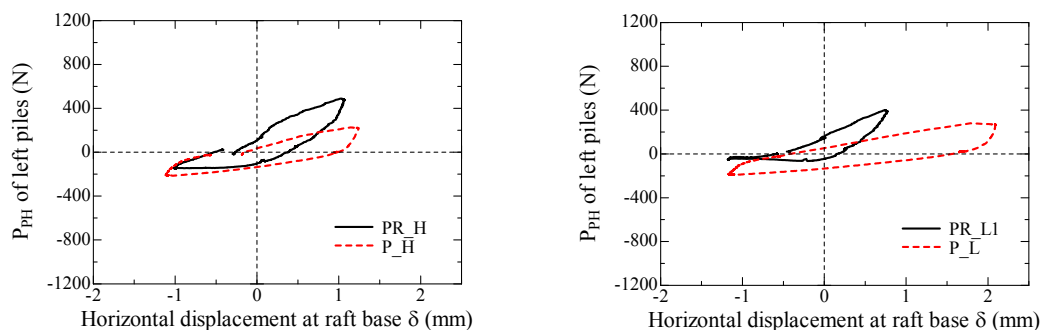
(a) Left pile (δ_{LDT}=±2mm, h/S=1) (b) Left pile (δ_{LDT}=±2mm, h/S=1.8)

Figure 5.4.3.4 Relationship between horizontal displacement at raft base δ and horizontal load carried by pile part P_{PH} for heavy case. (A.5.4.3.2)

Figure 5.4.3.3 and 5.4.3.4 show the relationship between the horizontal displacement at the raft base δ and the horizontal resistance of the left pile for δ_{LDT}=±2mm, h/S=1, 1.8. The results from the right pile and other loading steps are described in Appendix (A. 5.4.3.1, 5.4.3.2). The left pile was pushed in for the positive horizontal displacement and it was pulled out during the negative displacement. The horizontal resistance of the piled raft foundation was higher than that of the pile group in the push-in pile due to the increase of the confined stress around pile by the raft pressure. On the other hand, for the pull-out pile the horizontal resistance of the pile part in the piled raft gradually increased with horizontal displacement at the small displacement, however, it showed almost constant value and it was smaller than the pile group at the large displacement. The pull-out pile was pushed in during the previous loading step, and therefore the confined stress around piles was still high at the small horizontal displacement. However, the pull-out pile was rapidly moved upward in the piled raft foundation at the large horizontal displacement (Fig. 5.3.2.1, 5.3.2.2, 5.3.2.4, 5.3.2.5) resulting in the reduction of the confined stress around pile. In addition to this, the decrease of relative

161

displacement of pull-out pile against the soil also affected the pull-out pile response. The soil beneath the raft base moved with raft base during the loading, and the relative displacement of the pull-out pile was therefore decreased. Therefore, the horizontal resistance of the pull-out pile in the piled raft foundation was smaller than that in the pile group foundation.

In the horizontal loading tests on piled raft foundation and single pile done by Horikoshi et al. (2003a), average horizontal resistance of piles in the piled raft foundation was also larger than that of single pile. The higher average horizontal resistances were observed for both push-in and pull-out piles to the single pile. Nagao et al. (2002) reported that the although the horizontal load carried by the pile part was smaller than that of the pile group at the relatively small horizontal displacement, it was larger at the relatively large horizontal displacement due to the higher confined stress beneath the raft base for the piled raft foundation. They did not discuss the horizontal resistance of push-in pile and pull-out pile, however, they showed that the observed raft base pressure was almost same between the push-in and pull-out sides. From this fact, it can be said that the horizontal resistance of the push-in and pull-out pile were almost same for the piled raft foundation, and they were larger compared with the pile group foundation. Thus, the mobilization of pile horizontal resistance of piled raft foundation in the previous researches was significantly different from the present study The higher horizontal resistances were observed for both push-in and pull-out piles than the pile group in the previous researches, while the piled raft foundation in this study showed larger and smaller horizontal resistances than the pile group for push-in and pull-out piles respectively. This was due to the difference of base contact pressure distribution between two models. In this study relatively large rotation and moment load were applied to the foundation, which resulted in complex contact condition, i.e., different contact condition between push-in and pull-out sides.
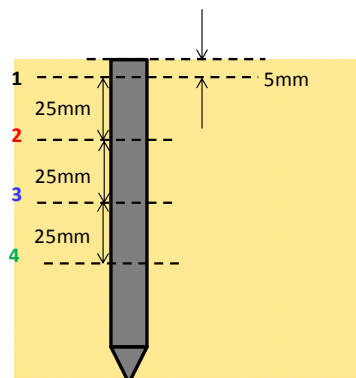
Figure 5.4.3.5 Depth at which horizontal subgrade reaciton of pile was estimated.
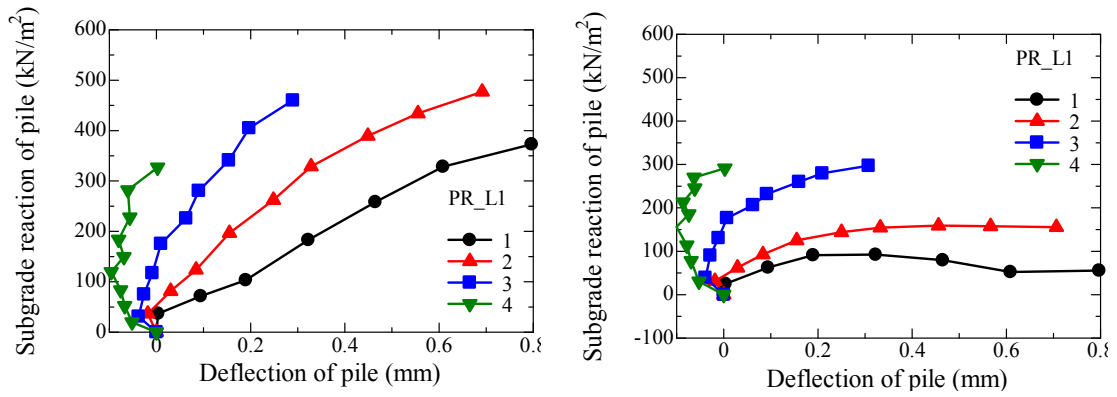
(a) Push-in ($\delta_{LDT}=\pm2$mm, h/S=1) (b) Pull-out ($\delta_{LDT}=\pm2$mm, h/S=1)

Figure 5.4.3.6 Relationship between pile deflection and subgrade reaction of pile for PR_L1.
(A. 5.4.3.3)
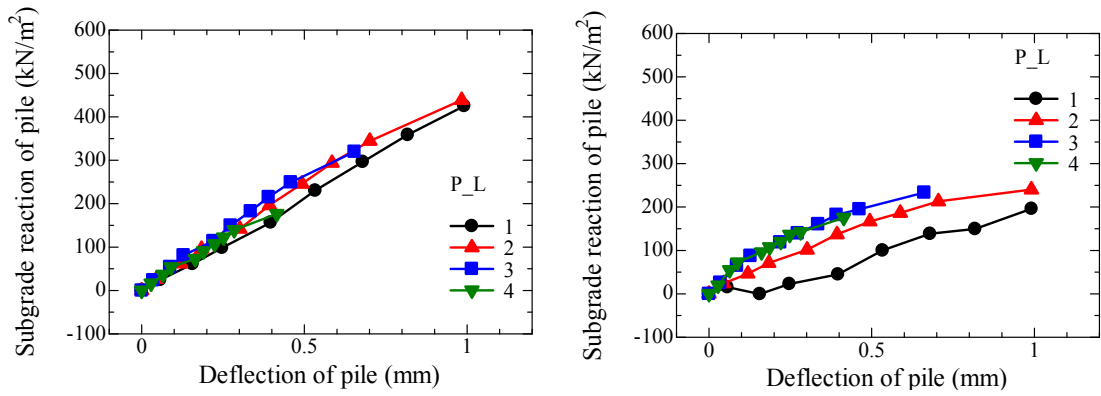
(a) Push-in ($\delta_{LDT}=\pm2$mm, h/S=1) (b) Pull-out ($\delta_{LDT}=\pm2$mm, h/S=1)

Figure 5.4.3.7 Relationship between pile deflection and subgrade reaction of pile for P_L.
(A. 5.4.3.4)
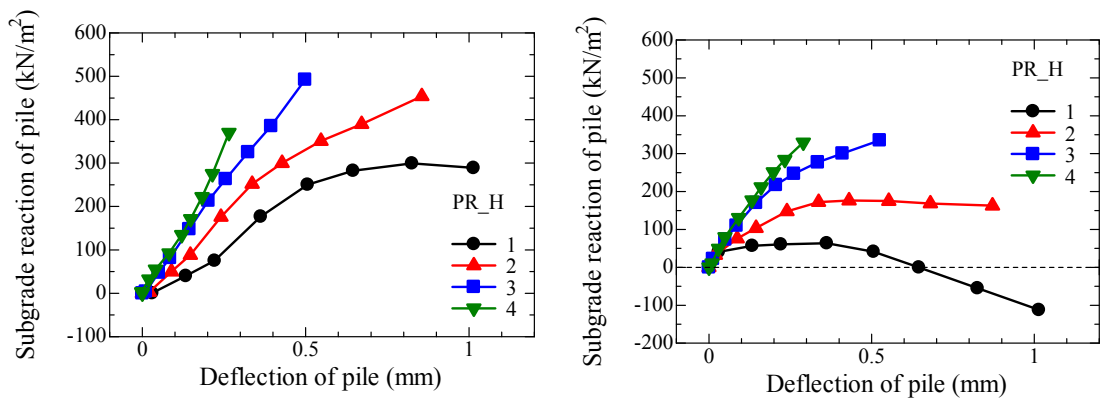
(a) Push-in ($\delta_{LDT}=\pm2$mm, h/S=1) (b) Pull-out ($\delta_{LDT}=\pm2$mm, h/S=1)

Figure 5.4.3.8 Relationship between pile deflection and subgrade reaction of pile for PR_H.
(A. 5.4.3.5)

163

(a) Push-in (δ_{LDT}=±2mm, h/S=1) (b) Pull-out (δ_{LDT}=±2mm, h/S=1)
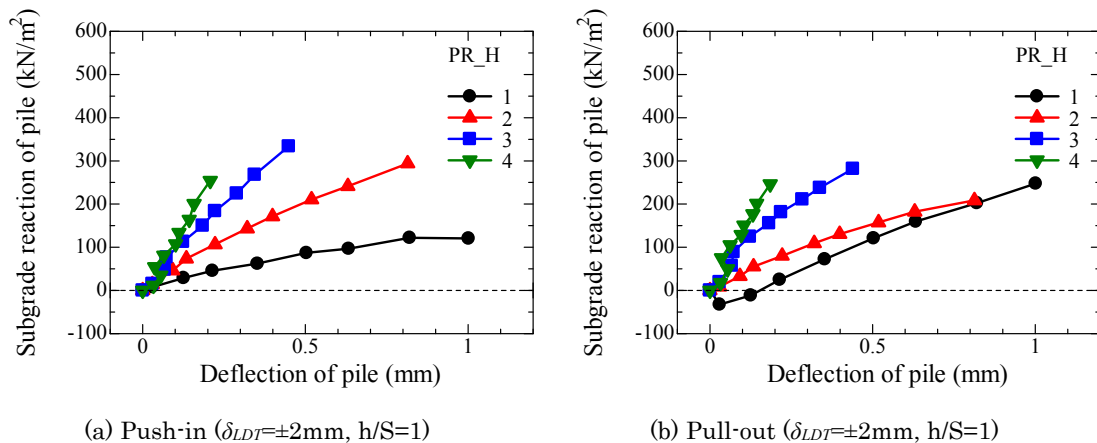
Figure 5.4.3.9 Relationship between pile deflection and subgrade reaction of pile for P_H.
(A. 5.4.3.6)

Next the horizontal subgrade reaction of pile will be examined. From the bending moment profile, the horizontal subgrade reaction of pile and the pile deflection can be estimated by second derivation and second integration of profile. From the observed bending moment profile, which was discussed in Section 5.5.2, the relationship between the pile deflection and horizontal subgrade reaction of pile was calculated as shown in Fig. 5.4.3.6 – 5.4.3.9. The results in these figures are from δ_{LDT}=±2mm, h/S=1 for the case of case of PR_L1, P_L, PR_H and P_H respectively. Results observed in other loading steps are summarized in Appendix (A.5.4.3.3-5.4.3.6).It was required for second integration to determine two integration constants. They were calculated using two boundary conditions: pile deflection at pile head was horizontal displacement at the raft base δ; pile deflection angel at pile head was rotation of the foundation θ. The subgrade reaction and deflection of pile were estimated at the depth shown in Fig. 5.4.3.5. Look at the pile group foundation (Fig. 5.4.3.7 and 5.4.3.9), the almost linear relationship between the subgrade reaction and pile deflection can be observed. Although the evaluated subgrade reaction was almost same between each depth during the small loading step, the subgrade reaction at shallower part gradually decreased with the increase of loading step procedures. In the shallower depth the displacement of pile was larger than the deeper, and therefore the soil near the ground surface was significantly disturbed by the pile, resulting in the smaller subgrade reaction at the shallower depth. It was also noted that the subgrade reaction of pull-out pile was slightly smaller than that of the push-in pile. This was because there was push-in pile in front of the pull-out pile, and the pull-out pile cannot obtain the sufficient resistance from the soil. Similar tendency was observed in the previous research as explained in Chapter 2, in which the resistance of the pull-out pile was smaller than that of push-in pile for the pile spacing

ratio of less than six (pile spacing ratio was five in the present study).

For the piled raft foundation, the subgrade reaction showed non-linear relation with the pile deflection. This was probably because the mobilization of the subgrade reaction became complex due to the base contact pressure. The totally different tendency in the subgrade reaction between the push-in pile and pull-out pile was observed in the piled raft foundation. The subgrade reaction of pull-out pile was significantly smaller than that of the push-in pile because the decrease of contact pressure in the pull-out side and the decrease of the relative displacement of the pull-out pile against the soil as explained in Fig. 5.4.3.3. and 5.4.3.4.
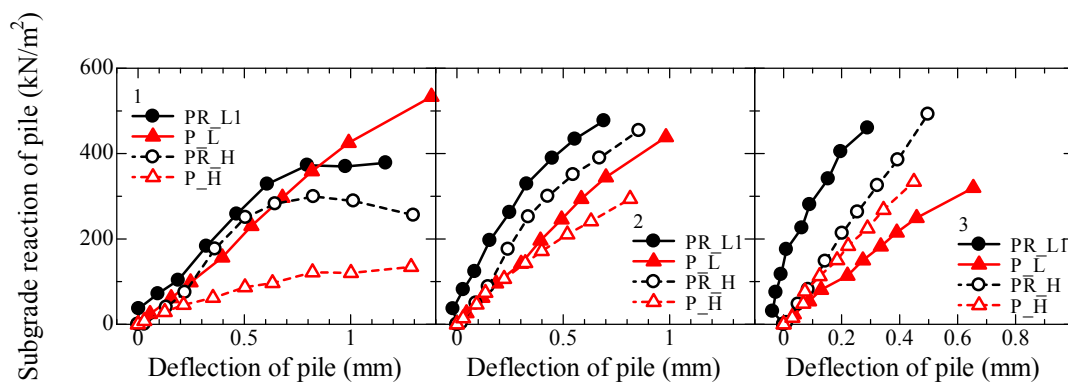
(a) Push-in (δ_{LDT}=±2mm, h/S=1)

Figure 5.4.3.10 Relationship between pile deflection and horizontal subgrade reaction of push-in pile at depth of 1, 2 and 3. (A. 5.4.3.7)

Figure 5.3.4.10 shows the relationship between the pile deflection and the subgrade reaction of push-in pile at the depth of 1, 2 and 3 (Fig. 3.4.3.5) observed in all foundations. The results in these figures are derived from the loading step of δ_{LDT}=±2mm, h/S=1. Results from other loading steps are summarized in Appendix (A.5.4.3.7). At the depth of 2 and 3, the subgrade reaction of pile was larger for the piled raft foundation than the pile group foundation due to the higher confined stress around piles in the piled raft foundation. As for the depth of 1 in the push-in pile, although the subgrade reaction was larger for the piled raft foundation at the small pile deflection, the subgrade reaction was larger for the pile group than the piled raft at the large pile deflection. The confined stress around pile at the shallower depth of 1 was also higher for the piled raft, however, the influence of the relative displacement of pile reduction was also significant near the ground surface. For the subgrade reaction described in Fig. 5.3.4.10 (c), the influence of the reduction of relative displacement of pile was larger than influence of the increase of confined stress, resulting in the smaller subgrade
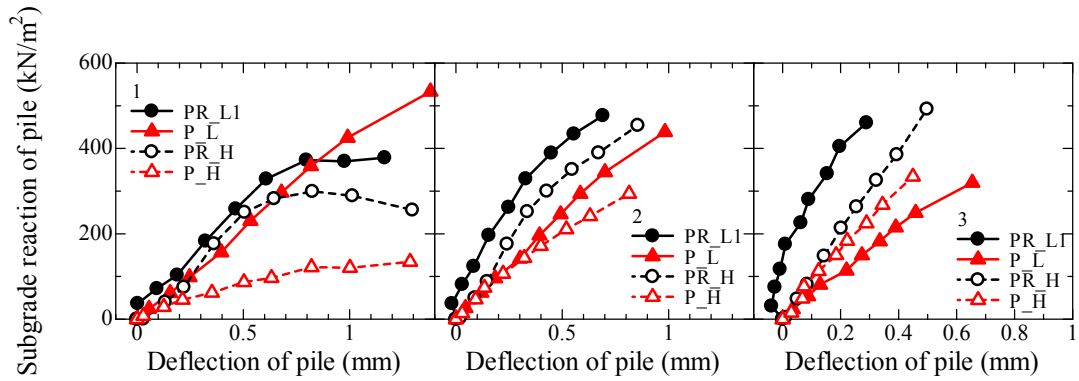
(a) Push-in (δ_{LDT}=±2mm, h/S=1)
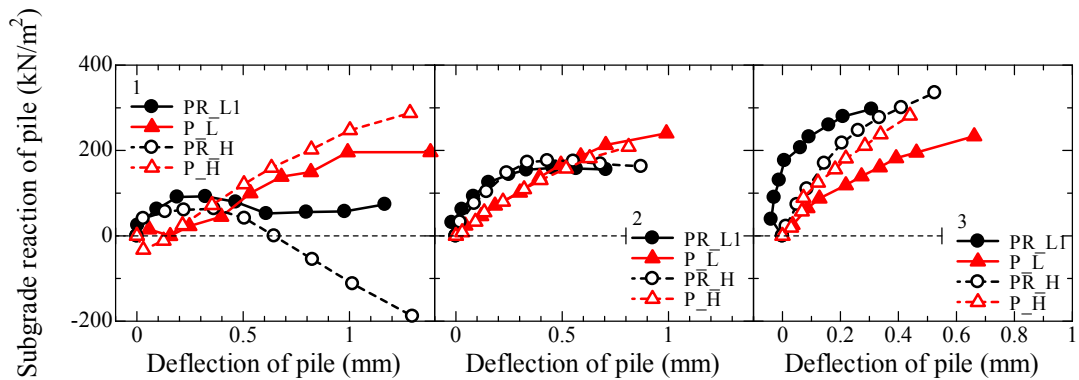
(b) Pull-out (δ_{LDT}=±2mm, h/S=1)

Figure 5.4.3.11 Relationship between pile deflection and horizontal subgrade reaction of pull-out pile at depth of 1, 2 and 3. (A. 5.4.3.8)

reaction of the piled raft at the large pile deflection.

Figure 5.3.4.11 shows the relationship between the pile deflection and the subgrade reaction of pull-out pile at the depth of 1, 2 and 3 (Fig. 3.4.3.5) observed in all foundations. The results in these figures are derived from the loading step of δ_{LDT}=±2mm, h/S=1. Results from other loading steps are summarized in Appendix (A.5.4.3.8). The subgrade reaction of the pile group foundation linearly increased with the pile deflection. However, the subgrade reaction of the piled raft foundation showed non-linear relationship with the pile deflection. The subgrade reaction increased at the small pile deflection showing higher subgrade reaction than the pile group. The pull-out pile was pushed in during the previous loading step, and it seemed that the confined stress around pile was higher at the small pile deflection. Therefore, the subgrade reaction of the piled raft foundation was higher than the pile group at the small pile deflection. However, the subgrade reaction decreased at the large pile deflection, and it was smaller than the pile group

foundation, especially for the shallower depth. This reduction of subgrade reaction of the piled raft foundation was attributed to the decrease of the confines stress and the decrease of the relative displacement of pull-out pile. As mentioned above, the influence of reduction of the relative displacement of pile was significant near the ground surface. Therefore, the larger reduction of the subgrade reaction of the piled raft can be clearly seen at the shallower depth of 1.

Mano et al. (2003) and Nagai and Tsuchiya (2004) also calculated the relationship between the subgrade reaction of pile and pile deflection from the bending moment profile. Mano et al. (2003) found that the subgrade reaction of pile was smaller for the piled raft foundation than that of the pile group foundation at the small horizontal displacement range because the relative displacement of pile against the soil was smaller for the piled raft foundation. However, larger subgrade reaction was observed in the piled raft than that in the pile group at the large horizontal displacement, especially for shallower depth. Nagai and Tsuchiya (2004) pointed out the 16-20 times larger pile subgrade reaction was observed for the piled raft than the pile group at just beneath the raft base. However, the heavily non-linear behavior of the subgrade reaction of pull-out pile observed in the present study could not be seen in above researches because the difference of base contact pressure distribution between two models. In this study relatively large rotation and moment load were applied to the foundation, which resulted in complex contact condition, i.e., different contact condition between push-in and pull-out sides.

Figure 5.4.3.12 shows the variation of the horizontal load increment ΔP_L and increment of resistance of the pile ΔP_{PH} with the horizontal displacement increment $\Delta \delta$ for the loading step of $\delta_{LDT}=\pm2$mm, h/S=1. And Fig. 5.4.3.13 shows the variation of the horizontal load increment of push-in pile and pull-out pile with $\Delta \delta$ for the same loading step of $\delta_{LDT}=\pm2$mm, h/S=1. Results from other loading steps are summarized in Appendix (A. 5.4.3.9 for Fig. 5.4.3.12 and A. 5.4.3.10 for Fig. 5.4.3.13). ΔP_L, ΔP_{PH}, and $\Delta \delta$ were estimated by the matter shown in Fig. 5.4.1.4. That is, they are the increment of horizontal load P_L, horizontal load carried by the pile part P_{PH} and the horizontal displacement at raft base δ from the beginning of each loading step respectively. The horizontal resistance of the pull-out pile in the piled raft foundation was almost same or slightly smaller than that of the pile group foundation, especially for large horizontal displacement. On the other hand, the horizontal resistance of the push-in pile was larger for the piled raft foundation than the pile group foundation due to the larger confines

stress around piles caused by the base pressure. The increment of the push-in pile was larger than the decrease of the pull-out pile, and therefore, the horizontal resistance of pile part in the piled raft foundation was larger than the pile group foundation as shown in Fig. 5.4.3.12. It was also noted that there was slight difference of the horizontal displacement between the light case and the heavy case. Therefore, it can be said that the difference of the total horizontal resistance of the piled raft foundation (Fig. 5.4.1.5) between the light case and heavy case was derived from the difference of the horizontal resistance of the raft part (Fig. 5.4.2.7).
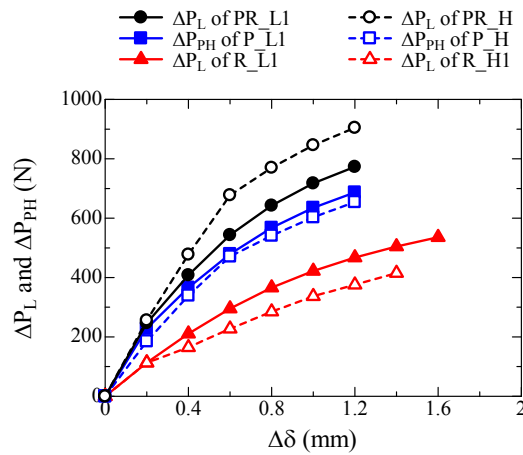
Figure 5.4.3.12 Variation of ΔP_L and ΔP_{PH} with $\Delta\delta$ for each loading step for. $\delta_{LDT}=\pm2$mm, h/S=1.
(A. 5.4.3.9)
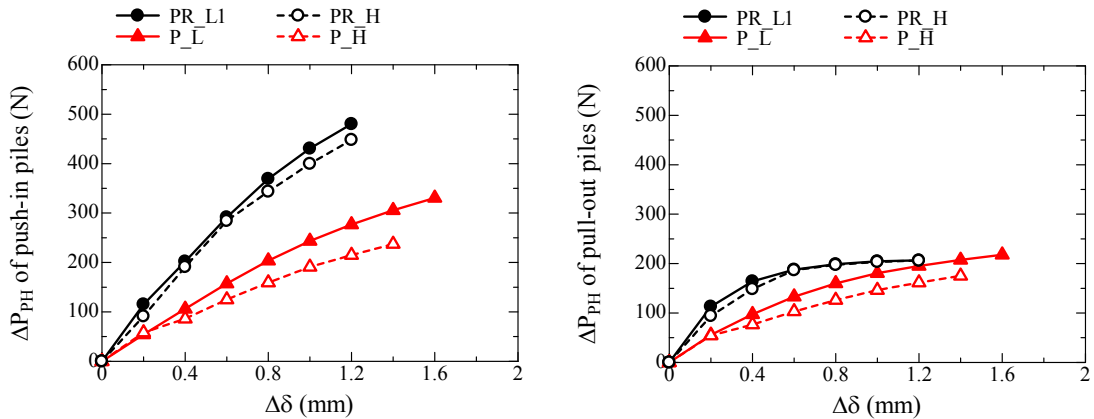
(a) Push-in ($\delta_{LDT}=\pm2$mm, h/S=1)   (b) Pul-out ($\delta_{LDT}=\pm2$mm, h/S=1)

Figure5.4.3.13 Relationship ΔP_{PH} of push-in and pull-out piles with $\Delta\delta$ for each loading step.
(A. 5.4.3.10)

Figure 5.4.3.14 shows relationship between $\Delta\delta$ and the normalized ΔP_{PH} by that of the pile group foundation for the loading step of $\delta_{LDT}=\pm2$mm, h/S=1. The results from other loading steps are shown in Appendix (A. 5.4.3.11). ΔP_{PH} of all piles, push-in pile and

(a) All piles ($\delta_{LDT}=\pm2$mm, h/S=1)   (b) Push-in & Pull-out piles ($\delta_{LDT}=\pm2$mm, h/S=1)
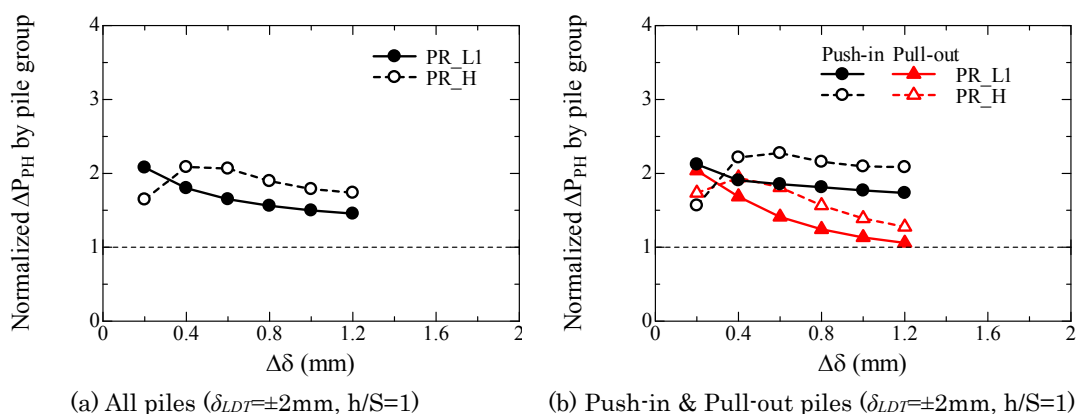
Figure 5.4.3.14 Relationship between $\Delta\delta$ and normalized ΔP_{PH} by that of pile group. (A. 5.4.3.11)
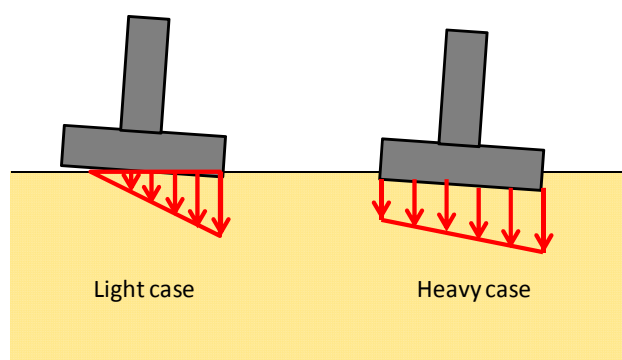
Figure 5.4.3.15 Predicted base contact pressure distribution for piled raft.

pull-out pile are shown in the figure. This normalized horizontal resistance represents the increased ratio of horizontal resistance of the pile part in the piled raft to that of the pile group foundation. The trend of normalized horizontal resistance of all piles and that of push-in pile was almost same because the horizontal resistance of push-in pile was dominant for the piled raft foundation as shown in Fig. 5.4.3.13. The ratio of push-in pile increased with the horizontal displacement because the base pressure at the push-in side gradually increased with the horizontal displacement. On the other hand, the ratio of the pull-out pile decreased with the horizontal displacement because the decrease of contact stress at the pull-out side and reduction of relative displacement of pile as explained above. Comparing the light case and heavy case, the ratio of push-in pile and pull-out pile was larger for the heavy case than the light case because the average base pressure was larger for the heavy case than the light case. In addition to this, the distribution of the raft pressure also affected to the phenomenon as shown in Fig. 5.4.3.15. The upward movement of pull-out pile was larger for the light case than the heavy case as shown in Fig. 5.3.2.4 and 5.3.2.5. Therefore, the raft pressure was heavily distributed, and the base pressure at the pull-out side became smaller. As a result, the heavy case showed higher horizontal resistance of push-in pile and pull-out pile as well.

169

Figure 5.4.3.16 shows the relationship between the $\varDelta\delta$ and normalized $\varDelta P_{PH}$ of heavy case by that of light case for the loading step of δ_{LDT}=±1mm, ±2mm and h/S=1. Results obtained from other loading steps are shown in Appendix (A. 5.4.3.12). This normalized horizontal resistance represents the influence of the safety factor of pile on the horizontal resistance of the pile part. For the pile group foundation, the horizontal resistance of the pile part in the heavy case was 30%-70% of the light case due to the lower safety factor of pile. Although the safety factor of the pile was also low for the PR_H, higher horizontal resistance of the pile part can be obtained for the PR_H compared with PR_L1. This was because the weak pile in the heavy case enhanced by the raft pressure. Thus, in addition to the horizontal resistance of the raft part, the raft base increased the pile resistance even for the relatively weak pile. Therefore, it can be said that the piled raft foundation had a significant advantages in the horizontal resistance compared with the pile group foundation.
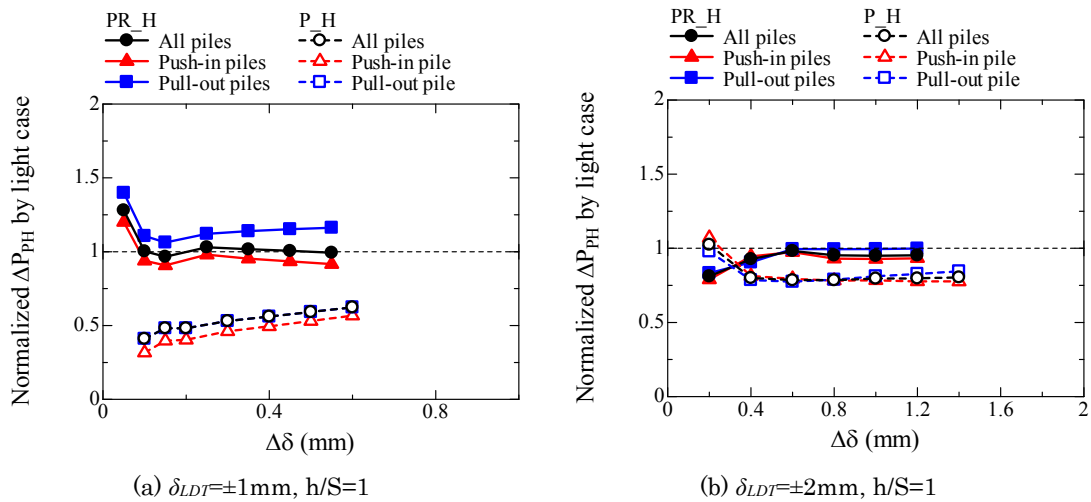
Figure 5.4.3.16 Relationship between $\varDelta\delta$ and normalized $\varDelta P_{PH}$ of heavy case by that of light case.

(A. 5.4.3.12)

Figure 5.4.3.17 shows the relationship between $\varDelta\delta$ and normalized $\varDelta P_{PH}$ of h/S=1.8 by that of h/S=1. This normalized resistance represents the influence of the loading height on the horizontal resistance of the pile part. From this figure it can be found that the higher loading height was, the smaller horizontal resistance of pile part was, because the relative large moment load with the horizontal load was applied to the foundation. And this trend can be clearly seen at the small horizontal displacement. However, for the pull-out pile the reduction of the horizontal resistance of the pile part by the higher loading height was clearly observed at the large horizontal displacement. This was

because the pull-out pile in the piled raft foundation rapidly moved upward at the large displacement, resulting in the decrease of the contact pressure. Consequently, the horizontal resistance of pull-out pile with higher loading height decreased with the horizontal displacement.

(a) $\delta_{LDT} = \pm 1mm$ (b) $\delta_{LDT} = \pm 2mm$
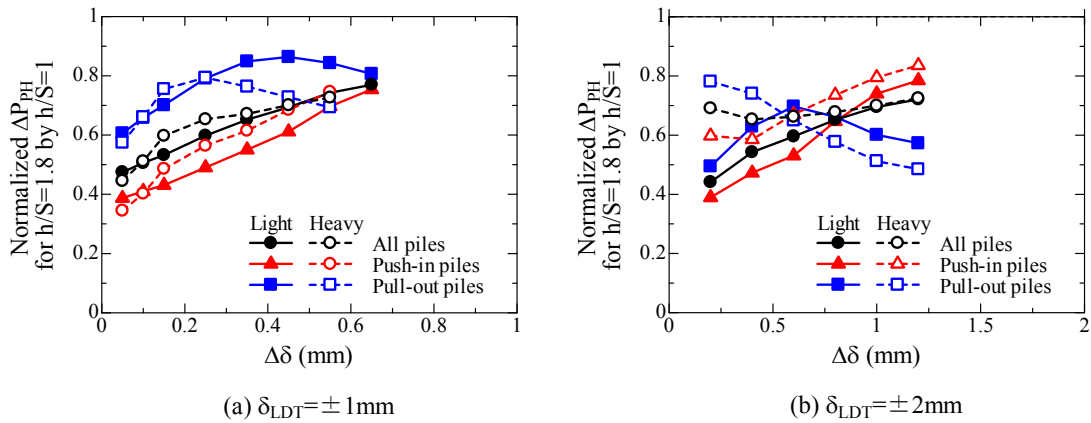
Figure 5.4.3.17 Relationship between $\Delta\delta$ and normalized ΔP_{PH} for h/S=1.8 by that for h/S=1.

Figure 5.4.3.18 shows the relationship between $\Delta\delta$ and ΔP_{PH} of all pile, push-in pile and pull-out pile for each loading step observed in PR_L1. The result from PR_H is shown in Appendix (A.5.4.3.13). The horizontal resistance of all piles, push-in pile and pull-out pile are shown in the figure. From this figure, it can be said that the large horizontal resistance was mobilized in the push-in pile during the first loading step, and the almost same horizontal resistance was shown in the other loading steps. The effect of the pre-vertical load was remained in the first loading step, but it was diminished after the first loading step. It should be noted that the horizontal resistances of the pull-out pile were almost same among all loading steps, implying that the pre-vertical load had a influence on only the push-in pile response.

(a) All piles (h/S=1)

(b) All piles (h/S=1.8)

(c) Push-in piles (h/S=1)

(d) Push-in piles (h/S=1.8)

(e) Pull-out piles (h/S=1)

(f) Pull-out piles (h/S=1.8)
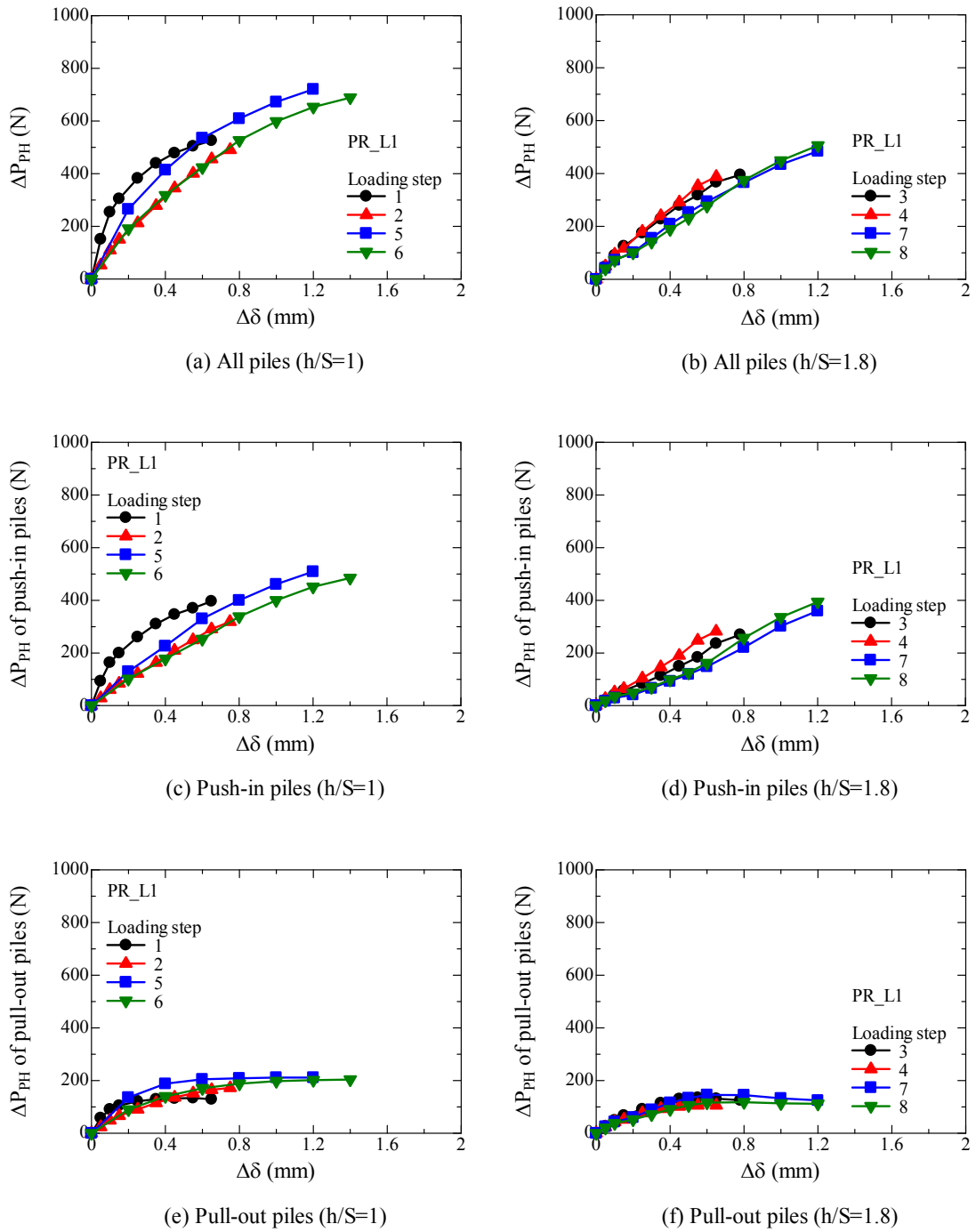
Figure 5.4.3.18 Relationship between $\Delta\delta$ and ΔP_{PH} for PR_L1 observed in each loading step.
(A. 5.4.3.13)

5.5 Moment resistance of piled raft

In this section, the moment resistance of the piled raft foundation will be examined. Firstly the moment resistance of overall foundation will be discussed, and then the loads acting on pile, which contributes the mobilization of the moment resistance of the piled raft foundation. Finally the moment resistance from the pile load and raft part will be discussed. The moment resistances from pile part such as the resistance from the variation of the pile head axial load and from the bending moment at pile head can be directly estimated by the pile load measured by the strain gauges. Although the moment resistance from the raft part cannot be measured directly, it can be evaluated by subtracting the moment resistance from pile part from the applied moment load. The applied moment load is estimated from not only the applied horizontal load ($P_L \times h$) but also the vertical load of the superstructure and foundation rotation ($W \times \Delta l$) as shown in Fig. 3.4.3.

5.5.1 Overall resistance of piled raft

Figure 5.5.1.1 and 5.5.1.2 show the relationship between the rotation of the foundation θ and moment load M_L for each foundation type. The black line and red line represent the result of h/S=1 and h/S=1.8 respectively. As been seen, the moment load was larger

(a) PR_L1

(b) P_L

(c) R_L1

(d) R_L2
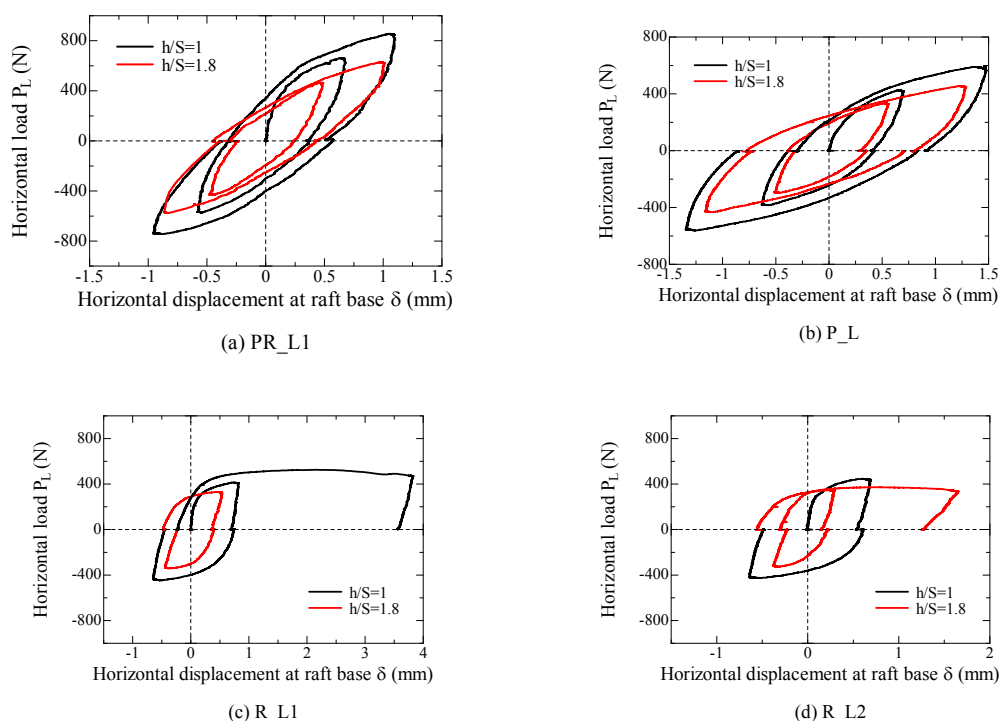
Figure 5.5.1.1 Relationship between horizontal displacement at raft base δ and horizontal load P_L for light case.

(a) PR_H

(b) P_H

(c) R_H1

(d) R_H2
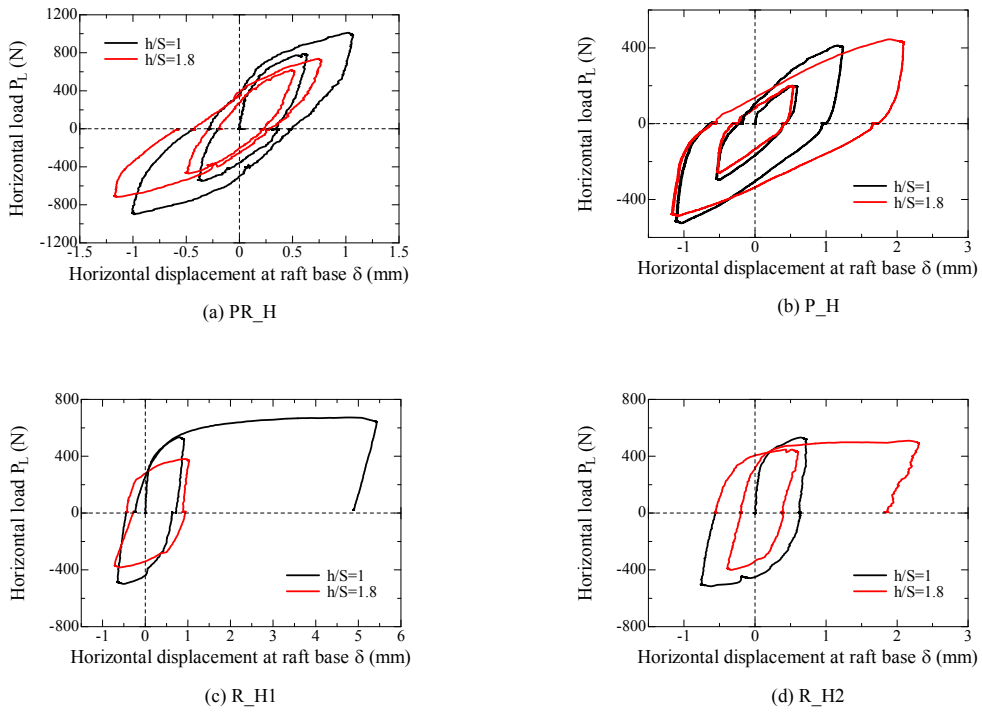
Figure 5.5.1.2 Relationship between horizontal displacement at raft base δ and horizontal load P$_L$ for heavy case.

(a) δ$_{LDT}$=±1mm, h/S=1

(b) δ$_{LDT}$=±1mm, h/S=1.8

(c) δ$_{LDT}$=±2mm, h/S=1

(d) δ$_{LDT}$=±2mm, h/S=1.8
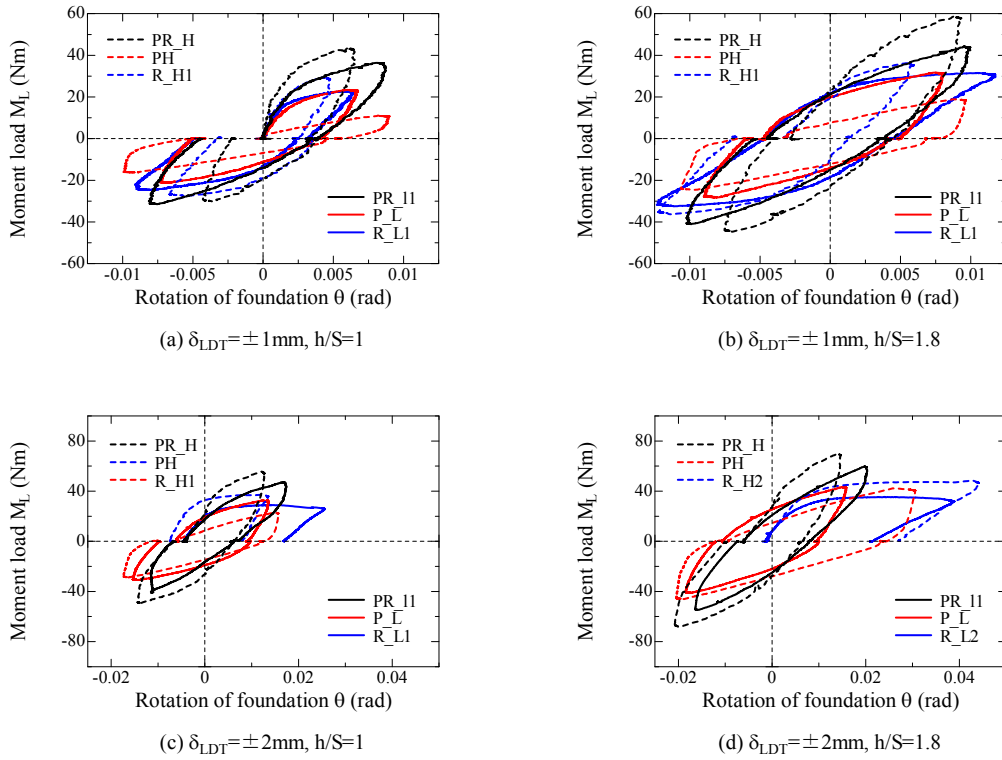
Figure 5.5.1.3 Relationship between rotation of foundation θ and moment load M$_L$ for each loading step.

for h/S=1.8 than h/S=1 because the relative horizontal load with the moment load was smaller for h/S=1.8. Figure 5.5.1.3 shows the rotation of the foundation θ and moment load M_L for each loading step. The raft foundation showed high moment resistance at the small rotation of foundation, but it was almost constant at the large moment resistance showing the clear failure of the foundation. On the other hand, the horizontal resistance of the pile group gradually mobilized with the horizontal displacement, and the moment resistance of the pile group was larger than that of the raft foundation at the large rotation. The piled raft foundation showed higher moment resistance than the pile group regardless the loading height and rotation level.
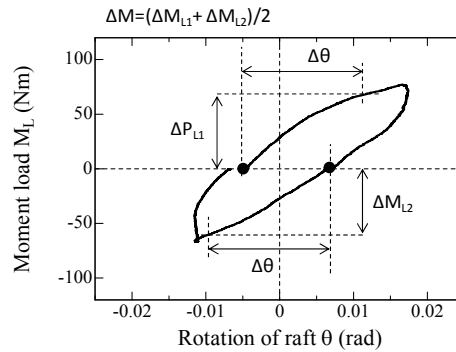
Figure 5.5.1.4 Definition of rotation increment $\Delta\theta$ and moment load increment ΔM.

(a) $\delta_{LDT}=\pm2$mm, h/S=1

(b) $\delta_{LDT}=\pm2$mm, h/S=1.8
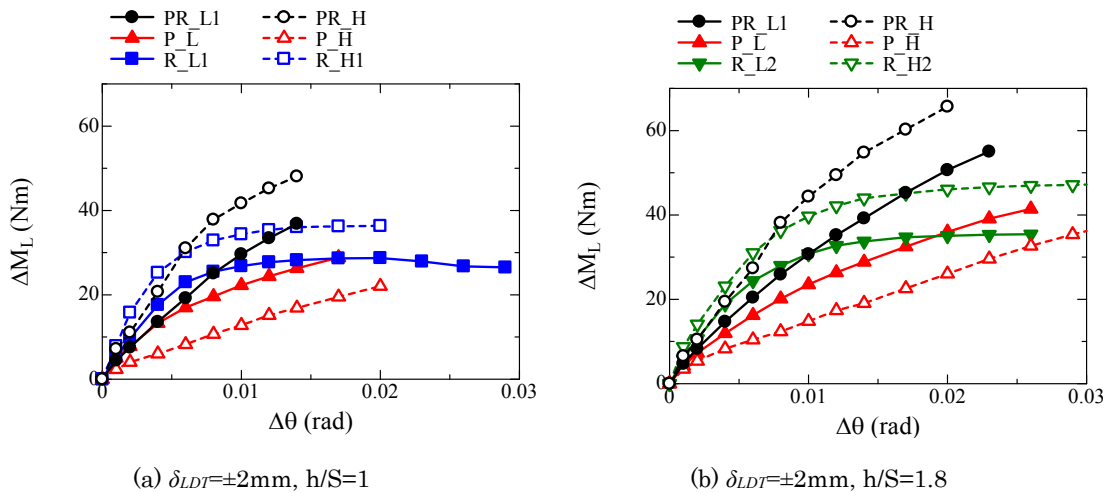
Figure 5.5.1.5 Relationship between $\Delta\theta$ and ΔM_L for each loading step.

Figure 5.5.1.5 shows relationship between the rotation increment $\Delta\theta$ and moment load increment ΔM_L where $\Delta\theta$ and ΔM_L are defined in Fig. 5.5.1.4. The result shown in this figure is from the loading step of $\delta_{LDT}=\pm2$mm, h/S=1 and 1.8. Results from other loading steps are summarized in Appendix (A. 5.5.1.1). As explained above, the moment resistance of the raft foundation was high at the small rotation range, however, the clear

failure of the foundation was clearly observed. And the moment resistance of the raft foundation was higher for the heavy case than the light case. For the pile group foundation, the moment resistance was gradually increased with the rotation of the foundation even for the relatively large rotation. And unlike the raft foundation, the moment resistance was higher for h/S=1 than h/S=1.8. This was because the safety factor of pile was smaller for heavy case than the light case (Fs=2.1 for light case and Fs=1.5 for heavy case) resulting in the weaker pile of heavy case. The moment resistance of the piled raft was almost same as the raft foundation at the small rotation, and it still increased with the rotation even for the large rotation. Although the piles in the piled raft also had a small safety factor in the heavy case, the mobilized moment resistance was larger for the heavy case than the light case. The reason for this will be discussed latter.

Figure 5.5.1.6 shows the relationship between $\Delta\theta$ and the normalized ΔM_L by that of the pile group foundation for the loading step of the loading step of δ_{LDT}=±2mm, h/S=1 and 1.8. Results from other loading steps are summarized in Appendix (A. 5.5.1.2). This normalized moment resistance represents the enhanced ratio of the moment resistance of the piled raft foundation to that of the pile group foundation. From this figure it can be said that the ratio of the raft foundation was large at the small rotation range, but it gradually decreased with the rotation because there was clear failure in the raft foundation. The piled raft foundation showed higher moment resistance than the pile group, particularly for the heavy case. Therefore, it seemed that the contribution of the raft part was larger for the piled raft with smaller safety factor of pile.

(a) δ_{LDT}=±2mm, h/S=1
(b) δ_{LDT}=±2mm, h/S=1.8
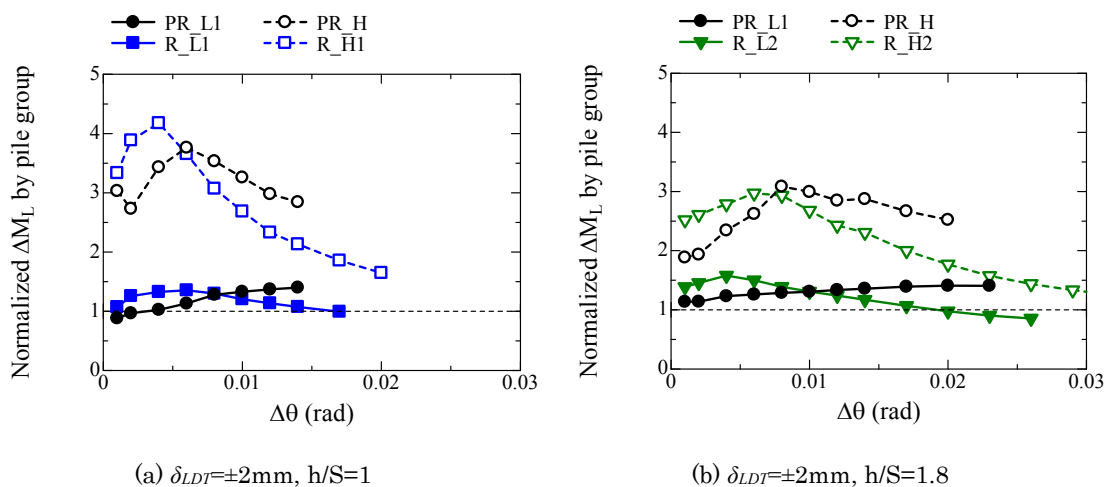
Figure 5.5.1.6 Relationship between $\Delta\theta$ and normalized ΔM_L by that of pile group. (A. 5.5.1.2)

Figure 5.5.1.7 shows relationship between $\Delta\theta$ and the normalized ΔM_L of heavy case by that of the light case for the loading step of the loading step of $\delta_{LDT}=\pm2$mm, h/S=1 and 1.8. Results from other loading steps are summarized in Appendix (A. 5.5.1.3). For the pile group foundation the moment resistance was larger for the light case in which the safety factor of the pile was larger. However, despite of the smaller safety factor of the pile part, the moment resistance was larger for the heavy case than the light case in the piled raft foundation. This was because the contribution from the raft part can be effectively mobilized for the smaller safety factor of the pile case owing to the relatively large settlement as explained in Fig. 5.3.1.4.

(a) $\delta_{LDT}=\pm2$mm, h/S=1 (b) $\delta_{LDT}=\pm2$mm, h/S=1.8
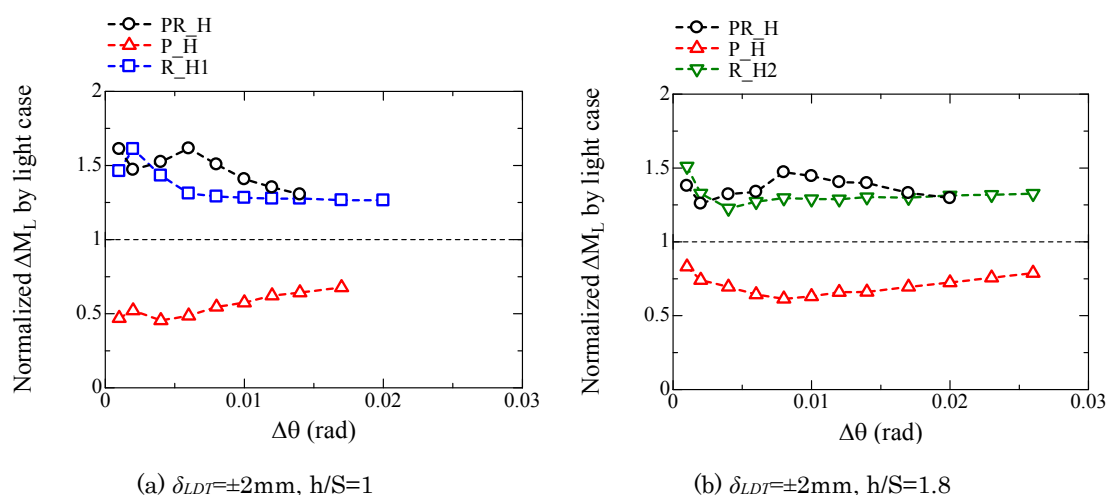
Figure 5.5.1.7 Relationship between $\Delta\theta$ and normalized ΔM_L of heavy case by that of light case. (A. 5.5.1.3)

Figure 5.5.1.8 and 5.5.1.9 show the relationship between $\Delta\theta$ and the normalized ΔM_L for each loading step. This figure compares with the moment resistances among the loading steps having same loading height. Therefore, the influence of loading procedures on the moment resistance of the foundation can be discussed using this figure. The moment resistance during the first loading step was larger than the others because the effect of the pre-vertical loading was remained in the first loading step. And the effect of the pre-vertical loading was diminished during the first loading because the soil around piles was disturbed by the loading.
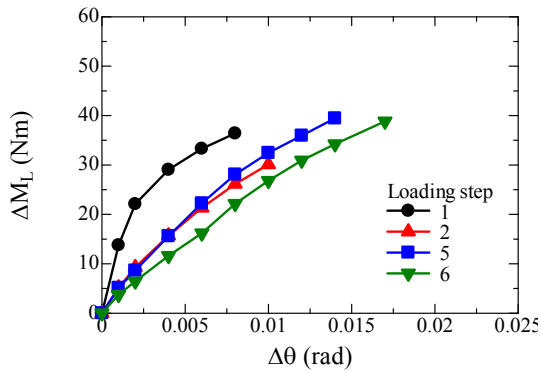
(a1) PR_L1 (h/S=1)
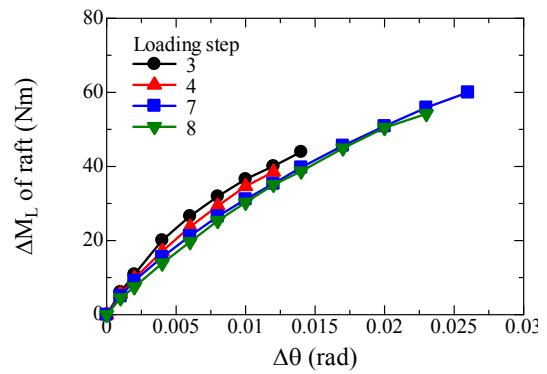
(a2) PR_L1 (h/S=1.8)
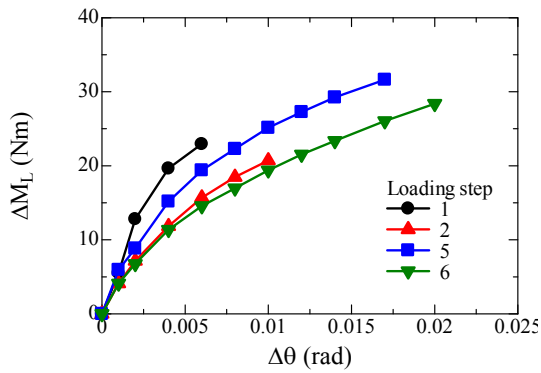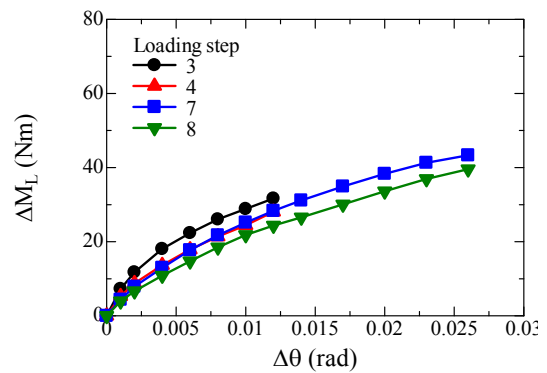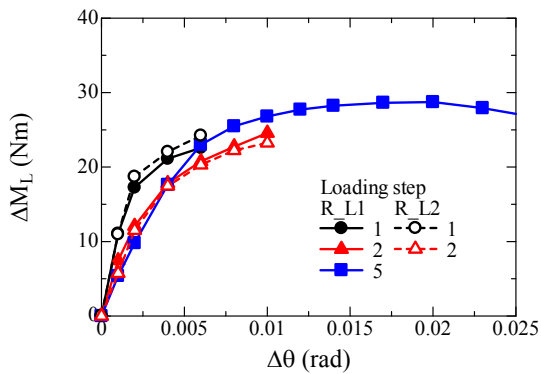
(b1) P_L (h/S=1)

(b2) P_L (h/S=1.8)
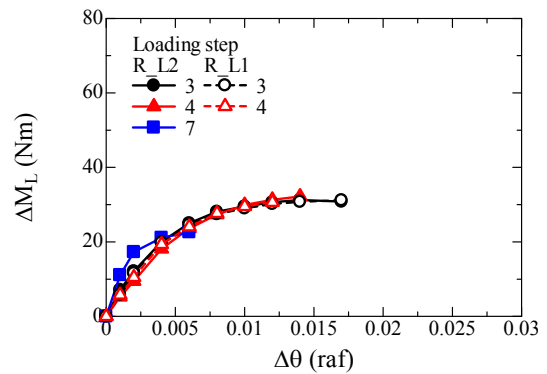
(c1) Raft (h/S=1)

(c2) Raft (h/S=1.8)

Figure 5.5.1.8 Relationship between $\Delta\theta$ and ΔM_L for light case observed in each loading step.
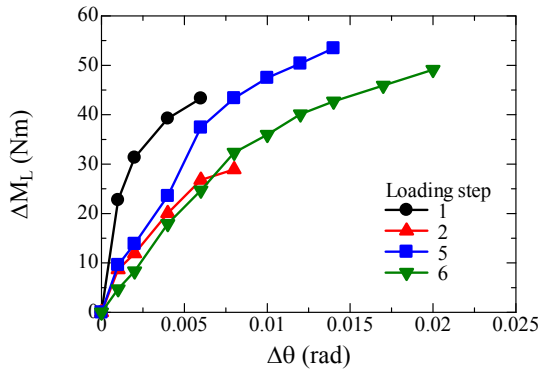
(a1) PR_L1 (h/S=1)
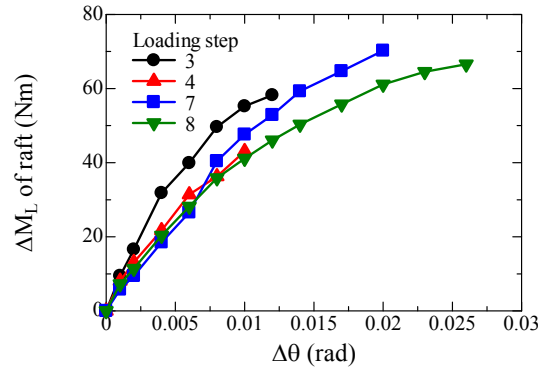
(a2) PR_L1 (h/S=1.8)
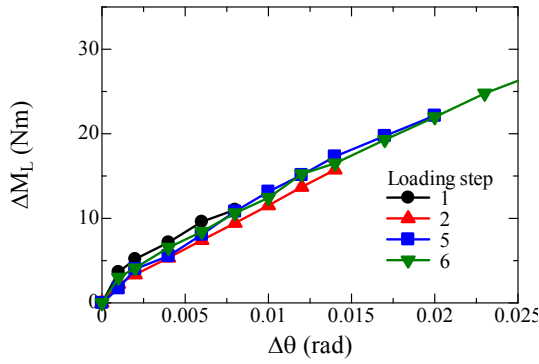
(b1) P_L (h/S=1)
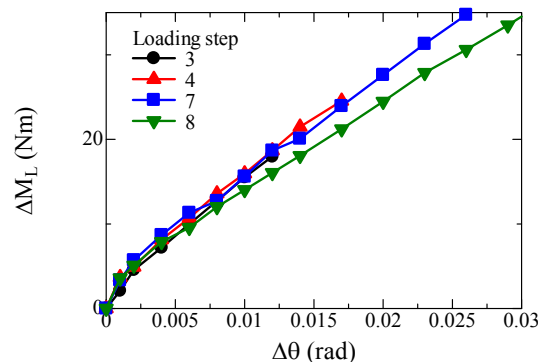
(b2) P_L (h/S=1.8)
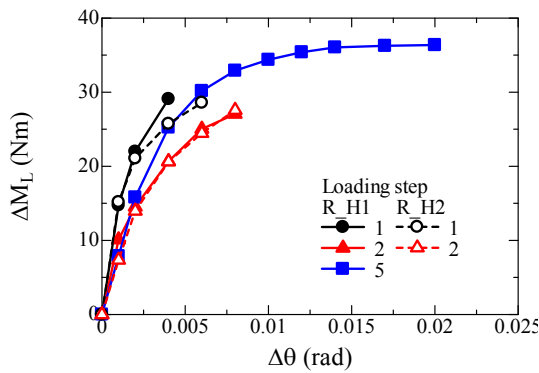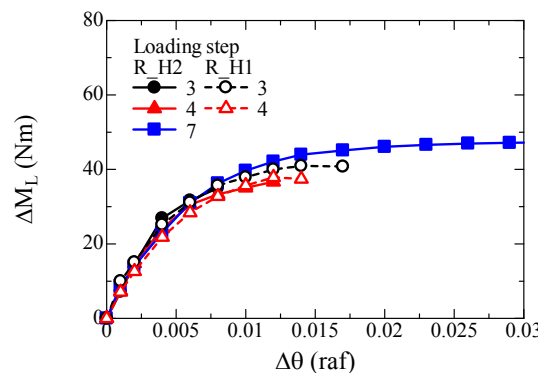
(c1) Raft (h/S=1)

(c2) Raft (h/S=1.8)

Figure 5.5.1.9 Relationship between $\Delta\theta$ and ΔM_L for heavy case observed in each loading step.

5.5.2 Loads acting on pile

The pile load is thought to be one of major factor of the moment resistance of the piled raft foundation. In this section the loads acting one pile such as the bending moment, axial load at pile head, end bearing load and shaft friction load will be examined.

5.5.2.1 Bending moment of pile

Figure 5.5.2.1 – 5.5.2.4 show the bending moment profile for the piled raft and pile group foundation. Figures (a) is the results at $\Delta\delta=\pm0.6$mm during the loading step 1 – 4 ($\delta_{LDT}=\pm1$mm), and Figures (b) is the results at $\Delta\delta=\pm1.2$mm during the loading step 5 – 8 ($\delta_{LDT}=\pm2$mm). Except for P_H, the bending moment at pile head showed opposite sign from the bending moment at deep ground. This kind of bending moment profile can be regarded as rigid pile head connection. However, the bending moment at pile head became zero or same sing as the bending moment at deep ground when the loading step proceeded. Therefore, it can be said the larger loading step was, the weaker the rigidity of the pile head connection was. For the P_H, the bending moment profiles can be regarded as the hinged pile head connection from the first loading step. Comparing the different loading height, there was no difference of bending moment at the deep ground, but the bending moment of h/S=1.8 was larger than that of h/S=1. Therefore, it can be said that the relative large moment load with the horizontal load may affect the bending moment at shallower part of the pile. For the piled raft foundation the bending moment of push-in pile was larger than that of the pull-out pile due to high confined stress around piles.
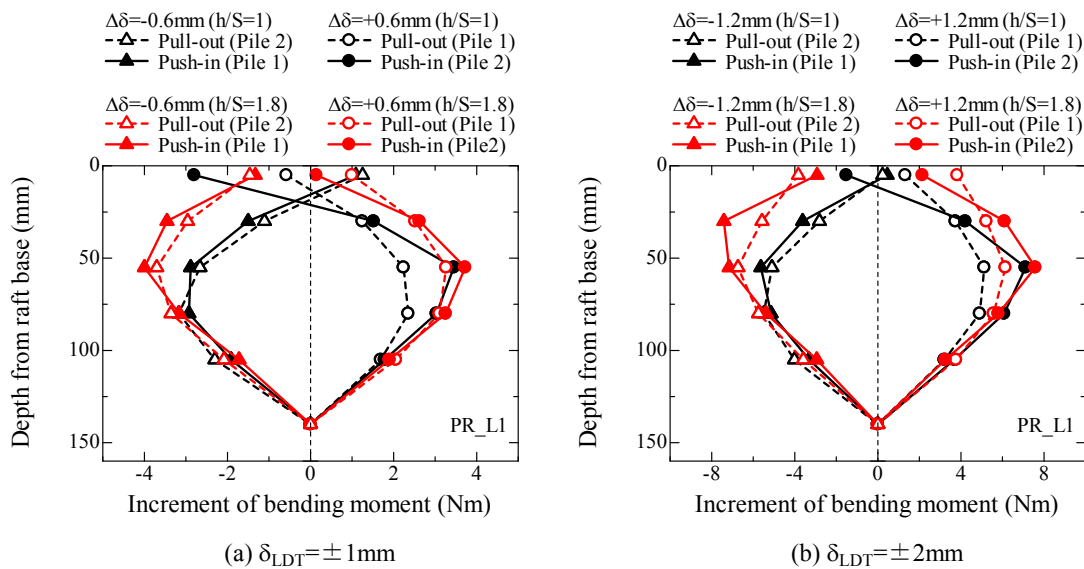
Figure 5.5.2.1 Profile of bending moment for PR_L1.

180

(a) $\delta_{LDT}=\pm 1mm$

(b) $\delta_{LDT}=\pm 2mm$
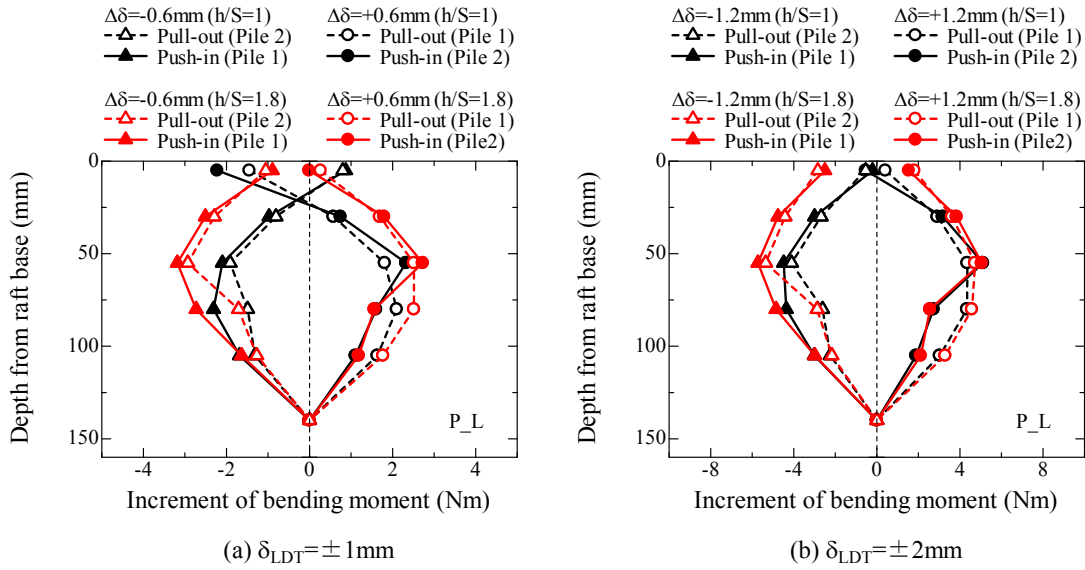
Figure 5.5.2.2 Profile of bending moment for P_L.

(a) $\delta_{LDT}=\pm 1mm$

(b) $\delta_{LDT}=\pm 2mm$
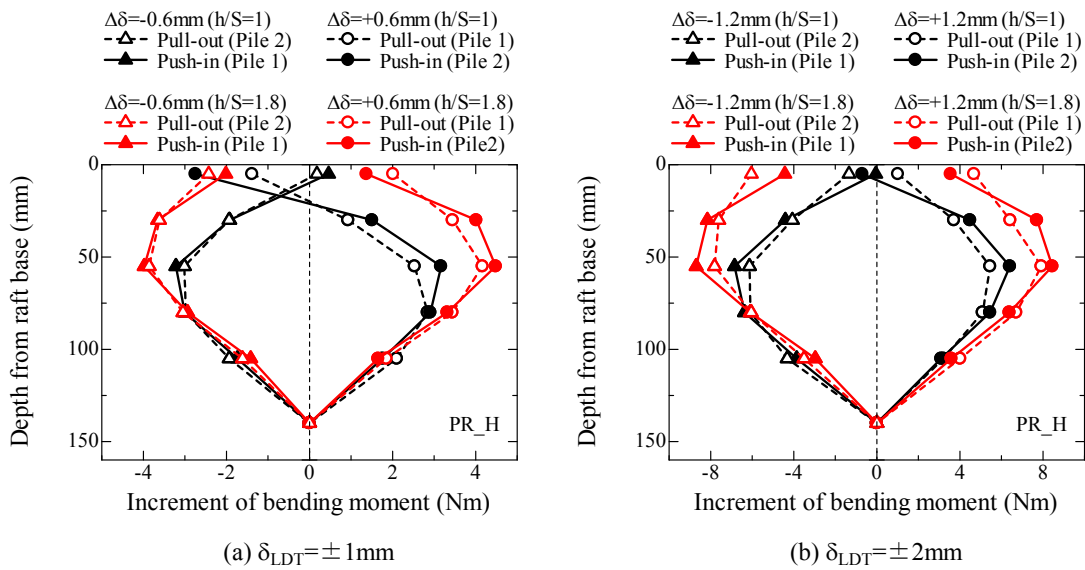
Figure 5.5.2.3 Profile of bending moment for PR_H.

181

(a) $\delta_{LDT} = \pm 1$mm
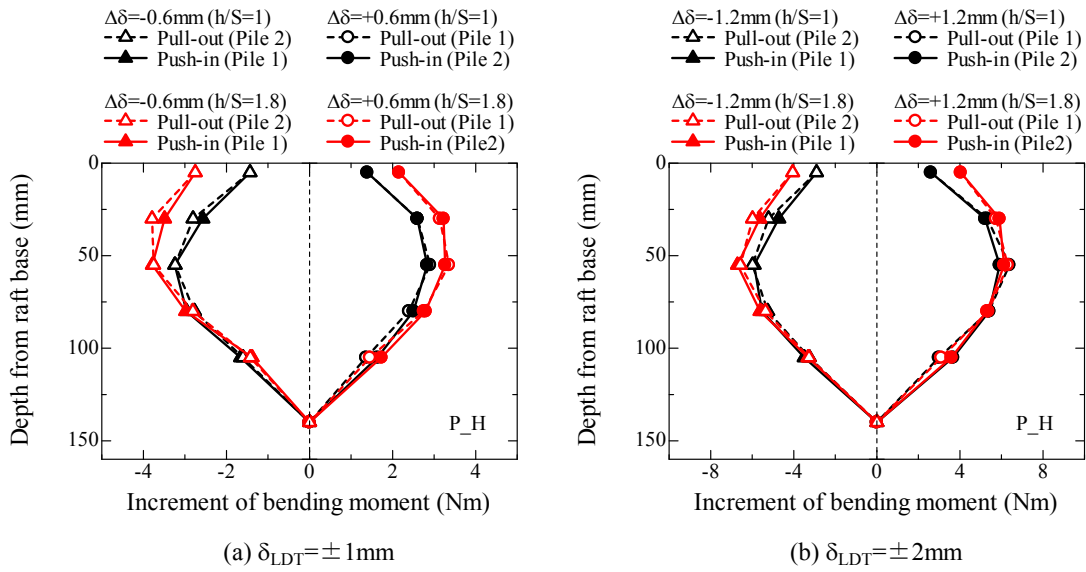
(b) $\delta_{LDT} = \pm 2$mm

Figure 5.5.2.4 Profile of bending moment for P_H.

(a) Push-in pile ($\delta_{LDT}=\pm 2$mm, h/S=1.8)

(b) Pull-out pile ($\delta_{LDT}=\pm 2$mm, h/S=1.8)
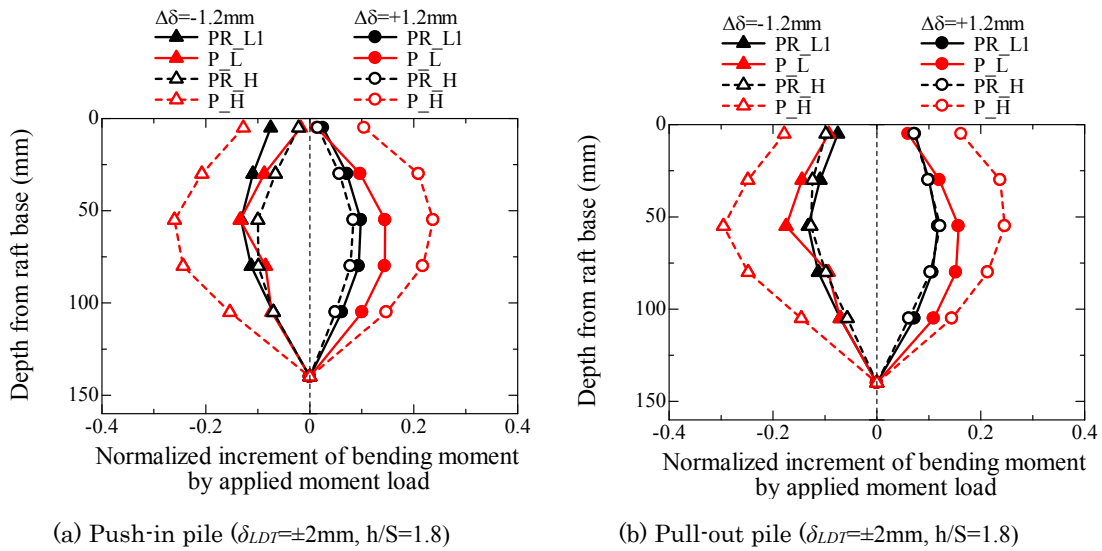
Figure 5.5.2.5 Profile of bending moment at $\Delta\delta=\pm 1.2$mm. (A. 5.5.2.1)

Figure 5.5.2.5 shows the bending moment profile of all foundation types at $\Delta\delta=\pm 1.2$mm for the loading step of $\delta_{LDT}=\pm 2$mm and h/S=1.8. Figure (a) and (b) represent the result of push-in pile and pull-out pile. The bending moment profile obtained from other loading step is summarized in Appendix (A. 5.5.2.1). The bending moment of push-in pile and pull-out pile are shown in the figure. The bending moment at the same horizontal displacement was larger for the piled raft foundation than the pile group foundation because large moment load was applied to the piled raft at the same displacement.

Figure 5.5.2.6 shows the normalized bending moment profile shown in Fig. 5.5.2.5 by

(g) Push-in pile ($\delta_{LDT}=\pm 2$mm, h/S=1.8)　　(h) Pull-out pile ($\delta_{LDT}=\pm 2$mm, h/S=1.8)
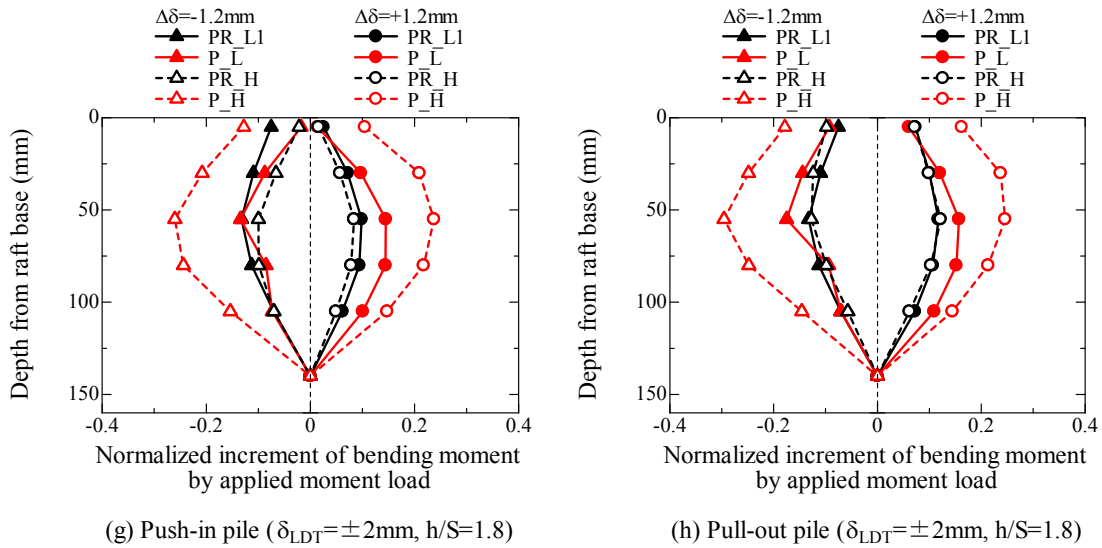
Figure 5.5.2.6 Profile of normalized bending moment by applied moment load at $\Delta\delta=\pm 1.2$mm.
(A. 5.5.2.2)

the applied moment load. The result shown in the figure is from loading step of $\delta_{LDT}=\pm 2$mm and h/S=1.8, and results observed in other loading steps are summarized in Appendix (A. 5.5.2.2). From this figure, it can be said that the relative bending moment acting on the pile with applied moment load can be restrained in the piled raft foundation compared with the pile group foundation. This was because the raft in the piled raft supported a part of the applied moment load and reduced the pile deformation and pile load. And this trend can be clearly seen for the heavy case. As explained in Chapter 3, because the safety factor or pile was small for the heavy case, the pile in the heavy case was thought to be easily deformed. However, the PR_H with small safety factor of pile can prevented the excessive pile deformation by the raft, and efficiently reduced the bending moment acting on pile.
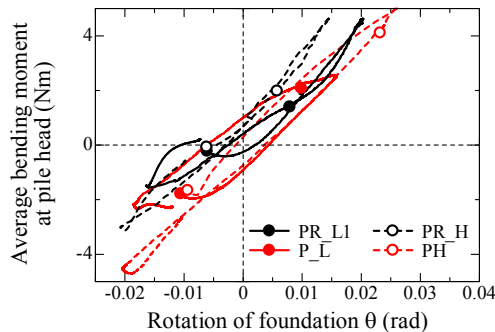
Figure 5.5.2.7 Relationship between rotation of foundaiton θ and average bending moment at pile head for $\delta_{LDT}=\pm 2$mm and h/S=1.8.

Figure 5.5.2.7 shows the relationship between the rotation of the foundation θ and bending moment at pile head for the loading step of $\delta_{LDT}=\pm 2$mm and h/S=1.8. The circular marks represent the beginning of each loading step.

5.5.2.2 Axial load of pile

Figure 5.5.2.8 – 5.5.2.11 show the variation of the axial load at pile head, the end bearing load and the shaft friction load of the left piles with the rotation of the foundation θ. The result from the right pile is summarized in Appendix (A. 5.5.2.8-5.5.2.11). And Figure 5.5.2.12 – 5.5.2.15 show the variation of the axial load at pile head, the end bearing load and the shaft friction load of the left piles with the settlement s. The result from the right pile is summarized in Appendix (A. 5.5.2.12-5.5.2.15).The result observed in the pre-vertical loading process is also shown in Fig. 5.5.2.12 – 5.5.2.15. The left pile consist of two piles, and therefore the pile load of left pile in these figures are represented as the average of two piles. Open marks in the figures represent the beginning of each loading step. The left pile was pushed in first and then pulled out. Except for P_H the end bearing load of pull-out pile reached at zero. Look at the relationship between the end bearing load and the settlement, pull-out pile in the piled raft foundation was further pulled out after the end bearing load reached zero. This trend shows the upward movement of pull-out pile was critical issues for the piled raft, which was already explained in Section 3.3.2. For the P_H, the end bearing load did not reach zero even for the large rotation of the foundation. As explained in Fig. 5.3.2.4 and 5.3.2.5, the settlement of push-in pile was dominant for the rotation of the foundation, and the upward displacement of the pull-out pile was quite small. Therefore, as been seen in Fig. 5.5.2.15 (c), the end bearing load did not reach the critical state for the pull-out side.

The end bearing load of push-in pile increased with the rotation of the foundation, and reached the peak value. As been seen in the relationship between the end bearing load and settlement, the end bearing load was significantly affected by the pre-vertical loading process, that is, the ultimate end bearing load during the horizontal loading tests was determined by the maximum end bearing load in the pre-vertical loading process. Therefore, after the end bearing load reached the maximum end bearing load in the pre-vertical loading, the end bearing load showed constant value and settlement rapidly increased. On the other hand, for the P_H the settlement of push-in pile was very large. Consequently, the relatively large end bearing load was mobilized compared with other cases. Therefore, the end bearing load in the push-in pile slightly increased at the large rotation of the foundation for P_H.
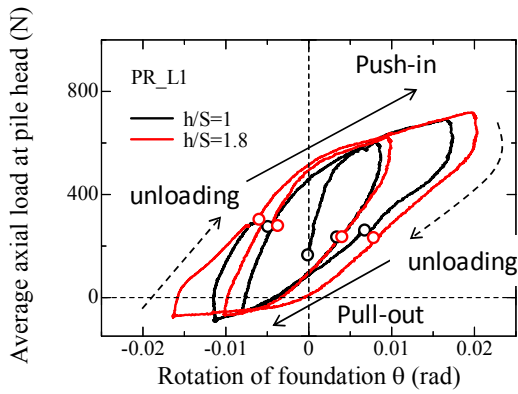
(a) Axial load at pile head (left pile)
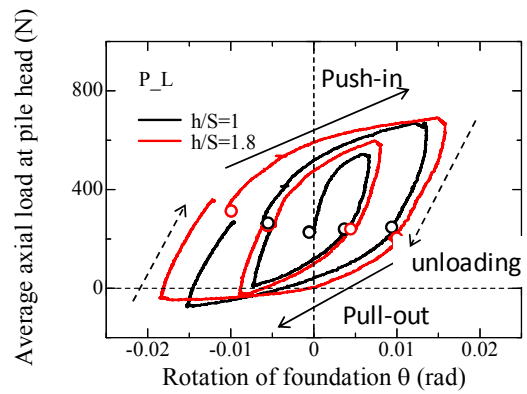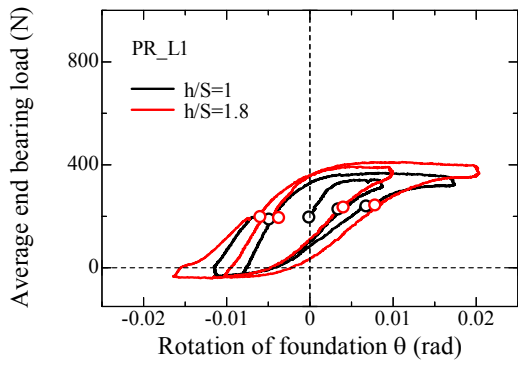
(a) Axial load at pile head (left pile)

(b) End bearing load (left pile)
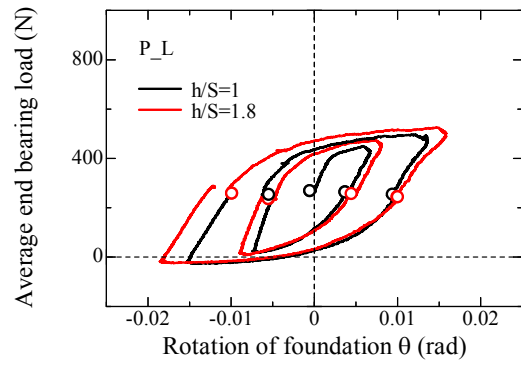
(b) End bearing load (left pile)
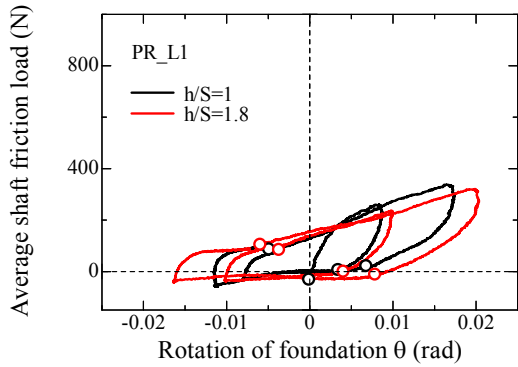
(c) Shaft friction load (left pile)
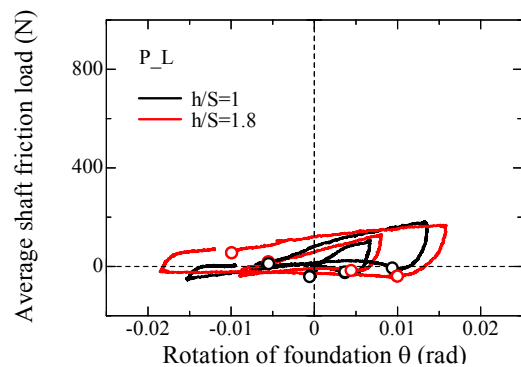
(c) Shaft friction load (left pile)

Figure 5.5.2.8 Variation of pile load with rotation of foundation θ for PR_L1. (A. 5.5.2.8)

Figure 5.5.2.9 Variation of pile load with rotation of foundation θ for P_L. (A. 5.5.2.9)
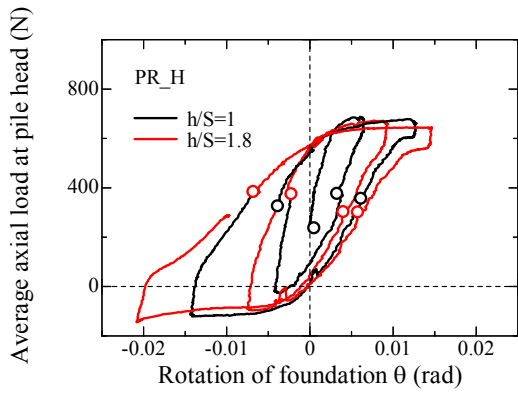
185

(a) Axial load at pile head (left pile)
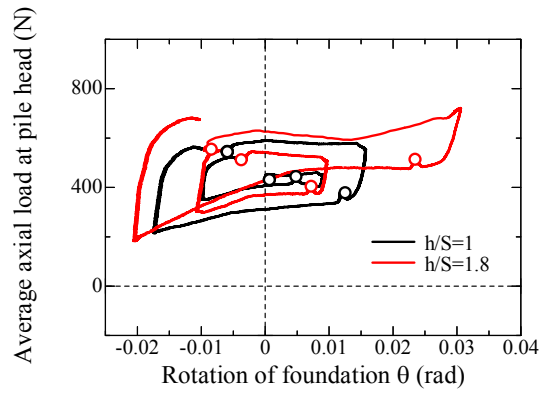
(a) Axial load at pile head (left pile)
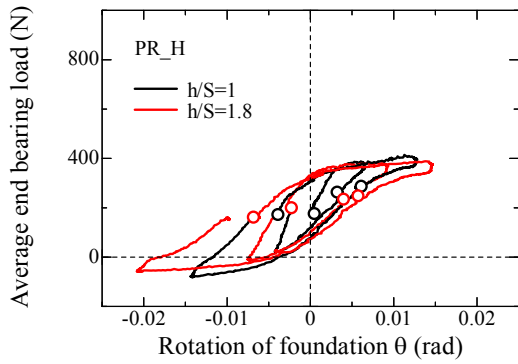
(b) End bearing load (left pile)
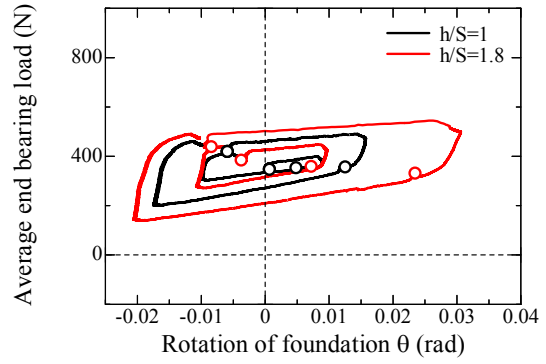
(b) End bearing load (left pile)
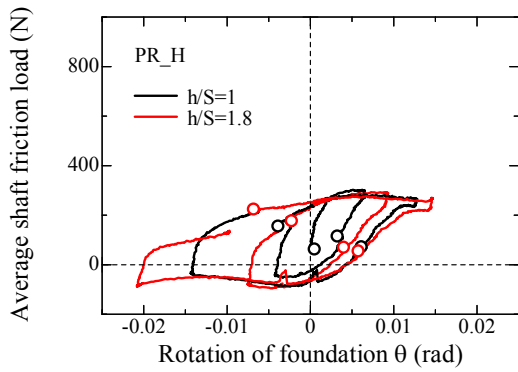
(c) Shaft friction load (left pile)
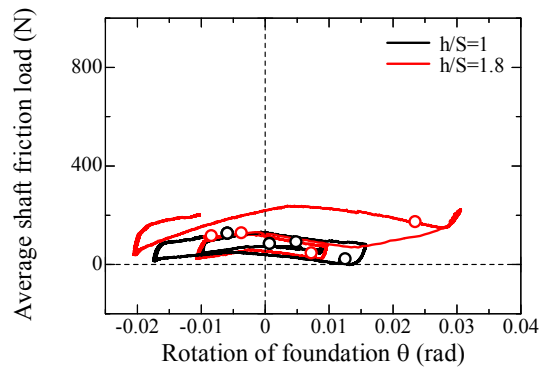
(c) Shaft friction load (left pile)

Figure 5.5.2.10 Variation of pile load with rotation of foundation θ for PR_H. (A. 5.5.2.10)

Figure 5.5.2.11 Variation of pile load with rotation of foundation θ for P_H. (A. 5.5.2.11)
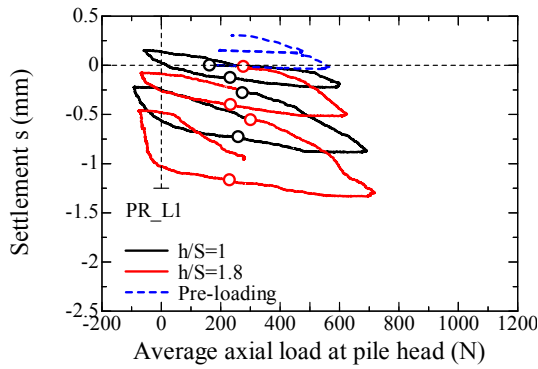
186
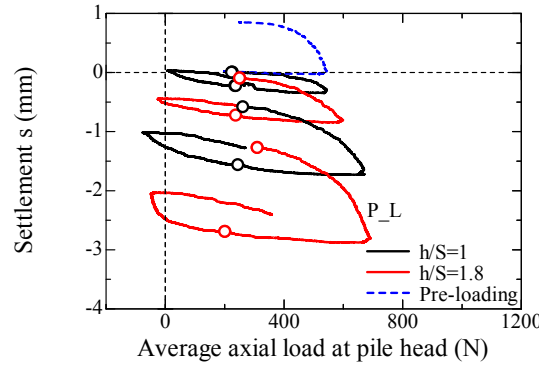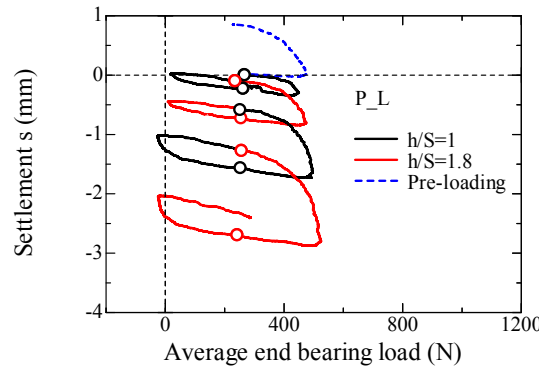
(a) Axial load at pile head (left pile)

(b) End bearing load (left pile)
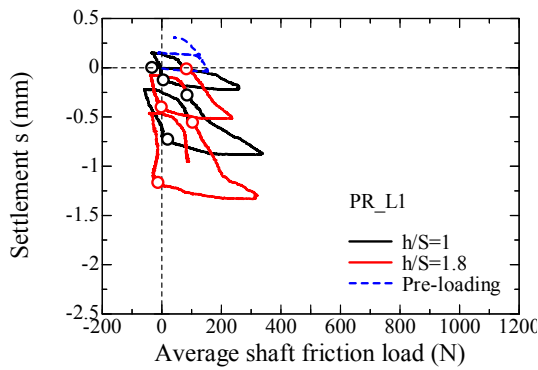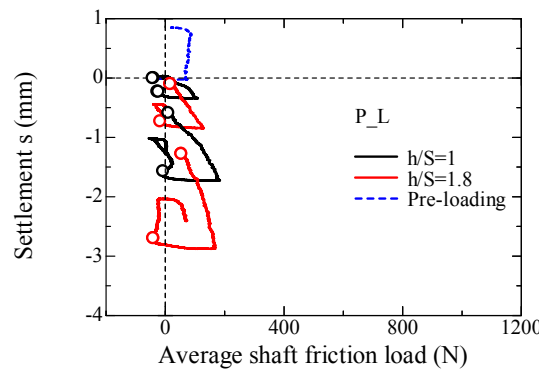
(c) Shaft friction load (left pile)

Figure 5.5.2.12 Variation of pile load with settlement for PR_L1. (A. 5.5.2.12)

(a) Axial load at pile head (left pile)

(b) End bearing load (left pile)

(c) Shaft friction load (left pile)

Figure 5.5.2.13 Variation of pile load with settlement for P_L. (A. 5.5.2.13)
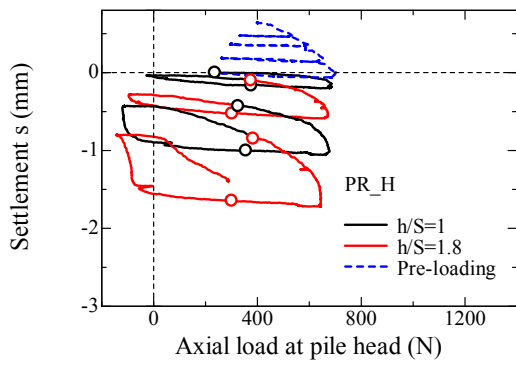
187

(a) Axial load at pile head (Left pile)

(a) Axial load at pile head (left pile)

(a) Axial load at pile head (Left pile)

(a) Axial load at pile head (left pile)

(c) End bearing load (Left pile)

(b) End bearing load (left pile)
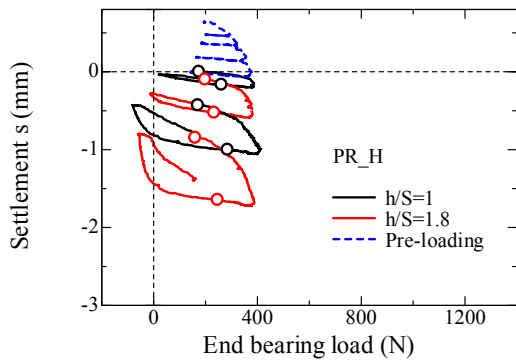
(c) End bearing load (Left pile)

(b) End bearing load (left pile)
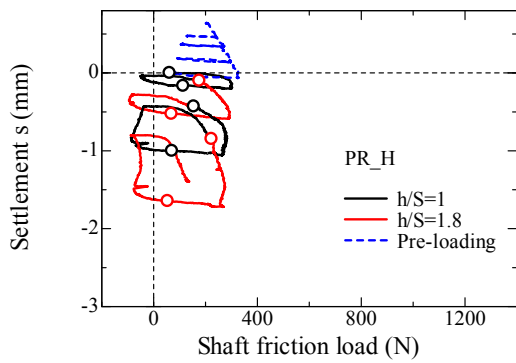
(e) Shaft friction load (Left pile)

(c) Shaft friction load (left pile)

Figure 5.5.2.14 Variation of pile load with settlement for PR_H. (A. 5.5.2.14)
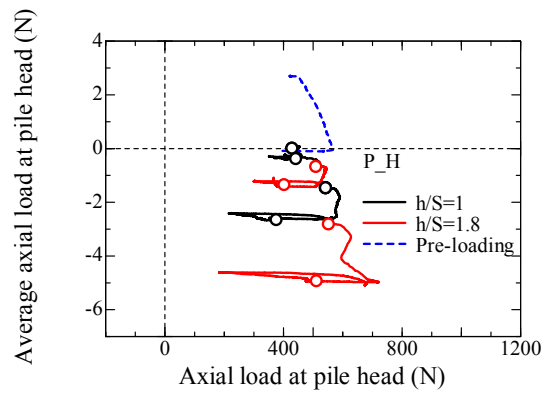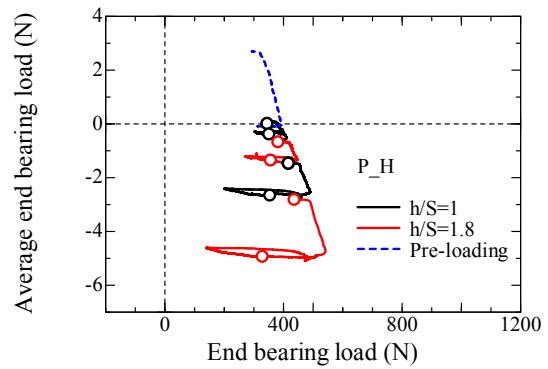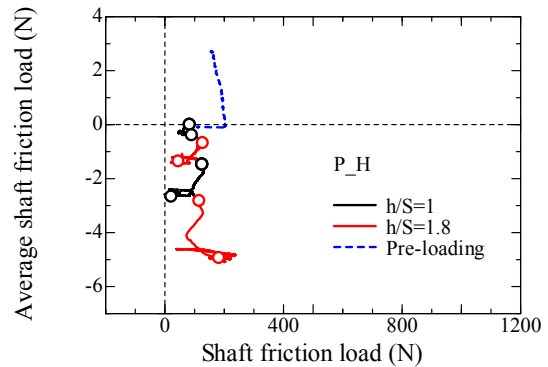
(e) Shaft friction load (Left pile)

(c) Shaft friction load (left pile)

Figure 5.5.2.15 Variation of pile load with settlement for P_H. (A. 5.5.2.15)

188

The shaft friction load of the pull-out pile reached at almost zero for all foundations. It was well known that the shaft friction load reached ultimate value by the relatively small displacement. Therefore, even for the P_H in which the upward displacement of pull-out pile was quite small, the shaft friction load reached at almost zero during the pile was pulled out. For the pile group case, although the shaft friction load showed almost constant value with the settlement during the pre-vertical loading process, that of push-in pile increased with the rotation and the settlement in the horizontal loading tests because the piles moved forward and the soil condition was shifted to the passive state. Furthermore, the raft base pressure at the push-in side was thought to be increased in the piled raft foundation. This influence of the raft part on the shaft friction load will be explained next figure.

To clarify the difference of pile load between the foundation type, the variation of the axial load at pile head, the end bearing load and the shaft friction load acting on left pile with rotation and settlement for each loading step are summarized in Fig. 5.5.2.16 and 5.5.17 respectively. These results are obtained from the loading step of δ_{LDT}=±2mm and h/S=1.8. Results from the right pile and other loading steps are summarized in Appendix (A. 5.5.2.16-5.2.2.19). The open marks in the figures represent the beginning of each loading step. The end bearing load of pull-out pile reached almost zero except for the P_H as shown in Fig. 5.5.2.8-5.5.2.15. In particular, the upward movement of the piled raft foundation was significant.

The end bearing load of push-in pile for all foundation types was involved in one envelope curve. Therefore, the larger end bearing load was mobilized in the pile group in which relatively large settlement was occurred. As explained in the previous chapter, the mobilized end bearing load was affected by the penetration depth in under the centrifugation, that is, the larger the penetration depth is, the larger the end bearing load is. Therefore, the larger end bearing load was mobilized for the light case compared with the heavy case in the penetration process and vertical loading process as explained in Chapter 4. However, there was slight difference of end bearing load between the light case and the heavy case as been seen in the Fig. 5.5.2.16, 5.5.2.17. This was because the relatively large pre-load, which was equivalent to the light case, was imposed to the heavy case during the pre-vertical loading process.

The initial end bearing load as represented as circular mark was smaller for the piled raft because a part of the vertical load was supported by the raft part and the vertical
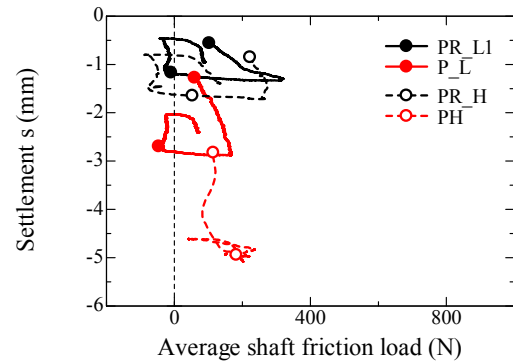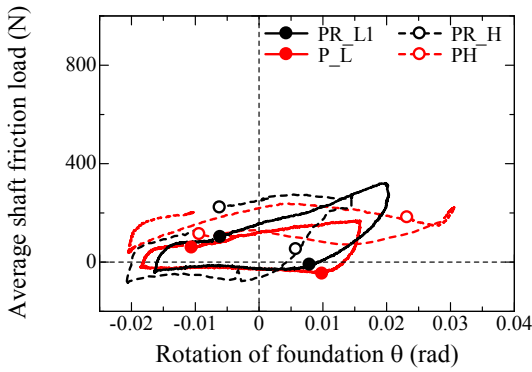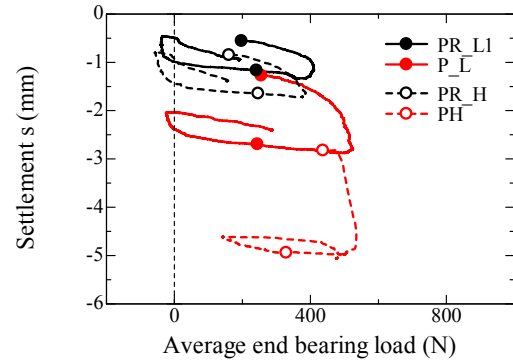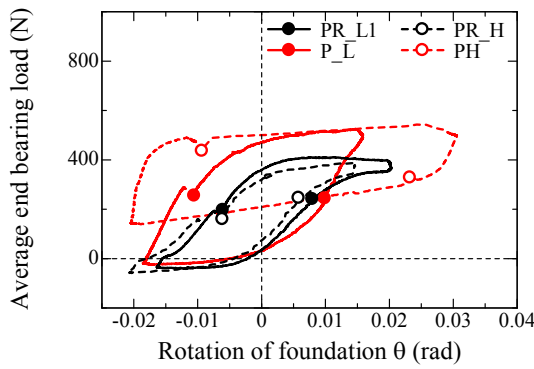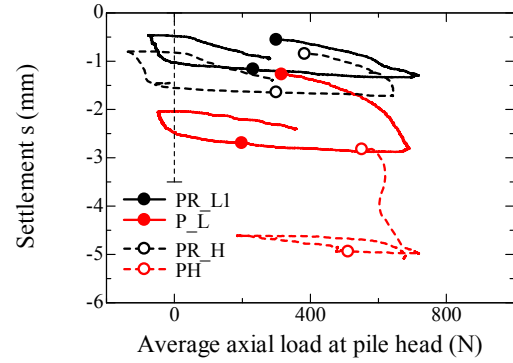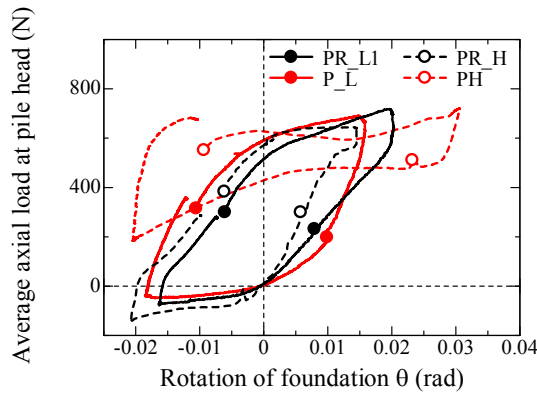
Figure 5.5.2.16 Variation of pile load with rotation of foundation θobserved in loading step 7 and 8 (δ_{LDT}=±2mm, h/S=1.8). (A. 5.5.2.16-5.5.2.19)

Figure 5.5.2.17 Variation of pile load with settlement observed in loading step 7 and 8 (δ_{LDT}=±2mm, h/S=1.8). (A. 5.5.2.16-5.5.2.19)

load acting on pile was reduced in the piled raft foundation. Therefore, the end bearing load of the pile group quickly reached ultimate bearing load, especially for P_H. Because the safety factor of pile was quite small for the P_H, the end bearing load reached ultimate value in quite small settlement, and the settlement of push-in pile was rapidly increased. Although the safety factor of pile was also small in PR_H, there was no clear yielding point in the end bearing load because the raft part supported a part of the vertical load and prevented the excessive settlement of push-in pile.

190

The shaft friction of the push-in pile increased with the settlement for both the piled raft and the pile group foundation. This was because piles moved forward and the soil condition was shifted to the passive state as explained in Fig. 5.5.2.8-5.5.2.15. The piled raft showed larger shaft friction load compared with the pile group foundation because the confined stress around piles increased by the raft base pressure in the push-in side. After the pile was pushed in, the push-in pile slightly moved upward and shaft friction load decreased during the unloading period. Except for the PR_H, the remained shaft friction load after unloading was almost zero as represented as circular marks. For the PR_H, the upward movement during the unloading period was smaller than other foundation types, and therefore the shaft friction load in the PR_H still showed positive value after the unloading.

In this section, the loads acting pile during the horizontal loading was examined. The moment resistance from each component such as pile load and raft part will be discussed in the next section.

5.5.3 Moment resistance of piled raft components

Figure 5.5.3.1 shows the method to calculate the moment resistance from the axial load acting on pile. The relationship between the rotation of the foundation θ and axial load at left pile head is described in the figure. The ΔP_{PI} and ΔP_{PO} in the figure represent the variation of axial load of push-in pile and pull-out pile respectively. From this figure, the axial load increment at the rotation increment $\Delta\theta$ for both positive and negative directions, and the average value of them was calculated. The moment resistance of the left pile was calculated by multiplying this average value with the distance between the
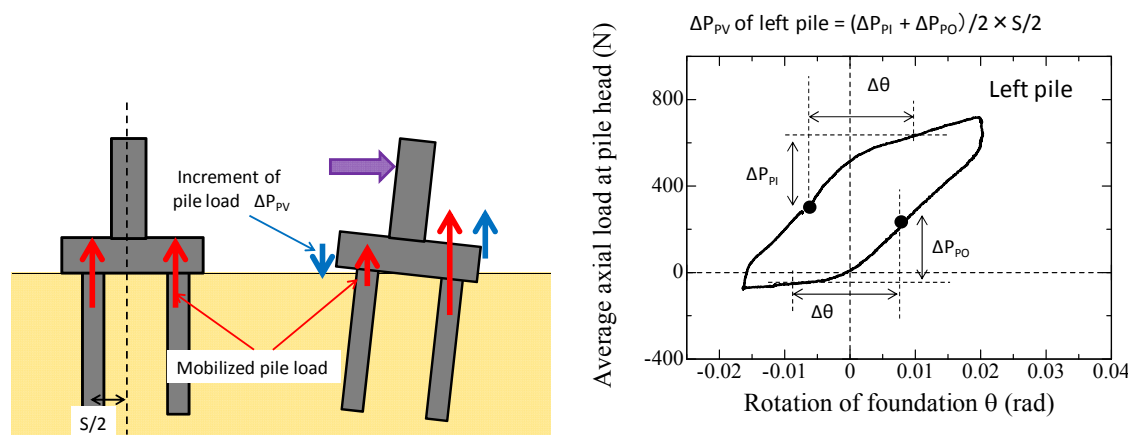
Figure 5.5.3.1 Calculation method to estimate moment resistance from pile load.

centre of the foundation and the left pile (S/2, where S is the pile spacing). The moment resistance of right pile was also calculated by the same matter as the left pile, and the sum of moment resistance of the left pile and right pile was defined as the moment resistance from the axial load at pile head. The moment resistance of the push-in pile an pull-out pile were calculated using the average ΔP_{PI} of right and left piles and average ΔP_{PO} of right and left piles. The moment resistances from the end bearing load and the shaft friction load were also estimated by the same method. The moment resistance from the raft part was calculated by subtracting the moment resistance of the pile part from the applied moment load. In this section, the moment resistance from the raft part will be examined.

(a) PR_L1

(b) P_L

(c) PR_H

(d) PR_H
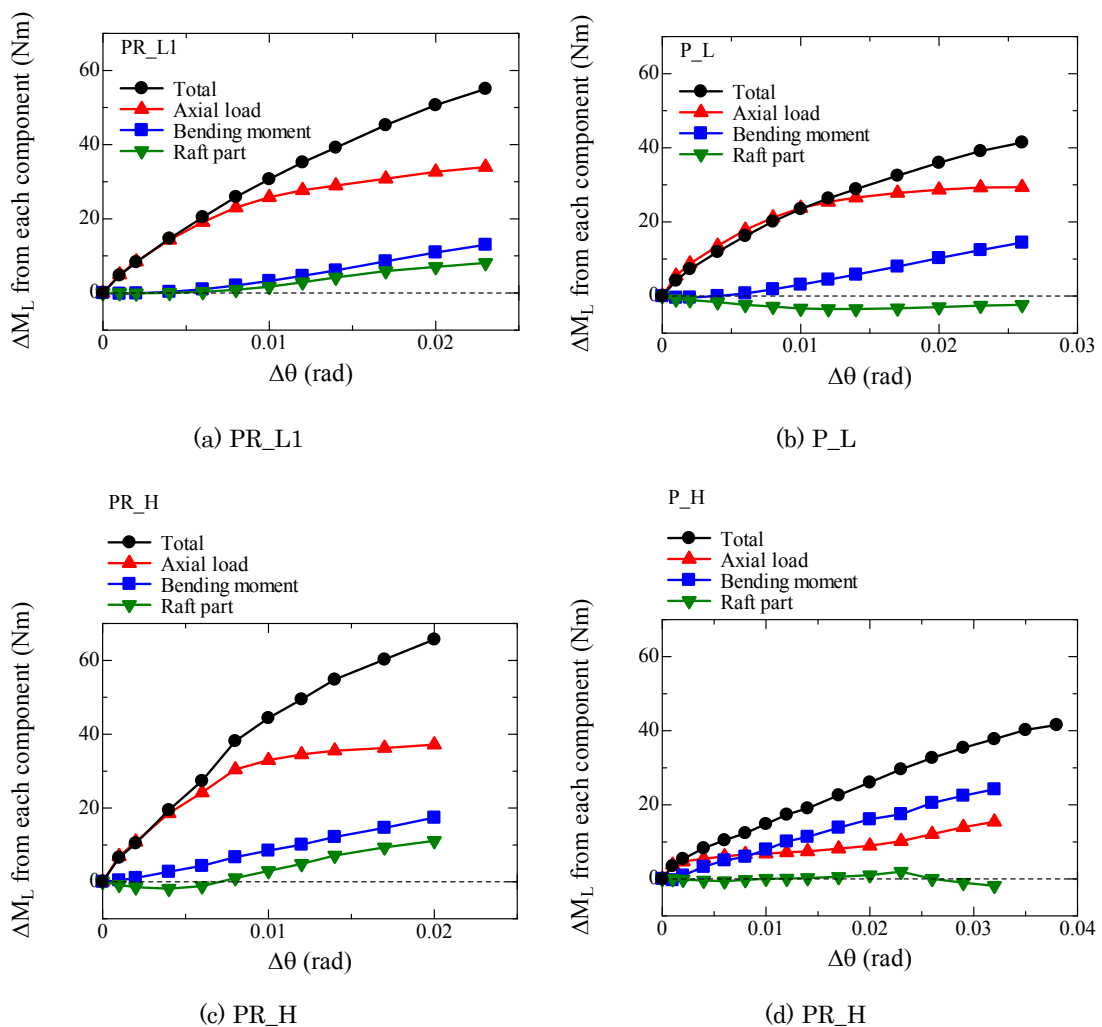
Figure 5.5.3.2 Relationship between Δθ and ΔML from axial load at pile head, bending moment at pile head and raft part.forδ_{LDT}=±2mm, h/S=1.8. (A. 5.5.3.1-5.5.3.4)

Figure 5.5.3.2 shows the relationship between $\Delta\theta$ and ΔM_L for each foundation type, where the $\Delta\theta$ and ΔM_L are defined in Fig. 5.5.1.4. The results shown in these figures are from δ_{LDT}=±2mm, h/S=1.8. The results from other loading steps are summarized in

Appendix (A. 5.5.3.1-5.5.3.4). The moment resistance from the axial load at pile head, bending moment at pile head and raft part are also shown in the figure. The moment resistance from raft part was also estimated for the pile group foundation. As been seen, the moment resistance from the raft part in the pile group foundation was almost zero for all loading step, implying that the calculated moment resistance of pile load had a high accuracy. Except for the P_H, the moment resistance of the foundation mainly consisted of the moment resistance of the axial load at pile head. This trend can be clearly seen at the small rotation of the foundation, and the moment resistance from the bending moment at pile head and raft part gradually increased with the rotation. On the other hand, the moment resistance from the axial load at pile head was relatively small for the P_H. The end bearing load in the push-in pile quickly reached ultimate value for the P_H as explained in Fig. 5.5.2.16 and 5.5.2.17. Therefore, the mobilized moment resistance from the axial load was small for the P_H.
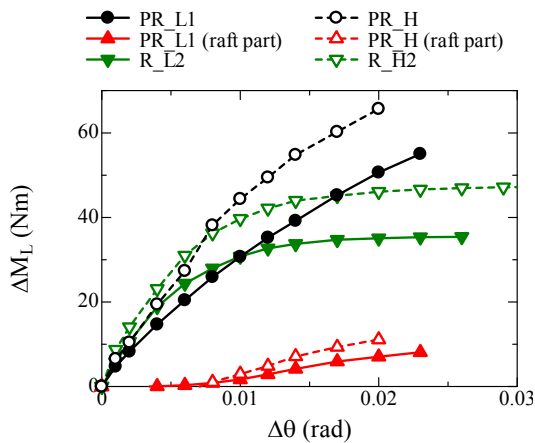
Figure 5.5.3.3 Relationship between $\Delta\theta$ and ΔM_L of piled raft, raft part in piled raft and raft foundation for. $\delta_{LDT}=\pm2$mm, h/S=1.8. (A. 5.5.3.5)
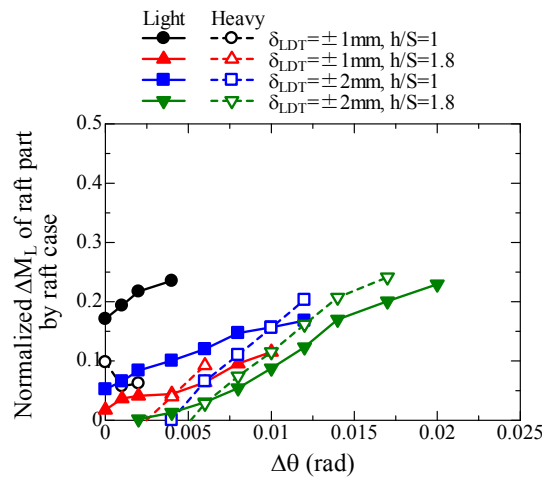
Figure 5.5.3.4 Relationship between $\Delta\theta$ and normalized ΔM of raft part by raft foundation.

5.5.3.1 Moment resistance of raft part

Figure 5.5.3.3 shows relationship between $\Delta\theta$ and the moment resistance from the raft part for $\delta_{LDT}=\pm2$mm, h/S=1.8. The results from other loading step are summarized in Appendix (A. 5.5.3.5). The moment resistances of the piled raft and the pile group foundations are also shown in the figure. The normalized moment resistance from the raft part by that of the raft foundation for each loading step is shown in the Fig. 5.5.3.4. This normalized resistance expressed the ratio of the moment resistance from the raft part in the piled raft to that of the raft foundation. The moment resistance of the raft foundation was almost same as that of the piled raft foundation at small rotation of the

foundation, but it showed almost constant value at the large rotation showing the clear failure of the raft foundation. The moment resistance from the raft part in the piled raft foundation was relatively small at the small rotation. However, there was no clear failure point like the raft foundation, and the moment resistance of the raft part still increased even at the large rotation. Therefore, the normalized horizontal resistance of the raft part increased with the rotation, and finally it showed about 20% of moment resistance of the raft foundation.

Figure 5.5.3.5 shows the relationship between $\Delta\theta$ and the moment resistance of the raft part of heavy case normalized by that of the light case for $\delta_{LDT}=\pm 2$mm, h/S=1 and 1.8. The results from other loading steps are summarized in Appendix (A. 5.5.3.6). The result of the raft foundation is also shown in the figure. From this figure it can be said that the higher moment resistance was observed in the heavy case than the light case, and the normalized moment resistance of the raft foundation was almost same with the rotation. On the other hand, the moment resistance of the raft part in the piled raft foundation was larger for the light case than the heavy case at the small rotation, and it gradually larger for the heavy case at the large rotation.
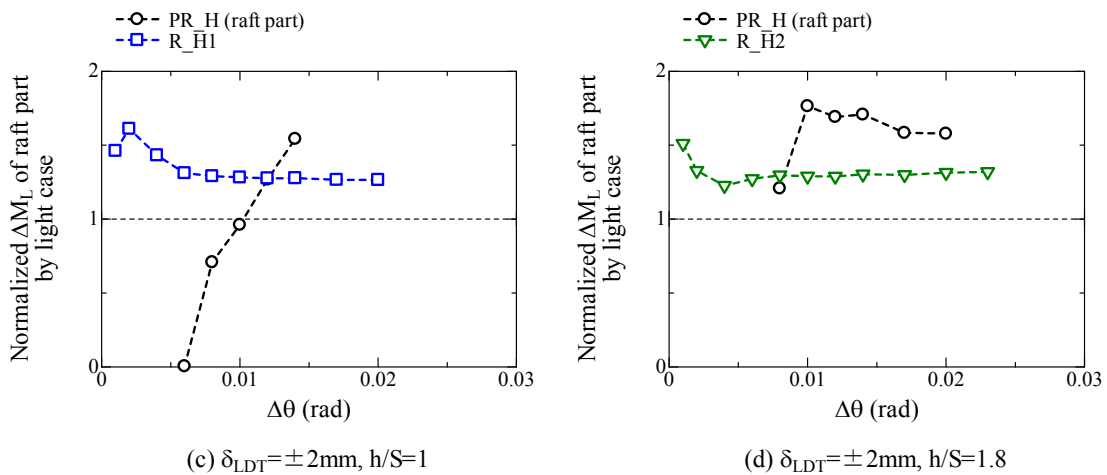
Figure 5.5.3.5 Relationship between $\Delta\theta$ and normalized ΔM of raft part normalized by light case for $\delta_{LDT}=\pm 2$mm, h/S=1 and 1.8. (A. 5.5.3.6)

Figure 5.5.3.6 and 5.5.4.7 show the relationship between $\Delta\theta$ and the moment resistance from the raft part in the piled raft foundation observed in each loading step for light case and the heavy case respectively. From this figure it can be said that the larger moment resistance of the raft part was observed in the first loading step compared with others. This was because the effect of pre-vertical loading was strongly remained in

the first loading step.

(a) PR_L1 (h/S=1)

(b) PR_L1 (h/S=1.8)
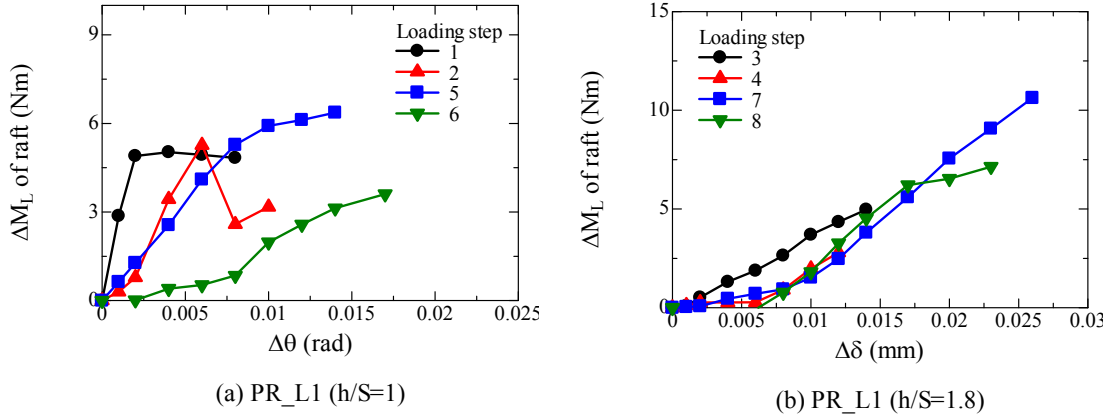
Figure 5.5.3.6 Relationship between $\Delta\theta$ and ΔM of raft part for light case observed in each loading step.

(a) PR_H (h/S=1)

(b) PR_H (h/S=1.8)
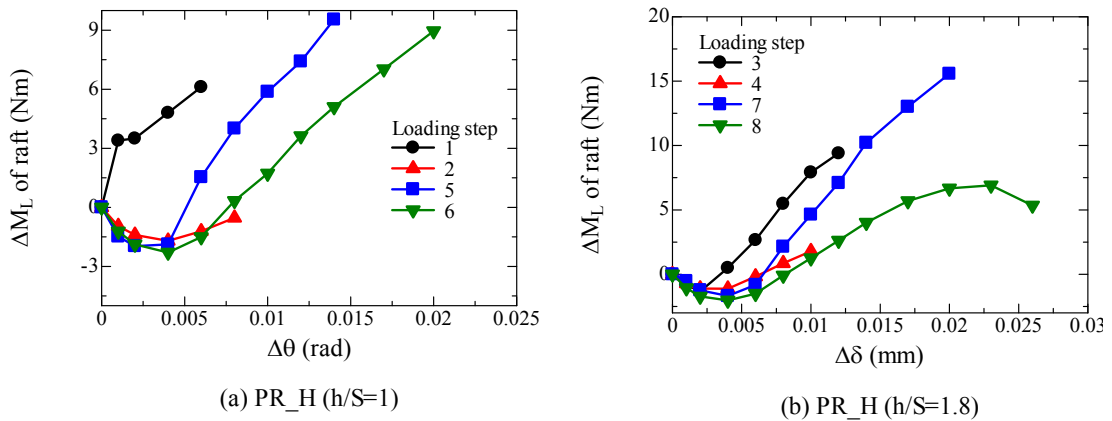
Figure 5.5.3.7 Relationship between $\Delta\theta$ and ΔM of raft part for heavy case observed in each loading step.

5.5.3.2 Moment resistance of pile part

In this section the moment resistance from the pile part will be examined. The moment resistance from the pile part can be divided into two parts such as that from the axial load at pile head and the bending moment at pile head.

Figure 5.5.3.8 show the relationship between the $\Delta\theta$ and the moment resistance from the bending moment at pile head for $\delta_{LDI}=\pm2$mm and h/S=1.8. The results from other loading steps are summarized in Appendix (A. 5.5.3.7). In the small loading step, the moment resistance from the bending moment at pile head showed negative value because the connection conditions of the pile head and the raft was rigid in the small loading step, and the mobilized bending moment at pile head was negative as shown in

195

Fig. 5.5.2.1 – 5.5.2.4. However, the rigidity of the pile head connection became weaker with the loading procedure resulting in the positive bending moment at the pile head.

(d) $\delta_{LDT}=\pm 2mm$, h/S=1.8
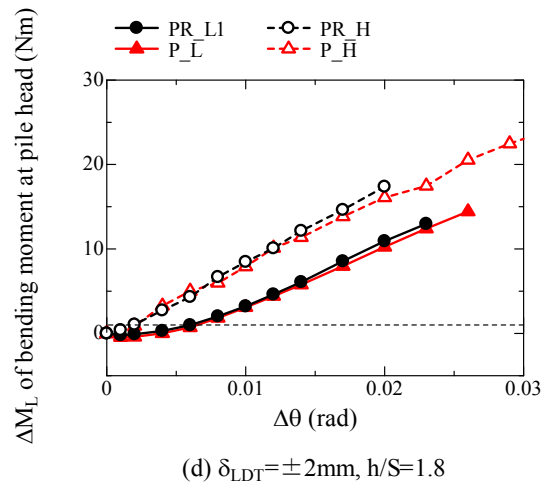
Figure 5.5.3.8 Relationship between $\Delta\theta$ and ΔM of bending moment at pile head for $\delta_{LDT}=\pm 2mm$ and h/S=1.8. (A. 5.5.3.7)

Figure 5.5.3.9 show the variation of the moment resistance from the axial load at pile head, the end bearing load and the shaft friction load with $\Delta\theta$ for $\delta_{LDT}=\pm 2mm$ and h/S=1.8. The results from other loading steps are summarized in Appendix (A. 5.5.3.8-5.5.3.11). These moment resistances from pile load are divided into push-in pile and pull-out pile in the figure. It was noted that the sum of the moment resistance from the end bearing load and the shaft friction load is the moment resistance from the axial load at pile head. It was observed that the moment resistance from the end bearing load was larger for the pull-out pile than the push-in pile in all foundation types. This was because the variation of the end bearing load in the pull-out pile was larger than that in the push-in pile.

Except for PR_H, the moment resistance from shaft friction load of pull-out pile was almost zero because the initial shaft friction load before the pile was pulled-out was almost zero as explained in Fig. 5.5.2.16 and 5.5.2.17. On the other hand, the initial shaft friction load before pulled out was positive for the PR_H, and therefore the moment resistance from the shaft friction load or pull-out pile was larger for the PR_H. As a result, the moment resistance from the axial load at pile head, which was determined by the sum of the moment resistance of the end bearing and the shaft friction loads, was larger for the PR_H compared with others.

196

(a) PR_L1

(b) P_L

(c) PR_H

(d) P_H
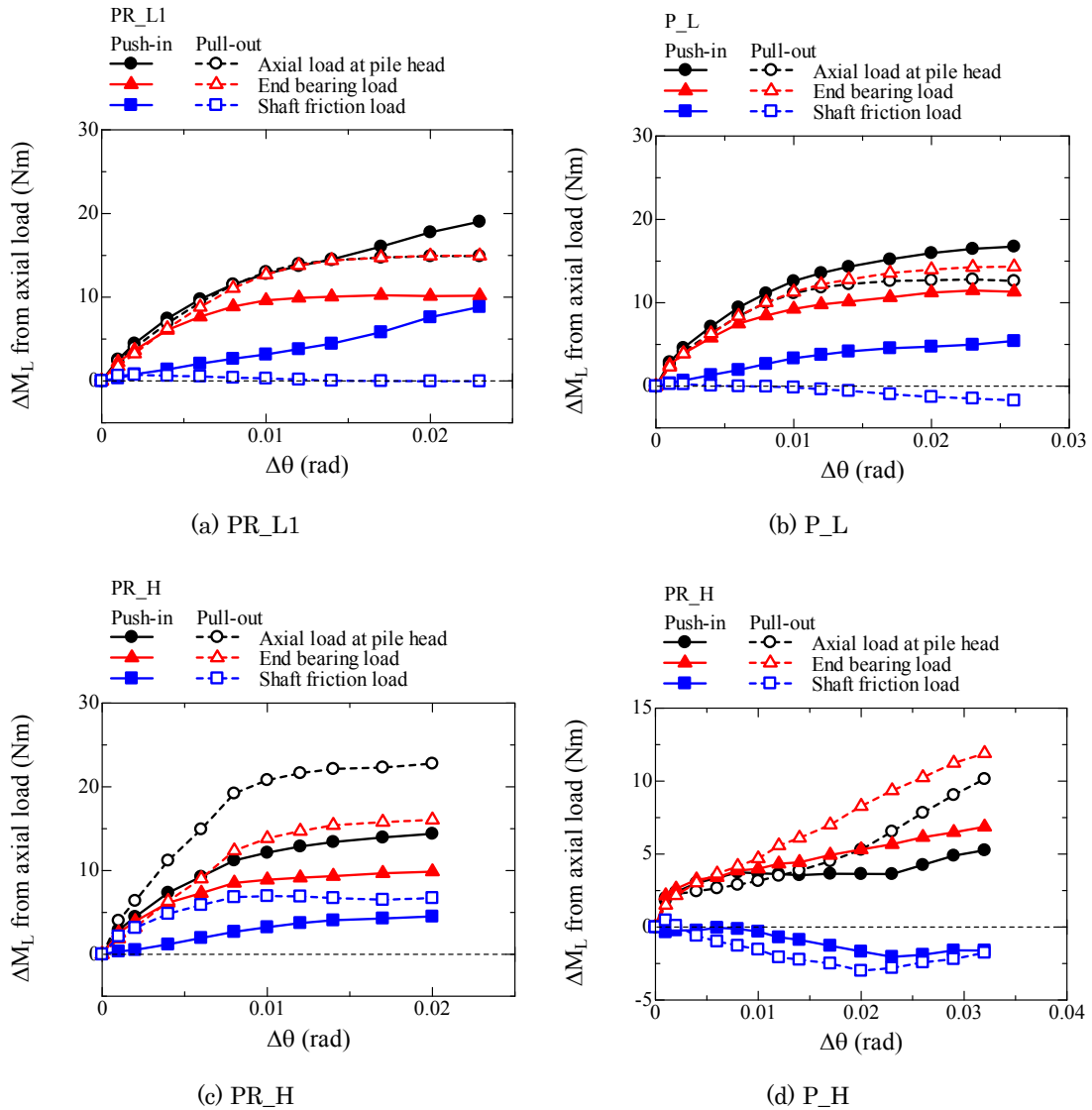
Figure 5.5.3.9 Relationship between $\Delta\theta$ and ΔM from axial load at pile head, end bearing load and shaft friction load for $\delta_{LDT}=\pm2$mm and h/S=1.8. (A. 5.5.3.8-5.5.3.11)

To discuss the difference of the mobilization of moment resistance from the pile load, the variation of moment resistance from the axial load at pile head, the end bearing load and shaft friction load with $\Delta\theta$ for $\delta_{LDT}=\pm2$mm and h/S=1.8 is described in Fig. 5.5.3.10. The results from other loading steps are summarized in Appendix (A. 5.5.3.12-5.5.3.15). The moment resistance from the end bearing load was almost same between the PR_L1 and P_L for both push-in and pull-out pile. Actually the moment resistance from the shaft friction load of push-in pile was larger for the PR_L1 than the P_L due to the increase of confined stress around piles, but this increment was not significant. And, the moment resistance from the shaft friction load of pull-out pile was almost zero for both the PR_L1 and the P_L as explained above. Furthermore, the moment resistance from the

(a) Axial load (push-in pile)　　(b) Axial load (pull-out pile)

(c) End bearing load (push-in pile)　　(d) End bearing load (pull-out pile)

(e) Shaft friction load (push-in pile)　　(f) Shaft friction load (pull-out pile)
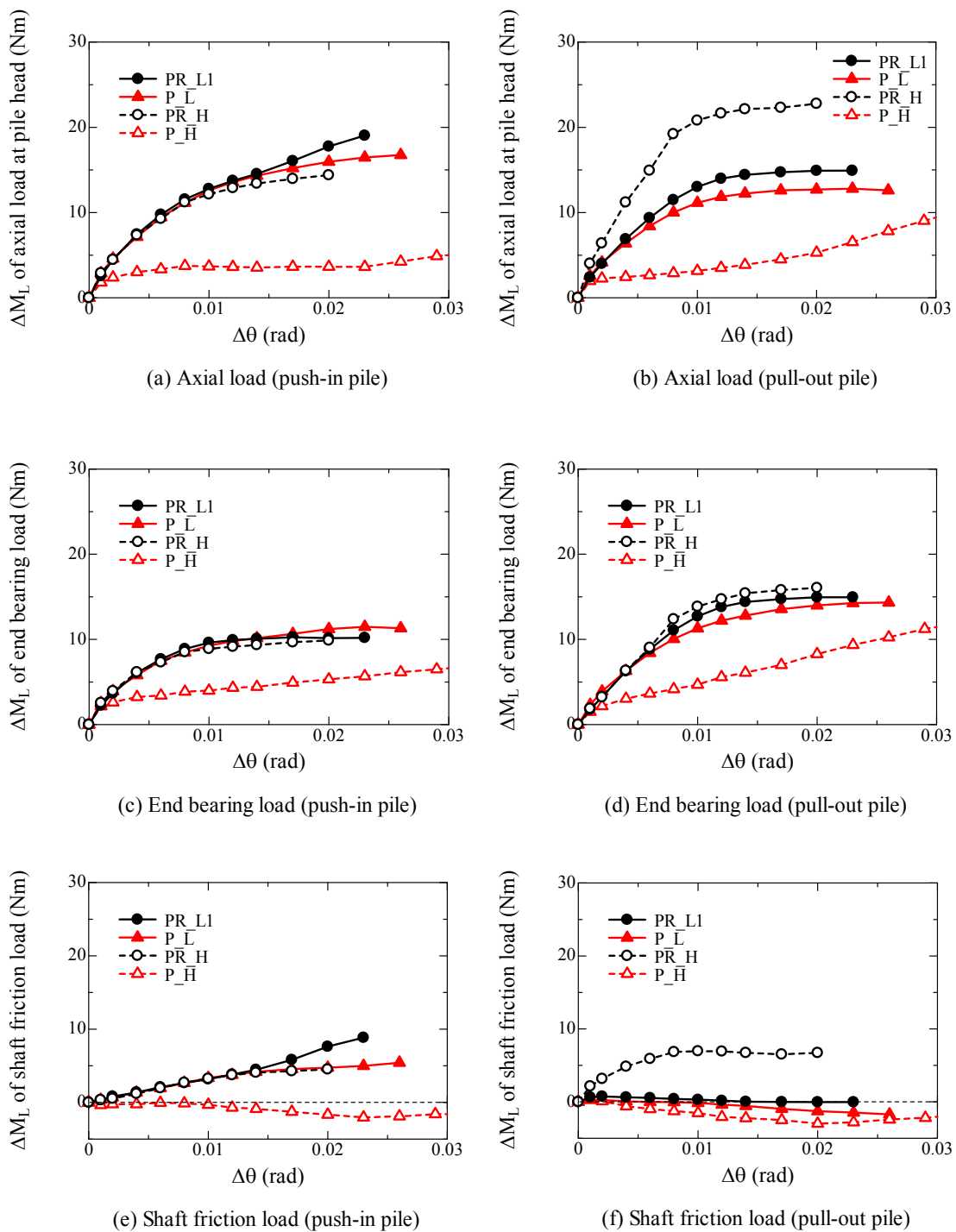
Figure 5.5.3.10 Relationship between $\Delta\theta$ and ΔM from pile load observed in $\delta_{LDT}=\pm2$mm and h/S=1 (loading step 7 and 8). (A. 5.5.3.12-5.5.3.15)

bending moment at pile head was also almost same between the PR_L1 and the P_L as shown in Fig. 5.5.3.8. From these facts, it can be said that the if the safety factor of the pile is sufficient, the moment resistance from the pile part was almost same between the

piled raft foundation and the pile group foundation.

Figure 5.5.3.11 shows the relationship between $\Delta\theta$ and moment resistance from the axial load by that of the pile group foundation for $\delta_{LDT}=\pm2mm$ and h/S=1.8. The results from other loading steps are summarized in Appendix (A. 5.5.3.16). The moment resistance of the axial load means the moment resistance of axial load, end bearing load and shaft friction load. This normalized resistance represents the increased ratio of moment resistance of piled raft to that of the pile group foundation. From this figure, it can be said that the moment resistance from the pile part (axial load at pile head) in the piled raft foundation was almost same as that of the pile group foundation. However, because the piled raft foundation can obtain the moment resistance from the raft part as shown in Fig. 5.5.3.2, the moment resistance of overall foundation was larger for the piled raft than the pile group foundation (Fig. 5.5.1.5、5.5.1.6).
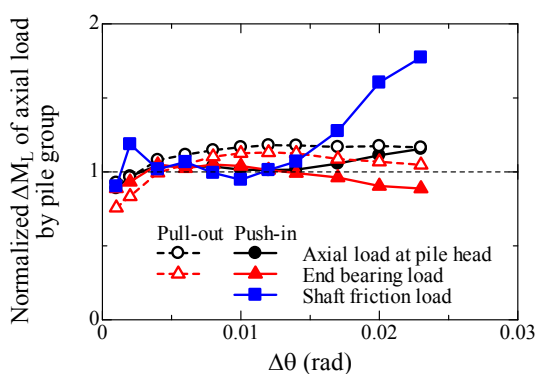
(d) P_L1 ($\delta_{LDT}=\pm2mm$, h/S=1.8)

Figure 5.5.3.11 Relationship between $\Delta\theta$ and normalized ΔM from pile load by pile group for PR_L1 for $\delta_{LDT}=\pm2mm$ and h/S=1.8. (A. 5.5.3.16)

Next the moment resistance of heavy case, in other words, the smaller safety factor of the pile, will be focused. The moment resistance from the end bearing load and the shaft friction load for both push-in pile and pull-out pile were significantly larger for the piled raft foundation than the pile group foundation. This was because although the pile group foundation with small safety factor of pile reached ultimate state in the quite small rotation and settlement, the piled raft foundation prevented the clear failure of piles and the excessive settlement. Therefore, larger moment resistance from the axial load can be obtained for the piled raft than the pile group foundation. In particular, although the moment resistance from the shaft friction load of the pull-out pile was almost zero for all foundation except for the PR_H, it was relatively large in the PR_H. Consequently, despite of the small safety factor of pile, the PR_H showed higher moment resistance

199

than the piled raft and pile group with large safety factor of pile (Fig. 5.5.1.5, 5.5.1.7).

5.6 Summary

In this chapter the mechanical behavior of the piled raft foundation subjected to horizontal and moment loads in sand was examined. The much focus was placed on the influence of the raft base pressure on the pile response. The following findings are derived from the present chapter.

The piled raft foundation can restrain the settlement caused by the alternate horizontal loading. In particular, even if the safety factor of the pile was small, the settlement of the push-in pile was effectively reduced for the piled raft foundation compared with the pile group foundation because the raft in the piled raft prevented the excessive settlement of push-in pile. However, the smaller settlement of push-in pile enhanced the pull-out displacement of pull-out piles, resulting in the larger upward movement than that of the pile group foundation. Therefore, it can be said that the upward movement of the pull-out pile was critical issue for the small scale piled raft with narrow pile spacing.

The settlement of the heavy case, in other words, the case with the small safety factor of the pile, was larger than that of the light case for both the pile group and the piled raft. This relatively large settlement of heavy case made the contact condition between the raft and the ground surface better.

The horizontal resistance of the piled raft foundation was higher than the pile group foundation, especially for the piled raft with small safety factor of pile because the larger contribution of the raft part can be mobilized. The horizontal resistance of the push-in pile was larger for the piled raft foundation than the pile group foundation due to the increase of the confined stress around pile. The horizontal subgrade reaction at relatively deep part (more than the raft width) was also enhanced by the raft pressure.

On the other hand, the horizontal resistance of the pull-out pile was smaller for the piled raft foundation than the pile group foundation. As explained above, the upward displacement of pull-out pile was critical for the piled raft foundation, and therefore the base contact stress rapidly reduced around the pull-out pile. In addition to this, the relative displacement of pull-out pile against the soil decreased during the loading because the soil beneath the raft base moved with the raft part. Consequently, the

horizontal resistance of the pull-out pile was smaller for the piled raft. The subgrade reaction of pull-out pile in the piled raft was also smaller than that of the pile group, especially near the raft base.

The moment resistance of the piled raft foundation was higher than the pile group foundation, especially for the heavy case, in other words, for the foundation with small safety factor of pile.

If the safety factor of the pile was sufficient, the moment resistance from the pile part was almost same between the piled raft foundation and the pile group foundation. The pile group with small safety factor showed quite small moment resistance because the pile load reached ultimate state in a small rotation and settlement. Despite of the small safety factor of pile, the piled raft foundation showed large moment resistance than the pile group and the piled raft having the large safety factor of pile. The raft part prevented the clear failure of the pile and prevented the excessive settlement of the foundation. Furthermore, the raft pressure enhanced the pile resistance, resulting in the higher moment resistance of the piled raft foundation.

Thus, the piled raft foundation with small safety factor of pile can be expected to the large contribution of the raft such as the resistance of the raft part, suppression of excessive settlement and enhancement of the pile capacity.

CHAPTER 6

CONCLUSIONS AND RECOMMENDATION

6.1 Conclusions

The main objective in this research was to examine the mechanical behavior of the piled raft foundation subjected to horizontal and the moment load was examined. Firstly the centrifuge modeling technique of the piled raft foundation was proposed, by which the behavior of the piled raft foundation can be evaluated in detail. Using proposed centrifuge technique the mechanical behavior of the piled raft foundation was examined. The much focus was placed on clarifying the influence of the raft pressure on the pile response. Because the foundation was experienced some vertical loading process during preparation, the vertical response of the piled raft foundation was also discussed to verify the initial condition of the horizontal loading tests. The following findings are derived from the present research.

Chapter 1 Introduction and Chapter 2 Literature review

The design concept of the piled raft foundation and the limitation of the piled raft foundation were presented, and the objectives and thesis stream in the present thesis is showed in Chapter 1. The researches on the laterally loaded pile group, which is the component of the piled raft and researched on the vertically and laterally loaded piled raft are introduced in Chapter 2. From the literature review, the current problem of the piled raft foundation is indicated.

The piled raft foundation has been recognized as the economical foundation system with the combined effect of the raft and pile. However, the behavior of the piled raft foundation is not still well understood due to the complex interaction of raft-ground-pile, especially when relatively large moment load and rotation are acting on the piled raft because the interaction varies during loading. It is crucial for the seismic design of the piled raft to clarify the mechanical behavior of the piled raft foundation subjected to horizontal and moment load in highly seismic area such as Japan.

To address above issue, physical modeling plays an important role because it can make the clear boundary conditions and can easily simulate the piled raft subjected to the horizontal load. However, research on the laterally loaded piled raft with physical modeling approach is new topic, and there should be rooms in the modeling techniques to improve and obtain reliable test results.

Therefore the centrifuge modeling technique was firstly proposed, and the mechanical behavior of the piled raft foundation subjected to horizontal and moment load was

examined using proposed technique.

Chapter 3 Development of centrifuge modeling of piled raft foundation

Chapter 3 explained the basic principal of centrifuge and proposed the modeling technique on the piled raft. In particular, the measurement accuracy of the strain gauge was carefully discussed because shared loads between the raft and the piles are generally estimated by the strain gauge. Followings are the basic findings and the modeling technique proposed in this chapter.

In the present study the model piles were installed as the "displacement pile", that is, the level model ground was firstly made, and the piles were penetrated into the ground in the centrifugation. Preparing the model foundation by this method, the uniform contact condition between the raft base and the ground surface can be made, and relatively large shaft friction can be expected. The concept of the piled raft is to reduce the settlement using a few friction piles. Therefore, the piled raft foundation installed as "displacement pile" introduced in the present thesis can model the actual piled raft concept accurately.

It was found that the proportion of the vertical load carried by the raft (RVLP) increased with the piled raft settlement. The initial RVLP before the horizontal loading tests was controlled by applying the pre-load to the foundation.

The pile calibration technique was proposed, by which the forces acting on the pile can be evaluated accurately. However, it was found that the axial strain measured by the gauge included the error due to the interference strain when the pile was subjected to bending moment. The method to improve the measurement accuracy of strain gauge was proposed. That is, the axial strain was corrected by removing the interference strain using the relationship between the bending strain and interference strain observed in the pile calibration. It was also confirmed that the validity of the calibration number obtained by the present calibration method and the effectiveness of correction method. This implied that he shared load between the raft and piles can be evaluated with high accuracy.

Chapter 4 Vertical response of the piled raft

The piled raft foundation subjected to vertical load was examined in the present chapter. The foundations experienced the three vertical loading processes such as the penetration process, the vertical loading process and the pre-vertical loading process before the horizontal loading tests. The main objectives of the present chapter was not only to examine the mechanical behavior of the piled raft foundation subjected to vertical load but also to verify the initial conditions of the foundation before the horizontal

loading tests. Followings are the findings in this chapter.

The piled raft foundation showed higher vertical resistance than the pile group foundation, which was attributed to the mobilized resistance of the raft part and the increase of the vertical resistance of the pile part.

Initially the coefficient of the subgrade reaction of raft part in the piled raft foundation was relatively smaller than that of the raft foundation because the contact condition between the raft base and the ground was poor. However, it increased with the settlement, in other words, the vertical load carried by the raft part.

The vertical resistance of the pile part in the piled raft was higher than that of the pile group due to the influence of raft base pressure on the pile response. There was no influence of the raft base on the ultimate end bearing load and the coefficient of the subgrade reaction of end bearing load. On the other hand, the raft base pressure enhanced the ultimate shaft friction load and the coefficient of the subgrade reaction of shaft friction. The additional shaft friction load had a linear relationship with the base pressure, and it can be simply estimated using elastic theory.

The proportion of the vertical load carried by the raft part (RVLP) can be controlled by applying the vertical load. The almost same RVLP of 30% was prepared for the piled raft cases by applying the vertical load before the horizontal loading tests.

The variation of the RVLP depended on the vertical load of the foundation. The piles in the piled raft acted a kind of anchor and prevented the free-heaving of the raft part during the unloading. This anchoring effect can be clearly seen for the piled raft with small vertical load of the foundation. Therefore, the RVLP increased during the unloading for the piled raft with small vertical load.

Chapter 5 Mechanical behavior of piled raft subjected to horizontal and moment loads

In this chapter the mechanical behavior of the piled raft foundation subjected to horizontal and moment loads in sand was examined. The much focus was placed on the influence of the raft base pressure on the pile response. The following findings are derived from the present chapter.

The piled raft foundation can restrain the settlement caused by the alternate

horizontal loading. In particular, even if the safety factor of the pile was small, the settlement of the push-in pile was effectively reduced for the piled raft foundation compared with the pile group foundation because the raft in the piled raft prevented the excessive settlement of push-in pile. However, the smaller settlement of push-in pile enhanced the pull-out displacement of pull-out piles, resulting in the larger upward movement than that of the pile group foundation. Therefore, it can be said that the upward movement of the pull-out pile was critical issue for the small scale piled raft with narrow pile spacing.

The settlement of the heavy case, in other words, the case with the small safety factor of the pile, was larger than that of the light case for both the pile group and the piled raft. This relatively large settlement of heavy case made the contact condition between the raft and the ground surface better.

The horizontal resistance of the piled raft foundation was higher than the pile group foundation, especially for the piled raft with small safety factor of pile because the larger contribution of the raft part can be mobilized. The horizontal resistance of the push-in pile was larger for the piled raft foundation than the pile group foundation due to the increase of the confined stress around pile. The horizontal subgrade reaction at relatively deep part (more than the raft width) was also enhanced by the raft pressure.

On the other hand, the horizontal resistance of the pull-out pile was smaller for the piled raft foundation than the pile group foundation. As explained above, the upward displacement of pull-out pile was critical for the piled raft foundation, and therefore the base contact stress rapidly reduced around the pull-out pile. In addition to this, the relative displacement of pull-out pile against the soil decreased during the loading because the soil beneath the raft base moved with the raft part. Consequently, the horizontal resistance of the pull-out pile was smaller for the piled raft. The subgrade reaction of pull-out pile in the piled raft was also smaller than that of the pile group, especially near the raft base.

The moment resistance of the piled raft foundation was higher than the pile group foundation, especially for the heavy case, in other words, for the foundation with small safety factor of pile.

If the safety factor of the pile was sufficient, the moment resistance from the pile part

was almost same between the piled raft foundation and the pile group foundation. The pile group with small safety factor showed quite small moment resistance because the pile load reached ultimate state in a small rotation and settlement. Despite of the small safety factor of pile, the piled raft foundation showed large moment resistance than the pile group and the piled raft having the large safety factor of pile. The raft part prevented the clear failure of the pile and prevented the excessive settlement of the foundation. Furthermore, the raft pressure enhanced the pile resistance, resulting in the higher moment resistance of the piled raft foundation.

Thus, the piled raft foundation with small safety factor of pile can be expected to the large contribution of the raft such as the resistance of the raft part, suppression of excessive settlement and enhancement of the pile capacity.

6.2 Recommendation

The present research clarified that the mechanical behavior of the piled raft foundation subjected to lateral and moment loads by centrifuge model tests. The model foundations used in the present research assume the civil engineering structure such as a viaduct foundation, which has relatively small raft with short piles. A couple of findings derived from the present research contributes further expansion of application of the piled raft foundation into civil engineering structure.

In particular, the piled raft foundation in sand, where the bearing capacity of the raft can be fully expected, can restrain the excess settlement by the raft part. However, the uplift of the pull-out pile might be large for the piled raft foundation. Larger uplift of pile causes the increase of the rotation which is considerable for foundation design. In case of same pile number, increase of the vertical load of superstructure is effective to prevent the rotation of the foundation caused by the pile uplift. This finding suggests the possibility of piled raft foundation, which can ensure enough horizontal and moment resistances with fewer piles compared with the conventional pile group foundation.

To establish the design code of the piled raft foundation and to accelerate the application of the piled raft foundation into civil engineering field, the numerical approach is required. In addition to this the shaking table test is also needed in a highly seismic area such as Japan.

LITERATURE CITED

1. American Petroleum Institute. 1993. API Recommended Practice for Planning and Constructing Fixed Offshore Platforms, load and resistance factor design first edition.

2. Architectural Institute of Japan. 2001. *Recommendations for Design of Building Foundation.*

3. Balakumar, V., Kalaiarasi, V. and Ilamparuthi, K. 2005. Experimental and analytical study on the behaviour of circular piled-raft on sand, *Proceedings of 16th International Conference on Soil Mechanics and Foundation Engineering*, 1943-1946.

4. Broms, B. B. 1964a. Lateral resistance of piles in cohesive soils. *Journal of Soil Mechanics and Foundation Division, ASCE*, **90** (SM2), 27-63.

5. Broms, B. B. 1964b. Lateral resistance of piles in cohesionless soils. *Journal of Soil Mechanics and Foundation Division, ASCE*, **90** (SM3), 123-156.

6. Broms, B. B. 1965. Design of laterally loaded piles, *Journal of Soil Mechanics and Foundation Division*, ASCE, **91** (SM3), 79-99.

7. Brown, D. A. and O'Neill, M. W. 1987. Cyclic lateral loading of a large-scale pile group. *Journal of Geotechnical Engineering*, **113**, 1326-1343.

8. Brown, D. A. and Reese, L. C. 1988. Lateral load behavior of pile group in sand. *Journal of Geotechnical Engineering*, **114**, 1261-1276.

9. Brown, P. T. and Wiesner, T. J. 1975. The behaviour of uniformly loaded piled strip footings, *Soils and Foundations*, **15** (4), 13-21.

10. Burland, J. B., Broms, B. B. and De Mello, V. F. B., 1977. Behaviour of foundations and structures. *Proc.of 9th ICSMFE* , **2**, 496-546.

11. Butterfield, R. and Banerjee, P. K. 1971. The elastic analysis of compressible piles and pile groups, *Geotechnique,* **21**(2), 43-60.

12. Butterfield, R. and Banerjee, P. K. 1971. The problem of pile group and pile cap interaction. *Geotechnique*, **21** (2), 135-142.

13. Chang, Y. L. 1937. Discussion on "Lateral pile loading tests" by Feagin. *Transaction, ASCE*, **102**, 272-278.

14. Chin, F. K. 1970. Estimation of the ultimate load of piles from tests not carried to failure, *Proceedings of 2nd South East Asian Conference Soil Engineering*, 81.

15. Chow, Y. K. and Teh, C. I. 1991. Pile-cap-pile-group interaction in non-homogeneous soil. *Journal of Geotechnical Engineering, ASCE*, **117** (11), 1655-1668.

16. Chow, Y. K. 1986. Analysis of vertically loaded pile groups, *International Journal for Numerical and Analytical Methods in Geomechanics*, **10** (1), 59-72.

17. Chow, Y. K. 1987a. Three-dimensional analysis of pile groups, *Journal of Geotechnical Engineering, ASCE*, **113** (6), 637-651.

18. Chow, Y. K. 1987b. Axial and lateral response of pile groups embedded in non-homogeneous soils, International, *Jounal for Numerical and Analytical Methods in Geomechanics*, **11** (6), 621-638.

19. Clancy, P. and Randolph, M. F. 1993. An approximate analysis procedure for piled raft foundations, *International Journal for Numerical and Analytical Methods in Geomechanics*, **17** (12), 849-869.

20. Cooke, R. W., Bryden Smith, D. W., Gooch, M. N. and Sillet, D. F. 1981. Some observations of the foundation loading and settlement of a multi-storey building on a piled raft foundation in London clay, *Proceedings of I.C.E, part 1*, **70**, 433-460.

21. Cooke, R. W. 1986. Piled raft foundations on stiff clays –a contribution of designing philosophy, *Geotechnique*, **36** (2), 169-203.

22. Cox, W. R., Dixon, D. A. and Murphy, B. S. 1984. Lateral load tests of 5.4mm diameter piles in very soft clay in side-by-side and in-line groups. Laterally loaded deep foundations: analysis and performance, ASTM, West Conshohocken, Pa.

23. Det Norske Veritas. 1980. Rules for the design, Construction and Inspection of Offshore Structure Appendix F: Foundations. Det Norske Veritas, Norway.

24. Durgunoglu, H. T. and Mitchell, J. K. 1975a. Static penetration resistance of soils: I. Analysis. *Proceedings of the Conference on In Situ Measurement of Soil Properties*, ASCE, **1**, 151‑171.

25. Durgunoglu, H. T. and Mitchell, J. K. 1975b. Static penetration resistance of soils: II. Evaluation of theory and implications for practice. *Proceedings of the Conference on In Situ Measurement of Soil Properties*, ASCE, **1**, 172‑189.

26. Endra, S. and Roman, D. H. 2003. Large displacement FEM modelling of the cone penetration test (CPT) in normally consolidated sand, *International Journal for Numerical and Analytical Methods in Geotechnics*, **27**, 585-602.

27. Ergun, M. U. 1995. Predicted and observed settlement of a piled raft foundation, *Proceedings of 11th Asian Region Conference on Soil Mechanics and Foundation Engineering*, 49-61.

28. Feagin, L. B. 1937. Lateral pile loading tests. *Transaction, ASCE*, **102**, 236-254.

29. Fraser, R. A. and Wardle, L. J. 1976. Numerical analysis of rectangular rafts on layered foundations, *Geotechnique*, **26** (4), 613.

30. Fukushima, S. and Tatsuoka, F. 1984. Strength and deformation characteristics of saturated sand at extremely low pressures, *Soils and Foundations*, **24** (4), 30-48.

31. Georgiadis, M., Anagnostopoulos, C. and Saflekou, S. 1991. Centrifugal testing of

laterally loaded piles in sand, *Canadian Geotechnical Journal*, **29**, 208-216.

32. Hain, S. J. 1975. Analysis of rafts and raft-pile foundations. *Proceedings of Symposium on Recent Development in Soil Mechanics*, 213-253.

33. Hain, S. J. and Lee, I. K. 1978. The analysis of flexible pile-raft systems, *Geotechnique*, **28** (1), 65-83.

34. Hamada, J., Tsuchiya, T. and Yamashita, K. 2009. Theoretical equations to evaluate the stress of piles on piled raft foundation during earthquake, *Journal of Structural Construction Engineering*, **74** (644), 1759-1767.

35. Hamada, J., Tsuchiya, T., Tanikawa, T. and Yamashita, K., 2012. Lateral loading model tests on piled rafts and their evaluation with simplified theoretical equations. *Proc.9th International Conference on Testing and Design Methods for Deep Foundations (IS-Kanazawa 2012)*, **1**, 467-476.

36. Hight, D. W. and Green, P. A. 1976. The performance of a piled raft foundation for a tall building in London, *Proceedings of 6th European Conference on Soil Mechanics and Foundation Engineering*, **2**, 234-237.

37. Hooper, J. A. 1973. Observations on the behaviour of a piled-raft foundation on London clay, *Proceedings of International Civil Engineering*, **55**, 855-877.

38. Hooper, J. A. 1979. Review of behaviour of piled raft foundations. CIRIA report in 83.

39. Hooper, J. A. and Levy, J. F. 1981. Behaviour of a flexible piled raft foundations, *Proceedings of 10th International Conference on Soil Mechanics and Foundation Engineering*, **2**, 735-740.

40. Horikoshi, K. and Randolph, M. F. 1996. Centrifuge modeling of piled raft foundations on clay, *Geotechnique*, **46** (4), 741-752.

41. Horikoshi, K. and Randolph, M. F. 1998. A contribution to optimum design of piled rafts, *Geotechnique*, **48** (3), 301-317.

42. Horikoshi, K., Matsumoto, T., Hashizume, Y., Watanabe, T. and Fukuyama, H. 2003a. Performance of piled raft foundations subjected to static horizontal loads, *International Journal of Physical Modelling in Geotechnics*, **3** (2), 37-50.

43. Horikoshi, K., Matsumoto, T., Hashizume, Y. and Watanabe, T. 2003b. Performance of piled raft foundations subjected to dynamic loads, *International Journal of Physical Modelling in Geotechnics*, **3** (2), 51-62.

44. Houque, E., Kamegai, Y., Hohata, Y., Siddiquee, M. S. A. and Tatsuoka, F. 1994. Cross-anisotropic elasticity of sands by large triaxial tests measuring local strains, 第 29 回地盤工学研究発表会講演概要集、pp.409-412.

45. Jaky, J. 1948. Pressure in Silos, *Proceedings of the 2nd International Conference On*

Soil Mechanics and Foundation Engineering, **1**, 103‑107.

46. Jendeby L, 1986. Friction piled foundations in soft clay, A study of load transfer and settlement, Ph.D. Thesis, Department of Geotechnical Engineering, Chalmers University of Tech, Goteborg.

47. Joustra, K., De Sitter, W. R. and Den Ouden, N. W. 1977. Tall building settlement and pile load measurements, *Proceedings of 9th International Conference on Soil Mechanics and Foundation Engineering*, **1**, 577‑580.

48. Kakurai, M., Yamashita, K. and Tomono, M. 1987. Settlement behavior of piled raft foundation on soft ground, P*roceedings of 8th Asian Region Conference on Soil Mechanics and Foundation Engineering*, 373‑376.

49. Katzenbach, R., Arslan, U., Moorman, C. and Reul, O. 1998. Piled raft foundation: interaction between piles and raft, *Darmstadt Geotechnics*, **4**, 279‑296.

50. Katzenbach, R, Arslan, U. and Moormann, C. 2000. Piled raft foundations projects in Germany, Design applications of raft foundations, 323‑392.

51. Katzenbach, R. and Turek, J. 2004. Combined pile‑raft foundation subjected to lateral loads, *Proceedings of International Conference on 16th Soil Mechanics and Geotechnical Engineering*, 2001‑2004.

52. Kishida, H. 1991. Soil‑piled raft foundation interaction, *Proceedings of the 9th Asian Regional Conference on Soil Mechanics and Foundation Engineering*, **2**, 331‑334.

53. Kitiyodom, P. and Matsumoto, T. 2002. A simplified analysis method for piled raft and pile group foundations with batter piles, International Journal for Numerical and Analytical methods in Geomechanics, 26, 1349‑1369.

54. Kitiyodom, P. and Matsumoto, T. 2003. A simplified analysis method for piled raft foundations in non‑homogeneous soils, International Journal for Numerical and Analytical methods in Geomechanics, 27, 85‑109.

55. Kuwabara, F. 1989. An elastic analysis for piled raft foundations in a homogeneous soil, *Soils and Foundations*, **28** (1), 82‑92.

56. Li, Y. and Peter, M. B. 1992. Lateral pile response to monotonic pile head loading. *Canadian Geotechnical Journal*, **29** (6), 955‑970.

57. Liu, J. L., Yuan, Z. L. and Zhang, K. P. 1985. Cap‑pile‑soil interaction of bored pile groups, *Proceedings of 11th International Conference on Soil Mechanics and Foundation Engineering*, 1433‑1436.

58. Llyas, T., Leung, C. F., Chow, Y. K. and Budi, S. S. 2004. Centrifuge model study of laterally loaded pile groups in clay. *Journal of Geotechnical and Geoenvironmental Engineering*, **130**, 274‑283.

59. Mandolini, A., Russo, G. and Viggiani, C. 2005. Pile foundations: Experimental

investigations, analysis and design, *Proceedings of 16th ICSMGE*, **1**, 177-213.

60. Matsuo, M., Morita, H., Tsukitani, T., Ookoshi, M. and Kobayashi, M. 2003. Behavior of building supported by piled-raft foundation on reclaimed ground (part 1 and 2), Annual report of Architectural Institute of Japan, 477-480.

61. Mayne, P. W. and Poulos, H. G. 1999. Approximate displacement influence factors for elastic shallow foundations, Journal of Geotechnical and Geoenvironmental Engineering, ASCE, 125 (6), 453-460.

62. McVay, M., Bloomquist, D., Vanderlaine, D. and Clausen, J. 1994. Centrifuge modeling of laterally loaded pile group in sand. *Geotechnical and Testing Journal*, **17** (2), 29-137.

63. McVay, M., Casper, R. and Shang, T. 1995. Lateral response of three-row groups in loose to dense sands at 3D and 5Dpile spacing. *Journal of Geotechnical Engineering*, **121** (5), 436-441.

64. McVay, M., Zhang, L., Molnit, T. and Lai, P. 1998. Centrifuge testing of large laterally loaded pile groups in sands. *Journal of Geotechnical and Geoenvironmental Engineering*, **124** (10), 1019-1026.

65. Meimon, Y., Baguelin, F. and Jezequel, J. F. 1986. Pile group behaviour under long time lateral monotonic and cyclic loading. *Proc. 3rd International Conference on Numerical Methods in Offshore Piling*, Inst. Francais Du Petrole, Nantes, France, 286-302.

66. Meyerhof, G. G. 1976. Bearing capacity and settlement of pile foundations, JGED, ASCE, 1 (GT3), 196-227.

67. Mindlin, R. D. 1936. Force at a point in the interior of a semi-infinite solid, *Physics*, **7**, 195-202.

68. Matsumoto, T., Fukumura, K., Kitiyodom, P., Horikoshi, K. and Oki, A. 2004a. Experimental and analytical study on behavior of model piled rafts in sand subjected to horizontal and moment loading, *International Journal of Physical Modelling in Geotechnics*, **4** (3), 1-19.

69. Matsumoto, T., Fukumura, Horikoshi, K. and Oki, A. 2004b. Shaking table tests on model piled rafts in sand considering influence of superstructures, *International Journal of Physical Modelling in Geotechnic*s, **4** (3), 20-38.

70. Matsumoto, T., Nemoto, H., Mikami, H., Yaegashi K., Arai T. and Kitiyodom, P. 2010. Load tests of piled raft models with different pile head connection conditions and their analysis, *Soils and Foundations*, **50** (1), 63-81.

71. Matlock, H. and Ripperger, E. A. 1956. Procedures and instrumentation for tests on a laterally loaded pile. *Proc. 8th Texas Conference on Soil Mechanics and Foundation*

Engineering, Special Publication No.29.

72. Morison, C. S. and Reese, L. C. 1986. A lateral load test of afull scale pile group in sand. *Geotechnical Centre, Report*, GR86-1.

73. Murchison, J. M. and O'Neill, M. W. 1984. Evaluation of p-y relationships in cohesionless soils, In analysis and design of pile foundations, ASCE, 174-191.

74. Ottaviani, M. 1975. Three-dimensional finite element analysis of vertically loaded pile groups, *Geotechnique*, **25** (2), 159-174.

75. Poulos, H. G. and Davis, E. H. 1968. The settlement behaviour of single axially loaded incompressible piles and piers, *Geotechnique*, **18**, 351-371.

76. Poulos, H. G. 1968. Analysis of the settlement of pile groups, *Geotechnique*, **18**, 449-471.

77. Poulos, H. G. and Davis, E. H. 1980. Pile foundation analysis and design. New York, John Wiley and Sons.

78. Poulos, H. G. 1989. Pile behaviour – Theory and application, *Geotechnique*, **39** (3), 365-415.

79. Poulos, H. G. 1991. Analysis of piled strip foundations, *Computing Methods and Advances in Geomechanics*, **1**, 183-191.

80. Poulos, H. G. 1994. An approximate numerical analysis of pile-raft interaction, *International Journal of Numerical Analytical Method in Geomechanics*, **1** (18), 73.

81. Poulos, H. G., Small, J. C., Ta, L. D., Sinha, J. and Chen, L. 1997. Comparison of some methods for analysis of piled rafts, *Proceedings of 14th International Conference on Soil Mechanics and Foundation Engineering*, **2**, 1119-1124.

82. Poulos, H. G. 2001. Piled raft foundations: design and applications, *Geotechnique*, **51** (2), 95-113.

83. Prakoso, W. A. and Kulhawy, F. H. 2000. Contribution to piled raft foundation design, *Journal of Geotechnical and Geoenvironmental Engineering*, ASCE, **127** (1), 17-24.

84. Randolph, M. G. 1983. Design of piled raft foundations, *CUED/D, soils TR 143*, Cambridge University.

85. Randolph, M. F. 1994. Design methods for pile groups and piled rafts, *Proceedings of 13th international Conference on Soil Mechanics and Foundation Engineering*, **5**, 61-82.

86. Randolph, M. F. and Wroth, C. P. 1978. Analysis of deformation of vertically loaded piles. *Journal of Geotechnical Engineering Division, ASCE*, 104 (GT12), 1465-1488.

87. Reese, L. C., Cox, W. R. and Koop, R. D. 1974. Analysis of laterally loaded piles in sand. *Proc. of Sixth Annual Offshore Technology Conference*, **2**, 473-483.

88. Remaud, D. and Garnier, J. 1998. Laterally loaded piles in dense sand. *Proc. of*

International Conference Centrifuge 98, 533-538.

89. Robert, L. M. and Duncan, J. M. 2001. Experimental evaluation of lateral-load resistance of pile caps, *Journal of Geotechnical and Geoenvironmental Engineering*, **127**, 185-192.

90. Rollins, K. M. and Weaver, T. J. 1998. Lateral load behavior of full-scale pile group in clay. *Journal of Geotechnical Engineering*, **124**, 468-478.

91. Ruesta, P. F. and Townsend, F. C. 1997. Evaluation of laterally loaded pile group at Roosevelt Bridge. *Journal of Geotechnical and Geoenvironmental Engineering*, **123** (12), 1153-1161.

92. Russo, G. 1996. Interazione tereno struttura per piaster su pli. Ph.D. Thesis, Department of Geotechnical Engineering, University of Napoli Federico II.

93. Russo, G. 1998. Numerical analysis of piled rafts, *International Journal of Analysis and Numerical Methods in Geomechanics*, **22** (6), 477-493.

94. Schofield, A. N. 1980. Cambridge Geotechnical Centrifuge Operations, *Geotechnique*, **30** (3), 227-268.

95. Scott, R. F. 1980. Analysis of centrifuge pile tests. Simulation of piles driving. Research Report, American Petroleum Institute, OSAPR Project 13.

96. Sherif, M. M., Sherif, G. B. and Hammam, A. H. 1995. Effect of method of pile installation on its behaviour, *Proceedings of 11th Asian Region Conference on Soil Mechanics and Foundation Engineering*, 253-267.

97. Siva, R. A. and Valsangkar, A. J. 1970. Generalized Solutions for Laterally Loaded Pile in Elasto-Plastic Soil. *Soils and Foundations*, **10** (3), 66-80.

98. Sommer, H., Tamaro, G. and De Benedittis, C. 1991. Messe Turm foundations fo the tallest building in Europe, *Proceedings of 4th International Conference on Piling and Deep Foundations*, 139-145.

99. Sparks, A. and Rollins, K. M. 1997. Passive resistance and lateral load capacity of a full-scale fixed-head pile group in clay. Civil and Environmental Engineering Report CEG 97-04, Brigham Young Univ., Provo, Utah.

100. Sparks, A. and Rollins, K. M. 1997. Passive resistance and lateral load caapcity of a full-scale fixed-head pile group in clay.

101. Ta, L. D. and Small, J. C. 1996. Analysis of piled raft systems in layered soils, *International Journal of Numerical and Analytical Methods in Geomechanics*, **20** (2), 105-123.

102. Takemura, J., Kondoh, M., Esaki, T., Kouda, M. and Kusakabe, O., 1999. Centrifuge model tests on double propped wall excavation in soft clay. *Soils and Foundations*, **39** (3), 75-87.

103. Tatsuoka, F., Sakamoto, M., Kawamura, T. and Fukushima, S. 1986. Strength and deformation characteristics of sand in plane strain compression at extremely low pressures, *Soils and Foundations*, **26** (1), 65-84.

104. Tejchman,, A. Gwizdala, K., Krasinski, A. and Slabek, A. Model tests of piled raft foundation, *Proceedings of 16th International Conference on Soil Mechanics and Foundation Engineering*, 2049-2052.

105. Terashi, M., Kitazume, M. and Kawabata, K. 1989.Centrifuge modeling of a lateral loaded pile, *Proc. of the 12th ICSMFE*, **2**, 991-994.

106. Terzaghi, K. 1955. Evaluation of coefficient of subgrade reaction. *Geotechnique*, **5**, 297-326.

107. Thaher, M. and Jessberger, H. L. 1991. The behaviour of pile-raft foundations, Investigation in centrifuge model tests, *Proceedings of Centrifuge 91*, 225-234.

108. Tokimatsu, K. and Yoshimi, Y. 1983. Empirical correlation of soil liquefaction based on SPT N-value and fines content, *Soils and Foundations*, **23** (4), 56-74.

109. Tomono, M., Kakurai, M. and Yamashita, K. 1987. Analysis of settlement behavior of piled raft foundations, Takenaka Technical Research Report, 37.

110. Van Impe, W. F. and De Clerq, Y. 1994. A piled raft interaction model, *Proceedings of 5th International Conference on Piling and Deep Foundations*, 1.3.1-1.3.10.

111. Wu, D., Broms, B. B. and Choa, V. 1998. Design of laterally loaded piles in cohesive soils using p-y curves, *Soils and Foundations*, **38** (2), 17-26.

112. Yamada, T., Yamashita, K., Kakurai, M. and Tsukatani, H. 2001. Long-term behaviour on raft foundation constructed by top-down method, *Proceedings of 5th International Conference on Deep Foundation Practice incorporating Piletalk*, 411-417.

113. Yamana H. 2009. Lateral resistance of pile-sheet pile combined foundation. Tokyo Institute of Technology, Master thesis.

114. Yamashita, K. and Kakurai, M. 1991. Settlement behavior of the raft foundation with friction piles, *Proceedings. Of 4th international Conference on Piling and Deep Foundations*, 461-466.

115. Yamashita, K. and Kakurai , M. 1994. Investigation of a piled raft foundation on stiff clay, *Proceedings of 13th International Conference on Soil Mechanics and Foundation Engineering*, **2**, 543-546.

116. Yamashita, K., Yamada, T. and Hamada, J. 2008. Recent case histories on monitoring settlement and load sharing of piled rafts in Japan, *Proceedings of the 5th international Geotechnical Seminar on Deep Foundations on Bored and Auger Piles*, 181-193.

117. Yamashita, K., Hamada, J. and Soga, Y. 2010. Settlement and load sharing of piled raft of a 162m high residential tower, *Proceedings of Sessions of GeoShanghai2010, ASCE Geotechnical Special Publication*, 205, 26-33.

118. Yamashita, K., Hamada, J. and Yamada, T. 2011. Field measurements on piled rafts with grid-form deep mixing walls on soft ground, *Geotechnical Engineering Journal of the SEAGS & AGSSEA*, **42** (2), 1-10.

119. Yamashita, K., Yamada, T. and Hamada, J. 2011. Investigation of settlement and load sharing on piled rafts by monitoring full-scale structures, *Soils and Foundations*, **51** (3), 513-532.

120. Yamashita, K. 2012. Field measurement on piled raft foundations in Japan. *Proc.9th International Conference on Testing and Design Methods for Deep Foundations (IS-Kanazawa 2012).*

121. Yamashita, K., Hamada, J., Onimaru, S. and Higashino, M. 2012. Seismic behavior of piled raft with ground improvement supporting a base-isolated building on soft ground in Tokyo, *Soils and Foundations*, **52** (5), 1000-1015.

122. Zeevaert, L. 1957. Compensated friction –pile foundation to reduce the settlement of buildings on the highly compressible volcanic clay of Mexico City, *Proceedings of 4th international Conference on Soil Mechanics and Foundation Engineering*, **3**, 81-86.

123. 石井雄輔、関崇夫、西山高士、藤森健史（2003）: 大型遠心せん断土槽実験によるパイルドラフト基礎の地震時挙動評価(その 3)簡易設計法の検討、日本建築学会大会学術講演梗概集、pp491-492.

124. 郭、落合英俊、安福規之、大野司郎、大嶺聖 (1996): 破砕性砂を対象とした一次元圧縮および低・中圧三軸試験、九州大学工業集報、第 69 巻 2 号.

125. 岸田英明、中井正一(1979): 地盤の破壊を考慮した杭の水平抵抗、日本建築学会論文報告集、No.281、pp.41-55.

126. 久保浩一(1961): 杭の横抵抗に関する実験的研究(その 2)、運輸技術研究所報告、Vol.11、No.12.

127. 久保浩一(1962): 杭の横抵抗に関する実験的研究(その 3)、運輸技術研究所報告、Vol.12、No.2.

128. 久保浩一(1964): 杭の横抵抗の新しい計算法、港湾空港技術研究所報告、Vol.2、No.3.

129. 久保浩一(1965): 垂直控え杭の横抵抗について、港湾空港技術研究所報告、Vol.4、No.2.

130. 久保田鉄工株式会社鋼管技術部・鋼管営業部(1977): くい頭回転高速水平抵抗模型実験報告書

131. 鈴木好秀、亀井敏雄、田中邦秀、中井正一、岸田英明(1976): 裏込め効果を考慮した群杭の水平抵抗、第 11 回土質工学研究発表会講演集、pp.625-628.

132. 土屋勉、池田篤則、水上大樹（2001）: 地震力を受けるパイルドラフトの挙動に関する解析的研究、日本建築学会北海道支部研究報告集 No.74、39-44.

133. 土屋富男、濱田純次、永野浩一、山下清　（2003）: 大型土槽を用いたパイルド・ラフト基礎の水平載荷実験（その 1－実験概要）、日本建築学会大会学術講演梗概集、B-1、pp.475-476.

134. 鉄道総合技術研究所: 鉄道構造物等設計標準・同解説、基礎構造物・抗土圧構造物編 永井宏、土屋勉（2004）: 水平力を受けるパイルド・ラフトの非線形ハイブリッド解析法、日本建築学会大会学術講演梗概集、B-1、pp.641-642.

135. 中井正一、真野英之、高梨晃一、石田理永（2002）: 水平力を受けるパイルドラフト基礎の遠心模型実験（その 2　振動実験）、日本建築学会大会学術講演梗概集、pp.663-664.

136. 永井宏、土屋勉（2004）: 杭頭拘束条件に着目したパイルド・ラフトの原位置水平載荷実験、日本建築学会構造系論文集、第 579 号、pp.47-53.

137. 長尾俊昌、桑原文夫、小林治男、渡邊徹（2002）: 小型基礎の原位置実験より得られたパイルド・ラフト基礎の水平挙動, 日本建築学会構造系論文集, 第 559 号, pp. 121-127.

138. 長尾俊昌、桑原文夫、小林治男、渡邊徹（2004）: 水平力を受けるパイルドラフト基礎の挙動解析, 日本建築学会構造系論文集, 第 577 号, pp. 63-68.

139. 永野浩一、濱田純次、土屋富男、山下清　（2003）: 大型土槽を用いたパイルド・ラフト基礎の水平載荷実験（その 2－実験結果）、日本建築学会大会学術講演梗概集、B-1、pp.475-476.

140. 西山高士、藤森健史、茶谷文雄（2003）: 大型遠心せん断土槽実験によるパイルドラフト基礎の地震時挙動評価(その 2)静的加力実験、日本建築学会大会学術講演梗概集、pp489-490.

141. 日本港湾協会: 港湾施設の技術上の基準・同解説

142. 日本道路協会: 道路橋示方書・同解説、IV 下部工編

143. 濱田純次、永野浩一、土屋富男、山下清　（2003）: 大型土槽を用いたパイルド・ラフト基礎の水平載荷実験（その 3－シミュレーション解析）、日本建築学会大会学術講演梗概集、B-1、pp.475-476.

144. 藤森健史、西山高士、若松邦夫（2003）: 大型遠心せん断土槽実験によるパイルドラフト基礎の地震時挙動評価(その 1)地震波加震実験、日本建築学会大会学術講演梗概集、pp487-488.

145. 真野英之、中井正一、高梨晃一（2002）: 水平力を受けるパイルドラフト基礎の遠心模型実験（その 1　静的載荷実験）、日本建築学会大会学術講演梗概集、pp.661-662.

146. 真野英之、中井正一、高梨晃一（2002）: 水平力を受けるパイルドラフト基礎の遠心模型実験（その 2　動的載荷実験）、日本建築学会大会学術講演梗概集、pp.663-664.

147. 真野英之、中井正一（2003）: 水平力を受けるパイルドラフト基礎のラフトの接地が杭応力へ与える影響、日本建築学会大会学術講演梗概集、pp.485-486.

148.山肩邦男、秋野矩之(1968): くいの横抵抗に関する弾塑性的考察、日本建築学会大会学術講演梗概集、pp.615-616.

149.山肩邦男、富永晃司(1969): 有限長くいの横抵抗に関する-考察、日本建築学会大会学術講演梗概集、pp.381-382.

150.山肩邦男、富永晃司(1970): くいの水平加力試験結果に関する実用的な弾塑性解析法、日本建築学会大会学術講演梗概集、pp.457-458.

APPENDIX

A. 3.6.1 Relationship between output value and applied bending strain for light case pile.

A. 3.6.2 Relationship between output value and applied bending strain for heavy case pile.

A. 3.6.3 Calibration number for light case pile

Gauge position	Pile 1	Pile 2	Pile 3	Pile 4	Theory
(1) (μ/mV)	544	538	554	608	513
(2) (μ/mV)	537	523	——	——	513
(3) (μ/mV)	525	533	——	——	513
(4) (μ/mV)	530	542	——	——	513
(5) (μ/mV)	548	530	——	——	513
(6) (μ/mV)	269	269	269	269	256
(7) (μ/mV)	151	146	147	140	325

A.3.6.4 Calibration number for heavy case pile

Gauge position	Pile 1	Pile 2	Pile 3	Pile 4	Theory
(1) (μ/mV)	——	——	548	543	513
(2) (μ/mV)	527	517	——	——	513
(3) (μ/mV)	520	529	——	——	513
(4) (μ/mV)	538	519	——	——	513
(5) (μ/mV)	577	515	——	——	513
(6) (μ/mV)	269	269	269	269	256
(1)' (μ/mV)	256	256	256	256	256
(7) (μ/mV)	224	135	147	195	325
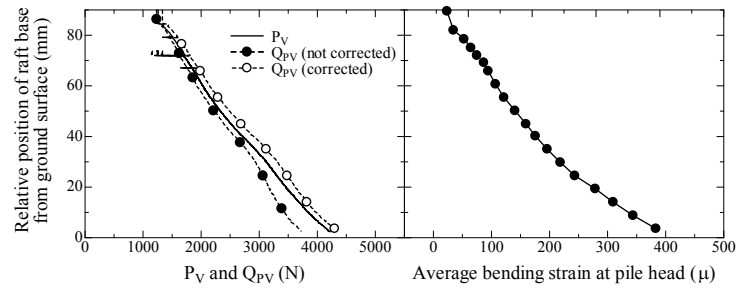
(a) Overall
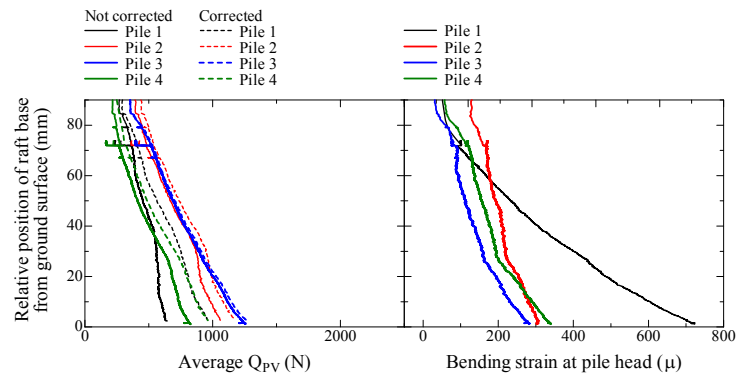
(b) Each pile

A. 3.6.5 Variation of P_V and Q_{PV} and bending strain at pile head with settlement for PR_L1 during penetration process.
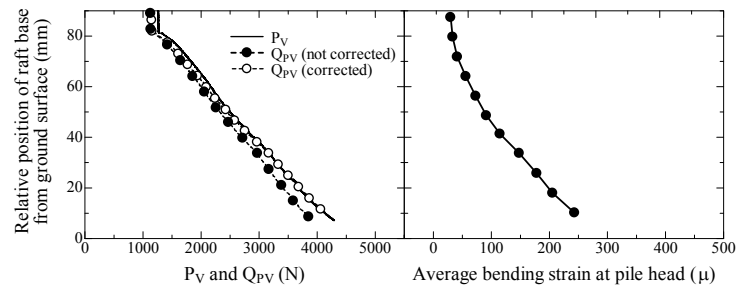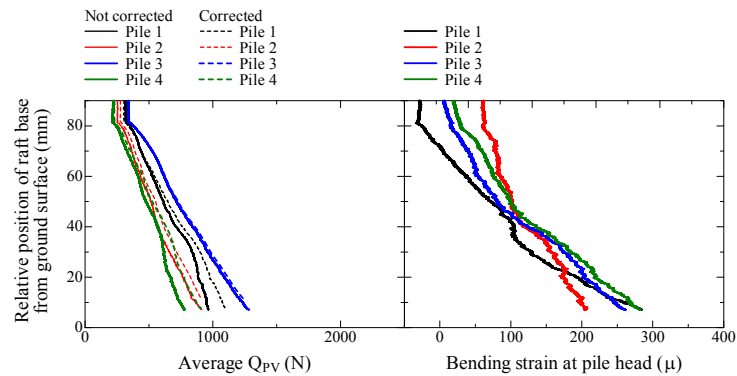
(a) Overall

(b) Each pile

A. 3.6.6 Variation of P_V and Q_{PV} and bending strain at pile head with settlement for PR_L2 during penetration process.
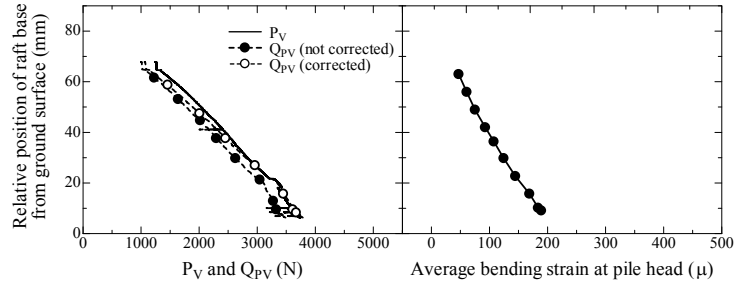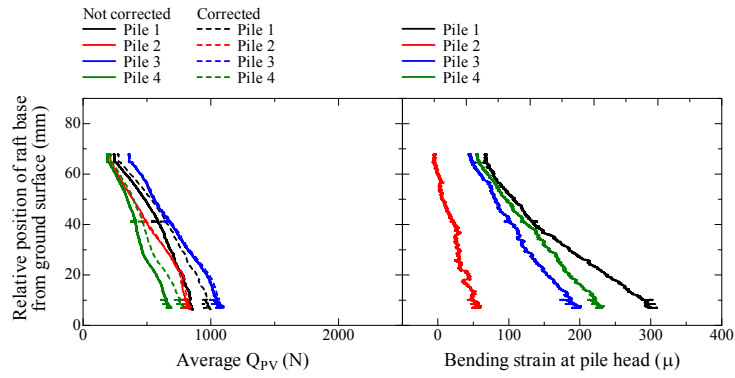
(a) Overall

(b) Each pile

A. 3.6.7 Variation of P_V and Q_{PV} and bending strain at pile head with settlement for P_L during penetration process.
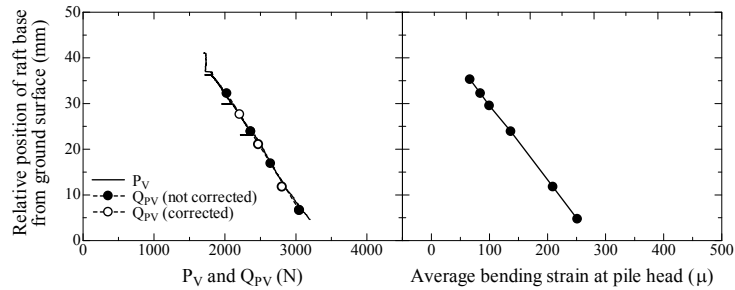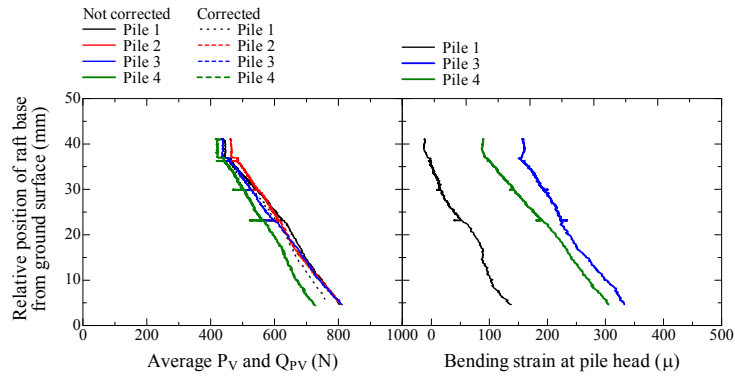
(a) Overall

(b) Each pile

A. 3.6.8 Variation of P_V and Q_{PV} and bending strain at pile head with settlement for PR_H during penetration process.
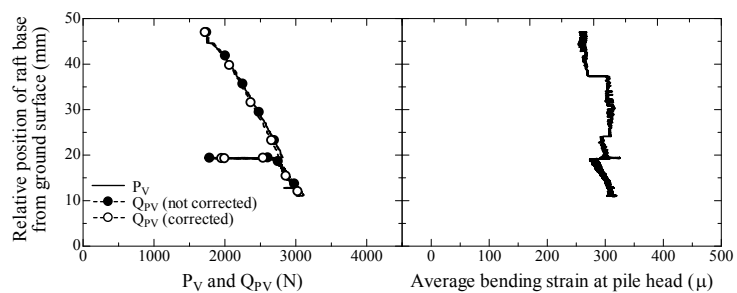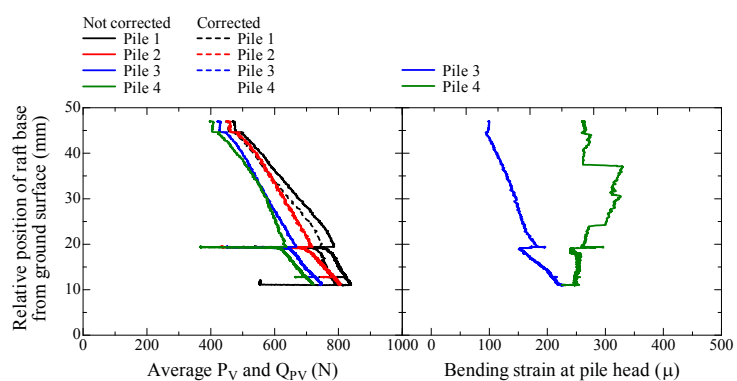
(a) Overall

(b) Each pile

A. 3.6.9 Variation of P_V and Q_{PV} and bending strain at pile head with settlement for P_H during penetration process.
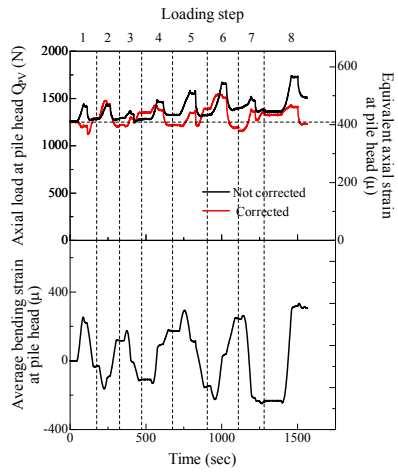
(a) Overall (P_L)
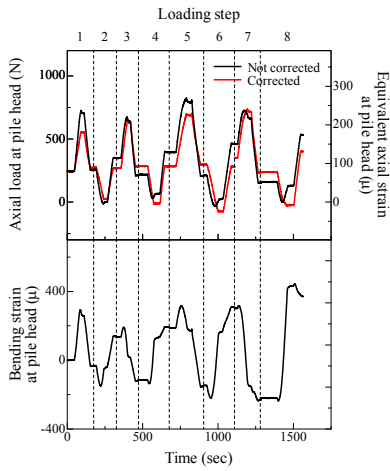
(b) Pile 1 (P_L)
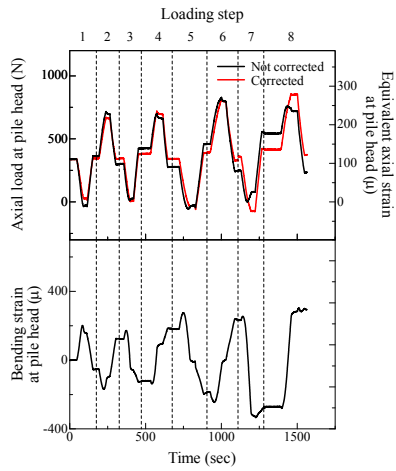
(c) Pile 2 (P_L)
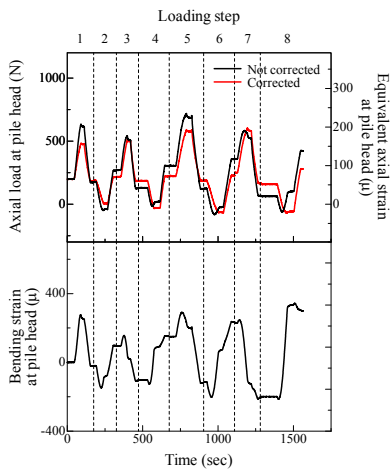
(d) Pile 3 (P_L)
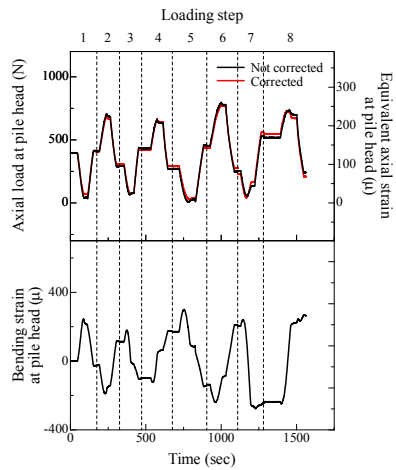
(e) Pile 4 (P_L)

A. 3.6.10 Variation of axial load and bending strain at pile head with time for P_L during horizontal loading test.
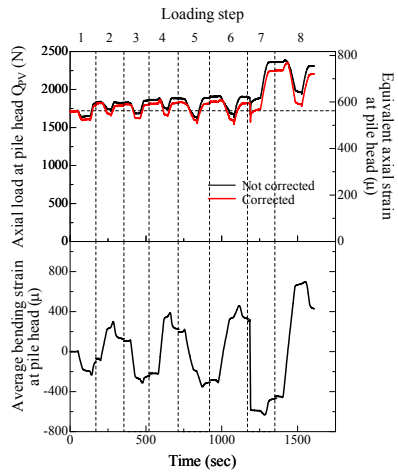
(a) Overall (P_H)
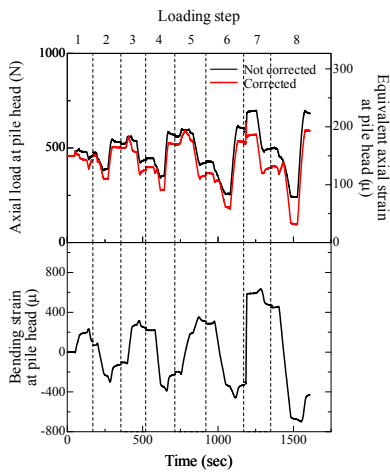
(b) Pile 1 (P_H)
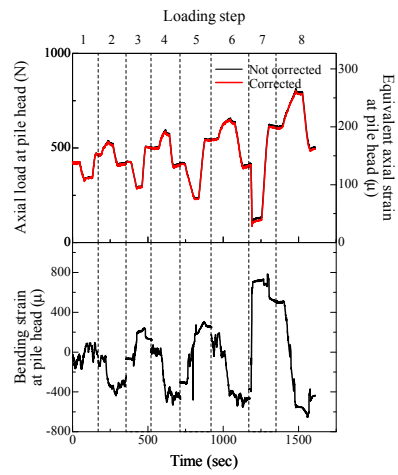
(c) Pile 2 (P_H)
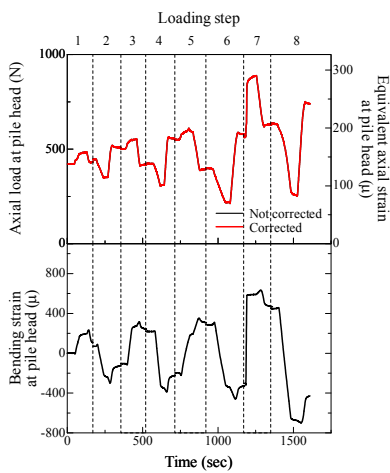
(d) Pile 3 (P_H)
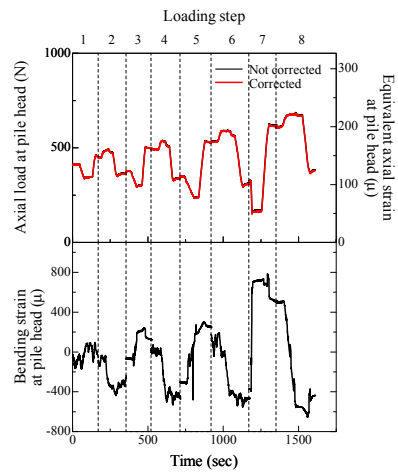
(e) Pile 4 (P_H)

A. 3.6.11 Variation of axial load and bending strain at pile head with time for P_H during horizontal loading test.
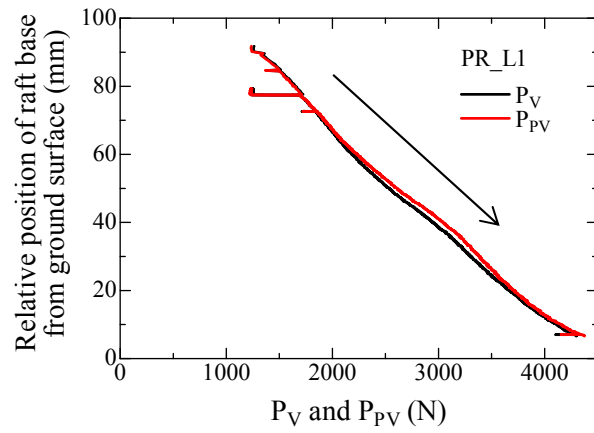
(a) PR_L1
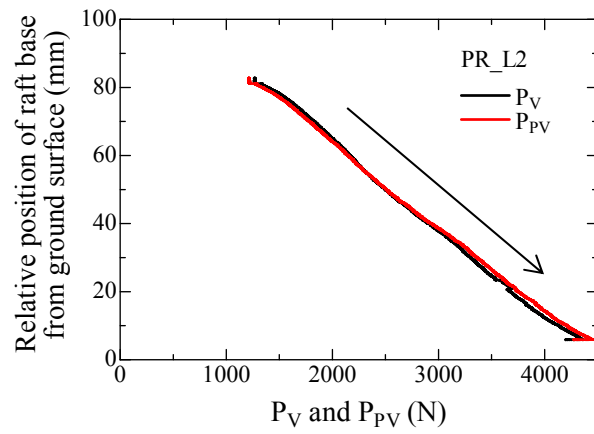
(b) PR_L2
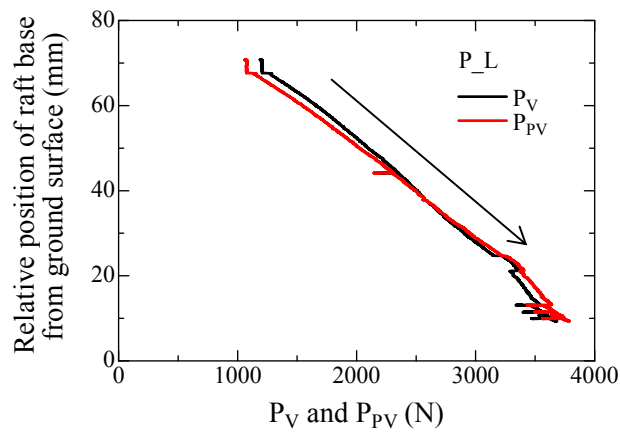
(c) P_L

A. 4.2.1.1 Variation of P_V, P_{PV} with settlement for light case observed in penetration process.
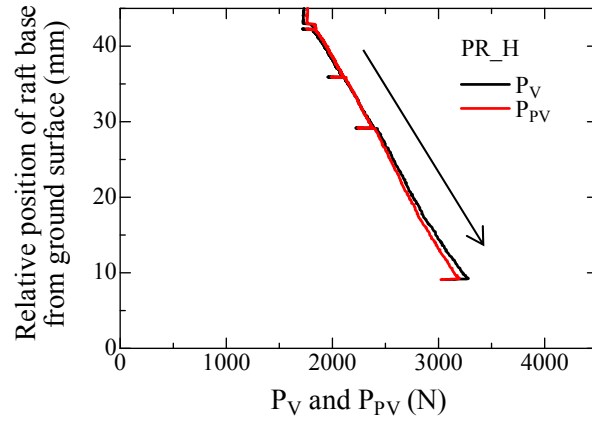
(a) PR_H
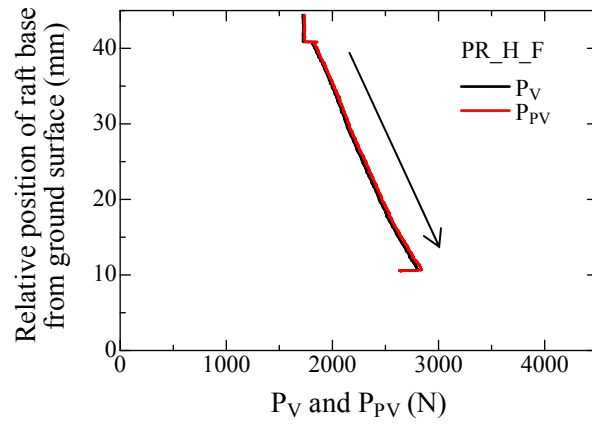
(b) PR_H_F
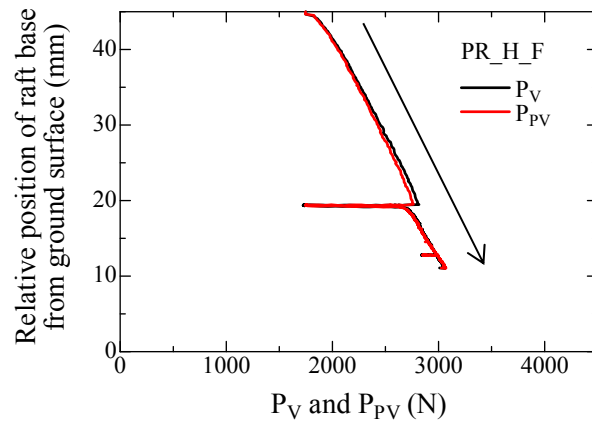
(c) P_H

A. 4.2.1.2 Variation of P_V, P_{PV} with settlement for heavy case observed in penetration process.
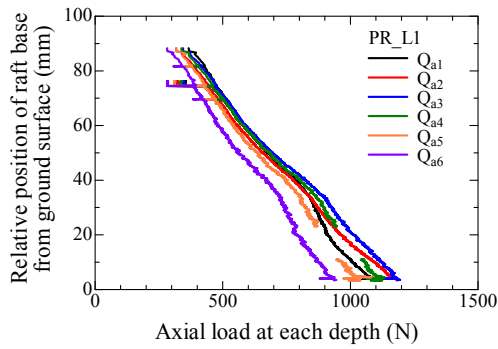
(a) AVerage of Pile 1 & Pile 2
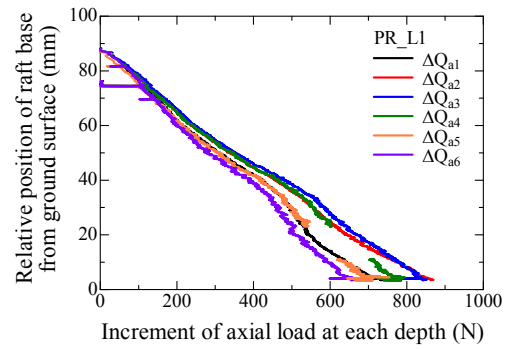
(d) AVerage of Pile 1 & Pile 2
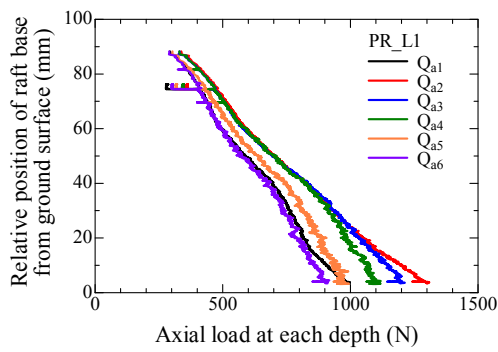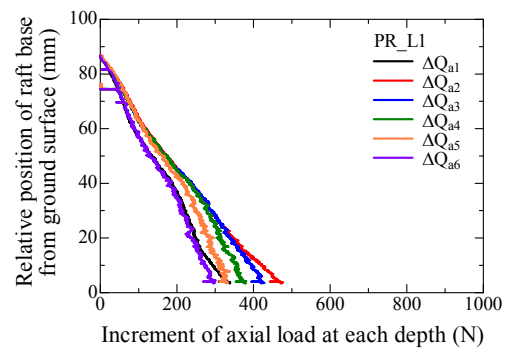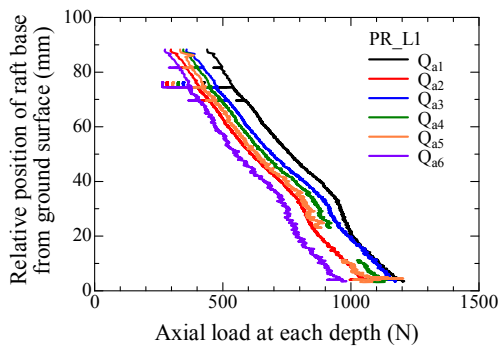
(b) Pile 1
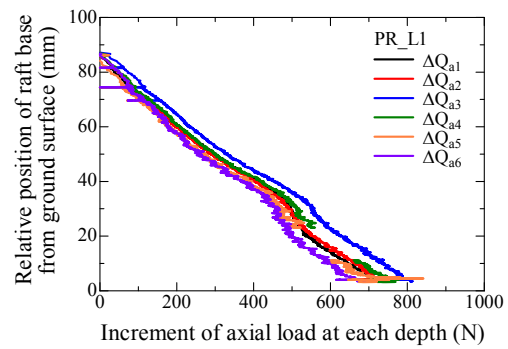
(e) Pile 1

(c) Pile 2

(f) Pile 2

A. 4.2.1.3 Variation of axial load and axial load increment at each depth with relative position of raft base from ground surface for PR_L1 during penetration process.
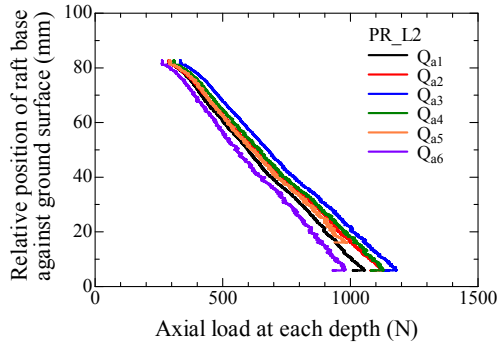
(a) Average of Pile 1 & Pile 2
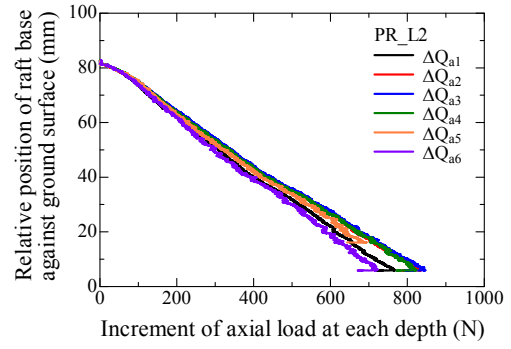
(d) Average of Pile 1 & Pile 2
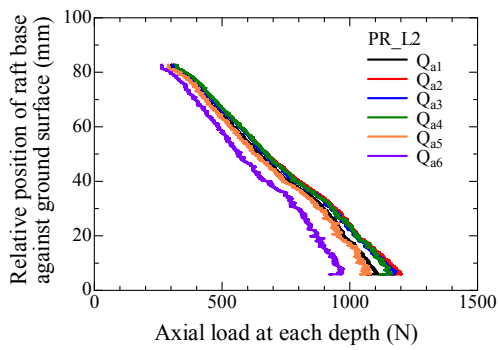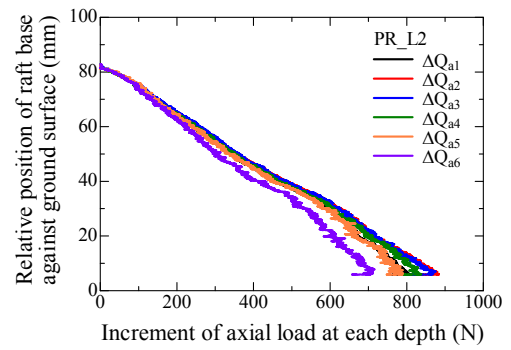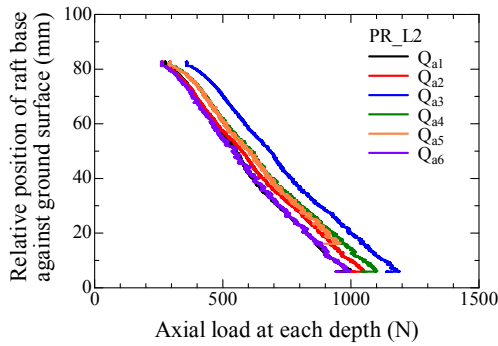
(b) Pile 1
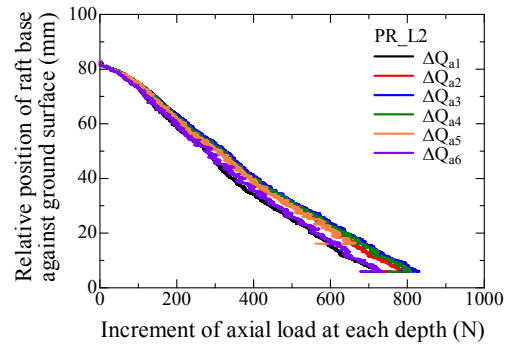
(e) Pile 1

(c) Pile 2

(f) Pile 2

A. 4.2.1.4 Variation of axial load and axial load increment at each depth with relative position of raft base from ground surface for PR_L2 during penetration process.
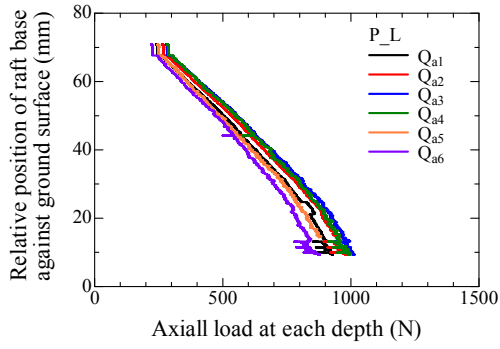
(a) Average of Pile 1 & Pile 2
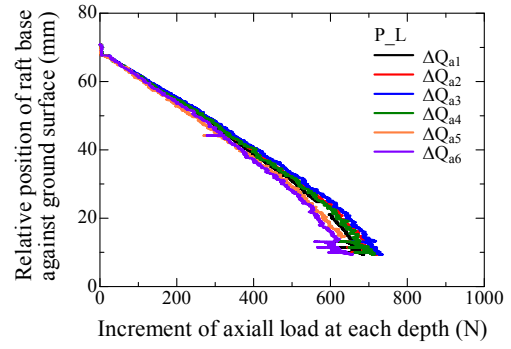
(d) Average of Pile 1 & Pile 2
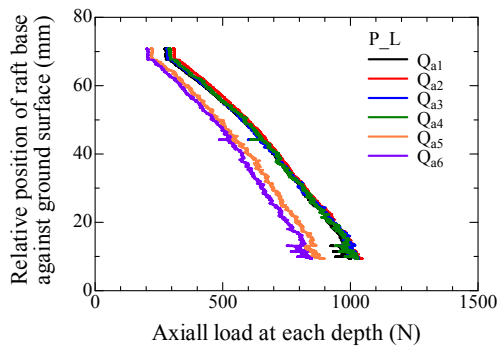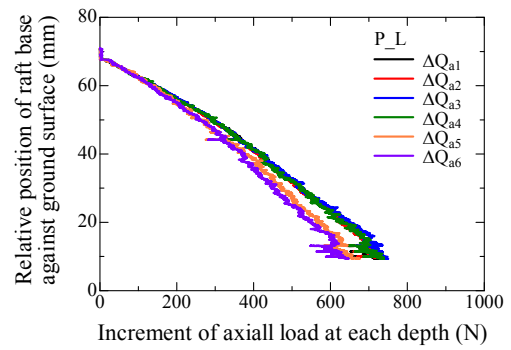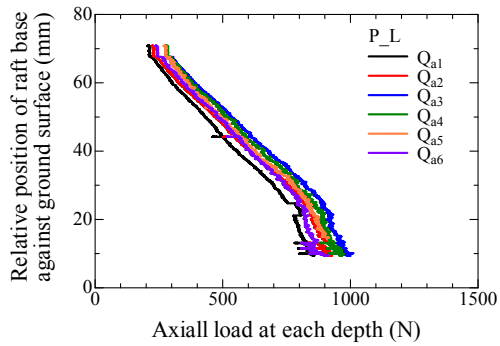
(b) Pile 1
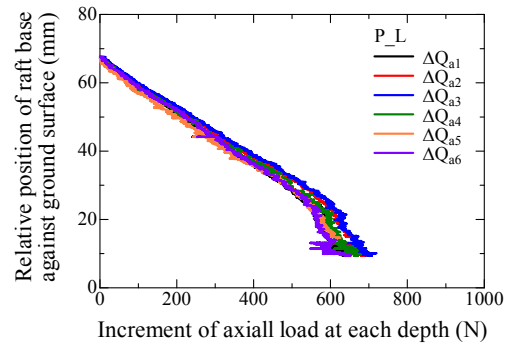
(e) Pile 1

(c) Pile 2

(f) Pile 2

A. 4.2.1.5 Variation of axial load and axial load increment at each depth with relative position of raft base from ground surface for P_L during penetration process.
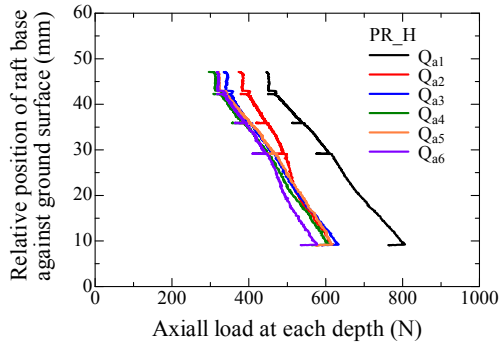
(a) Average of Pile 1 & Pile 2
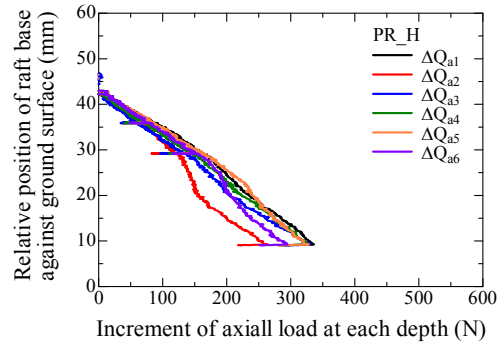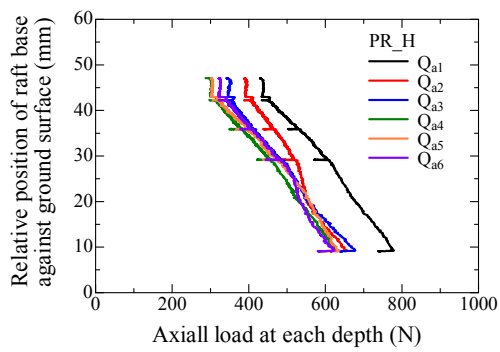
(e) Pile 1

(b) Pile 1
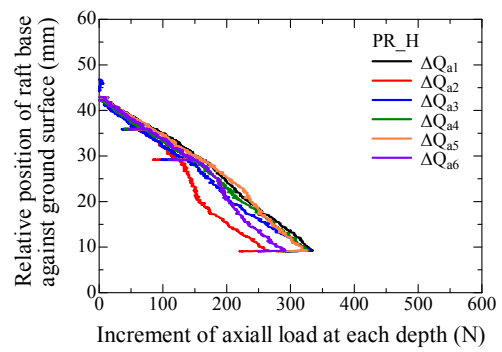
(e) Pile 1
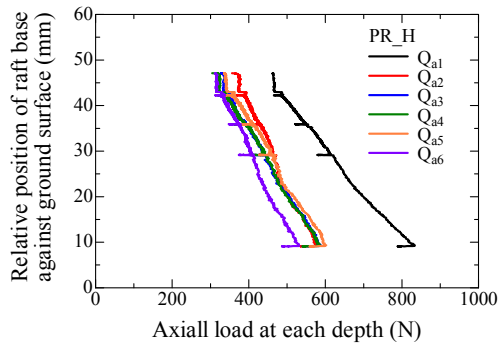
(c) Pile 2
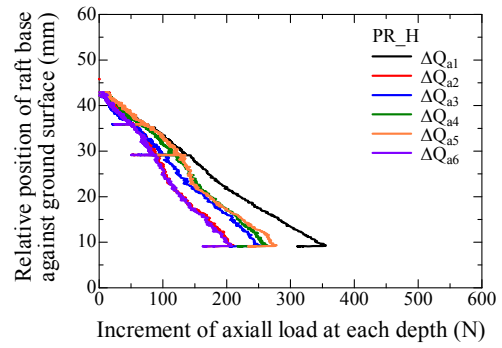
(f) Pile 2

A. 4.2.1.6 Variation of axial load and axial load increment at each depth with relative position of raft base from ground surface for PR_H during penetration process.
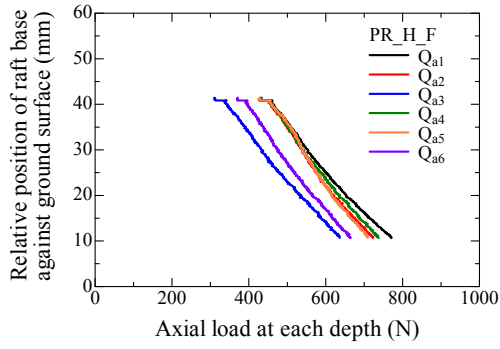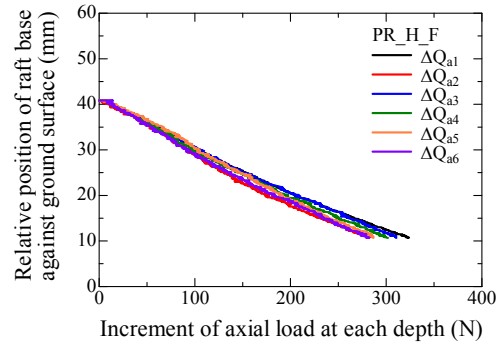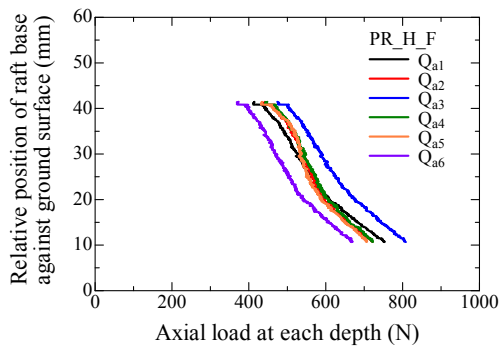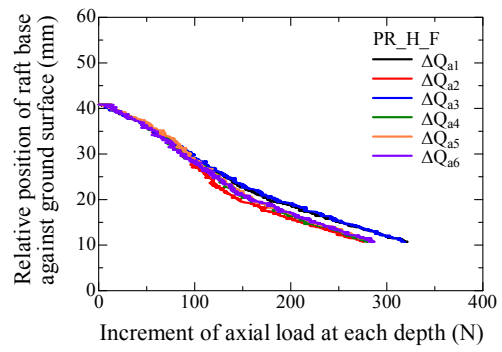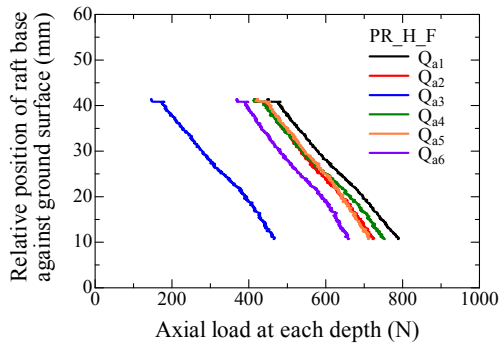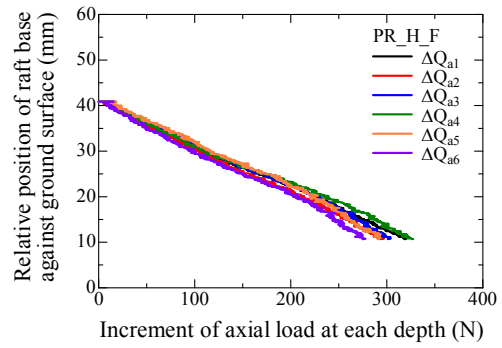
A. 4.2.1.7 Variation of axial load and axial load increment at each depth with relative position of raft base from ground surface for PR_H_F during penetration process.
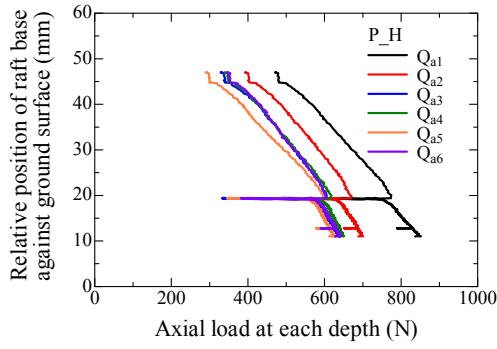
(a) Average of Pile 1 & Pile 2
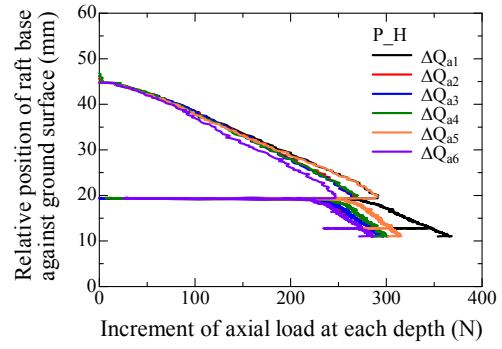
(d) Average of Pile 1 & Pile 2
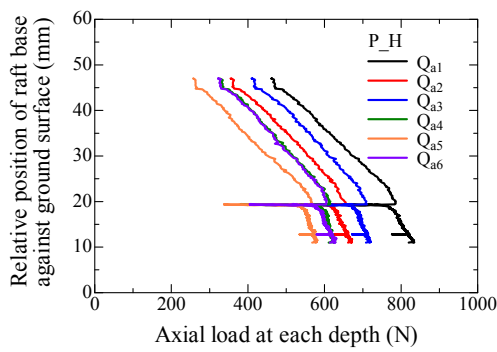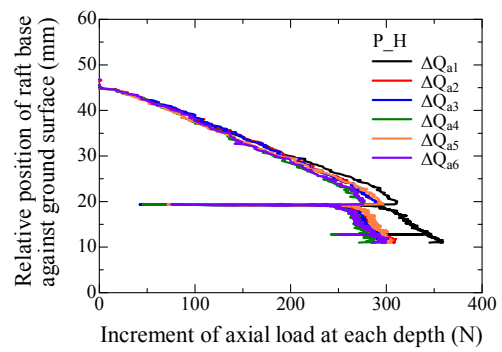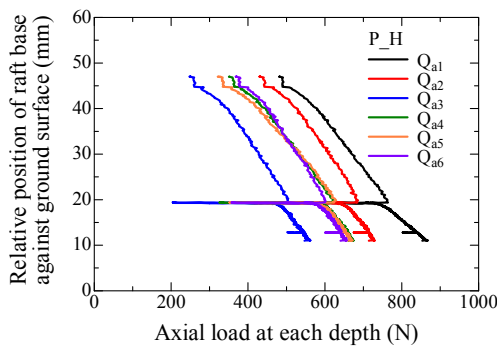
(b) Pile 1
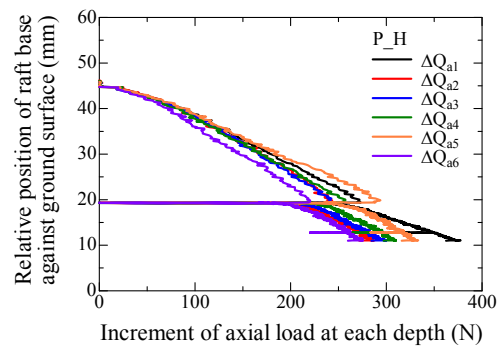
(e) Pile 1

(c) Pile 2

(f) Pile 2

A. 4.2.1.8 Variation of axial load and axial load increment at each depth with relative position of raft base from ground surface for P_H during penetration process.
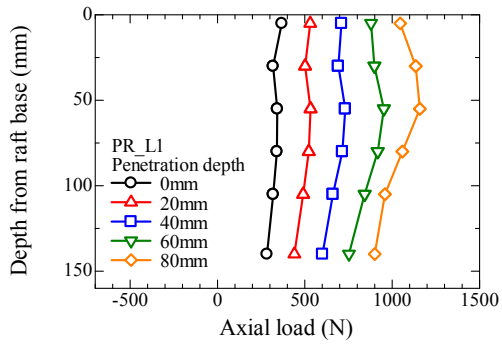
(a) Average of Pile 1 & Pile 2
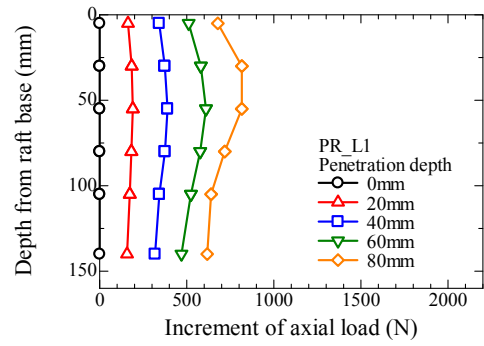
(d) Average of Pile 1 & Pile 2
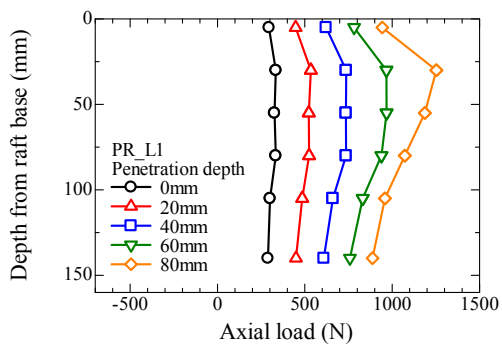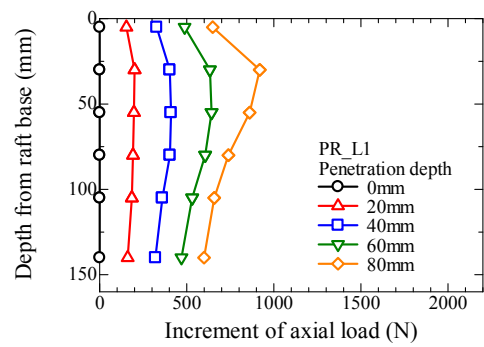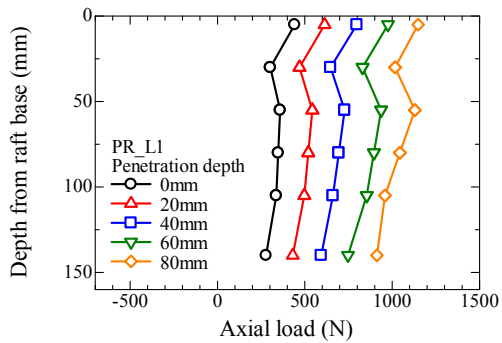
(b) Pile 1
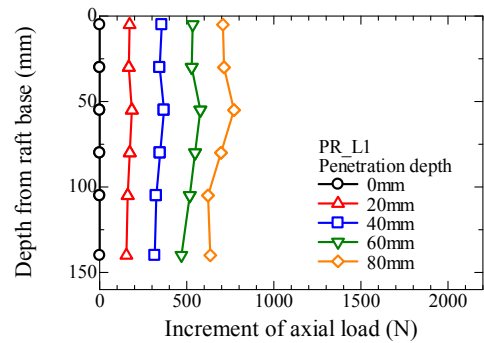
(e) Pile 1

(c) Pile 2

(f) Pile 2

A. 4.2.1.9 Profiles of axial load and axial load increment for PR_L1 during penetration process.
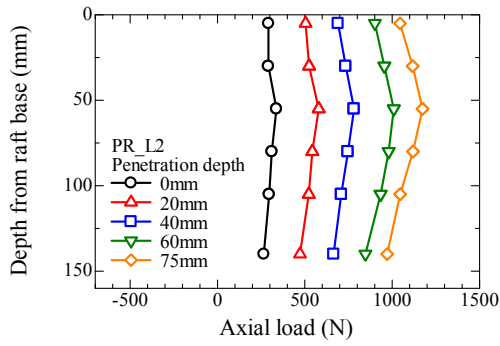
(a) Average of Pile 1 & Pile 2
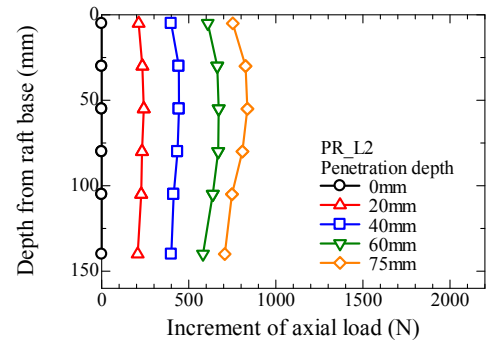
(d) Average of Pile 1 & Pile 2
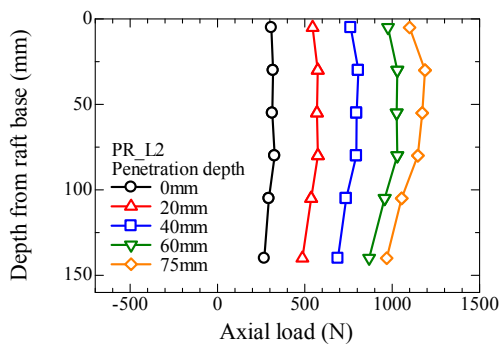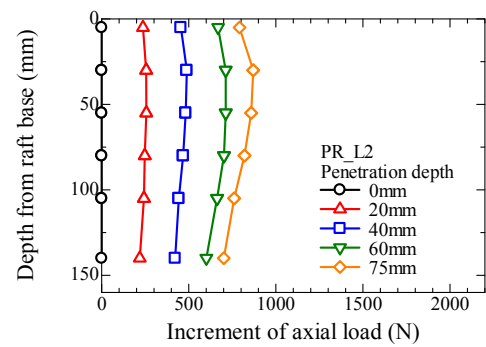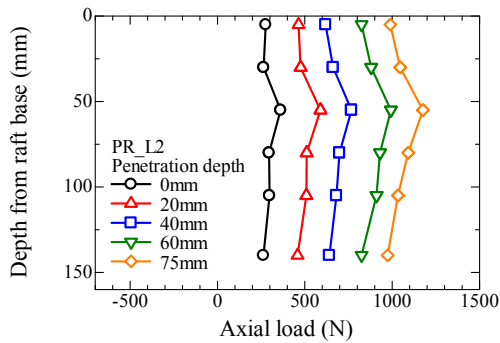
(b) Pile 1
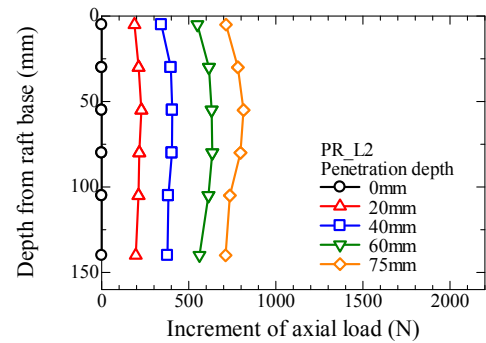
(e) Pile 1

(c) Pile 2

(f) Pile 2

A. 4.2.1.10 Profiles of axial load and axial load increment for PR_L2 during penetration process.
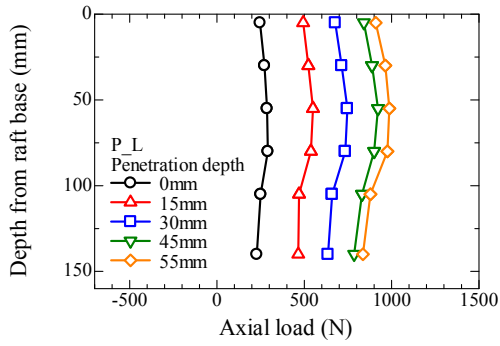
(a) Average of Pile 1 & Pile 2
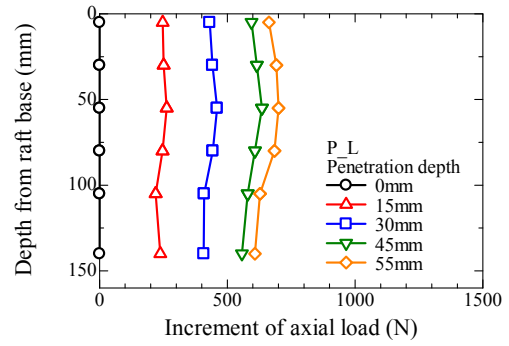
(d) Average of Pile1 & Pile2
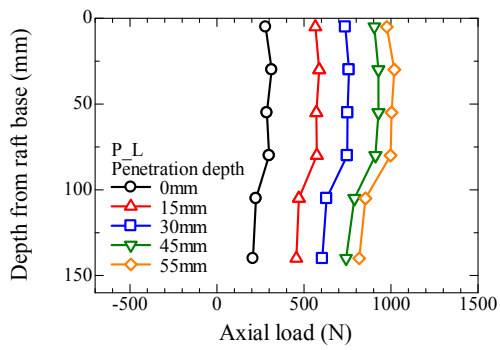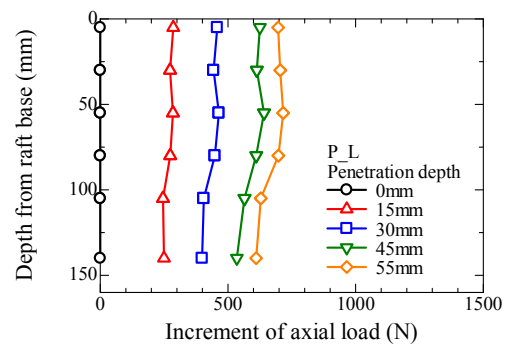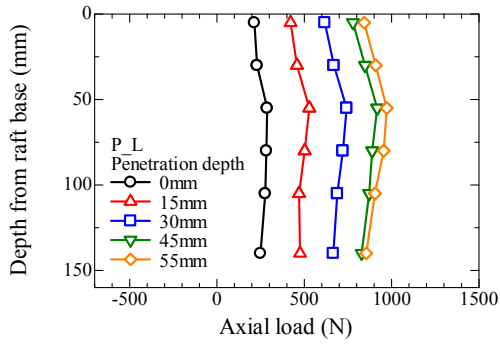
(b) Pile 1
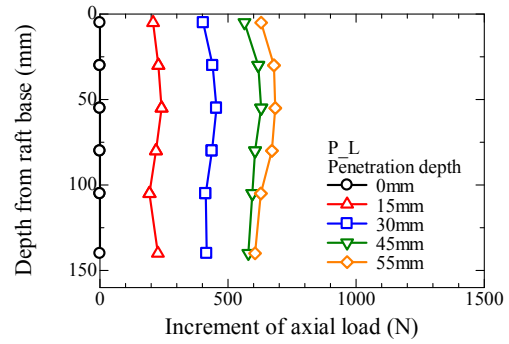
(e) Pile 1

(c) Pile 2

(f) Pile 2

A. 4.2.1.11 Profiles of axial load and axial load increment for P_L during penetration process.
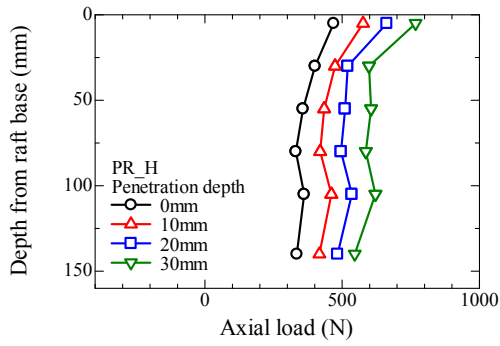
(a) Average of Pile 1 & Pile 2
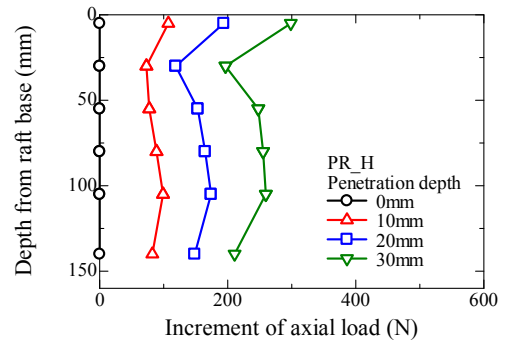
(d) Average of Pile 1 & Pile
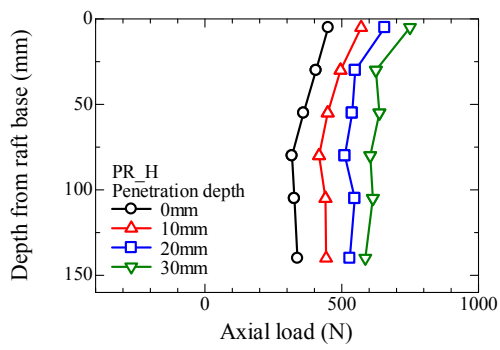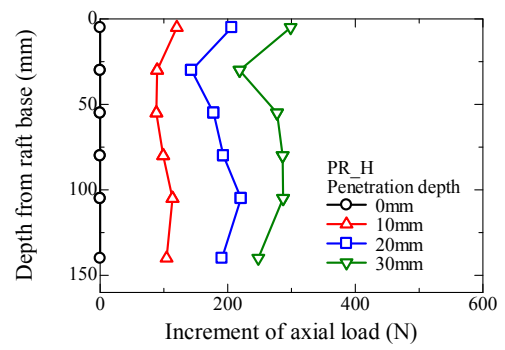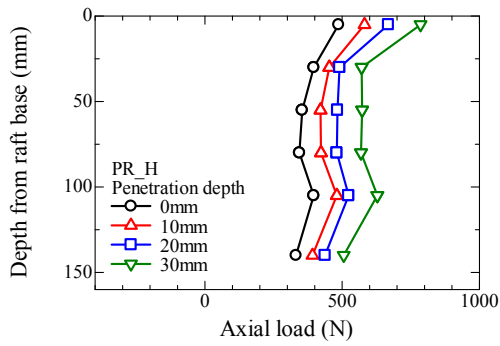
(b) Pile 1
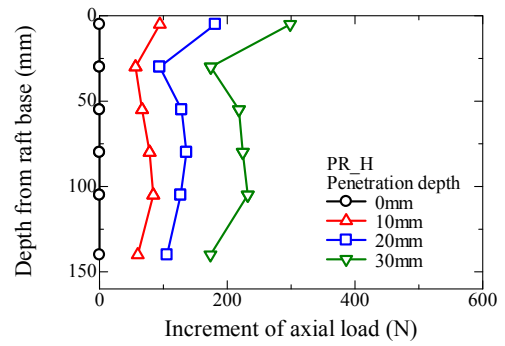
(e) Pile 1

(c) Pile 2

(f) Pile 2

A. 4.2.1.12 Profiles of axial load and axial load increment for PR_H during penetration process.
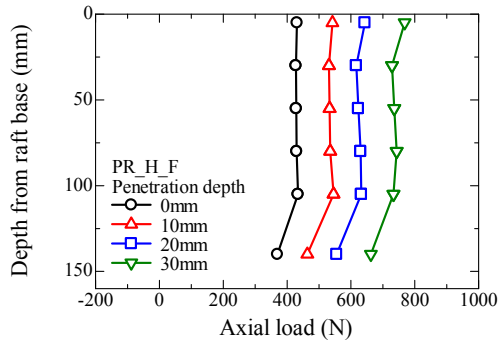
(a) Average of Pile 1 & Pile 2
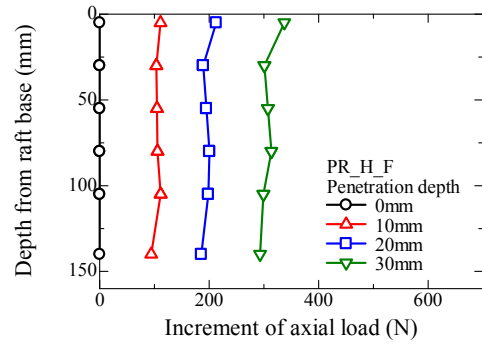
(d) Average of Pile 1 & Pile 2
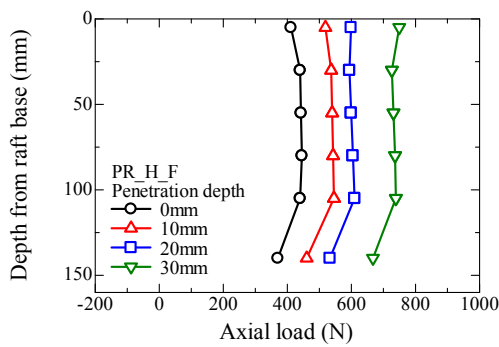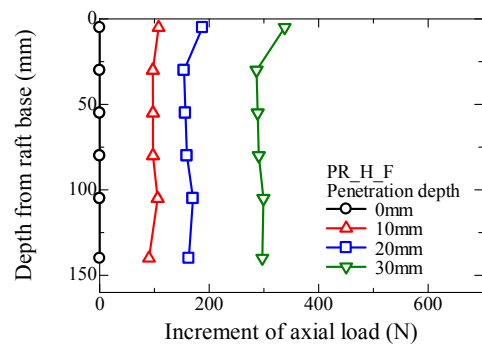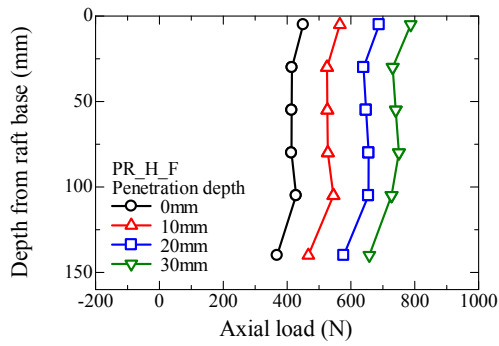
(b) Pile 1
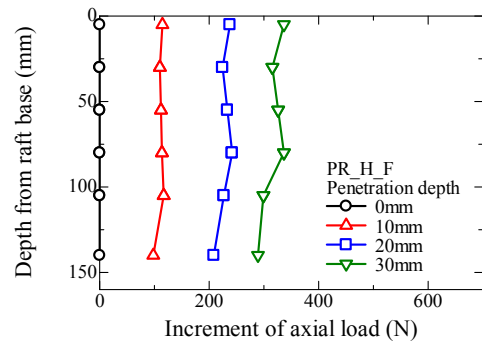
(e) Pile 1

(c) Pile 2

(f) Pile 2

A. 4.2.1.13 Profiles of axial load and axial load increment for PR_H_F during penetration process.
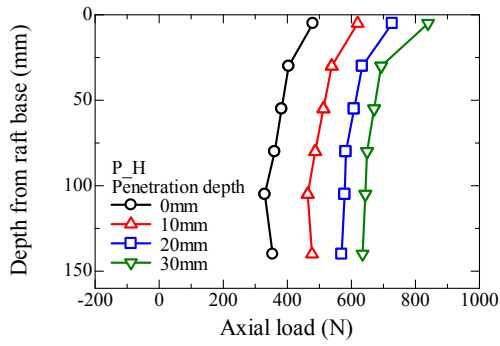
(a) Average of Pile 1 & Pile 2
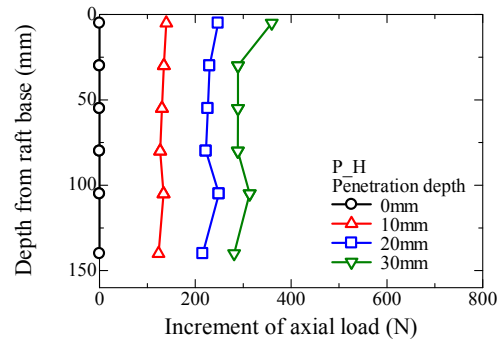
(d) Average of Pile 1 & Pile 2
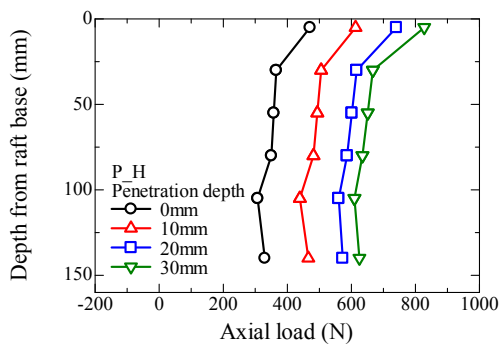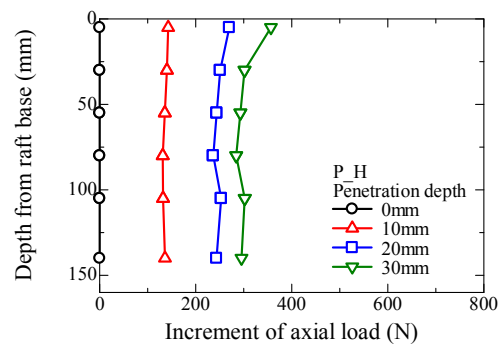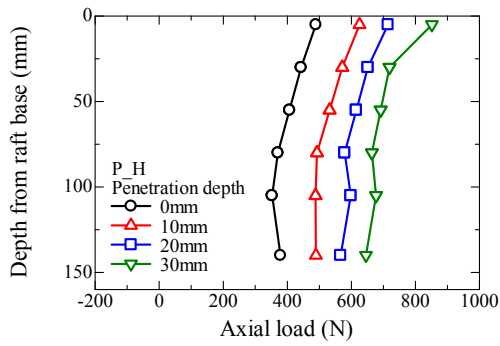
(b) Pile 1
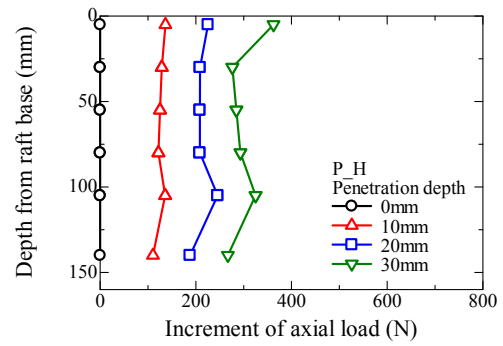
(e) Pile 1

(c) Pile 2

(f) Pile 2

A. 4.2.1.14 Profiles of axial load and axial load increment for P_H during penetration process.
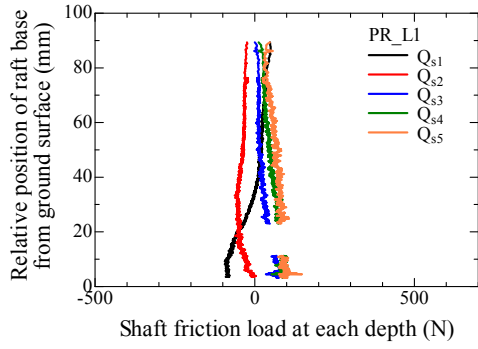
(a) Average of Pile 1 & Pile 2
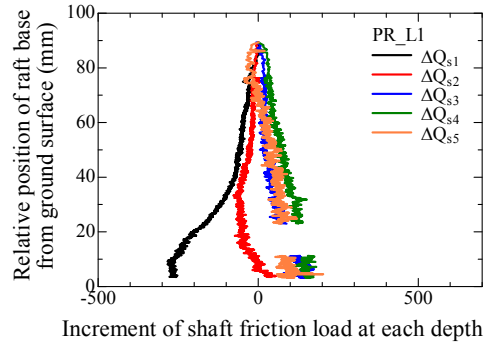
(d) Average of Pile 1 & Pile 2
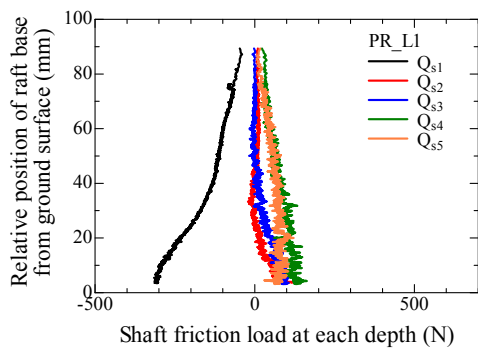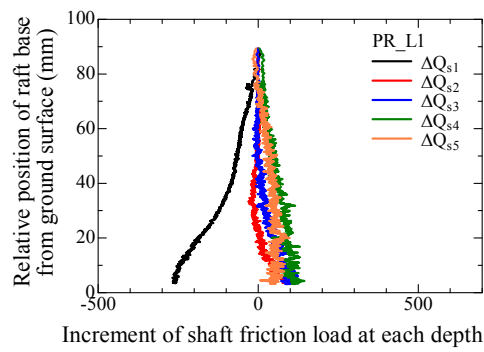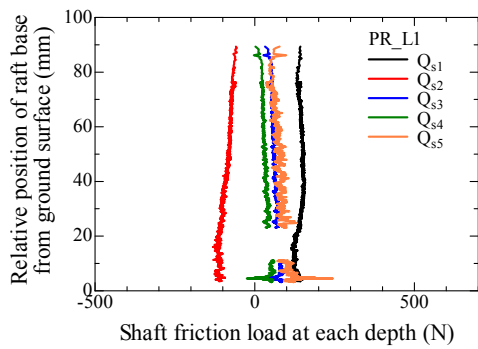
(b) Pile 1
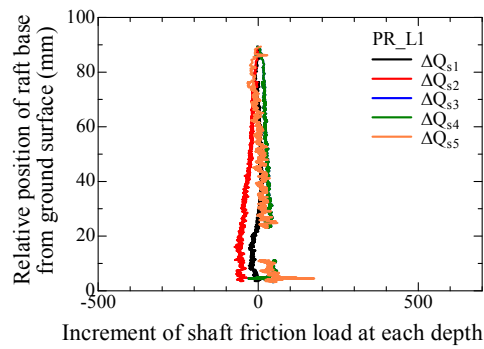
(e) Pile 1

(c) Pile 2

(f) Pile 2

A. 4.2.1.15 Variation of shaft friction load and shaft friction load increment at each depth with relative position of raft base from ground surface for PR_L1 during penetration process.

A22
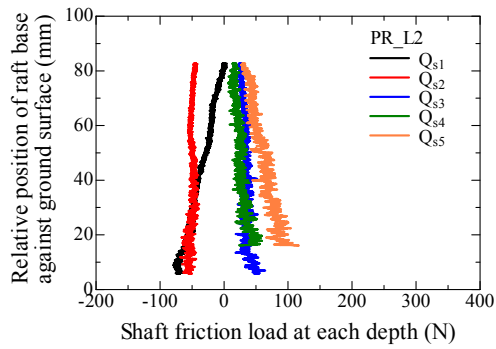
(a) Average of Pile 1 & Pile 2
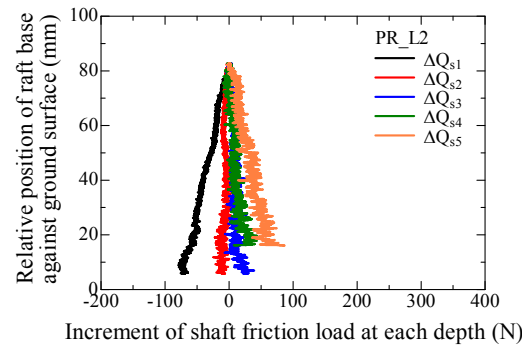
(d) Average of Pile 1 & Pile 2
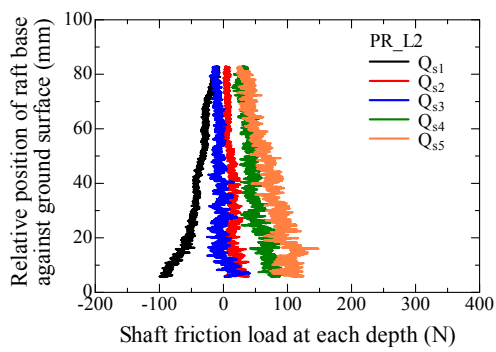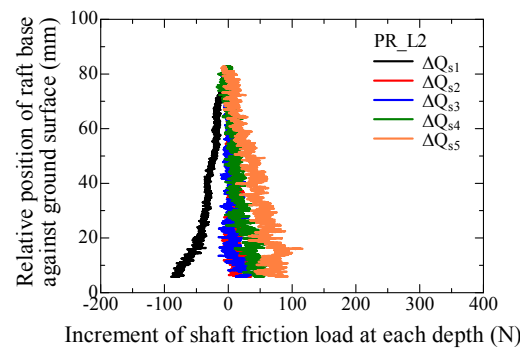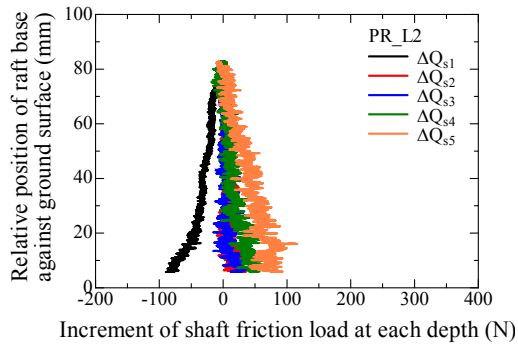
(b) Pile 1
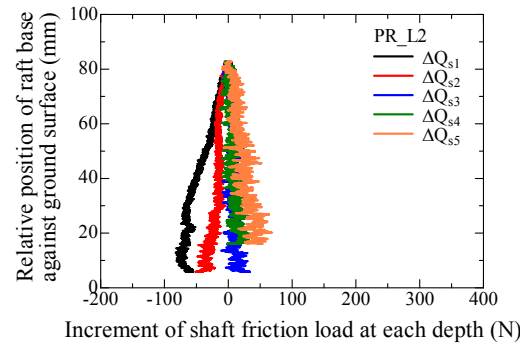
(e) Pile 1

(e) Pile 1

(f) Pile 2

A. 4.2.1.16 Variation of shaft friction load and shaft friction load increment at each depth with relative position of raft base from ground surface for PR_L2 during penetration process.
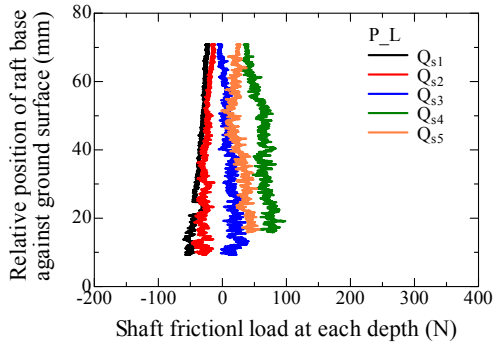
(a) Average of Pile 1 & Pile 2
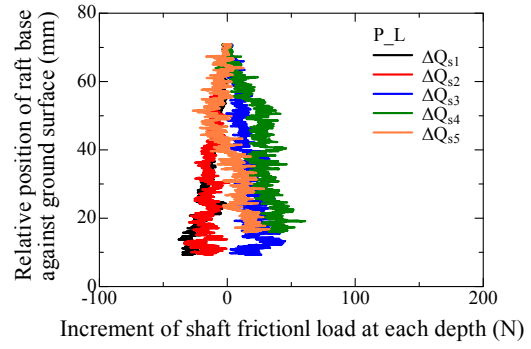
(d) Average of Pile 1 & Pile 2
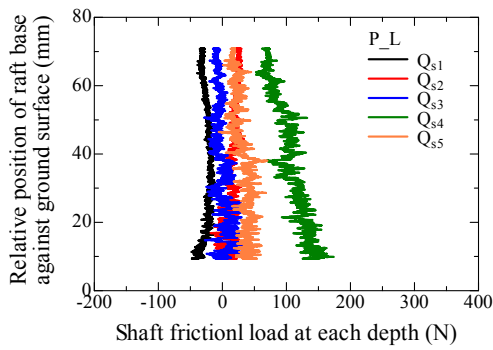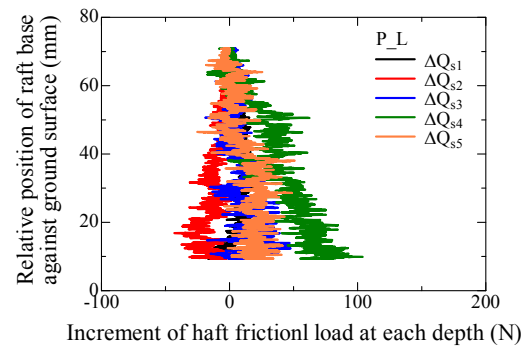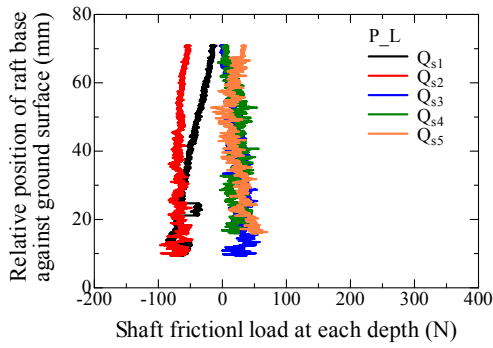
(b) Pile 1
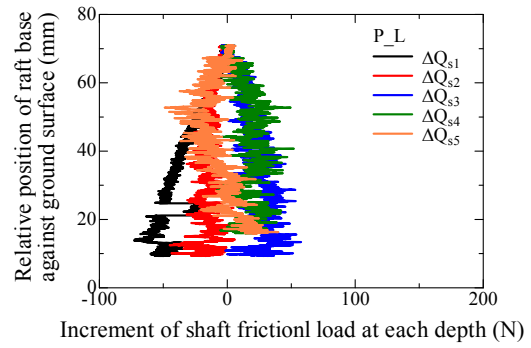
(e) Pile 1

(c) Pile 2

(f) Pile 2

A. 4.2.1.17 Variation of shaft friction load and shaft friction load increment at each depth with relative position of raft base from ground surface for P_L during penetration process.
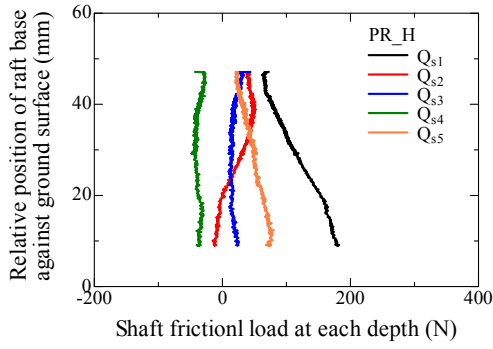
(a) Average of Pile 1 & Pile 2
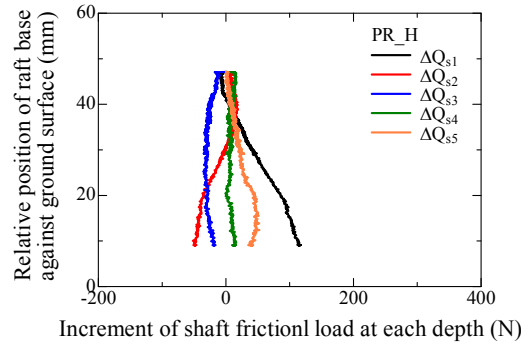
(d) Average of Pile 1 & Pile 2
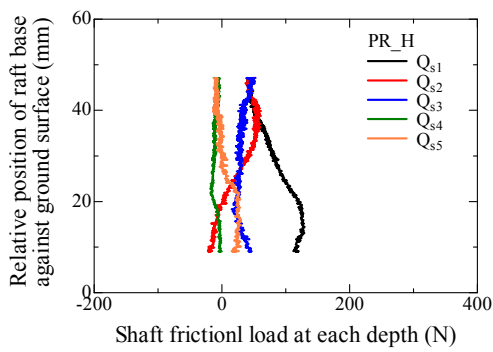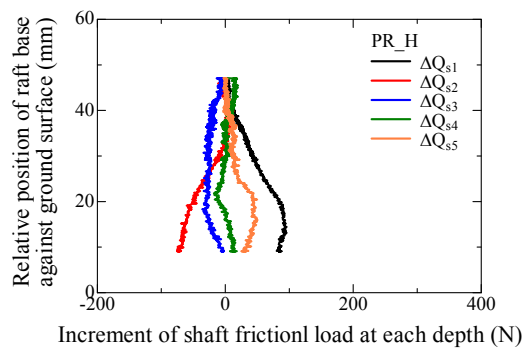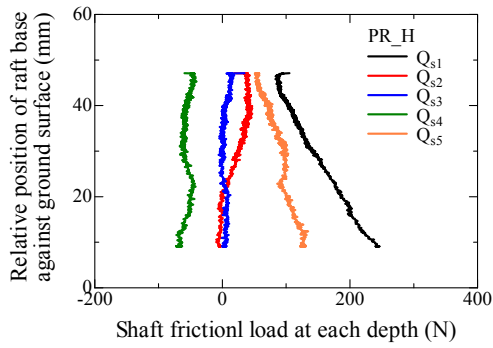
(b) Pile 1
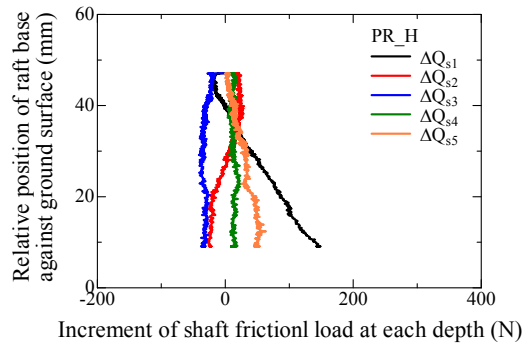
(e) Pile 1

(c) Pile 2

(f) Pile 2

A. 4.2.1.18 Variation of shaft friction load and shaft friction load increment at each depth with relative position of raft base from ground surface for PR_H during penetration process.
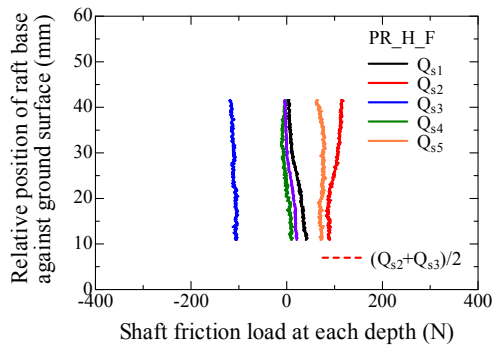
(a) Average of Pile 1 and Pile 2
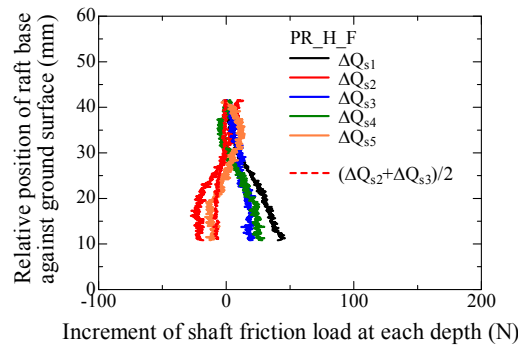
(b) Pile 1

(c) Pile 2

(d) Average of Pile 1 and Pile 2
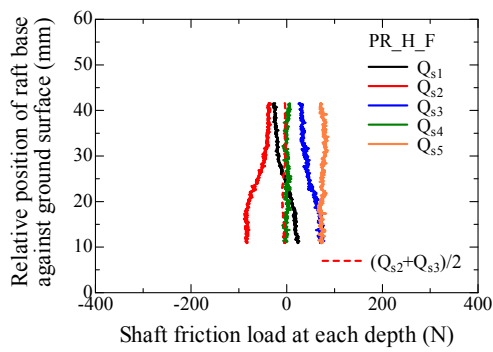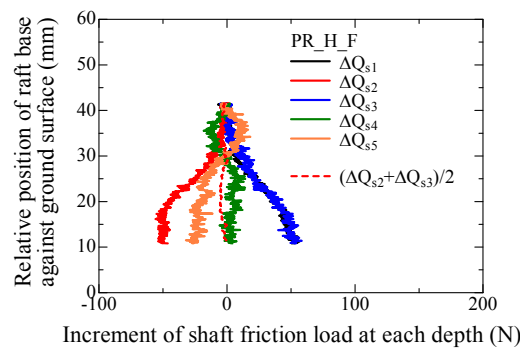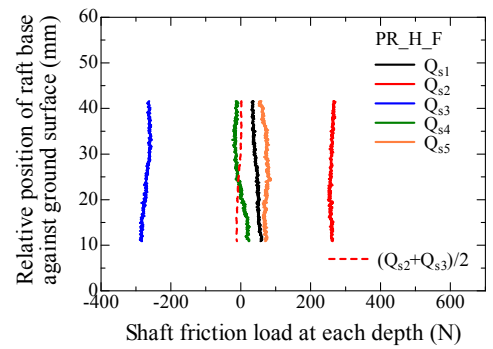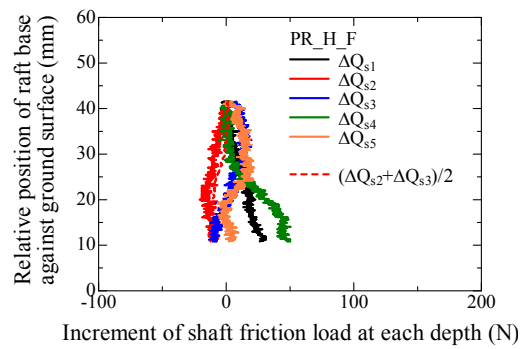
(e) Pile 1

(f) Pile 2

A. 4.2.1.19 Variation of shaft friction load and shaft friction load increment at each depth with relative position of raft base from ground surface for PR_H_F during penetration process.
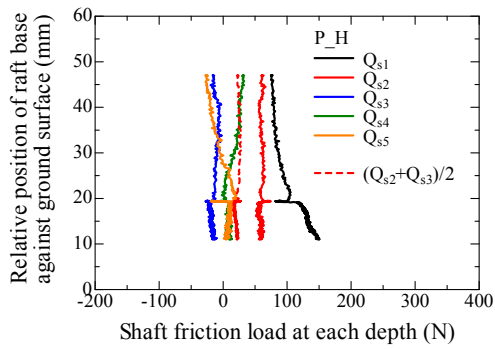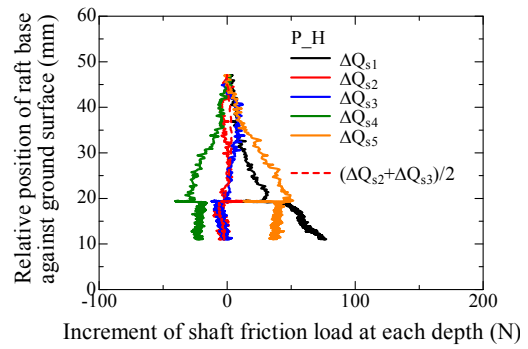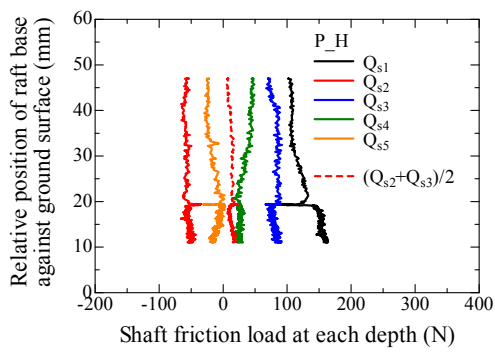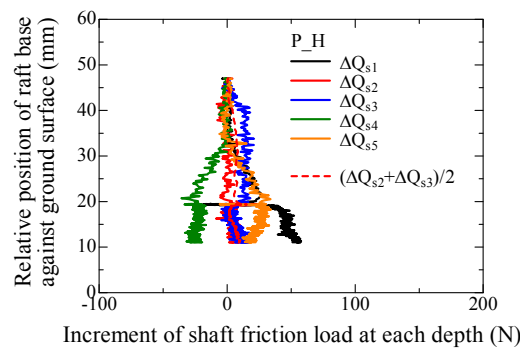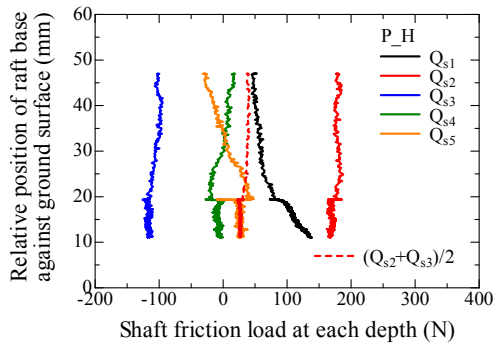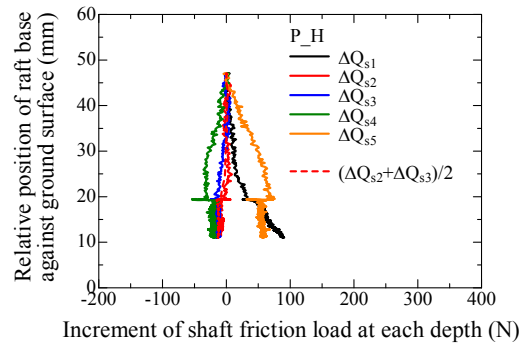
A. 4.2.1.20 Variation of shaft friction load and shaft friction load increment at each depth with relative position of raft base from ground surface for P_H during penetration process.
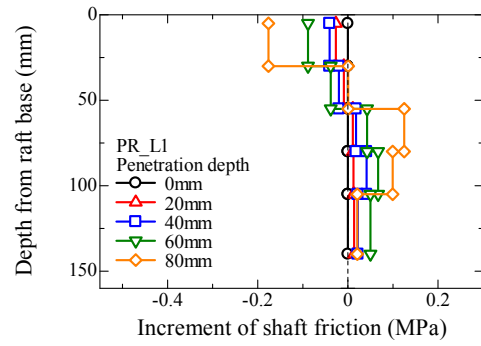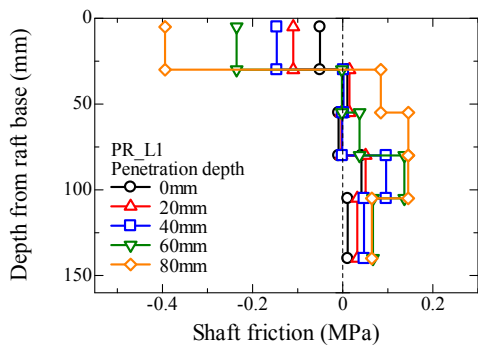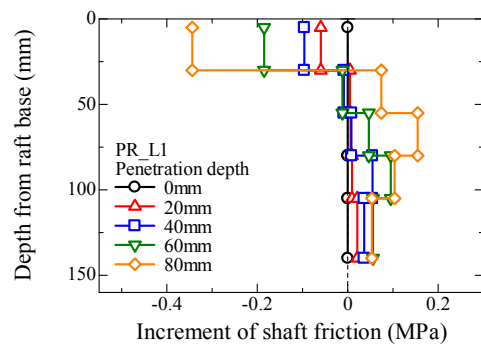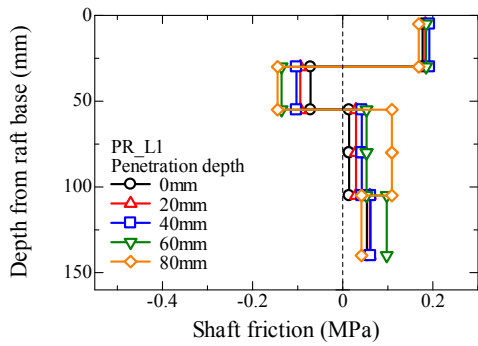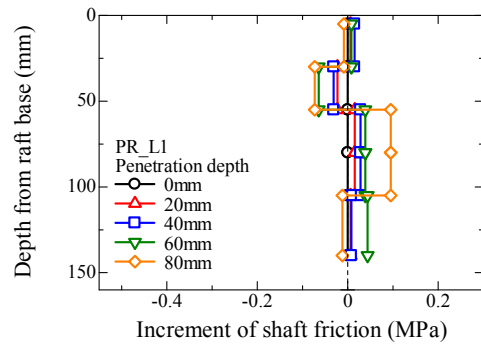
A. 4.2.1.21 Profiles of shaft friction and shaft friction increment at certain penetration depth for PR_L1 during penetration process.
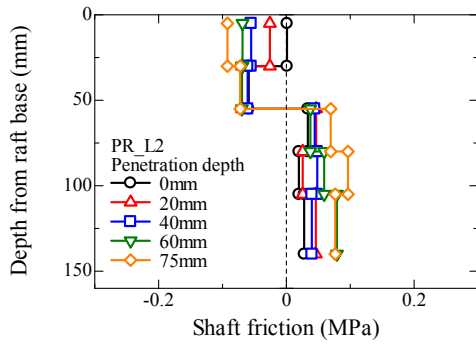
(a) Average of Pile 1 & Pile 2
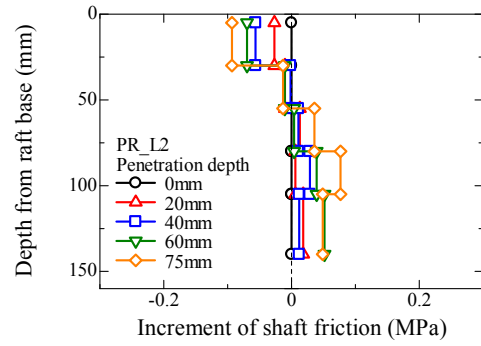
(d) Average of Pile 1 & Pile 2
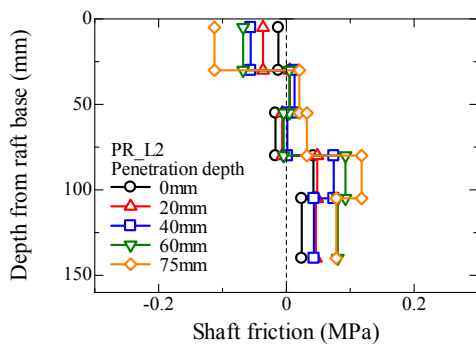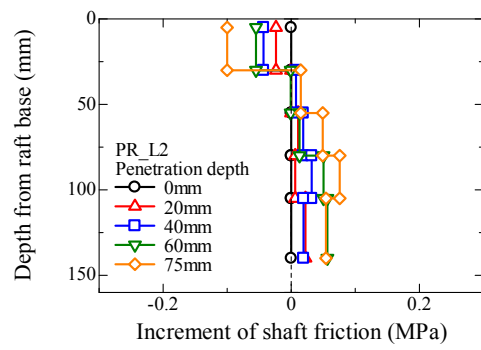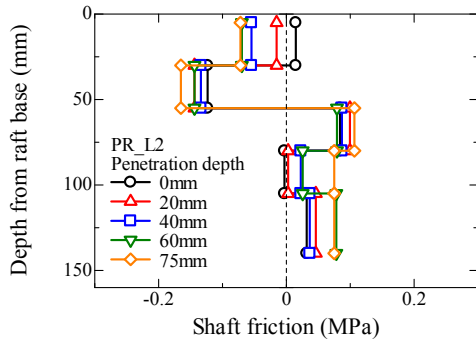
(b) Pile 1
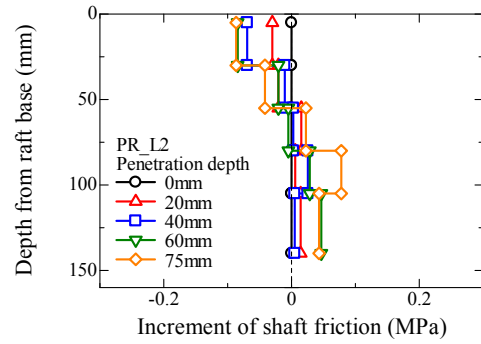
(e) Pile 1

(c) Pile 2

(f) Pile 2

A. 4.2.1.22 Profiles of shaft friction and shaft friction increment at certain penetration depth for PR_L2 during penetration process.
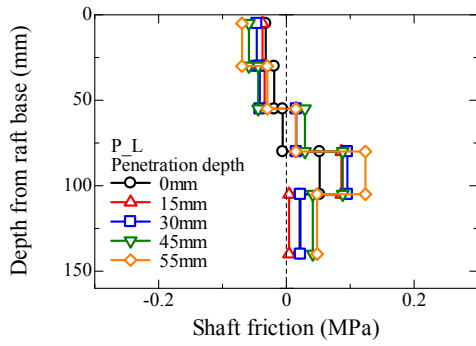
(a) Average of Pile 1 & Pile 2
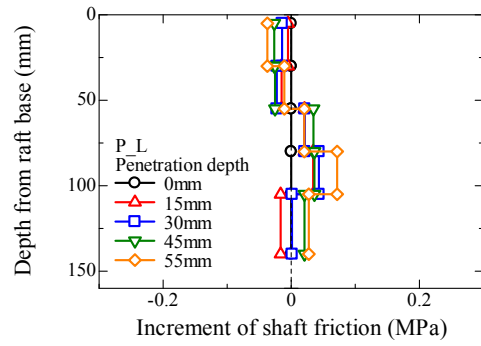
(d) Average of Pile 1 & Pile 2
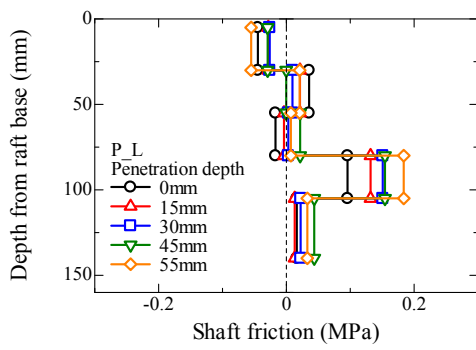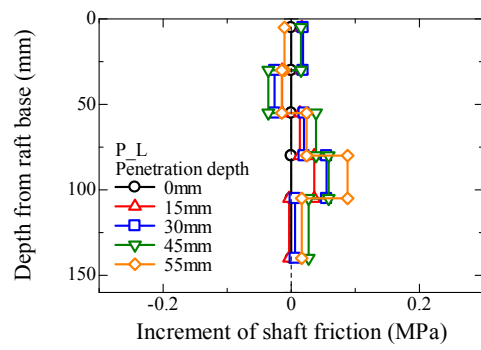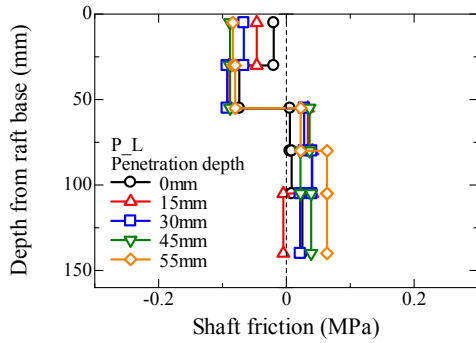
(b) Pile 1
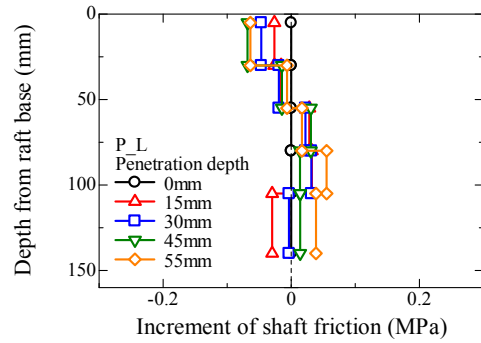
(e) Pile 1

(c) Pile 2

(f) Pile 2

A. 4.2.1.23 Profiles of shaft friction and shaft friction increment at certain penetration depth for P_L during penetration process.
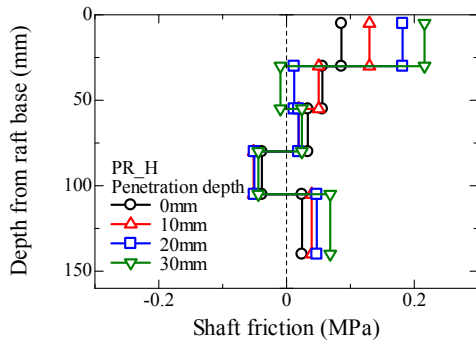
(a) Average of Pile 1 & Pile 2
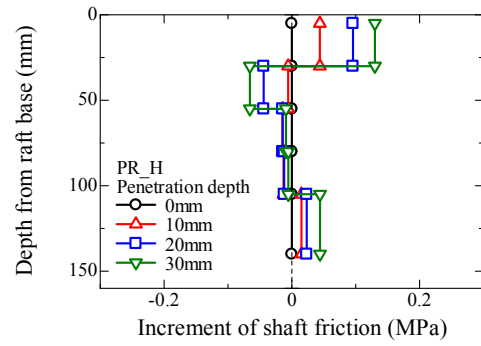
(d) Average of Pile 1 & Pile 2
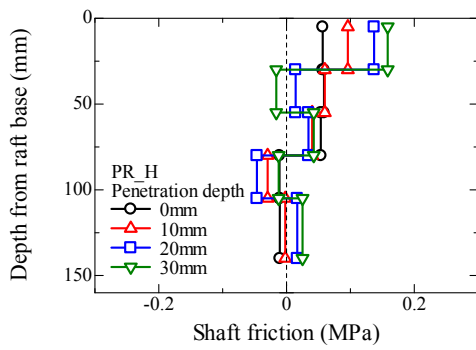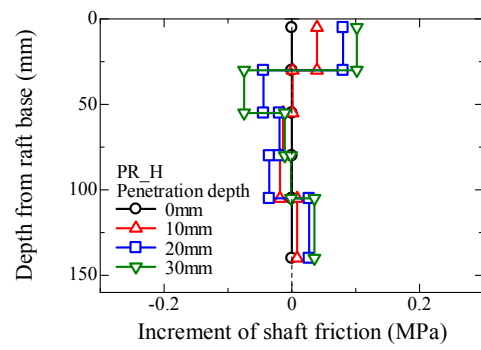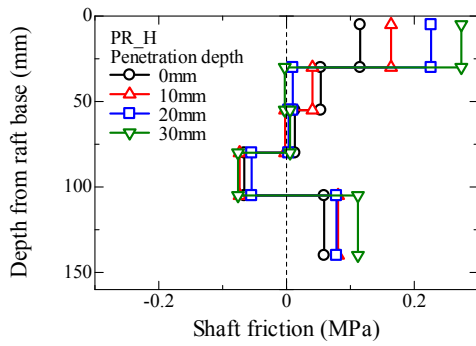
(b) Pile 1
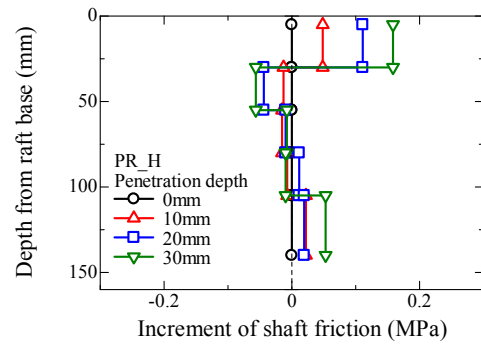
(e) Pile 1

(c) Pile 2

(f) Pile 2

A. 4.2.1.24 Profiles of shaft friction and shaft friction increment at certain penetration depth for PR_H during penetration process.
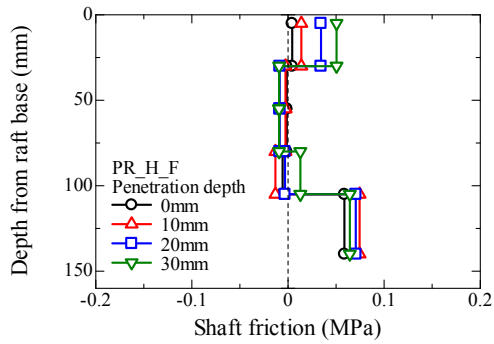
(a) Average of Pile 1 & Pile 2
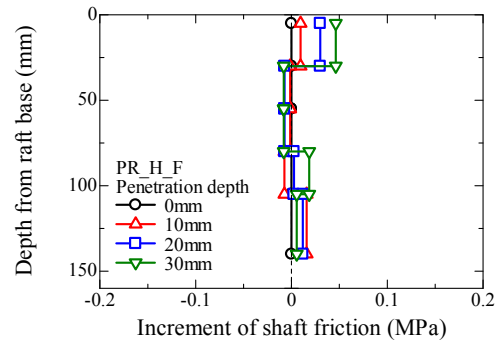
(d) Average of Pile 1 & Pile 2
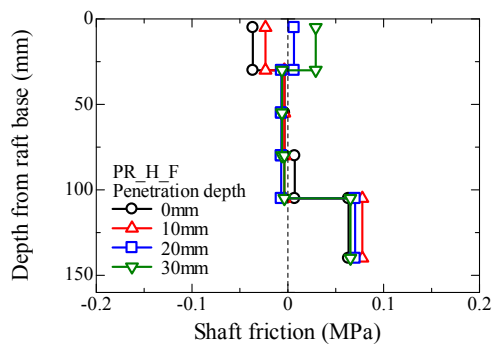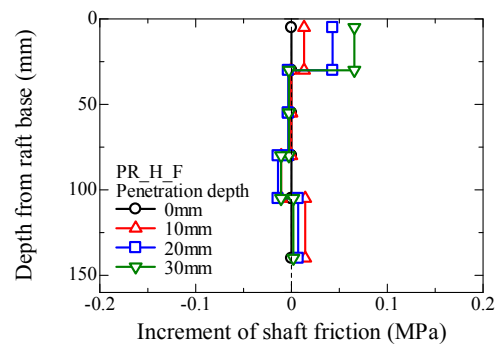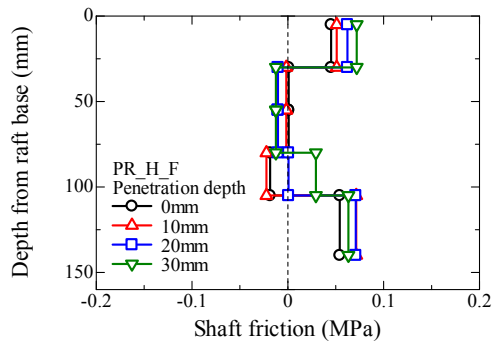
(b) Pile 1
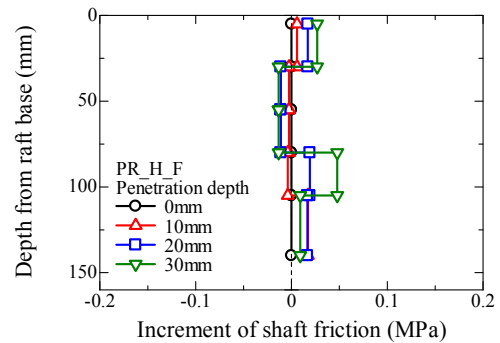
(e) Pile 1

(c) Pile 2

(f) Pile 2

A. 4.2.1.25 Profiles of shaft friction and shaft friction increment at certain penetration depth for PR_H _Fduring penetration process.
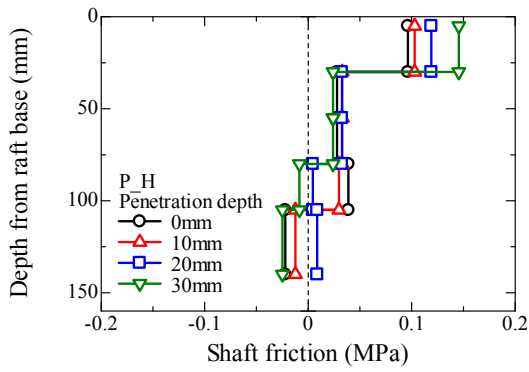
(a) Average of Pile 1 & Pile 2
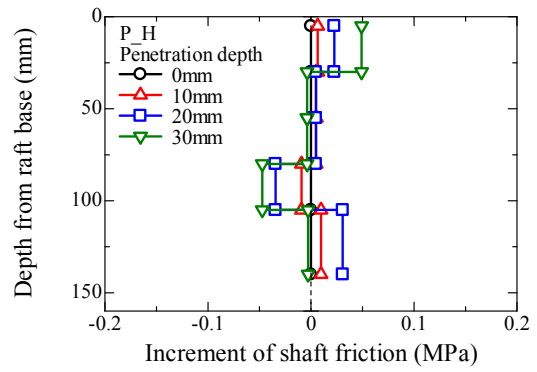
(d) Average of Pile 1 & Pile 2
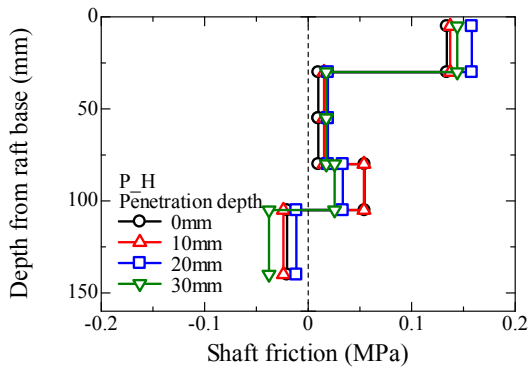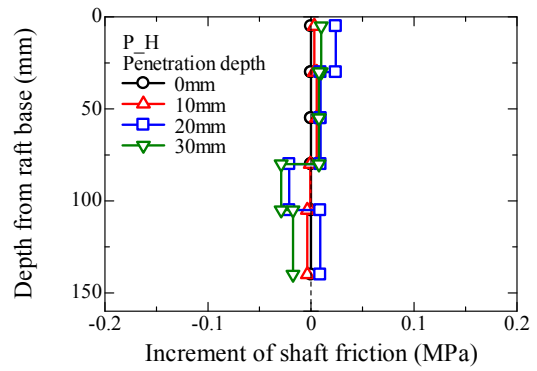
(b) Pile 1

(e) Pile 1
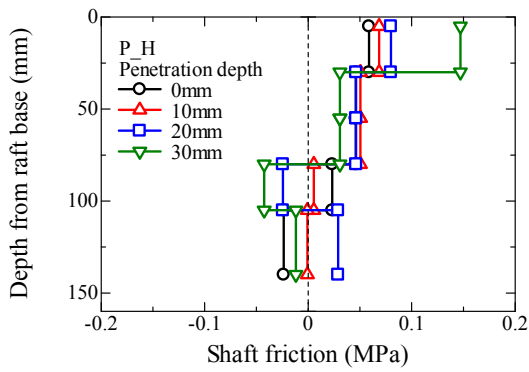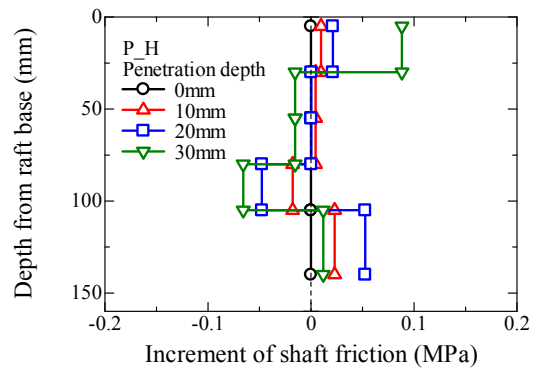
(c) Pile 2

(f) Pile 2

A. 4.2.1.26 Profiles of shaft friction and shaft friction increment at certain penetration depth for P_H during penetration process.
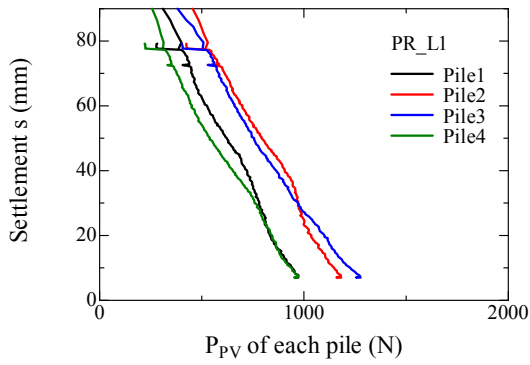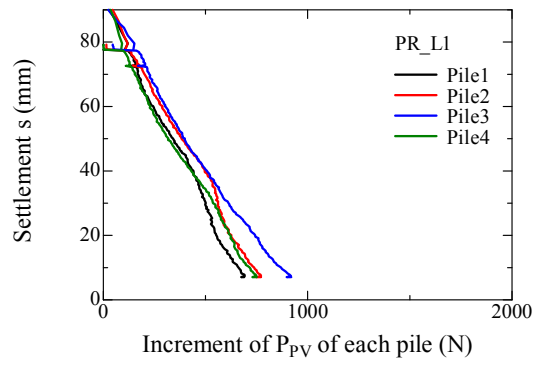
(a) P_{PV}

(a) P_{PV}
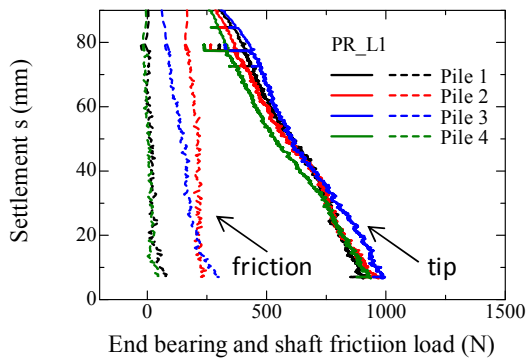
(b) End bearing and shaft friction loads
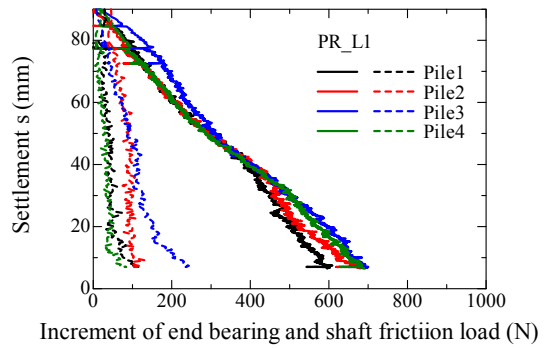
(b) End bearing and shaft friction loads

A. 4.2.2.1 Relationship between each pile load and settlement for PR_L1 observed in penetration process.

A. 4.2.2.2 Relationship between each pile load increment and settlement for PR_L1 observed in penetration process.
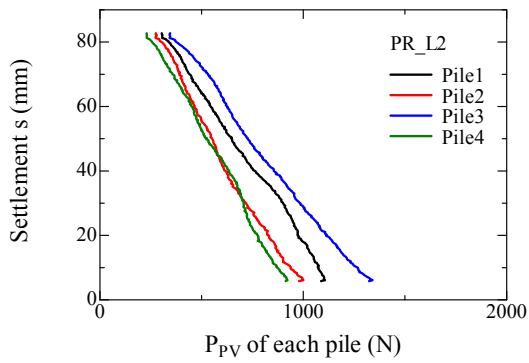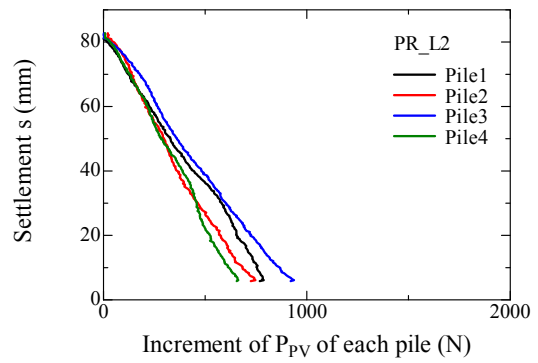
(a) P_{PV}

(a) P_{PV}
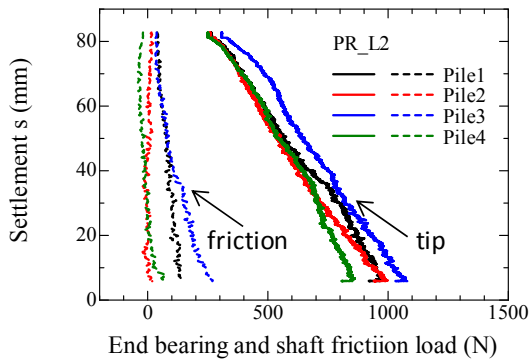
(b) End bearing and shaft friction loads
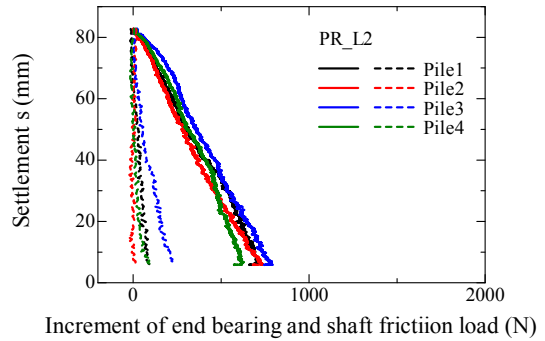
(b) End bearing and shaft friction loads

A. 4.2.2.3 Relationship between each pile load and settlement for PR_L2 observed in penetration process.

A. 4.2.2.4 Relationship between each pile load increment and settlement for PR_L2 observed in penetration process.
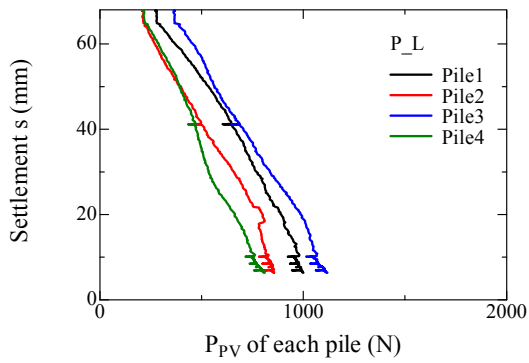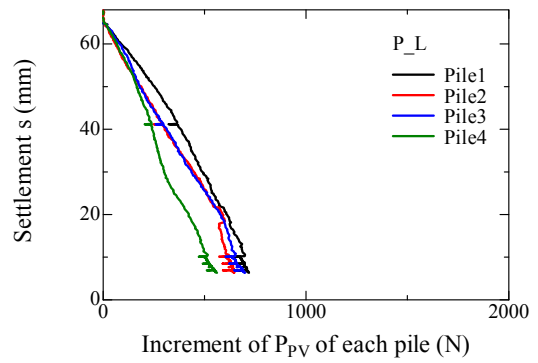
(a) P_{PV}

(a) P_{PV}
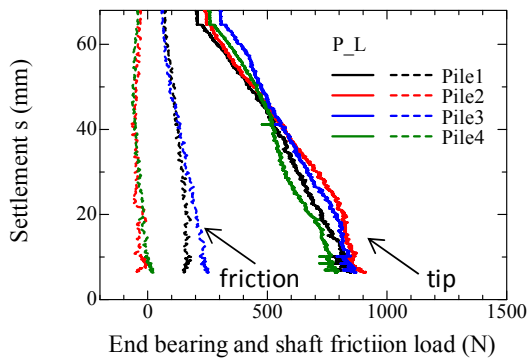
(b) End bearing and shaft friction loads
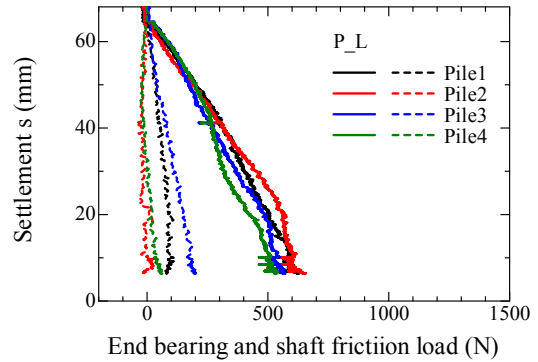
(b) End bearing and shaft friction loads

A. 4.2.2.5 Relationship between each pile load and settlement for P_L observed in penetration process.

A. 4.2.2.6 Relationship between each pile load increment and settlement for P_L observed in penetration process.
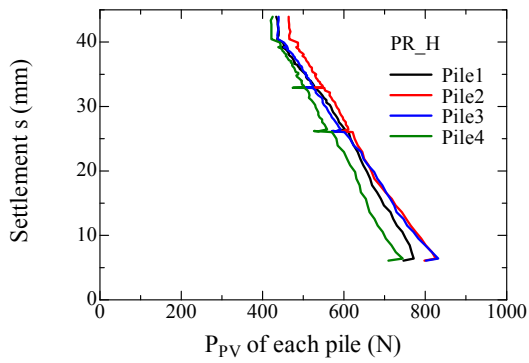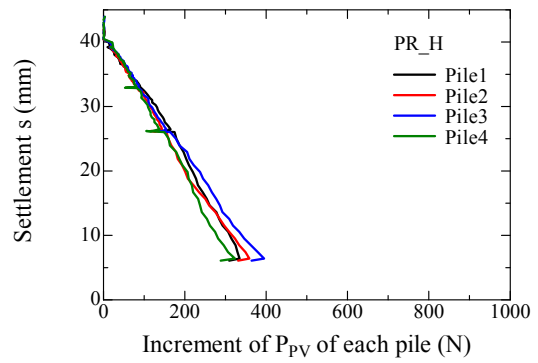
(a) P_{PV}

(a) P_{PV}
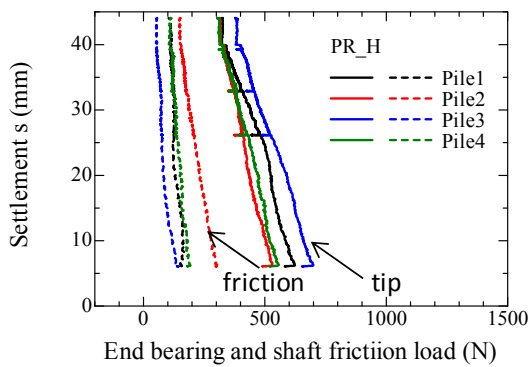
(b) End bearing and shaft friction loads
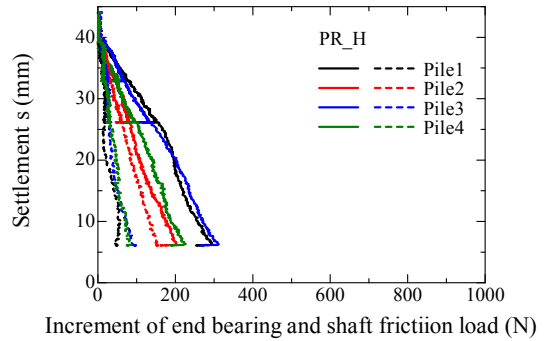
(b) End bearing and shaft friction loads

A. 4.2.2.7 Relationship between each pile load and settlement for PR_H observed in penetration process.

A. 4.2.2.8 Relationship between each pile load increment and settlement for PR_H observed in penetration process.
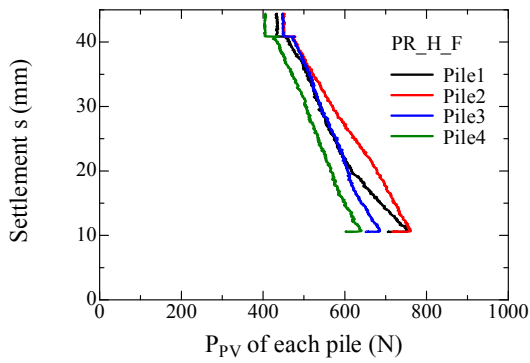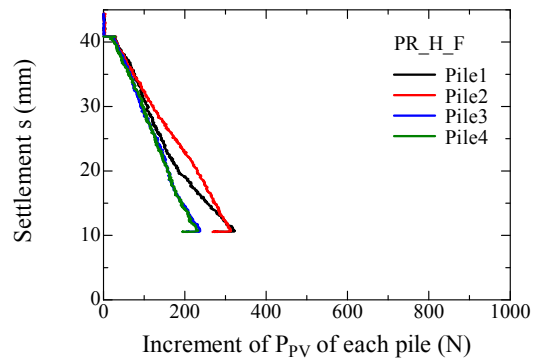
(a) P_{PV}

(a) P_{PV}
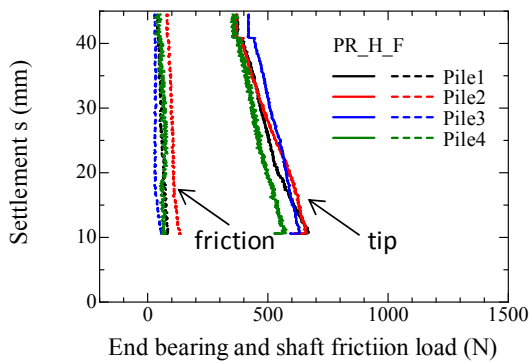
(b) End bearing and shaft friction loads
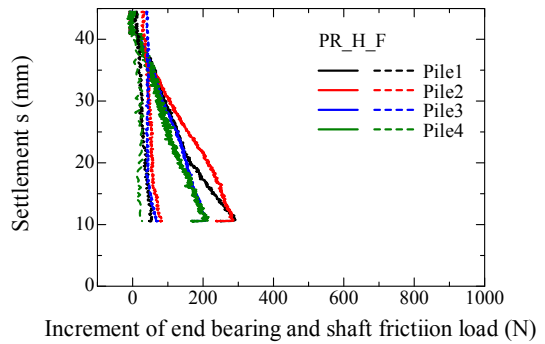
(b) End bearing and shaft friction loads

A. 4.2.2.9 Relationship between each pile load and settlement for PR_H_F observed in penetration process.

A. 4.2.2.10 Relationship between each pile load increment and settlement for PR_H_F observed in penetration process.
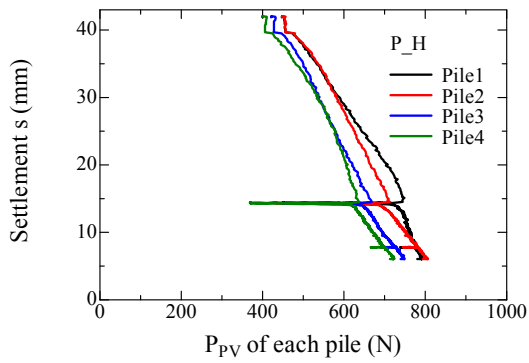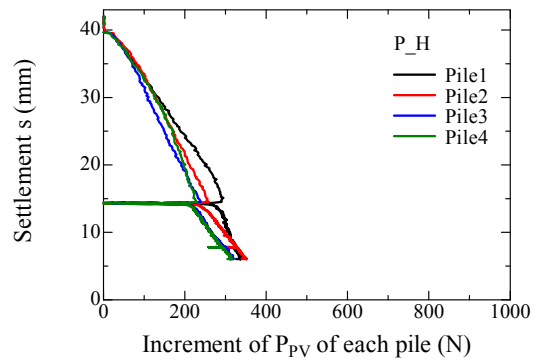
(a) P_{PV}

(a) P_{PV}
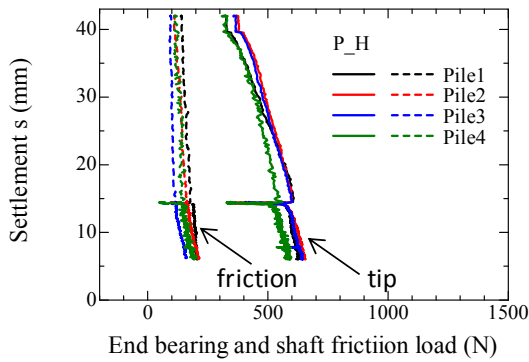
(b) End bearing and shaft friction loads
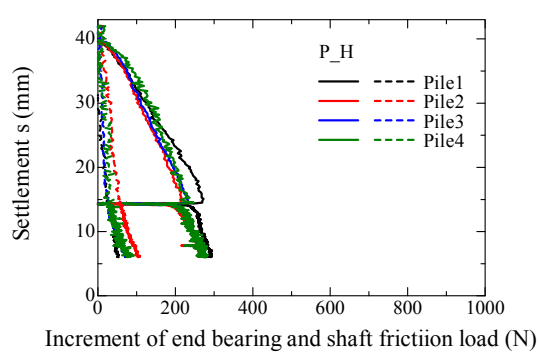
(b) End bearing and shaft friction loads

A. 4.2.2.11 Relationship between each pile load and settlement for P_H observed in penetration process.

A. 4.2.2.12 Relationship between each pile load increment and settlement for P_H observed in penetration process.
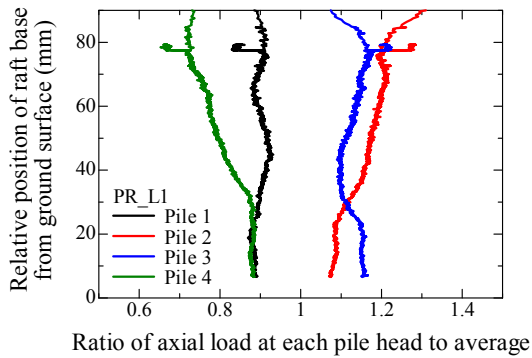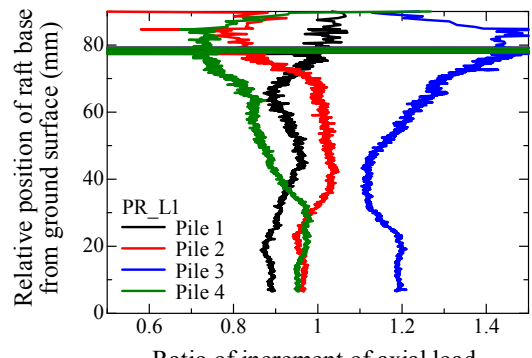
(a) Axial load at pile head
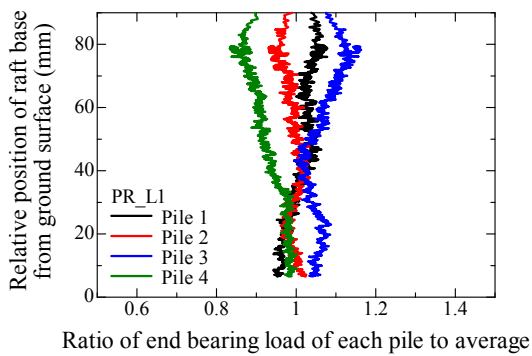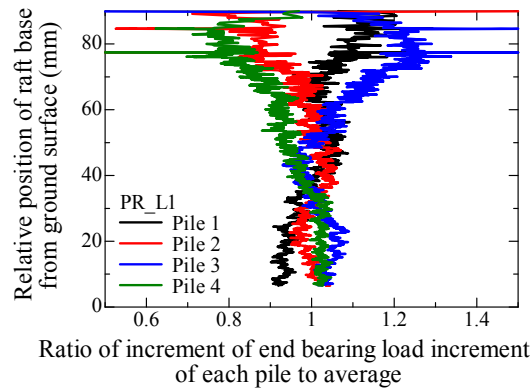
(b) End bearing load
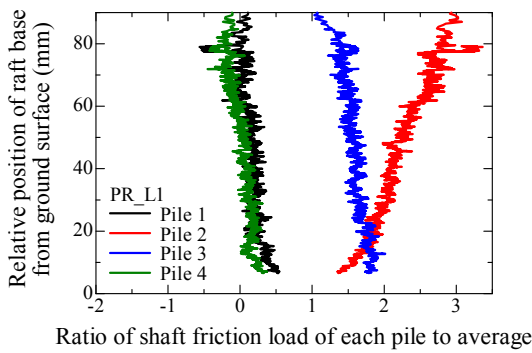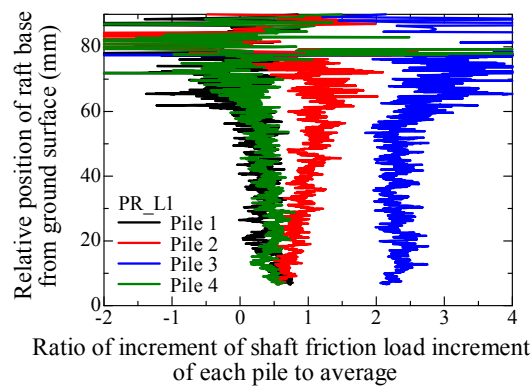
(c) Shaft friction load

A. 4.2.2.13 Relationship between variability of pile forces and relative position of raft base from ground surface for PR_L1 observed in penetration process.

(a) Axial load at pile head

(b) End bearing load

(c) Shaft friction load

A. 4.2.2.14 Relationship between variability of increment of pile forces and relative position of raft base from ground surface for PR_L1 observed in penetration process.
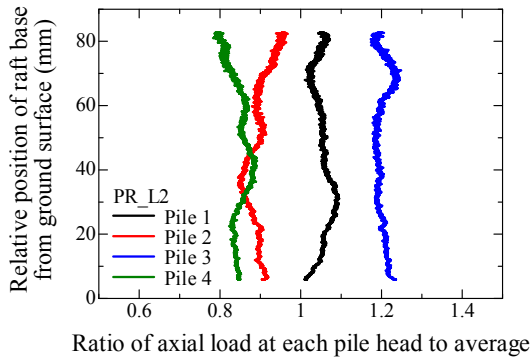
(a) Axial load at pile head
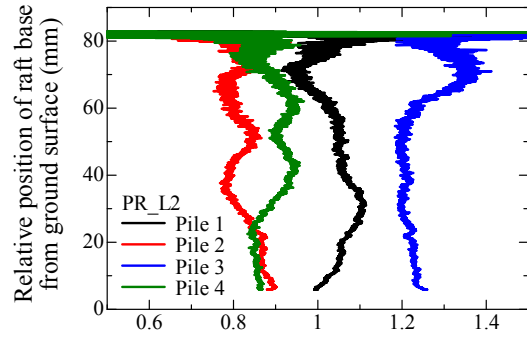
(a) Axial load at pile head
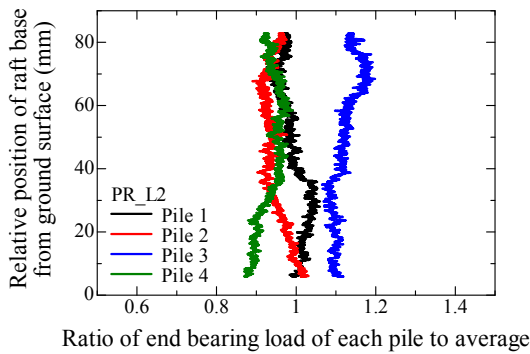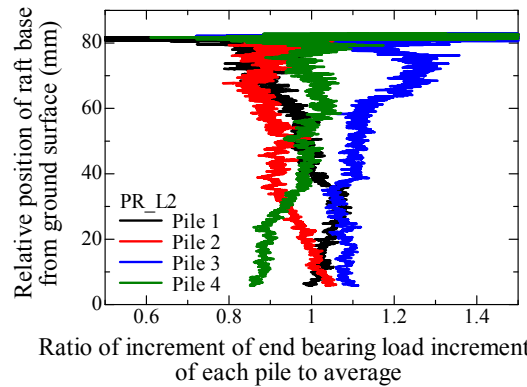
(b) End bearing load

(b) End bearing load
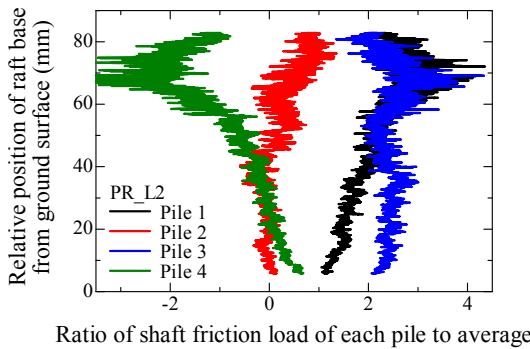
(c) Shaft friction load
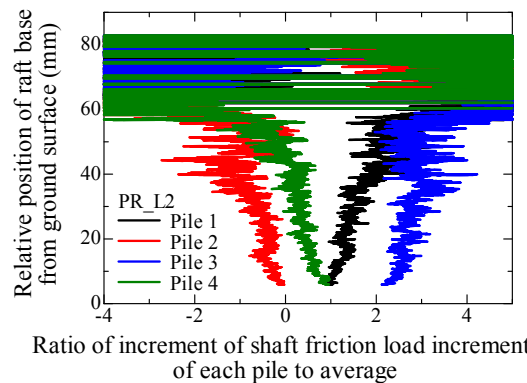
(c) Shaft friction load

A. 4.2.2.15 Relationship between variability of pile forces and relative position of raft base from ground surface for PR_L2 observed in penetration process.

A. 4.2.2.16 Relationship between variability of increment of pile forces and relative position of raft base from ground surface for PR_L2 observed in penetration process.
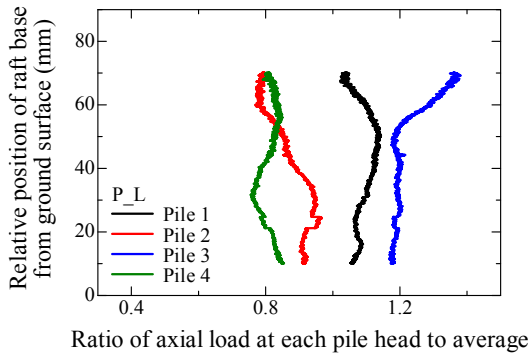
(a) Axial load at pile head
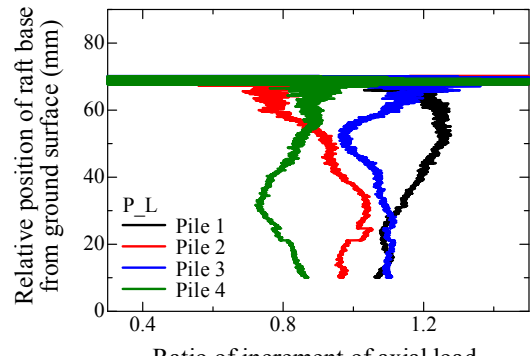
(a) Axial load at pile head
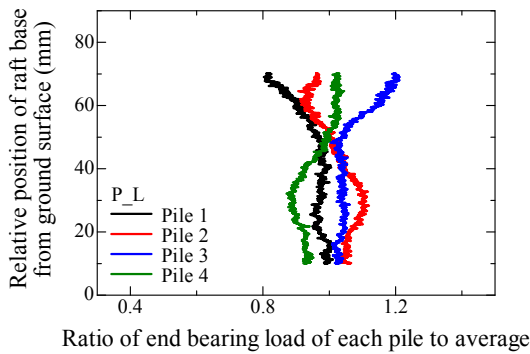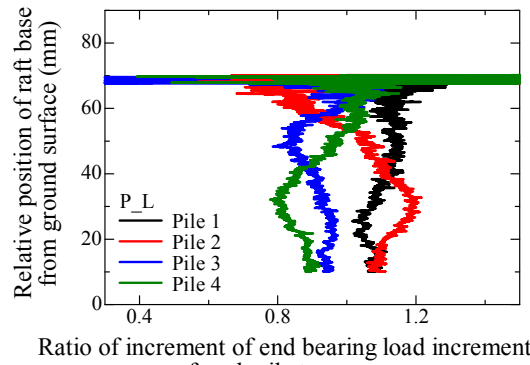
(b) End bearing load

(b) End bearing load
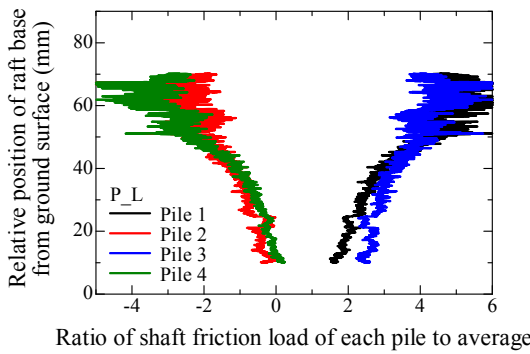
(c) Shaft friction load
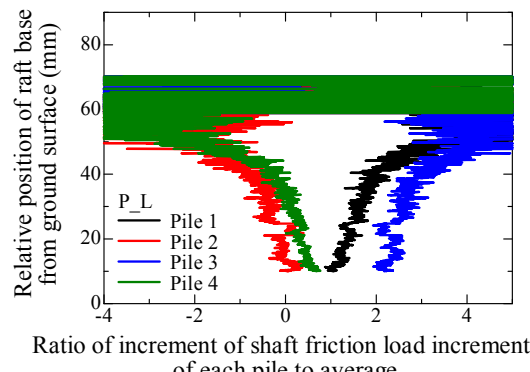
(c) Shaft friction load

A. 4.2.2.17 Relationship between variability of pile forces and relative position of raft base from ground surface for P_L observed in penetration process.

A. 4.2.2.18 Relationship between variability of increment of pile forces and relative position of raft base from ground surface for P_L observed in penetration process.
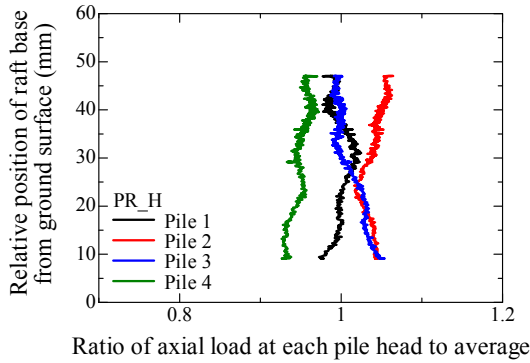
(a) Axial load at pile head
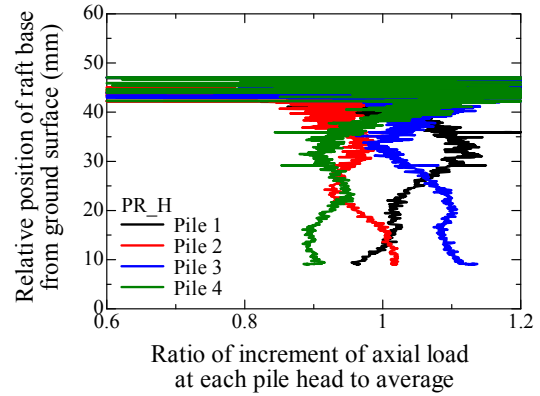
(a) Axial load at pile head
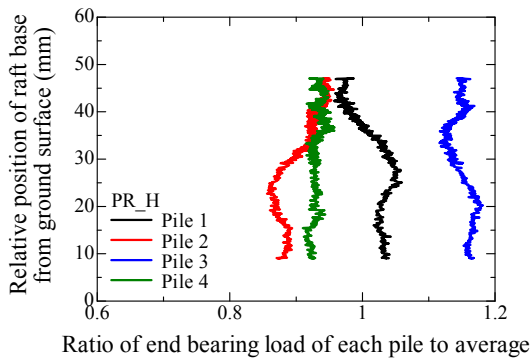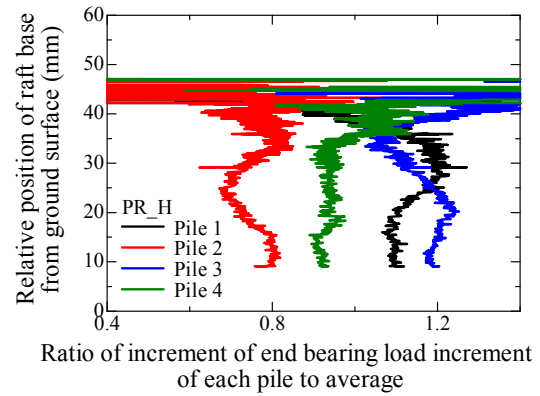
(b) End bearing load

(b) End bearing load
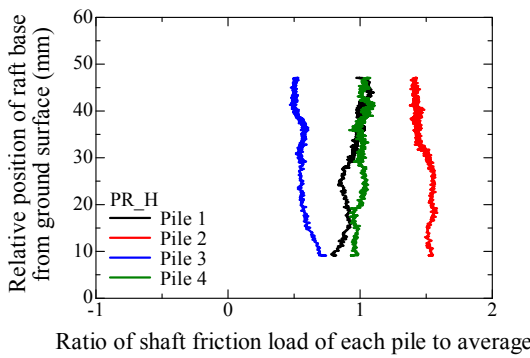
(c) Shaft friction load
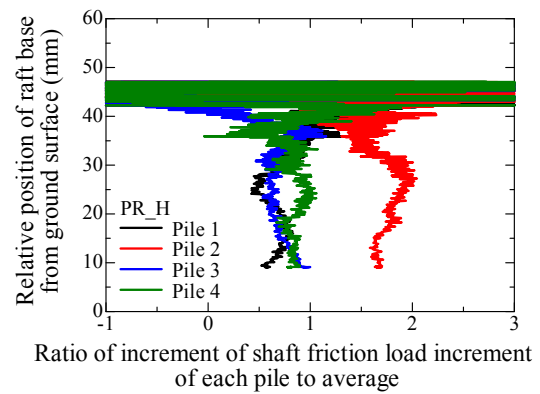
(c) Shaft friction load

A. 4.2.2.19 Relationship between variability of pile forces and relative position of raft base from ground surface for PR_H observed in penetration process.

A. 4.2.2.20 Relationship between variability of increment of pile forces and relative position of raft base from ground surface for PR_H observed in penetration process.
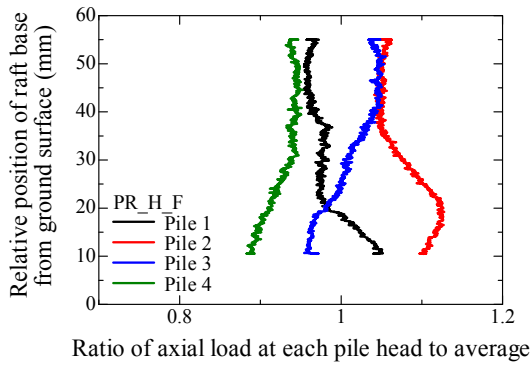
(a) Axial load at pile head
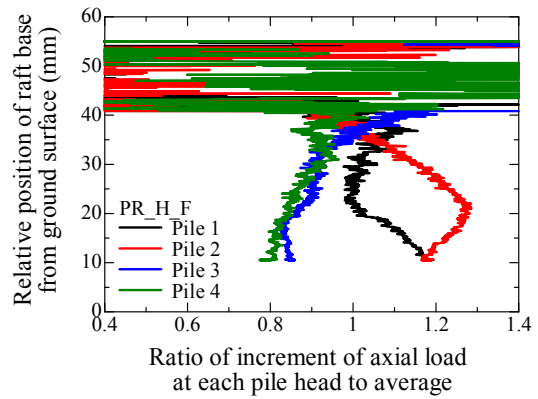
(a) Axial load at pile head
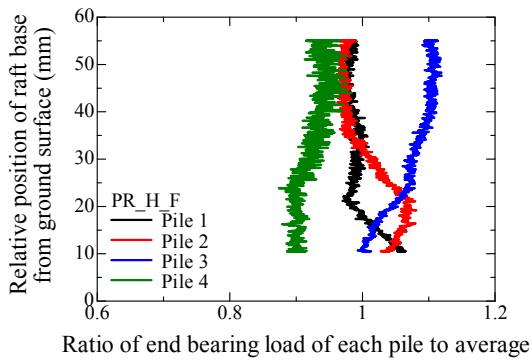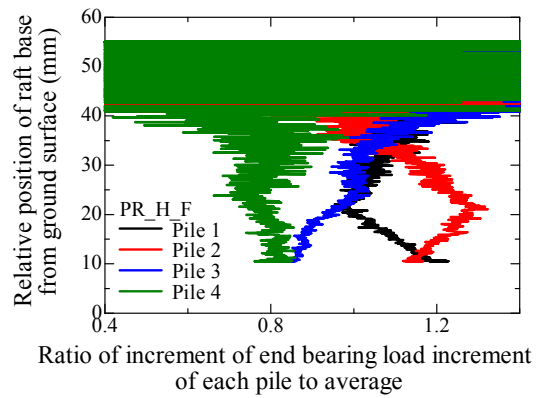
(b) End bearing load

(b) End bearing load
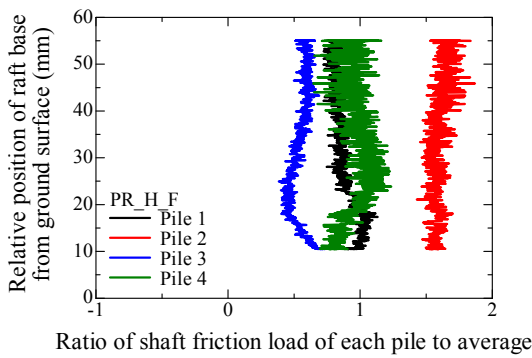
(c) Shaft friction load
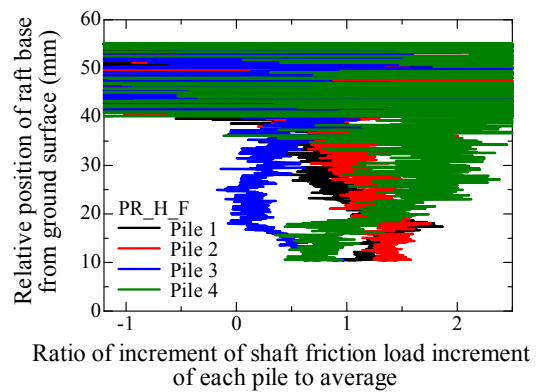
(c) Shaft friction load

A. 4.2.2.21 Relationship between variability of pile forces and relative position of raft base from ground surface for PR_H_F observed in penetration process.

A. 4.2.2.22 Relationship between variability of increment of pile forces and relative position of raft base from ground surface for PR_H_F observed in penetration process.

A44
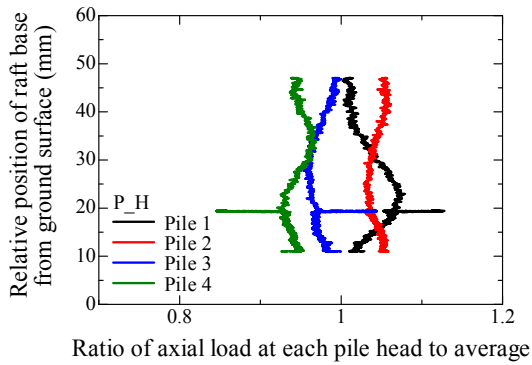
(a) Axial load at pile head
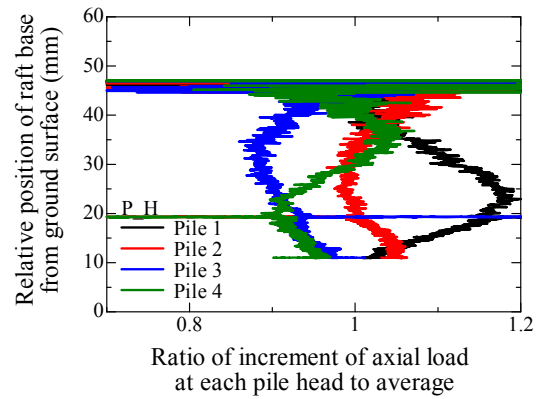
(a) Axial load at pile head
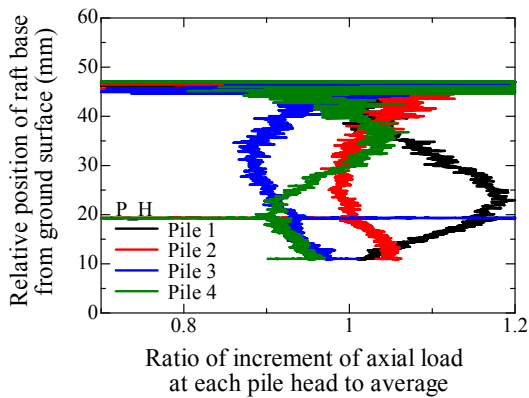
(a) Axial load at pile head
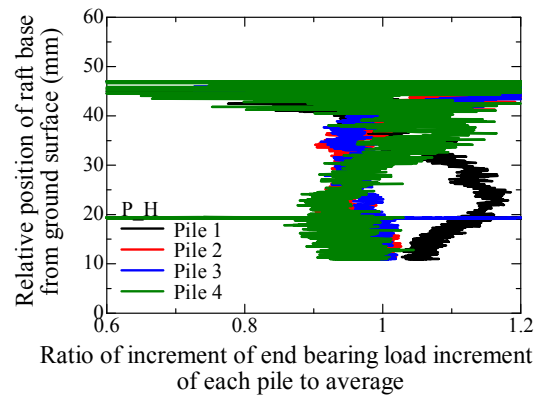
(b) End bearing load
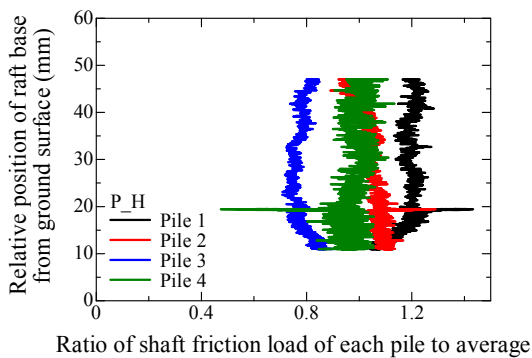
(c) Shaft friction load
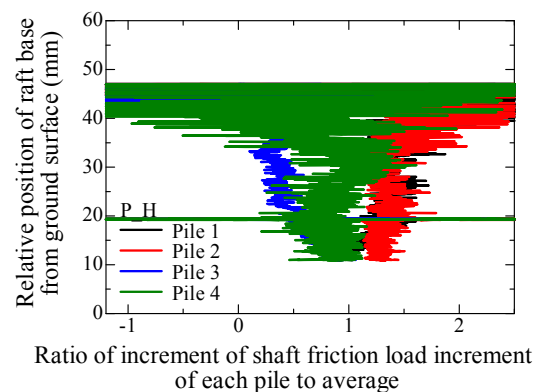
(c) Shaft friction load

A. 4.2.2.23 Relationship between variability of pile forces and relative position of raft base from ground surface for P_H observed in penetration process.

A. 4.2.2.24 Relationship between variability of increment of pile forces and relative position of raft base from ground surface for P_H observed in penetration process.

A45

(a) PR_L1

(b) PR_L2

(c) P_L
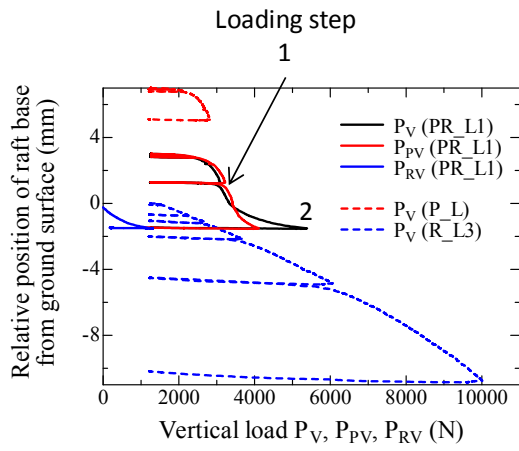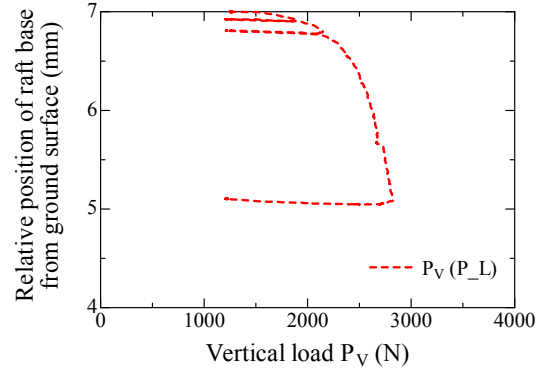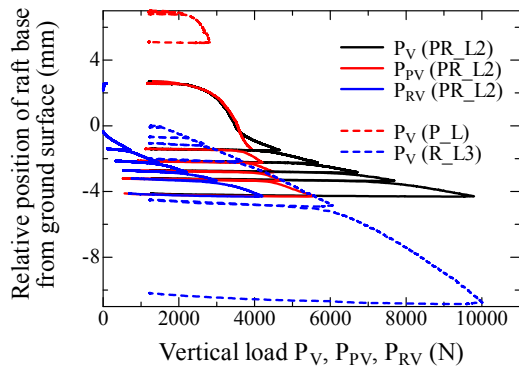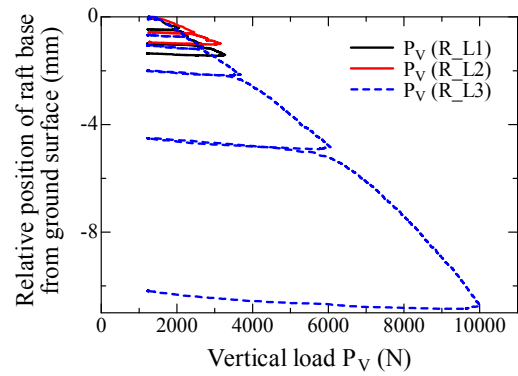
(d) Raft

A. 4.3.1.1 Variation of P_V, P_{PV} and P_{RV} for light case with settlement observed in vertical loading process.
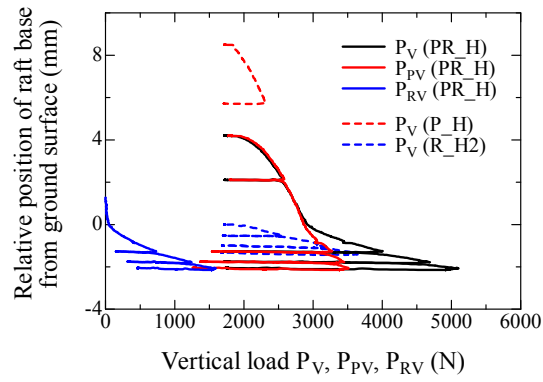
(a) PR_H
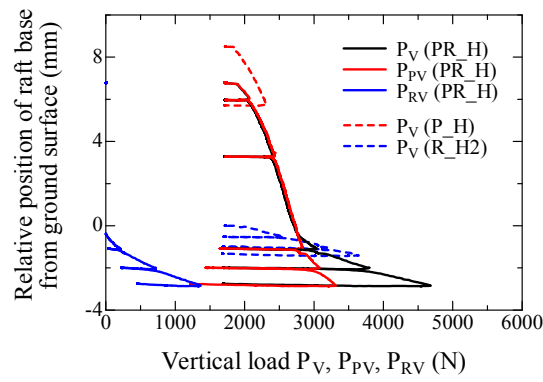
(b) PR_H_F
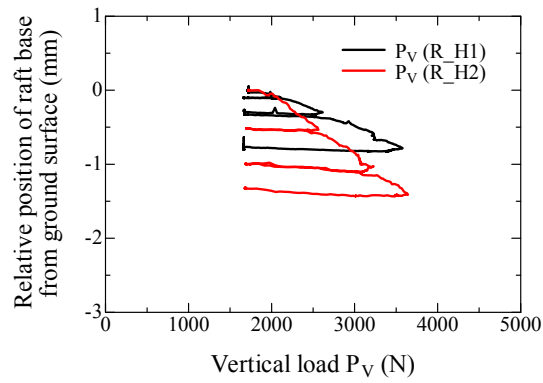
(c) Raft

A. 4.3.1.1 Variation of P_V, P_{PV} and P_{RV} for light case with settlement observed in vertical loading process.
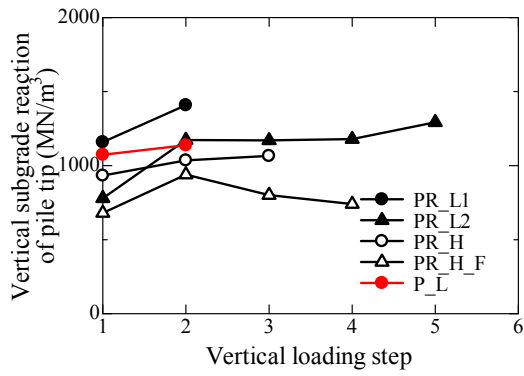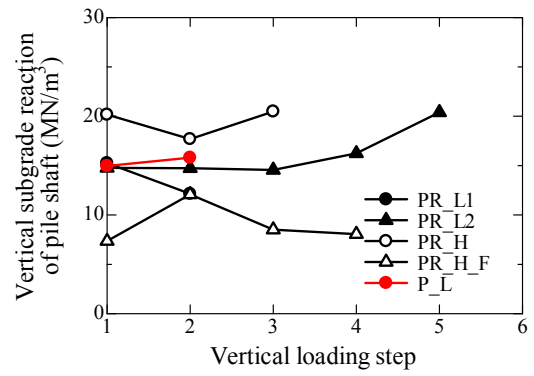
(a) Pile tip
(b) Pile shaft

A. 4.3.3.1 Variation of vertical subgrade reaction of pile with vertical loading step.
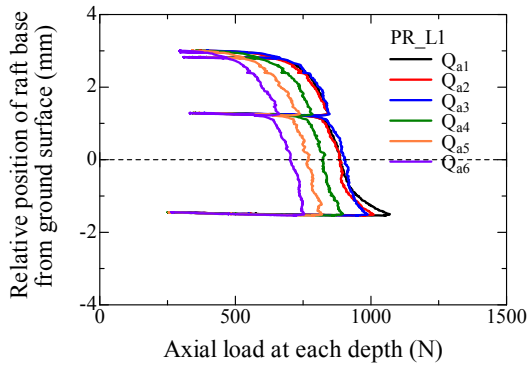
(a) Average of Pile 1 & Pile 2
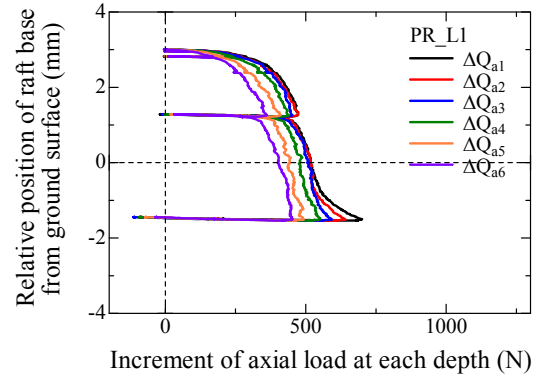
(d) Average of Pile 1 & Pile 2
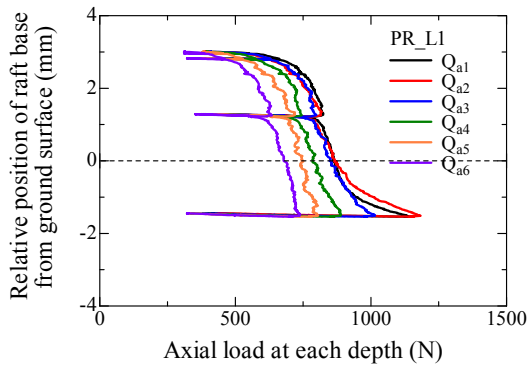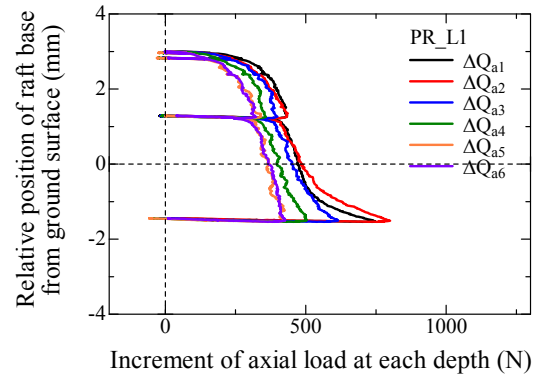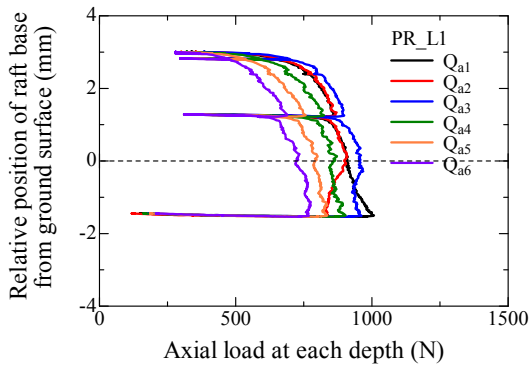
(b) Pile 1
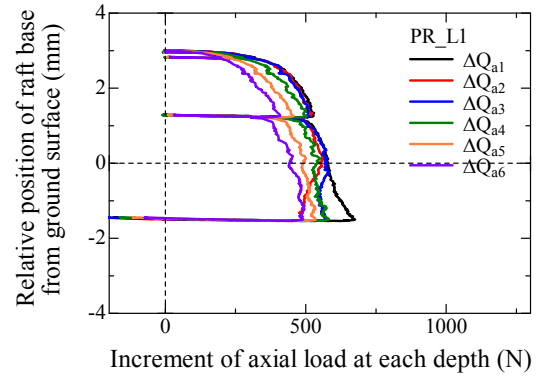
(e) Pile 1

(c) Pile 2

(f) Pile 2

A. 4.3.3.2 Relationship between variability of pile forces and relative position of raft base from ground surface for PR_L1 observed in penetration process.
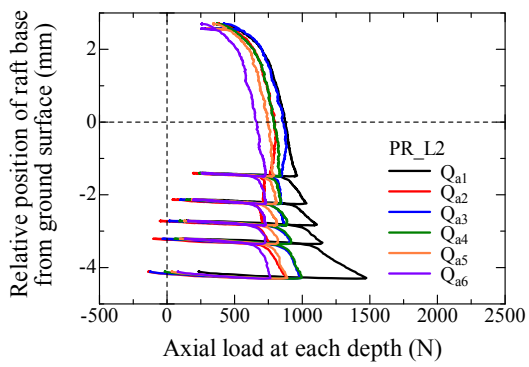
(a) Average of Pile 1 & Pile 2
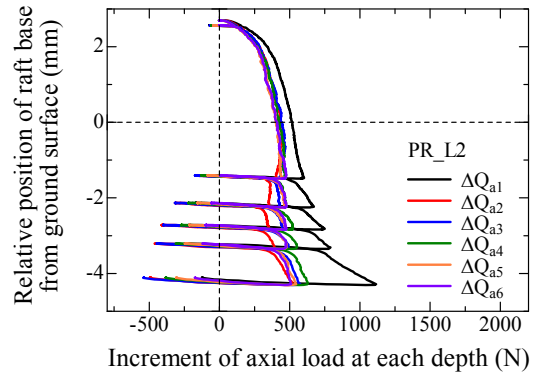
(b) Pile 1
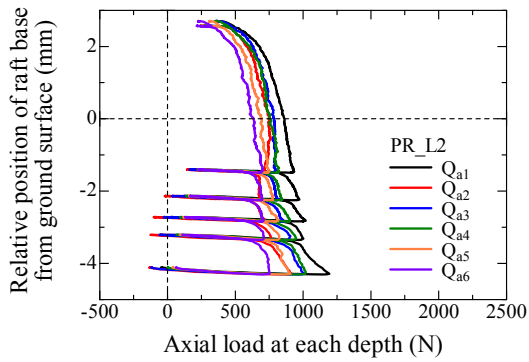
(c) Pile 2
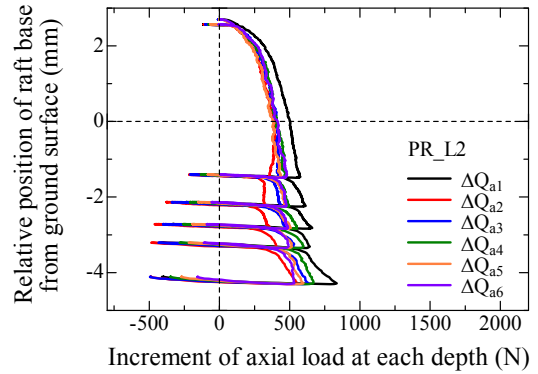
(d) Average of Pile 1 & Pile 2
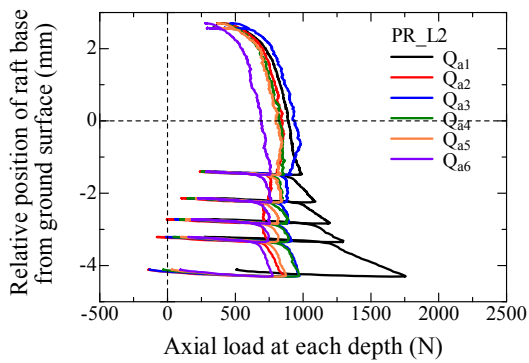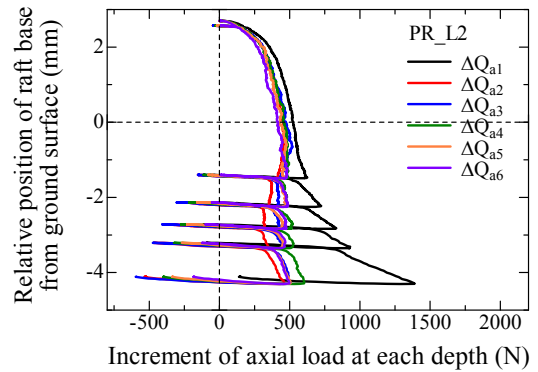
(e) Pile 1

(f) Pile 2

A. 4.3.3.3 Relationship between variability of pile forces and relative position of raft base from ground surface for PR_L2 observed in penetration process.
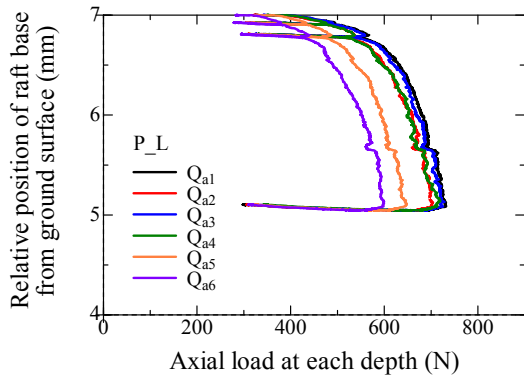
(a) Average of Pile 1 & Pile 2
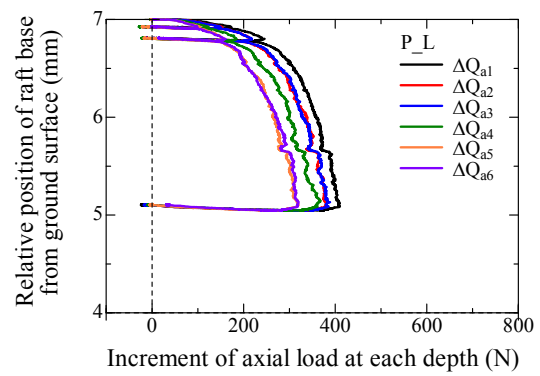
(d) Average of Pile 1 & Pile 2
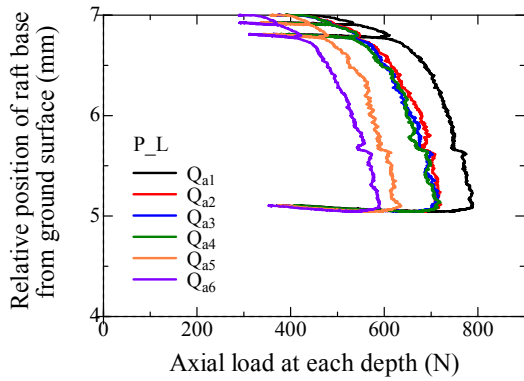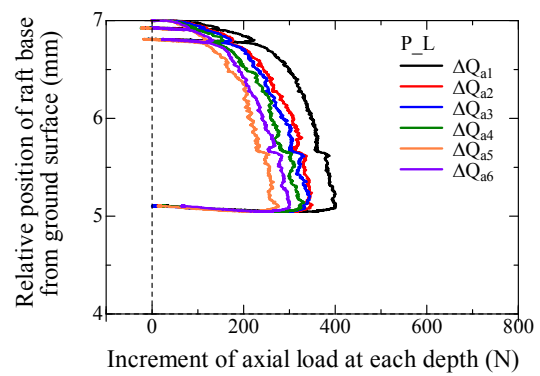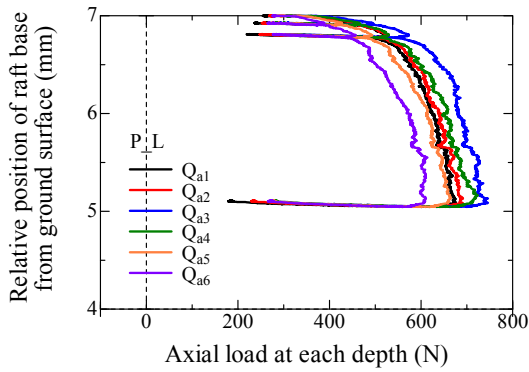
(b) Pile 1
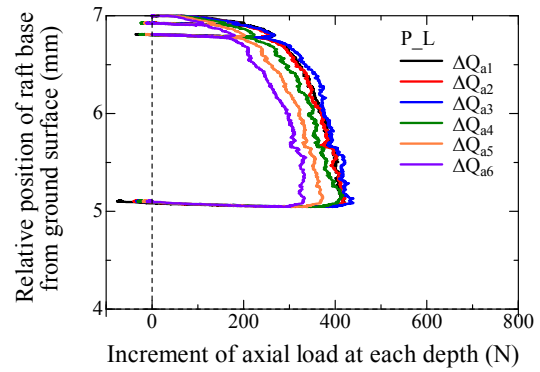
(e) Pile 1

(c) Pile 2

(f) Pile 2

A. 4.3.3.4 Relationship between variability of pile forces and relative position of raft base from ground surface for P_L observed in penetration process.
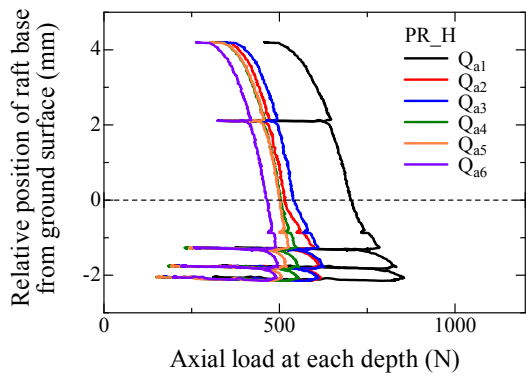
(a) Average of Pile 1 & Pile 2
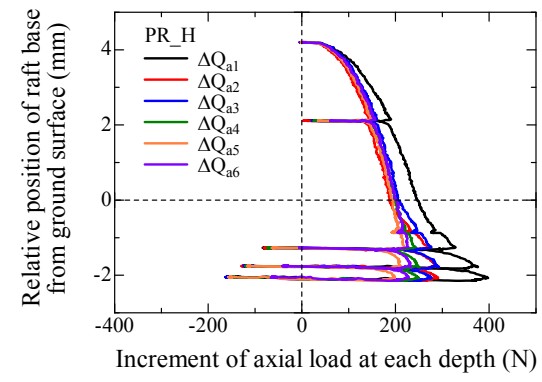
(a) Average of Pile 1 & Pile 2
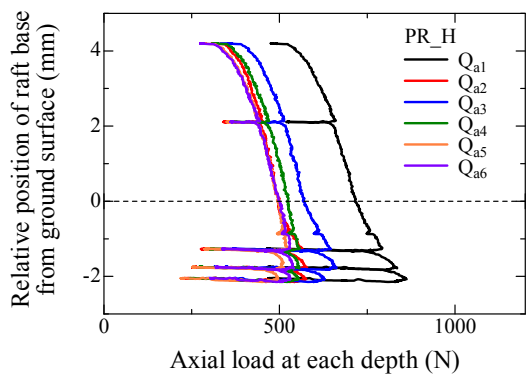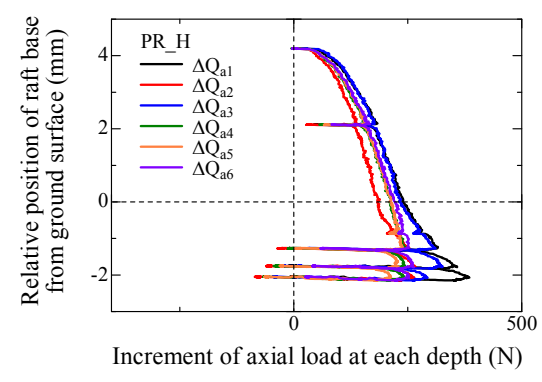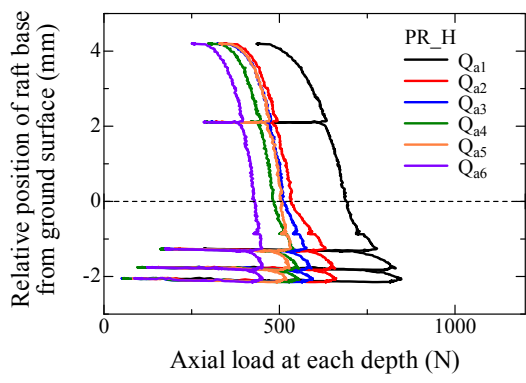
(b) Pile 1
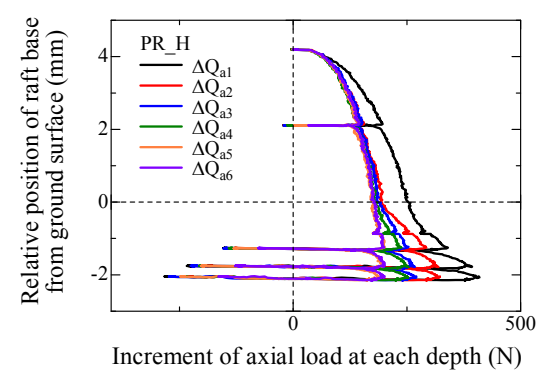
(b) Pile 1

(c) Pile 2

(c) Pile 2

A. 4.3.3.5 Relationship between variability of pile forces and relative position of raft base from ground surface for PR_H observed in penetration process.

A52
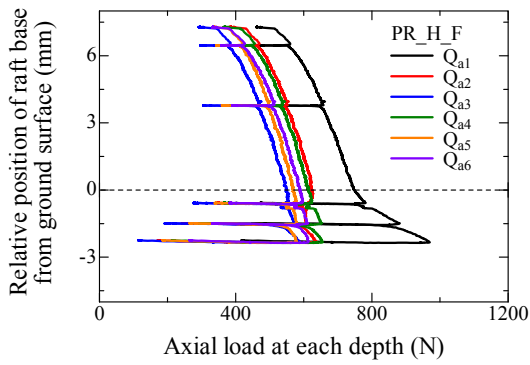
(a) Average of Pile 1 & Pile 2
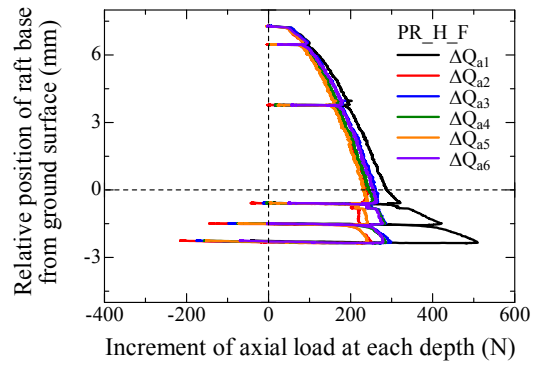
(d) Average of Pile 1 & Pile 2
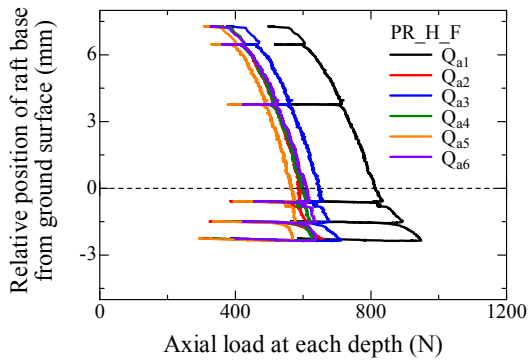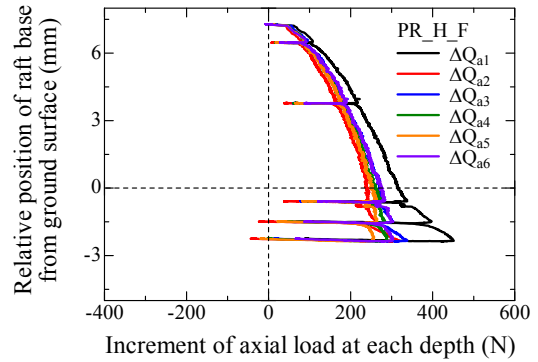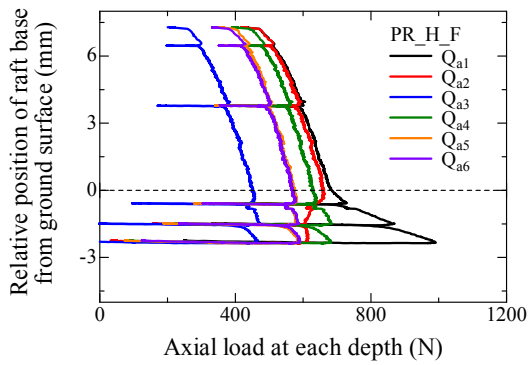
(b) Pile 1
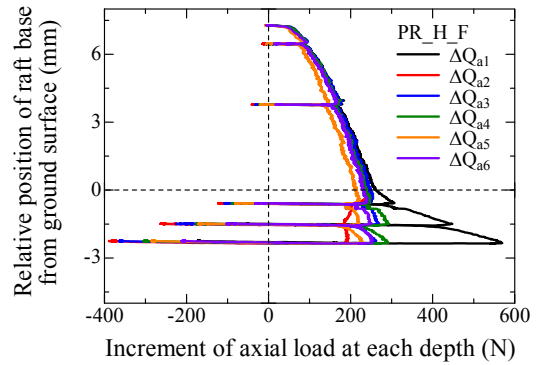
(e) Pile 1

(c) Pile 2

(f) Pile 2

A. 4.3.3.6 Relationship between variability of pile forces and relative position of raft base from ground surface for PR_H_F observed in penetration process.
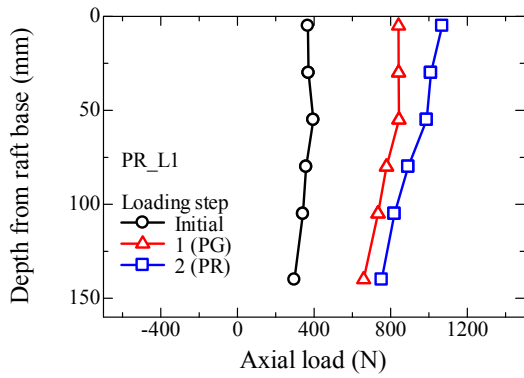
(a) Average of Pile 1 & Pile 2
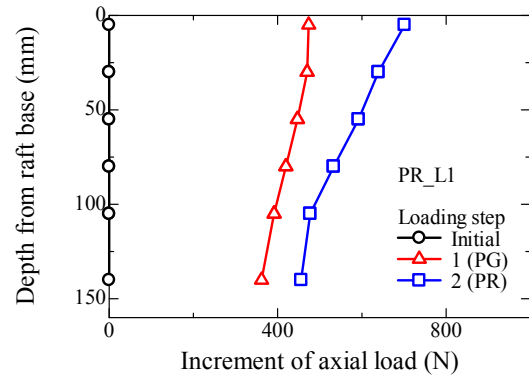
(d) Average of Pile 1 & Pile 2
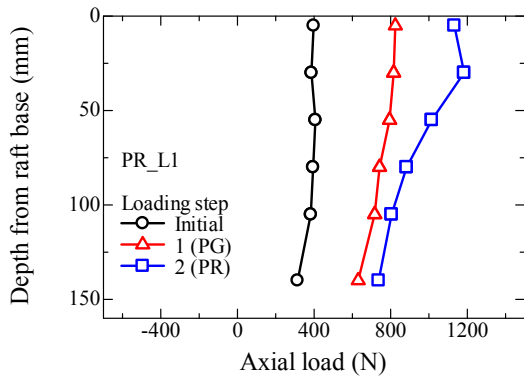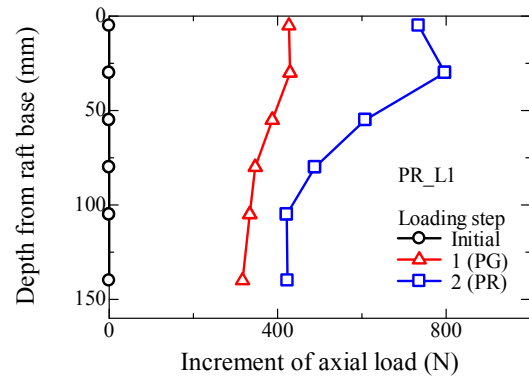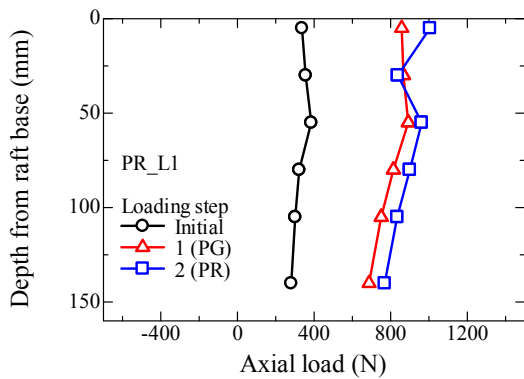
(b) Pile 1
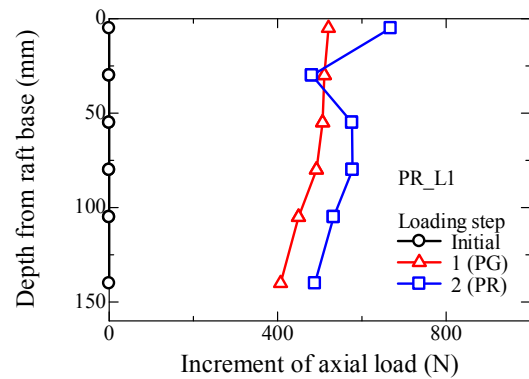
(e) Pile 1

(c) Pile 2

(f) Pile 2

A. 4.3.3.7 Profiles of axial load and axial load increment for PR_L1 during vertical loading process.
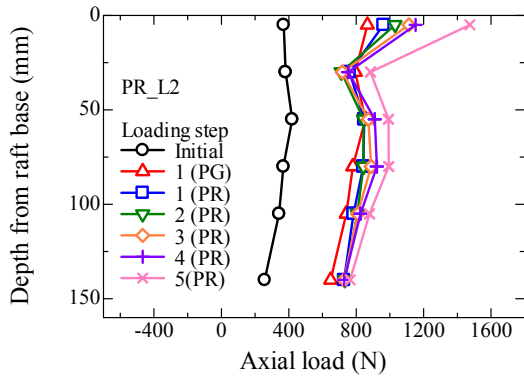
(a) Average of Pile 1 & Pile 2
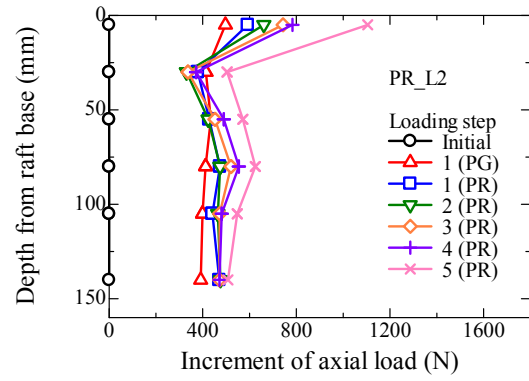
(d) Average of Pile 1 & Pl
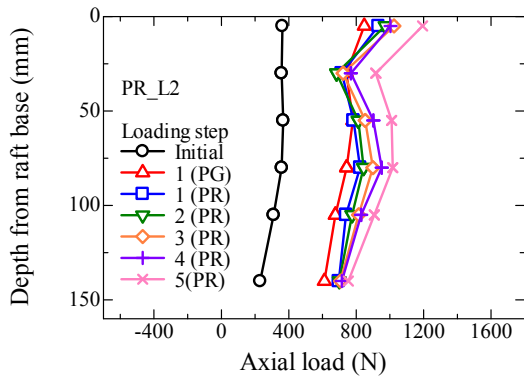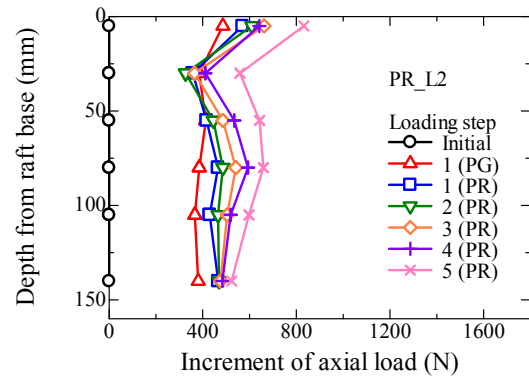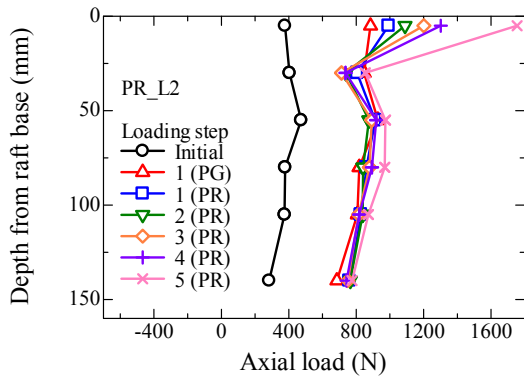
(b) Pile 1
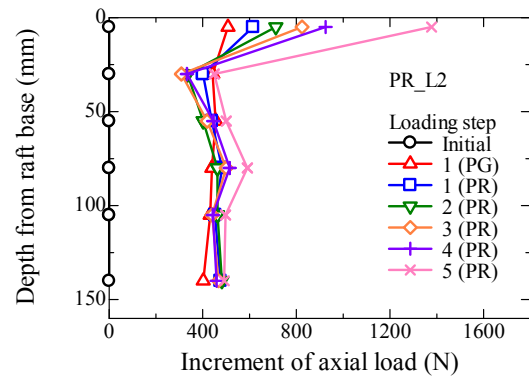
(e) Pile 1

(c) Pile 2

(f) Pile 2

A. 4.3.3.8 Profiles of axial load and axial load increment for PR_L2 during vertical loading process.
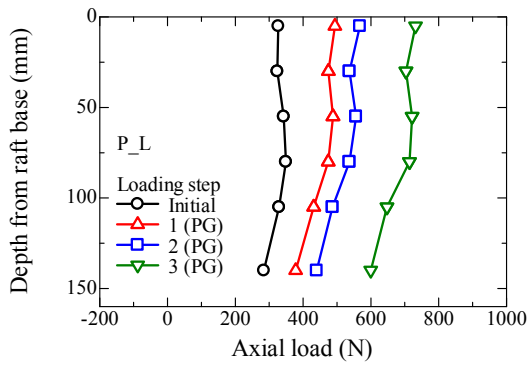
(a) Average of Pile 1 & Pile 2
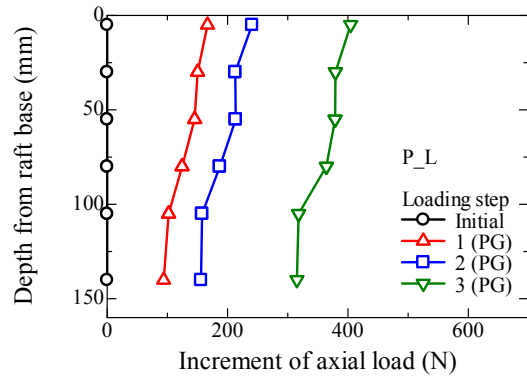
(d) Average of Pile 1 & Pile 2
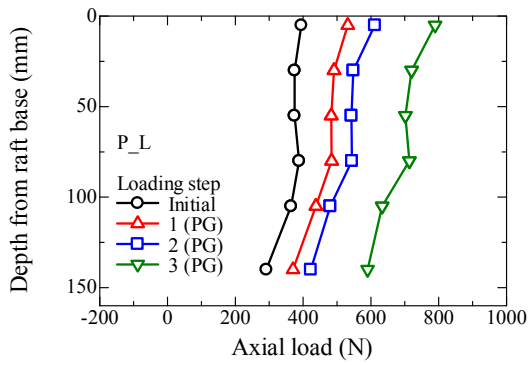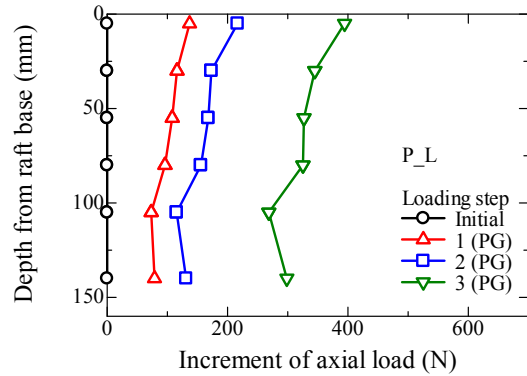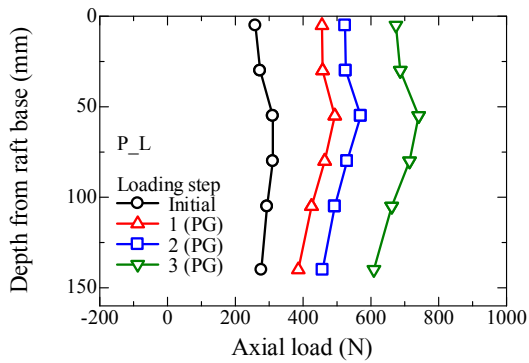
(b) Pile 1
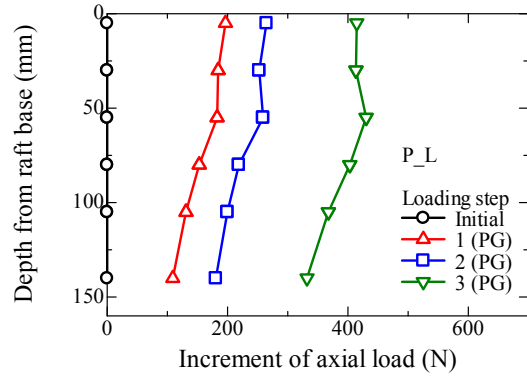
(e) Pile 1

(c) Pile 2

(f) Pile 2

A. 4.3.3.9 Profiles of axial load and axial load increment for P_L during vertical loading process.
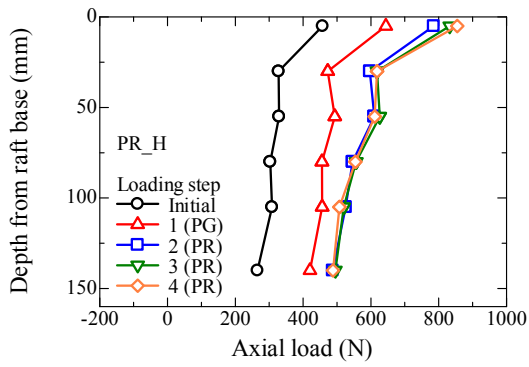
(a) Average of Pile 1 & Pile 2
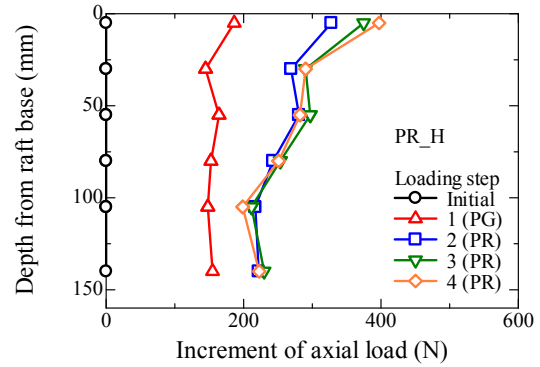
(d) Average of Pile 1 & Pile 2
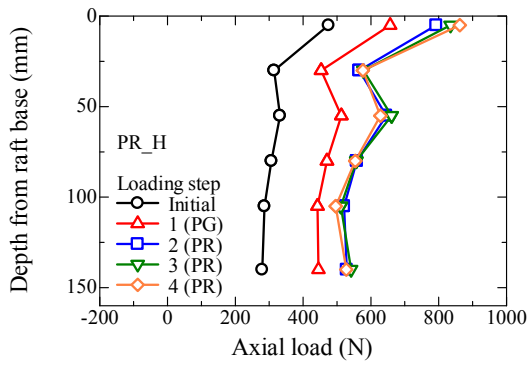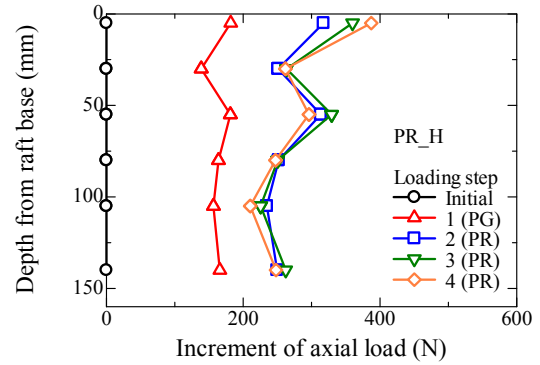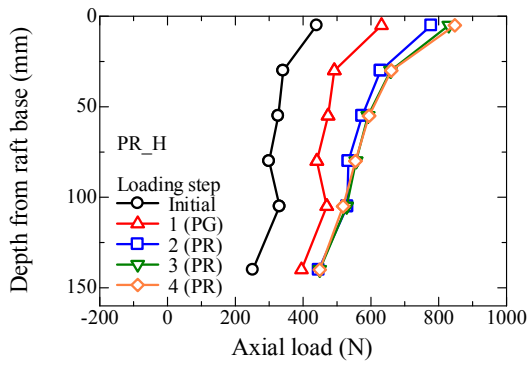
(b) Pile 1
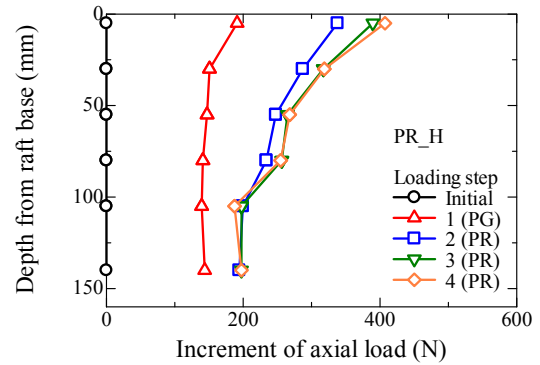
(e) Pile 1

(c) Pile 2

(f) Pile 2

A. 4.3.3.10 Profiles of axial load and axial load increment for PR_H during vertical loading process.
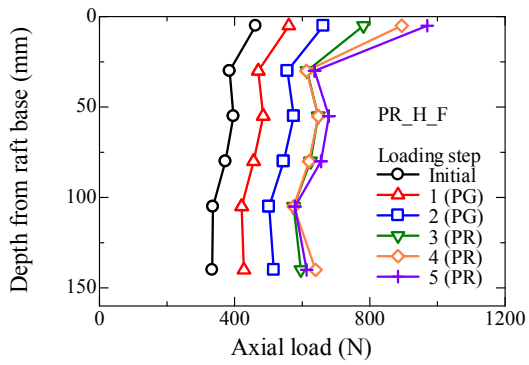
(a) Average of Pile 1 & Pile 2
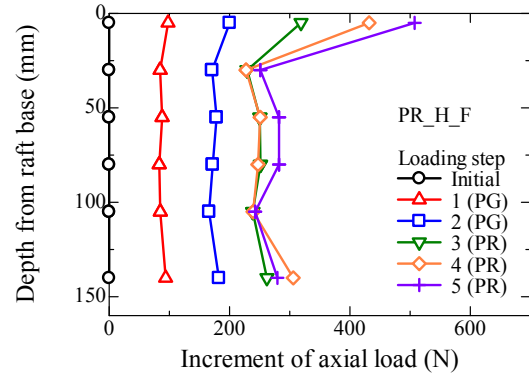
(d) Average of Pile 1 & Pile 2
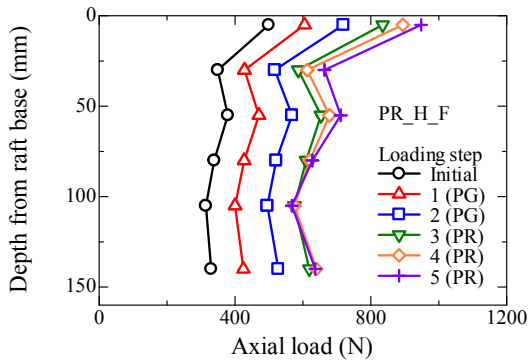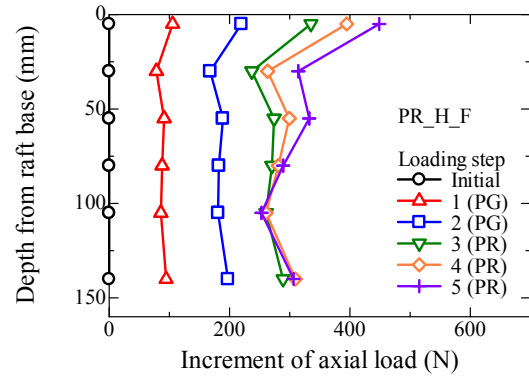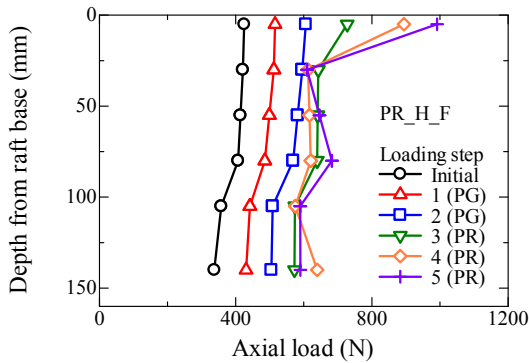
(b) Pile 1
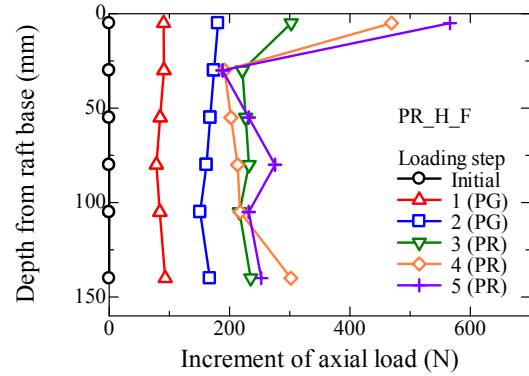
(e) Pile 1

(c) Pile 2

(f) Pile 2

A. 4.3.3.11 Profiles of axial load and axial load increment for PR_H_F during vertical loading process.
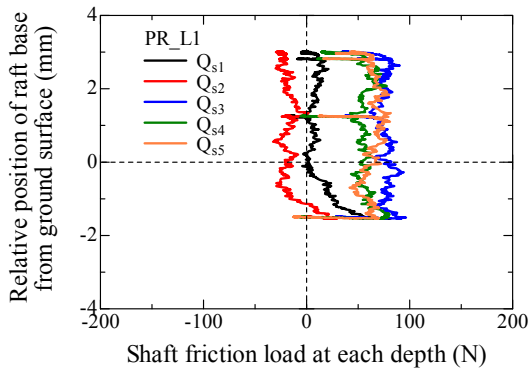
(a) Average of Pile 1 & Pile 2
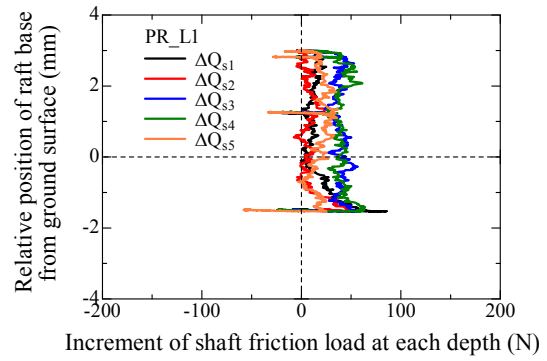
(d) Average of Pile 1 & Pile 2
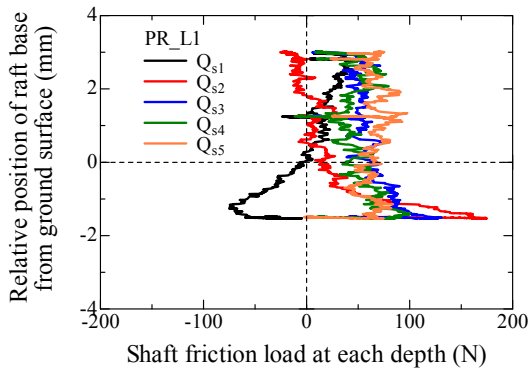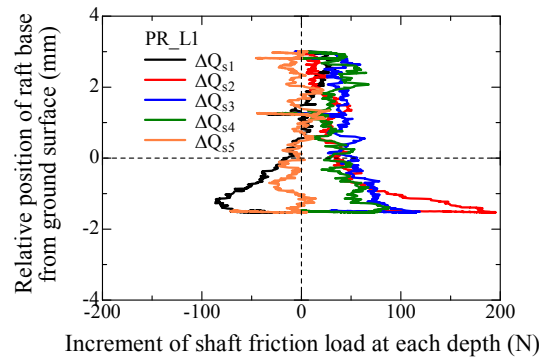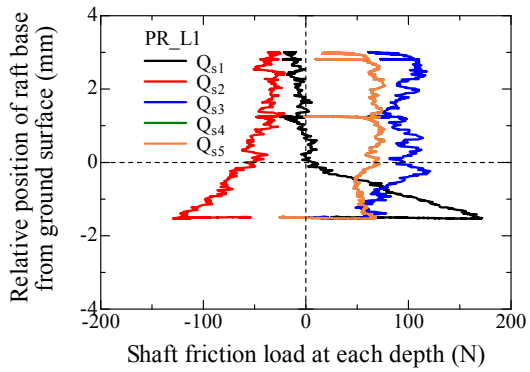
(b) Pile 1
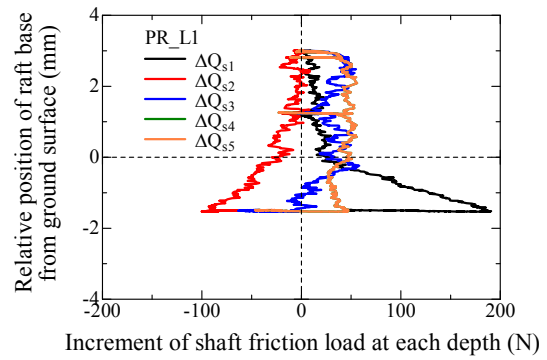
(e) Pile 1

(c) Pile 2

(f) Pile 2

A. 4.3.3.12 Variation of shaft friction load and shaft friction load increment at each depth with relative position of raft base from ground surface for PR_L1 during penetration process.
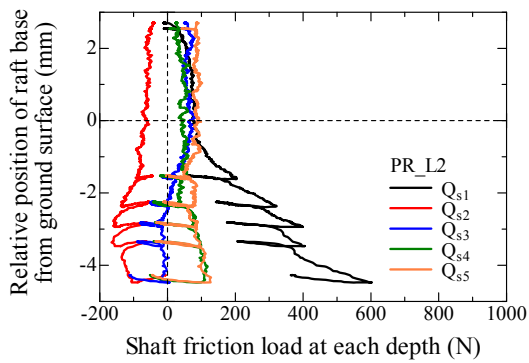
(a) Average of Pile 1 & Pile 2
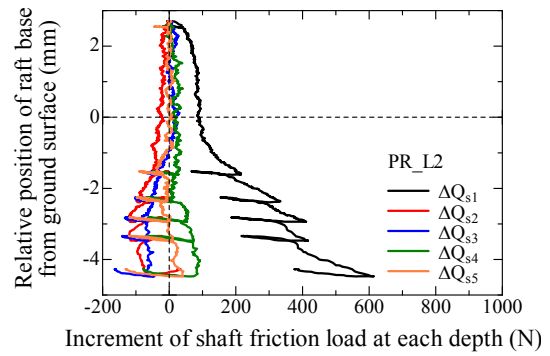
(d) Average of Pile 1 & Pile 2
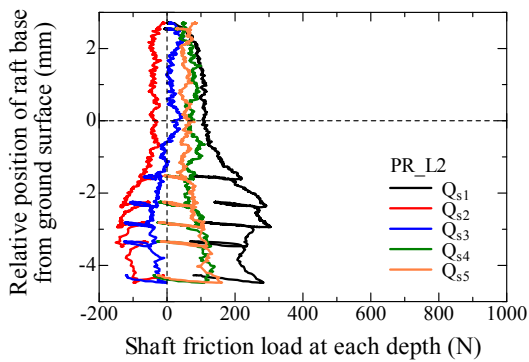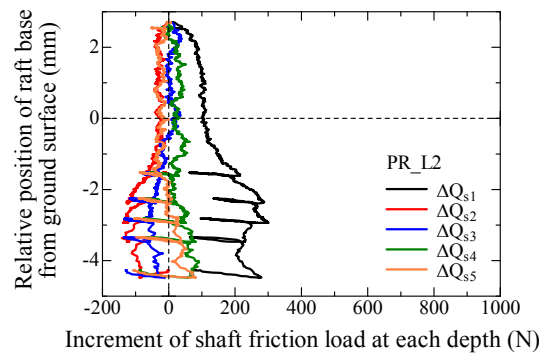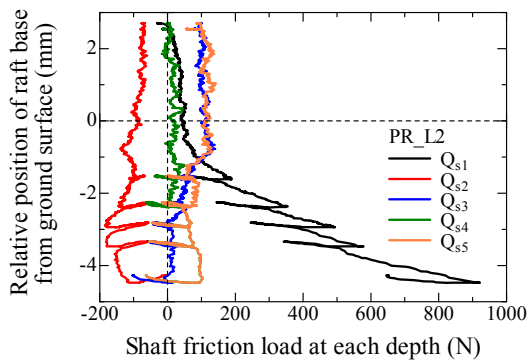
(b) Pile 1
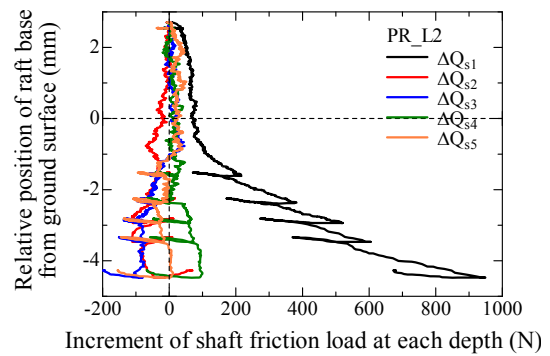
(e) Pile 1

(c) Pile 2

(f) Pile 2

A. 4.3.3.13 Variation of shaft friction load and shaft friction load increment at each depth with relative position of raft base from ground surface for PR_L2 during penetration process.
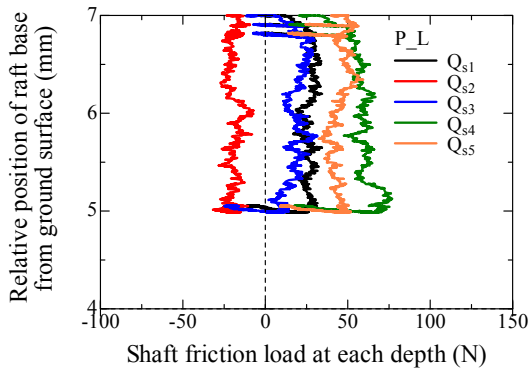
(a) Average of Pile 1 & Pile 2
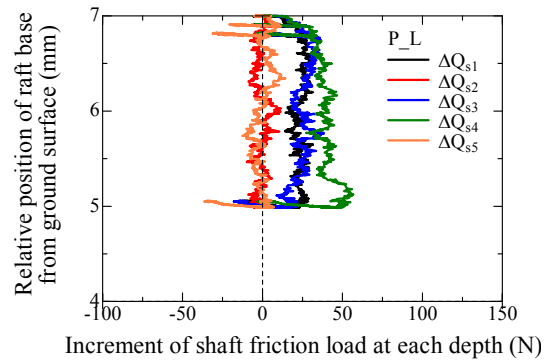
(d) Average of Pile 1 & Pile 2
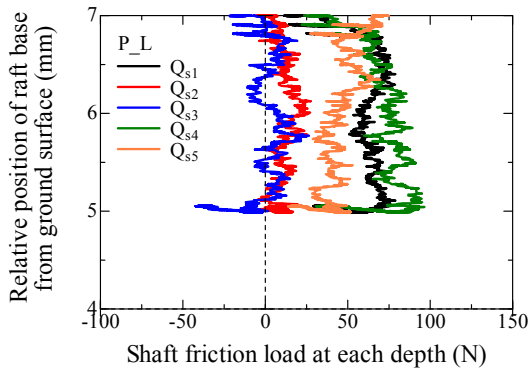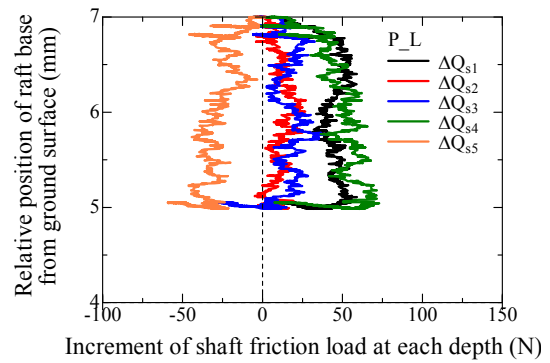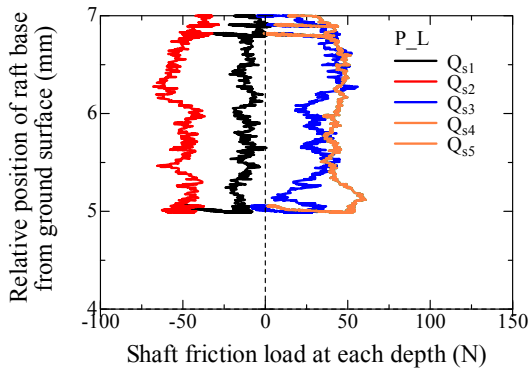
(b) Pile 1
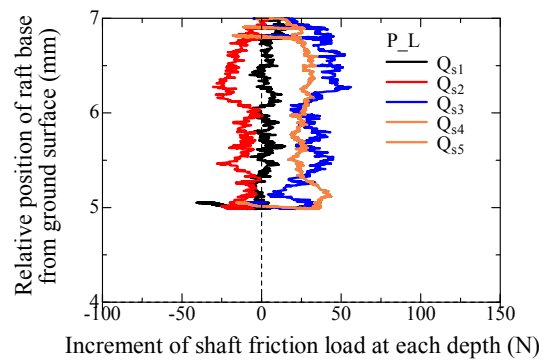
(e) Pile 1

(c) Pile 2

(f) Pile 2

A. 4.3.3.14 Variation of shaft friction load and shaft friction load increment at each depth with relative position of raft base from ground surface for P_L during penetration process.
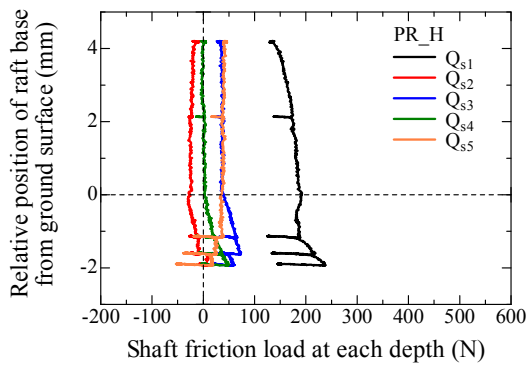
(a) Average of Pile 1 & Pile 2
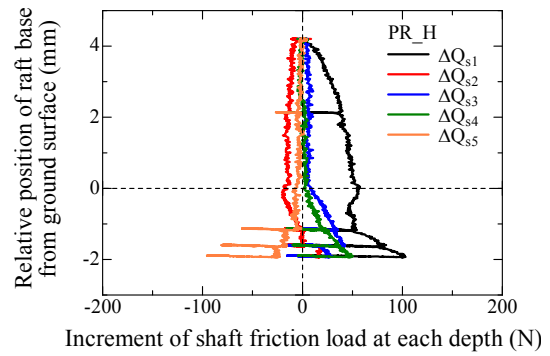
(a) Average of Pile 1 & Pile 2
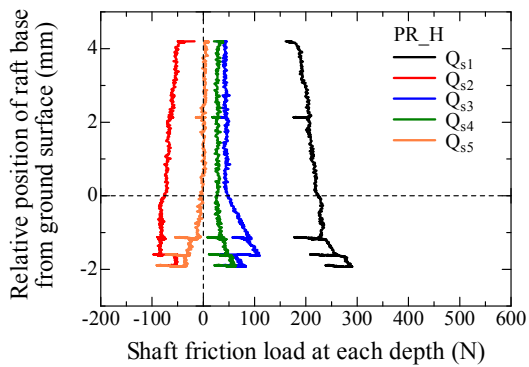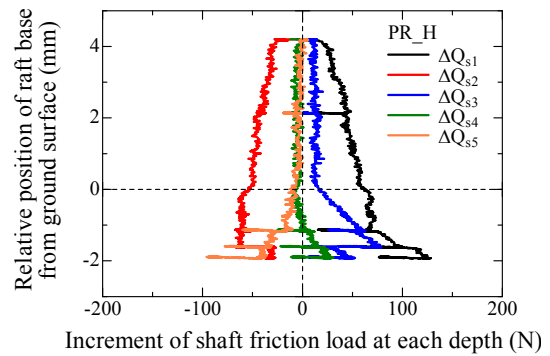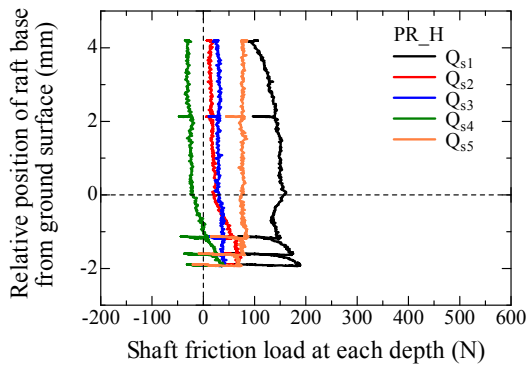
(b) Pile 1
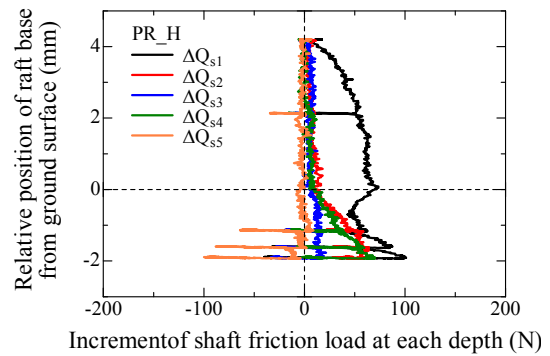
(b) Pile 1

(c) Pile 2

(c) Pile 2

A. 4.3.3.15 Variation of shaft friction load and shaft friction load increment at each depth with relative position of raft base from ground surface for PR_H during penetration process.
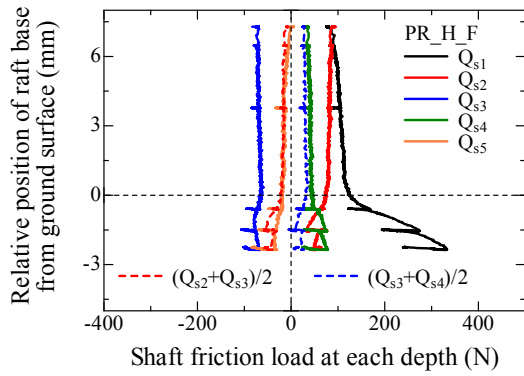
(a) Average of Pile 1 & Pile 2
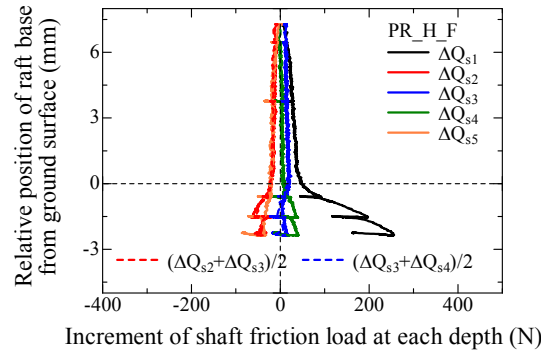
(d) Average of Pile 1 & Pile 2
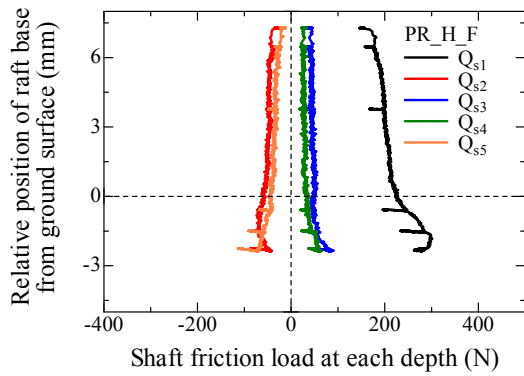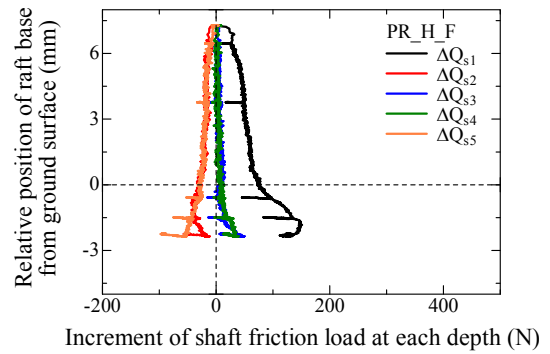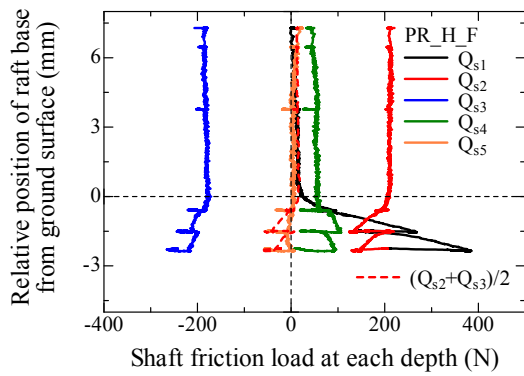
(b) Pile 1
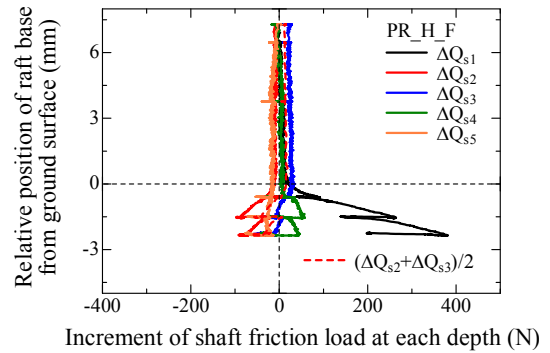
(e) Pile 1

(c) Pile 2

(f) Pile 2

A. 4.3.3.16 Variation of shaft friction load and shaft friction load increment at each depth with relative position of raft base from ground surface for PR_H_F during penetration process.
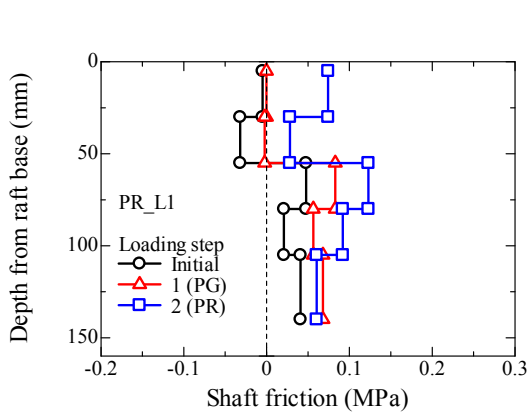
(a) Average of Pile 1 & Pile 2
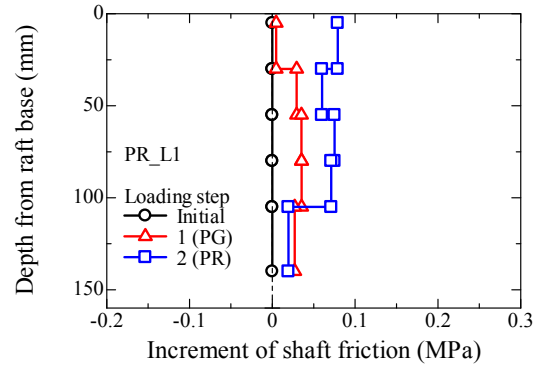
(d) Average of Pile 1 & Pile 2
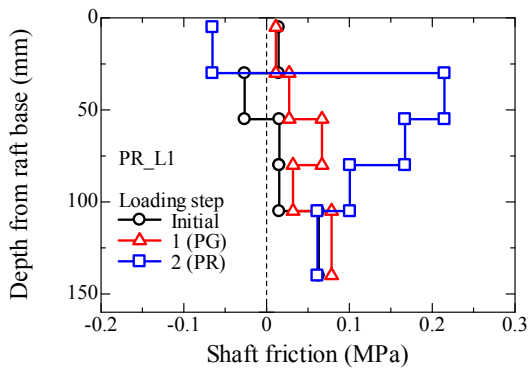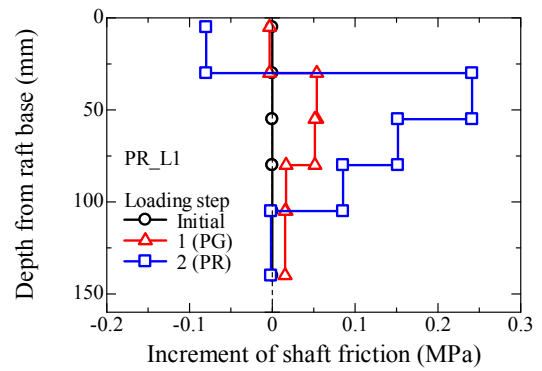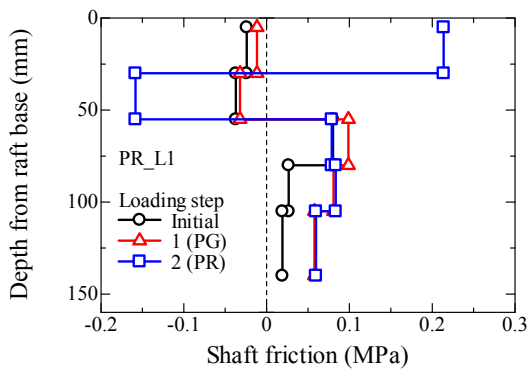
(b) Pile 1
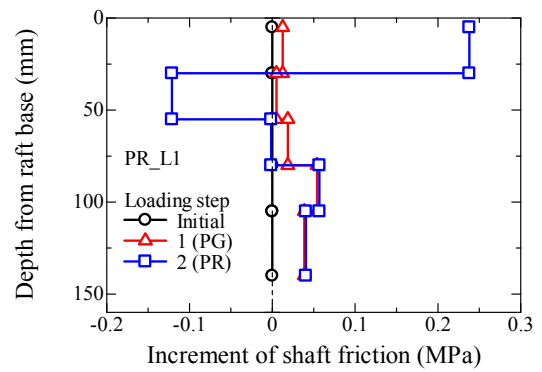
(e) Pile 1

(c) Pile 2

(f) Pile 2

A. 4.3.3.17 Profiles of shaft friction and shaft friction increment for PR_L1 during vertical loading process.
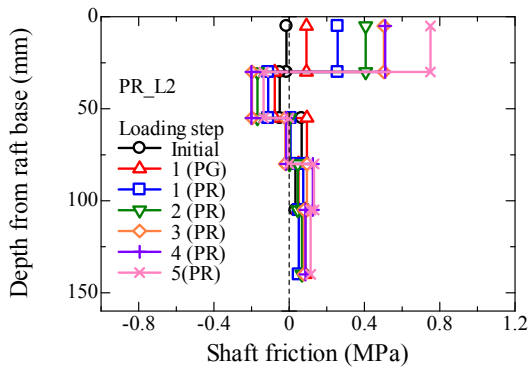
(a) Average of Pile 1 & Pile 2
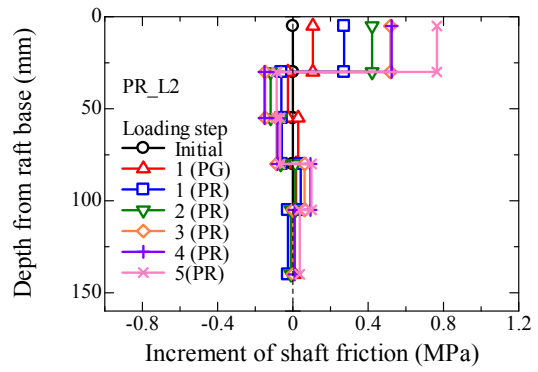
(d) Average of Pile 1 & Pile 2
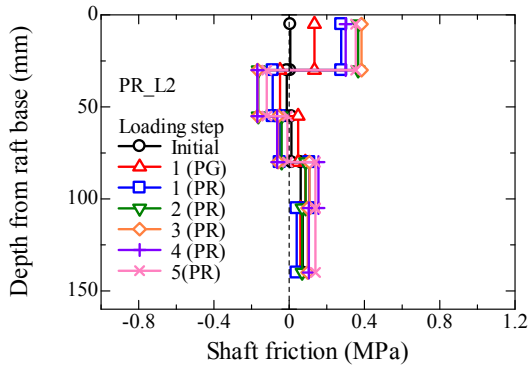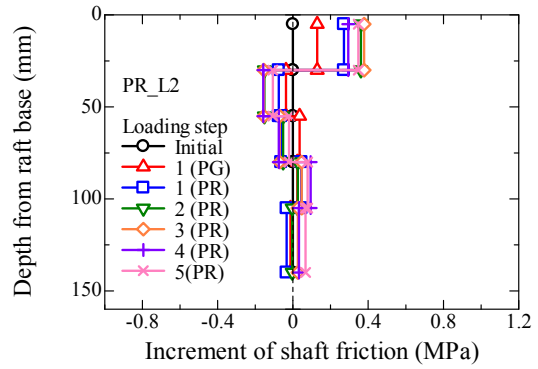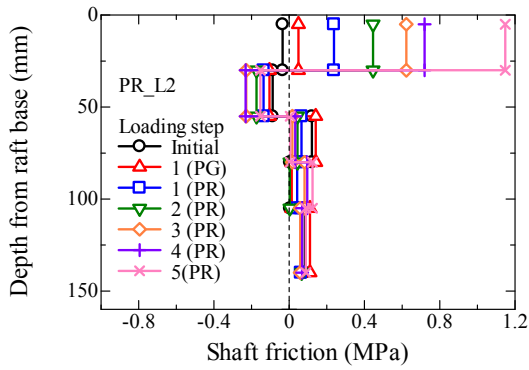
(b) Pile 1
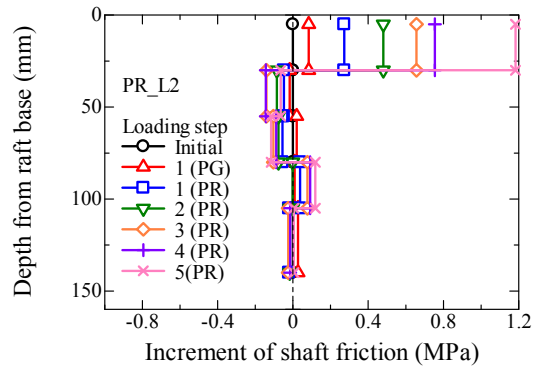
(e) Pile 1

(c) Pile 2

(f) Pile 2

A. 4.3.3.18 Profiles of shaft friction and shaft friction increment for PR_L2 during vertical loading process.
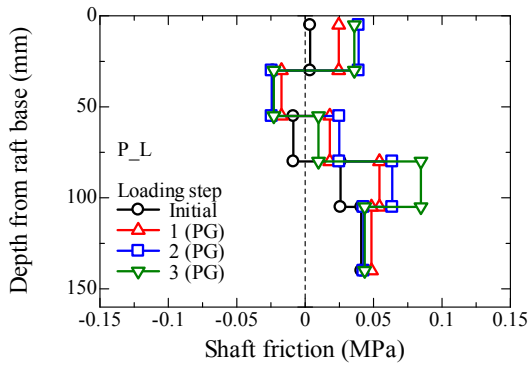
(a) Average of Pile 1 & Pile 2
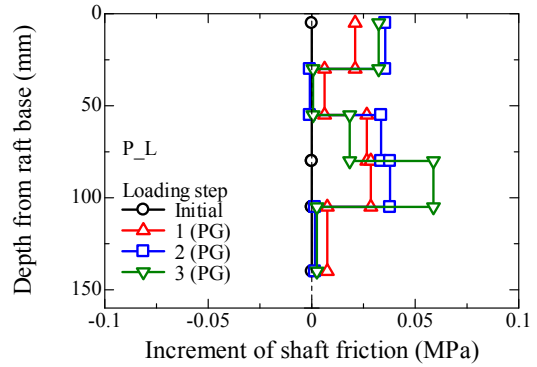
(d) Average of Pile 1 & Pile 2
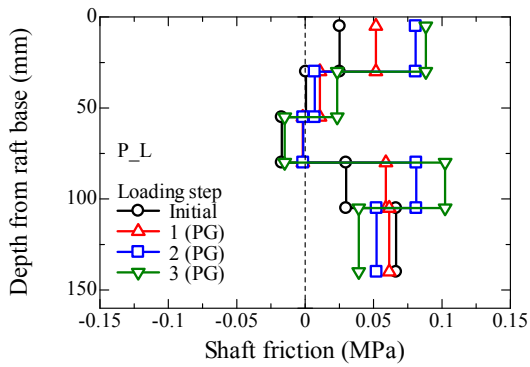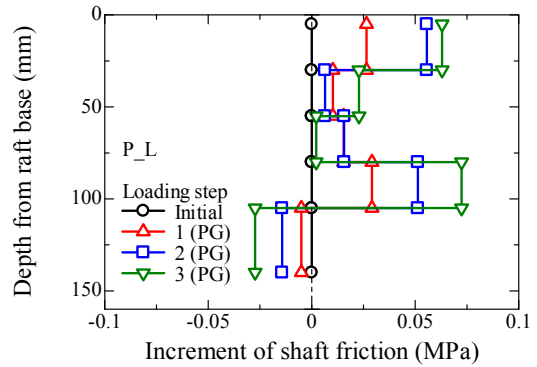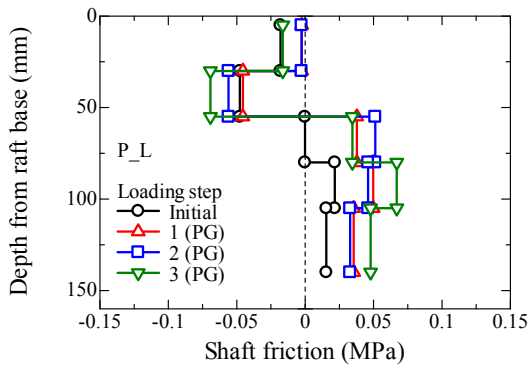
(b) Pile 1
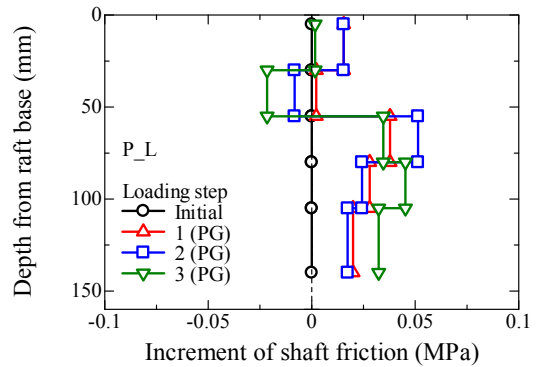
(e) Pile 1

(c) Pile 2

(f) Pile 2

A. 4.3.3.19 Profiles of shaft friction and shaft friction increment for P_L during vertical loading process.
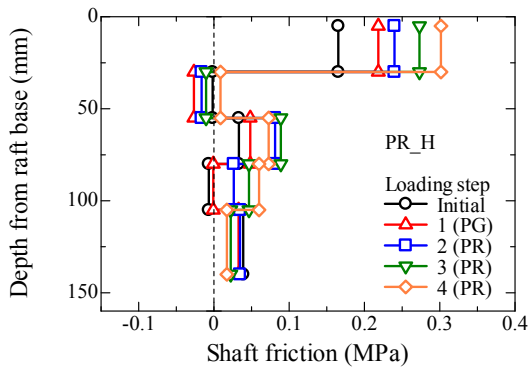
(a) Average of Pile 1 & Pile 2
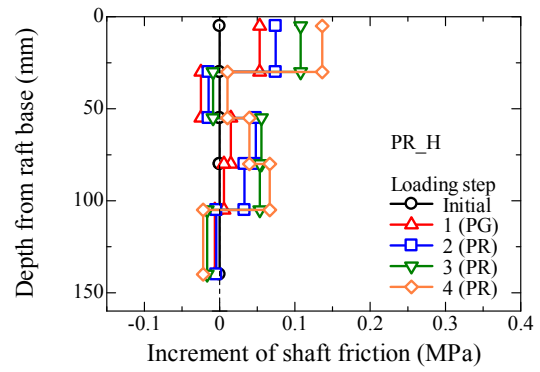
(d) Average of Pile 1 & Pile 2
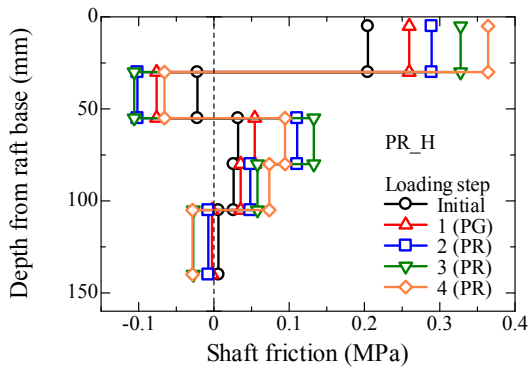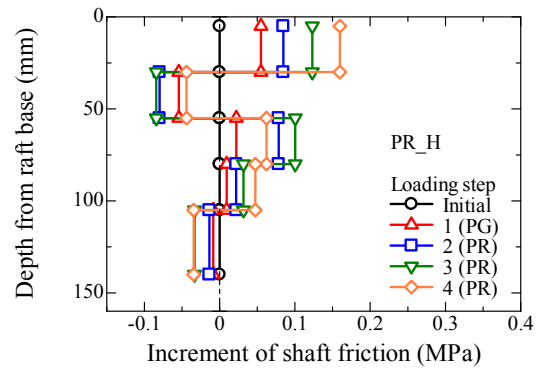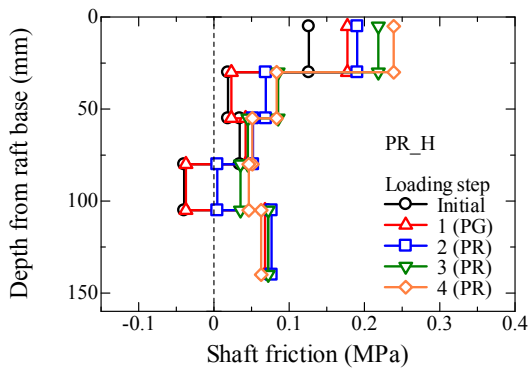
(b) Pile 1
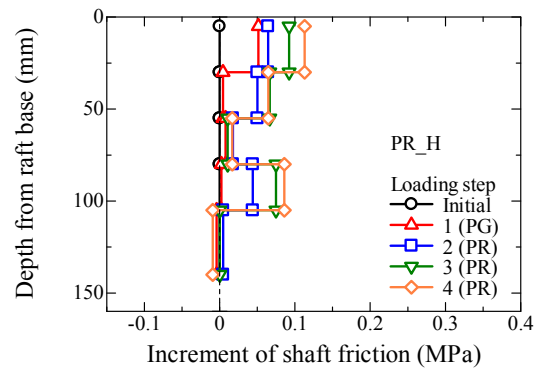
(e) Pile 1

(c) Pile 2

(f) Pile 2

A. 4.3.3.20 Profiles of shaft friction and shaft friction increment for PR_H during vertical loading process.
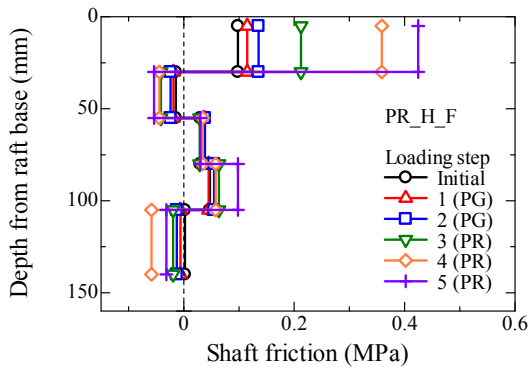
(a) Average of Pile 1 & Pile 2
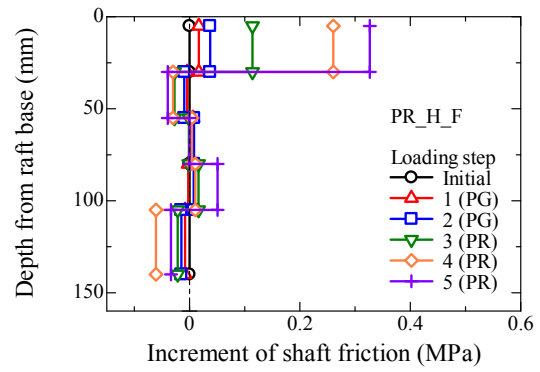
(d) Average of Pile 1 & Pile 2
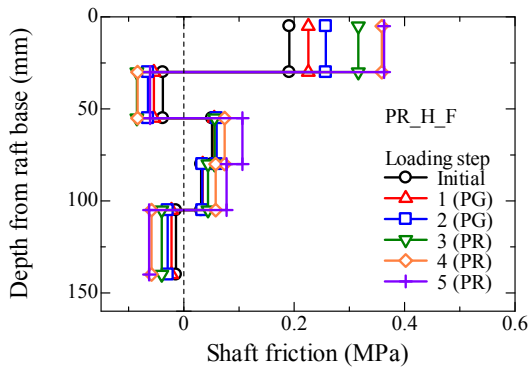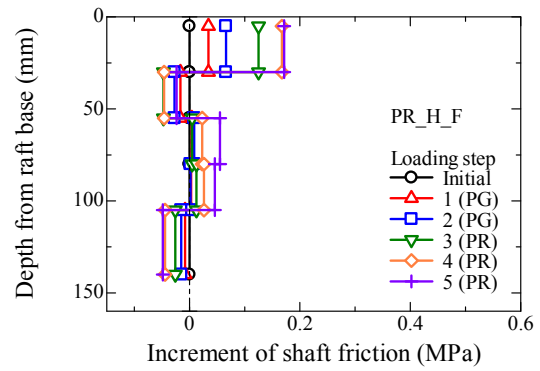
(b) Pile 1

(e) Pile 1
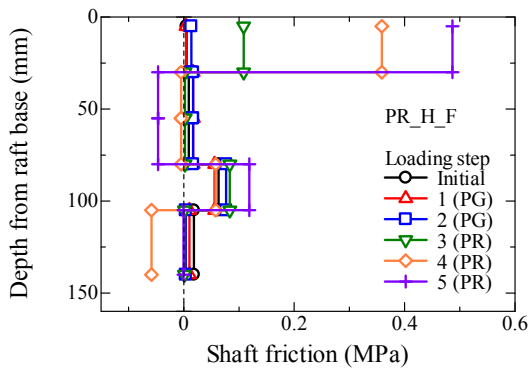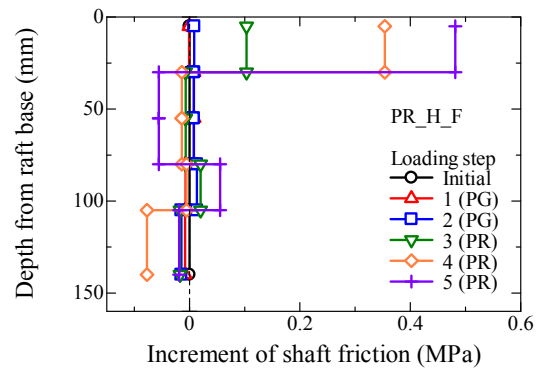
(c) Pile 2

(f) Pile 2

A. 4.3.3.21 Profiles of shaft friction and shaft friction increment for PR_H_F during vertical loading process.
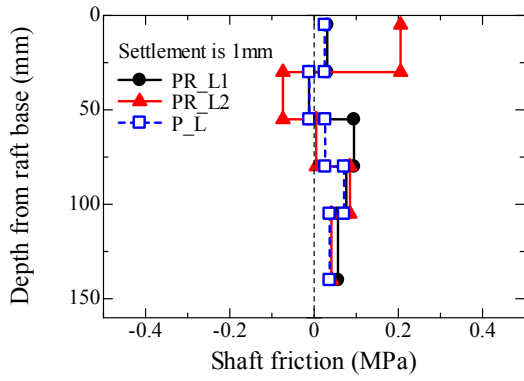
(a) Light case (Absolute value)
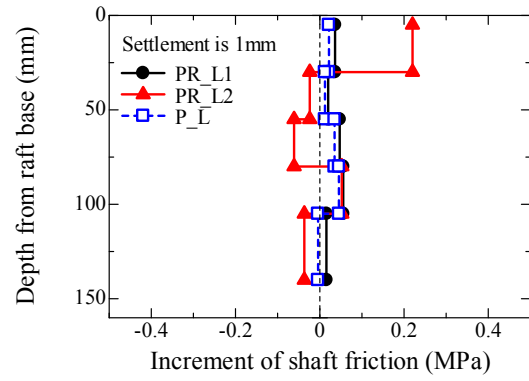
(c) Light case (Increment value)
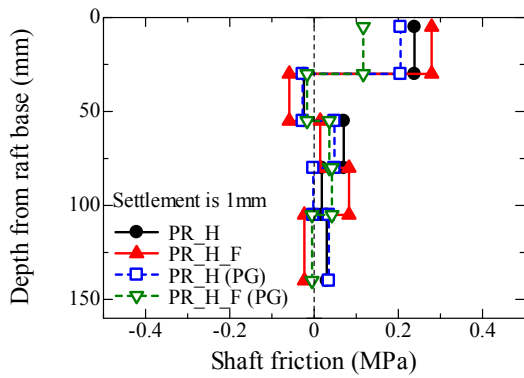
(b) Heavy case (Absolute value)
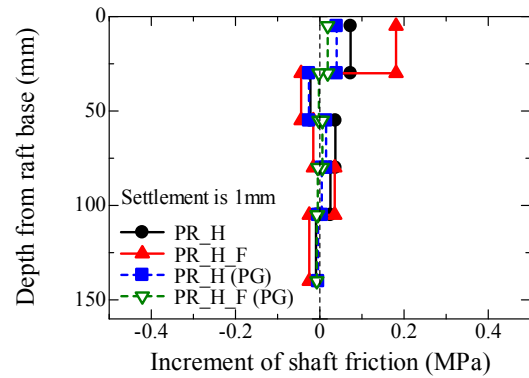
(d) Heavy case (Increment value)

A. 4.3.3.22 Profile of shaft friction at settlement of 1mm.
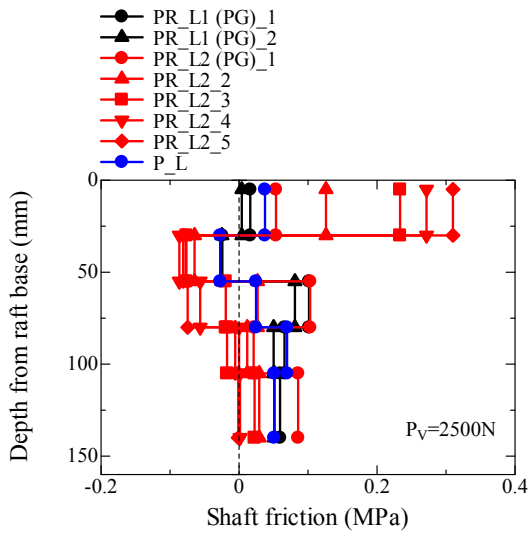
(a) Light case (Absolute value)
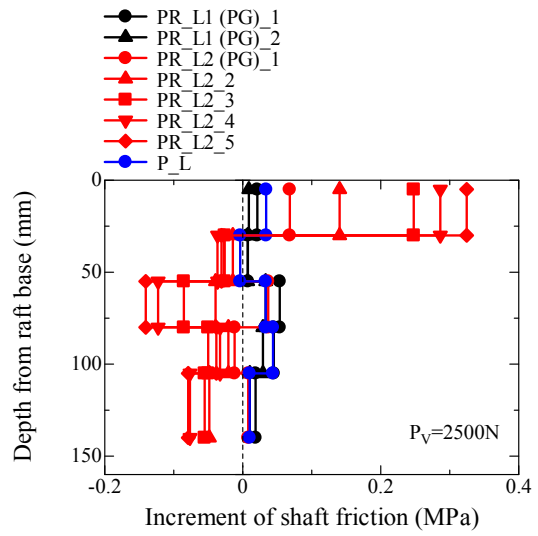
(c) Light case (Increment value)
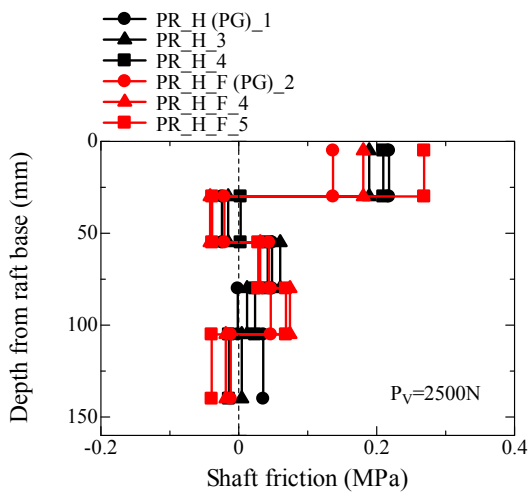
(b) Heavy case (Absolute value)
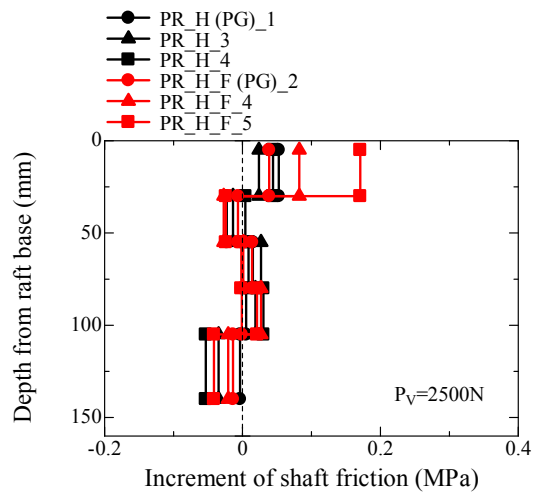
(d) Heavy case (Increment value)

A. 4.3.3.23 Profile of shaft friction at P_V of 2500N.

(a) PR_L1

(b) P_L

(c) R_L1 & R_L2

(d) PR_H

(e) P_H
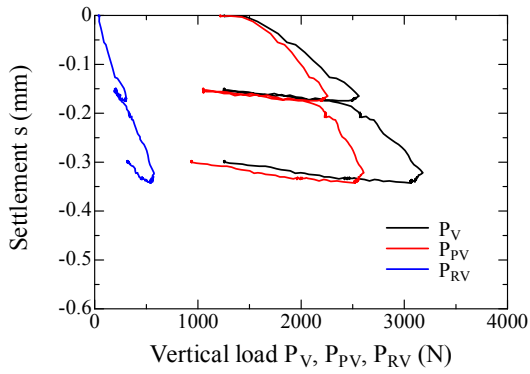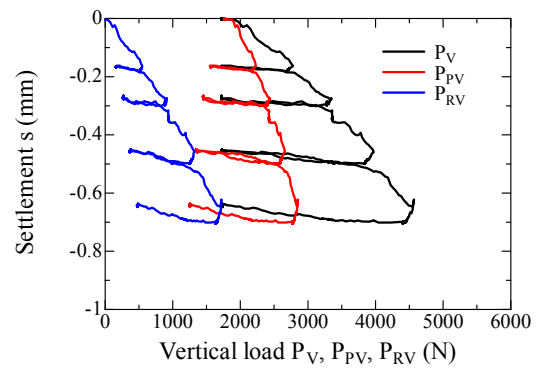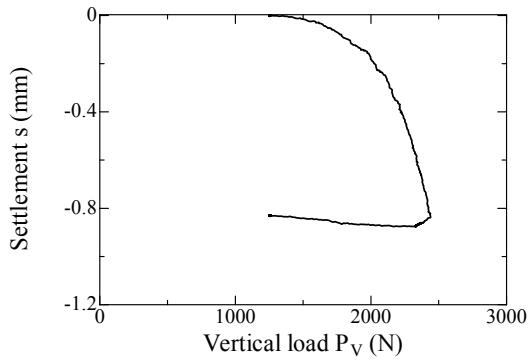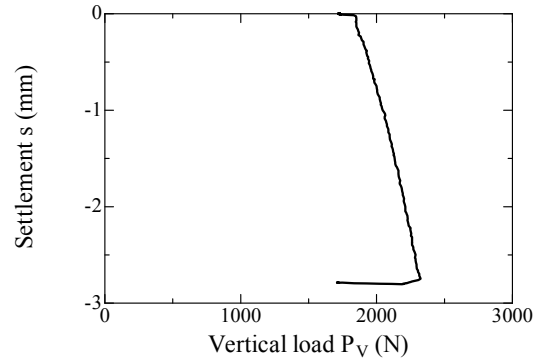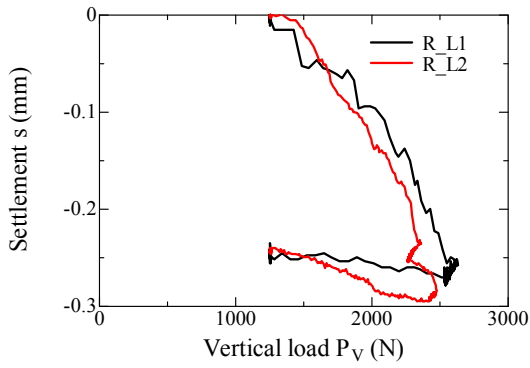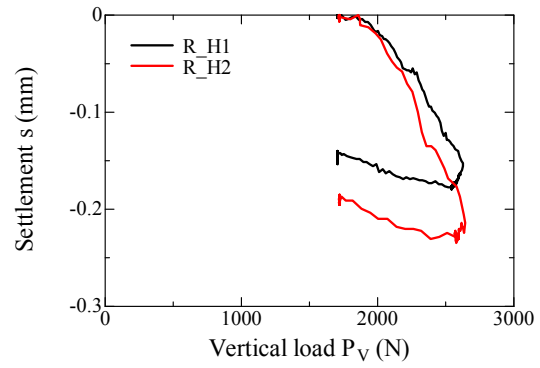
(f) R_H1 & R_H2

A. 4.4.2.1 Variation of P_V, P_{PV} and P_{RV} with settlement during pre-vertical loading process.
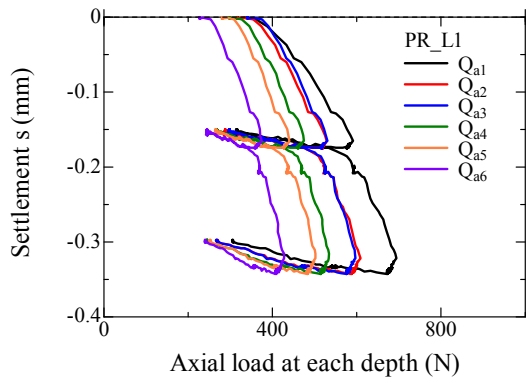
(a) Average of Pile 1 & Pile 2
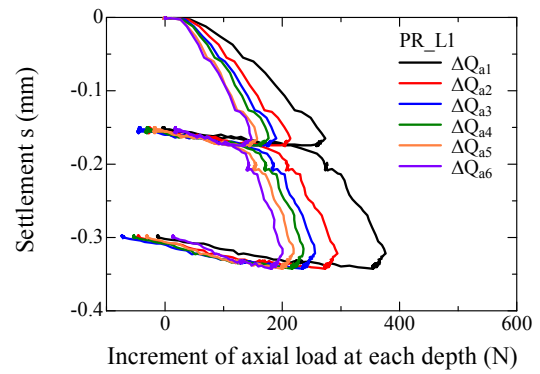
(d) Average of Pile 1 & Pile 2
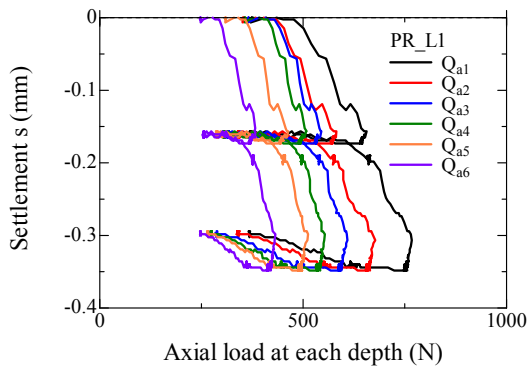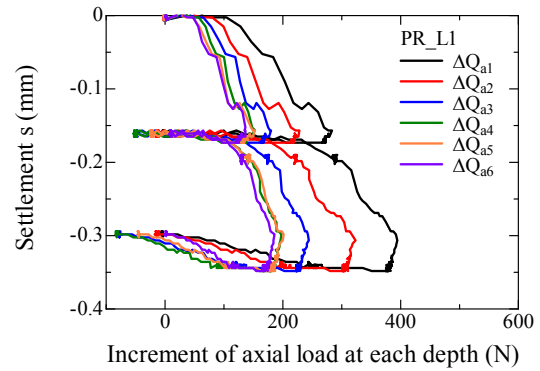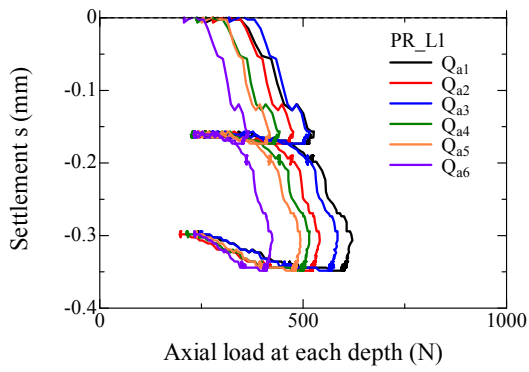
(b) Pile 1
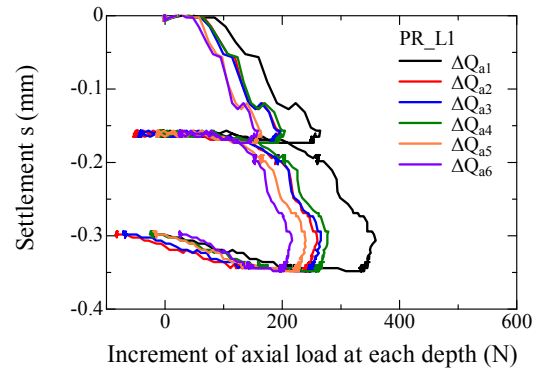
(e) Pile 1

(c) Pile 2

(f) Pile 2

A. 4.4.2.2 Variation of axial load at each depth Q_{an} with settlement s during pre-vertical loading process for PR_L1.

.
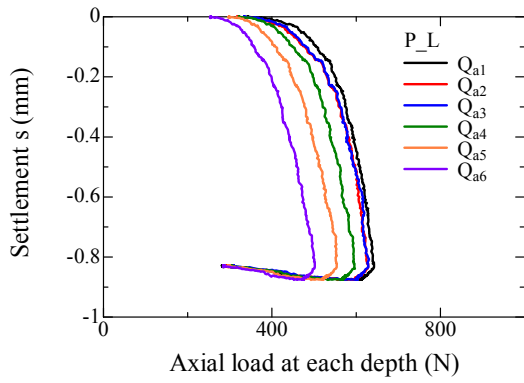
(a) Average of Pile 1 & Pile 2
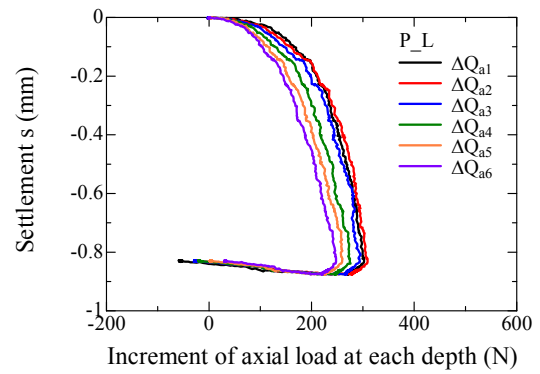
(d) Average of Pile 1 & Pile 2
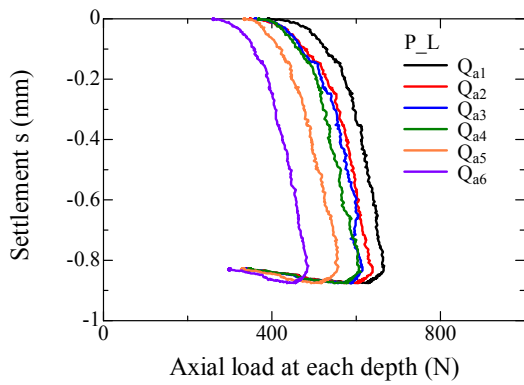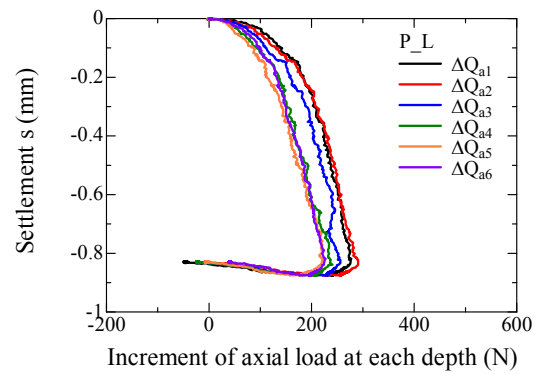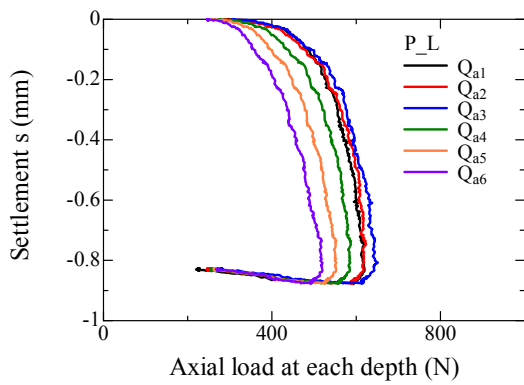
(b) Pile 1
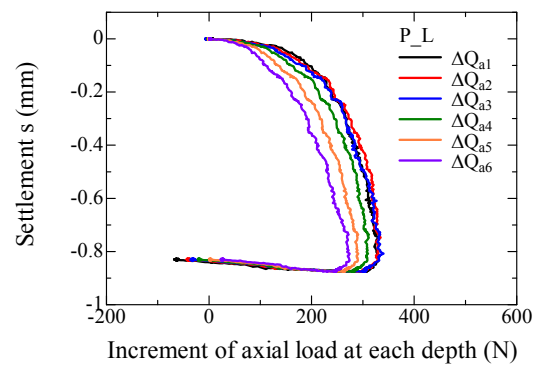
(e) Pile 1

(c) Pile 2

(f) Pile 2

A. 4.4.2.3 Variation of axial load at each depth Q_{an} with settlement s during pre-vertical loading process for P_L.

.
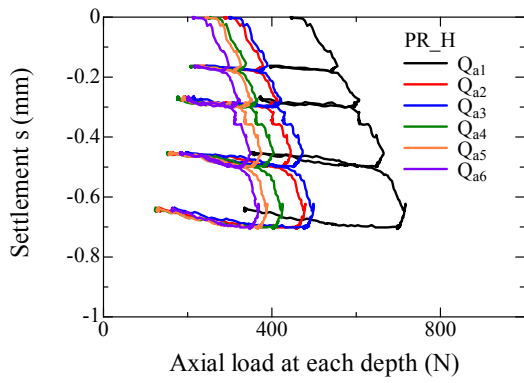
A. 4.4.2.4 Variation of axial load at each depth Q_{an} with settlement s during pre-vertical loading process for PR_H.

.

(a) Average of Pile 1 & Pile 2

(d) Average of Pile 1 & Pile 2

(b) Pile 1

(e) Pile 1

(c) Pile 2

(f) Pile 2

A. 4.4.2.5 Variation of axial load at each depth Q_{an} with settlement s during pre-vertical loading process for P_H.

.
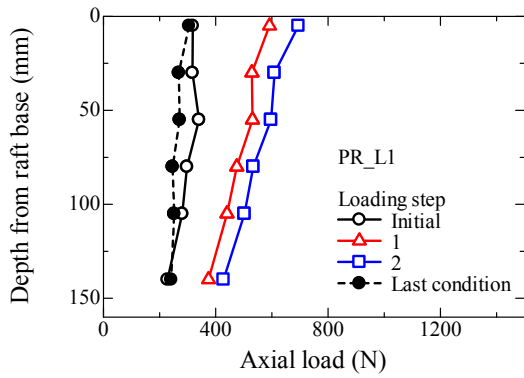
(a) Average of Pile 1 & Pile 2
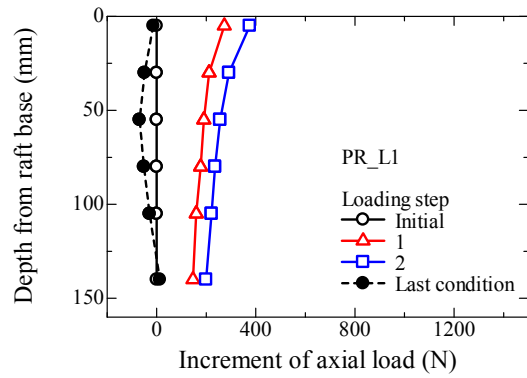
(d) Average of Pile 1 & Pile 2
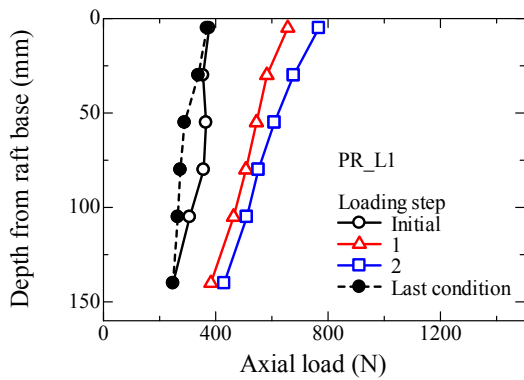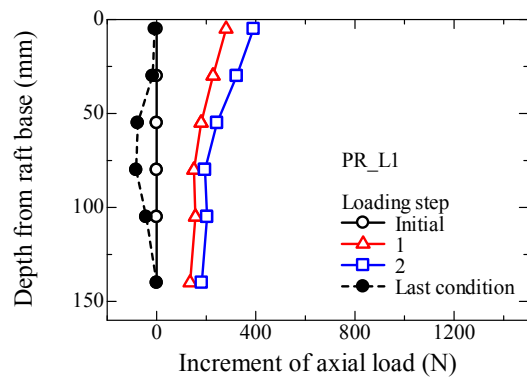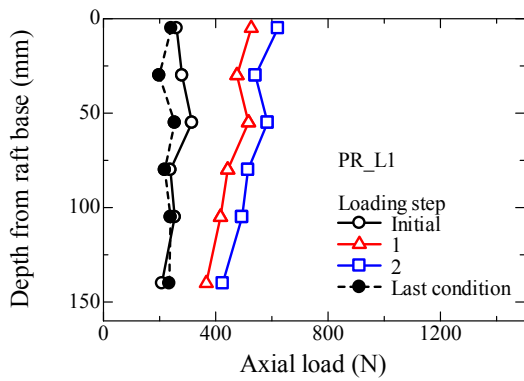
(b) Pile 1
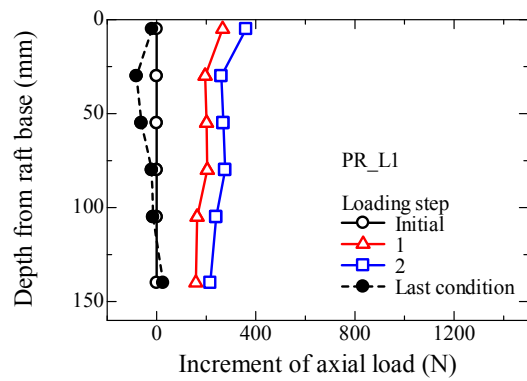
(e) Pile 1

(c) Pile 2

(f) Pile 2

A. 4.4.2.6 Profiles of axial load during pre-vertical loading process for PR_L1.

.
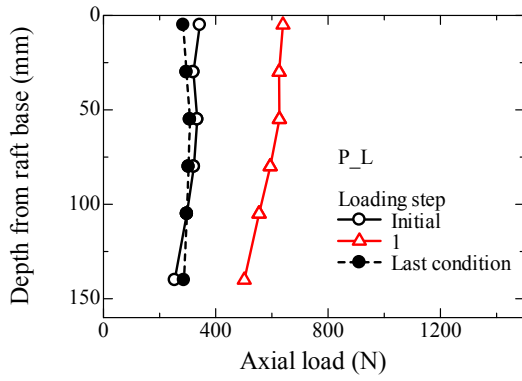
(a) Average of Pile 1 & Pile 2
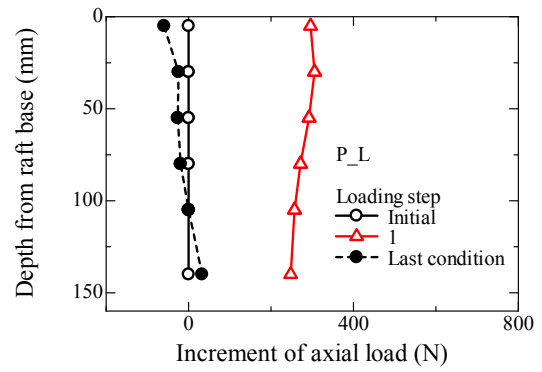
(d) Average of Pile 1 & Pile 2
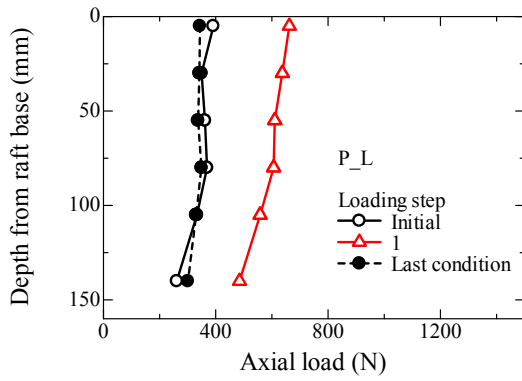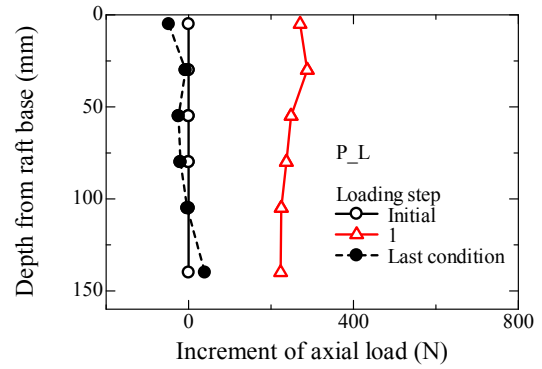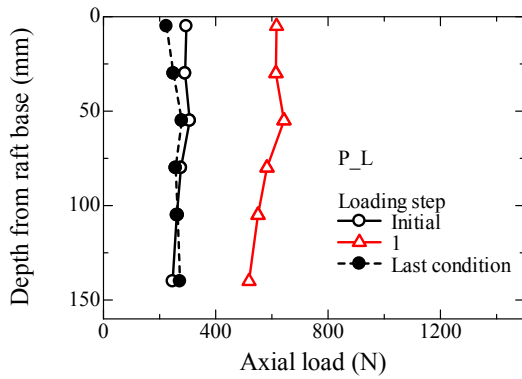
(b) Pile 1
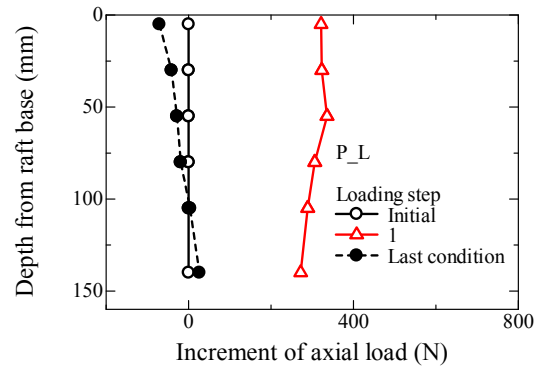
(e) Pile 1

(c) Pile 2

(f) Pile 2

A. 4.4.2.7 Profiles of axial load during pre-vertical loading process for P_L.

.
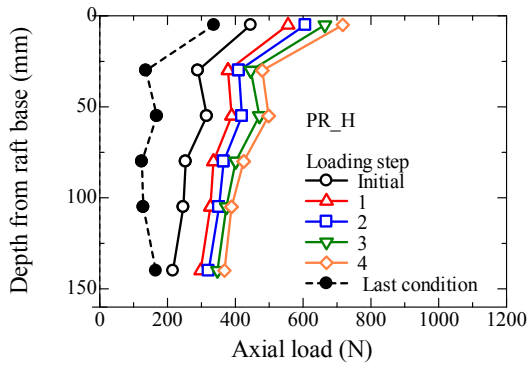
(a) Average of Pile 1 & Pile 2
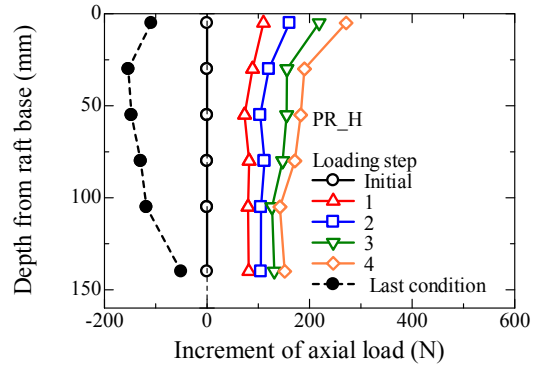
(d) Average of Pile 1 & Pile 2
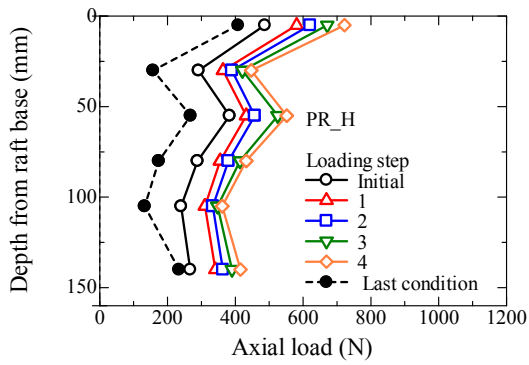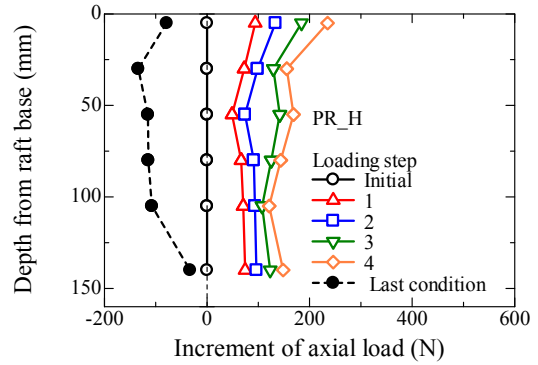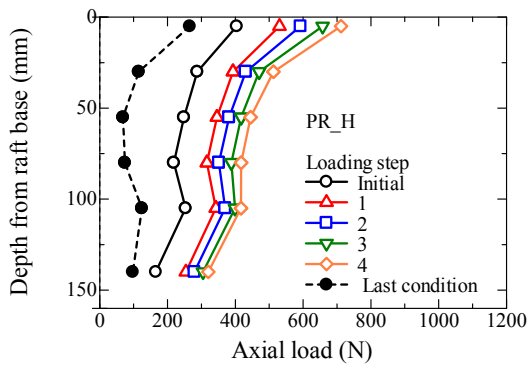
(b) Pile 1
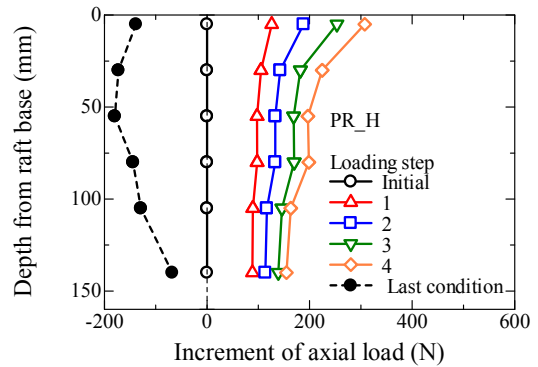
(e) Pile 1

(c) Pile 2

(f) Pile 2

A. 4.4.2.8 Profiles of axial load during pre-vertical loading process for PR_H.

.
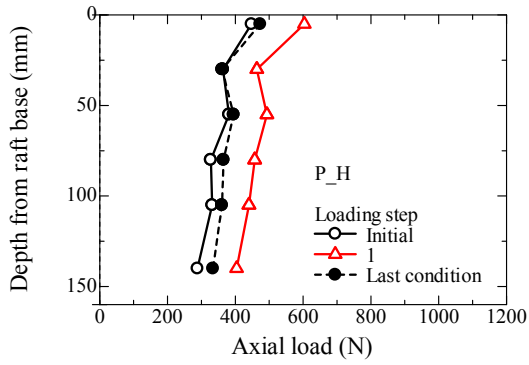
(a) Average of Pile 1 & Pile 2
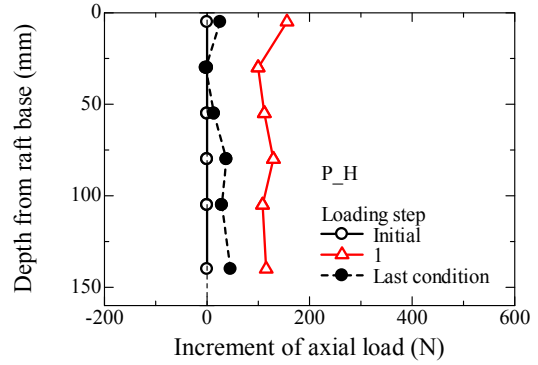
(d) Average of Pile 1 & Pile 2
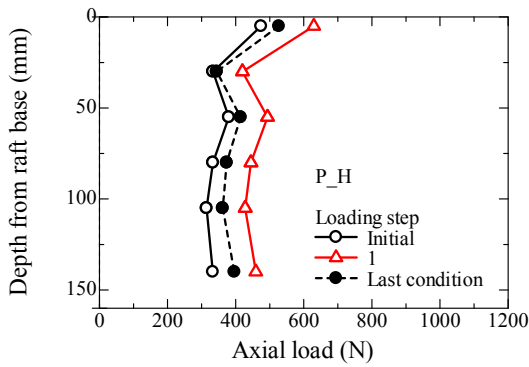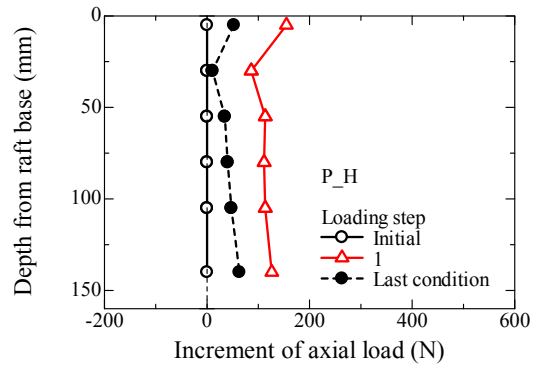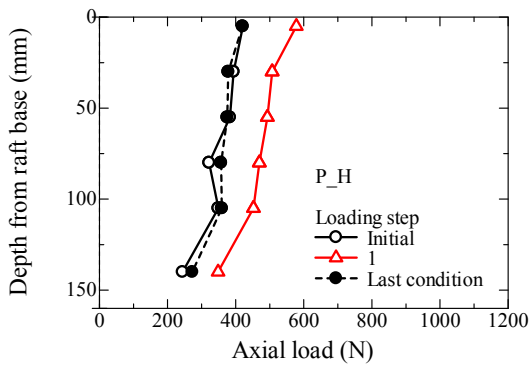
(b) Pile 1
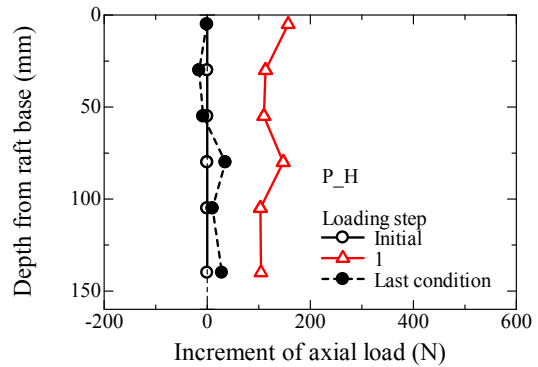
(e) Pile 1

(c) Pile 2

(f) Pile 2

A. 4.4.2.9 Profiles of axial load during pre-vertical loading process for P_H.

.
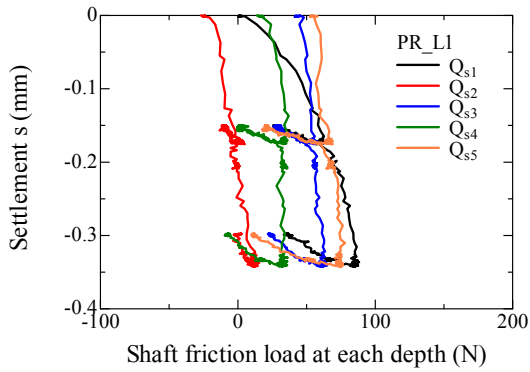
(a) Average of Pile 1 & Pile 2
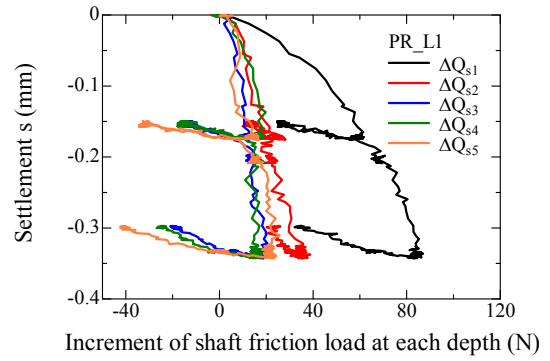
(d) Average of Pile 1 & Pile 2
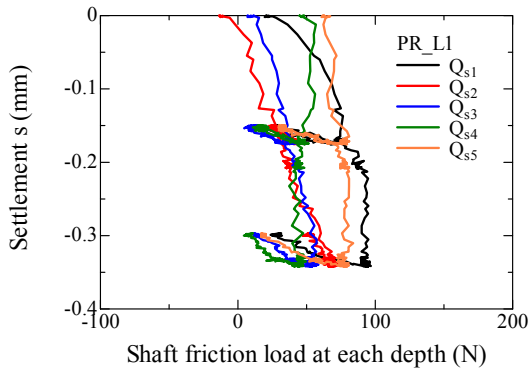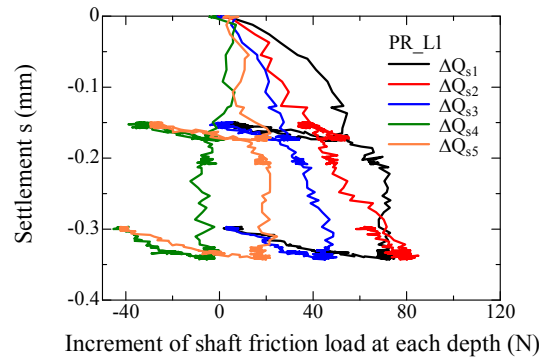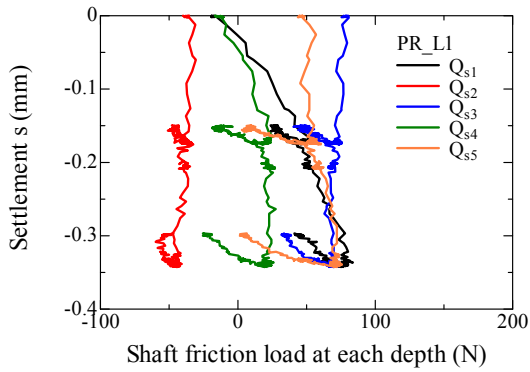
(b) Pile 1
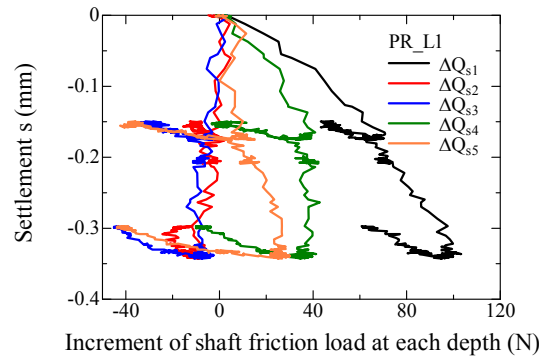
(e) Pile 1

(c) Pile 2

(f) Pile 2

A. 4.4.2.10 Variation of shaft friction load at each depth with settlement s for PR_L1 during pre-vertical loading process.

.
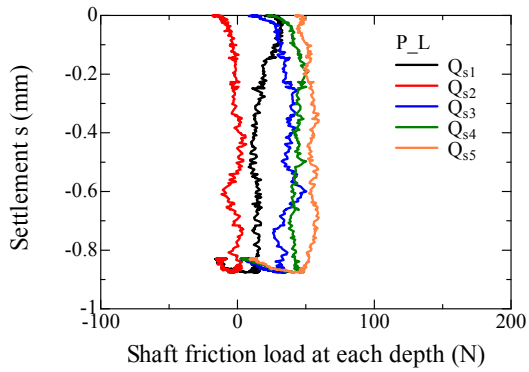
(a) Average of Pile 1 & Pile 2
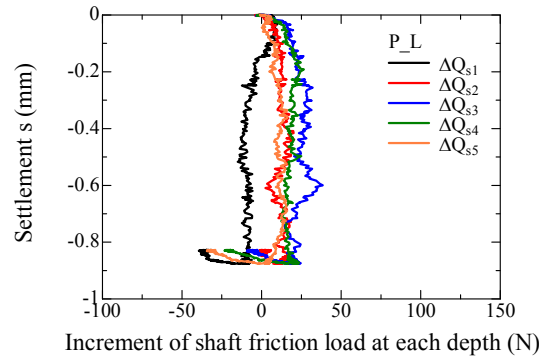
(d) Average of Pile 1 & Pile 2
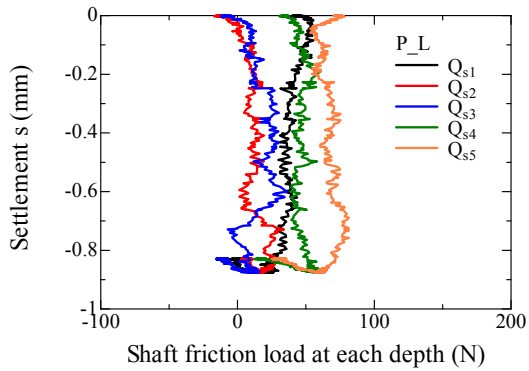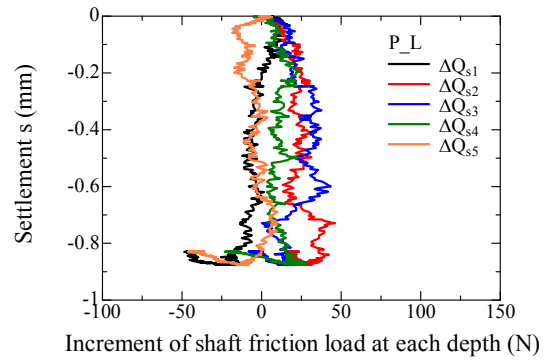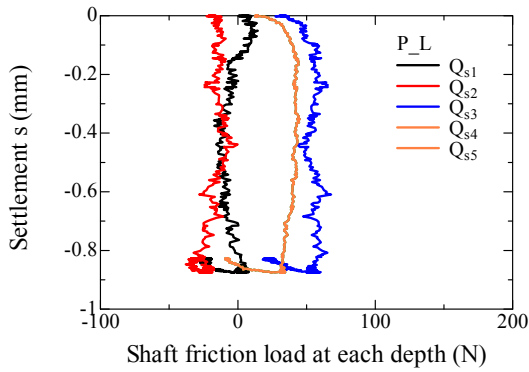
(b) Pile 1
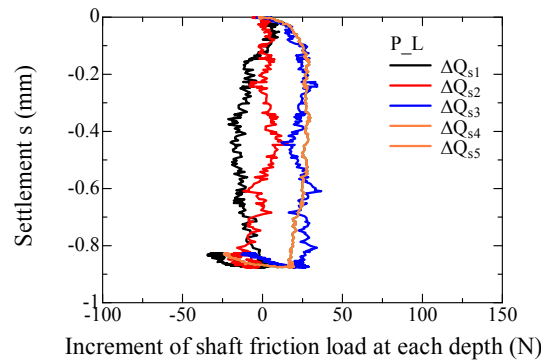
(e) Pile 1

(c) Pile 2

(f) Pile 2

A. 4.4.2.11 Variation of shaft friction load at each depth with settlement s for P_L during pre-vertical loading process.

.
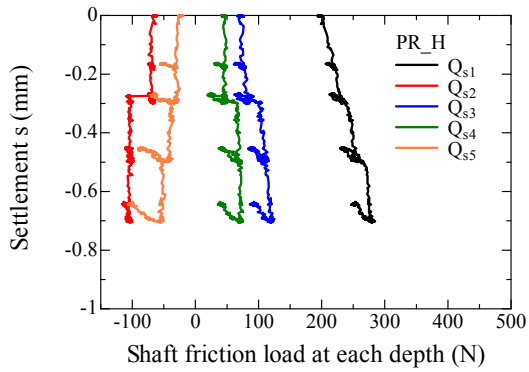
(a) Average of Pile 1 & Pile 2
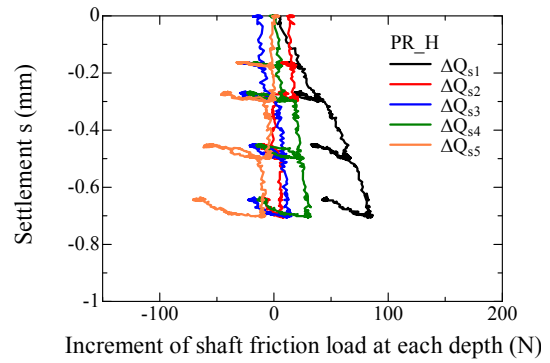
(d) Average of Pile 1 & Pile 2
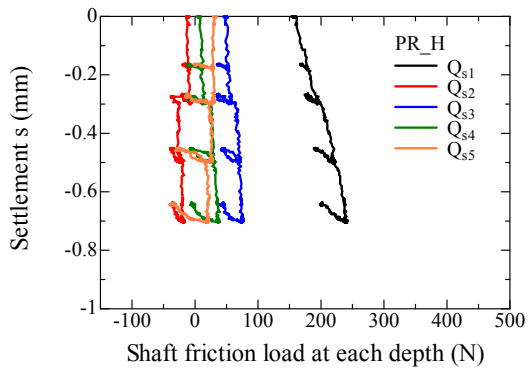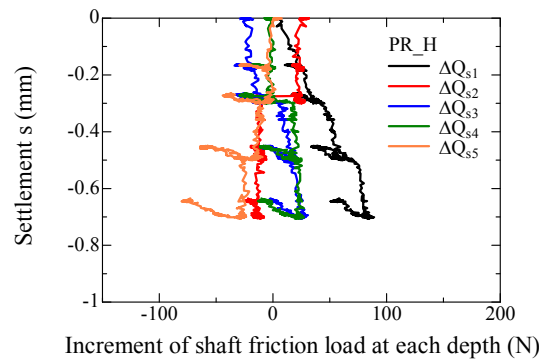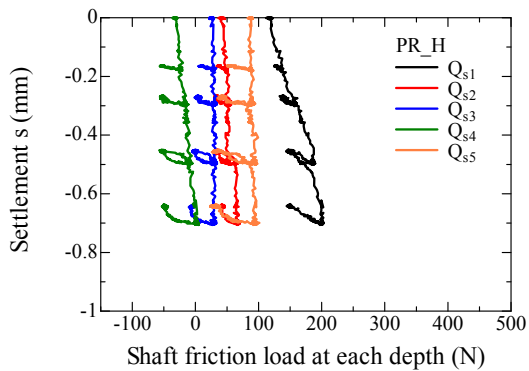
(b) Pile 1
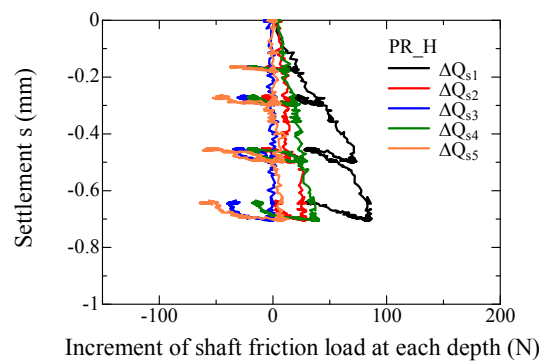
(e) Pile 1

(c) Pile 2

(f) Pile 2

A. 4.4.2.12 Variation of shaft friction load at each depth with settlement s for PR_H during pre-vertical loading process.

.
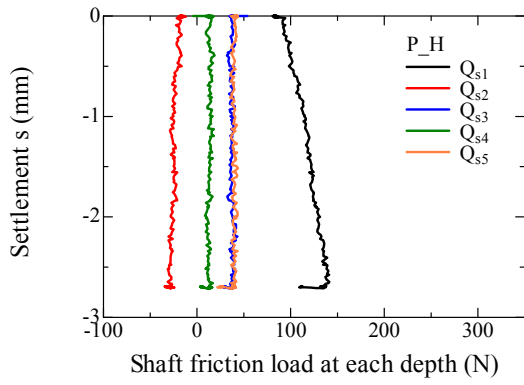
(a) Average of Pile 1 & Pile 2
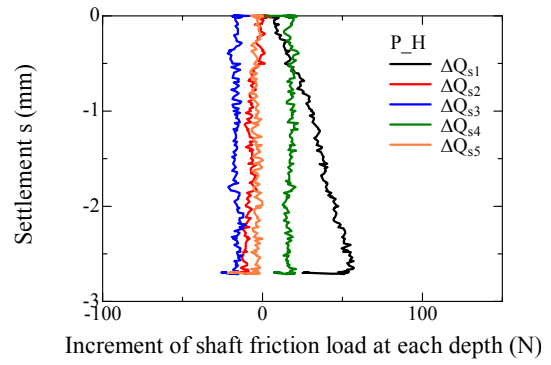
(d) Average of Pile 1 & Pile 2
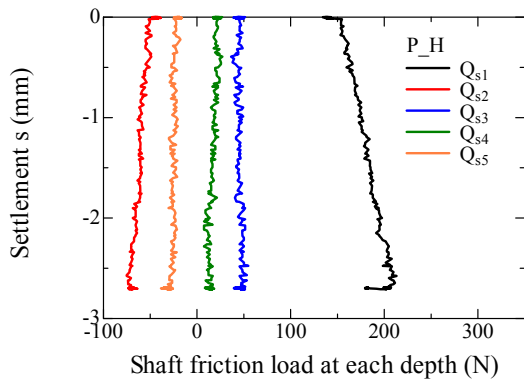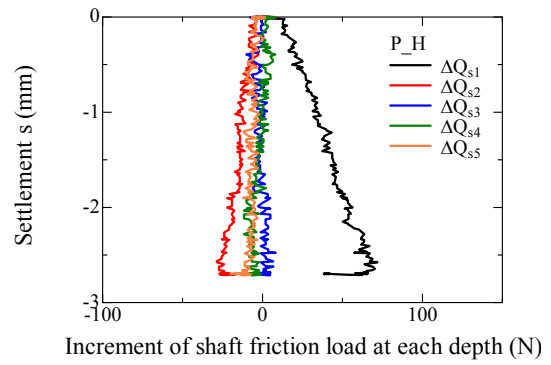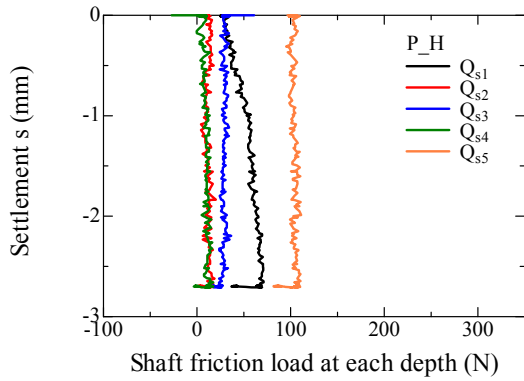
(b) Pile 1
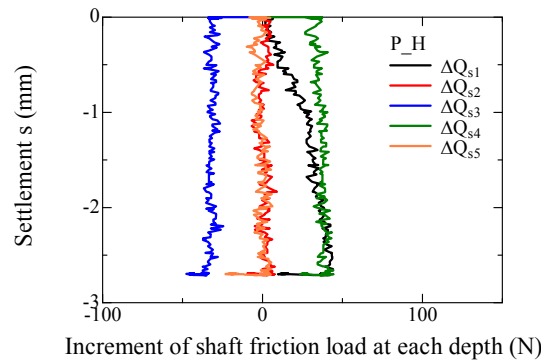
(e) Pile 1

(c) Pile 2

(f) Pile 2

A. 4.4.2.13 Variation of shaft friction load at each depth with settlement s for P_H during pre-vertical loading process.

.
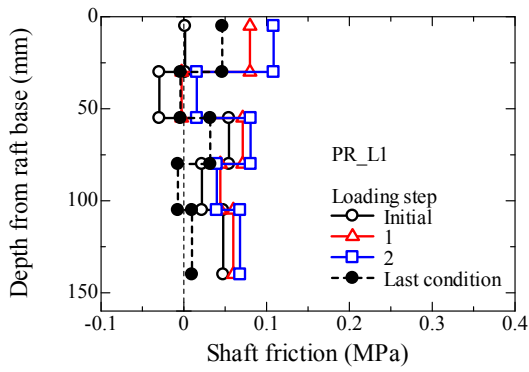
(a) Average of Pile 1 & Pile 2
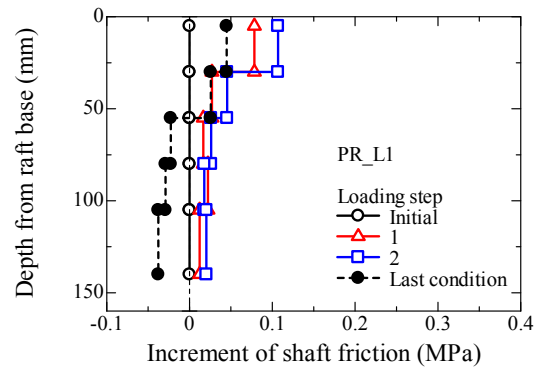
(d) Average of Pile 1 & Pile 2
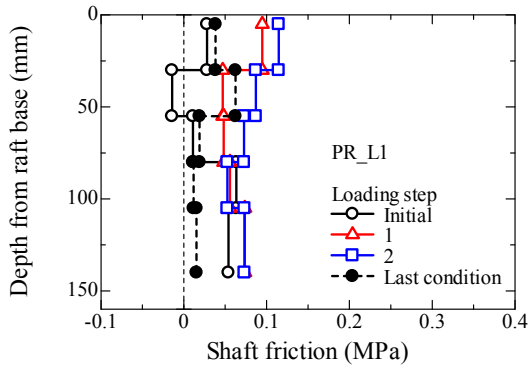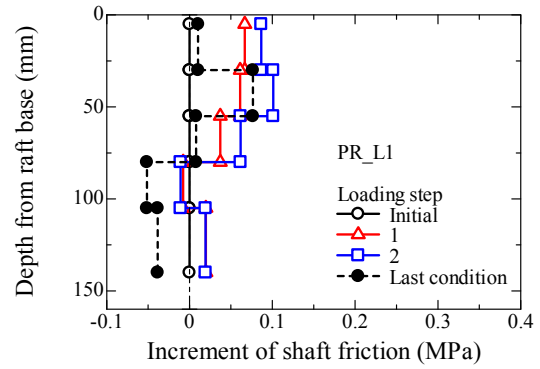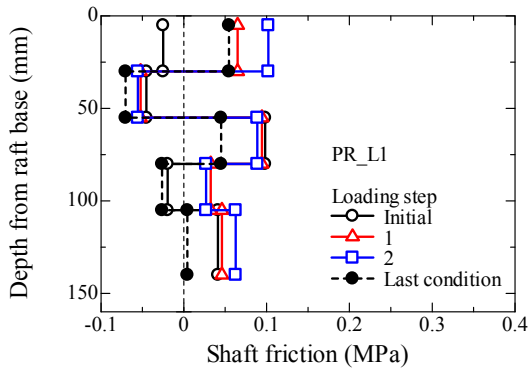
(b) Pile 1
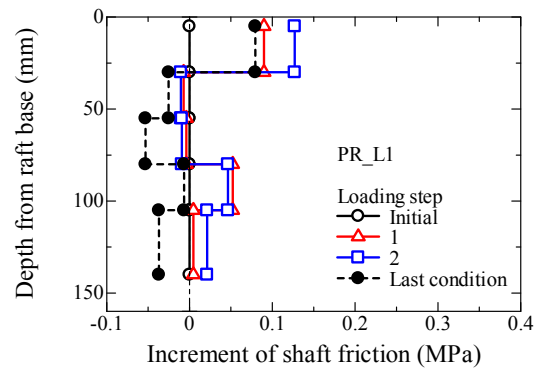
(e) Pile 1

(c) Pile 2

(f) Pile 2

A. 4.4.2.14 Profiles of shaft friction for PR_L1 during pre-vertical loading process.
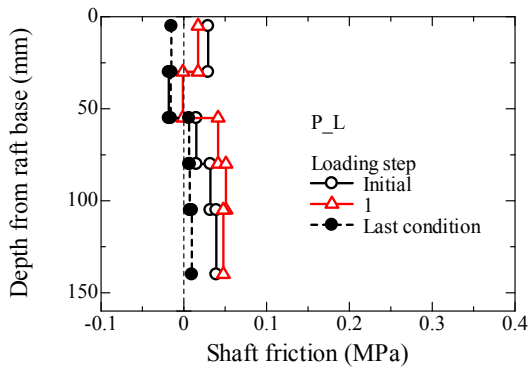
(a) Average of Pile 1 & Pile 2
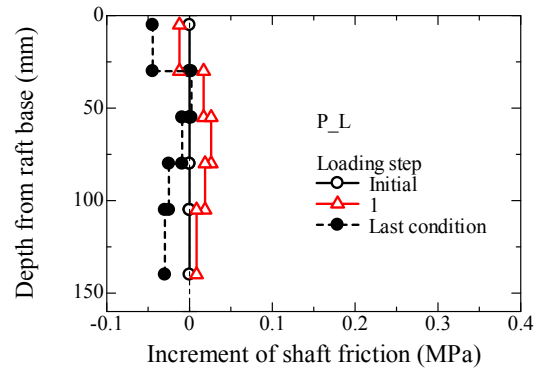
(d) Average of Pile 1 & Pile 2
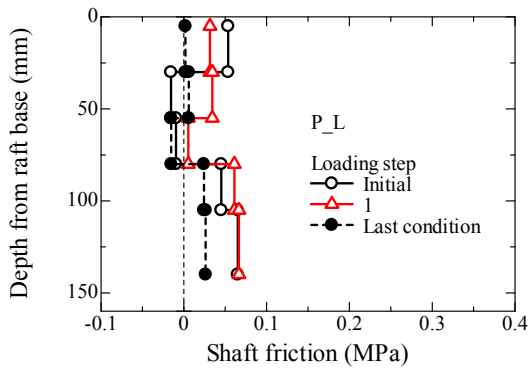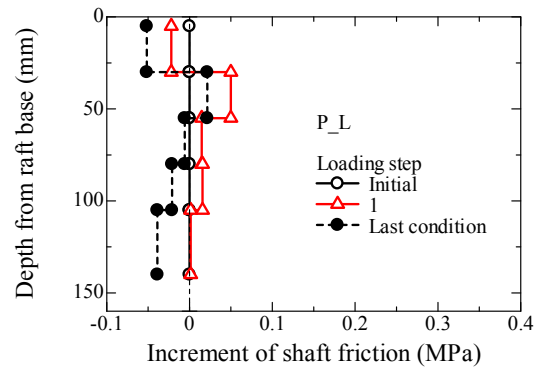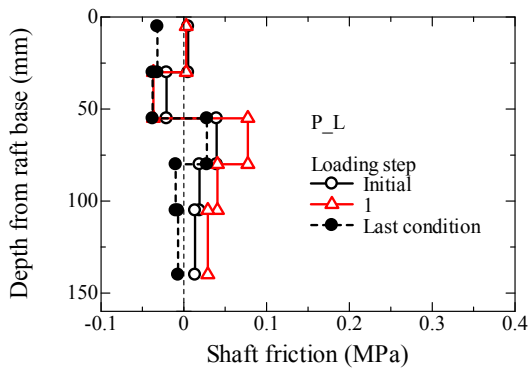
(b) Pile 1
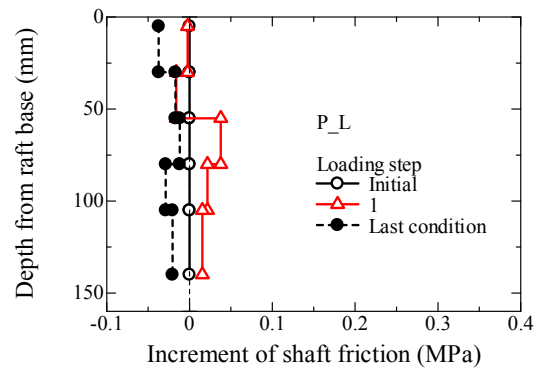
(e) Pile 1

(c) Pile 2

(f) Pile 2

A. 4.4.2.15 Profiles of shaft friction for P_L during pre-vertical loading process.
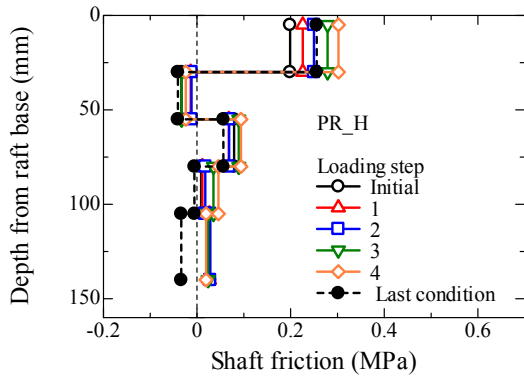
(a) Average of Pile 1 & Pile 2
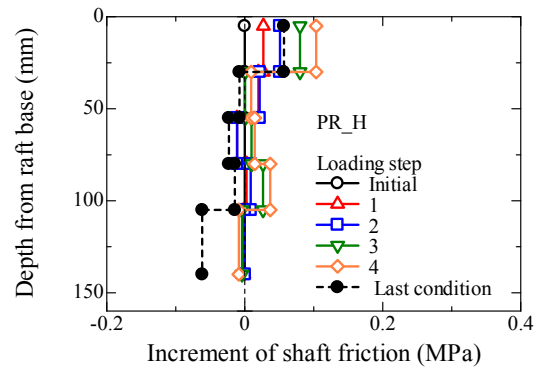
(d) Average of Pile 1 & Pile 2
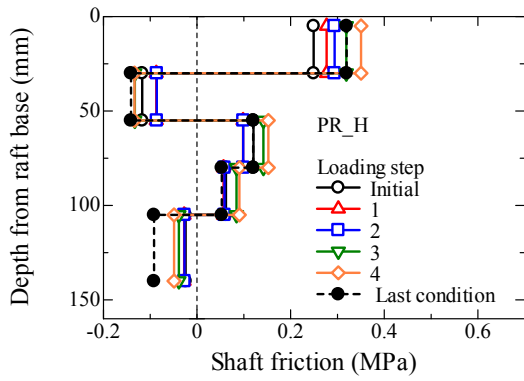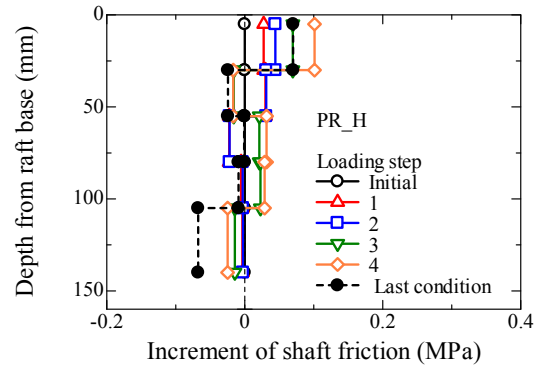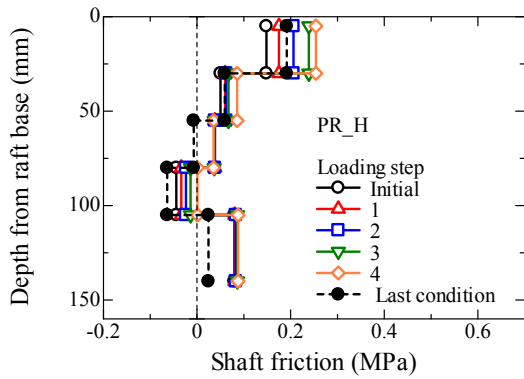
(b) Pile 1
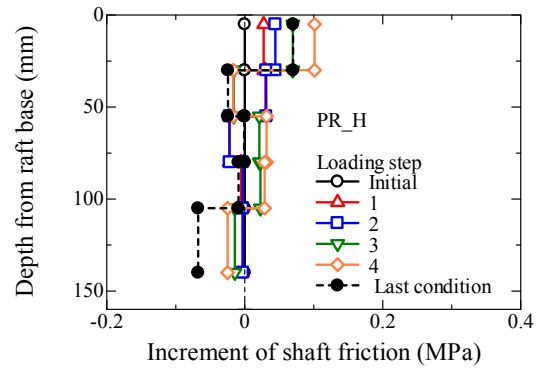
(e) Pile 1

(c) Pile 2

(f) Pile 2

A. 4.4.2.16 Profiles of shaft friction for PR_H during pre-vertical loading process.
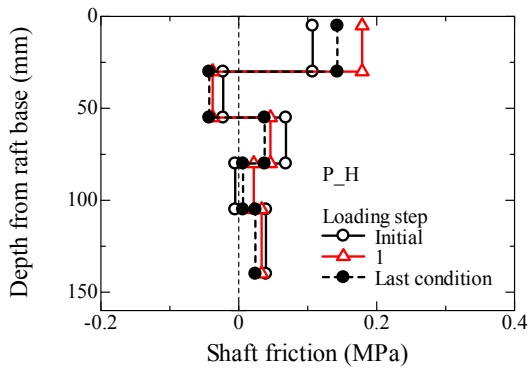
(a) Average of Pile 1 & Pile 2
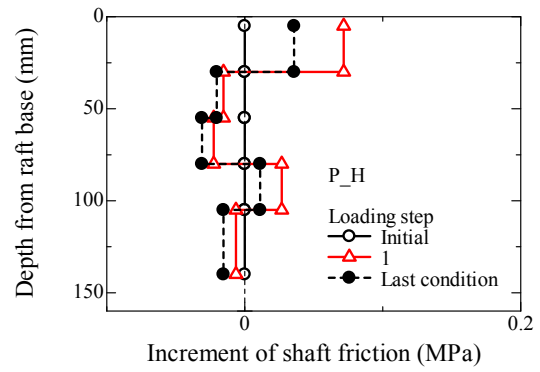
(d) Average of Pile 1 & Pile 2
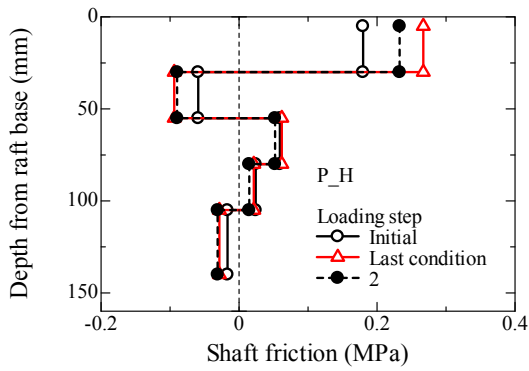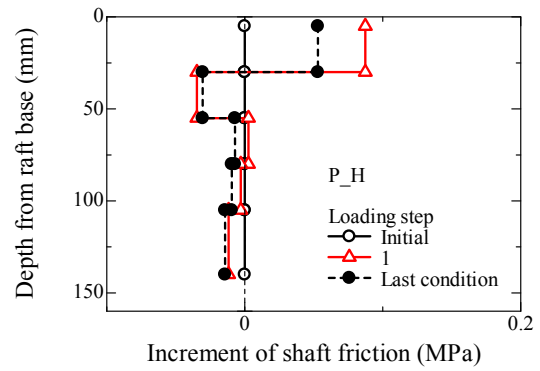
(b) Pile 1

(e) Pile 1
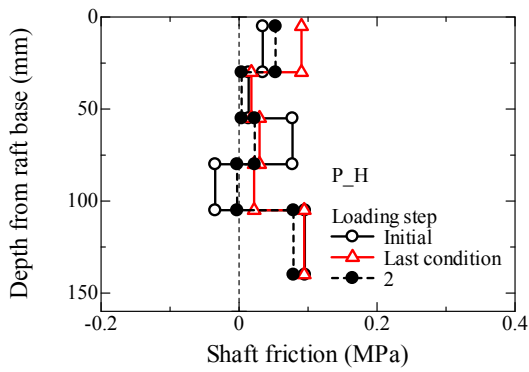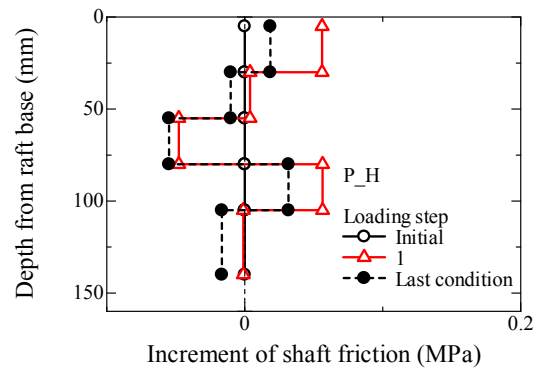
(c) Pile 2

(f) Pile 2

A. 4.4.2.17 Profiles of shaft friction for P_H during pre-vertical loading process.
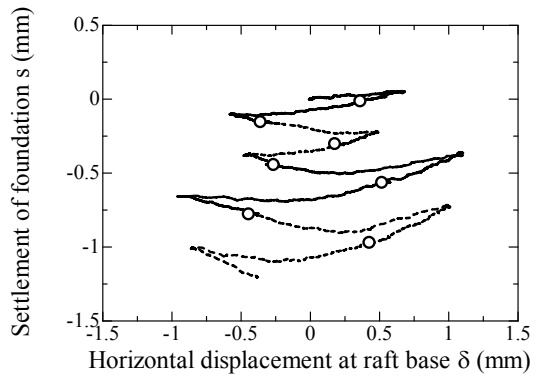
(a) PR_L1
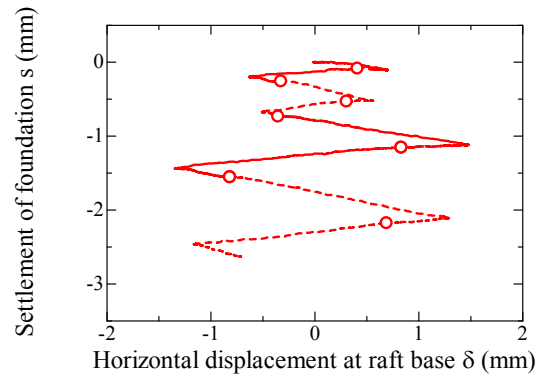
(b) P_L
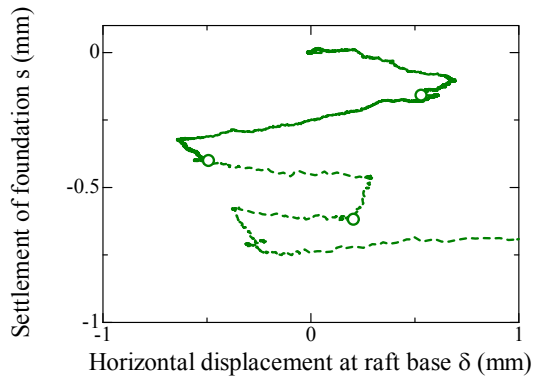
(c) R_L2
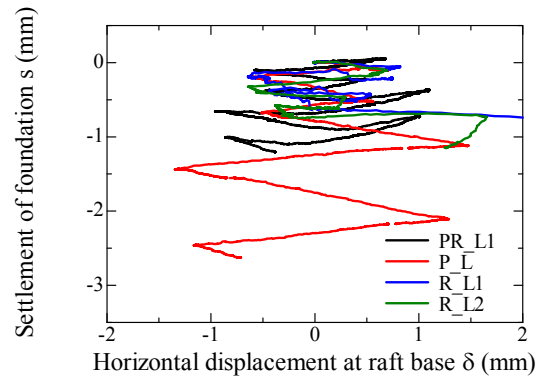
(d) Light case

A. 5.3.1.1 Relationship between horizontal displacement at raft base δ and settlement s for light case.
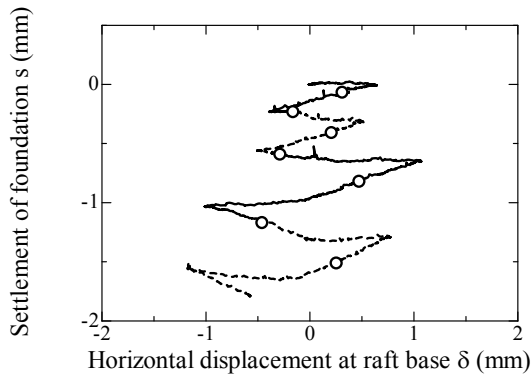
(a) PR_H
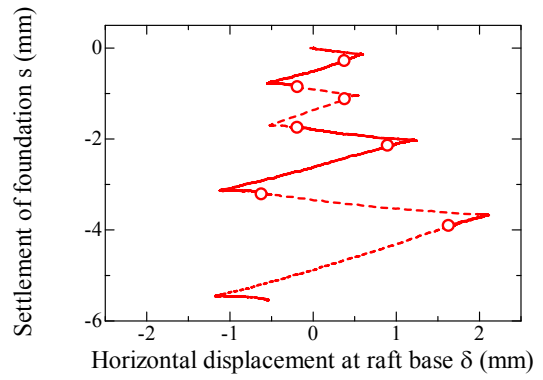
(b) P_H
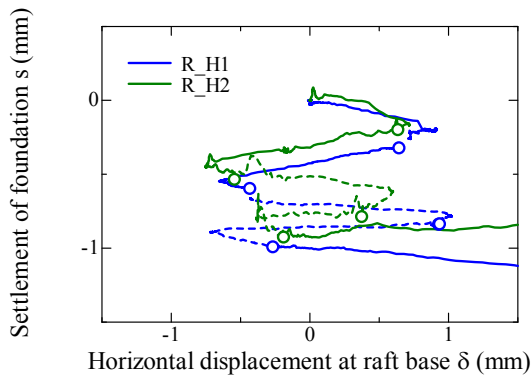
(c) R_H1 & R_H2
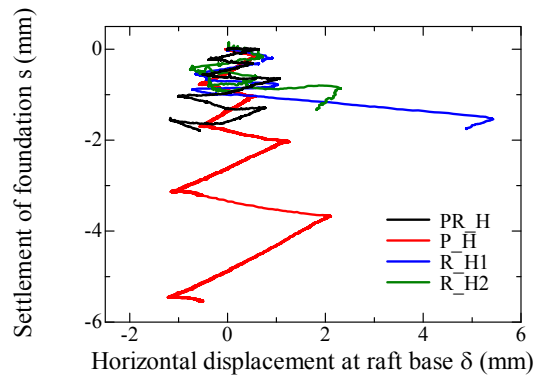
(d) Heavy case

A. 5.3.1.2 Relationship between horizontal displacement at raft base δ and settlement s for heavy case.
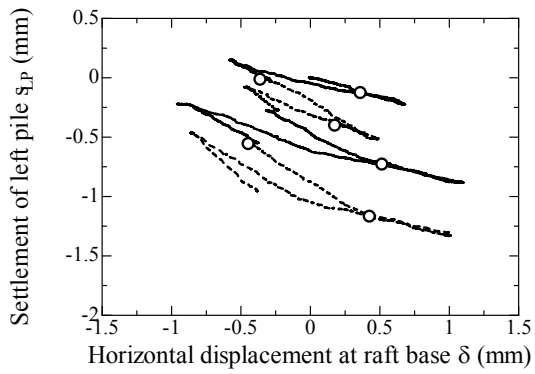
(a) PR_L1 (left pile)
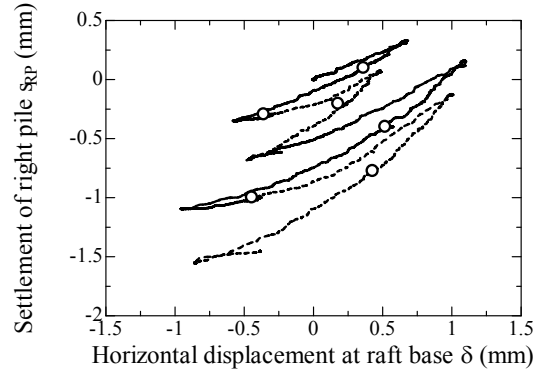
(b) PR_L1 (right pile)
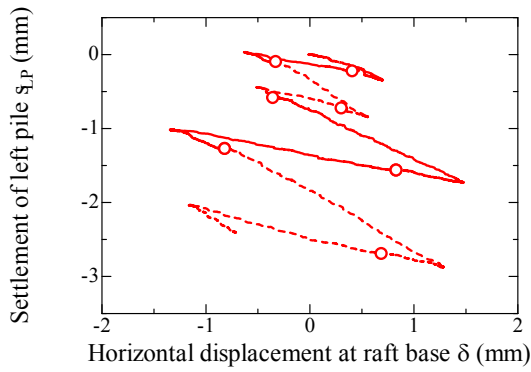
(c) P_L (left pile)
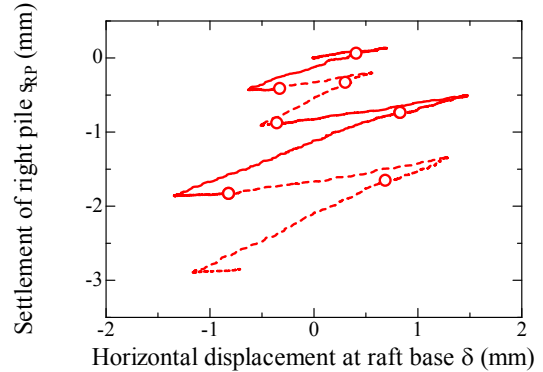
(d) P_L (right pile)
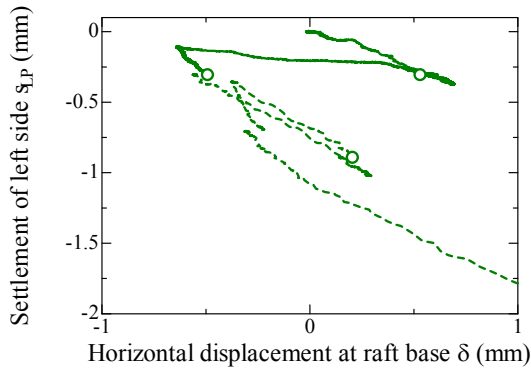
(e) R_L2 (left side)
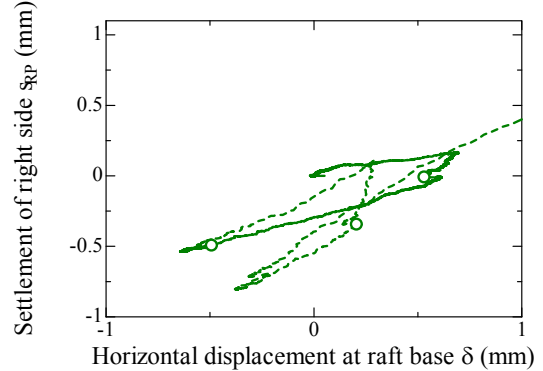
(f) R_L2 (right side)

A. 5.3.2.1 Relationship between horizontal displacement at raft base δ and settlement of righ pile s_{RP} and left pile s_{LP} for light case.

A90
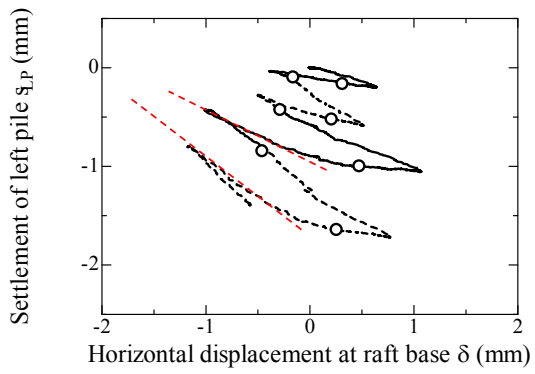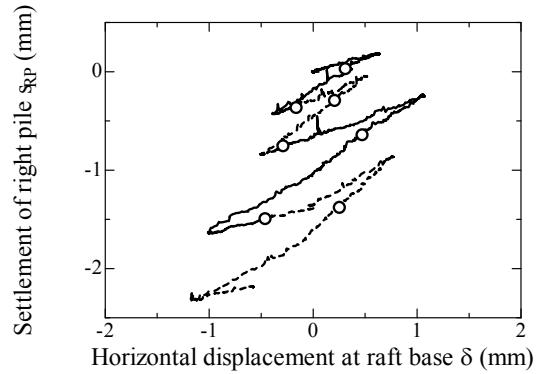
(a) PR_H (left pile)

(b) PR_H (right pile)
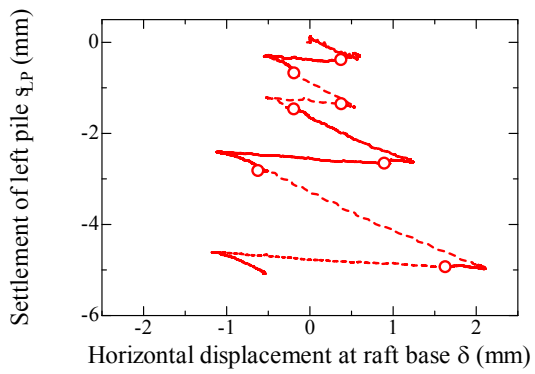
(c) P_H (left pile)
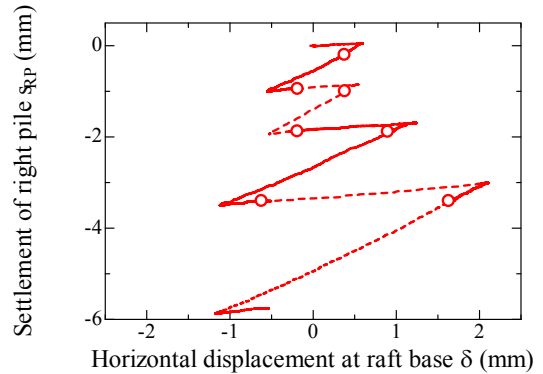
(d) P_H (right pile)
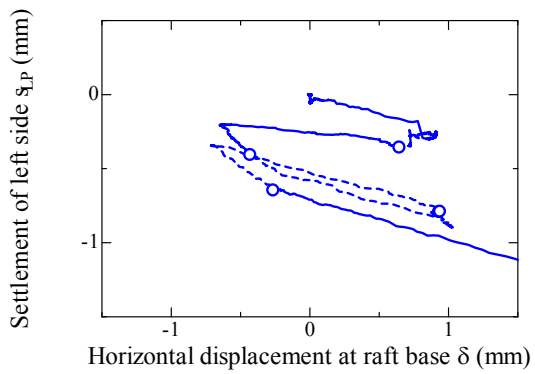
(e) R_H1 (left side)
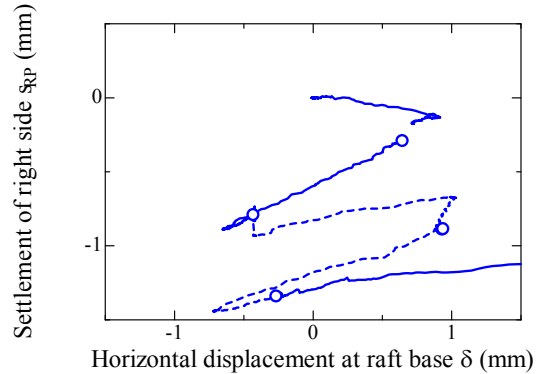
(f) R_H1 (right side)

A. 5.3.2.2 Relationship between horizontal displacement at raft base δ and settlement of righ pile s_{RP} and left pile s_{LP} for heavy case.
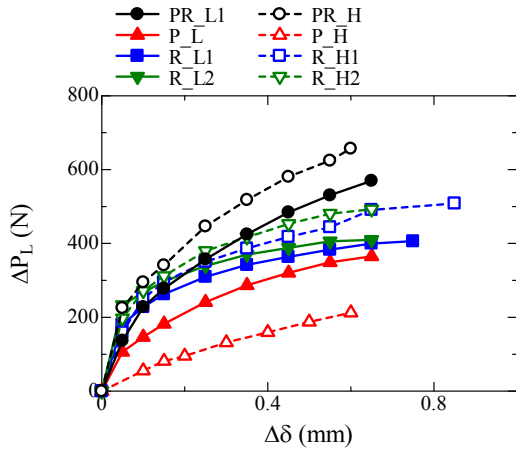
(a) $\delta_{LDT}=\pm 1mm$, h/S=1
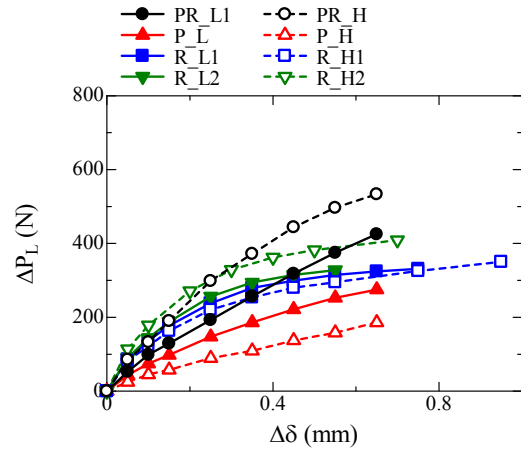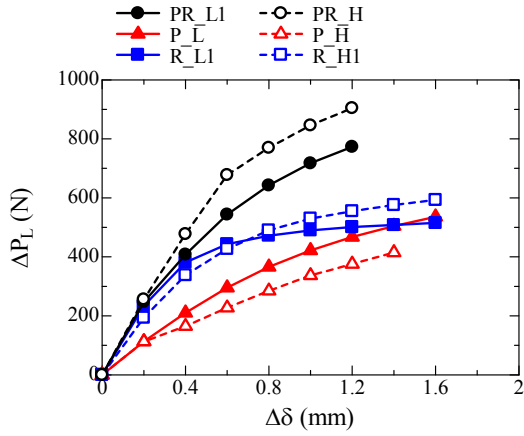
(b) $\delta_{LDT}=\pm 1mm$, h/S=1.8
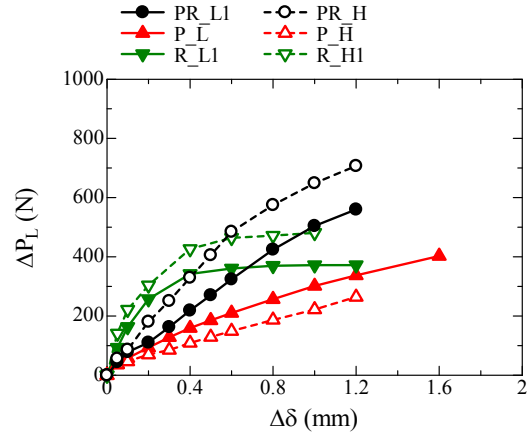
(c) $\delta_{LDT}=\pm 2mm$, h/S=1

(d) $\delta_{LDT}=\pm 2mm$, h/S=1.8

A. 5.4.1.1 Relationship between $\Delta\delta$ and ΔP_L observed in each loading step.

(a) $\delta_{LDT}=\pm1mm$, h/S=1

(b) $\delta_{LDT}=\pm1mm$, h/S=1.8

(c) $\delta_{LDT}=\pm2mm$, h/S=1
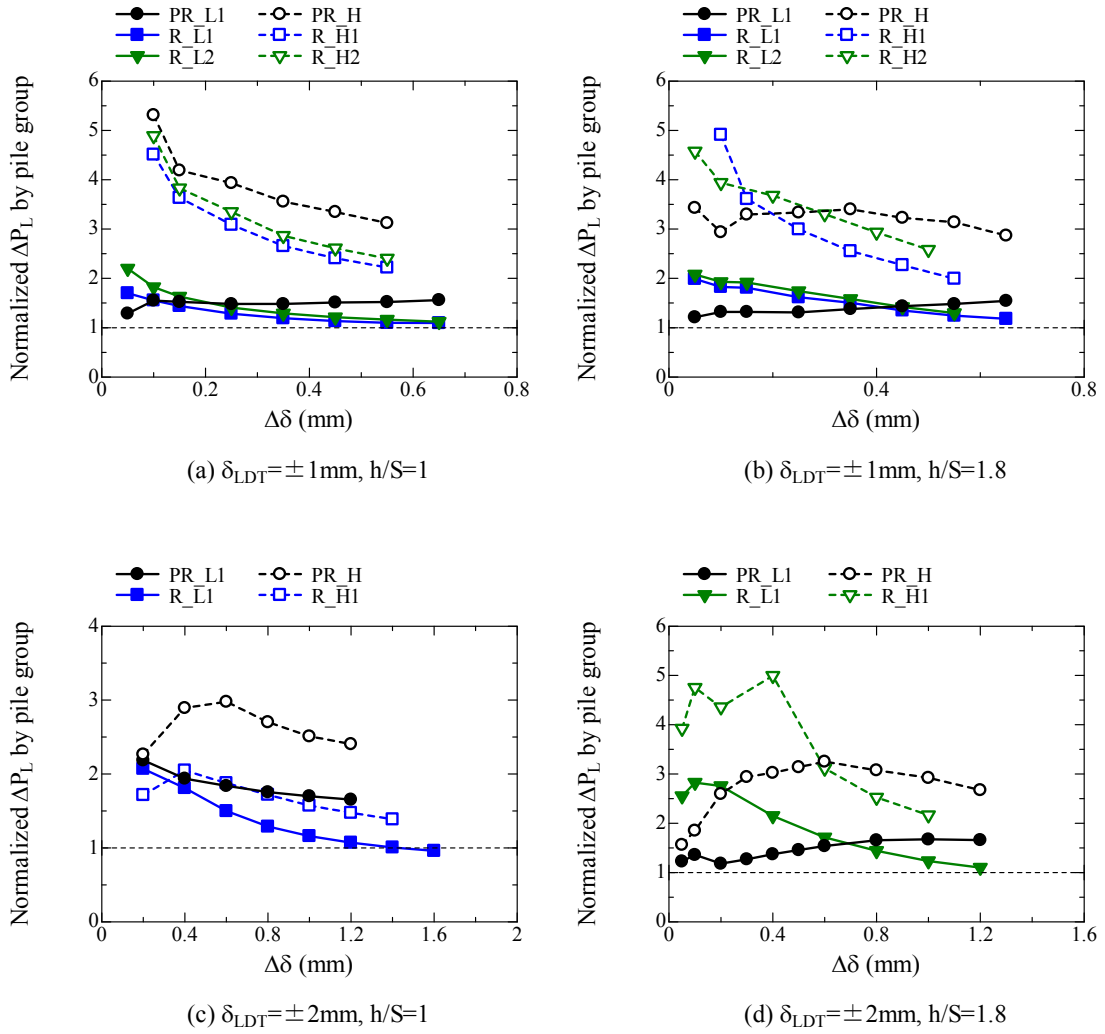
(d) $\delta_{LDT}=\pm2mm$, h/S=1.8

A. 5.4.1.2 Relationship between $\Delta\delta$ and normalized ΔP_L by that of pile group for each loading step.
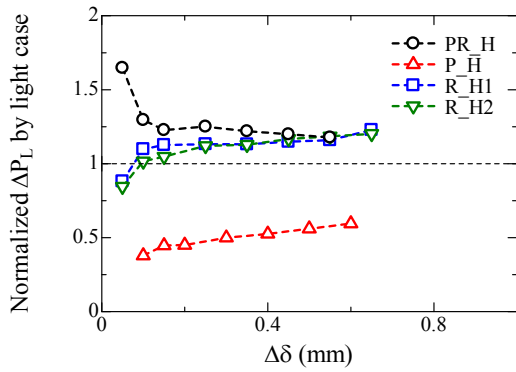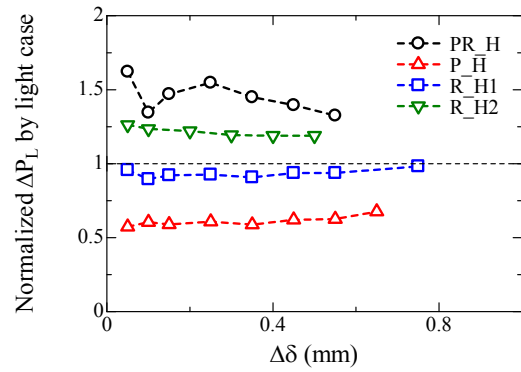
(a) $\delta_{LDT}=\pm 1mm$, h/S=1
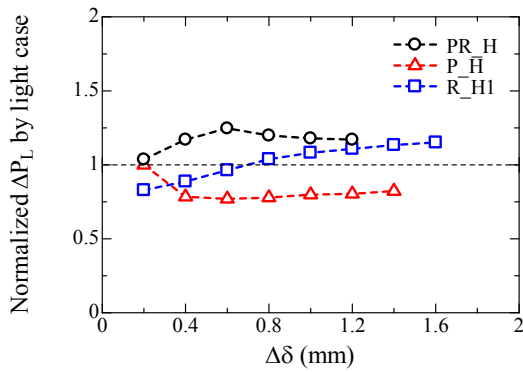
(b) $\delta_{LDT}=\pm 1mm$, h/S=1.8
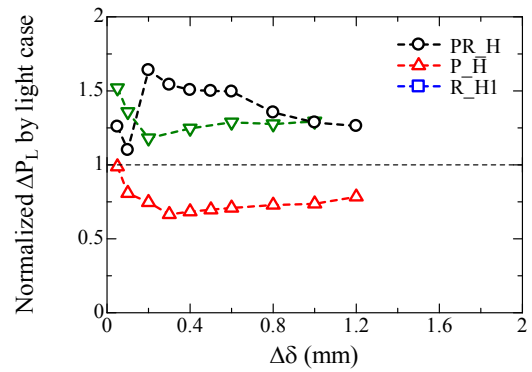
(c) $\delta_{LDT}=\pm 2mm$, h/S=1

(d) $\delta_{LDT}=\pm 2mm$, h/S=1.8

A. 5.4.1.3 Relationship between $\Delta\delta$ and normalized ΔPL of heavy case by that of light case for each loading step.
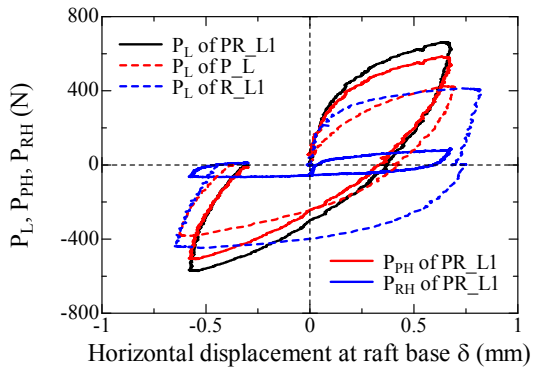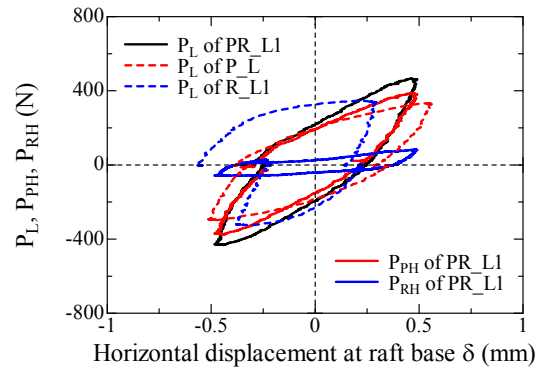
(a) $\delta_{LDT}=\pm 1$mm, h/S=1

(b) $\delta_{LDT}=\pm 1$mm, h/S=1.8
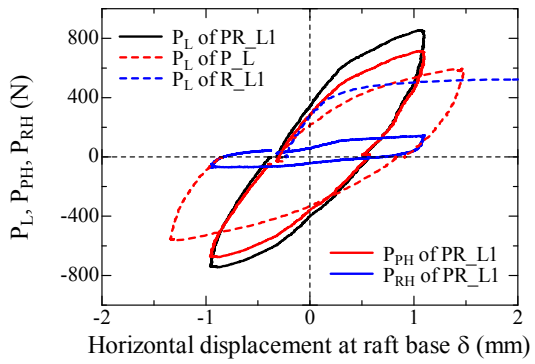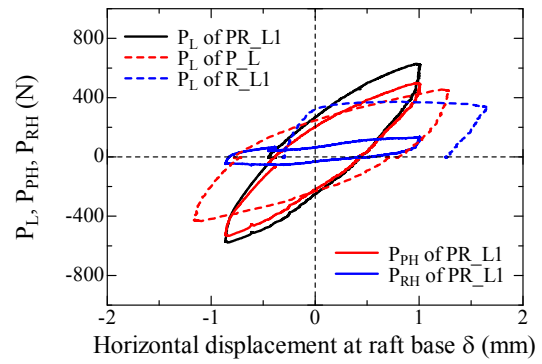
(c) $\delta_{LDT}=\pm 2$mm, h/S=1

(d) $\delta_{LDT}=\pm 2$mm, h/S=1.8

A. 5.4.2.1 Variation of horizontal load P_L and horizontal load carried by raft P_{RH} and piles P_{PH} with horizontal displacement at raft base δ for light case.

(a) $\delta_{LDT}=\pm 1$mm, h/S=1

(b) $\delta_{LDT}=\pm 1$mm, h/S=1.8

(c) $\delta_{LDT}=\pm 2$mm, h/S=1

(d) $\delta_{LDT}=\pm 2$mm, h/S=1.8
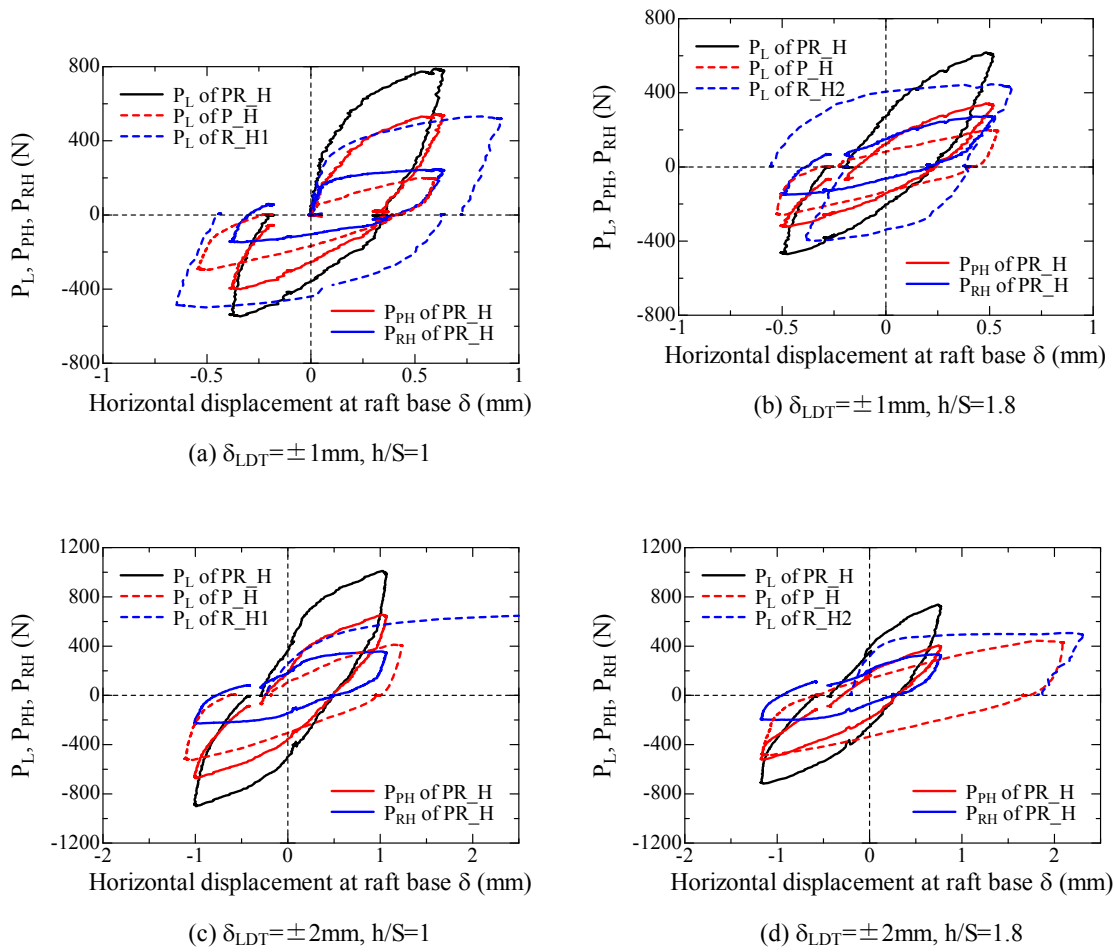
A. 5.4.2.2 Variation of horizontal load P_L and horizontal load carried by raft P_{RH} and piles P_{PH} with horizontal displacement at raft base δ for heavy case.
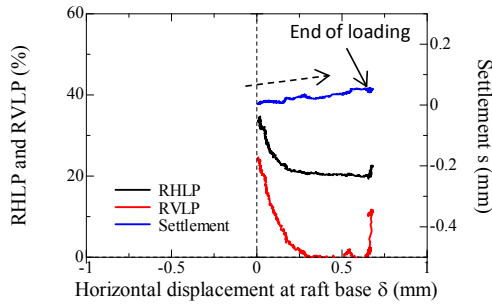
(a) Loading step 1 (δ_{LDT}=+1mm, h/S=1)
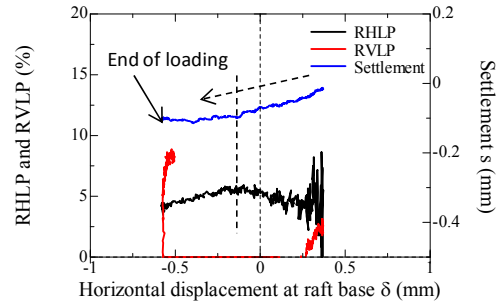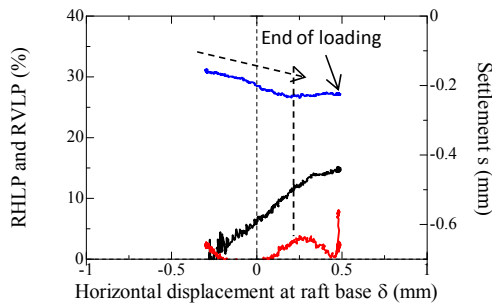
(b) Loading step 2 (δ_{LDT}=-1mm, h/S=1)

(c) Loading step 3 (δ_{LDT}=+1mm, h/S=1.8)
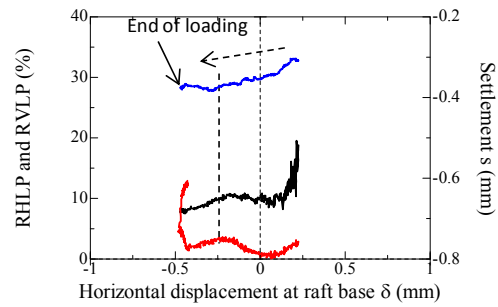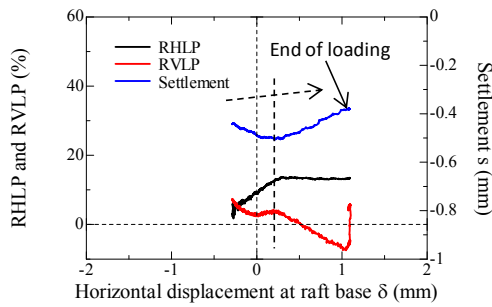
(d) Loading step 4 (δ_{LDT}=-1mm, h/S=1.8)

(e) Loading step 5 (δ_{LDT}=+2mm, h/S=1)
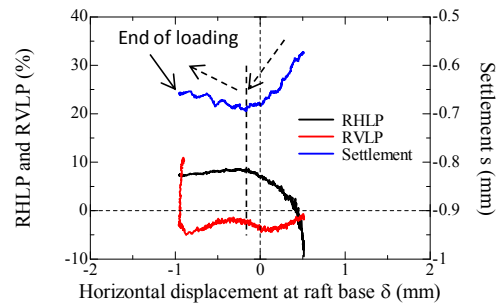
(f) Loading step 6 (δ_{LDT}=-2mm, h/S=1)
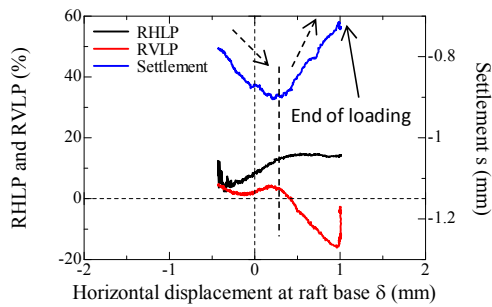
(g) Loading step 7 (δ_{LDT}=+2mm, h/S=1.8)
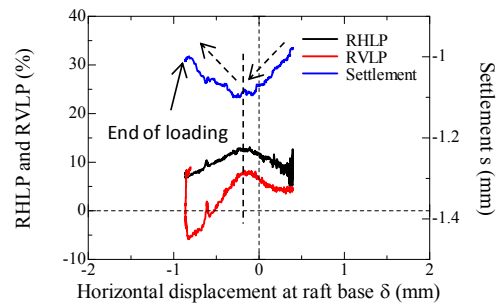
(h) Loading step 8 (δ_{LDT}=-2mm, h/S=1.8)

A. 5.4.2.3 Variation of RHLP, RVLP and settlement s for light case.
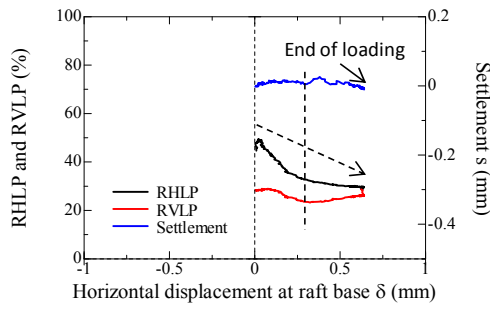
(a) Loading step 1 (δ_{LDT}=+1mm, h/S=1)
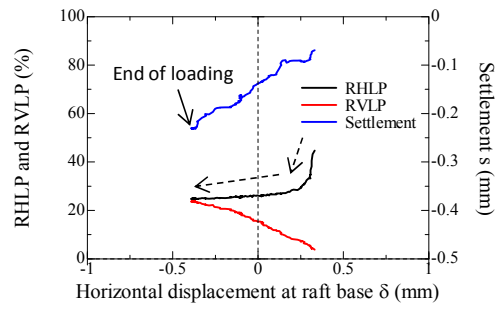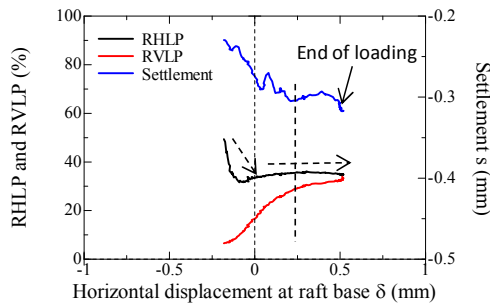
(b) Loading step 2 (δ_{LDT}=-1mm, h/S=1.8)

(c) Loading step 3 (δ_{LDT}=+1mm, h/S=1.8)
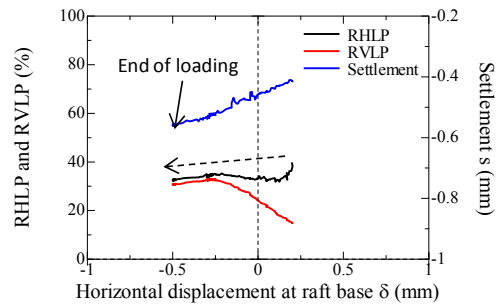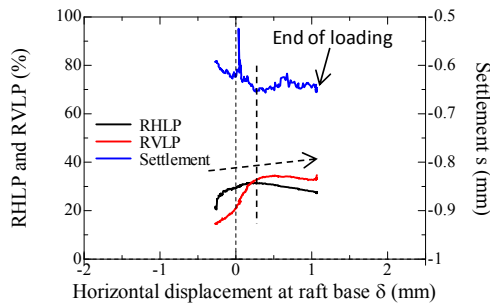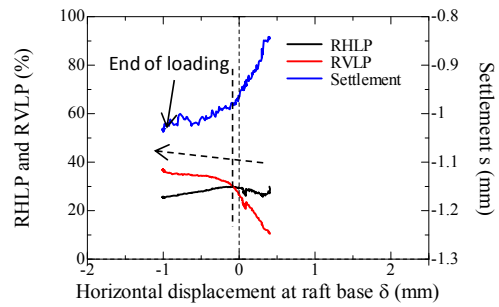
(d) Loading step 4 (δ_{LDT}=-1mm, h/S=1.8)

(e) Loading step 5 (δ_{LDT}=+2mm, h/S=1)

(f) Loading step 6 (δ_{LDT}=-2mm, h/S=1)
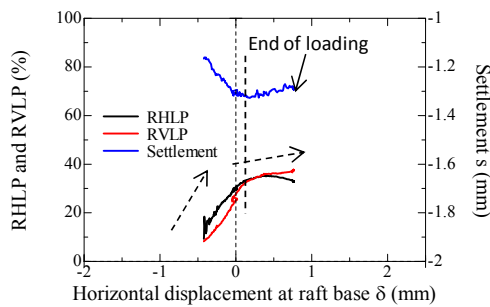
(g) Loading step 7 (δ_{LDT}=+2mm, h/S=1.8)
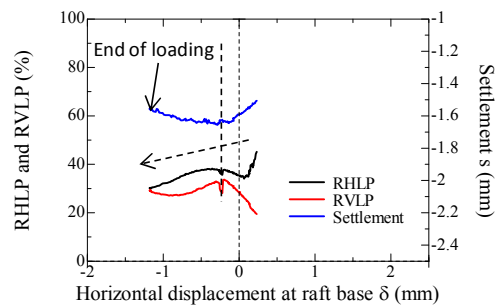
(h) Loading step 8 (δ_{LDT}=-2mm, h/S=1.8)

A. 5.4.2.4 Variation of RHLP, RVLP and settlement s for heavy case.
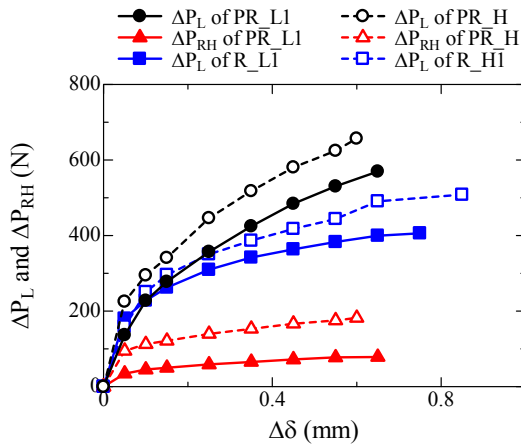
(a) $\delta_{LDT}=\pm 1mm$, h/S=1
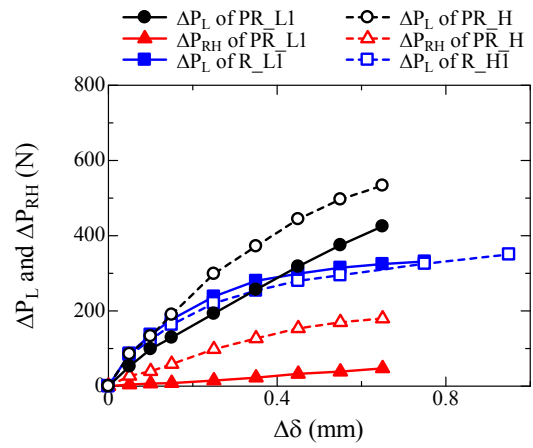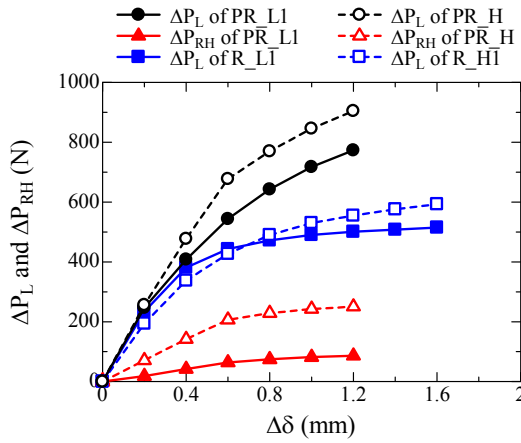
(b) $\delta_{LDT}=\pm 1mm$, h/S=1.8
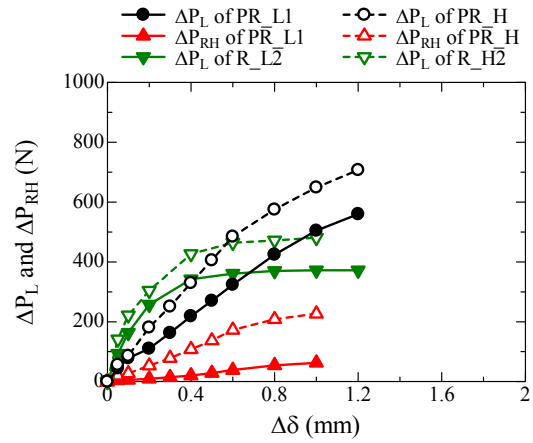
(c) $\delta_{LDT}=\pm 2mm$, h/S=1

(d) $\delta_{LDT}=\pm 2mm$, h/S=1.8

A. 5.4.2.5 Variation of ΔP_L and ΔP_{RH} with $\Delta\delta$ for each loading step..
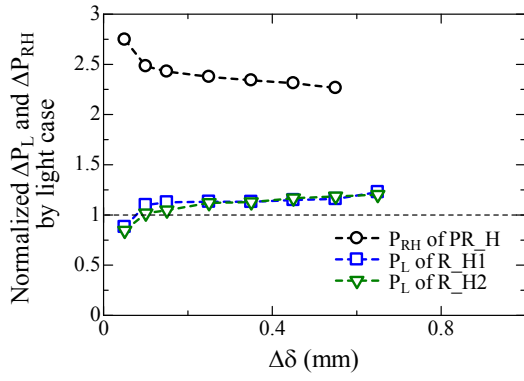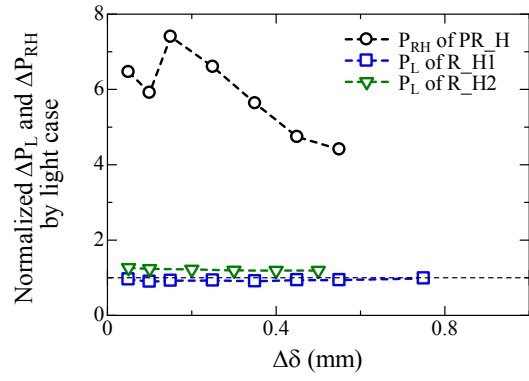
(a) $\delta_{LDT}=\pm 1mm$, h/S=1
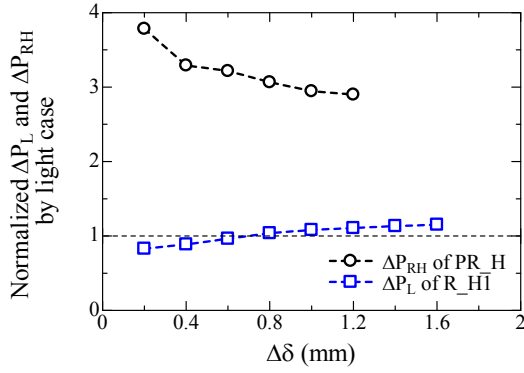
(b) $\delta_{LDT}=\pm 1mm$, h/S=1.8
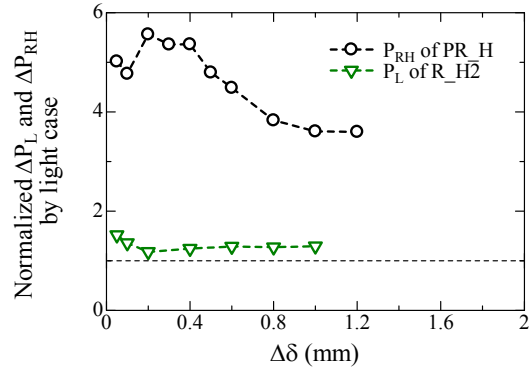
(c) $\delta_{LDT}=\pm 2mm$, h/S=1

(d) $\delta_{LDT}=\pm 2mm$, h/S=1.8

A. 5.4.2.6 Variation of normalized ΔP_L and ΔP_{RH} of heavy case by those of light case with $\Delta\delta$.
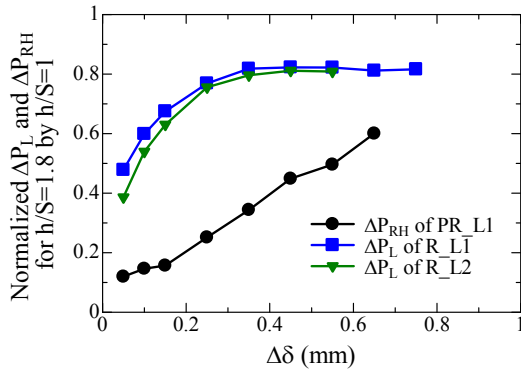
(a) Light case ($\delta_{LDT}=\pm 1$mm)
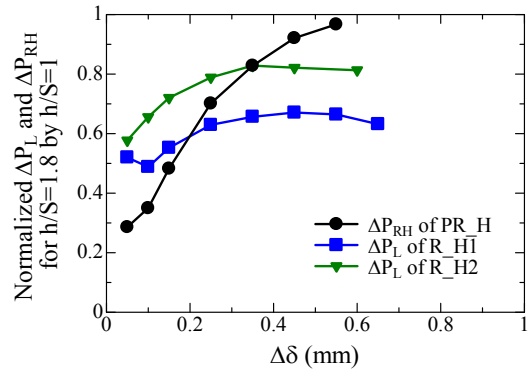
(b) Heavy case ($\delta_{LDT}=\pm 1$mm)
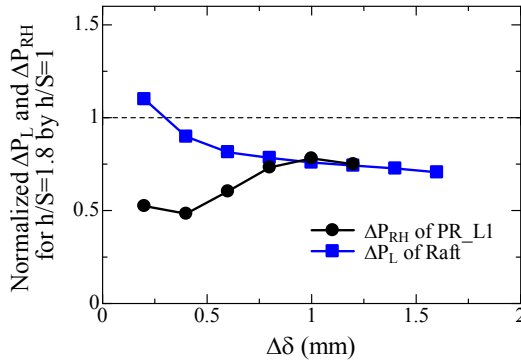
(c) Light case ($\delta_{LDT}=\pm 2$mm)
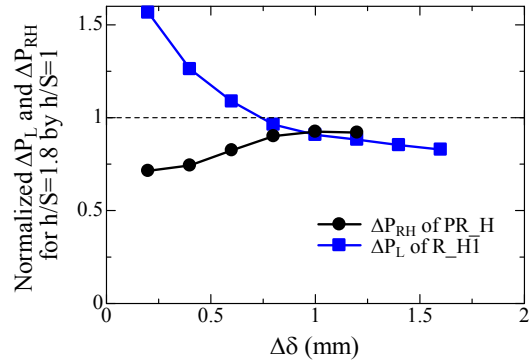
(d) Heavy case ($\delta_{LDT}=\pm 2$mm)

A. 5.4.2.7 Variation of normalized ΔP_L and ΔP_{RH} of heavy case by those of light case with $\Delta\delta$.
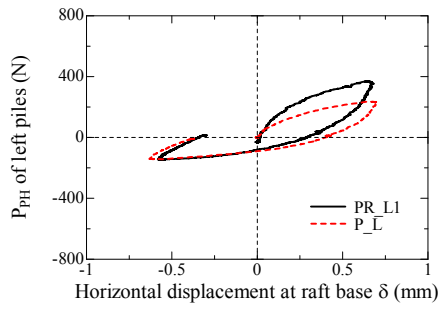
(a) Left piles ($\delta_{LDT}=\pm 1$mm, h/S=1)
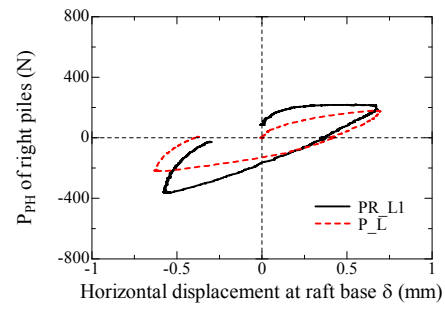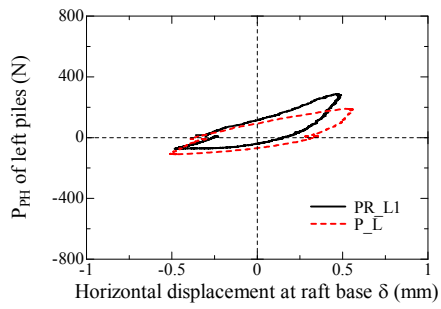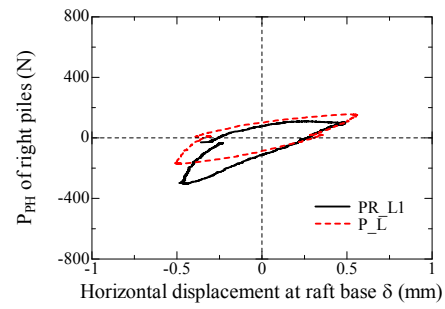
(b) Right piles ($\delta_{LDT}=\pm 1$mm, h/S=1)

(c) Left piles ($\delta_{LDT}=\pm 1$mm, h/S=1.8)

(d) Right piles ($\delta_{LDT}=\pm 1$mm, h/S=1.8)
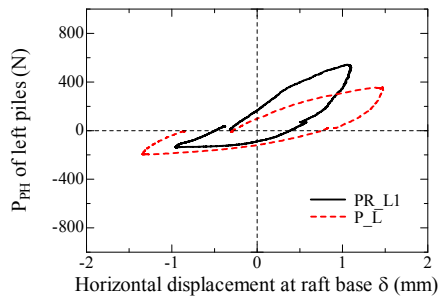
(e) Left piles ($\delta_{LDT}=\pm 2$mm, h/S=1)
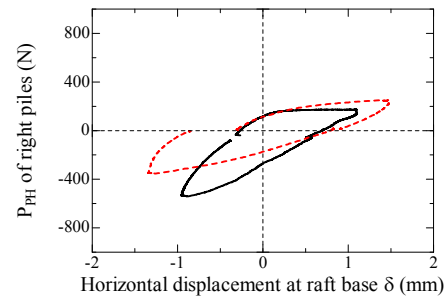
(f) Right piles ($\delta_{LDT}=\pm 2$mm, h/S=1)
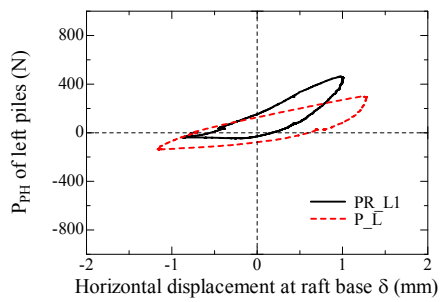
(g) Left piles ($\delta_{LDT}=\pm 2$mm, h/S=1.8)
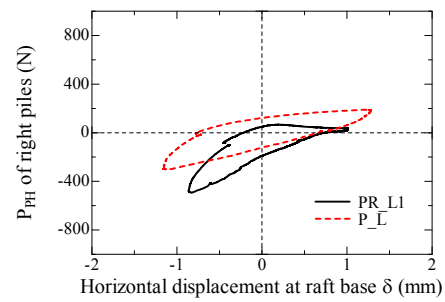
(h) Right piles ($\delta_{LDT}=\pm 2$mm, h/S=1.8)

A. 5.4.3.1 Relationship between horizontal displacement at raft base δ and horizontal load carried by pile part P_{PH} for light case.

A102
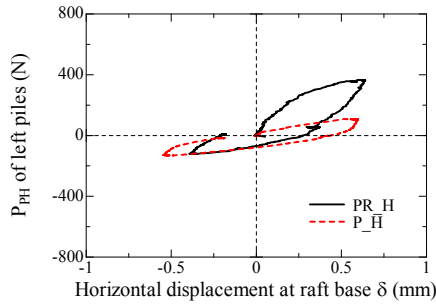
(a) Left piles ($\delta_{LDT}=\pm1$mm, h/S=1)
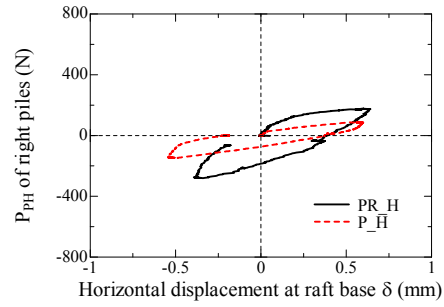
(b) Right piles ($\delta_{LDT}=\pm1$mm, h/S=1)
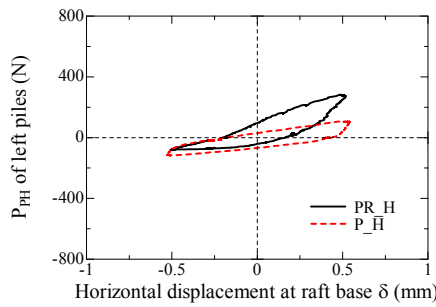
(c) Left piles ($\delta_{LDT}=\pm1$mm, h/S=1.8)
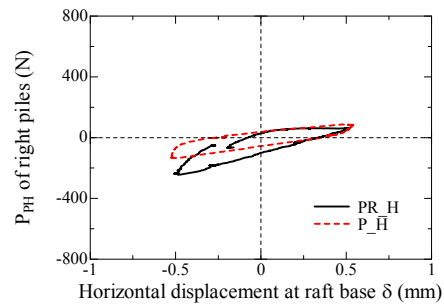
(d) Right piles ($\delta_{LDT}=\pm1$mm, h/S=1.8)
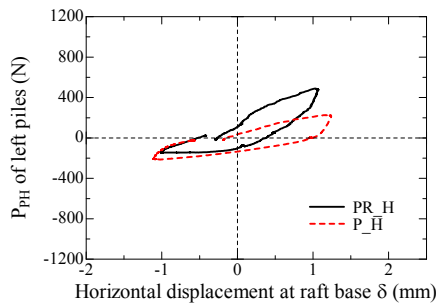
(e) Left piles ($\delta_{LDT}=\pm2$mm, h/S=1)
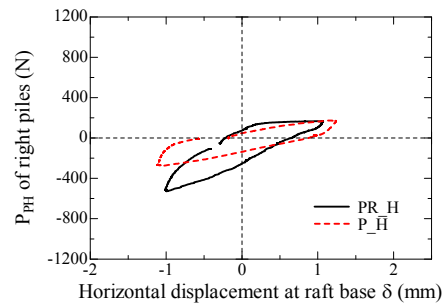
(f) Right piles ($\delta_{LDT}=\pm2$mm, h/S=1)
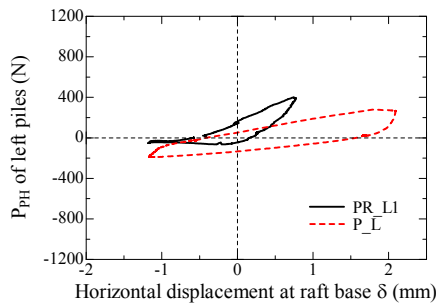
(g) Left piles ($\delta_{LDT}=\pm2$mm, h/S=1.8)
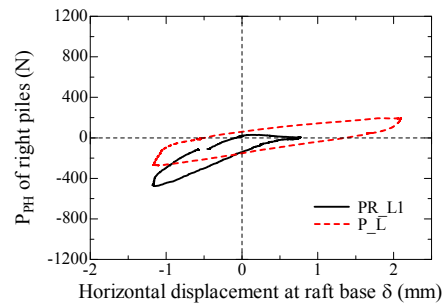
(h) Right piles ($\delta_{LDT}=\pm2$mm, h/S=1.8)

A. 5.4.3.2 Relationship between horizontal displacement at raft base δ and horizontal load carried by pile part P_{PH} for heavy case.
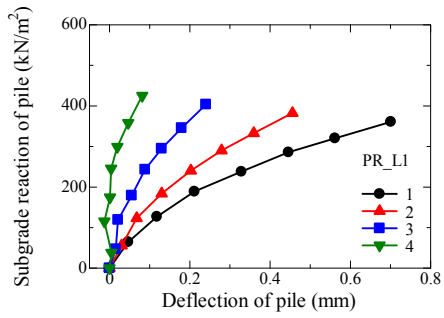
(a) Push-in pile ($\delta_{LDT}=\pm 1mm$, h/S=1)
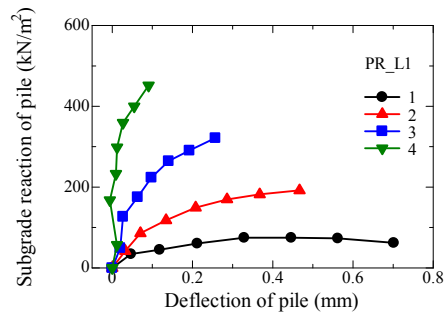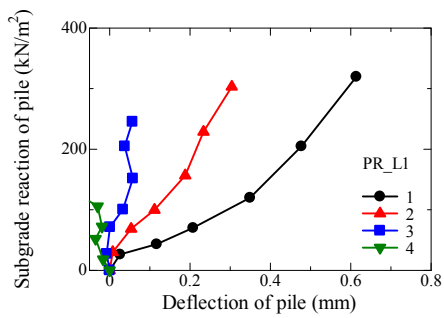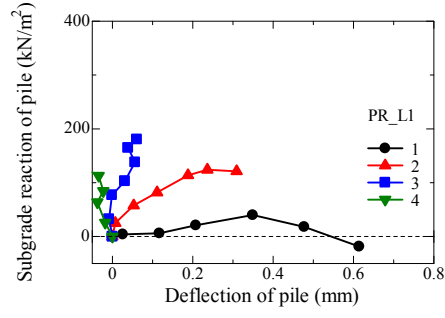
(b) Pull-out pile ($\delta_{LDT}=\pm 1mm$, h/S=1)

(c) Push-in pile ($\delta_{LDT}=\pm 1mm$, h/S=1.8)

(d) Pull-out pile ($\delta_{LDT}=\pm 1mm$, h/S=1.8)
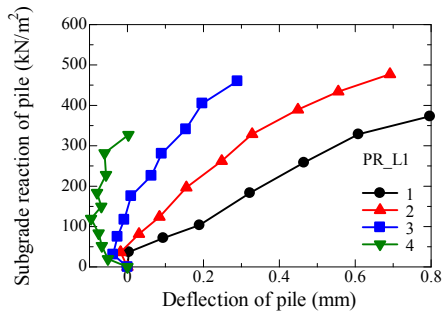
(e) Push-in pile ($\delta_{LDT}=\pm 2mm$, h/S=1)
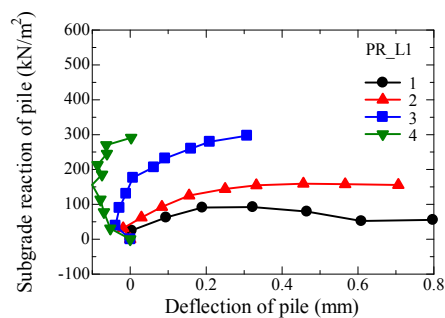
(f) Pull-out pile ($\delta_{LDT}=\pm 2mm$, h/S=1)
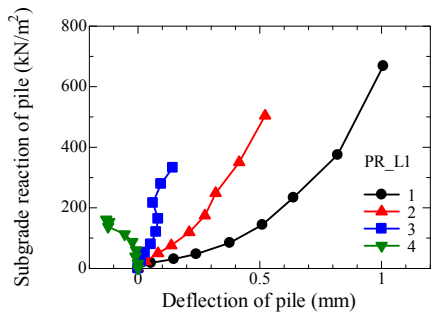
(g) Push-in pile ($\delta_{LDT}=\pm 2mm$, h/S=1.8)
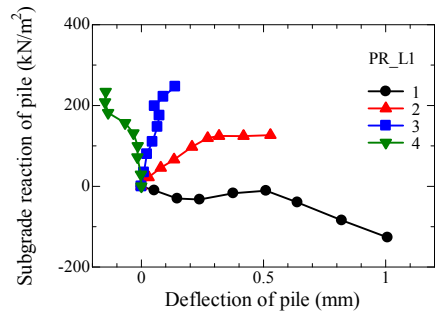
(h) Pull-out pile ($\delta_{LDT}=\pm 2mm$, h/S=1.8)

A. 5.4.3.3 Relationship between pile deflection and subgrade reaction of pile for PR_L1.
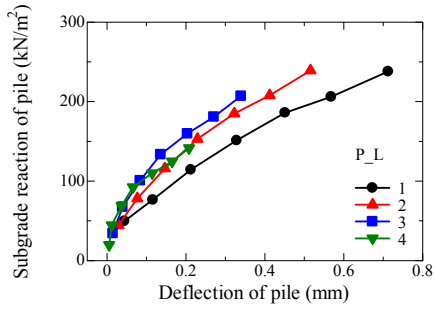
(a) Push-in pile ($\delta_{LDT}=\pm 1$mm, h/S=1)
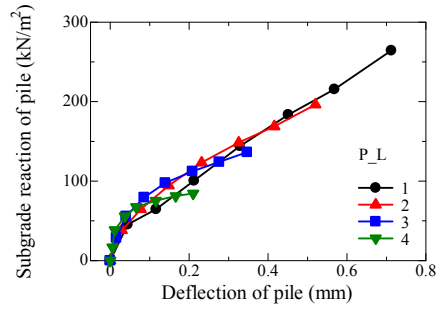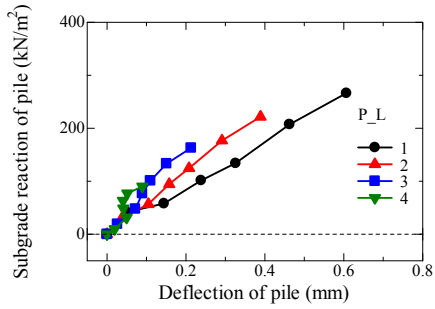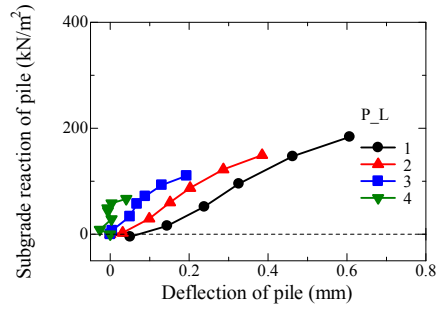
(b) Pull-out pile ($\delta_{LDT}=\pm 1$mm, h/S=1)

(c) Push-in pile ($\delta_{LDT}=\pm 1$mm, h/S=1.8)

(d) Pull-out pile ($\delta_{LDT}=\pm 1$mm, h/S=1.8)
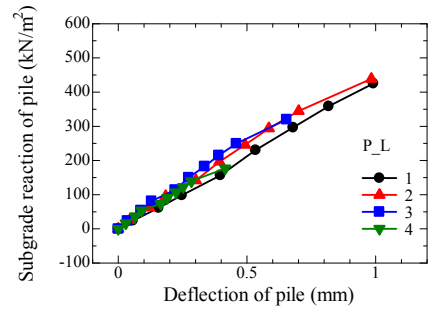
(e) Push-in pile ($\delta_{LDT}=\pm 2$mm, h/S=1)
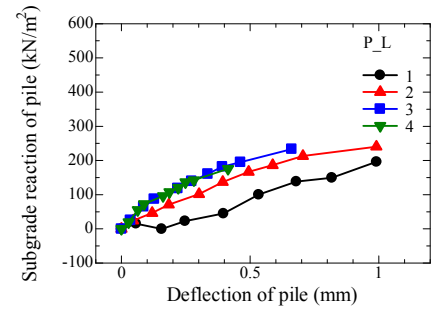
(f) Pull-out pile ($\delta_{LDT}=\pm 2$mm, h/S=1)
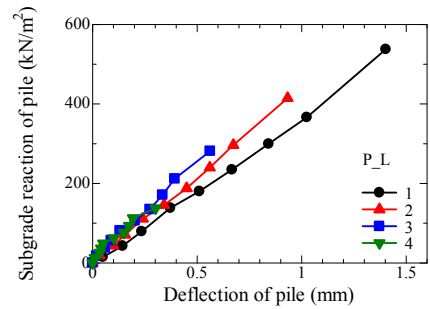
(g) Push-in pile ($\delta_{LDT}=\pm 2$mm, h/S=1.8)
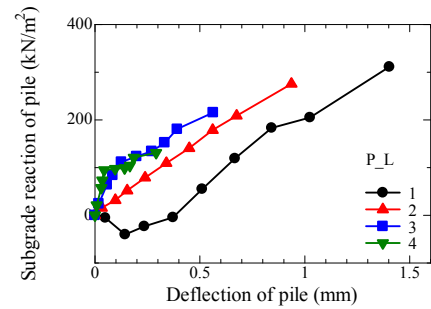
(h) Pull-out pile ($\delta_{LDT}=\pm 2$mm, h/S=1.8)

A. 5.4.3.4 Relationship between pile deflection and subgrade reaction of pile for P_L.
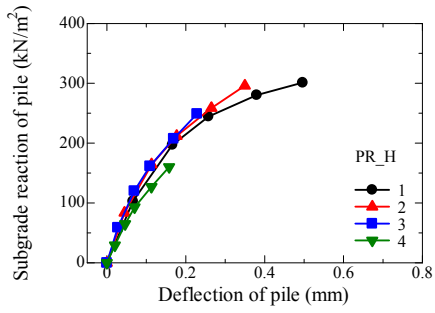
(a) Push-in pile ($\delta_{LDT}=\pm 1$mm, h/S=1)
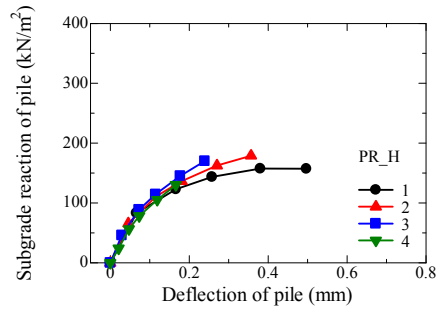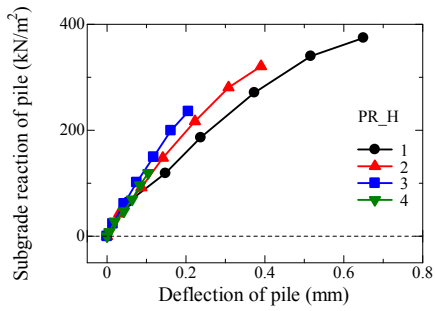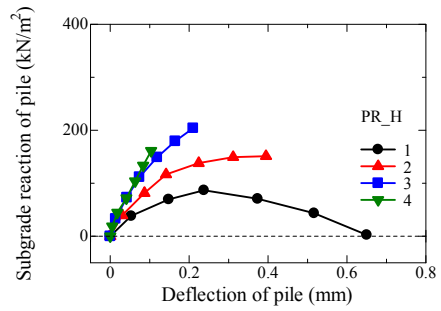
(b) Pull-out pile ($\delta_{LDT}=\pm 1$mm, h/S=1)

(c) Push-in pile ($\delta_{LDT}=\pm 1$mm, h/S=1.8)

(d) Pull-out pile ($\delta_{LDT}=\pm 1$mm, h/S=1.8)
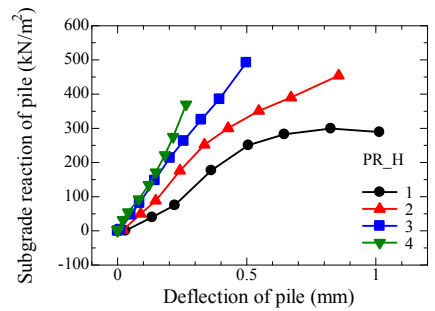
(e) Push-in pile ($\delta_{LDT}=\pm 2$mm, h/S=1)
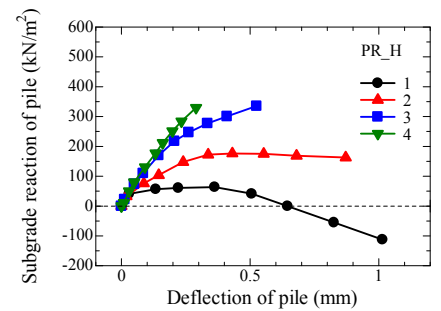
(f) Pull-out pile ($\delta_{LDT}=\pm 2$mm, h/S=1)
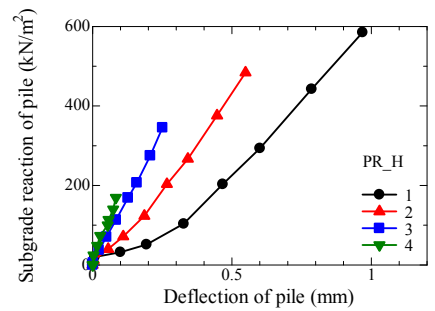
(g) Push-in pile ($\delta_{LDT}=\pm 2$mm, h/S=1.8)
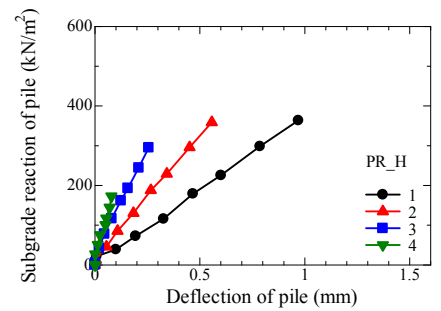
(h) Pull-out pile ($\delta_{LDT}=\pm 2$mm, h/S=1.8)

A. 5.4.3.5 Relationship between pile deflection and subgrade reaction of pile for PR_H.
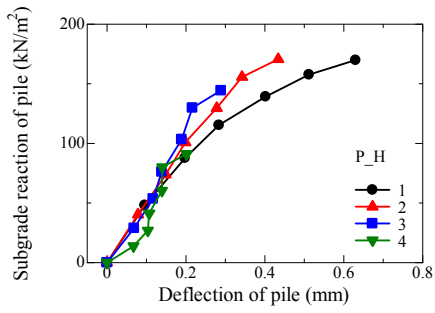
A106

(a) Push-in pile ($\delta_{LDT}=\pm 1$mm, h/S=1)
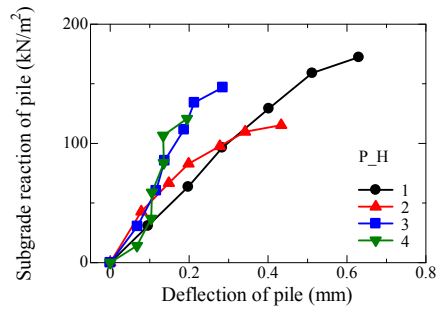
(b) Pull-out pile ($\delta_{LDT}=\pm 1$mm, h/S=1)
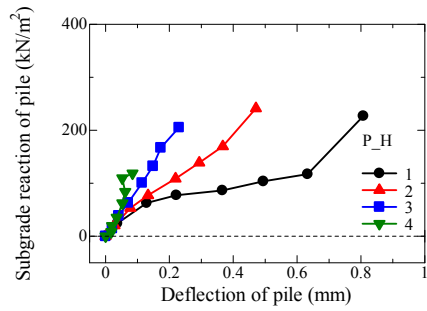
(c) Push-in pile ($\delta_{LDT}=\pm 1$mm, h/S=1.8)
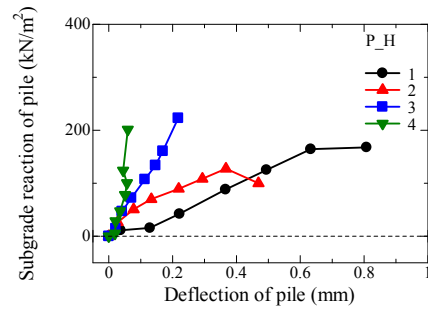
(d) Pull-out pile ($\delta_{LDT}=\pm 1$mm, h/S=1.8)
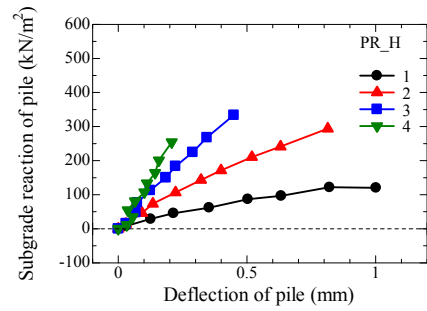
(e) Push-in pile ($\delta_{LDT}=\pm 2$mm, h/S=1)
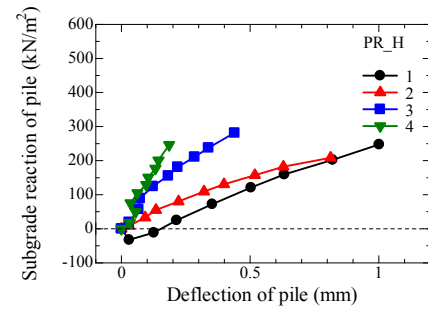
(f) Pull-out pile ($\delta_{LDT}=\pm 2$mm, h/S=1)
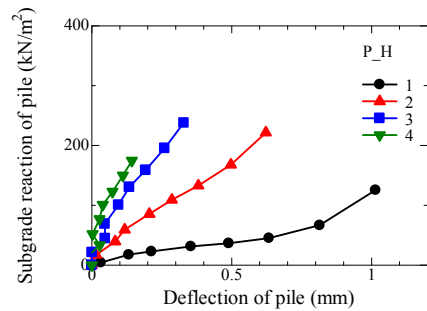
(g) Push-in pile ($\delta_{LDT}=\pm 2$mm, h/S=1.8)
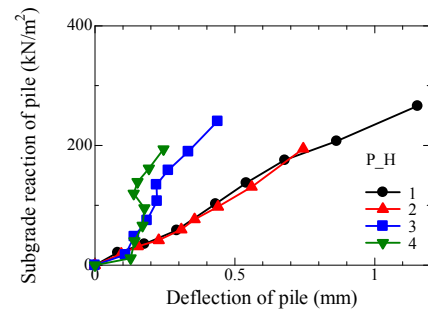
(h) Pull-out pile ($\delta_{LDT}=\pm 2$mm, h/S=1.8)

A. 5.4.3.6 Relationship between pile deflection and subgrade reaction of pile for P_H.
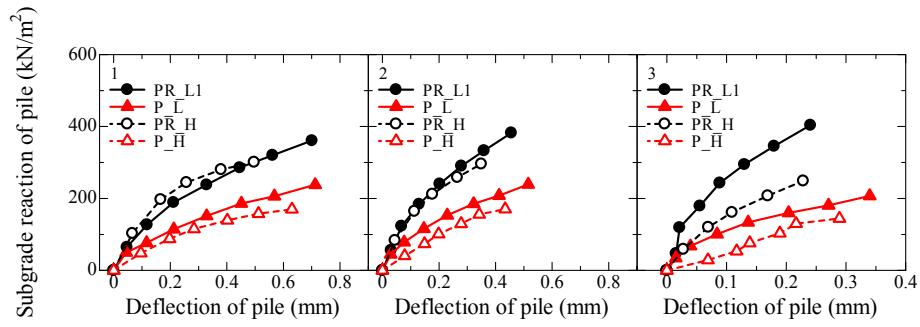
(a) Push-in pile ($\delta_{LDT}=\pm 1$mm, h/S=1)
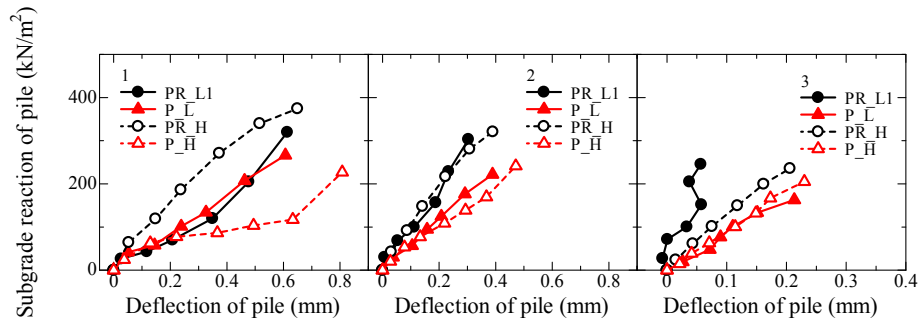
(b) Push-in pile ($\delta_{LDT}=\pm 1$mm, h/S=1.8)
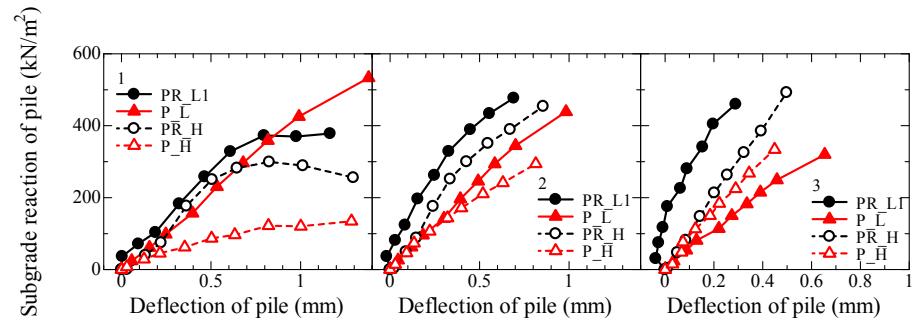
(c) Push-in pile ($\delta_{LDT}=\pm 2$mm, h/S=1)
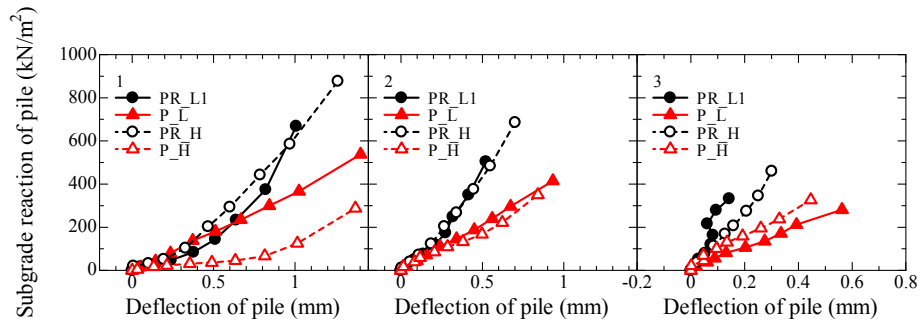
(d) Push-in pile ($\delta_{LDT}=\pm 2$mm, h/S=1.8)

A. 5.4.3.7 Relationship between pile deflection and horizontal subgrade reaction of push-in pile at depth of 1, 2 and 3.
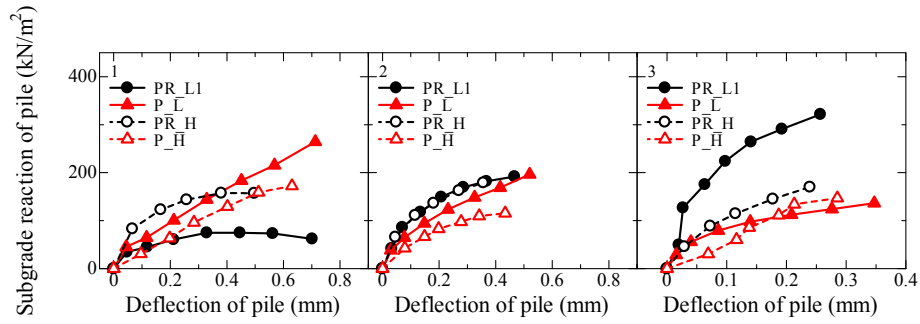
(a) Pull-out pile ($\delta_{LDT}=\pm1$mm, h/S=1)
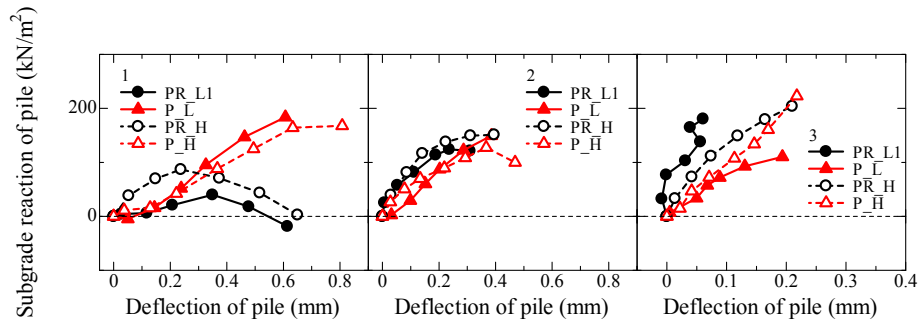
(b) Pull-out pile ($\delta_{LDT}=\pm1$mm, h/S=1.8)
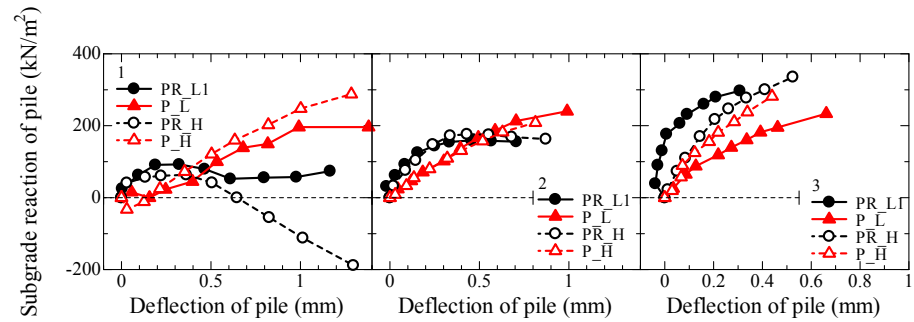
(c) Pull-out pile ($\delta_{LDT}=\pm2$mm, h/S=1)
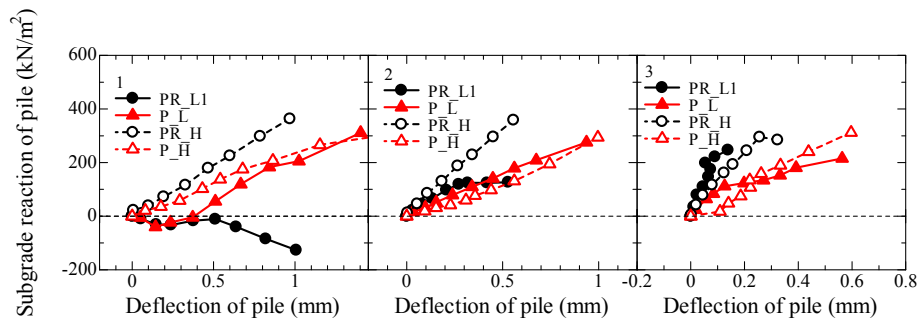
(d) Pull-out pile ($\delta_{LDT}=\pm2$mm, h/S=1.8)

A. 5.4.3.8 Relationship between pile deflection and horizontal subgrade reaction of pull-out pile at depth of 1, 2 and 3.
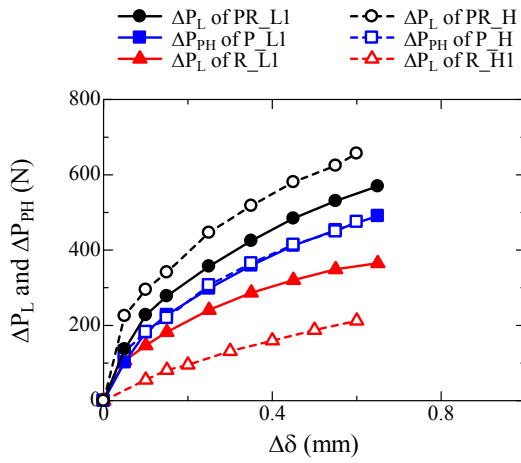
(a) $\delta_{LDT}=\pm 1$mm, h/S=1
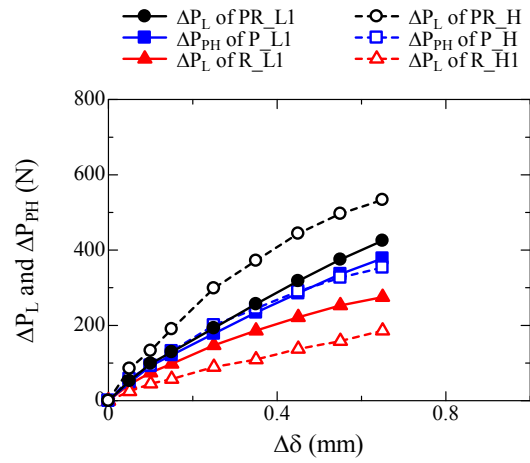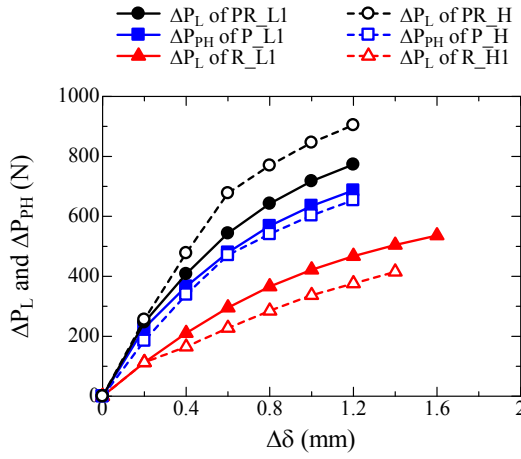
(b) $\delta_{LDT}=\pm 1$mm, h/S=1.8
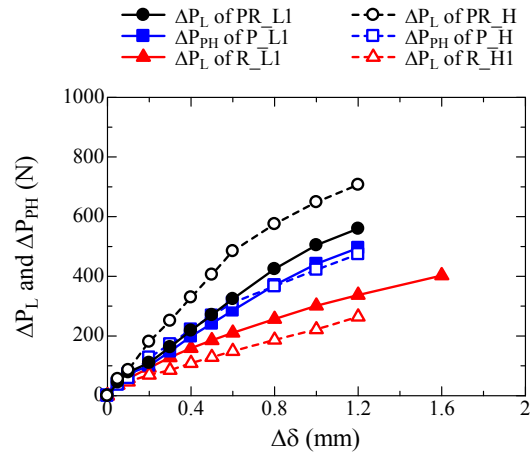
(c) $\delta_{LDT}=\pm 2$mm, h/S=1

(d) $\delta_{LDT}=\pm 2$mm, h/S=1.8

A. 5.4.2.9 Variation of ΔP_L and ΔP_{PH} with $\Delta\delta$ for each loading step.
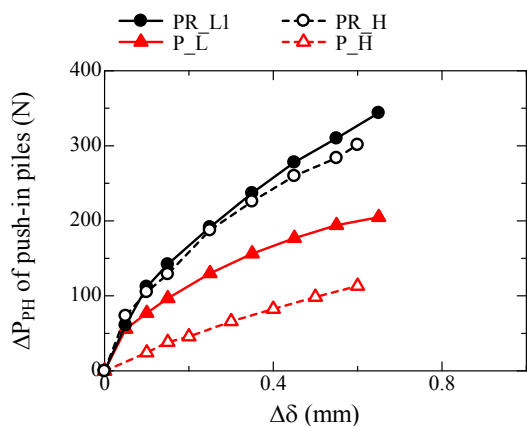
(a) Push-in piles ($\delta_{LDT}=\pm 1mm$, h/S=1)
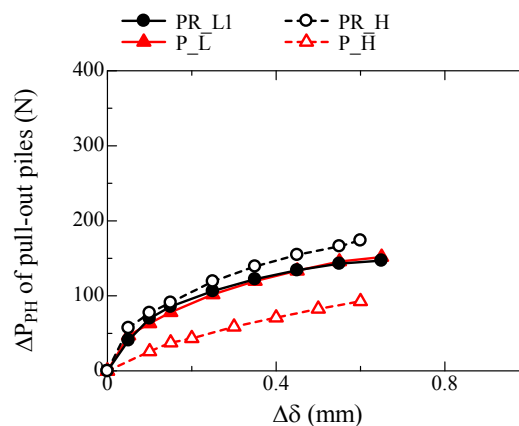
(b) Pull-out piles ($\delta_{LDT}=\pm 1mm$, h/S=1)
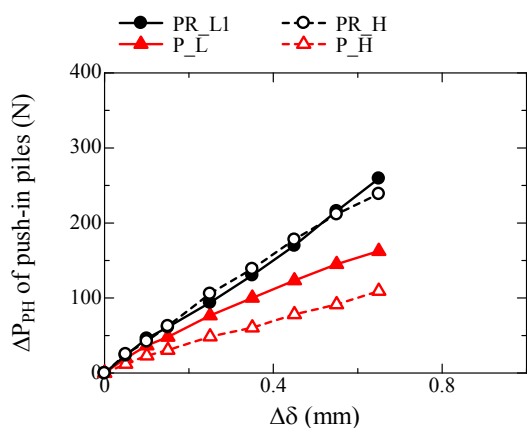
(c) Push-in piles ($\delta_{LDT}=\pm 1mm$, h/S=1.8)
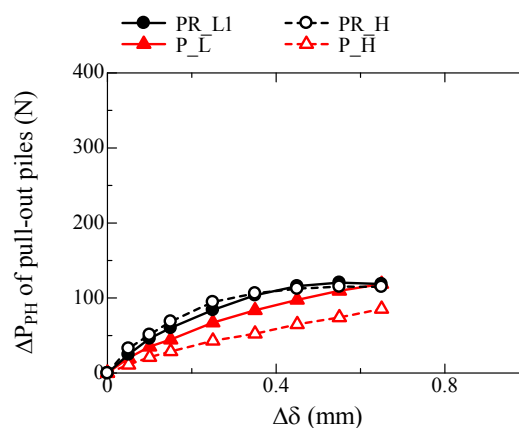
(d) Pull-out piles ($\delta_{LDT}=\pm 1mm$, h/S=1.8)
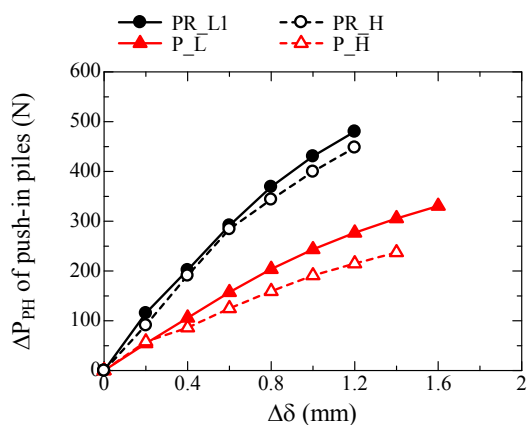
(e) Push-in piles ($\delta_{LDT}=\pm 2mm$, h/S=1)
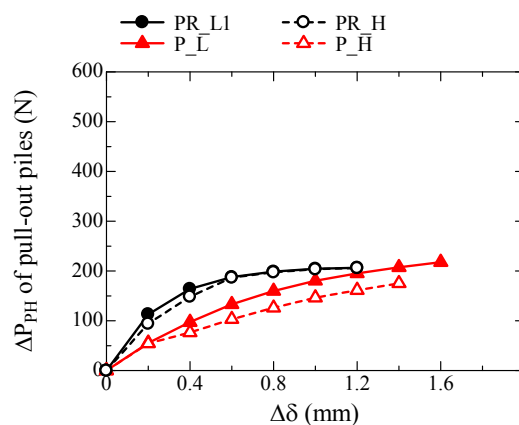
(f) Pull-out piles ($\delta_{LDT}=\pm 2mm$, h/S=1)

A. 5.4.2.10 Relationship ΔP_{PH} of push-in and pull-out piles with $\Delta\delta$ for each loading step.
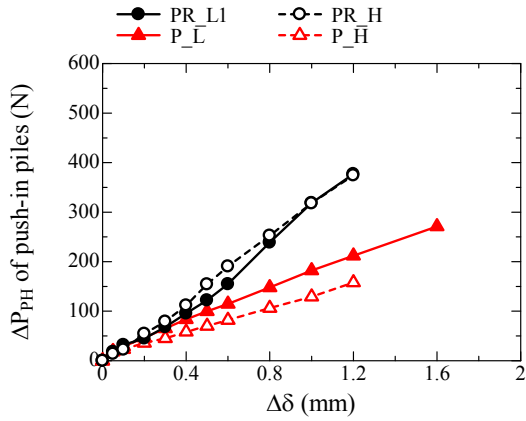
(g) Push-in piles ($\delta_{LDT}=\pm2$mm, h/S=1.8)
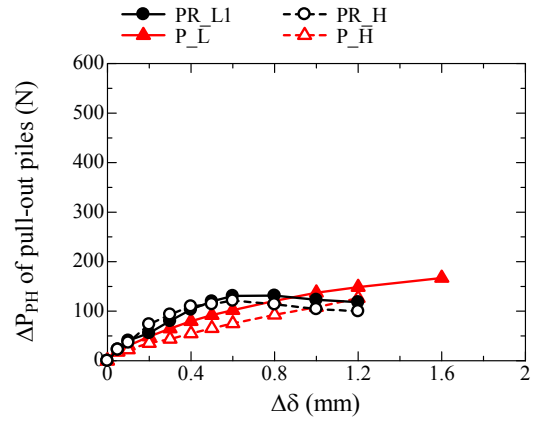
(h) Pull-out piles ($\delta_{LDT}=\pm2$mm, h/S=1.8)

A. 5.4.2.10 Relationship ΔP_{PH} of push-in and pull-out piles with $\Delta\delta$ for each loading step.
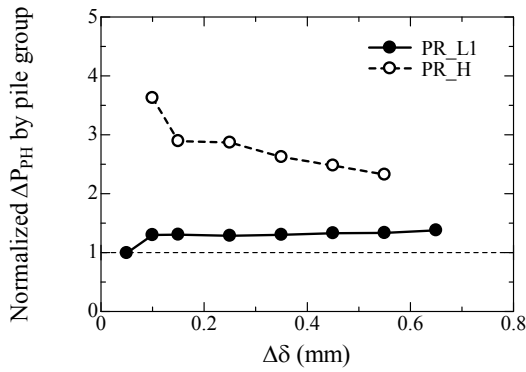
(a) All piles ($\delta_{LDT}=\pm1$mm, h/S=1)
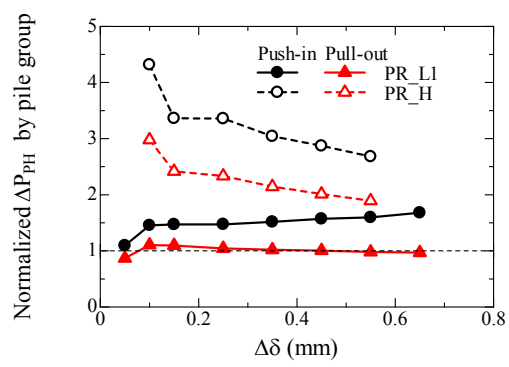
(b) Push-in & pull-out piles ($\delta_{LDT}=\pm1$mm, h/S=1)
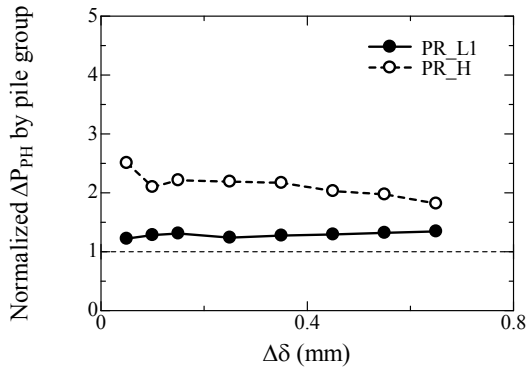
(c) All piles ($\delta_{LDT}=\pm1$mm, h/S=1.8)
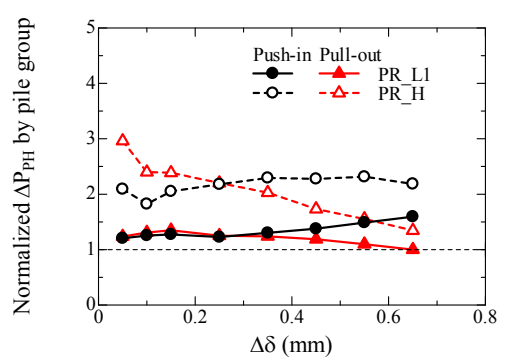
(d) Push-in & pull-out piles ($\delta_{LDT}=\pm1$mm, h/S=1.8)

A. 5.4.2.11 Relationship between $\Delta\delta$ and normalized ΔP_{PH} by that of pile group.
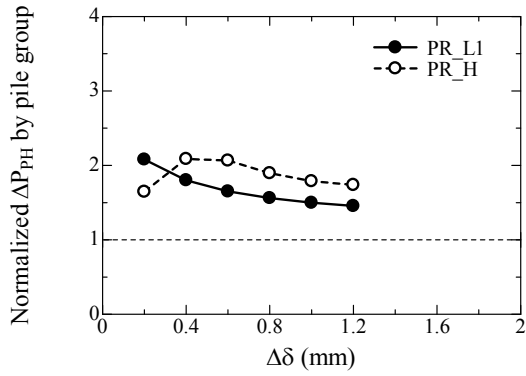
(e) All piles ($\delta_{LDT}=\pm 2mm$, h/S=1)
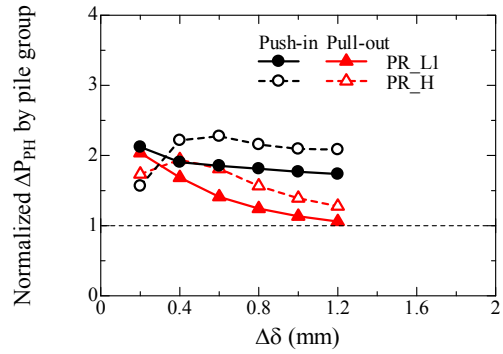
(f) Push-in & pull-out piles ($\delta_{LDT}=\pm 2mm$, h/S=1)
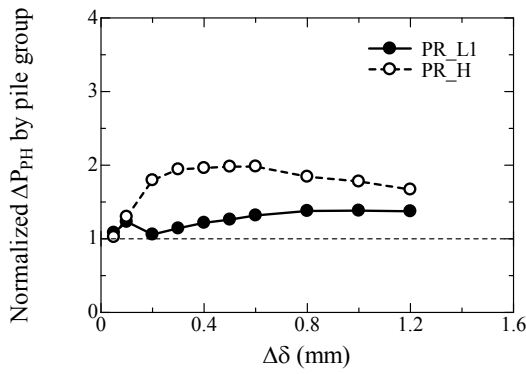
(g) All piles ($\delta_{LDT}=\pm 2mm$, h/S=1.8)
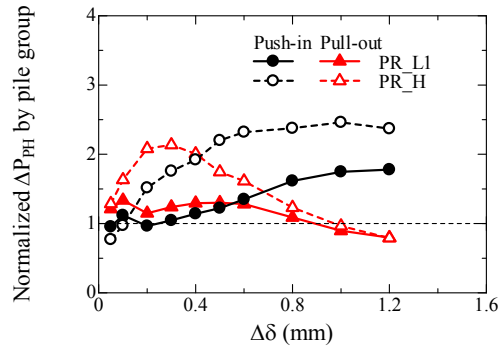
(h) Push-in & pull-out piles ($\delta_{LDT}=\pm 2mm$, h/S=1.8)

A. 5.4.2.11 Relationship between $\Delta\delta$ and normalized ΔP_{PH} by that of pile group.
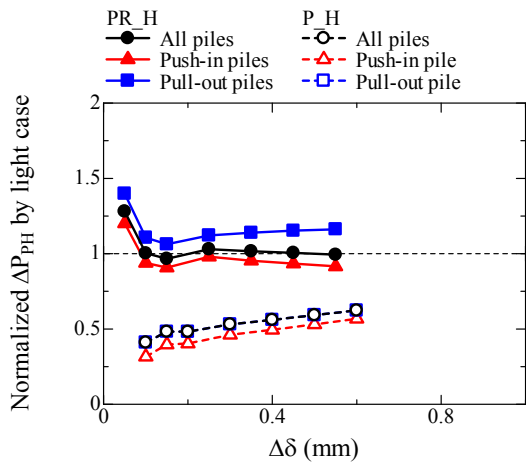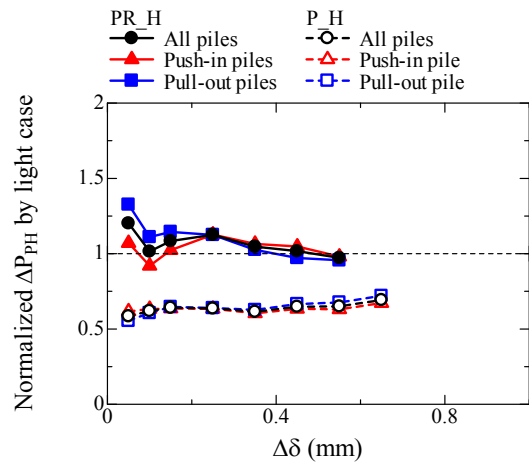
(a) $\delta_{LDT}=\pm 1mm$, h/S=1

(b) $\delta_{LDT}=\pm 1mm$, h/S=1.8
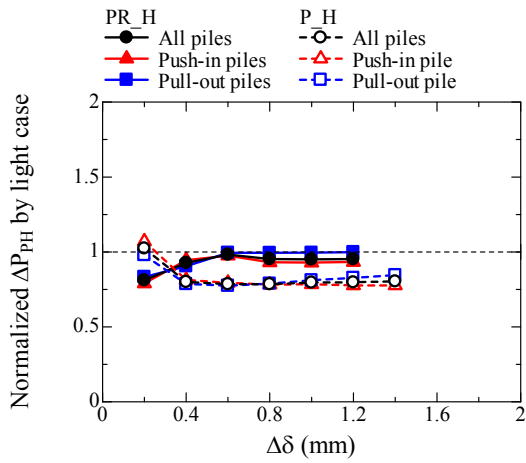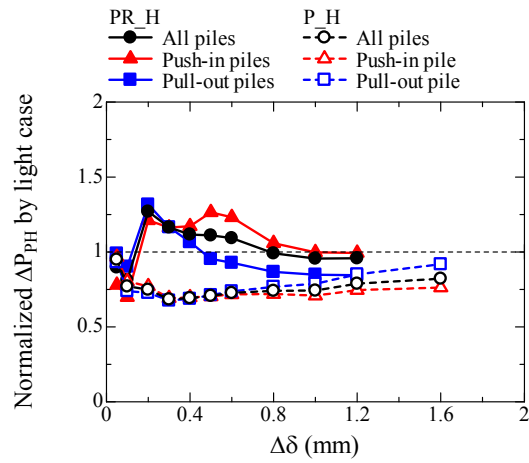
(c) $\delta_{LDT}=\pm 2mm$, h/S=1

(d) $\delta_{LDT}=\pm 2mm$, h/S=1.8

A. 5.4.2.12 Relationship between $\Delta\delta$ and normalized ΔP_{PH} of heavy case by that of light case
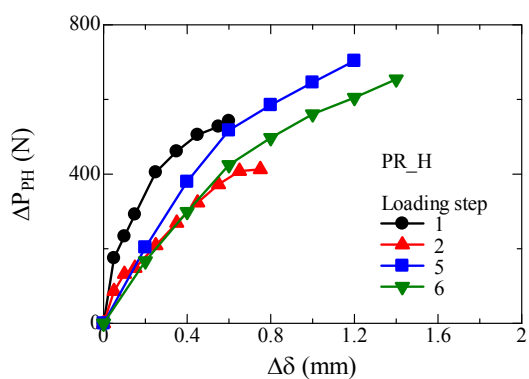
(a) All piles (h/S=1)
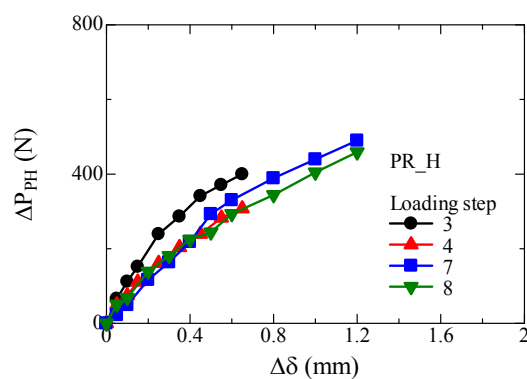
(b) All piles (h/S=1.8)
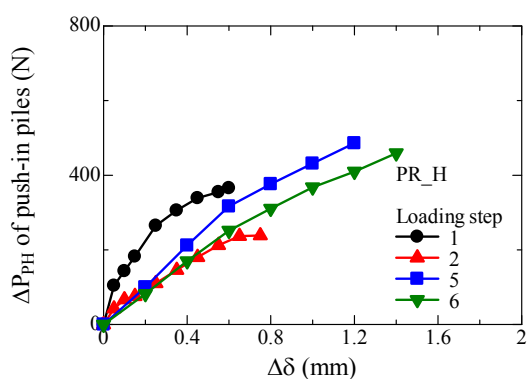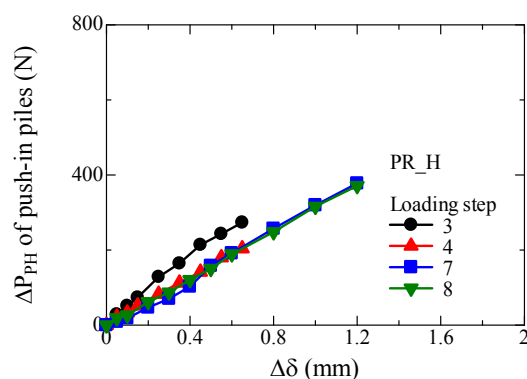
(c) Push-in piles (h/S=1)
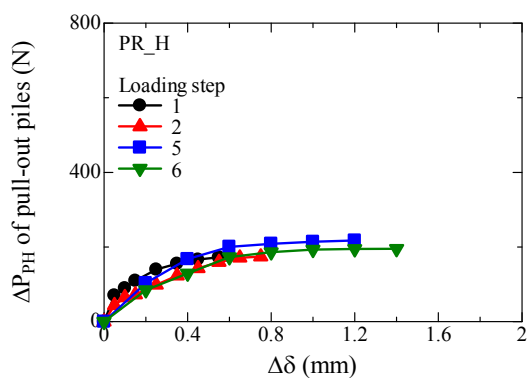
(d) Push-in piles (h/S=1.8)
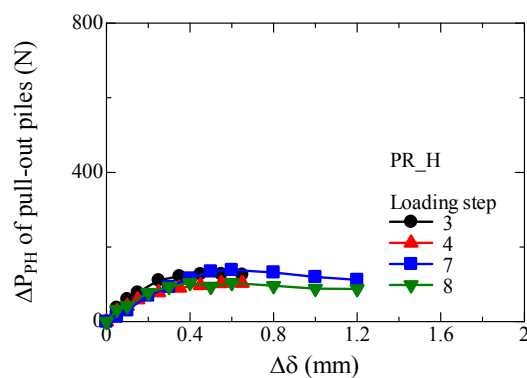
(e) Pull-out piles (h/S=1)

(f) Pull-out piles (h/S=1.8)

A. 5.4.2.13 Relationship ΔP_{PH} of push-in and pull-out piles with $\Delta\delta$ for each loading step (PR_H).
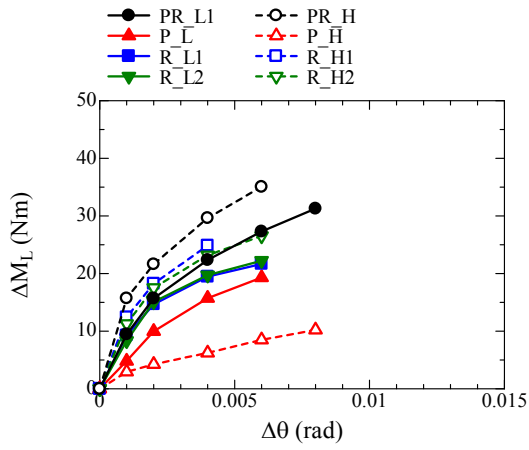
(a) $\delta_{LDT}=\pm 1$mm, h/S=1
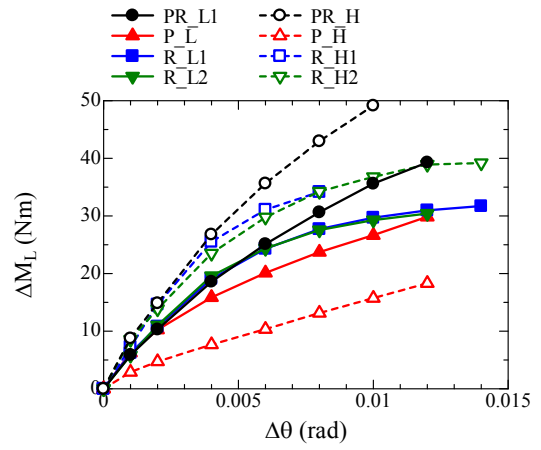
(b) $\delta_{LDT}=\pm 1$mm, h/S=1.8
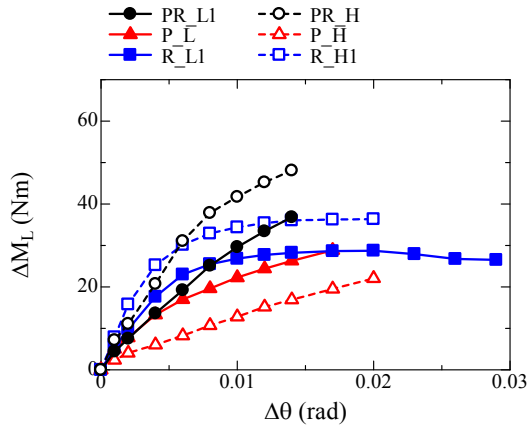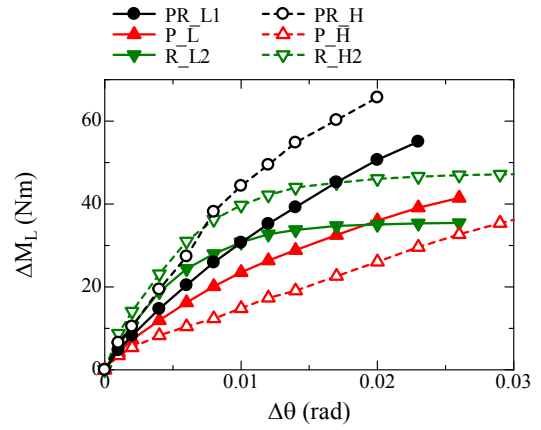
(c) $\delta_{LDT}=\pm 2$mm, h/S=1

(d) $\delta_{LDT}=\pm 2$mm, h/S=1.8

A. 5.5.1.1 Relationship between $\Delta\theta$ and ΔM_L for each loading step.
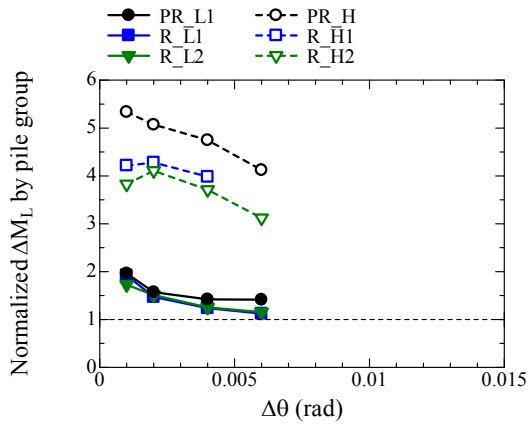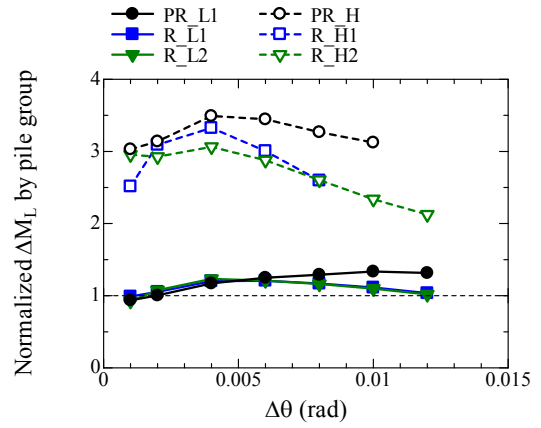
(a) $\delta_{LDT}=\pm 1mm$, h/S=1
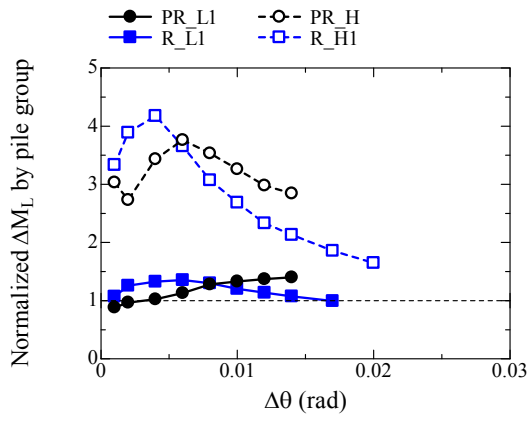
(b) $\delta_{LDT}=\pm 1mm$, h/S=1.8
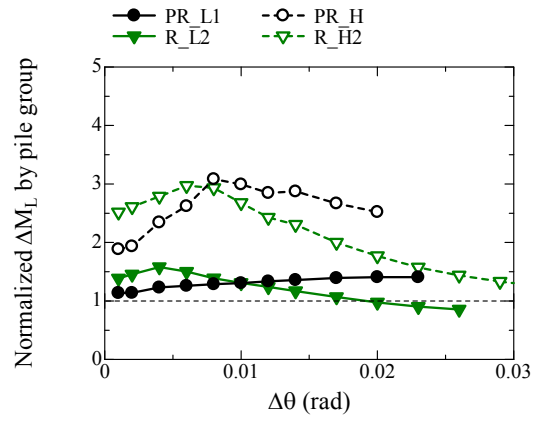
(c) $\delta_{LDT}=\pm 2mm$, h/S=1

(d) $\delta_{LDT}=\pm 2mm$, h/S=1.8

A. 5.5.1.2 Relationship between $\Delta\theta$ and normalized ΔM_L by that of pile group.
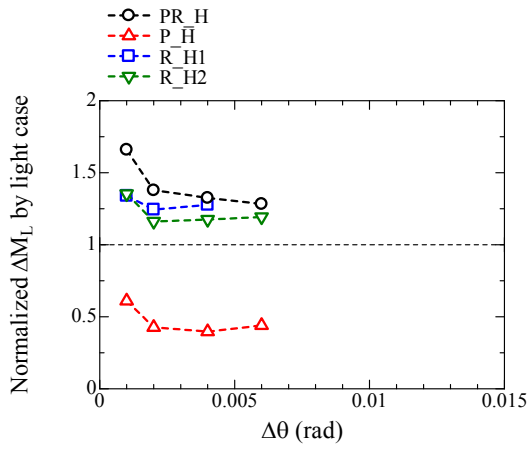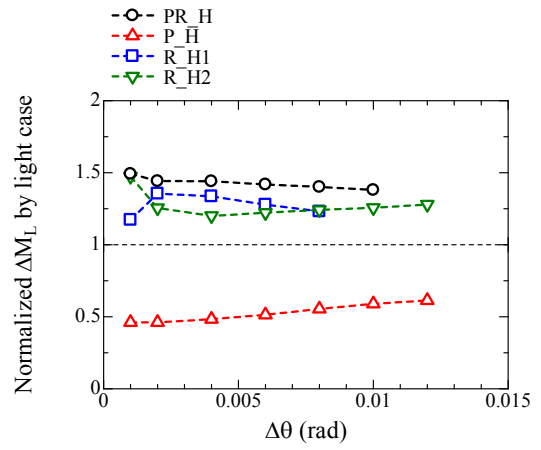
(a) $\delta_{LDT}=\pm1mm$, h/S=1
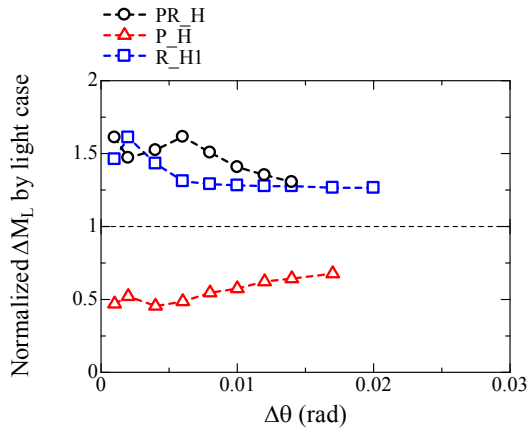
(b) $\delta_{LDT}=\pm1mm$, h/S=1.8
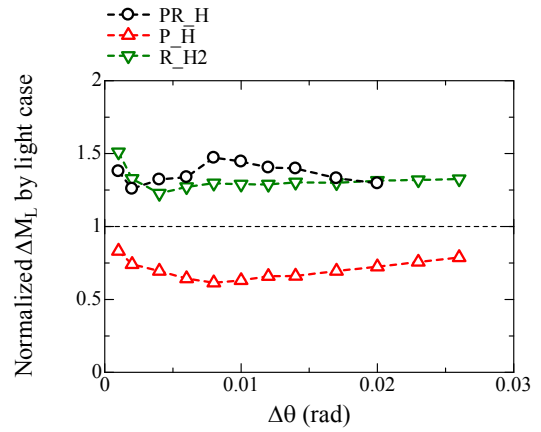
(c) $\delta_{LDT}=\pm2mm$, h/S=1

(d) $\delta_{LDT}=\pm2mm$, h/S=1.8

A. 5.5.1.3 Relationship between $\Delta\theta$ and normalized ΔM_L of heavy case by that of light case.
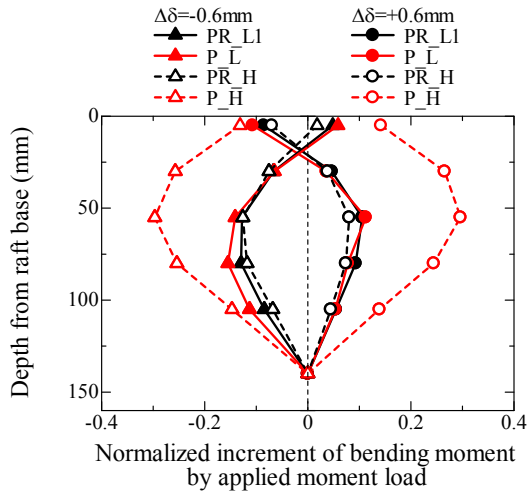
(a) Push-in pile ($\delta_{LDT}=\pm 1$mm, h/S=1)
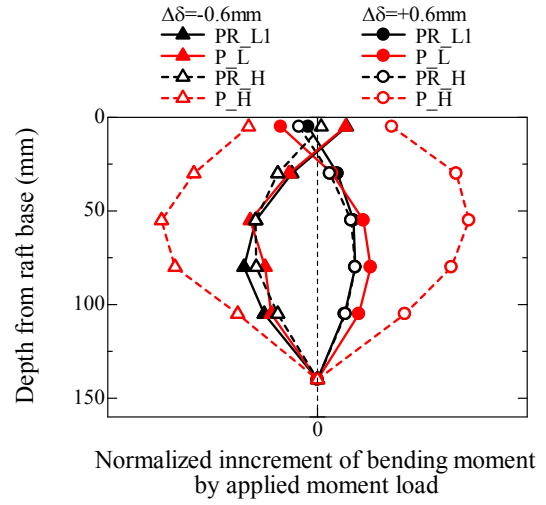
(b) Pull-out pile ($\delta_{LDT}=\pm 1$mm, h/S=1)
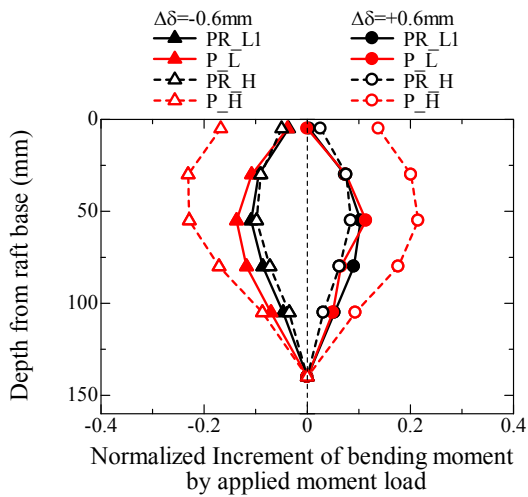
(c) Push-in pile ($\delta_{LDT}=\pm 1$mm, h/S=1.8)
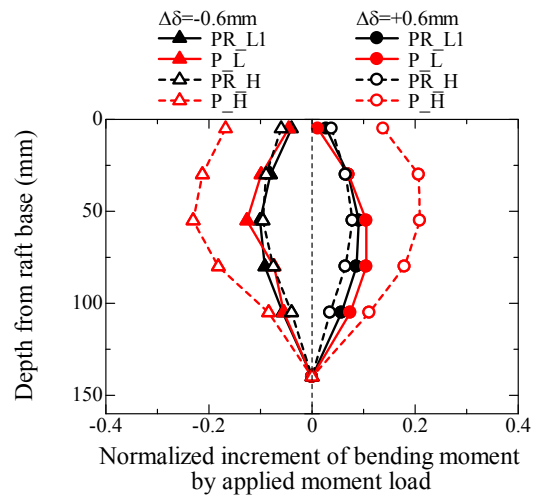
(d) Pull-out pile ($\delta_{LDT}=\pm 1$mm, h/S=1.8)

A. 5.5.2.1 Profile of bending moment at $\Delta\delta=\pm 0.6$mm, ± 1.2mm.
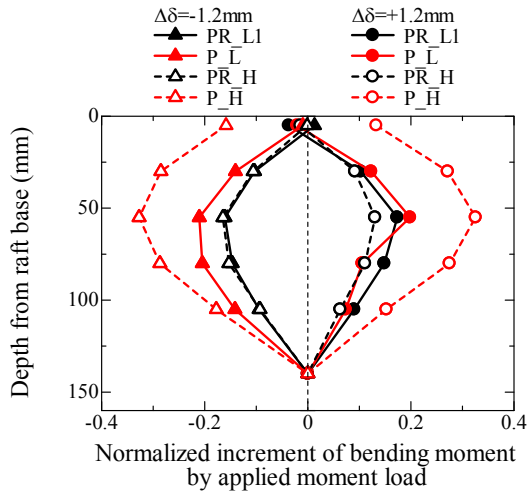
A119

(e) Push-in pile ($\delta_{LDT}=\pm2$mm, h/S=1)

(f) Pull-out pile ($\delta_{LDT}=\pm2$mm, h/S=1)

(g) Push-in pile ($\delta_{LDT}=\pm2$mm, h/S=1.8)

(h) Pull-out pile ($\delta_{LDT}=\pm2$mm, h/S=1.8)

A. 5.5.2.1 Profile of bending moment at $\Delta\delta=\pm0.6$mm, ±1.2mm.
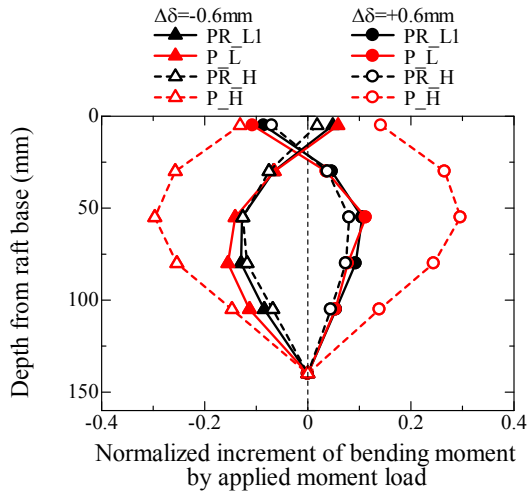
(a) Push-in pile ($\delta_{LDT}=\pm 1$mm, h/S=1)
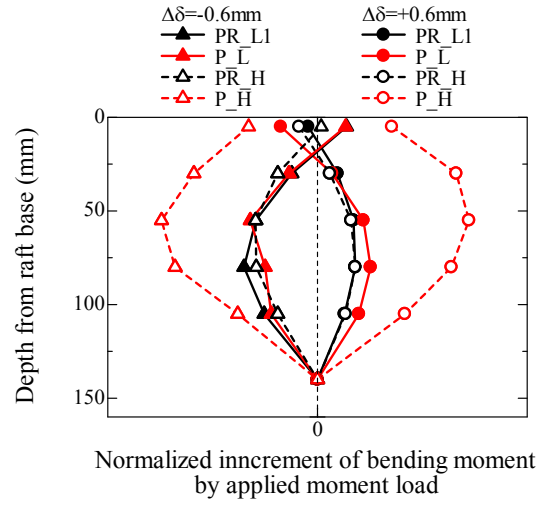
(b) Pull-out pile ($\delta_{LDT}=\pm 1$mm, h/S=1)
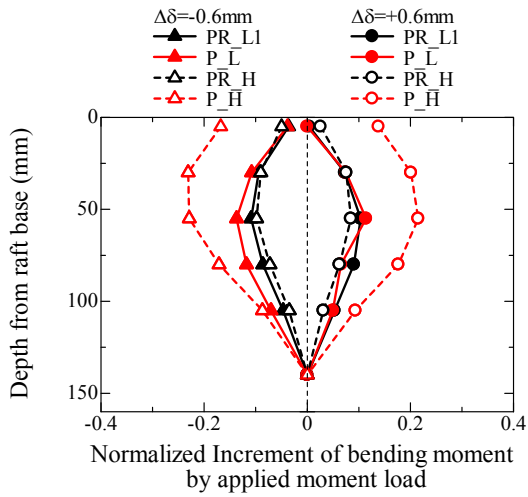
(c) Push-in pile ($\delta_{LDT}=\pm 1$mm, h/S=1.8)
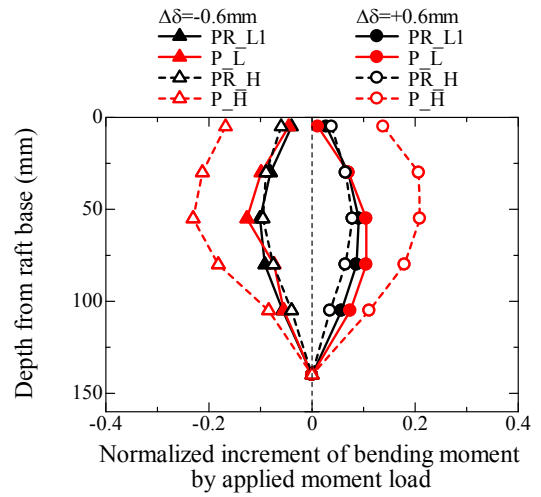
(d) Pull-out pile ($\delta_{LDT}=\pm 1$mm, h/S=1.8)

A. 5.5.2.2 Profile of normalized bending moment by applied moment load at $\Delta\delta=\pm 0.6$mm, ± 1.2mm.
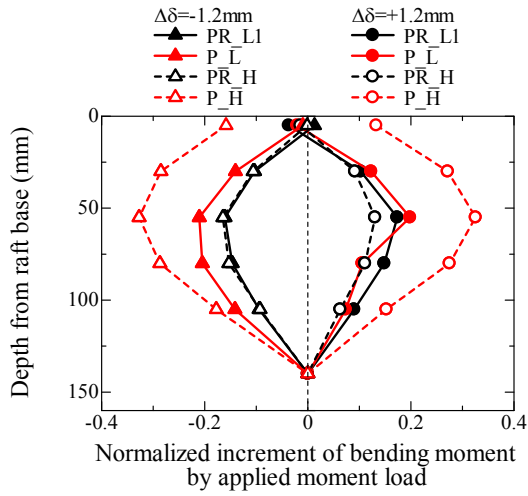
(e) Push-in pile ($\delta_{LDT}=\pm 2mm$, h/S=1)
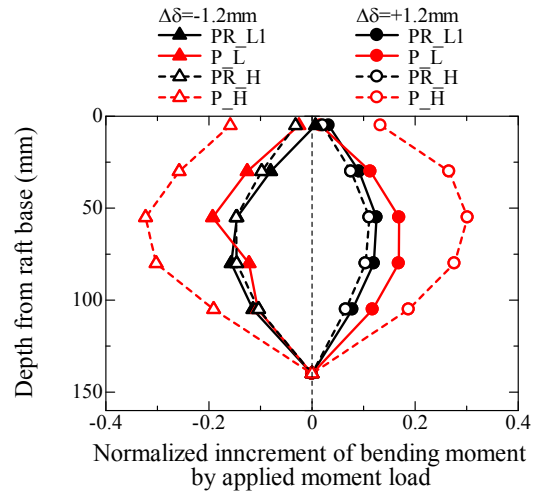
(f) Pull-out pile ($\delta_{LDT}=\pm 2mm$, h/S=1)
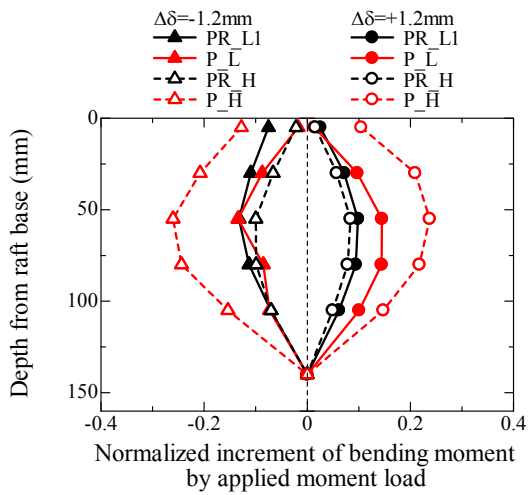
(g) Push-in pile ($\delta_{LDT}=\pm 2mm$, h/S=1.8)
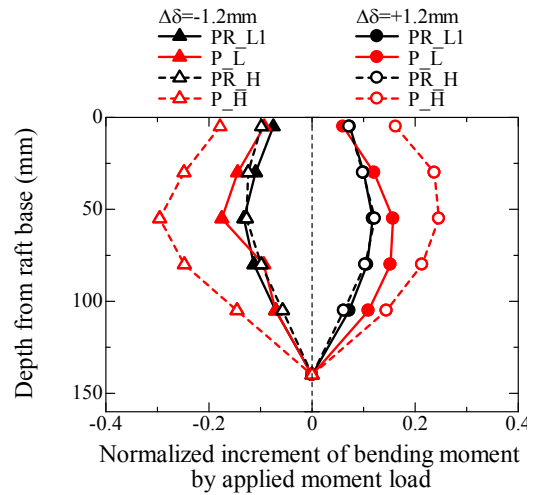
(h) Pull-out pile ($\delta_{LDT}=\pm 2mm$, h/S=1.8)

A. 5.5.2.2 Profile of normalized bending moment by applied moment load at $\Delta\delta=\pm 0.6mm$, $\pm 1.2mm$.
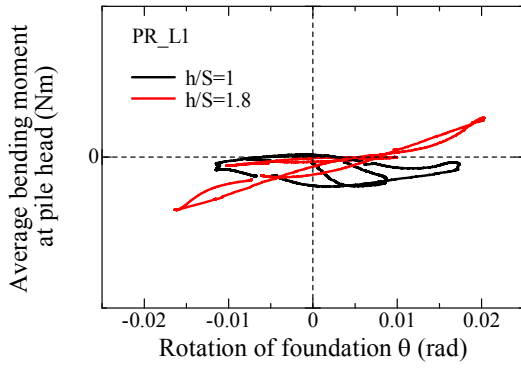
(a) All piles
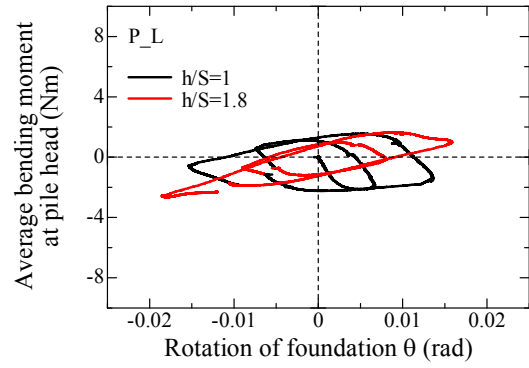
(a) All piles
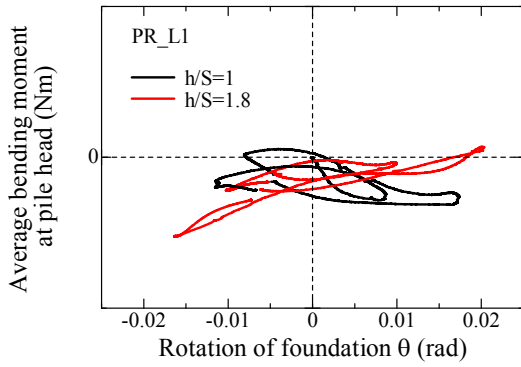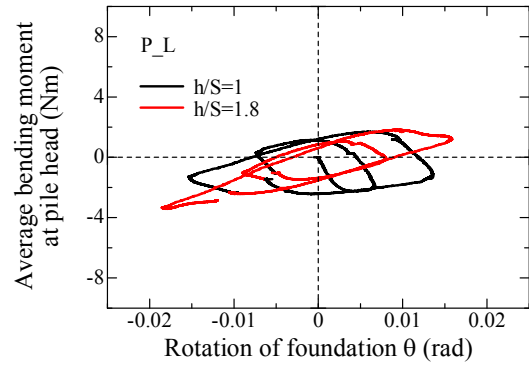
(b) Left pile

(b) Left pile
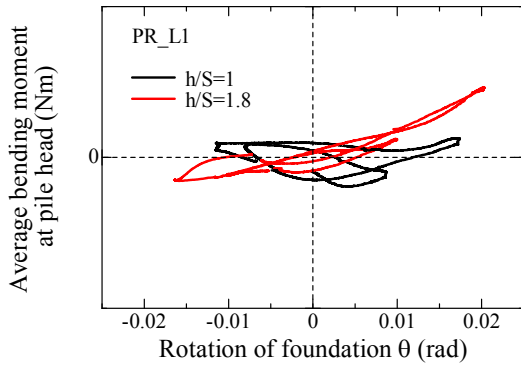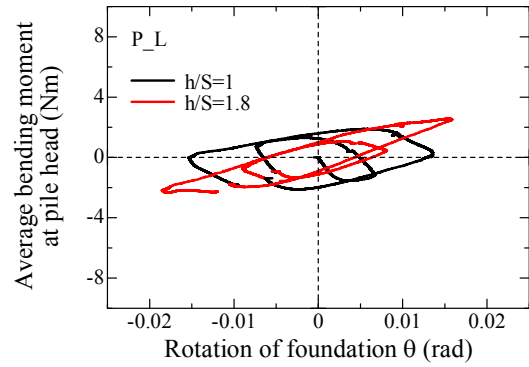
(c) Right pile

(c) Right pile

A. 5.5.2.3 Relationship between rotation of foundaiton θ and average bending moment at pile head for PR_L1.

A. 5.5.2.4 Relationship between rotation of foundaiton θ and average bending moment at pile head for PR_L1.
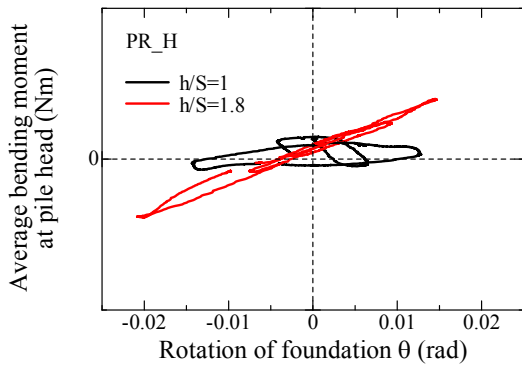
(a) All piles
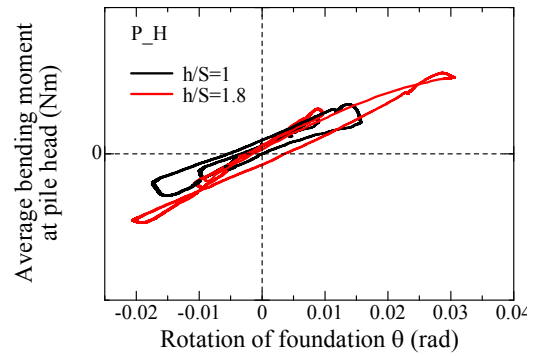
(a) All piles
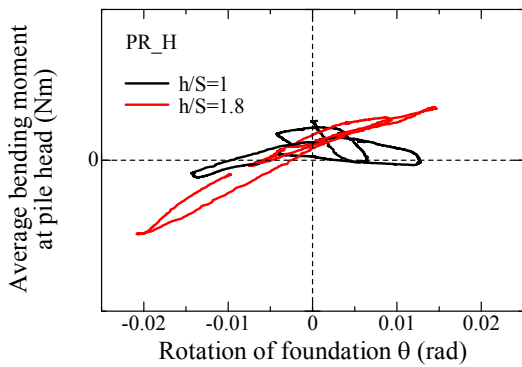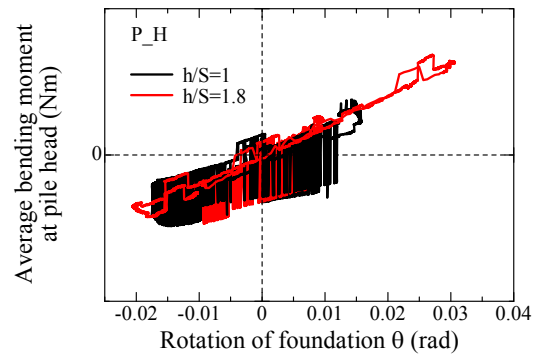
(b) Left pile

(b) Left pile
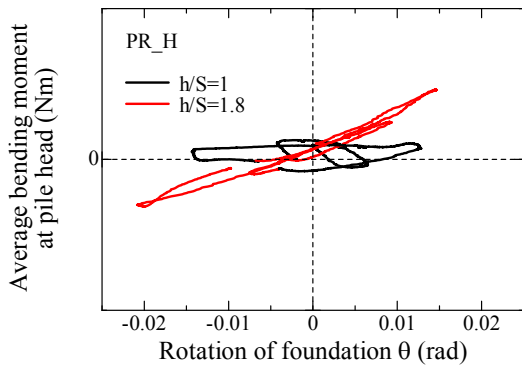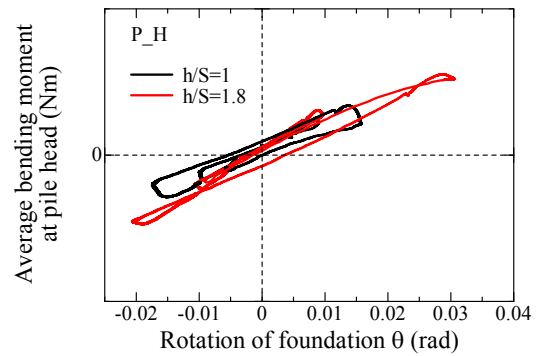
(c) Right pile

(c) Right pile

A. 5.5.2.5 Relationship between rotation of foundaiton θ and average bending moment at pile head for PR_H.

A. 5.5.2.6 Relationship between rotation of foundaiton θ and average bending moment at pile head for P_H.
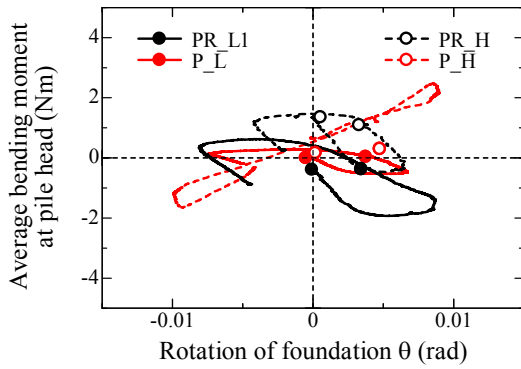
(a) $\delta_{LDT}=\pm 1$mm, h/S=1 (all pile)
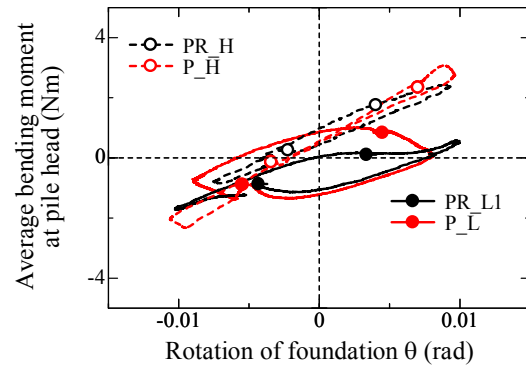
(d) $\delta_{LDT}=\pm 1$mm, h/S=1.8 (all piles)
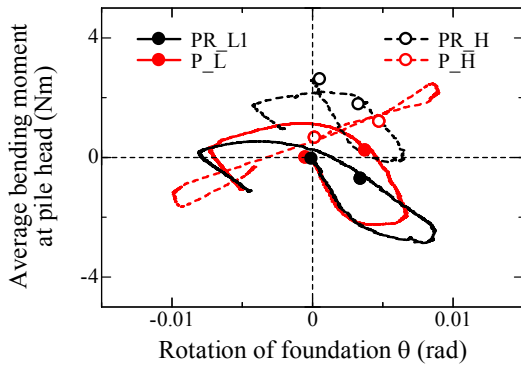
(b) $\delta_{LDT}=\pm 1$mm, h/S=1 (left pile)
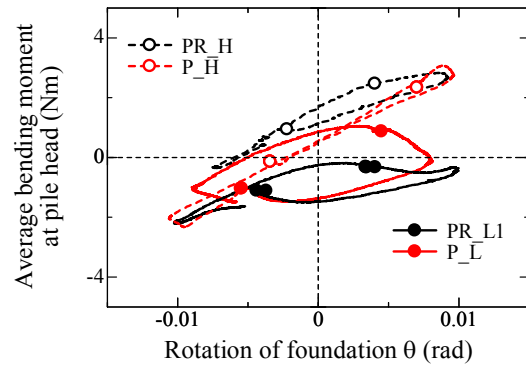
(e) $\delta_{LDT}=\pm 1$mm, h/S=1.8 (left piles)
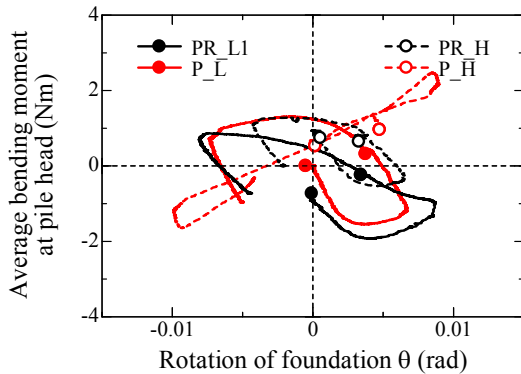
(c) $\delta_{LDT}=\pm 1$mm, h/S=1 (right pile)
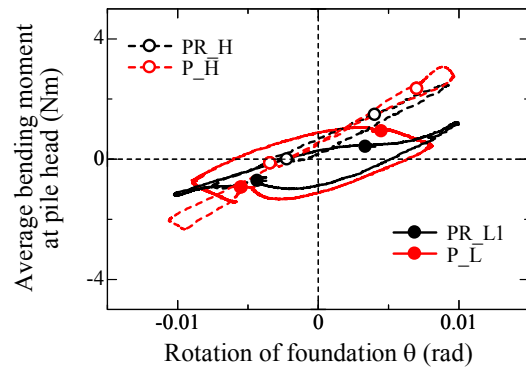
(f) $\delta_{LDT}=\pm 1$mm, h/S=1.8 (right piles)

A. 5.5.2.7 Relationship between rotation of foundaiton θ and average bending moment at pile head for each loading step.
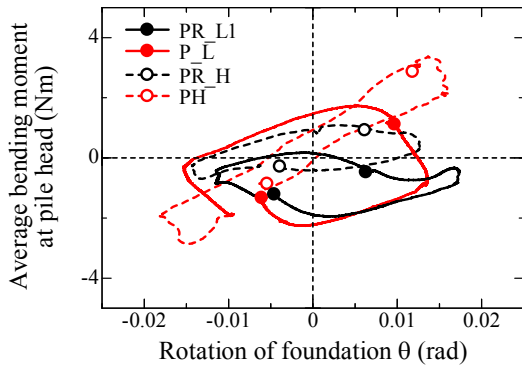
(g) $\delta_{LDT}=\pm 2$mm, h/S=1 (all piles)
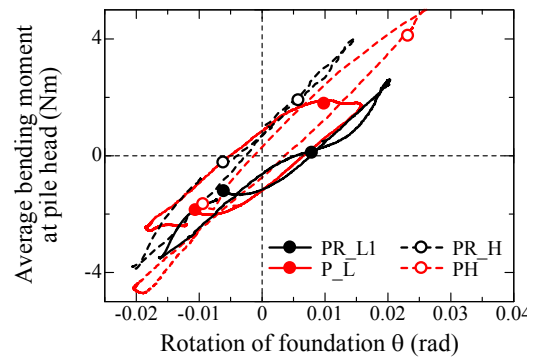
(j) $\delta_{LDT}=\pm 2$mm, h/S=1.8 (all piles)
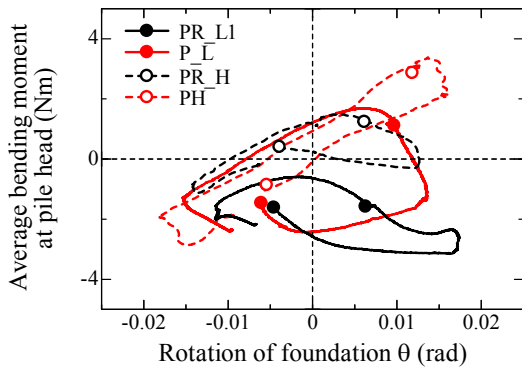
(h) $\delta_{LDT}=\pm 2$mm, h/S=1 (left pile)
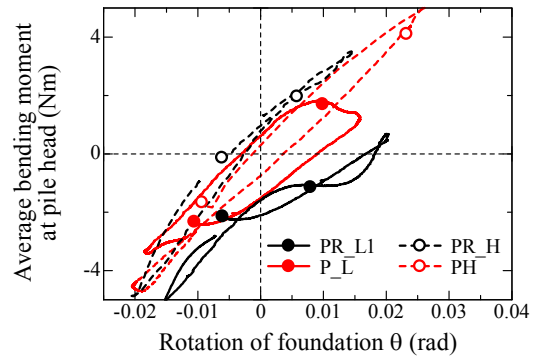
(k) $\delta_{LDT}=\pm 2$mm, h/S=1.8 (left pile)
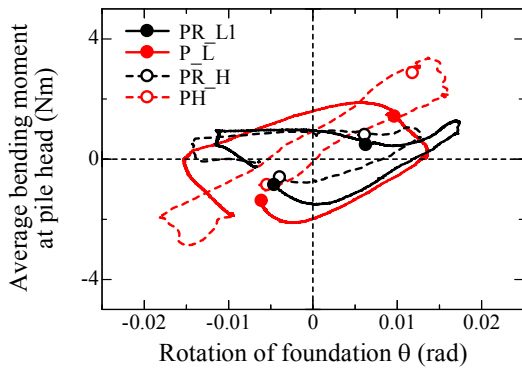
(i) $\delta_{LDT}=\pm 2$mm, h/S=1 (right piles)
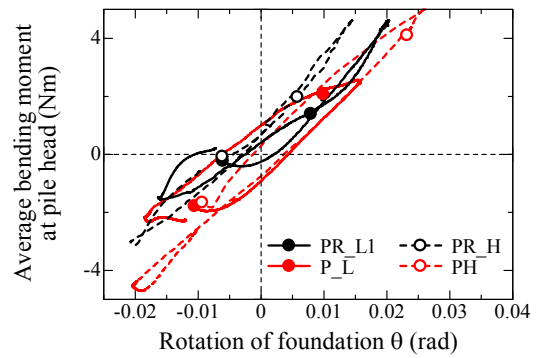
(l) $\delta_{LDT}=\pm 2$mm, h/S=1.8 (right pile)

A. 5.5.2.7 Relationship between rotation of foundaiton θ and average bending moment at pile head for each loading step.
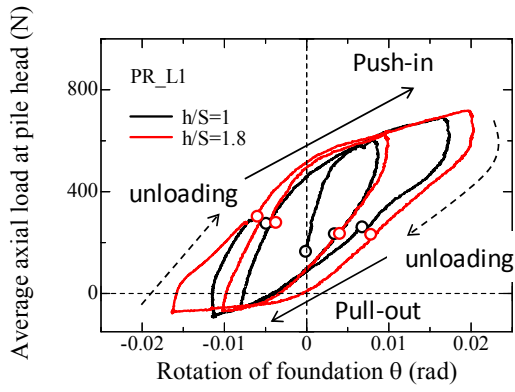
(a) Axial load at pile head (Left pile)
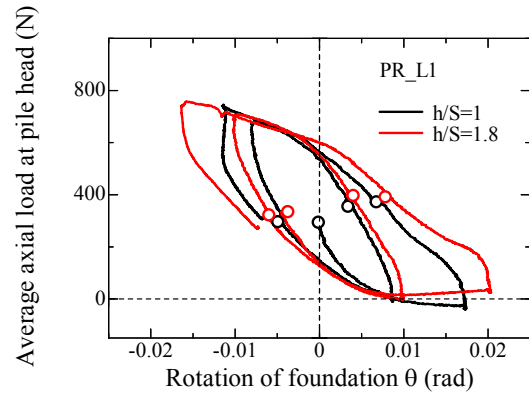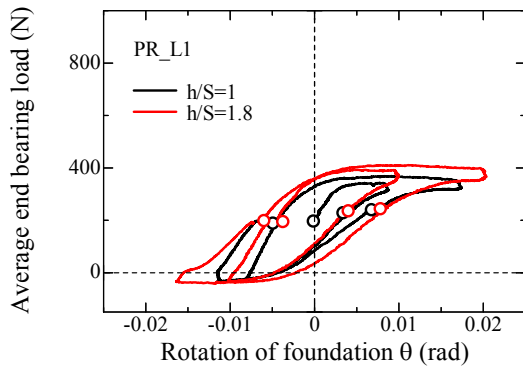
(b) Axial load at pile head (Right pile)

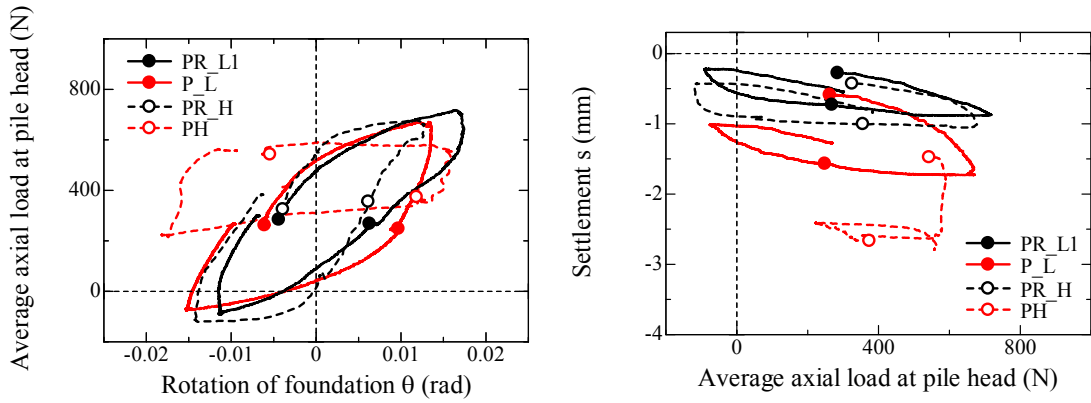(c) End bearing load (Left pile)
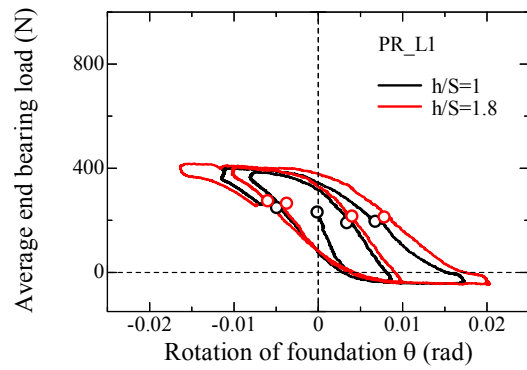
(d) End bearing load (Right pile)
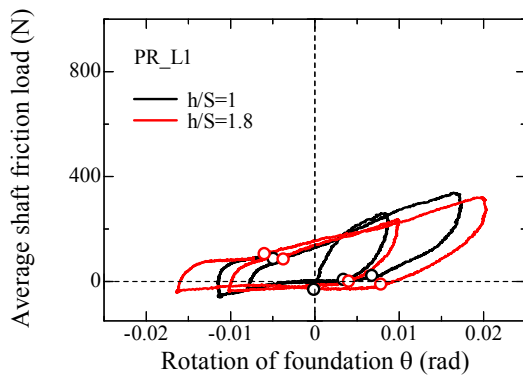
(e) Shaft friction load (Left pile)
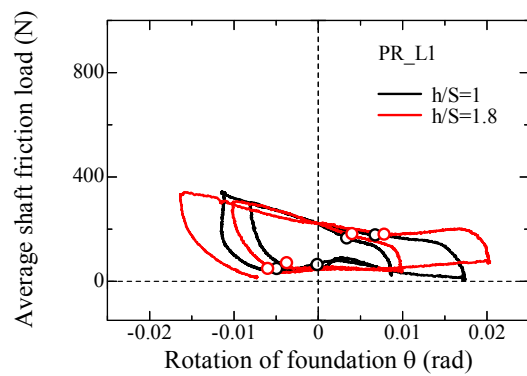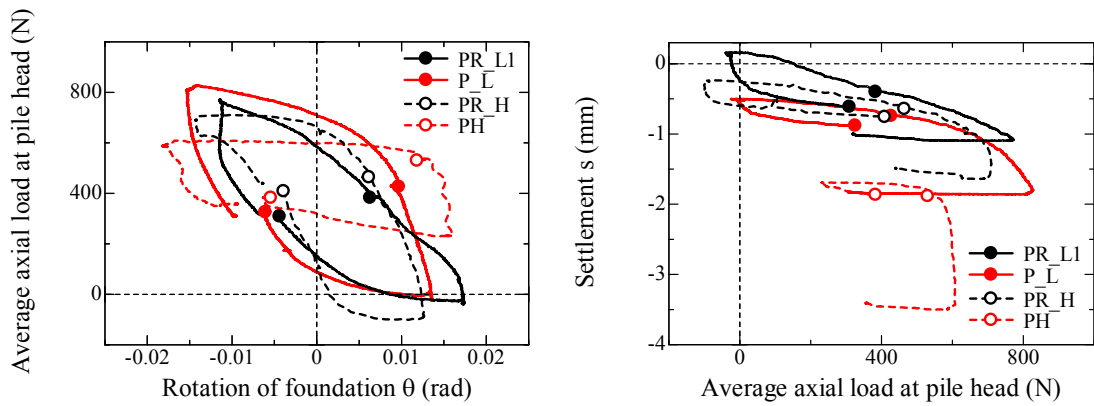
(f) Shaft friction load (Right pile)

A. 5.5.2.8 Variation of pile load with rotation of foundation θ for PR_L1.
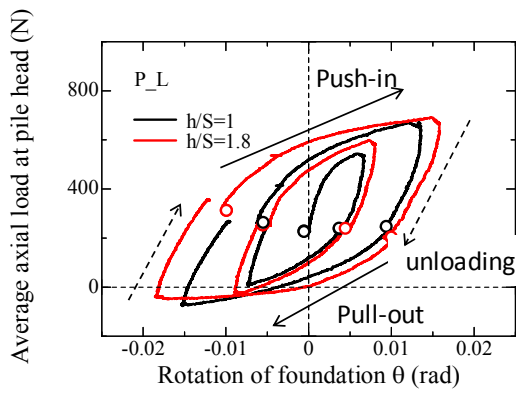
(a) Axial load at pile head (Left pile)
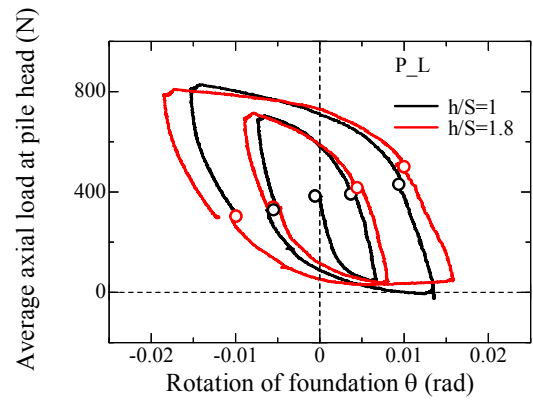
(b) Axial load at pile head (Right pile)
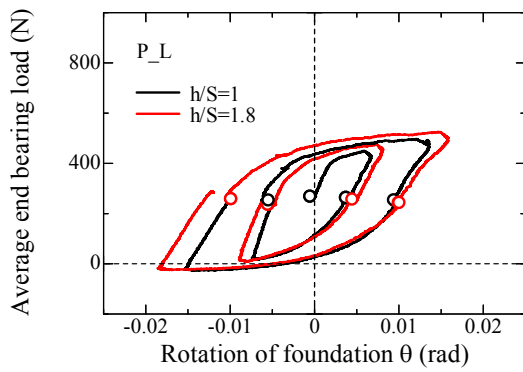
(c) End bearing load (Left pile)
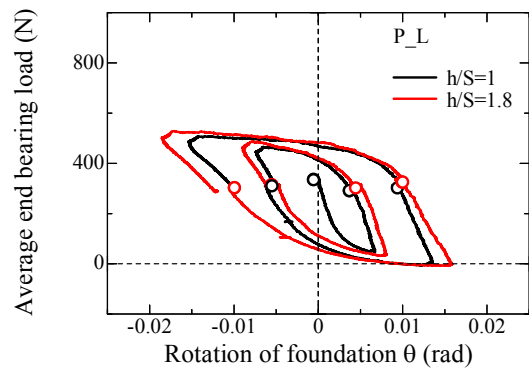
(d) End bearing load (Right pile)
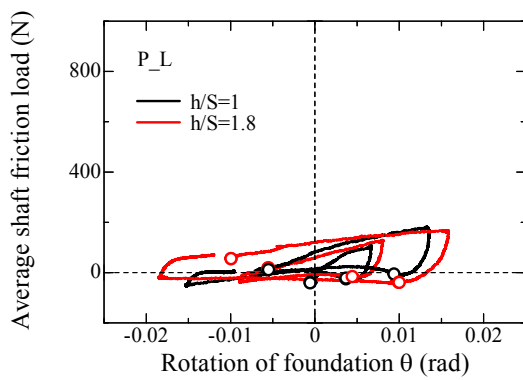
(e) Shaft friction load (Left pile)
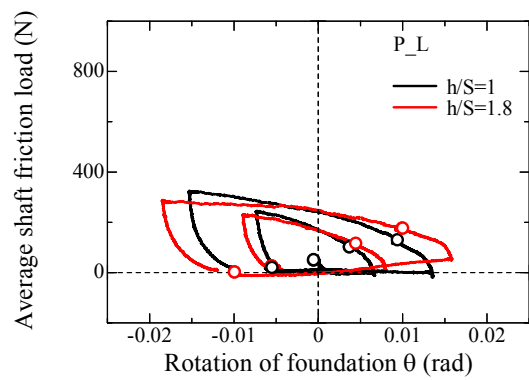
(f) Shaft friction load (Right pile)

A. 5.5.2.9 Variation of pile load with rotation of foundation θ for P_L.
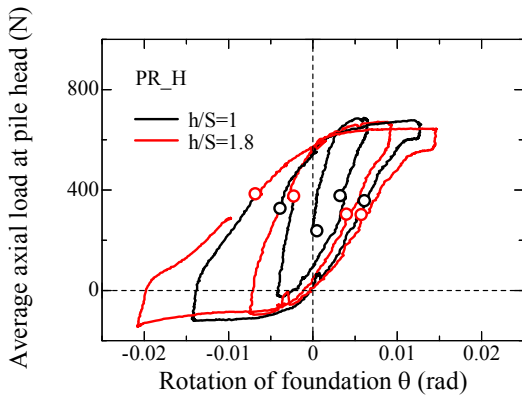
(a) Axial load at pile head (Left pile)
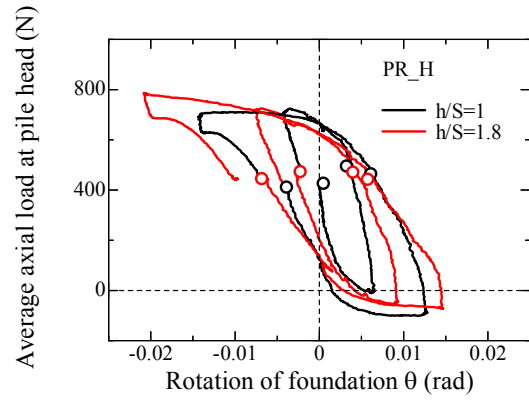
(b) Axial load at pile head (Right pile)
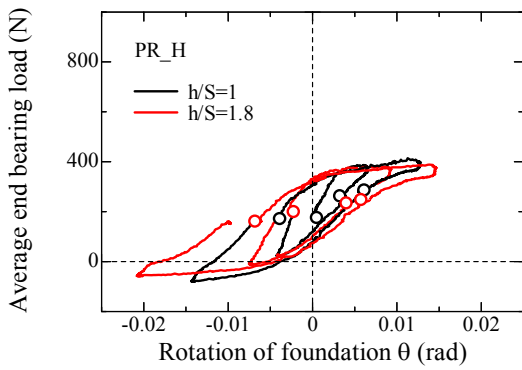
(c) End bearing load (Left pile)
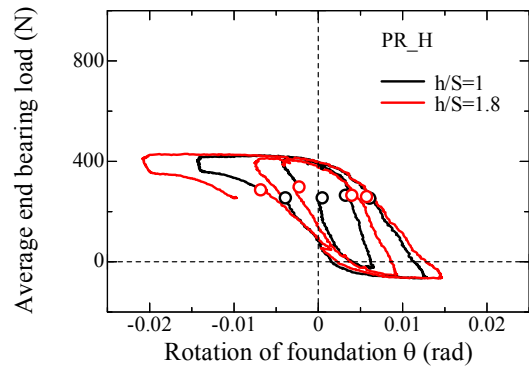
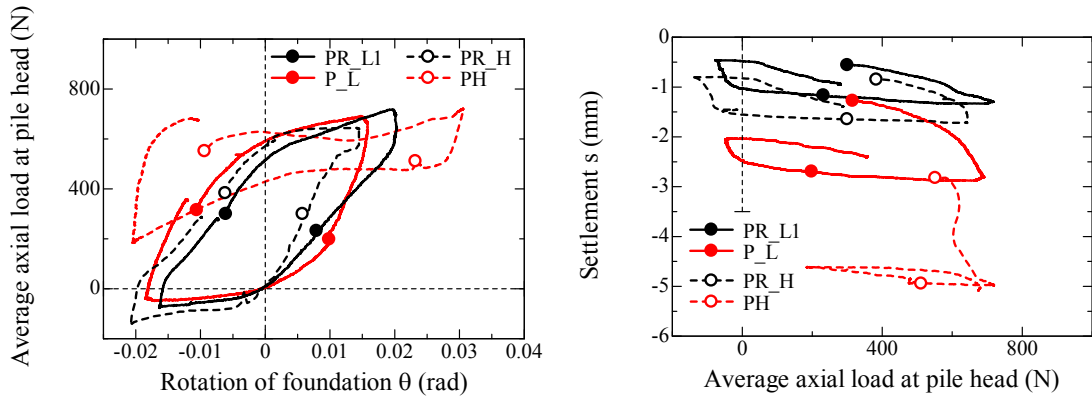(d) End bearing load (Right pile)
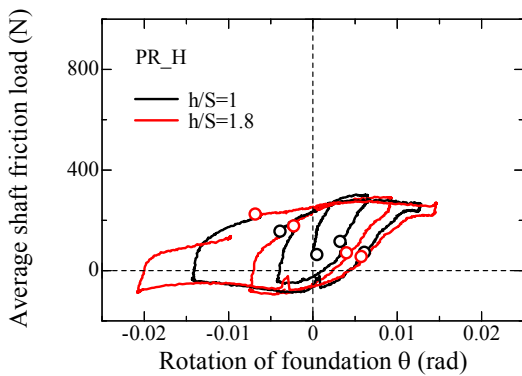
(e) Shaft friction load (Left pile)
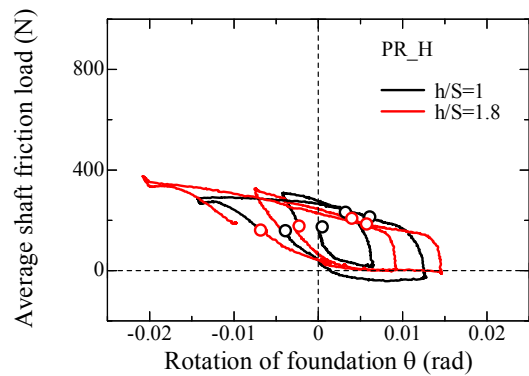
(e) Shaft friction load (Right pile)

A. 5.5.2.10 Variation of pile load with rotation of foundation θ for PR_H.
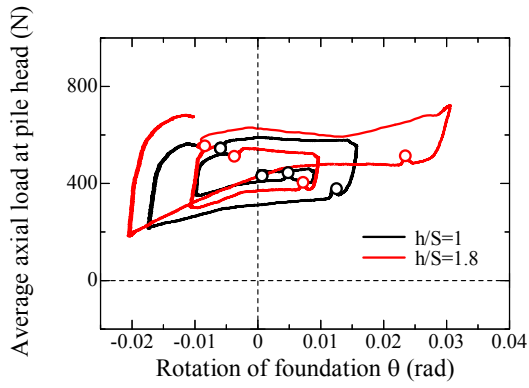
(a) Axial load at pile head (Left pile)
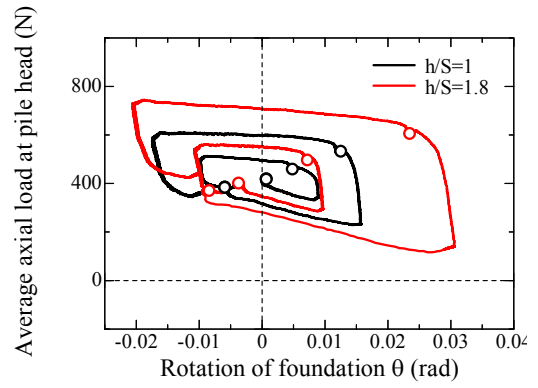
(b) Axial load at pile head (Right pile)
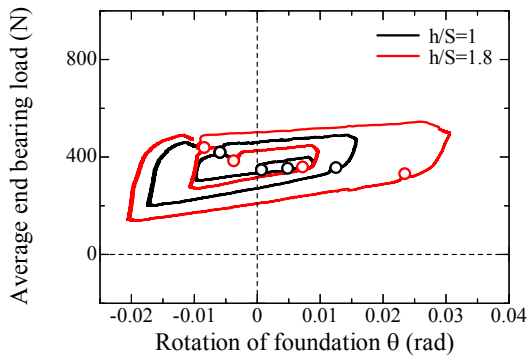
(c) End bearing load (Left pile)
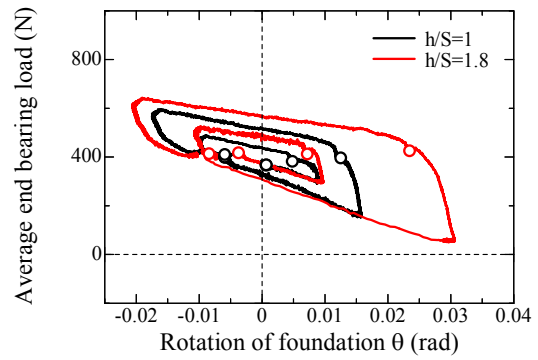
(d) End bearing load (Right pile)
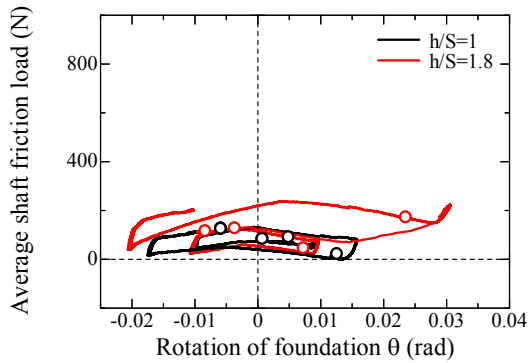
(e) Shaft friction load (Left pile)
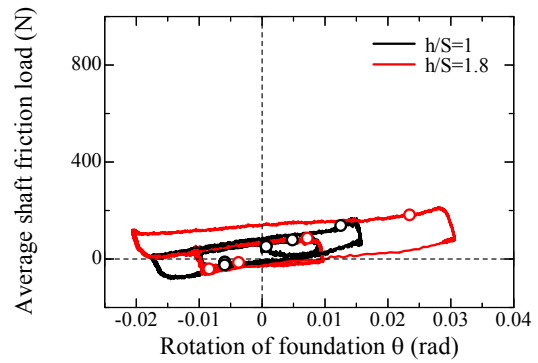
(f) Shaft friction load (Right pile)

A. 5.5.2.11 Variation of pile load with rotation of foundation θ for P_H.
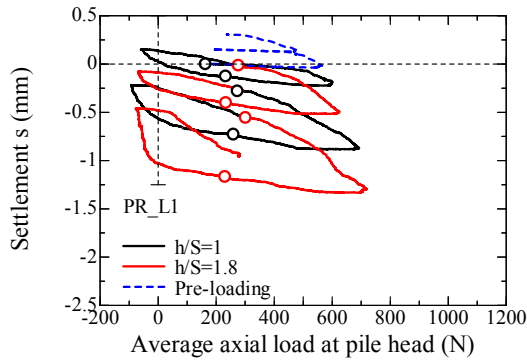
A130

(a) Axial load at pile head (Left pile)
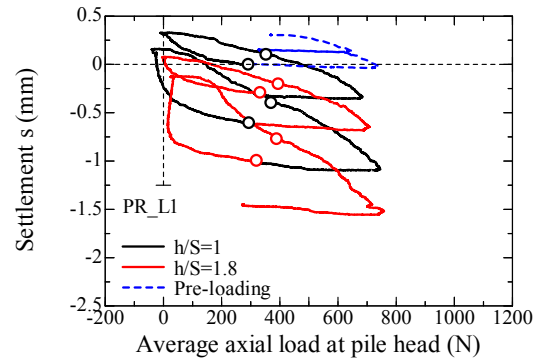
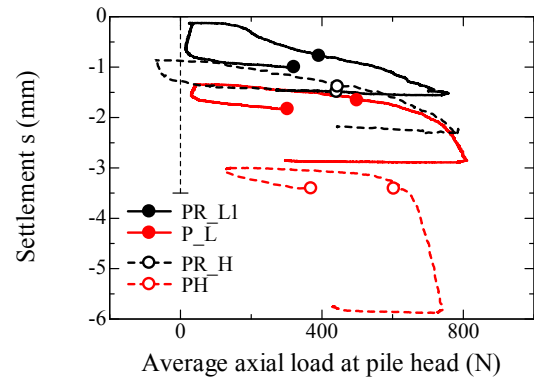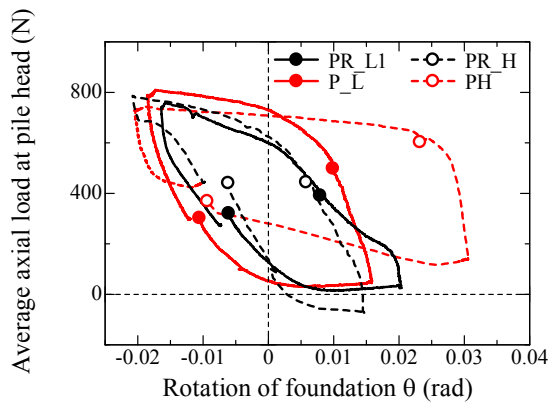(b) Axial load at pile head (Right pile)
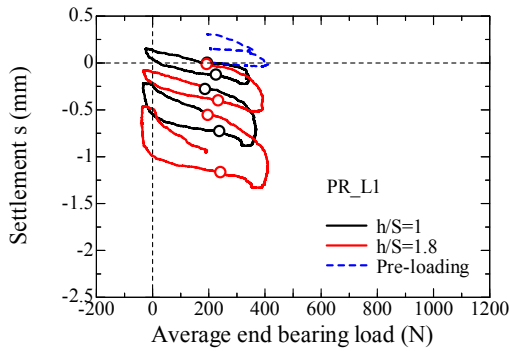
(c) End bearing load (Left pile)
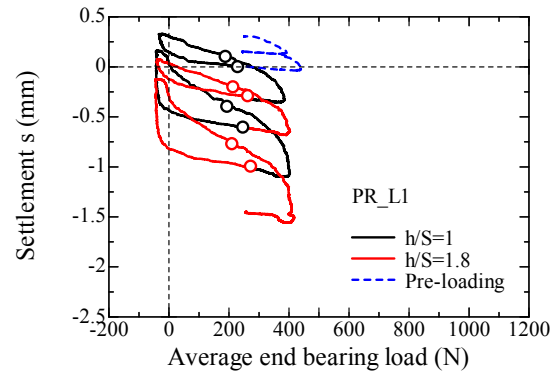
(d) End bearing load (Right pile)
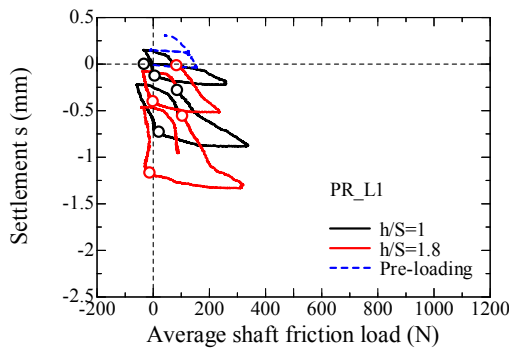
(e) Shaft friction load (Left pile)
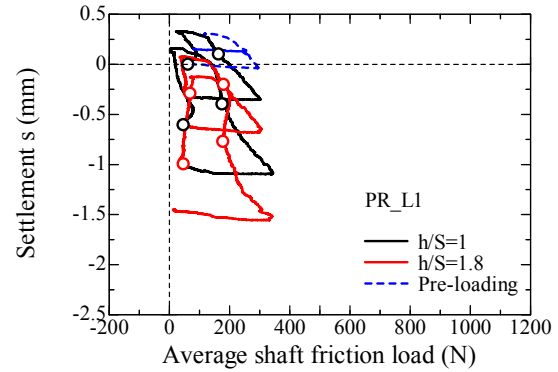
(f) Shaft friction load (Right pile)

A. 5.5.2.12 Variation of pile load with settlement for PR_L1.
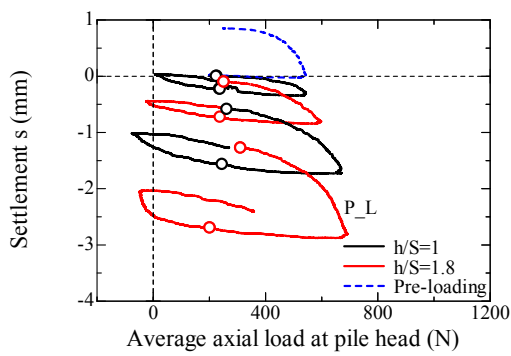
(a) Axial load at pile head (Left pile)
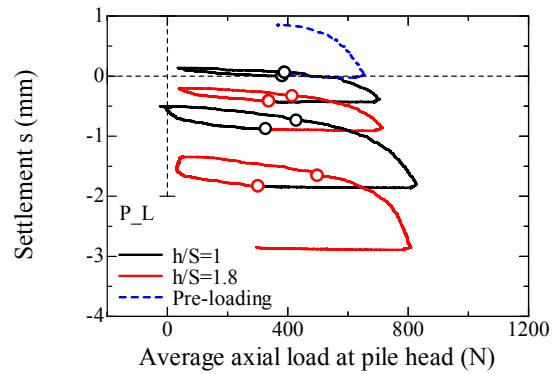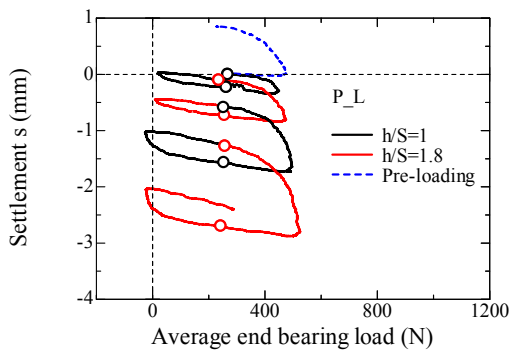
(b) Axial load at pile head (Right pile)

(c) End bearing load (Left pile)
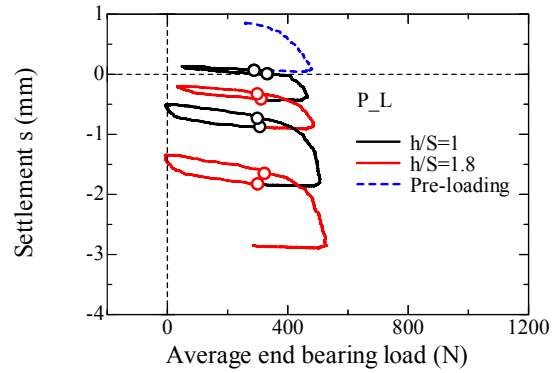
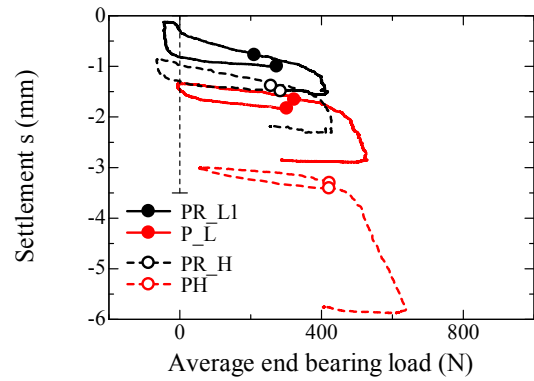(d) End bearing load (Right pile)
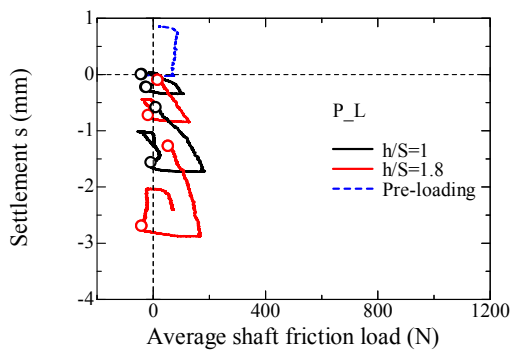
(e) Shaft friction load (Left pile)
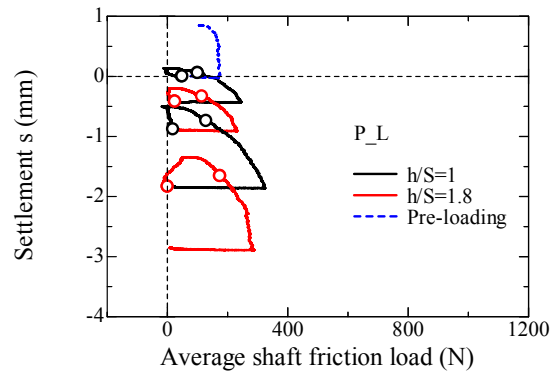
(f) Shaft friction load (Right pile)

A. 5.5.2.13 Variation of pile load with settlement for P_L.
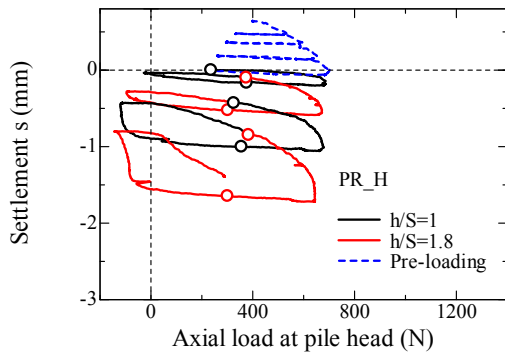
(a) Axial load at pile head (Left pile)
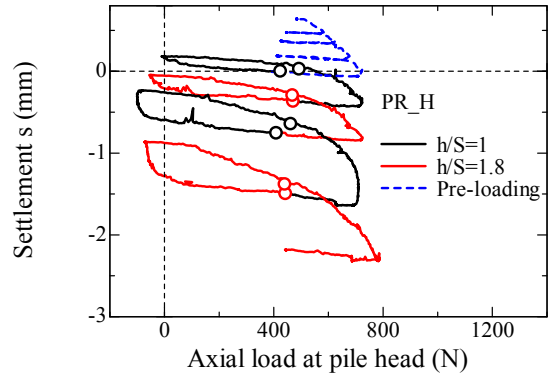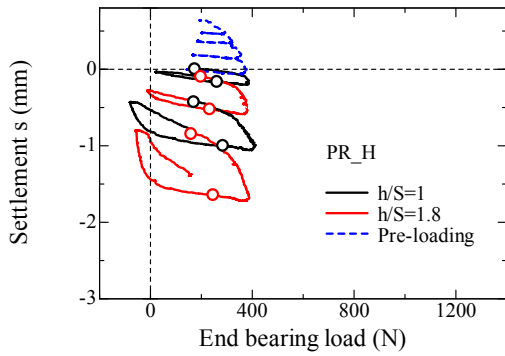
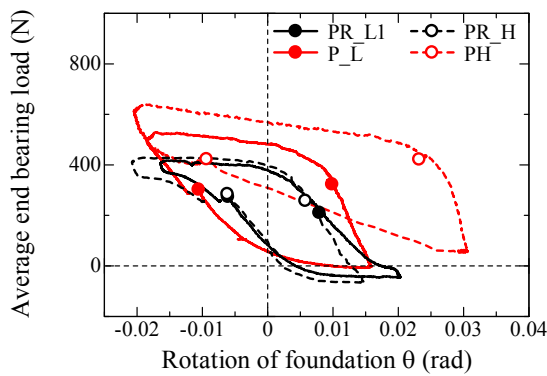(b) Axial load at pile head (Right pile)

(c) End bearing load (Left pile)
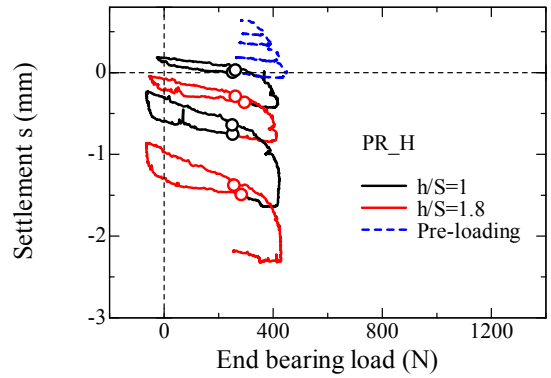
(d) End bearing load (Right pile)
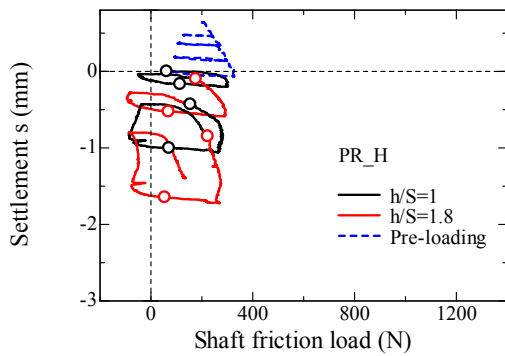
(e) Shaft friction load (Left pile)
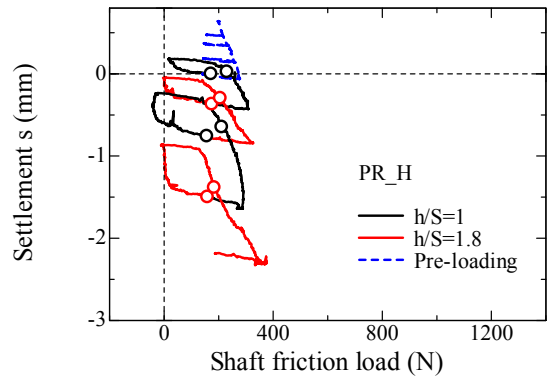
(f) Shaft friction load (Right pile)

A. 5.5.2.14 Variation of pile load with settlement for PR_H.
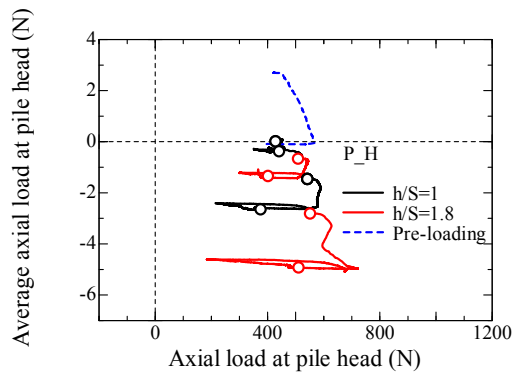
(a) Axial load at pile head (Left pile)
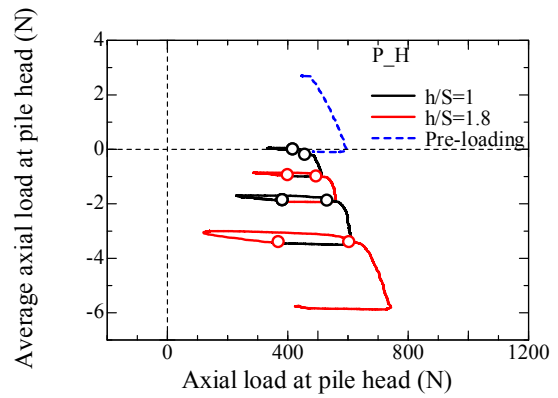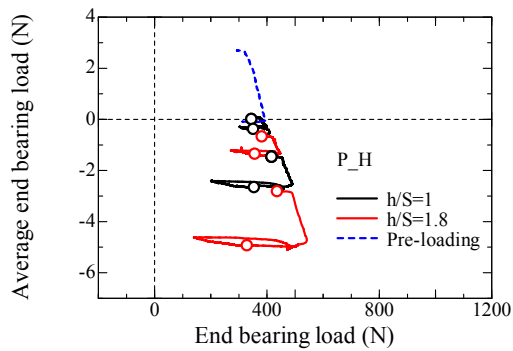
(b) Axial load at pile head (Right pile)

(c) End bearing load (Left pile)
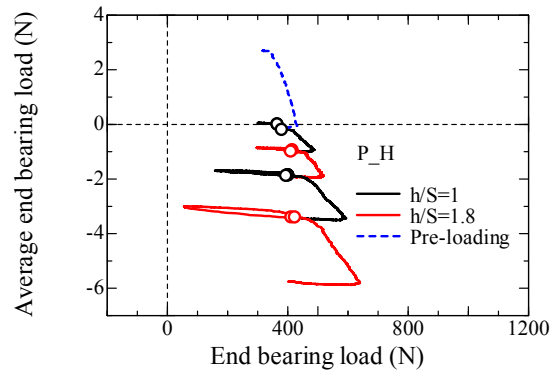
(d) End bearing load (Right pile)
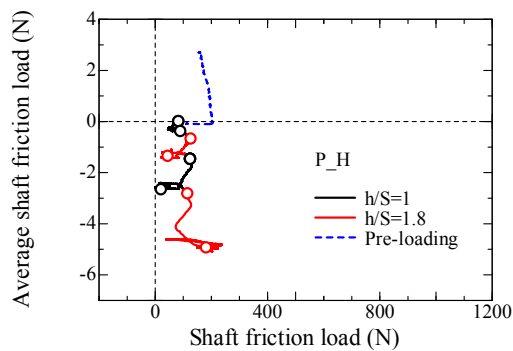
(e) Shaft friction load (Left pile)
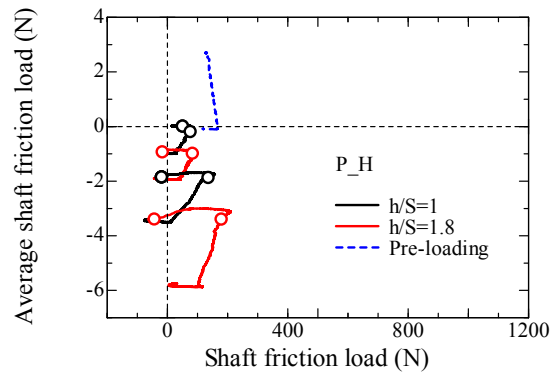
(f) Shaft friction load (Right pile)

A. 5.5.2.15 Variation of pile load with settlement for P_H.
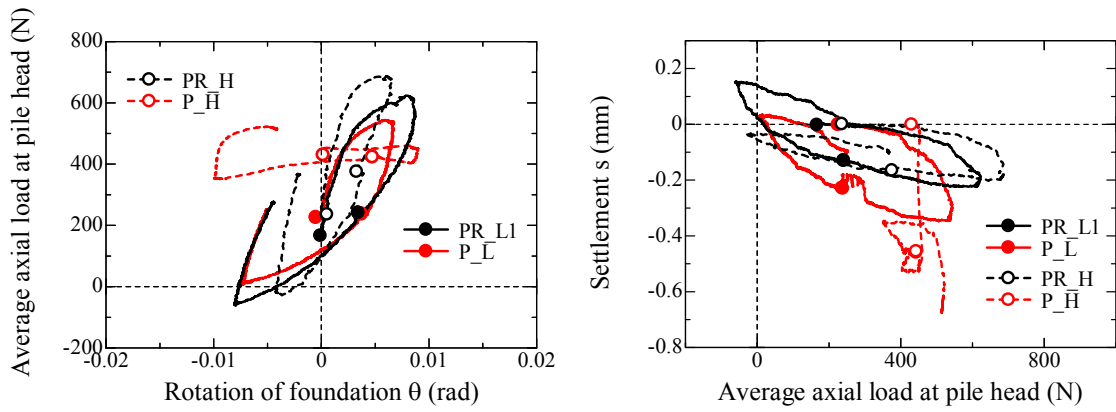
A134

(a) Axial load at pile head (Left pile)
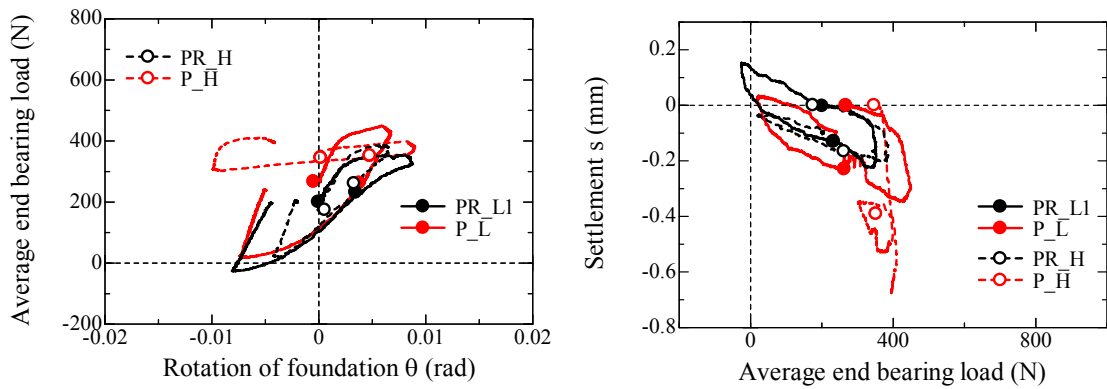
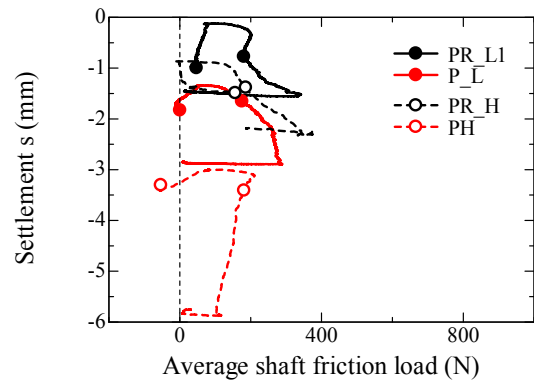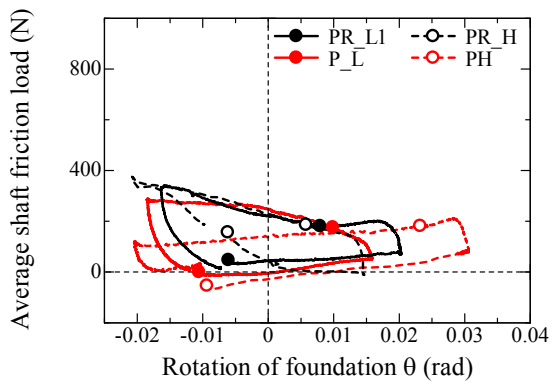(b) End bearing load (Left pile)
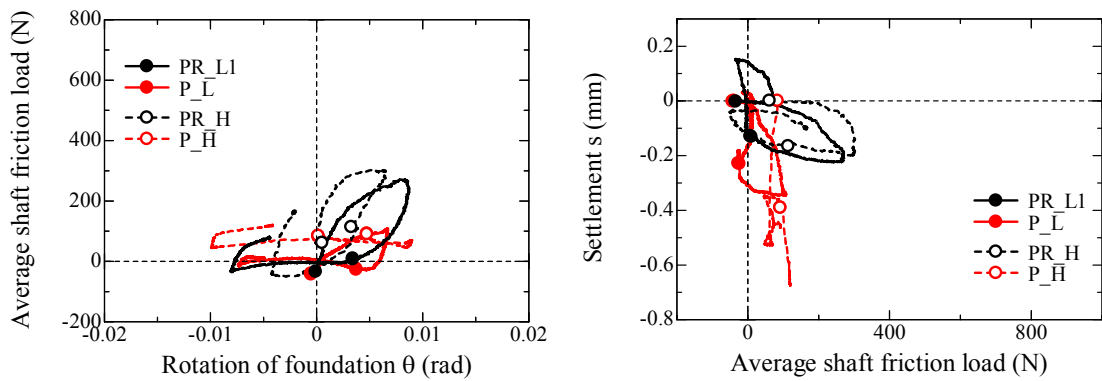
(c) Shaft friction load (Left pile)

A. 5.5.2.16 Variation of pile load with rotation of foundation θ or settlement observed in loading step 1 and 2 (δ$_{LDT}$=±1mm, h/S=1).

A135
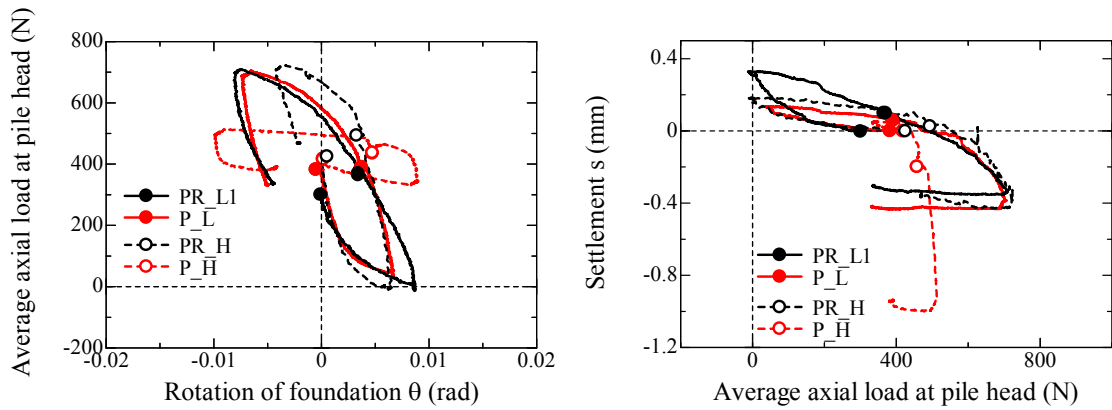
(d) Axial load at pile head (Right pile)
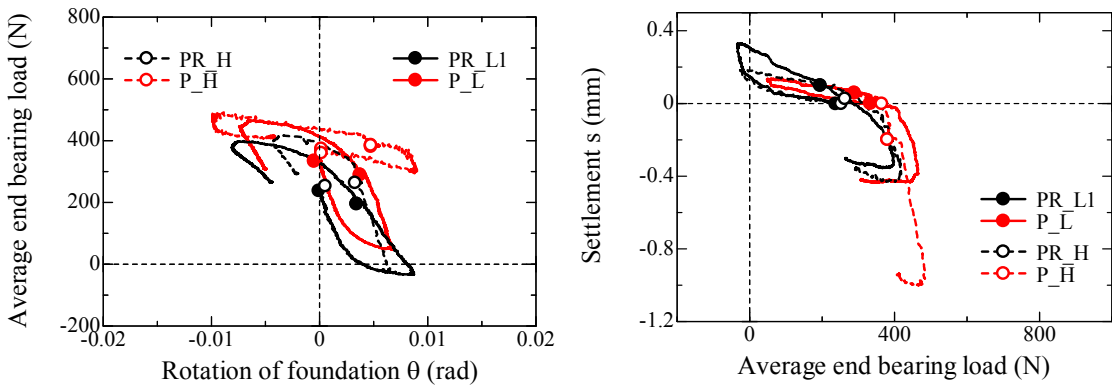
(e) End bearing load (Right pile)
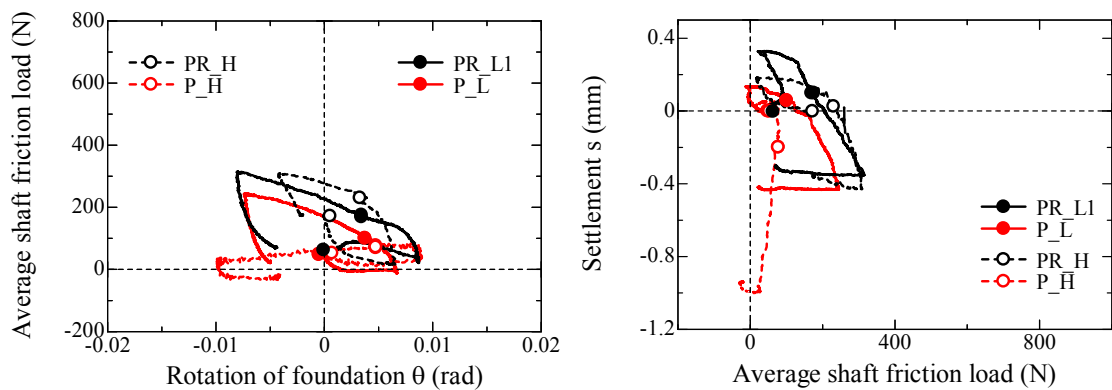
(f) Shaft friction load (Right pile)

A. 5.5.2.16 Variation of pile load with rotation of foundation θ or settlement observed in loading step 1 and 2 (δ_{LDT}=±1mm, h/S=1).
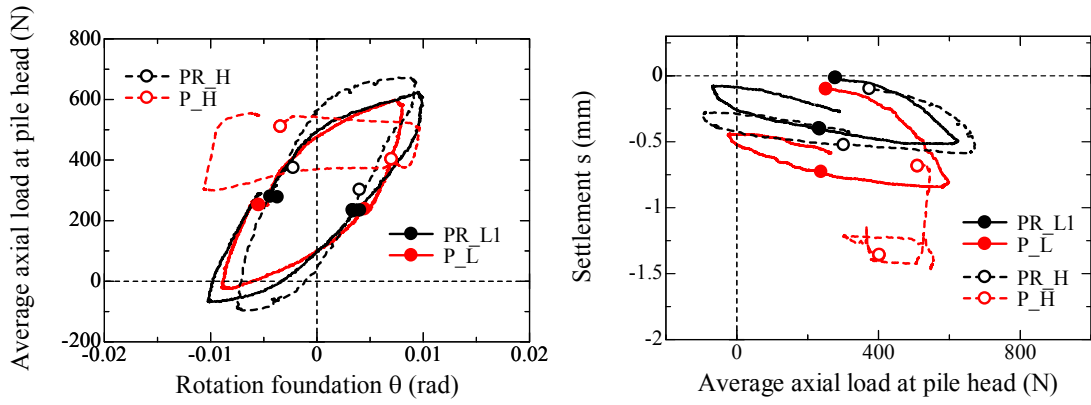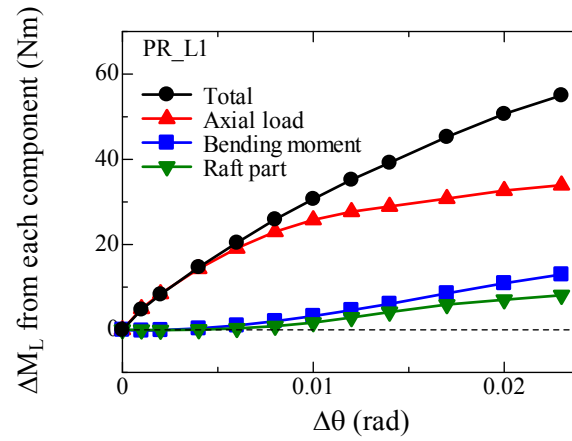
(a) Axial load at pile head (Left pile)
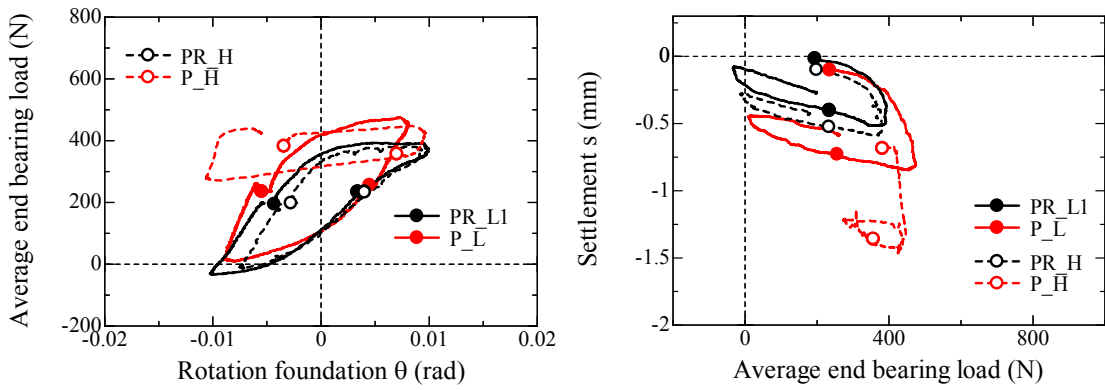
(b) End bearing load (Left pile)
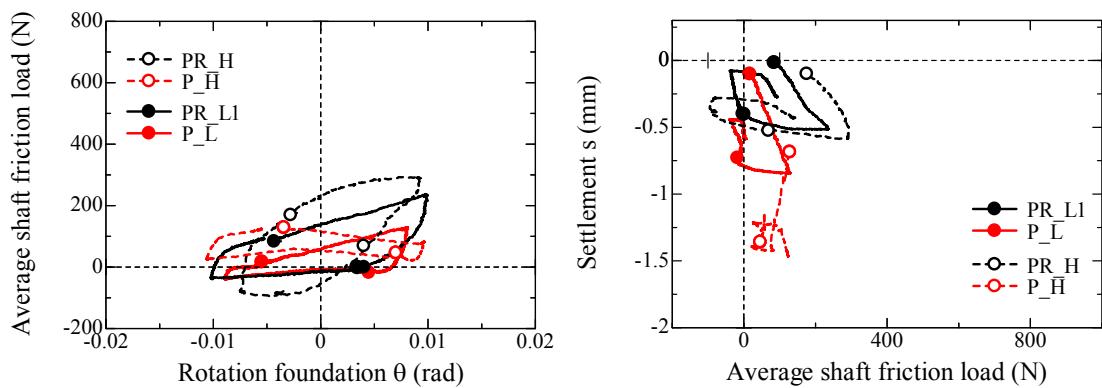
(c) Shaft friction load (Left pile)

A. 5.5.2.17 Variation of pile load with rotation of foundation θ or settlement observed in loading step 3 and 4 (δ$_{LDT}$=±1mm, h/S=1.8).
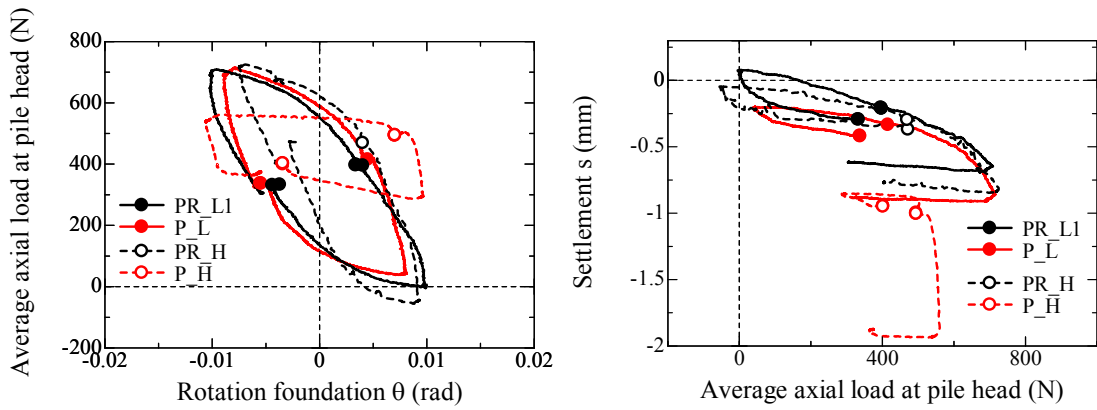
(d) Axial load at pile head (Right pile)
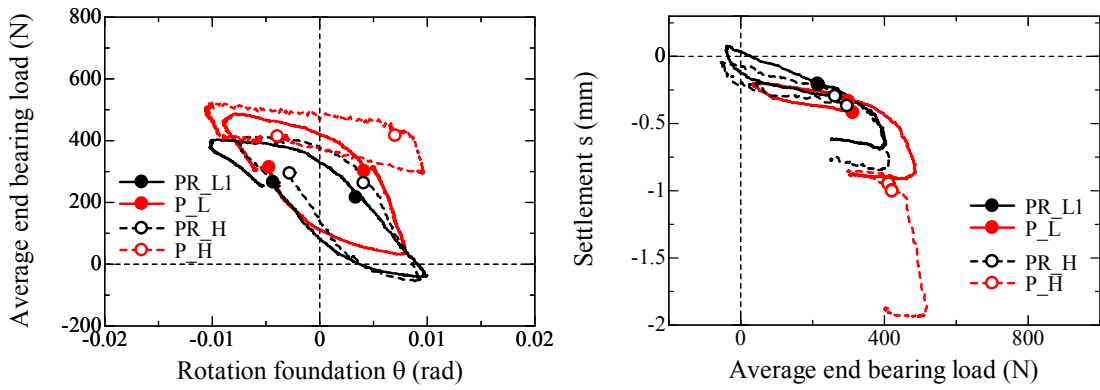
(e) End bearing load (Right pile)
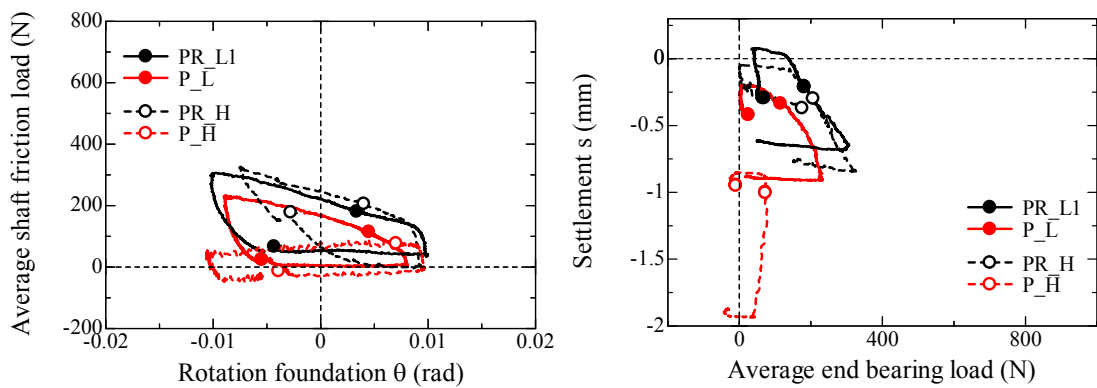
(f) Shaft friction load (Right pile)

A. 5.5.2.17 Variation of pile load with rotation of foundation θ or settlement observed in loading step 3 and 4 (δ_LDT=±1mm, h/S=1.8).

A138

(a) Axial load at pile head (Left pile)
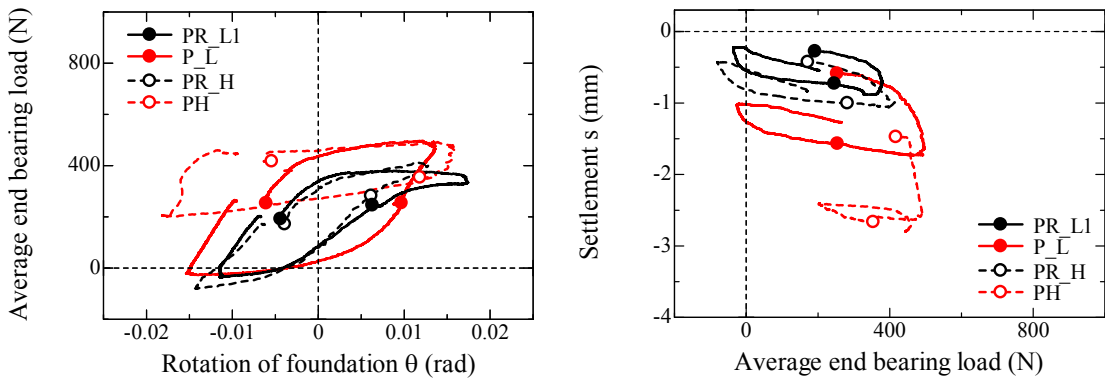
(b) End bearing load (Left pile)
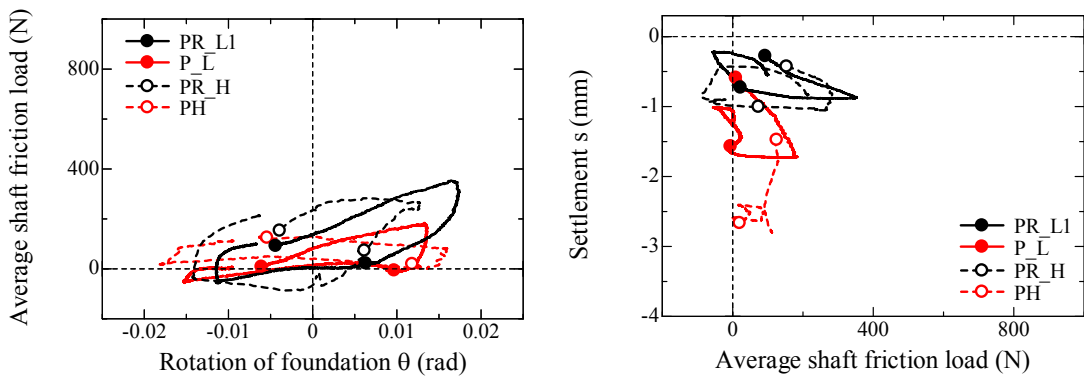
(c) Shaft friction load (Left pile)

A. 5.5.2.18 Variation of pile load with rotation of foundation θ or settlement observed in loading step 5 and 6 (δ_LDT=±2mm, h/S=1).

(d) Axial load at pile head (Right pile)
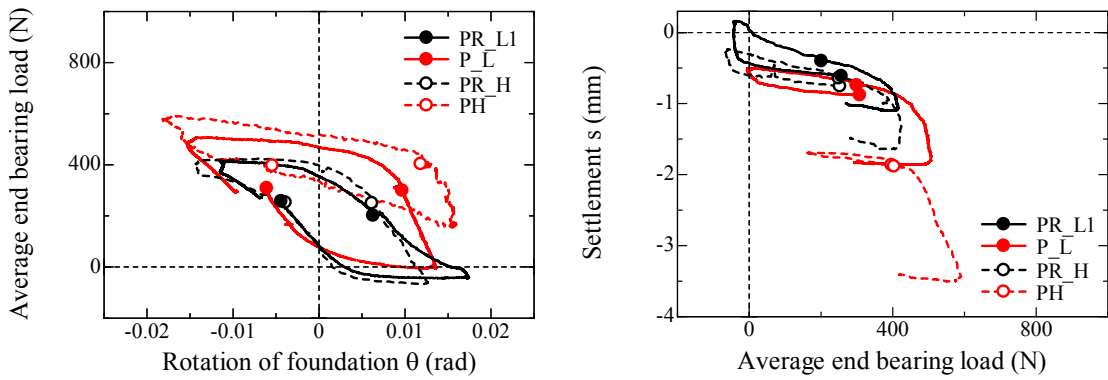
(e) End bearing load (Right pile)
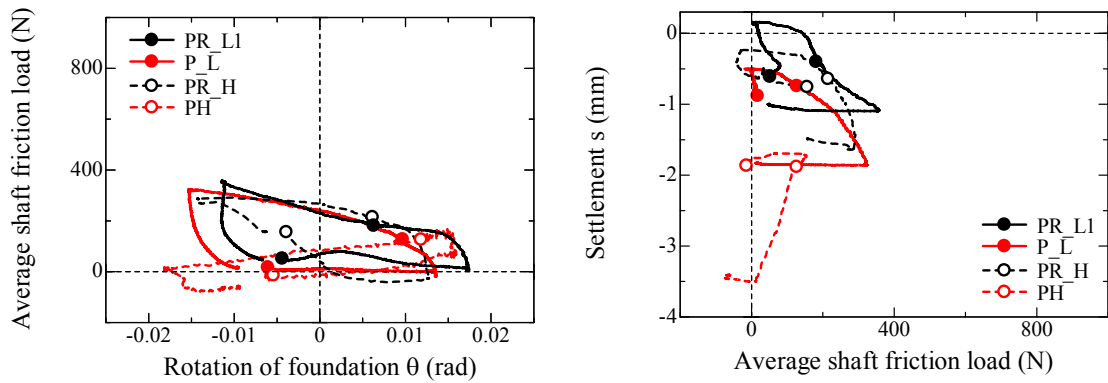
(f) Shaft friction load (Right pile)

A. 5.5.2.18 Variation of pile load with rotation of foundation θ or settlement observed in loading step 5 and 6 (δ$_{LDT}$=±2mm, h/S=1).

A140

(a) Axial load at pile head (Left pile)
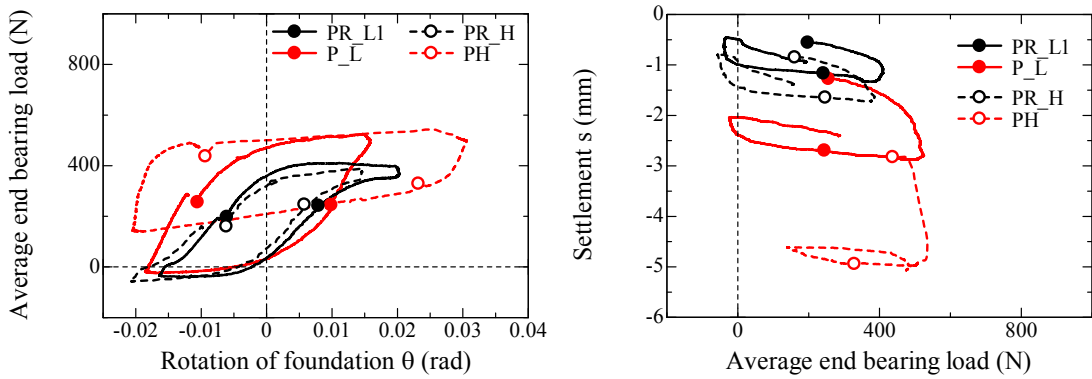
(b) End bearing load (Left pile)
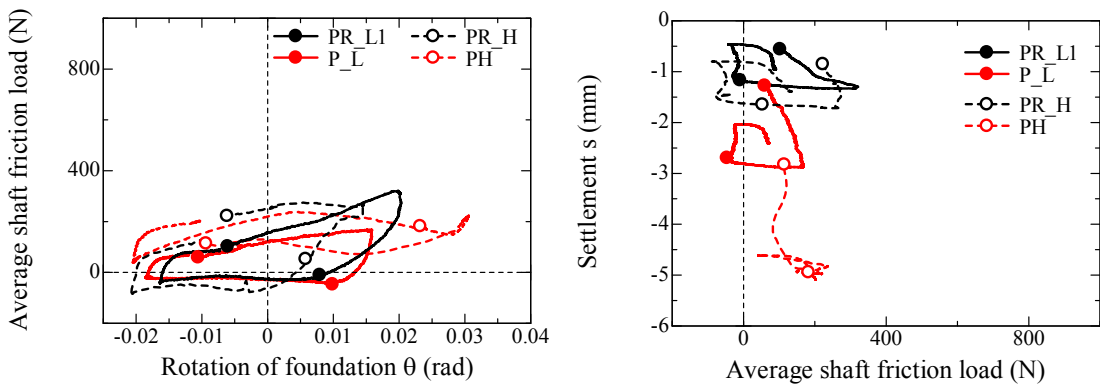
(c) Shaft friction load (Left pile)

A. 5.5.2.19 Variation of pile load with rotation of foundation θ or settlement observed in loading step 7 and 8 (δ$_{LDT}$=±2mm, h/S=1.8).

A141

(d) Axial load at pile head (Right pile)

(e) End bearing load (Right pile)

(f) Shaft friction load (Right pile)

A. 5.5.2.19 Variation of pile load with rotation of foundation θ or settlement observed in loading step 7 and 8 (δ$_{LDT}$=±2mm, h/S=1.8).
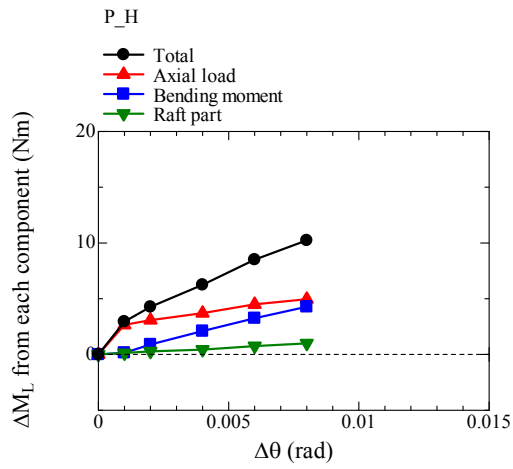
A142
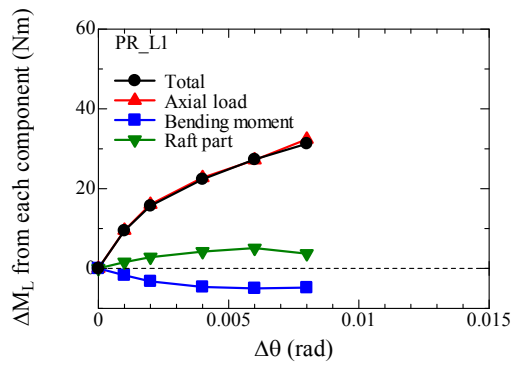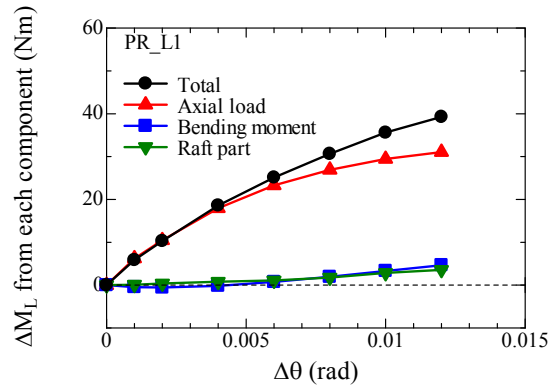
(a) $\delta_{LDT}=\pm 1mm$, h/S=1
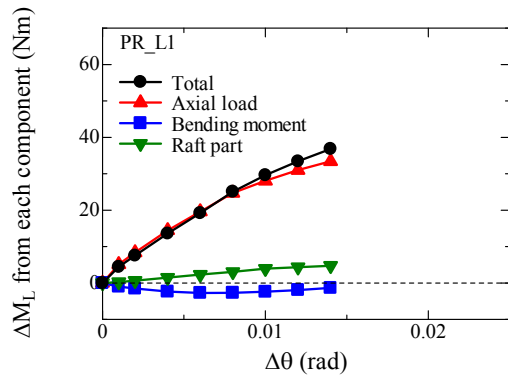
(b) $\delta_{LDT}=\pm 1mm$, h/S=1.8

(c) $\delta_{LDT}=\pm 2mm$, h/S=1
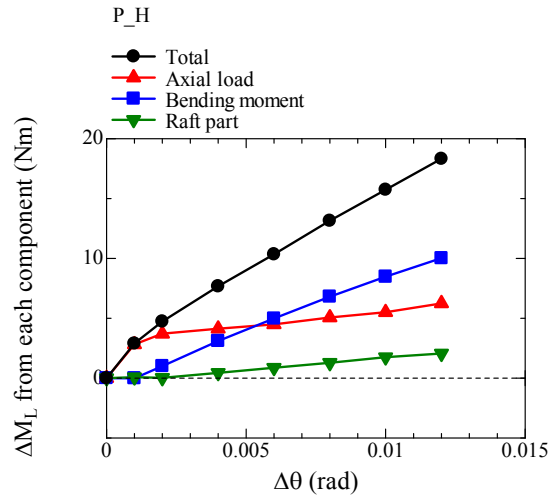
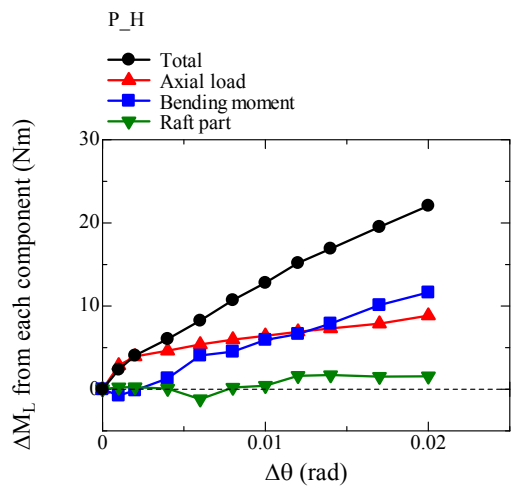(d) $\delta_{LDT}=\pm 2mm$, h/S=1.8

A. 5.5.3.1 Relationship between $\Delta\theta$ and ΔM_L from axial load at pile head, bending moment at pile head and raft part.for PR_L1.
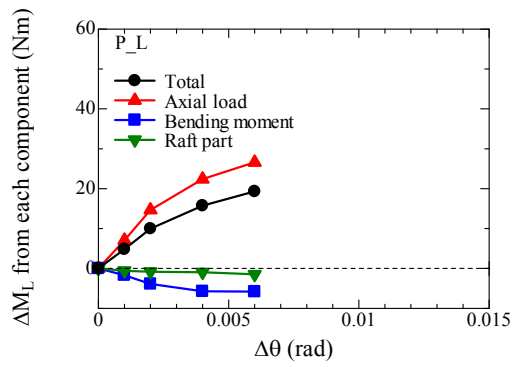
(a) $\delta_{LDT}=\pm1$mm, h/S=1
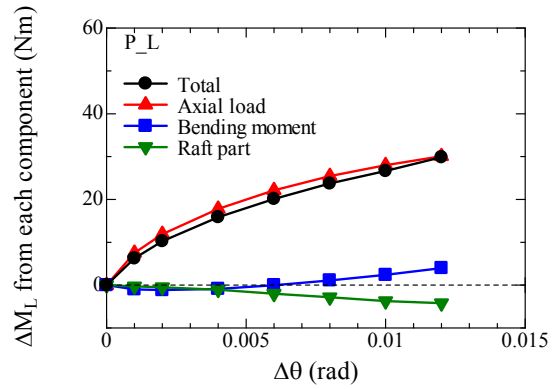
(b) $\delta_{LDT}=\pm1$mm, h/S=1.8
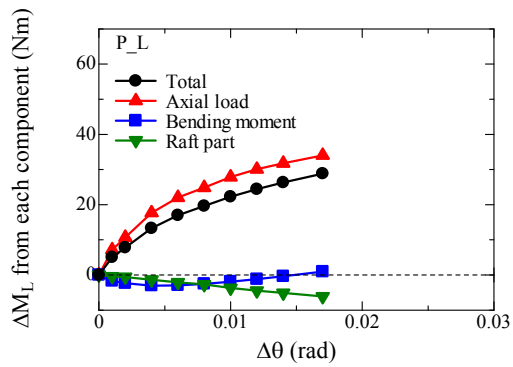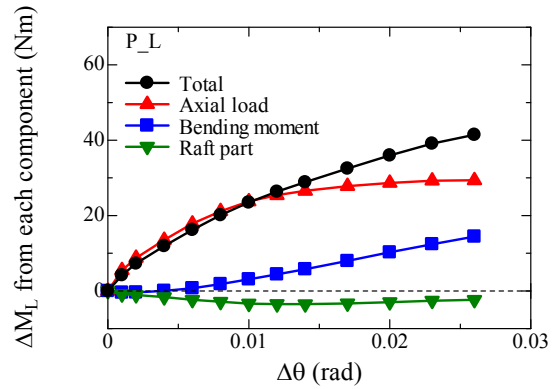
(c) $\delta_{LDT}=\pm2$mm, h/S=1

(d) $\delta_{LDT}=\pm2$mm, h/S=1.8

A. 5.5.3.2 Relationship between $\Delta\theta$ and ΔM_L from axial load at pile head, bending moment at pile head and raft part.for P_L.
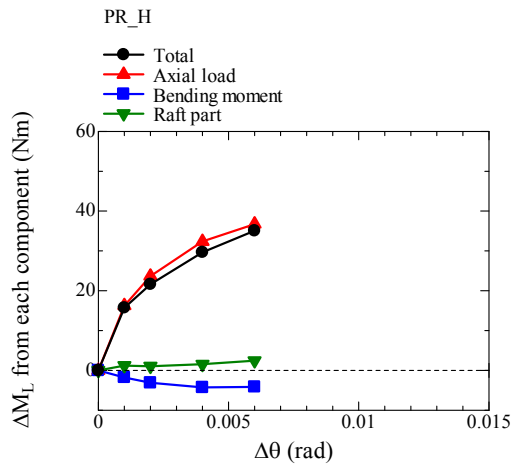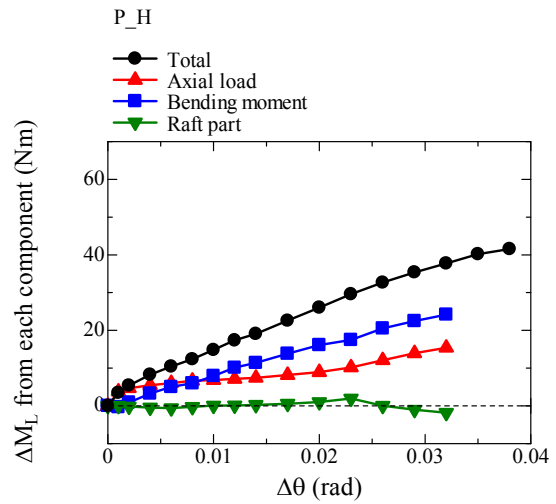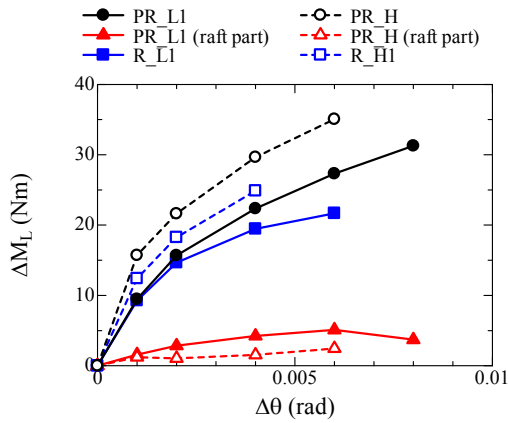
(a) $\delta_{LDT}=\pm 1$mm, h/S=1
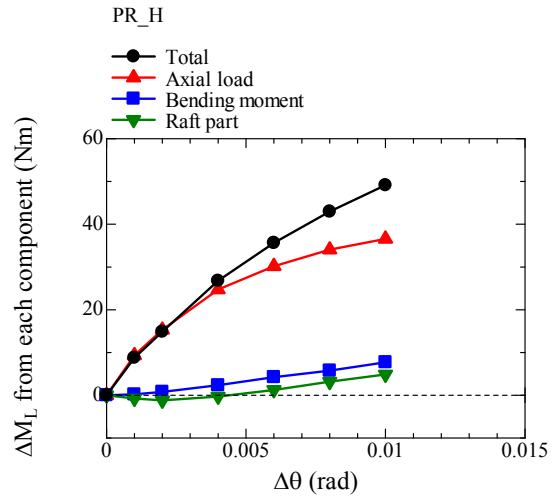
(b) $\delta_{LDT}=\pm 1$mm, h/S=1.8
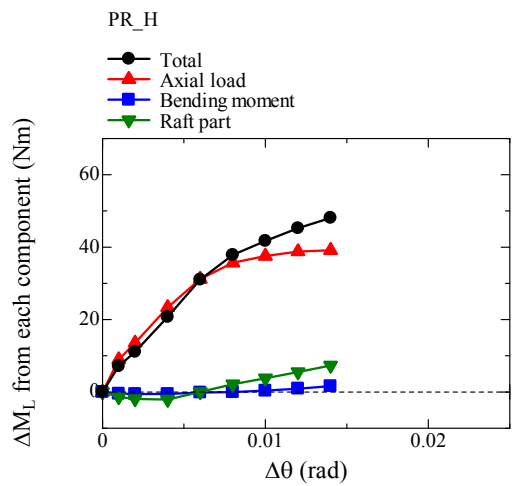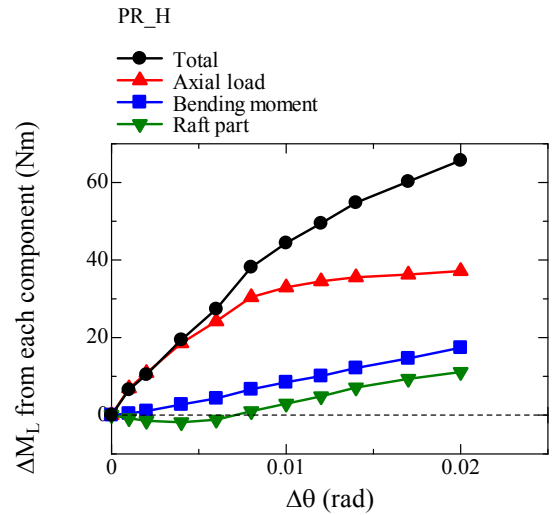
(c) $\delta_{LDT}=\pm 2$mm, h/S=1
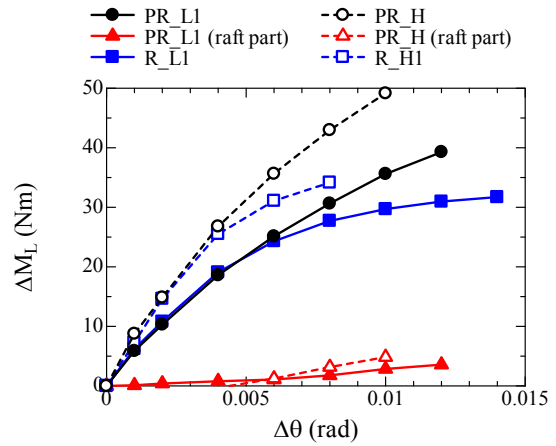
(d) $\delta_{LDT}=\pm 2$mm, h/S=1.8

A. 5.5.3.3 Relationship between $\Delta\theta$ and ΔM_L from axial load at pile head, bending moment at pile head and raft part.for PR_H.

A145

(a) $\delta_{LDT}=\pm 1mm$, h/S=1

(b) $\delta_{LDT}=\pm 1mm$, h/S=1.8

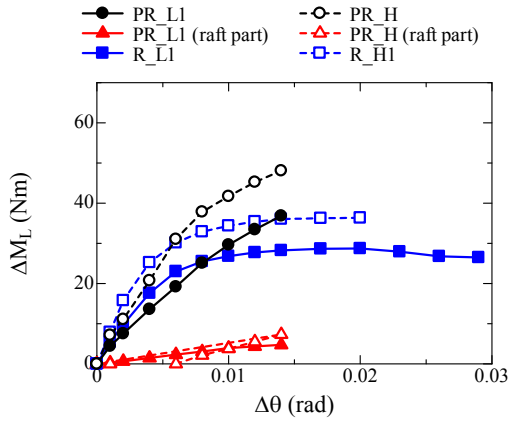(c) $\delta_{LDT}=\pm 2mm$, h/S=1

(d) $\delta_{LDT}=\pm 2mm$, h/S=1.8

A. 5.5.3.4 Relationship between $\Delta\theta$ and ΔM_L from axial load at pile head, bending moment at pile head and raft part.for P_H.
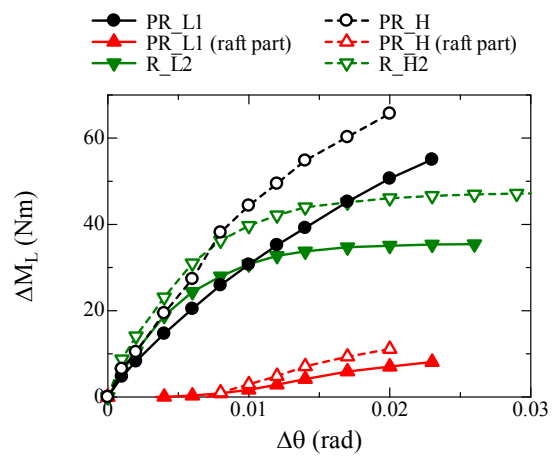
(a) $\delta_{LDT}=\pm 1$mm, h/S=1

(b) $\delta_{LDT}=\pm 1$mm, h/S=1.8

(c) $\delta_{LDT}=\pm 2$mm, h/S=1

(d) $\delta_{LDT}=\pm 2$mm, h/S=1.8

A. 5.5.3.5 Relationship between $\Delta\theta$ and ΔM_L of piled raft, raft part in piled raft and raft foundation for each loading step.